COORDINATION CHEMISTRY OF NIOBIUM(V) AND TANTALUM(V) WITH HARD O-DONOR LIGANDS: A SOLUTION AND SOLID STATE INVESTIGATION

by

Alebel Nibret Belay

A thesis submitted to meet the requirements for the degree of

Doctor of Philosophy (PhD)

in the

Department of Chemistry

in the Faculty of

Natural- and Agricultural Sciences

at the

University of the Free State

Supervisor: Dr. Johan Venter

Co-Supervisor: Prof. Andreas Roodt

February 2018

The Lord is my shepherd, I shall not want (Ps 23:1).

እግዚአብሔር እረኛዬ ነው፤ የሚያሳጣኝም የለም (መዝሙረ ዳዊት 23 ፥1) ።

Acknowledgements

First of all, I would like to thank Almighty God for giving me the strength, knowledge, ability and opportunity to undertake this research study and to persevere and complete it satisfactorily, without his blessings, this achievement would not have been possible.

I would like to express my deepest sense of gratitude to my supervisors, Prof Andreas Roodt and Dr. Johan A. Venter for their excellent guidance, fruitful comment, suggestion and constant support throughout my period of study at University of the Free State. And also their ability to inspire and stimulate the study of chemistry has meant the difference between a dream and reality.

I especially thank Prof Andreas Roodt for the systematic guidance and great effort he put into training me in the scientific field. This is great opportunity for me working on this project and I am very grateful for all the time he spends helping me understand crystallography and kinetics as well.

Again, I would like to thank Dr. Johan A.Venter was always there when I needed him and have inspired me to keep going through to the end and his encouragement.

My thanks further go to Dr. Gertruida J.S.Venter for tireless reading my chapters and she was collected most of my crystal structures, Dr. Ruben M. Drost for his fruitful discussion related to my work, while Dr. Linette Twigge was assisting for NMR training and data analysis as well.

I would like to thank the members of Prof Andreas Roodt's research group, past and present, for sharing their knowledge and experience. Additionally, my thanks further go to especially the crystallographic data collection team for providing such a pleasant atmosphere in which to work.

Furthermore, senior experimental and technical staff and research students in the Inorganic Chemistry Department, as well as finance staff members, Tessa Swarts and Callie Laubscher for all your help and co-operation over the years, none of this work would have been possible.

To all my friends (outside chemistry) I truly want to say thank you. Your constant inquiries into the welfare of me and my studies are truly appreciated, even if I know you don't have a clue what I am talking about.

Last but not least, I take this opportunity to express the profound gratitude deep from my heart to my beloved all family (my wife, Tsegenet Tesfahun Atalie and son, Yohannes Alebel Nibret), parents (my mam, dad and brothers, Adanech Mekonnen Zeleke, Nibret Belay Yimam and Demelash Nibret Belay as well as Kumilachew Mekonnen Ayenew), friends and relatives for their encouragement, love and moral support through the years.

There is no elevator to success. You have to take the stairs.

Declaration

(I) ''I, Alebel Nibret Belay, declare that the Doctoral Degree research thesis that I herewith submit for the Doctoral Degree qualification in Inorganic Chemistry at the University of the Free State is my independent work, and that I have not previously submitted it for a qualification at another institution of higher education.''

(II) ''I, Alebel Nibret Belay, that I am aware that the copyright is vested in the University of the Free State.''

(III) ''I, Alebel Nibret Belay, hereby declare that all royalties as regards intellectual property that was developed during the course of and/or in connection with the study at the University of the Free State, will accrue to the University.''

Alebel Nibret Belay   Signature…………………….

Dedication

This work is dedicated to my family; past, present and future…

I dedicate this work to:

My respected parents who have supported and encouraged me all of time.

My wife Tsegenet Tesfahun Atalie for her patience, efforts and generous support.

My sweet baby Yohannes Alebel Nibret.

List of publications and conferences

This thesis is based on the work reported in the following papers and conferences:

1. **A.N. Belay**, R. Koen, J.A. Venter, R.M. Drost, Tris(N-nitroso-N-phenylhydroxyl-aminato-k^2 O,O') Oxido Niobium(V), $C_{18}H_{15}N_6O_7Nb$. *Z. Kristallogr. NCS*., **2016**, 231(2), 513-515. DOI: 10.1515/ncrs-2015-0172.

2. **A.N**. **Belay**, J.A. Venter, A. Roodt, The crystal structure of triphenylphosphineoxide-2,5-dichloro-3,6-dihydroxycyclohexa-2,5-diene-1,4-dione (2/1), $C_{42}H_{32}Cl_2O_6P_2$, *Z. Kristallogr. NCS*., **2017**, 232(2), 163-164. DOI: 10.1515/ncrs-2016-064.

3. **A.N. Belay**, J.A. Venter, G.J.S.Venter, A. Roodt, Kinetics and structural studies of niobium(V) 2,5-dichloro-3,6-dihydroxy-1,4-benzoquinonato complexes. Intend to be submitting to *J. Chem. Soc., Dalton Trans*., at the beginning of 2018.

4. **A.N. Belay**, J.A. Venter, G.J.S. Venter, A. Roodt, Investigation of solid state structural differences between niobium(V)- and tantalum(V) 2-hydroxpyridinato-N-oxide complexes. Intend to be submitting to *Journal of Coordination Chemistry* at the beginning of 2018.

5. **A.N. Belay**, J.A. Venter, A. Roodt, The crystal structure and IR spectroscopic properties of 2,5-dichloro-3,6-dihydroxycyclohexa-2,5-diene-1,4-dione-4-N,N-dimethylamino-pyridinium, ($2½(caH_2)(DMAP)_6.11H_2O$). Intend to be submitting to *Journal of Chemical Crystallography* at the beginning of 2018.

Conferences:

1. Synthesis and characterization of Nb(V) complexes with O,O' bidentate ligands, presented at: *Indaba8 Serendipity vs Prediction Conference*, 16-21 August 2015 Skukuza in the Kruger National Park, South Africa (Funded by the International Union of Crystallography (IUCr) and the International Council for Science (ICSU)).

2. Crystal structures and characterization of $(Et_4N)[MCl_6]$ (M = Nb and Ta) as novel synthons to pursue coordination chemistry with O,O'-bidentate ligands, presented at: *the first Pan African Conference of Crystallography*, at Dschang (Cameroon), 06-10 October, 2016 which won a prize for the presentation (Funded by Cameroon Crystallography Association

(CCrA) and the International Union of Crystallography (IUCr) in collaboration with UNESCO and ICSU.

3. Coordination Chemistry: Niobium(V) and Tantalum(V) with O,O'-bidentate ligands, presented at: *the 24th Congress and General Assembly of the International Union of Crystallography (IUCr)* in Hyderabad, India, 21-28 Aug 2017, was on this latter occasion invited to take part in a formal round table discussion at the IUCr2017 meeting, this contributed to expanding science in Africa, as well as selected to be the Ethiopian representative on the steering committee for the future African Crystallographic Association (AfCA) (Funded by The World Academy of Sciences (TWAS)).

Overall, this thesis is structured as follows: Chapter **1** present general introduction and the motivation, Chapter **2** literature review, Chapter **3** new synthon method (experimental part), Chapter **4**, **5** and **6** which describe solid state crystal structures of selected complexes, co-crystals as well as free ligands including results and discussion, Chapter **7** evaluation and comparison with related studies, Chapter **8** mechanistic study (solution state) of selected complex, Chapter **9** evaluation of study and future work, Chapter **10** supplementary crystallographic data (Appendixes **A-C**) and kinetic data (Appendix **D**). Overall, the references of each chapter are independently sited.

Table of Contents

List of Figures

[NbO(ca)$_2$(H$_2$O)OPPh$_3$]$^-$ (0.013 M) in acetonitrile (CD$_3$CN) at 25 °C. Insert (a) illustrates the relative integrals of the signals at X, Y andZ and the chemical shifts of the different signals. X = decreasing *cis*-[NbO(ca)$_2$(MeCN)OPPh$_3$]$^-$, Y = decreasing *cis*-[NbO(ca)$_2$(H$_2$O)OPPh$_3$]$^-$ and Z = increasing liberated free triphenylphosphineoxide (OPPh$_3$) (signal at 32.6 ppm).   214

List of Tables

Abbreviations and Symbols

Abbreviations	Meaning
phen	1,10-Phenanthroline
terpy	2,2': 6',2"-Terpyridine
dipyno	2,2'-Dipyridyl-N-oxide
dhbqH$_2$	2,5-Dihydroxy-1,4-benzoquinone
hopoH	2-Hydroxypyridine-N-oxide (1-hydroxy-2-pyridone).
mpoH	2-Mercaptoypyridine-N-oxide (2-pyridinethiol-1-oxide or pyrithione)
Brpy	3-Bromopyridine
Clpy	3-Chloropyridine
dmap	4-(Dimethylamino)pyridine
Mepy	4-Methylpyridine
qno	8-Hydroxyquinolin-N-oxide
phenbq	9,10-Phenanthrenequinone
MeCN	Acetonitrile
pKa	Acid dissociation constant
a-py	a-Pyridoin
ATR-FTIR	Attenuated total reflection-fourier transform infrared spectroscopy
(L, L') or Bid	Bidentate ligand
CSD	Cambridge structural database
δ	Chemical shift
caH	Chloranilate anion
ca	Chloranilate dianion
cupfH	Cupferron (the ammonium salt of N-nitroso-N-phenylhydroxylamine)
DMF	Dimethylformamide
DMSO	Dimethylsulfoxide
eq	Equation
K	Equilibrium constant

ε	Extinction coefficient
X	Generally halogen, (F, Cl, Br, I) also a leaving group
η	Hapticity
^{i}Pr	Isopropyl
MeOH	Methanol
^{n}Bu	n-Butyl
neocupfH	Neocupferron (N-Nitroso-N-(1-naphthyl)hydroxylamine ammonium salt)
$NbCl_5$	Niobium pentachloride
NMR	Nuclear magnetic resonance spectroscopy
k_{obs}	Observed rate constant
picoH	Picolinic acid-N-oxide
py	Pyridine
k	Rate constant
μ	Signifies a bridging ligand
SXRD	Single crystal X-ray diffraction.
ν	Stretching frequency on IR
$TaCl_5$	Tantalum pentachloride
tBu	Tertiary butyl
$Et_4(N^+)Cl^-$ or TEAC	Tetraethylammoniumchloride
THF	Tetrahydrofuran
Et_3N	Triethylamine
$OPPh_3$	Triphenylphosphineoxide
UV-Vis	Ultraviolet-visible spectroscopy
caH_2	Undissociated chloranilic acid (2,5-Dichloro-3,6-dihydroxy-2,5-cyclohexadiene-1,4-dione)
ppm	Units of chemical shift (parts per million)

Abstract

This thesis describes the study directed towards the synthesis, characterization and substitution kinetics of novel niobium(V) and tantalum(V) complexes containing selected O,O'-bidentate ligands that could potentially be used for the separation of niobium from tantalum. There is also a search for complexes that will be attractive and useful as advanced materials for high technology applications and in the nuclear power environment. The study included systematic assessment of the physical and chemical behaviour of the free ligands, co-crystals and complexes as well as the factors which govern their stability, reactivity, coordination geometry, bond lengths and angles, π-π stacking interaction and inter- and intramolecular networks of hydrogen bonds. It became evident that the crystal stabilization was influenced by intermolecular π-π interactions and inter- and intramolecular hydrogen and halogen bond networks, producing a stabilized crystal lattice.

A range of Nb(V) and Ta(V) complexes such as cis-(Et$_4$N)[NbO(ca)$_2$(H$_2$O)OPPh$_3$]·3H$_2$O··THF (**5**), (Et$_4$N)$_4$[Nb$_4$O$_4$(ca)$_2$(μ^2-O)$_2$Cl$_8$]·2CH$_3$CN (**6**), [NbO(cupf)$_3$] (**7**), [NbO(hopo)$_3$]·MeOH (**8**), [TaO(hopo)$_3$]·MeOH (**9**), [Ta(hopo)$_4$]Cl·2MeCN·2H$_2$O (**10**) (where ca = 2,5-dichloro-3,6-dihydroxy-1,4-benzoquinonato, cupf = N-nitroso-N-phenylhydroxylaminato, hopo = 2-hydroxypyridinato-N-oxide) as well as two co-crystals [OPPh$_3$½(caH$_2$)] (**2**) and [(2½(caH$_2$)(DMAP)$_6$·11H$_2$O)] (**4**) were prepared and characterised by IR (ATR), NMR (^{1}H, ^{13}C and ^{31}P), UV-Vis spectroscopy and single crystal X-ray diffraction. Additionally, two free ligands, [½(caH$_2$)·H$_2$O] (**1**) and [hopoH] (**3**), were characterised by single crystal X-ray diffraction.

The six-, seven- and eight coordinate geometries show different coordination modes as observed in complexes (**5**) and (**7**) (D_{5h} pentagonal bipyramidal geometry), (**6**) (a regular octahedral coordination mode), (**8**) (C_{3v}-capped octahedral geometry), (**9**) (C_2-capped trigonal prismatic geometry) and (**10**) (D_2-square antiprismatic geometry). Therefore, these different geometries found in complexes (**5**), (**6**), (**7**), (**8**), (**9**) and (**10**) describe the shape of complexes with six, seven and eight oxygen atoms bound to the niobium(V) and tantalum(V) metal centres, with the differences playing a possible key role to increase the potential of a new type of separation of niobium from tantalum.

Starting with the selected complex, *cis*-[NbO(ca)$_2$(H$_2$O)(OPPh$_3$)]$^-$, the substitution of the triphenyl-phosphineoxide by pyridine-type ligands such as pyridine (py), 4-N,N-dimethyl-aminopyridine (DMAP), 4-methylpyridine (4-Mepy), 3-chloropyridine (3-Clpy) and 3-bromopyridine (3-Brpy) in acetonitrile media at 31.2 °C were determined and evaluated. These entering monodentate ligands could be arranged in terms of their increasing reactivity values: 3-Brpy < 3-Clpy < 4-Mepy < py < DMAP, defined by the values of k_f = 0.147(4) x 10^{-2}; 0.206(7) x 10^{-2}; 0.181(6) x 10^{-2}; 0.131(2) x 10^{-2} and 2.032(2) x 10^{-2} M^{-1}s^{-1} respectively. The *pseudo* first-order rate constants were dependent on concentration and temperature. From the observed kinetic results a suitable mechanism was proposed.

Activation parameters were determined for the reaction of the complex, *cis*-[NbO(ca)$_2$(H$_2$O)(OPPh$_3$)]$^-$, with 4-N,N-dimethylaminopyridine (DMAP) as entering ligand. The activation parameters for these triphenylphosphineoxide substitution reactions were calculated as 51.5(9) k J mol^{-1} and -108(3) J K^{-1} mol^{-1} for the standard change of enthalpy ($\Delta H^{\neq}_{(kf)}$) and the standard change of entropy ($\Delta S^{\neq}_{(kf)}$) respectively. The negative entropy of activation implies a more ordered state and presumably this substitution reaction could involve an associative ligand substitution mechanism.

Although only part of a preliminary study, a range of novel Nb(V) and Ta(V) complexes with O,O'-, O,N- and N,N'-bidentate ligands were synthesised and characterised by IR (ATR), NMR (^{1}H and ^{13}C) and UV-Vis spectroscopy. The reaction of [NbCl$_6$]$^-$ with chloranilic acid (caH$_2$) in solution gave *cis*-[NbO(ca)$_2$(H$_2$O)]$^-$, which react further with added triphenylphosphineoxide (OPPh$_3$) to give the final product, *cis*-[NbO(ca)$_2$(H$_2$O)OPPh$_3$]$^-$.

Knowledge obtained from this study should contribute to the understanding of the chemical and physical properties of the various Nb(V) and Ta(V) complexes and identify possible differences to apply in future for developing potential separation methods for niobium from tantalum.

Keywords: Niobium(V), Tantalum(V), Coordination geometry, O,O'-bidentate ligands, Pyridine derivatives, Separation, Substitution kinetics, Spectroscopic studies and X-ray crystallography.

Opsomming

Hierdie tesis beskryf die studie wat gerig was op die sintese, karakterisering en substitusie-kinetika van nuwe niobium(V) en tantalum(V) komplekse wat geselekteerde O,O'-bidentate ligande bevat wat moontlik gebruik kan word vir die skeiding van niobium en tantalum. Daar is ook 'n soektog na komplekse wat aanloklik en nuttig as gevorderde stowwe vir hoë tegnologie toepassings en in die kernkrag omgewing sal wees. Die studie het 'n sistematiese beoordeling van die fisiese en chemiese gedrag van die vry ligande, ko-kristalle en komplekse asook die faktore wat hulle stabiliteit, reaktiwiteit, koördinasiegeometrie, bindingslengtes- en hoeke, π-π stapelingsinteraksie en inter- sowel as intramolekulêre netwerke van waterstofbindings ingesluit. Dit het duidelik geword dat die kristalstabilisasie beïnvloed is deur intermolekulêre π-π interaksies asook inter- en intramolekulêre netwerke van waterstof- en halogeenbindings, wat 'n gestabiliseerde kristalrooster tot gevolg het.

'n Reeks van Nb(V) en Ta(V) komplekse soos cis-(Et$_4$N)[NbO(ca)$_2$(H$_2$O)OPPh$_3$]·3H$_2$O·THF (**5**), (Et$_4$N)$_4$[Nb$_4$O$_4$(ca)$_2$(μ^2-O)$_2$Cl$_8$]·2CH$_3$CN (**6**), [NbO(cupf)$_3$] (**7**), [NbO(hopo)$_3$]·MeOH (**8**), [TaO(hopo)$_3$]·MeOH (**9**), [Ta(hopo)$_4$]Cl·2MeCN·2H$_2$O (**10**) (waar ca = 2,5-dichloro-3,6-dihidroksi-1,4-bensokwinonato, cupf = N-nitroso-N-fenielhidroksielaminato, hopo = 2-hydroksipiridinato-N-oksied) sowel as twee ko-kristalle, [OPPh$_3$½(caH$_2$)] (**2**) en [(2½(caH$_2$)(DMAP)$_6$·11H$_2$O)] (**4**) is berei en gekarakteriseer deur IR (ATR), KMR (^{1}H, ^{13}C en ^{31}P), UV-Vis spektroskopie en enkelkristal X-straaldiffraksie. Bykomend is twee vry ligande, [½(caH$_2$)·H$_2$O] (**1**) en [hopoH] (**3**), gekarakteriseer deur enkelkristal X-straaldiffraksie.

Die ses-, sewe- en agtgekoördineerde geometrieë vertoon verskillende wyses van koördinering soos waargeneem in komplekse (**5**) en (**7**) (D_{5h} pentagonale bipiramidale geometrie), (**6**) ('n gewone oktahedriese koördinering), (**8**) (C_{3v}-gekroonde oktahedriese geometrie), (**9**) (C_2-gekroonde trigonale prismatiese geometrie) en (**10**) (D_2-vierkantig antiprismatiese geometrie). Die verskillende geometrieë soos waargeneem in komplekse (**5**), (**6**), (**7**), (**8**), (**9**) en (**10**) beskryf die vorm van komplekse met ses, sewe en agt suurstofatome gebonde aan die niobium(V) en tantalum(V) metaalsentrums, waar die verskille 'n moontlike sleutelrol kan speel om die potensiaal van 'n nuwe tipe skeiding van niobium van tantalum te vergroot.

Beginnende met die gekose kompleks, *cis*-[NbO(ca)$_2$(H$_2$O)(OPPh$_3$)]$^-$, is die substitusie van trifenielfosfienoksied deur piridien tipe ligande soos piridien (py), 4-N,N-dimetiel-aminopiridien (DMAP), 4-metielpiridien (4-Mepy), 3-chloropiridien (3-Clpy) en 3-bromopiridien (3-Brpy) in asetonitrielmedium by 31.2 ^{o}C bepaal en ge-evalueer. Hierdie inkomende monodentate ligande kan gerangskik word in terme van hulle toenemende reaktiwiteitswaardes: 3-Brpy < 3-Clpy < 4-Mepy < py < DMAP, gedefinieer deur die waardes van k_f = 0.147(4) x 10^{-2}; 0.206(7) x 10^{-2}; 0.181(6) x 10^{-2}; 0.131(2) x 10^{-2} en 2.032(2) x 10^{-2} M^{-1}s^{-1} respektiewelik. Die *pseudo* eerste-orde tempokonstantes was afhanklik van konsentrasie en temperatuur. Vanaf die waargenome kinetiese resultate kon 'n toepaslike meganisme voorgestel word.

Aktiveringsparameters is bepaal vir die reaksie van die kompleks, *cis*-[NbO(ca)$_2$(H$_2$O)(OPPh$_3$)]$^-$ met 4-N,N-dimetielaminopiridien (DMAP) as inkomende ligand. Die aktiveringsparameters vir hierdie trifenielfosfienoksied substitusiereaksies is bereken as 51.5(9) k J mol^{-1} en -108(3) J K^{-1} mol^{-1} vir die standaard entalpieverandering ($\Delta H^{\neq}_{(kf)}$) en die standaard entropieverandering ($\Delta S^{\neq}_{(kf)}$) respektiewelik. Die negatiewe aktiveringsentropie impliseer 'n meer geordende toestand en dat hierdie substitusiereaksie moontlik volgens 'n assosiatiewe meganisme van ligandsubstitusie plaasvind.

Alhoewel slegs deel van 'n voorlopige studie, is 'n reeks nuwe Nb(V) en Ta(V) komplekse met O,O'-, O,N- en N,N'-bidentate ligande berei en gekarakteriseer met behulp van IR (ATR), KMR (^{1}H and ^{13}C) en UV-Vis spektroskopie. Die reaksie van [NbCl$_6$]$^-$ met chlooranilieksuur (caH$_2$) in oplossing lewer *cis*-[NbO(ca)$_2$(H$_2$O)]$^-$, wat verder met bygevoegde trifenielfosfienoksied (OPPh$_3$) reageer om die finale produk *cis*-[NbO(ca)$_2$(H$_2$O)OPPh$_3$]$^-$ te lewer.

Kennis wat met hierdie studie ingewin is behoort te lei tot 'n beter insig en begrip van die chemiese en fisiese eienskappe van die verskeie Nb(V) en Ta(V) komplekse en om moontlike verskille te identifiseer om in die toekoms toe te pas vir die ontwikkeling van metodes vir die skeiding van niobium en tantalum.

Sleutelwoorde: Niobium(V), Tantalum(V), Koördinasiegeometrie, O,O'-bidentate ligande, Piridienderivate, Skeiding, Substitusiekinetika, Spektroskopiese studies en X-straal-kristallografie.

1 Background and Aim of the study

1.1 Introduction

Niobium (atomic number 41) and tantalum (atomic number 73) occur in nature almost entirely as single isotopes (Nb^{93} and Ta^{181}), and they commonly substitute for one another in minerals because they both have similar ionic radii and occur mostly in the pentavalent state.[1] These similarities in chemical and physical properties are the reason for the difficult separation of these two elements during the processing of tantalum and niobium containing minerals. In recent times attempts have been made not only to quantify the chemical separation process but also to take into account other variables such as yields, the price of reaction components, safety in handling chemicals, hardware demands and ease of product workup and purification. The current tantalum and niobium separation methods are very expensive, high reaction temperatures are required, toxic waste gasses such as chlorine and phosgene are evolved, the use of dangerous acids such as hydrofluoric acid (HF) are required, hazardous waste products (eg. metal fluorides) are formed and these procedures are very laborious.[2,3]

This thesis, which attempts to avoid very strong acids such as HF and to reduce expensive instrumentation costs and as well as tedious procedures, aims to expand knowledge of the range of O,O'-bidentate ligands known to coordinate to Nb and Ta and design a different strategy which is characterized by being a novel, safe and more environment friendly way to separate the two metals. This approach investigates the synthesis and characterization of niobium(V) and tantalum(V) complexes chelated with various tailored organic mono-, bi- and multidentate ligands. In the past few years of this broader study, ligands used include the N,N'-, N,O-, O,O'-,

---

[1] R.L. Parker, M. Fleischer, *A review of the geochemistry of niobium and tantalum*, U.S. Government Printing Office Washington, DC, 1-43, 1968.

[2] W. Urbaniak, K. Jurek, K. Witt, A. Goracko, *CHEMIK*, **65**, 273-282, 2011.

[3] W.R. Cullen, S.J. Rettig, E.B. Wickenheizer, *J. Organomet. Chem.*, **370**, 141-148, 1989.

S,S'-and S,O- bidentate ligands such as acetylacetone, 8-hydroxyquinoline and tropolone type ligands, with relative success. The products obtained from these reactions were studied and crystalline products collected for single crystal X-ray diffraction analysis.

The results of these tantalum(V) and niobium(V) complexes have been shown that the different chelating behavior might be exploited as a possible separation technique. Niobium(V) like tantalum(V) can be regarded as hard metal centers and their halide species are known to readily hydrolyze.[4] As previously stated, this group 5 metals and their behaviour towards different ligands, which include mono- (halido and pseudo halido) and bidentate hard ligands with O,O'- and N,O-donor atoms were investigated in our group,[5,6,7,8] but in a vast majority of the cases, these compounds were synthesized under an inert atmosphere and favored a *mono-* chelated moiety.[9,10,11] The instability of these complexes in ambient conditions can be ascribed to the hydrolyzation of the metal synthon, eg. $NbCl_5$ or $TaCl_5$.[12] However, some exceptions are observed where *mono-* coordination of the bidentate ligand had taken place in hydrous conditions, but this seems to be an exception, rather than the norm.[13]

Niobium and tantalum pentahalides are scarcely soluble in non-coordinating solvents, and easily susceptible to hydrolysis by traces of moisture and are difficult to handle and store. This could probably be the main reason why the coordination chemistry of group 5 metals are significantly less developed than that of other transition metal halides (e.g. group 4 metal tetrahalides), and the data reported in the literature up to 2007 were sparse and incomplete.[14] The reactivity of niobium and tantalum pentahalides with limited, stoichiometric amounts of oxygen donor ligands was

[4] J.B. Lambert, *Kirk-Othmer Encyclopedia of Chemical. Technology. John Wiley & Sons, Inc., New York, NY*, 1-23, 2011.

[5] A.N. Belay, R. Kone, R.M. Drost, J.A. Venter, *Z.kristallogr. NCS*, **231**(2), 513-515, 2016.

[6] L. Herbst, H.G. Visser, A. Roodt, *Advanced Materials Research,* **1019**, 412-418, 2014

[7] R. Koen, A. Roodt, H.G. Visser, *Advanced Materials Research,* **1019**, 426-432, 2014.

[8] A.N. Belay, J.A. Venter, A. Roodt, *Z.kristallogr. NCS*, **232**(2), 163-164, 2017.

[9] H.O. Davies, T.J. Leedlam, A.C. Jones, *Polyhedron*, **18**, 3165-3172, 1999.

[10] P. Wendrup, V.G. Kessler, *J. Chem. Soc.*, *Dalton Trans.*, 574-579, 2001.

[11] L. Herbst, H.G. Visser, C. Pretorius, A. Roodt, *Acta Cryst.*, **E68**, m1392-m1394, 2012.

[12] D. Soria, J. Grundy, M. Coles, P. Hitchcock, *J. Organomet. Chem.*, **690**, 2278-2284, 2005.

[13] R. Kergoat, J.E. Guerchais, *J. Less Common Met.*, **39**, 91-98, 1975.

[14] F. Marchetti, G. Pampaloni, S. Zacchini, *J. Chem. Soc.*, *Dalton Trans.*, 4343-4351, 2007.

scarcely investigated in the past, and only a few coordination adducts of MCl$_5$ (M = Nb, Ta) with O-donors were isolated and characterised.[15] Therefore, it is essential to increase our knowledge and obtain improvement of stability of the various niobium(V) and tantalum(V) complexes, which are crucial to furthering the separation process to an industrial level.

1.2 Coordination mode of selected bidentate ligands (L,L')

Bidentate and multidentate ligands play an important role in organometallic and coordination chemistry, because of enhancing the stability of complexes and enforcing constrained coordination environments in comparison to their analogues containing monodentate ligands.[16]

1.2.1 Coordination mode of chloranilic acid ligand (caH$_2$)

Chloranilic acid or 2,5-dichloro-3,6-dihydroxy-2,5-cyclohexadiene-1,4-dione, caH$_2$ (Figure 1.1-1.3) are a sub-class of the quinoid compounds which are promising for the synthesis of novel functional materials. It was considered a unique multifunctional ligand system because they possess coordination, hydrogen bonding and ionic interaction sites, together with redox active π-electronic structures, affording rich coordination chemistry and also acts as strong proton donors and acceptors.[17]

[15] K. Feenan, G.W.A. Fowles, *J. Chem. Soc.*, 2449-2451, 1965.

[16] H. Kawaguchi, T. Matsuo, *J. Organomet. Chem.*, **689**, 4228-4243, 2004.

[17] K. Molcanov, B. Kojic-Prodicand, A. Meden, *Croat. Chem. Acta*, **82**(2), 387-396, 2009.
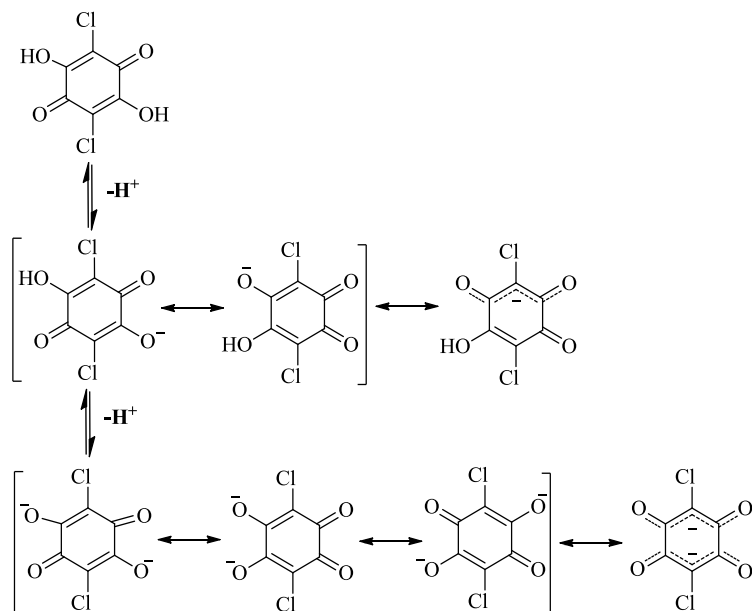
Figure 1.1 Dissociation of chloranilic acid (caH$_2$) to the monoanion (caH) and dianions (ca), with resonance structures shown in brackets (pKa_1 = 0.76 and pKa_2 = 2.58).[18]

The coordination modes referred to in Figure 1.2 are (A) monodentate and the less common, not observed in this study, (B) terminal bidentate and common, observed in this study, (C) bridging (bis) bidentate and the most common, observed in this study, (D) bis-carbanion bidentate and less common, not observed in this study, and (E) π-bonded bidentate and less common, not observed in this study.
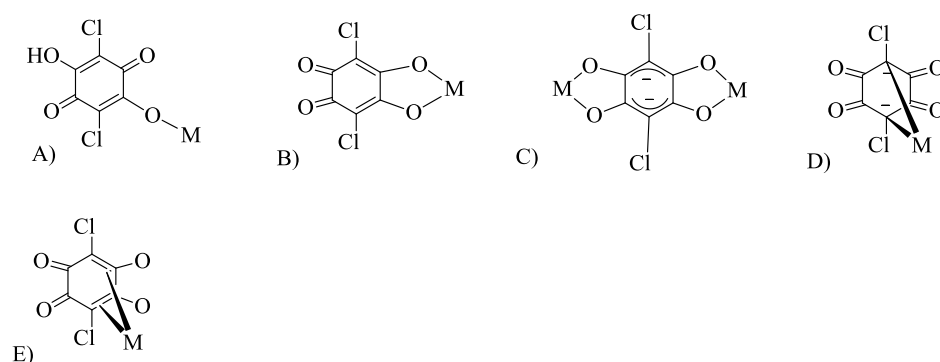
Figure 1.2 Five coordination modes of chloranilic acid (caH$_2$).[19]

---

[18] I.M. Sahar, *Transition Met. Chem.*, **24**, 306-310, 1999.

Figure 1.3 shows that the four oxygen donors along with delocalized orbitals of tetraoxolene enable the ligand to bind to metal ions in different coordination modes. The organic molecule can not only coordinate to metal ions via oxygen donors, but also through carbanions and π-bonding to bind metal ions to its carbon skeleton (Figure 1.2). In fact, there are five possible coordination modes for caH_2 and its analogues which are shown in Figure 1.2. With the help of hydrogen bonding exerted by the ligand itself and some guest molecules, for instance water, coordination polymers with 1D, 2D, and 3D structures composed of mono or dinuclear complex units are accessible.[20,21,22]
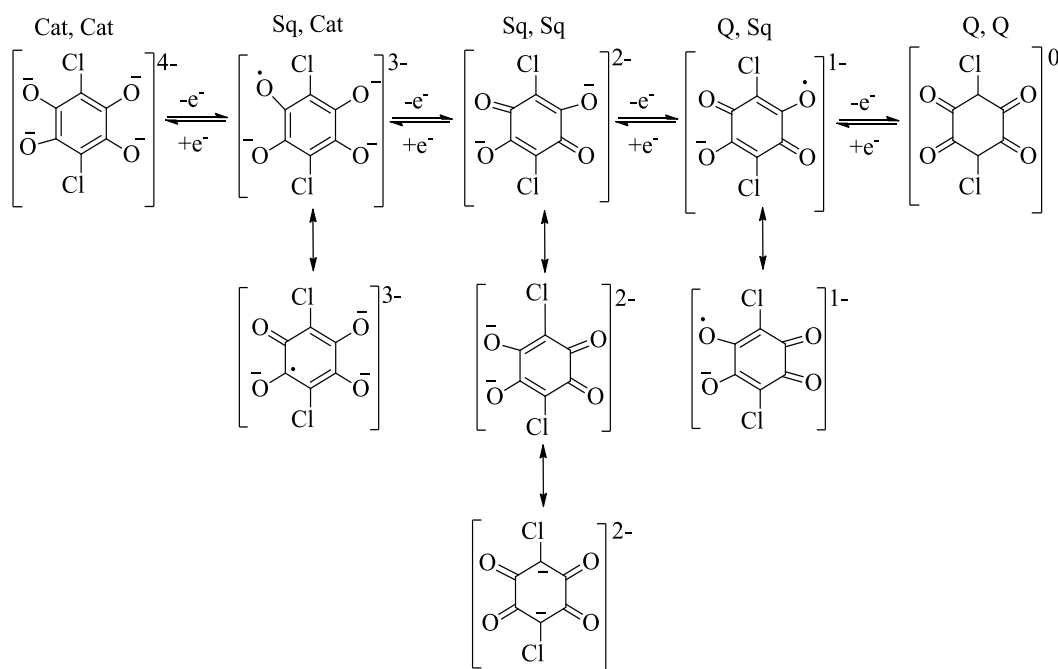
Figure 1.3 Oxidation states of chloranilic acid (caH_2) and their possible resonances structures, where the abbreviations "Cat", "Sq", and "Q" represents catecholate, semiquinone, and quinone respectively.[23]

[19] S. Kitagawa, S. Kawata, *Coord. Chem. Rev.*, **224**, 11-34, 2002.

[20] M. Kawahara, M.K. Kabir, K. Yamada, K. Adachi, H. Kumagai, Y. Narumi, K. Kindo, S. Kitagawa, S. Kawata, *Inorg. Chem.,* **43**(1), 92-100, 2004.

[21] T.T. Luo, Y.H. Liu, H.L. Tsai, C.C. Su, C.H. Ueng, K.L. Lu, *Eur. J. Inorg. Chem.*, **21,** 4253-4258, 2004.

[22] P.C.A. Bruijnincx, M. Viciano-Chumillas, M. Lutz, A.L. Spek, J. Reedijk, G. Koten, R.J.M.K. Gebbink, *Chem. Eur. J.,* **14**(18), 5567-5576, 2008.

[23] D. Guo, J.K. Mccusker, *Inorg. Chem.,* **46**(8), 3257-3274, 2007.

In mono-nuclear tetraoxolene complexes, electronic interaction takes place between the metal ion and the ligand, resulting in tautomers among which the metal ion and ligand have different oxidation states respectively (Figure 1.3). Nevertheless, in the dinuclear complexes with a bis-bidentate coordinating quinone, valence electrons of each metal centre are able to communicate through the delocalized orbitals of the ligand, and of course, interact with electrons in the frontier orbitals of the ligand as well. [24,25,26] Moreover, caH_2 is a well-known quinone derivative, which can coordinate metal ions as both bidentate and bis-bidentate modes allowing a variety of structures. Previously, they reported those bidentate mode of chloranilic acid forms mononuclear complexes with various transition metal ions.[27,28] But, the unsubstituted 2, 5-dihydroxyquinone behaves as a weak organic acid with p*Ka* values of 2.73 and 5.18, respectively.[29]

This thesis describes how new niobium and tantalum complexes with the caH_2 ligands were studied in terms of their reactivity and kinetic behaviour as part of a mechanistic study where differences in the outcome of those complexes would be exploited. Selected complexes could be subjected to competitive reactions in an attempt to enrich the reaction mixture with one of the two metal complexes. Positive results will be refined and optimized till the maximum separation is obtained.

[24] C. Carbonera, A. Dei, J.F. Latard, C. Sangregorio, L. Sorace, *Angew.Chem, Int. Ed.,* **43**(24), 3136-3138, 2004.

[25] A. Dei, D. Gatteschi, L. Pardi, U. Russo, *Inorg. Chem.,* **30**(12), 2589-2594, 1991.

[26] P. Gupta, A. Das, F. Basuli, A. Castineiras, W.S. Sheldrick, H. Mayer-Figge, S. Bhattacharya, *Inorg. Chem.,* **44**(6), 2081-2088, 2005.

[27] K. Nagayoshi, M.K. Kabir, H. Tobita, K. Honda, M. Kawahara, M. Katada, K. Adachi, H. Nishikawa, I. Ikemoto, H. Kumagai, Y. Hosokoshi, K. Inoue, S. Kitagawa, S. Kawata, *J. Am. Chem. Soc.*, **125**, 221, 2003.

[28] M.K. Kabir, N. Miyazaki, S. Kawata, K. Adachi, H. Kumagai, K. Inoue, S. Kitagawa, K. Iijima, *Coord. Chem. Rev.*, **198**, 157-169, 2000.

[29] K. Wallenfels, K. Friedrich, *Chem. Ber.*, **93**, 3070-3082, 1960.

1.2.2   Coordination mode of cupferron (cupfH)

The ammonium salt of N-phenyl-N-nitroso-hydroxylamine, known as cupferron (cupfH), is one of the most important and versatile reagents used in separations. Although more than fifty years have passed since its introduction by Baudisch,[30] considerable interest still centres on its use, as shown by recent publications.[31] The reagent is readily soluble in water, alcohol, ethyl acetate and chloroform. The ligand is considered to be bidentate, with coordination to the oxygen of the nitroso group and to the negatively charged oxygen. The acidity of the free acid derived from cupferron is due to the presence of the electronegative -NO group and the phenyl group. In addition, cupferron is a biologically active compound, known to display carcinogenic, genotoxic, mutagenic and DNA-damaging effects.[32,33]

The knowledge of the chemistry of cupferron and its analogues containing N-nitrosohydroxylamine fragments could contribute to a better understanding of the interaction of nitrogen oxide with metal centres of biologically important species, and during the last 20 years only one review concerning organic chemistry of N-nitrosohydroxylamine derivatives has been made available[34] and there have been no special revision on coordination chemistry except the one published by McCleverty in 1979.[35] Because it acts as a good ligand to hard transition metal centres to form stable complexes, it would form part of a range of related ligands, which include substituted cupferrate ligands like neocupferron, 2-methylcupferrate, 4-methylcupferrate, 3,5-dichlorocupferrate, and 3-acetylcupferrate, which are a prime focus of this PhD study. Four types of coordination of ionized N-nitrosohydroxylamine derivatives to the metallic cations or centres can be proposed (Figure 1.4) and only three of them (**A-C**) have so far been identified by X-ray structural analysis.[36]

---

[30] O. Baudisch, *Chem.-Ztg*., **33**, 1298-1300, 1909.

[31] R.C. Mehrotra, G. Wilkinson, Comprehensive Coordination chemistry, Pergamon, Oxford, U.K, in ed., **2**, Chap. 15.9, 1987.

[32] M. Shiino, Y. Watanabe, K. Umezawa, *Bioorg. Med. Chem.*, **9**, 1233-1240, 2001.

[33] M. Shiino, Y. Watanabe, K. Umezawa, *Bioorg. Chem*., **31**, 129-135, 2003.

[34] J.A. Hrabie, L.K. Keefer, *Chem. Rev.,* **102**(4), 1135-1154, 2002.

[35] J.A. McCleverty, *Chem. Rev*, **79**(1), 53-76, 1979.

[36] O. Kovalchukova, M. Ryabov, *Asian J. Chem*., **28**(9), 1873-1890, 2016.
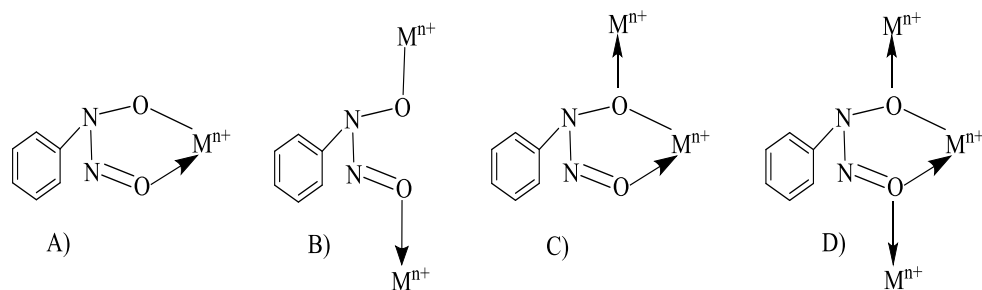
Figure 1.4 Coordination modes of the ammonium salt of N-nitroso-N-phenylhydroxylamine, cupferron (cupfH).

The coordination modes of cupferron, as shown in Figure 1.4 include (A) bidentate chelating (monometallic biconnective, O,O'-η^2), observed in this study, but (B) bidentate bridging (μ-O,O'), (C) bimetallic triconnective bridging (O,O'-η^2, O'- η^1) as well as (D) trimetallic tetraconnective bridging (μ-O,O', O,O'-η^2) are not observed in this study.

1.2.3 Coordination mode of 2-hydroxypyridine-N-oxide (hopoH)

The 2-hydroxypyridine-N-oxide (hopoH) ligand is capable of bidentate coordination with metals and act as a strong bidentate chelating agent for hard metals.[37] Based on a CSD search, 2-mercaptopyridine-N-oxide (mpoH)[38] and 2-hydroxypyridine-N-oxide (hopoH)[39] are the most studied ligands in the 2-substituted pyridine-N-oxide family after pyridine carboxylic acid N-oxides. Each ligand coordinates to the metal centres or cations with two, three and four ligands per metal with the general formula ML_2, ML_3 and ML_4. The molecular complexes described in the literature consider several potential donor sites for the aromatic N-oxides, such as the π-system of the heterocyclic group, the oxygen atom of the N-oxide group, or ring substituents, which interact with different acceptors.[40,41]

[37] X. Li, L. Yi-Zhi, L. San-Hui, C. Xue-Tai, Z. Jain-Hao, *Acta.Cryst.*, **E61**, m364-m366, 2005.

[38] U. Casellato, S. Sitran, S. Tamburini, P.A. Vigato, R. Graziani, *Inorg. Chim. Acta*, **95**, 37-42, 1984.

[39] A.E.V. Gorden, J. Xu, G. Szigethy, A. Oliver, D.K. Shuh, K.N. Raymond, *J. Am. Chem. Soc.,* **129**, 6674-6675, 2007.

[40] J.L. Yue, A.E. Martell, *Inorg. Chim. Acta*, **214**, 103-111, 1993.

[41] P.J. Sun, Q. Fernando, H. Freiser, *Anal. Chem.*, **36**, 2485-2486, 1964.

In this study we have successfully synthesized and characterized new [MO(L)$_3$] and [M(L)$_4$]$^+$ complexes (where M = Nb or Ta and L = hopoH and mpoH) (Chapter 3). Figure 1.5 shows the coordination modes of 2-hydroxypyridine N-oxide (hopoH), where (A) is the most common and is observed in this study while (B) is less common and is not observed in this study.
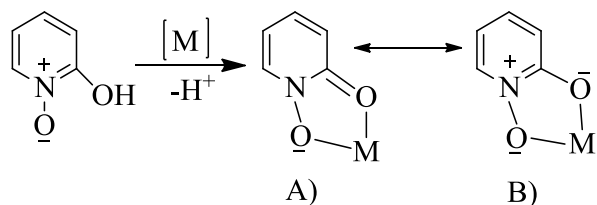
Figure 1.5 Coordination modes of 2-hydroxypyridine N-oxide (hopoH).

1.3 Motivation of this thesis

The interest in the two heaviest elements of group 5, niobium and tantalum, is essentially related to the multiple uses of these elements in advanced materials for high technology applications. It is of utmost importance to be able to separate niobium and tantalum in the most effective, novel and environmental friendly way. Niobium's low thermal neutron capture cross section makes it an attractive metal for nuclear power application where it is used with zirconium to produce zirconium alloys for nuclear reactors. High purity zirconium metal has low mechanical strength at high temperatures and the addition of niobium in small concentrations imparts high mechanical strength to the zirconium metal used for cladding and assembly components in both light and heavy water-cooled reactors. The presence of tantalum as impurity in the niobium metal in these applications must be very low, due to the high thermal neutron capture cross section of tantalum that is twenty times that of niobium and thus reduces niobium's effectiveness as cladding material. However, tantalum's ability to absorb neutrons, high mechanical strength and high corrosion resistance make it ideal for use in the production of control rods in the nuclear reactor.[42]

---

[42] http://www.grandviewmaterials.com/product/niobium-products, accessed on 10 July 2015.

Tantalum production is highly dependent on its demand in the electronic industry for the manufacturing of capacitors, rectifiers, pyroelectric infrared sensors, etc. which account for more than 60% of the total global tantalum consumption. Purity levels of at least 99.99% are required for tantalum or tantalum compounds to be used in electronic applications and electro-optical components. It is clear that effective separation of the two metals are essential, but niobium and tantalum are chemically similar and are associated with each other in nature which makes it very difficult to separate. For many years, the separation of tantalum from niobium involved the fractional crystallization of potassium heptafluorotantalate from potassium oxypentafluoroniobate monohydrate in dilute hydrofluoric acid solutions.[43]

This works well, but has two major disadvantages, namely its extreme toxicity, and the issue of disposing of HF-containing hazardous waste in an environmentally friendly manner. Despite this, HF dissolution is still a part of most of the industrial tantalum/niobium refining processes. This method has been supplanted by solvent extraction from fluoride-containing solutions and by the use of solvent extractants such as octanol, bis(2-ethylhexyl)phosphoric acid (DEHPA), alamine 336, methyl isobutyl ketone (MIBK), tri-*n*-butyl phosphate (TBP) or cyclohexanone. Perhaps the most significant disadvantage of the solvent extraction separation method is that it introduces a separate hydrometallurgical step into the flow-sheet for niobium production.

Moreover, numerous analytical methods have been used to determine trace amounts of niobium and tantalum in industrial, geological and other materials. These include X-ray fluorescence (XRF),[44] inductively coupled plasma (ICP) mass spectrometry (MS),[45] ICP atomic emission spectrometry (AES),[46,47] atomic absorption spectrometry (AAS),[48] neutron activation analysis (NAA) and reversed phase high performance liquid chromatography (RP-HPLC).[49,50,51]

[43] O.S. Ayanda, F.A. Adekola, *JMMCE*., **10**(3), 245-256, 2011.

[44] B.T. Eddy, *Report Council for Mineral Technology (MINTEK)*, **M129**, 1-27, 1984.

[45] S.M. Eggins, J.D. Woodhead, L.P.J. Kinsley, G.E. Mortimer, P. Sylvester, M.T. McCulloch, J.M. Hergt, M.R. Handler, *Chem. Geol.*, **134**(4), 311-326, 1997.

[46] O.N. Grebneva, I.V. Kubrakova, T.F. Kudinova, N.M. Kuzmin, *Spectrochim.Acta B*, **52B**, 1151-1159, 1997.

[47] J.E. Sanchez-Uria, C. Garcia-Ortiz, A. Menendez-Garcia, A. Sanz-Medel, *Mikrochim.Acta,* **II**, 195-202, 1987.

[48] R.K. Malhotra, K. Satyanarayana, G. Srinivasan, D.S.R. Murty, *Atom. Spectrosc.*, **8**, 164-166, 1987.

[49] S. Oszwaldowski, *Analyst,* **120**, 1751-1758, 1995.

The main disadvantage of ICP-AES, ICP-MS and NAA methods are high costs, using of dangerous strong acids in high concentration (HF, HCl and H_2SO_4), whilst for XRF and AAS, low sensitivity limits (detection limits). Therefore, by attempting a different strategy, a novel, safe and more environment friendly way to separate the two metals might emerge.

Overall, as mentioned in earlier paragraphs, the main focus of this thesis is on the coordination of O,O'-bidentate ligands to tantalum and niobium centers, for a potentially enhanced separation of these metals. On conducting an in-depth literature study into bidentate coordination reactions, no meaningful solid and solution state investigations of this type was found for niobium and tantalum complexes. Hopefully, this study will contribute to a better understanding of separation methods for industrial processing.

1.4 The Aim of the study

This study aims to synthesise, identify and further investigate various niobium(V) and tantalum(V) complexes containing selected hard O,O'-bidentate ligands, but especially focussing on chloranilic acid (caH$_2$), 2-hydroxypyridine N-oxide (hopoH) as well as the ammonium salt of N-nitroso-N-phenylhydroxylamine, cupferron (cupfH), which could potentially be utilized for the selective separation of niobium from tantalum. Another objective is to find out if new niobium(V) and tantalum(V) complexes can be obtained conveniently with high percent yield from the direct reaction of commercially available niobium and tantalum pentachloride at atmospheric conditions. Furthermore, our special interest was to obtain distinct physico-chemical properties (chemical differences) of the tri- and tetra O,O'-bidentate ligands coordinated to niobium(V) and tantalum(V) centers, since the literature reveals only limited examples of this type of compounds.[52] If the niobium and tantalum complexes would display differences in their coordinating behaviour, either by solubility, stability, density, coordination modes, reaction

[50] H. Wang, H.S. Zhang, J.K. Cheng, P.H. Qiu, *Microchem. J.*, **55**, 332-339, 1997.

[51] M. Rehkämper, *Chem. Geol.*, **113**, 61-69, 1994.

[52] L.G. Hubert-Pfalzgraf, M. Postel, J.G. Riess, R.D. Gillard, J.A. McCleverty, *Pergamon Press,* Oxford, **3**, 585-697, 1982.

kinetics, etc., it could allow exploitation of these leading to the development of new separation methods for these two identical twin metals.

Investigation of the reaction mechanism and analysis thereof will also help in the development of a process to clarify the chemical behaviour of the metal itself during substitution reaction kinetics.

Specific objectives:

➢ To synthesize a range of novel niobium(V) and tantalum(V) complexes with hard O,O'-bidentate ligands, using the new synthon tetraethylammonium chloride as counter-ion that has led to stable starting materials, $(Et_4N)[NbCl_6]$ and $(Et_4N)[TaCl_6]$, as well as high percentage yields in atmospheric conditions. We postulate that a difference in physical and chemical properties between niobium and tantalum, as well as a certain coordination mode for these metals that may differ, will allow for a better understanding of and ease of separation of niobium from tantalum.

➢ Characterization of the newly synthesized niobium(V) and tantalum(V) complexes by utilizing their solid state and solution properties. This would be done utilizing thin layer chromatography (TLC), UV-Vis spectroscopy, stopped-flow spectroscopy, nuclear magnetic resonance (NMR) spectroscopy (^{1}H-, ^{13}C- and ^{31}P), ATR-FTIR spectroscopy and single crystal X-ray diffraction studies.

➢ A mechanistic study of the newly synthesised niobium(V) complexes. Solution behavioural substitution kinetic studies of selected niobium(V) complexes, successfully characterized by X-ray crystallographic determination, give valuable insight into the mechanism of coordination of pyridine type ligands, which leads to better understanding of the reaction mechanism, as well as to physical and chemical differences between niobium and tantalum for a specific ligand system. These differences could easily be identified and potentially utilized in the separation of niobium from tantalum.

> Finally, a study of the stability of the niobium(V) and tantalum(V) bidentate complexes, especially looking at the role of the electronic and steric effects of the bidentate ligands on stability and comparison with related studies.

Figure 1.6 shows proposed structures of selected O,O'-bidentate ligands, whereas Figure 1.7 shows the molecular structures of selected O,O'- N,O- and S,O- bidentate ligands for the synthesis of niobium(V) and tantalum (V) complexes.
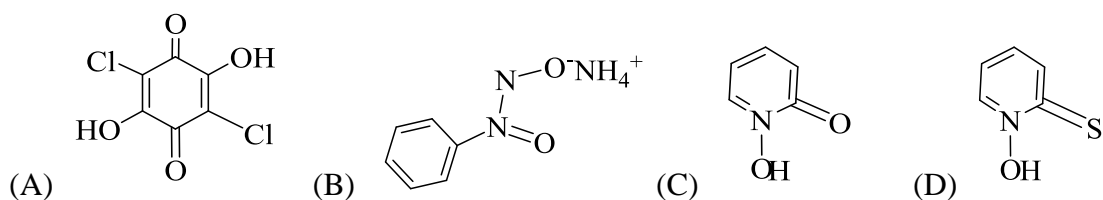
Figure 1.6 Molecular structures of: (A) chloranilic acid (caH$_2$), C$_6$H$_2$Cl$_2$O$_4$, (B), cupferron (cupfH), C$_6$H$_9$N$_3$O$_2$, (C) 2-hydroxypyridine N-oxide (hopoH), C$_5$H$_5$NO$_2$, and (D) 2-mercaptopyridine N-oxide (mpoH), C$_5$H$_5$NOS.
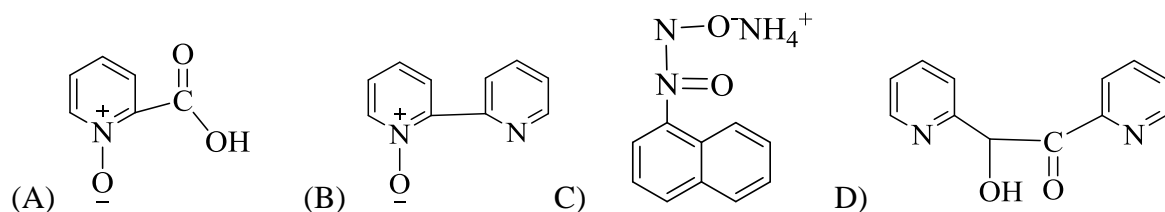
Figure 1.7 Molecular structures of: (A) picolinic acid N-oxide (picoH), C$_6$H$_5$NO$_3$, (B) 2, 2'-dipyridyl-N-oxide (dipyno), C$_{10}$H$_8$N$_2$O, (C) neocupferron (neocupfH), C$_{10}$H$_{11}$N$_3$O$_2$ and (D) pyridoin (α-py), C$_{12}$H$_{10}$N$_2$O$_2$.

2 Literature Overview of Niobium and Tantalum

2.1 History of niobium and tantalum

The story of niobium's discovery is a bit confusing.[1] The first governor of Connecticut, John Winthrop the younger, discovered a new mineral around 1734. He named the mineral columbite $((Fe, Mn, Mg)(Nb, Ta)_2O_6)$ and sent a sample of it to the British Museum in London, England. The columbite sample was displayed in the museum's mineral collection for years until it was analysed by Charles Hatchett in 1801. Hatchett could tell that there was an unknown element in the columbite, but he was not able to isolate it. He named the new element columbium, and the fate of columbium took a drastic turn in 1809 when William Hyde Wollaston, an English chemist and physicist, compared the minerals columbite and tantalite $((Fe, Mn)(Ta, Nb)_2O_6)$ and declared that columbium was actually the element tantalum. This confusion arose because tantalum and niobium are similar metals, are always found together and are very difficult to isolate.[2]

Columbium was rediscovered by Heinrich Rose in 1844 when he produced two new acids, niobic acid (H_3NbO_4) and pelopic or tantalic acid (H_3TaO_4), from samples of columbite and tantalite. He could distinguish between these two elements by their differences in valence state, with columbium exhibiting +3 and +5 oxidation states and tantalum only +5 as stable entity. Moreover, he renamed columbium as niobium after Niobe, the daughter of Tantalus from the Greek mythology to signify their close relationship. These acids showed high similarity to each other and it took another twenty-two years and a Swiss chemist named Jean Charles Galissard de

---

[1] W.H. Wollaston, Phil. *Trans. Royal Society*, **99**, 246-252, 1809.
[2] M.H. Cockbill, *Analyst*, **87**, 611-629, 1962.

Marignac (1817-1894) to prove that these were two distinct compounds, produced from two different elements.

Metallic niobium was finally isolated in 1864 by the Swedish chemist Christian Wilhelm Blomstrand, later to be achived by Moissan and Goldschmidt as well. Blomstrand reduced niobium chloride with hydrogen to form niobium, while Moissan and Goldschmidt reduced the oxide with carbon in an electrical furnace and with aluminum powder, respectively. The name niobium was officially adopted as the international name in 1949 at the 15th International Union of Chemistry Congress held in Amsterdam. The columbium name has however been accepted and used for a long time by the metallurgical and chemical industry in the U.S., resulting in the continued use of the name.[3,4,5]

Niobium occurs naturally in several minerals, mostly associated with tantalum but also includes those of many rare earth elements. Niobium metal is never found in the free elemental form, but occurs mostly as hydroxide, silicate, or borate, or as its oxy salt, niobate, which is mostly associated with isomorphous tantalate. Some of these minerals are loparite $((Ce,Na,Ca)(Ti,Nb)O_3)$,[6] bariomicrolite $(Ba(Ta,Nb)_2(O,OH)_7)$, bariopyrochlore $((Ba,Sr)_2(Nb,Ti)_2$-$(O,OH)_7)$, betafite $((Ca,Na,U)_2(Ti,Nb,Ta)_2O_6(OH))$, bismutomicrolite $((Bi,Ca)$-$(Ta,Nb)_2O_6(OH))$, bornemanite $(BaNa_4Ti_2NbSi_4O_{17}(F,OH).Na_3(PO_4))$, calciobetafite $(Ca_2(Nb,Ti)_2(O,OH)_7)$, ceriopyrochlorece $((Ce,Ca,Y)_2(Nb,Ta)_2O_6(OH,F))$, and koppite $((Na, Ca)_2(Nb, Ti, Ta)_2O_6 (OH, F, O))$.[7] All of them are complexes of hydroxide minerals and their composition may vary with location.[8] Currently, niobium is primarily obtained from the minerals columbite and pyrochlore $((Ca, Na)_2Nb_2O_6(O,OH, F))$. Niobium minerals are slightly paramagnetic and radioactive because of uranium-thorium impurities.

[3] W.P.Griffith, P.J.T. Morris, *Notes Rec. R. Soc. Lond.*, **57**(3), 299-316, 2003.

[4] N.N. Greenwood, *Catal. Today*, **78**, 5-11, 2003.

[5] R.M.F. Sousa, L.E. Fernandes, W.Guerra, *Química Novana Escola,* **35**, 68-69, 2013.

[6] J.W. Anthony, R.A. Bideaux, K.W. Bladh, M.C. Nichols, *Mineral Data Publishing*, Handbook of Mineralogy, Mineralogical Society of America, Chantilly, VA 20151-1110, USA, 2001.

[7] http://nature.berkeley.edu/classes/eps2/wisc/mineral.html, accessed on 13 November 2015.

[8] P.Patnaik, *McGraw-Hill*, Handbook of inorganic chemicals, manuals, 626-911, 2002.

Tantalum was discovered by the Swedish chemist Anders Gustaf Ekeberg in 1802, when he was examining new mineral samples, namely yttrotantalite found in Ytterby, Sweden.[9] The name "tantalum" was derived from the Greek mythology, after Tantalus. He is most famously known to have revealed the divine secrets of the gods to ordinary mortals.

Niobium and tantalum naturally occur in combination with oxygen and one or more other metals as niobates and tantalite in various types of deposits. Of these, the important ones are niobites-tantalites as pegmatite, pyrochlore as carbonates, and niobium-tantalum bearing cassiterite as placer deposits.[10] Tantalum-containing minerals are tantalite, wodginite, microlite (the tantalum rich member of the pyrochlore series), and columbite.[11] Columbite, tantalite, columbite-tantalite (Coltan), pyrochlore, and euxenite constitute the major primary sources for niobium and tantalum and are located in Canada, Brazil, Nigeria, Zaire (now the Democratic Republic of Congo) and Russia.[12,13]

2.2 Physical properties

Niobium is a shiny gray transition metal and has a high melting point of 2470 °C, is corrosion resistant, has good ductility at room temperature, and acquires a blue colour when exposed to air for a long period. It is resistant to corrosion due to the formation of an oxide film on its surface, and has multiple oxidation states, of which +5 is the most common state. In ambient temperature conditions, it does not react with hydrogen, air, water, or acids, except hydrofluoric acid and mixtures thereof with nitric acid. On the other hand, under increased temperature niobium reacts with most non-metallic species and generates products that are non-stoichiometric and includes interstitial elements. Under these conditions, it is also resistant to attack by molten bases.[14,15]

---

[9] A.G. Ekeberg, *Ann. Chem.*, **43**, 276-307, 1802.

[10] C.K. Gupta, T.K. Mukherjee, *Hydrometallurgy in Extraction Processes*, volume I, CRC Press, Boca Raton, Florida, USA.141-143, 1990.

[11] F. Habashi, *Handbook of Extractive Metallurgy*, volume III, Wiley-Vch, Quebec, Canada,1403-1431, 1997..

[12] N. Thakur, http://knol.google.com/k/narayan thakur/niobiumand-tantalum/2kwb871ek26nr/66, retrieved on 23 September 2009.

[13] Congo, war-torn heart of Africa, December 1, 2008, retrieved 18/10/2012.

[14] R. Grill, A. Gnadenberger, *Int. J. Refract. Metals. Hard. Mater.*, **24**(4), 275-282, 2006.

[15] R. Grill, *International Study Centre-Bulletin,* **129**, 6-8, 2007.

Niobium is characterized by having only one stable isotope, which has a body centered cubic (BCC) crystalline structure. It is a refractory metal because of the very high melting point of 2470 ^{o}C and it offers lower density and low thermal neutron cross-section compared to other refractory metals, which makes niobium useful in nuclear reactors. With its small capture cross-section for fast neutrons, niobium is highly recommended in nuclear reactors because of its good high temperature creep strength, its resistance to corrosion by liquid sodium-potassium alloys, and its outstanding compatibility with nuclear fuels. However, due to the poor oxidation resistance of niobium-base alloys at high temperatures, they must be coated before use in nuclear environments. A niobium 1% zirconium alloy is used as a construction material in nuclear engineering, where its low neutron absorption coefficients, along with its good resistance to liquid sodium or lithium are utilized.[16]

Tantalum is a very hard, malleable, ductile, lustrous transition metal, has a silvery-bluish color when unpolished but a bright silvery color when polished, and is found in the earth's crust at a concentration of little over 2 ppm. It has a strong affinity for oxygen and occurs almost exclusively as an oxide in association with niobium due to its close chemical similarity and atomic diameter.[17] It crystallizes in a body-centred cubic lattice with an atomic radius of 146 picometer. Tantalum has one stable isotope, ^{181}Ta, which is long-lived (half-life 1.2×10^{15} years).[18]

Niobium and tantalum have strong geochemical coherence because of their similar ionic radius and identical valance state ($Nb^{+5} = 0.69$ Å and $Ta^{+5} = 0.68$ Å). Both elements are lithophilic, showing strong affinity for oxygen and are enriched in the earth's curst.[19] The abundance of niobium in the earth's crust is estimated to be 20 ppm and its average concentration in sea water

[16] G. Barbato, *Electrodeposition of Tantalum and Niobium using Ionic Liquid*, M.Sc. dissertation, University of Toronto, 2009.

[17] A.N. Zelikman, O.E. Krein, G.V. Samsonov, *Israel Program for Scientific Translations*, Metallurgy of Rare Metals, 99-154, 1966.

[18] http://www.chemistryexplained.com/elements/P-T/Tantalum.html#ixzz4RF2x1xsV, accessed on November 27, 2016.

[19] D.A. Brobst, W.P. Pratt, *Geological Survey Professional Paper*, U.S. Government Printing Office, **820**, 75-84 1973.

is 1.0 x 10^{-2} mg.L^{-1}. Those of tantalum are 2 ppm and 2.5 x 10^{-6} mg.L^{-1}.[20] Both elements are also found in the solar system including the lunar surface, and the radionuclides niobium-94 (^{94}Nb) and -95 (^{95}Nb) occur in the fission products of uranium-235 (^{235}U).[21] Since the mechanical and physical properties of Nb are influenced by the purity of the metal, even small quantities of interstitial impurities may promote degradation of the properties of the metal. The main impurities of Nb products in accordance with specifications of the American Society for Testing and Materials (ASTM) are oxygen, nitrogen, hydrogen, carbon, iron, molybdenum and tungsten.[22]

2.3 Chemical properties

Niobium metal is resistant to attack by most common chemicals. It doesn't combine with oxygen or most other active elements except at high temperatures and it doesn't react with most strong acids unless they are hot and concentrated.[23] At normal temperature niobium is stable in contact with air. Oxidation start to take place during heating to 200-300 °C and at 500 °C fast oxidation occurs with formation of Nb_2O_5.[24] Niobium oxides dissolve very slowly in HF solutions. Because of oxide films on the surface, niobium has an excellent corrosion resistance in mineral and organic acids of all concentrations at 10-150 °C. However, the metal slowly dissolves in hydrofluoric acid and intensively in a mixture of hydrofluoric and nitric acids. It also dissolves in hot solutions of sodium and potassium hydroxides. Niobium reacts with most non-metals at high temperatures; it reacts with fluorine at room temperature, with chlorine and hydrogen at 200 °C, and with nitrogen at 400 °C, giving products that are frequently interstitial and nonstoichiometric.[25] Niobium is able to form oxides with oxidation states of +5 (Nb_2O_5), +4 (NbO_2) and +3 (Nb_2O_3),[26] as well as with the rarer oxidation state +2 (NbO).[27]

---

[20] K.H. Wedepohl, *Handbook of Geochemistry*, **2**, 231-243, 1974.

[21] Idaho National Engineering Laboratory, U.S. Department of Energy, DOE/LLW-238, 1996.

[22] O.S. Ayanda, F.A. Adekola, *J. Mine. Mate. Chara. Eng.,* **10**, 245-256, 2011.

[23] http://www.chemistryexplained.com/elements/L-P/Niobium.html#ixzz4REzQ2DAE, accessed on 27 November 2016.

[24] A.N. Zelikman, B.G. Korshunov, Moscow, *Metallurgy*, 432-433, 1991.

[25] I. Nowak, M. Ziolek, *Chem. Rev.,* **99**(12), 3603-3624, 1999.

[26] A.F. Holleman, E. Wiberg, N. Wiberg, *Lehrbuch der Anorganischen Chemie,* Walter de Gruyter, German, 91-100 ed., 1075-1079, 1985.

The most stable oxidation state of niobium is +5, the pentoxide, which along with the dark green non-stoichiometric dioxide, is the most common of the oxides. Tantalum, however, is one of the most unreactive metals. At room temperature, it reacts only with fluorine gas and certain fluorine compounds. At higher temperatures, tantalum becomes more reactive. Above 150 °C, it reacts with acids and alkalis. Tantalum is not attacked by concentrated bases or acids (other than hydrofluoric acid or fuming sulfuric acid) at 25 °C because of its adhering, corrosion-resistant oxide film.[28]

Both niobium and tantalum have very little cationic behaviour, but they form many complexes in oxidation states II, III, IV, and V. In oxidation states II and III, M-M bonds are fairly common and in addition there are numerous compounds in lower oxidation states where metal atom clusters exist. The oxides are numerous and structurally elaborated. Both Nb_2O_5 and Ta_2O_5 are relatively inert white solids. Concentrated HF is the only acid that attacks them, but they can be dissolved by fusion with hydrogen sulphate, carbonate, or hydroxide. The two pentaoxides are obtained by roasting the hydrous oxides (so called niobic and tantalic acids). The hydrous oxides themselves are gelatinous white precipitates obtained on neutralizing acid solutions of Nb(V) and Ta(V) halides. Their composition is variable owing to inconsistencies in the water content which varies depending on the method of preparation and drying.[29] Niobic acid ($Nb_2O_5.nH_2O$) exhibits a high acidity, equivalent to the acidity of 70% sulphuric acid and it is widely used as a catalyst[30] in reactions with participation or elimination of water such as esterification, hydration, dehydration, hydrolysis, and others. On heating, the hydrated pentoxide slowly loses water, after which the Nb_2O_5 goes through a series of structural changes. Finally it loses some of the oxygen atoms with formation of oxygen deficient, non-stoichiometric niobium oxides. Both of the pentoxides, but especially Nb_2O_5, have complex structural relationships.[31] They are built of MO_6 octahedral sharing edges and corners, but can be arranged in an almost unlimited number of

[27] N.N. Greenwood, A. Earnshaw, *Chemistry of the Elements,* 2nd ed., Butterworth-Heinemann, Oxford, 976-999 1997.

[28] http://www.chemistryexplained.com/elements/P-T/Tantalum.html#ixzz4RF4XaapV, accessed on 27 November 2016.

[29] F.A. Chernyshkova, *Russian Chem. Rev*., **62**, 743-749, 1993.

[30] K. Tanabe, *Catal. Today*, **8**(1), 1-11, 1990.

[31] E.I. Ko, J.G. Weissman, *Catal. Today*, **8**, 27-36, 1990.

ways. The Ta_2O_5 phase exists with an excess of Ta atoms from $TaO_{2.5}$ to nearly TaO_2. Tantalum dioxide has the rutile structure as does NbO_2 at higher temperature, but either of two similar phases with alternating bonding (2.74 Å) and non-bonding (3.30 Å) Nb-Nb bond distance may be obtained at low temperature. Niobate and tantalite isopolyanions can be obtained by fusing the oxides in an excess of alkali (hydroxide or carbonate) and dissolving the melts in water. The solutions are stable only at higher pH; precipitation occurs below ~7 for niobates and ~10 for tantalates. At pH > 14.5, mononuclear $NbO_2(OH)_4^{3-}$ anions are likely to be present in dilute aqueous solution. At lower pH the only species that appears to be present in solution are the $[H_xM_6O_{19}]^{(8-x)-}$ ions (x = 1, 2, or 3),[32] despite frequent claims for others. The structure of the $M_6O_{19}^{8-}$ ions (M = Nb or Ta) is found in crystals and is believed to persist in solutions.

The oxometalates are commonly synthesized by solid state reactions from appropriate mixtures of binary or ternary starting materials with carbon or NbO and Nb as reducing agents, at temperatures above 1500 K, using sealed Au, Pt, or Nb ampoules or quartz ampoules protected by corundum crucibles. Fluxes such as alkali or alkaline earth halides or borates have been used successfully to reduce reaction temperatures and to obtain single-crystal specimens. However, some fluxes can lead to composition changes, for example, phosphates give NbP instead. The compounds are created by dissolving the pentoxide in basic hydroxide solutions or by melting it in another metal oxide. Examples are lithium niobate ($LiNbO_3$) and lanthanum niobate ($LaNbO_4$). In the lithium niobate, the niobate ion NbO_3^- is not alone but part of a trigonally distorted perovskite-like structure, while the lanthanum niobate contains lone NbO_4^{-3} ions.[16] Lithium niobate, which is ferroelectric, is used extensively in mobile telephones and optical modulators, and for the manufacture of surface acoustic wave devices. It belongs to the ABO_3 structure ferroelectrics like lithium tantalate and barium titanate.[33]

Niobium forms halogen compounds in the +5, +4, and +3 oxidation states of the type NbX_5, NbX_4, and NbX_3, although multicore complexes and substoichiometric compounds are also

---

[32] N. Etexebarria, L.A. Fernández, J.M. Madariaga, *J. Chem. Soc, Dalton Trans.*, 3055-3059, 1994.

[33] T. Volk, M. Wohlecke, *Defects, Photorefraction and Ferroelectric Switching*, Springer, 1-9, 2008.

formed.[34] Simple binary halides are known for oxidation states IV and V, while those in lower states are cluster compounds. The pentafluorides are made by direct fluorination of the metals or the pentachlorides. The fluorides of niobium(V) and tantalum(V) have tetranuclear structures in the solid state, while the corresponding heavier halides are dinuclear in the solid state and mononuclear in the vapour phase.

Niobium pentafluoride (NbF_5) is a white solid with a melting point of 79 °C and niobium pentachloride ($NbCl_5$) is a yellowish white solid with a melting point of 203.4 °C. Both are hydrolysed by water and react with additional niobium at elevated temperatures by forming the black and highly hygroscopic niobium tetrafluoride (NbF_4) and niobium tetrachloride ($NbCl_4$). The trihalogen compounds can be obtained by reduction of the pentahalogens with hydrogen, but the dihalogen compounds do not exist.[26] However, the monochloride (NbCl) has been observed spectroscopically at high temperatures.[35] Fluorides of niobium can be isolated after its separation from tantalum.[36]

Niobium pentachloride is used in organic chemistry as a Lewis acid in activating alkenes for carbonylene and Diels-Alder reactions. The pentachloride is also used to generate the organometallic compound niobocene dichloride ((C_5H_5)$_2NbCl_2$), which in turn is used as a starting material for other organoniobium compounds.[37] Niobium sulphide as well as a few interstitial compounds of niobium with silicon are also known. An overview of oxidation states and stereochemistry (excluding the cluster compounds) of niobium and tantalum were previously reported.[38] The most important physicochemical properties of niobium and tantalum are listed in Table 2.1.

---

[34] A. Agulyansky, *Chemistry of Tantalum and Niobium Fluoride Compounds*, 1st ed., Elsevier, Amsterdam, 1-11, 2004.

[35] R.S. Ram, N. Rinskopf, J. Lievin, P.F. Bernatha, *J. of Mol. Spectrosc.,* **228**, 544-553, 2004.

[36] D.J. Soisson, J.J. McLafferty, J.A. Pierret, *Staff-Industry Collaborative Report,* Tantalum and Niobium Industrial and Engineering Chemistry, **53**(11), 861-868.1961.

[37] C.R. Lucas, J.A. Labinger, J. Schwartz, J. Robert, *Inorganic Syntheses,* Reagents for Transition Metal Complex and Organometallic Syntheses, New York, J. Wiley & Sons, **28**, 267-270, 1990.

[38] F.A. Cotton, G. Wilkinson, C.A. Murillo, M. Bochmann, *Advanced Inorganic Chemistry*, 6th ed., 895-896, 1999.

Table 2.1 Physicochemical properties of niobium and tantalum.[39,40,41,42]

Properties	Niobium (Nb)	Tantalum (Ta)
Atomic number	41	73
Atomic weight (g.mol^{-1})	92.906	180.947
Stable isotopes	^{93}Nb	^{181}Ta
Normal state	solid metal	solid metal
Group, period and block	5, 5 and d	5, 6 and d
Lattice structure	body-centred cubic (bcc)	body-centred cubic (bcc)
Density @ STP (g.cm^{-3})	8.57	16.69
Atomic radius (nm) or (Å)	0.147 or 1.47	0.146 or 1.46
Ionic radius (nm) or (Å)	0.069 or 0.69 (+5)	0.069 or 0.69 (+5)
Atomic volume (cm^3.mol^{-1})	10.80	10.90
Stable valence states	+5 and +3	+5
Melting point (ºC)	2470 ± 10	3017
Boiling point (ºC)	~4744	5458
Electron configuration	[Kr] 4d^4 5s^1	[Xe] 4f^{14} 5d^3 6s^2
Electronegativity (Pauling scale)	1.6	1.5
Ionization potential (eV)	6.77	7.89
Ionization energy (1st) (kJ.mol^{-1})	664	761
Ionization energy (2nd) (kJ.mol^{-1})	1382	1500
Ionization energy (3rd) (kJ.mol^{-1})	2416	2100
Specific heat capacity @ 25ºC (J.mol^{-1}.K^{-1})	24.60	25.36
Standard molar entropy (J.K^{-1}.mol^{-1})	36.4	41.5
Enthalpy of fusion (kJ.mol^{-1})	27.2	31.4
Enthalpy of vaporization (kJ.mol^{-1})	696.6	753.1
Thermal conductivity (W.m^{-1}.K^{-1})	53.7	57.5
Thermal expansion (µm.m^{-1}.K^{-1})	7.3	6.3

---

[39] http://www.gordonengland.co.uk/elements/nb.htm, accessed on 10 November 2015.
[40] A.S.M. Gloss, *Metals Handbook*, American Society for Metals, Metals Park, Ohio, 8th ed., 41-1236, 1961.
[41] D.L. Kepert, London, Academic Press, *The early transition metals*, 142-254, 1972.
[42] H.G. Lang, *Book Review*, *ISIS,* **93**(2), 356-357, 2002.

2.4 Uses and applications of niobium and tantalum

The interest in the two heaviest elements of group 5, niobium and tantalum, is essentially related to the multiple uses of these elements in advanced materials for high technology applications. Niobium was first applied as a material in the industry in 1933 to stabilize stainless steels against intergranular corrosion. In early 1960's, research showed that niobium contains microalloying properties that promote significant improvements in the resistance to corrosion of steels. Later, around 1970, Nb began to be used in several advanced applications, especially at high temperatures, in the form of super alloys, and in the last four decades Nb has been employed on industrial scale.[43,44,45]

Tantalum is inert to body fluids, and it is an ideal material for surgical uses in bone repair and internal suturing. It's also widely used in electronics, for the manufacture of capacitors because it readily forms an oxide film that acts as an efficient insulator. The demand for niobium and tantalum in various applications has increased steadily over the past two decades due to their importance in the production of modern industrial materials and high-tech consumer products, ranging from super alloys to electronic devices such as cell phones.[46] Niobium is used in superconducting magnets, commemorative coins, medical devices, jewellery, arc-tube seals, capacitors, optical lenses, barometers, nuclear applications, superconducting RF cavities, electromagnetic radiation detectors, as well as in nickel-, cobalt-, and iron-based super-alloys which are used in jet engine components, rocket sub-assemblies, and heat resistant and combustion equipment.[47]

The demand of the construction industry will continue to grow due to urbanization, population growth, and replacement of very old infrastructure combined with the need for lighter structures,

[43] C.E.D. Rowe, *Tantalum-Niobium International Study Centre Bulletin,* **97**, 2-5, 1999.

[44] R.A. Graham, R.C. Sutherlin, C. Wah, *Niobium Science and Technology*, Florida, 337-355, 2001.

[45] M. Oliveira, S. Jansto, H. Mohrbacher, J. Patel, M. Stuart, *30 Years of Niobium steel development in China*, 119-145, 2013.

[46] K. Hayes, R. Burge, *Coltan Mining in the Democratic Republic of Congo*, Fauna, Flora International, Cambridge, UK, 15-51, 2003.

[47] Wikipedia, http://en.wikipedia.org/wiki/Niobium, retrieved on 05 September 2009.

result in greater use of high quality steel containing niobium.[48,49,50] In the automotive industry, increased employment of niobium led to a series of innovations in the manufacturing of parts requiring several types of steels, for example, steels with high strength low alloy, called HSLA. The manufacture of parts from HSLA steels help to reduce fuel consumption, reduce CO_2 emissions, and increase passenger safety. Therefore, in view the increased production of cars worldwide, the demand for niobium in the automotive industry is expected to grow significantly in the coming years.[14,44]

In the energy sector a strong growth in production and consumption of natural gas by the year 2035 is forecasted. For example, an increase around 20% in OECD countries (The Organisation for Economic Co-operation and Development) and up to 68% in non-OECD countries, according to information from the EIA (US Energy Information Administration). Consequently, the increase in production of Nb will be directly linked to the growth in demand for HSLA steel, depending on the need of transporting natural gas over long distances and under high pressure requiring steel tubes with increased mechanical strength. This will increase the participation of niobium in energy production. In the petroleum industry, the use of HSLA is higher, so that the increase in offshore drilling platforms entails the need for more stringent performance of the steels according to the harshest conditions in increasingly deep wells. In addition, another use is as an element of orthopaedic implants in combination with other biocompatible metals.[51,52]

Niobium and tantalum powders are used for electronics and in the nanotechnology industries as nanostructured materials, due to their high purity, containing only small amounts of contaminants like oxygen and metals of low density. Moreover, niobium additives are used to stabilize and improve modern stainless steels,[53] and super alloys containing tantalum and niobium are

[48] G. Aggarwal, S.J. Park, I. Smid, *Int. J. Ref. Met. Hard Mat.*, **24**(3), 253-262, 2006.

[49] G. Tither, *International Symposium Niobium*, Orlando, Florida, 2001.

[50] IAMGOLD, http://www.iamgold.com/English/Operations/OperatingMines/Niobec-Niobium-Mine/Niobium-101/default.aspx, 2012.

[51] B.A. Alberich, B.L. Martí, J. Lafuente, C.E. Guibelaldedel, *Radiología,* **55**(2), 99-106, 2013.

[52] J. Grabis, R. Munter, Y. Blagoveshchenskiy, V. Gorkunov, L. Yamshchikov, *Proceedings of the Estonian Academy of Sciences,* **61**(2), 137-145, 2012.

[53] G. Tither, *International Symposium on Tantalum and Niobium*, Proceedings, Brussels, 129, 1995.

successfully applied in gas turbine engines and in the aerospace industry.[54] Niobium nitride (NbN), which becomes a superconductor at low temperature, is used in detectors for infrared light. Niobium-titanium alloys are used for superconducting magnets in magnetic resonance imaging equipment used for the detection of abnormalities in soft tissue. Other fields of application are catalysis (both homogeneous and heterogeneous),[55,56] ferroelectrics, superconductors,[57] as well as in organic synthesis processes as catalysts and promoters.[34]

In general, reported literature shows a number of products and applications of niobium and tantalum in the industrial and technological sector.[58,59,60,61,62,63,64]

2.5 Extraction and separation of niobium and tantalum

The close similarity in the chemical behaviour of the compounds of niobium and tantalum has rendered their separation extremely difficult. Although many processes have been investigated, the method most in use appears to be that developed by Marignac as long ago as 1866, or a modification of it.[65] The method of extraction of niobium and tantalum compounds from their natural ores does not differ from the process followed in the quantitative examination of the ores, and consists of fusing the material with an alkali or alkali salt, extracting the fused mixture of niobates and tantalates with water, and hydrolysing the solution by boiling, whereupon a comparatively insoluble mixture of niobic and tantalic acids or their anhydrides is obtained. This mixture yields the pentoxides, Nb_2O_5 and Ta_2O_5, when ignited.

---

[54] T. Carneiro, E.A. Lori, *International Symposium on Tantalum and Niobium*, Proceedings, Brussels, 235, 2000.

[55] I. Nowak, M. Ziolek, *Chem. Rev.*, **99**, 3603-3624, 1999.

[56] M. Ziolek, *Catal. Today*, **78**, 47-64, 2003.

[57] I.E. Wachs, J.M. Jehng, G. Deo, H. Hu, N. Arora, *Catal. Today,* **28**, 199-205, 1996.

[58] L.G.O, Silva, *M.Sc. Dissertation*, University of Campinas, Brazil, 1994.

[59] L. Herbst*, A solution and solid state study of niobium Complexes,* M.Sc. Dissertation, University of the Free State, South Africa, 2012.

[60] R.L. Moss, E. Tzimas, H. Kara, P. Willis, J. Kooroshy, *Energy Policy*, **55**, 556-564, 2013.

[61] R. Scanlan, Proceedings, *International Symposium on Tantalum and Niobium*, Brussels, 205, 2000.

[62] D.L. Kepert, *The Early Transition Metals*, Academic Press, London, 142, 1972.

[63] http://www.grandviewmaterials.com/product/niobium-application accessed on July 10, 2015.

[64] http://www.grandviewmaterials.com/product/tantalum-application accessed on July 10, 2015.

[65] M.C. Marignac, *Ann. Chem. Phys*, **9**(4), 249-259, 1866.

Only those metals which give rise to acidic oxides demand special separation.[66] Amuda *et al*[67] reported gravitational, magnetic and electrostatic separation techniques with leaching as adjunct beneficiation techniques to generate the various secondary ore concentrates. Agulyansky[34] reported the use of 2-octanol for the separation of niobium and tantalum. This process consists of the collective extraction of tantalum and niobium (5-7 extraction stages), scrubbing (6-9 stages), niobium stripping (5-7 stages), and tantalum stripping (4-6 stages). Sulphuric acid is added to Ta_2O_5 (50-60 $g.L^{-1}$) and Nb_2O_5 (30 $g.L^{-1}$) solutions in order to obtain an optimal acidity level. The optimal H_2SO_4 concentration for tantalum extraction is about 2.5-3.5 M while niobium begins to move into the organic phase between 4-5 M concentrations of H_2SO_4. Vin and Khopkar[68] developed a method for the reversed-phase extractive chromatographic separation of niobium and tantalum with bis(2-ethylhexyl)phosphoric acid (DEHPA). Niobium was extracted from between 1-10 M hydrochloric acid and stripped with 3 M sulphuric acid containing 2% hydrogen peroxide, while tantalum was extracted from between 0.1-2 M hydrochloric acid and was stripped with 0.1 M hydrochloric acid containing 2 M tartaric acid.

2.6   The main methods of separation of niobium and tantalum

2.6.1   Marignac process

The Marignac process is based on the fractional crystallisation of the alkali metal double fluorides, which enables the sparingly soluble K_2TaF_7 to be separated from a solution containing K_2NbOF_5. The main disadvantage of this process is that it necessitates working with hydrofluoric acid.[69] This process,[70] developed in 1866, is considered to be the first industrial separation process for the niobium and tantalum metals and is based on the difference in solubility of the fluoride complexes of tantalum and niobium. It involves the addition of an excess of potassium

[66] W.R. Schoeller, A.R. Powell, *Analysts of Minerals and Ores of the Rarer Elements*, London, Charles Griffin & Company, Ltd., 115-143, 1919.

[67] M.O.H Amuda, D.E. Esezobor, G.I. Lawal, *JM M CE*, **6**(1), 67-75, 2007.

[68] Y.Y. Vin, S. M Khopkar, *Talanta*, Elsiver, **38**(9), 971-975, 1991.

[69] K. Fritz, S. Waldemar, *Process for Separating Niobium and Tantalum from each other*, US patent, US2976114 A, 1961.

[70] H. Manuspiya, *Electrical Properties of Niobium Based Oxides Ceramics and Single Crystal Fibers Grown by the Laser-Heated Pedestal Growth Technique*, PhD. Dissertation, the Pennsylvania State University, USA, 2003.

fluoride to the hydrofluoric acid solutions of the metal ores to precipitate complex fluorides of the two metals. The potassium tantalum fluoride, K_2TaF_7, is only sparingly soluble in dilute hydrofluoric acid (HF), whereas the potassium niobium oxyfluoride, K_2NbOF_5, has very high solubility. Potassium niobium fluoride, K_2NbF_7, is not formed in this process as it is only stable in concentrated HF. The Marignac process has been replaced by other industrial processes because only the purity of the tantalum produced was adequate. The purity of niobium produced by this process was unsatisfactory due to the presence of titanium in the mineral concentrate.

2.6.2   Liquid-liquid extraction (solvent extraction)

Liquid-liquid extraction is the only method available for the separation of the rare earth elements to obtain individual metals. This method is very effective for the separation of dissolved components and enables the production of high-purity products, in addition to its advantages of being a low-cost and simple method.[71] During this process an organic solution is mixed with the filtrate produced from the leaching process. However, intensive mixing is required to establish sufficient contact time between the organic and the aqueous phase. In 1950, the U.S. Bureau of Mines and Ames Laboratory of Iowa State University developed the solvent extraction process.[72,73] This process utilises the extractant, methyl isobutyl ketone (MIBK), for the separation of niobium and tantalum. The solvent extraction is ideal for large-scale operations and satisfactory for the production of pure niobium compounds. It is also relatively simple when compared to Marignac's process. Industrial separation processes involve the use of various acids in combination with HF and a choice of four solvents, either tributyl phosphate (TBP), MIBK, cyclohexanone (CHN), or 2-octanol (2-OCL). Some of these combinations have been reported in the literature,[74,75,76,77] e.g. HF-nitric acid (HNO_3)-MIBK[78]

[71] A. Agulyansky, L. Agulyansky, V.F. Travkin, *Chem. Eng. Proc.,* **43**, 1231-1237, 2004.

[72] Japan Mining Industry Association, *Study Report of High-purity Rare Metals*, 1991.

[73] J.R. Werning, K.B. Higbie, J.T. Grace, B.F. Speece, H.L. Gilbert, *Ind.Eng. Chem*, **46**(4) 644-652, 1954.

[74] O.M. El hussaini, N. M. Rice, *Liquid-liquid extraction of niobium and tantalum from aqueous sulphate/fluoride solutions by a tertiary amine*, Hydrometallurgy, **72**, 259-267, 2004.

[75] A.D. Damodaran, S.G. Deshpande, A.A. Majmudar, M.S. Sastri, *Bhabha Atomic Research Center*, Trombay, Bombay, **36**(5) 306-318, 1969.

[76] H. Konghak, *Korean. J. Chem. Eng.*, **29**, 305-343, 1991.

[77] H.H. Htet, T.L. Kay, *World Acad. Sci. Eng. Techn.*, **46**, 133-135, 2008.

and HF-hydrochloric acid (HCl)-MIBK.[79] Although these combinations involve different chemicals, they all still work on the same principle, varying only in terms of the back extraction of either niobium or tantalum. The ores are finely ground and dissolved in HF. The acidity is adjusted to greater than 8 M with sulphuric acid (H_2SO_4) in order to dissolve the accompanying elements such as iron, manganese and titanium along with the niobium and tantalum. After removal of the remaining insoluble elements like the rare earth metals by filtration, the acid solution is extracted with MIBK. Initially both niobium and tantalum are extracted into the organic phase while most of the impurities remain in the aqueous phase. This organic phase is then mixed with a new aqueous phase containing 3 M H_2SO_4. The niobium is back extracted into the aqueous phase due to the lower acidity of the aqueous phase. The back extracted aqueous niobium is again re-extracted with MIBK to remove any traces of tantalum that could be present. This ensures that complete separation of niobium (aqueous phase) and tantalum (organic phase). To precipitate niobium oxide hydrate from the aqueous phase, ammonia is added and the niobium oxide hydrate is removed by filtration. The niobium oxide obtained after drying is of high purity.[64]

2.6.3   Chlorination

Chlorination is a process for the breakdown of ores and concentrates of many of the refractory metals,[79] and even some of the commonly used metals. Important features of chlorination include the high reactivity of chlorine, relative ease in gasifying many of the constituents of the concentrates due to high volatility of most of the chlorides, and high water solubility of most of the chlorides. The chlorides formed can also be readily separated due to differences in their vapour pressures, or due to differences in reactivity with oxygen and/or water vapour and in their reducibility with hydrogen. Thus, the chlorination process is suitable not only for breakdown of the ore or concentrate but also for the separation/purification of various elements co-occurring in the concentrate and for reduction to metallic form.

---

[78] C.H. Faye, W.R. Inman, *Research Report MD210*, Dept. Mines and Technical Surveys, Ottawa, London, 287-309, 1956.

[79] C.K. Gupta, A.K. Suri, *Extractive Metallurgy of Niobium*, CRC Press, 1-16, 1994.

Direct chlorination of refractory metal oxides Nb_2O_5 and Ta_2O_5 to their pentachlorides is thermodynamically unfavourable and takes place only in the presence of a reducing agent binding the released oxygen. The process is usually carried out in the presence of different forms of carbon[80,81,82,83,84] or carbon monoxide[85] and is known as carbochlorination. In all cases the reaction is carried out at a high temperature, up to 1000 ºC, and is therefore very energy consuming. Processes using one reagent acting as both the chlorinating and the reducing agent are also known, for example, carbochlorination of Nb_2O_5[86] or Ta_2O_5[87] with carbon tetrachloride vapours at temperatures up to 580 ºC.

Chlorination with CCl_4 proceeds under milder conditions than with chlorine, although the temperature is still rather high.[88] The selective chlorination of materials containing niobium and tantalum in oxidised form which is described in French Patent No. 973,896,[69] is carried out in the absence of reducing gases, but at very high temperatures of about 1200 °C and the process therefore entails the use of very unstable solutions, and the digestion with sulfuric acid is a lengthy process.[68] In general, the use or formation of such toxic and ozone depleting compounds as chlorine, phosgene, and chlorocarbons during the processes makes them dangerous and environmentally harmful.

2.6.4   Alkaline fusion

Alkaline fusion is also one of the processes used for the breakdown of concentrates of mineral ores. A large number of alkaline fluxes, such as caustic soda, soda ash, caustic potash, potassium carbonate, and a mixture of these, with or without addition of oxidizing agents, such as sodium

---

[80] O.K. Mehra, H.S. Zahed, P.K. Jena, *Trans. Indian Inst. Met.,* **19**, 53-56, 1966.

[81] P. Meubus, *Metall. Trans*, **10B**(1), 93-101, 1979.

[82] M.C. Ruiz, J. Gonzalez, J. Rivarola, *Canad. Metallurg. Quart.*, **36**(2), 103-110, 1997.

[83] J. Gonzalez, F. Gennari, A. Bohe, M.C. Ruiz, J. Rivarola, D.M. Pasquevich, *Thermochim. Acta*, **311**(2), 61-69, 1998.

[84] J. Gonzalez, A. Bohe, D.M. Pasquevich, M.C. Ruiz, *Canad. Metallurg. Quart.*, **41**(1), 29-40, 2002.

[85] E. Allain, M. Djona, I. Gaballah, *Metall. Mater. Trans.*, **28B**(2), 223-233, 1997.

[86] P.K. Jena, E.A. Brocchi, R.I. Garcia, *Metall. Mater. Trans.*, **28B**(1), 39-45, 1997.

[87] P.K. Jena, E.A. Brocchi, M.P.A.C. Lima, *Metall. Mater. Trans.*, **32B**(5), 801-810, 2001.

[88] B.A. Shainyan, Yu. S. Danilevich, Yu.L. Garmazov, A.L. Finkelstein, T.S. Aisueva, V.K. Turchaninov, *JMMCE* **7**(2), 163-173, 2008.

nitrate and sodium peroxide, have been used by a large number of investigators.[89] Alkaline fusion in combination with acid leaching was one of the first methods to be adopted on an industrial scale to achieve simultaneous breakdown of columbite and tantalite concentrate and upgrading of niobium and tantalum values by leaching out of iron, manganese, tin, titanium and silicon.

2.6.5   Leaching

Leaching is the process of extracting a substance from a solid material by dissolving it in a liquid. This process is commonly referred to as extraction, particularly in the chemical industry. In the chemical processing industry, leaching has a variety of commercial applications, including separation of metal from ore using acid.[89] In industrial leaching, solvent and solids are mixed, allowed to approach equilibrium, and the two phases are separated. Liquids and solids pass countercurrently (a change in the direction of flow of a fluid) through the next adjacent stages. The solvent phase, called the extract, becomes more concentrated as it dissolves the increasingly solute-rich solids in the stagewise fashion. The raffinate becomes less concentrated in soluble material as it moves towards the fresh solvent phase.[90]

Odo *et al*.[91] reported a high percentage of pure tantalum and niobium extracted from tin slag using a double leaching process by applying HCl and NaOH. Figure 2.1 shows the processing of tantalum and niobium (columbium) metals.[92]

[89] M.H. Cockbill, *Analyst*, **87**, 611-629, 1962.

[90] Xi. Wang, S. Zheng, H. Xu, Yi. Zhang, *Hydrometallurgy*, **98**, 219-223, 2009.

[91] J.U. Odo, W.C. Okafor, S.O. Ekpe, C.C. Nwogbu, *IJSRP*, **4**(11), 2014.

[92] L.D. Cunningham, *Columbium (niobium) and Tantalum*, From Minerals Yearbook. Volume I. Metals and M inerals. U.S. Bureau of Mines, 435-460, 1992.
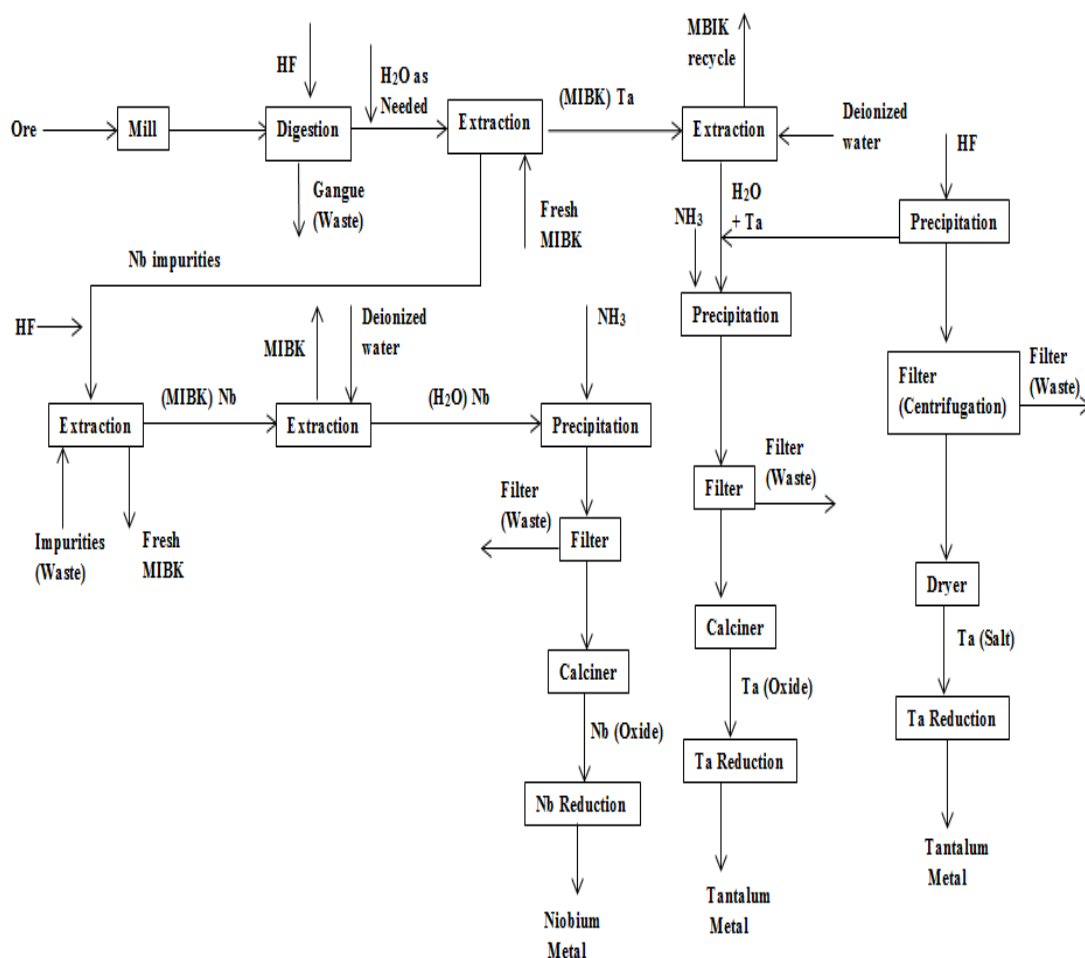
Figure 2.1 The processing of tantalum and niobium (columbium) metals.

2.7 Bidentate ligands

2.7.1 Niobium and tantalum complexes containing *β*-diketones

β-Diketones are some of the most widely used ligands in coordination chemistry.[93,94] They are known for their interesting chemical and physical properties in addition to their keto-enol tautomerism. The simplest aliphatic *β*-diketone is known as acetylacetone (Hacac, 2, 4-pentanedione), which forms strongly bound complexes with multiple metal cations (alkali

---

[93] R.C. Maurya, S. Rajput, *J. Mol. Struct.*, **687**, 35-44, 2004.
[94] V.D. John, K. Krishnankutty, *Appl. Organomet. Chem.*, **20**, 477-482, 2006.

and transition metals). These compounds can exist as keto and enol tautomers in solution as well as in solid state since the presence of the ketone and the enol forms in equilibrium. The equilibrium in the case of *β*-diketones is strongly shifted towards the enol form due to the formation of the distinct resonance structure as a six-membered ring.

The keto-enol equilibrium (Figure 2.2) is affected by a number of factors with the most important being solvent polarity and the presence of substituents with distinct properties (both terminal and those in the methylene group).[95] The capacity to form stable complexes with most metals is a direct consequence of the occurrence of such compounds in the enol form. Generally, research is stimulated by the versatility of these compounds as NMR shift reagents,[96] laser chelates,[97] extraction agents,[98] and chemical and photochemical catalysts.[99]
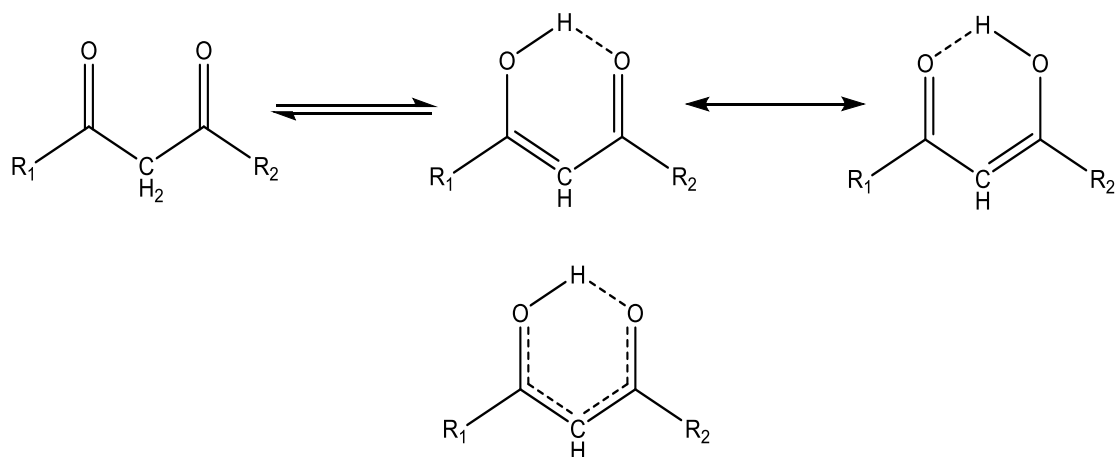
Figure 2.2 Proposed keto-enol tautomerism of a *β*-diketone.[100]

[95] U. Wlodzimierz, J. Katarzyna, W. Katarzyna, G. Andrzej, *CHEMIK,* **65**(4), 273-282, 2011.

[96] C.C. Hinckley, *J. Am. Chem. Soc.*, **91**(18), 5160-5162, 1969.

[97] C. Brecher, A. Lempicki, H. Samelson, *J. Chem. Phys.,* **42**, 1081-1096, 1969.

[98] A.M. Poskanzerand, B.M. Foremn, *J. Inorg. Nuc. Chem.*, **16**, 323-336, 1961.

[99] B. Marciniak, G.E. Buonocore, *J. Photochem. Photobiol. A. Chem.*, **52**(1), 1-25, 1990.

[100] http://www.masterorganicchemistry.com/2010/04/12/keto-enol-tautomerism-key-points/, accessed on 04 December, 2016.

2.7.2 Tetrakis(β-diketonate), (O,O'-, and O,N-)niobium(V) and tantalum(V) complexes

Only one crystal structure of tetrakis-tantalum(V) complexes with β-diketonate is reported in literature.[101,102] Very few of the corresponding tetrakis complexes of the metal ions in the higher +5 oxidation state exist, being restricted to N,N',[103] S,S', or mixed S,O[104] chelates. One report in the literature deals with the preparation and use in MOCVD of a tetrakis 2,2,6,6-tetramethylheptane-3,5-dionate (tmhd) complex of Ta(V), [Ta(tmhd)$_4$]Cl.[102] In contrast, there are some crystal structures of tetrakis-(β-diketonate) niobium and tantalum(IV) complexes, with in depth literature study into the eight coordinate tetrakis-chelate complexes of the type M^{IV}(chelate)$_4$ (where, M = Nb, Ta) reported in section 2.7.3. The complexes of this type include [Nb(β-diketonate)$_4$], [Ta(β-diketonate)$_4$],(where β-diketonate = acetylacetonate, thenoyltrifluoro-acetylacetonate and benzoylmethanate).[105]

2.7.2.1 Hexachloridotantalate(V) tetrakis(2,2,6,6-tetramethylheptane-3,5-dionato) tantalate(V), [Ta(tmhd)$_4$][TaCl$_6$]

In 2005, Davies *et al*.[106] published the structure for a tetrakis-[Ta(tmhd)$_4$][TaCl$_6$] complex, where tmhdH is 2,2,6,6-tetramethylheptane-3,5-dione (Figure 2.3). The goal of their study was the preparation of β-diketonate complexes of various metal ions for the metal-organic chemical vapour deposition (MOCVD) of metal oxides or nitrides at low temperatures. They reported the first complex of tantalum in the +5 oxidation state containing four chelating diketonate anions to be characterised using X-ray crystallography. The reactions were performed under a dry, inert atmosphere using standard Schlenk techniques and the yield of [Ta(tmhd)$_4$] [TaCl$_6$] was between 10-20 % and purity of this compound was poor due to the use of acetonitrile as solvent. They decided to modify the synthetic approach by omitting the use of such a solvent. In the absence of

[101] I. Kobayashi, N.K. Kaishi, *J. Chem. Soc, Japan,* **12**, 1515-1517, 1992.

[102] The Cambridge Structural Database, C.R. Groom, I.J. Bruno, M.P. Lightfoot, S.C. Ward, *Acta. Cryst*., **B72**, 171-179, 2016.

[103] E.L. Muetterties, C.M. Wright, *J. Amer. Chem. Soc.*, **87**(21), 4706-4717, 1965.

[104] R.C. Fay, *Coord. Chem. Rev.*, **154,** 99-124, 1996.

[105] R.L. Deustscher, D.L. Kepert, *Inorg. Chim. Acta,* **4**(4), 645-650, 1970.

[106] H.O. Davies, A.C. Jones, M.A. Motevalli, E.A. McKinnell, P.O. Brien, *Inorg. Chem. Com*, **8**, 585-287, 2005.

solvent, solid $TaCl_5$ reacted with four molar equivalents of neat tmhdH, refluxed for 30 min and was allowed to cool slowly at room temperature. The product [Ta(tmhd)$_4$] [TaCl$_6$] was isolated in good yield and structurally characterised.

The Ta-O bond lengths vary from 2.009(9) to 2.145(11) Å, with an average Ta-O bond distance of 2.075(9) Å whereas Ta-Cl bond distances vary from 2.303(5) to 2.345(4) Å. The average O-Ta-O bite angle is 77.5(4)°. This is an extremely tight bite angle and the tightest observed in compounds of this nature.[107,108] Moreover, these Ta-O angles indicate that the shape of the TaO$_8$ core approximates that of a dodecahedron.
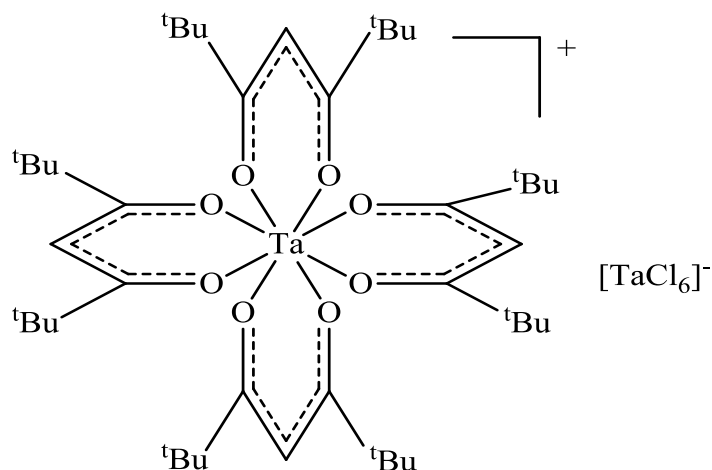
Figure 2.3 Proposed structure of [Ta(tmhd)$_4$][TaCl$_6$].

2.7.2.2 Trichloridehydronium ditetrakis(tropolonato)niobate(V), [Nb(trop)$_4$]$_2$[H$_3$OCl$_3$]

In 1975, Davis *et al.*[109] published the crystal structure of tetrakis-niobium(V) complex with tropolonato ligands (tropH). The cation compound, [Nb(trop)$_4$]$_2$[H$_3$OCl$_3$] (Figure 2.4), crystallizes in the monoclinic space group *C2/c*. They reported that the Nb-O bond lengths vary from 2.070(11) to 2.111(11) Å, with the average Nb-O bond distance being 2.0745(7) Å. This

---

[107] H.O. Davies, A.C. Jones, P.O. Brien, T.J. Leedham, A.J.P. White, D.J. Williams, *Polyhedron*, **18**, 3165-3172, 1999.

[108] D.P. Graddon, *Coord. Chem. Rev.*, **4**(1), 1-28, 1969.

[109] A.R. Davis, F.W.B. Einstein. *Inorg. Chem.*, **14**(12), 3030-3035, 1975.

describes an irregular bicapped trigonal prism, distorted towards a dodecahedron. The O-Nb-O bite angles vary from 70.2(5) to 73.1(4) Å with the average O-Nb-O bite angle 71.2(4)°. The mean O$^{...}$O separation in the four tropolonato ligands was 2.432(17) Å, which is significantly and unexpectedly smaller than the values reported for other tropolonate complexes.[110,111] Compared to other interligand contacts in the NbO$_8$ polyhedron, two interligand O…O contacts were very short (2.41(1) and 2.47(2) Å).[112,113] The species [H$_3$OCl$_3$]$^{2-}$ contains the H$_3$O$^+$ cation hydrogen-bonded to the three chloride ions placed at the corners of the base of a flattened trigonal prism. This twofold axis passes through one of the chloride ions and correlates the other two; the oxygen atom is disordered on either side of the twofold axis at the apex of the trigonal prism. The other two peaks were refined as a CH$_3$CN molecule randomly disordered between two sites on either side of the twofold axis. They conclude that the tropolonate ligands reveals that increasing strength of the complexing bonds is accompanied by lengthening of the C-O bonds and also some shortening of the C1-C7 bonds.[117,118]

$[H_3OCl_3]^{2-}$
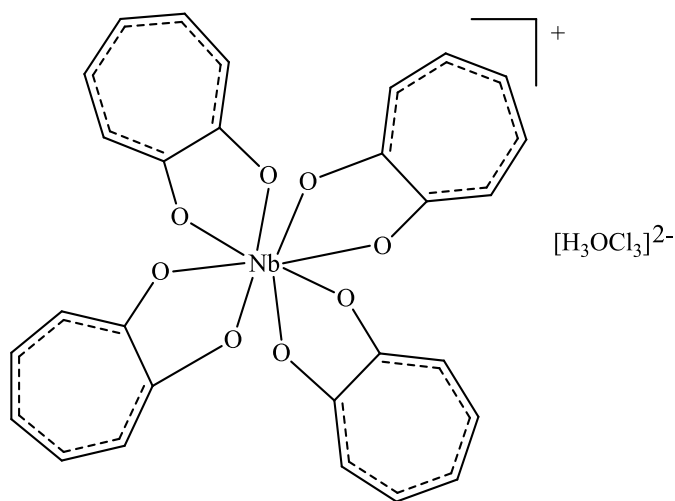
Figure 2.4 Proposed structure of [Nb(trop)$_4$]$_2$[H$_3$OCl$_3$].

[110] L.J. Guggenberger, E.L. Muetterties, *J. Am. Chem.,* SOC, **94**(23), 8046-8055, 1972.

[111] T.J. Anderson, M.A. Neuman, G.A. Nelson, *Inorg. Chem.*, **13**, 158-163, 1974.

[112] W.D. Bonds, R.D. Archer, W.C. Hamilton, *Inorg. Chem.*, **10**, 1764, 1971.

[113] M.C. Poore, D. R. Russell, *J. Chem. Sco. D,* 18-19, 1971.

2.7.2.3 Tetrakis(tropolonato)tantalate(V) chloride, [Ta(trop)₄][Cl]

In 1965, Muetterties *et al.*[103,114] published the crystal structure of group 3, 4, and 5 metals with tropolone (tropH) ligand. The [Ta(trop)$_4$]$^+$ [Cl]$^-$ (Figure 2.5) complex geometries shows the D_2 square antiprism and the D_{2d} dodecahedron. The hydrolytic stabilities of [Nb(trop)$_4$]$^+$ and [Ta(trop)$_4$]$^+$ differ rather significantly. The niobium cation is stable only in strongly acidic media. With increasing pH or increasing temperature, the niobium chelate undergoes partial hydrolysis to [NbO(trop)$_3$] which separates from solution. This reaction is reversed by addition of concentrated hydrochloric acid. In basic solution, the niobium cation is rapidly and completely hydrolysed; initial hydroxide attack is on the ligand not the metal atom.

$$H_2O + \left[Nb(trop)_4\right]^+ \xrightarrow{\ pH > 3,\ 60\,^oC\ } \left[NbO(trop)_3\right] + tropH + H^+$$
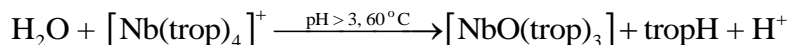
In contrast, [Ta(trop)$_4$]$^+$ is resistant to hydrolysis provided the pH is not appreciably above 7. They conclude that fast ligand exchange between [Ta(trop)$_4$]$^+$ and labelled tropolone was also observed in non-aqueous media. Exchange was about 71% complete in ethanol and 45% in acetonitrile within 0.5 hr for much less concentrated solutions than those employed for the aqueous exchange. Furthermore, they reconfirmed that percentage hydrolysis results varied for the various [Ta(trop)$_4$]$^+$ salts in different other anions such as [Ta(trop)$_4$]$^+$ [Cl]$^-$, [Ta(trop)$_4$]$^+$ [ClO$_4$]$^-$, [Ta(trop)$_4$]$^+$ [PF$_4$]$^-$, and [Ta(trop)$_4$]$_2^+$ [B$_{12}$Cl$_{12}$]$^{2-}$; 3%, 5%, 6% and 10.5% respectively.
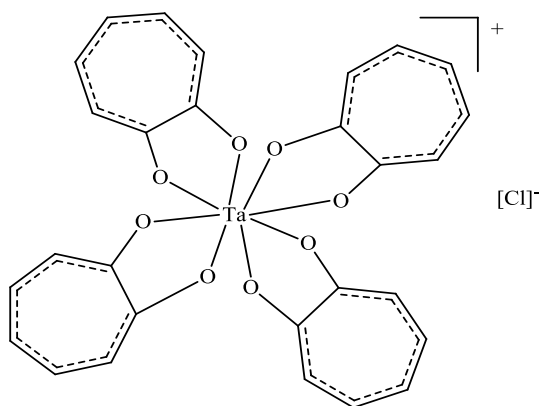
Figure 2.5 Proposed structure of [Ta(trop)₄][Cl].

---

[114] R. Koen, *High oxidation state niobium and tantalum coordination chemistry*, PhD. Dissertation, University of the Free State, South Africa, 2016.

2.7.3 Tetrakis(*β*-diketonate) niobium(IV) complexes

2.7.3.1 Tetrakis(hexafluoroacetylacetonato)niobium(IV), [Nb(hfacac)$_4$]

In 1998, Calderazzo *et al.*[115] published a structures of niobium(IV) and zirconium(IV) complex with hexafluoroacetylacetone (hfacacH) as ligand. They reported that the hexafluoroacetylacetonate derivatives of zirconium(IV) and niobium(IV) are not isotypical compounds, that the central metal atom in both complexes shows a square antiprismatic coordination, the coordination modes of the ligands are different and slight deviations from the *D$_4$(llll)* and *C$_2$(llss)* ideal geometries have been observed in the case of niobium and zirconium. A graphic postulation of this formation compound of Nb(hfacac)$_4$ is illustrated in Figure 2.7. The crystal and molecular structures of Zr(hfacac)$_4$ and Nb(hfacac)$_4$ show similar geometries at the metal, but (Nb(hfacac)$_4$ crystallized in the orthorhombic space group *Pna*2$_1$ and Zr(hfacac)$_4$ crystallized in a monoclinic space group *P*2$_1$/*n*.

Average bond distances and angles of Nb(hfacac)$_4$ were Nb-O = 2.114 Å and O-Nb-O = 81.4° respectively whereas, average bond distances and angles of Zr(hfacac)$_4$ were Zr-O = 2.175 Å and O-Zr-O = 75.9° respectively. Moreover, the *β*-diketonato derivatives of niobium (IV) were very sensitive to oxygen and only slightly soluble in common organic solvents whereas, Nb (hfacac)$_4$ was more soluble and more volatile than the corresponding unsubstituted derivative.[116]

[115] F. Calderazzo, U. Englert, C. Maichle-Mossmer, F. Marchetti, G. Pampaloni, D. Petroni, C. Pinzino, J. Strahle, G. Tripepi, *Inorg. Chim. Acta*, **270**, 177-188, 1998.

[116] R.L. Deutscher, D.L. Kepert, *Inorg. Chim. Acta*, **4**, 645-650, 1970.
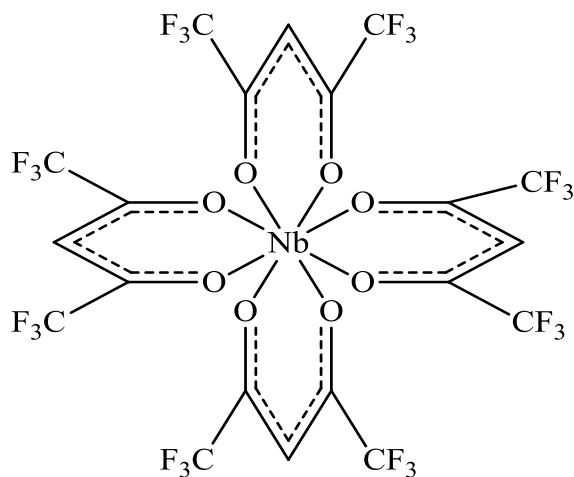
Figure 2.6 Proposed structure of [Nb(hfacac)4].

2.7.3.2 Tetrakis(2,2,6,6-tetramethyl-3,5-heptanedionato)niobium(IV), [Nb(tmhd)4]

In 1975, Pinnavaia *et al.*[117] published the structure for a tetrakis-[Nb(tmhd)4] complex, where tmhd is the 2,2,6,6-tetramethyl-3,5-heptanedionate (sometimes called dipivaloylmethanate (dpm)), indicating that the complex is square antiprismatic (Figure 2.7). The compound crystallizes in the monoclinic space group *P*2/*c* with four molecules in a unit cell. In addition, X-ray powder diffraction patterns revealed that Nb(dpm)4 was not isomorphous with Zr(dpm)4. Since the latter complex is expected to adopt a $D_2(ssss)$ tructure analogous Zr(acac)4,[118] the lack of isomorphism between the niobium and zirconium dpm complexes raised the possibility of a $D_4(llll)$ structure existing for Nb(dpm)4. This led to the single crystal X-ray diffraction determination of its molecular structure. The Nb-O bond lengths vary from 2.118(8) Å to 2.144(8) Å, with an average Nb-O bond distance of 2.133(9) Å.

The O-Nb-O bite angles vary from 79.4(3)° to 80.0(3)° with the average O-Nb-O bite angle of 79.8(3)°. They concluded that the coordination polyhedron of each Nb(dpm)4 molecule was unequivocally a square antiprism, and the bidentate span lateral (*l*) edges. Due to the two half-

---

[117] T.J. Pinnavaia, B.L. Barnett, G. Podolsky, A. Tulinsky, *J. Am. Chem. Soc.*, **97**(10), 2712-2717, 1975.

[118] J.V. Silverton, J.L. Hoard, *Inorg. Chem*, **2**(2), 243-249, 1963.

molecules in the asymmetric unit lying on twofold axes, they were required crystallographically to have only C_2 symmetry. Nevertheless, D_4 symmetry is nearly achieved.
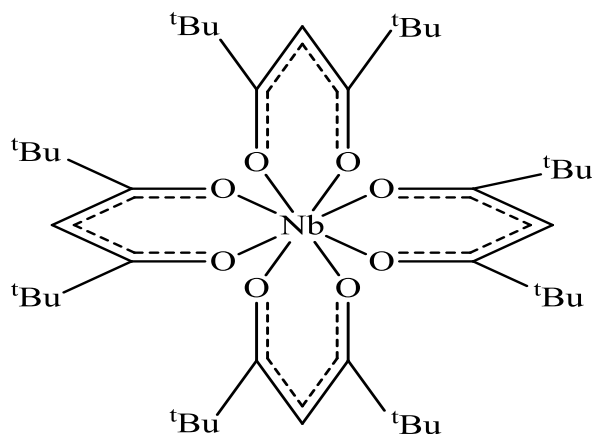
Figure 2.7 Proposed structure of [Nb(dpm)$_4$].

2.7.4   Tris-niobium(V) and tantalum(V) complexes with O,O'- and O,N-bidentate ligands

2.7.4.1   Hexafloridotantalate(V) tris(3-methyl-2,4-pentanedionato)fluorido tantalate(V), [TaF(mpd)$_3$][TaF$_6$]

In 2007, Marchetti *et al.*[119] published the crystal structure of tris-tantalum(V) complexes with acetylacetone (acacH) and 3-methyl-2,4-pentanedione(mpdH) respectively. The molecular structure of [TaF(mpd)$_3$][TaF$_6$] was isolated and characterized by spectroscopic, analytical, and X-ray analyses as the ionic complex (Figure 2.8). They reported the Ta-O bond lengths as 2.005(3)-2.056(4) Å in the range observed for the Ta-O$_{ketone}$, and the O-Ta-O bite angle as 77.53(14)°.

This bond distance was significantly shorter than those observed in other halo-β-diketonates: Ta(η^5-C$_5$Me$_5$)F$_3$(dibenzoylmethanate) [2.049(4)–2.120(4) Å],[120] *trans*,*cis*-TaCl$_2$(OMe)$_2$(acac)-

[119] F. Marchetti, G. Pampaloni, S. Zacchinib, *Dalton Trans.,* **38**, 4343-4351, 2007.
[120] H.W. Roesky, F. Schrumpf, M. Noltemeyer, *Z. Naturforsch.*, **44B**, 1369-1372, 1989.

[2.026(10)-2.083(12)Å],[113] *trans, cis*-TaCl$_2$(OMe)$_2$(tmhd), tmhdH = 2,2,6,6-tetramethylheptane-3,5-dione, [2.051(10)-2.055(9) Å],[114] and [Ta(tmhd)$_4$][TaCl$_6$] [2.018(8)-2.134(8) Å, mean values].[112]

In general, the [TaF(mpd)$_3$]$^+$ cation shows a seven coordinated tantalum centre with a capped trigonal prismatic coordination geometry. The Ta-F interaction [1.909(5) Å] was slightly longer than the ones present in the [TaF$_6$]$^-$ anion [1.893(3)-1.897(3) Å], probably because of the higher steric hindrance due to the presence of the three bulky acetylacetonates. On the other hand, the reactions of TaCl$_5$ or TaBr$_5$ with acetylacetone proceed without formation of by-products and the [TaF$_6$]$^-$ ion was more stable than [TaCl$_6$]$^-$ and [TaBr$_6$]$^-$.[121]
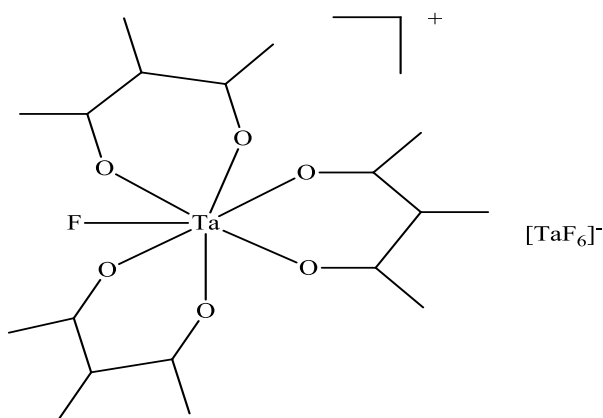
Figure 2.8 Proposed structure of [TaF(mpd)$_3$][TaF$_6$].

2.7.4.2 Pyridiniumtris(catecholato)tantalum(V) (A) and pyridiniumtris(catecholato)-niobium(V) (B), [Ta(cat)$_2$(cat-H)(py)] and [Nb(cat)$_2$(cat-H)py]

In 2005, Boyle *et al.*[122] published two crystal structures of tris-tantalum and -niobium (V) complexes with 1,2-dihydroxybenzene, catechol ligand (cat-H$_2$) in pyridine (py). [Ta(cat)$_2$(cat-H)py] and [Nb(cat)$_2$(cat-H)py] were mononuclear wherein each metal centre formally adopts a

[121] D.R. Lide, *CRC Handbook of Chemistry and Physics*, 86th ed., CRC Press, Boca Raton, FL, USA, 9-996, 2005.

[122] T.J. Boyle, L.J. Tribby, T.M. Alam, S.D. Bunge, *Polyhedron*, **24**, 1143-1152, 2005.

seven coordination capped-trigonal prism involving three chelating catechol ligands, with one being cat-H, along with a coordinated pyridine ligand (Figure 2.9).

The Nb-O bond lengths vary from 1.995(2) Å to 2.124 (2)Å, with an average Nb-O bond distance of 2.034(3) Å and Nb-N bond distance of 2.326(3) Å. The O-Nb-O bite angles vary from 74.38(9)° to 76.02(9)° with the average O-Nb-O bite angle being 75.44(3)°, whereas the Ta-O bond lengths vary from 2.003(5) Å to 2.084(5) Å, with the average Ta-O bond distance of 2.025(5) Å and Ta-N bond distance of 2.308(6) Å. The O-Ta-O bite angles vary from 75.28(19)° to 76.80(2)° with an average O-Ta-O bite angle of 75.88(2)°.

The complexes **(A)** and **(B)** crystallize in the triclinic space group $P\bar{1}$ at 273(2) K and monoclinic space group $P2_1/c$ at 168(2) K, respectively. It was concluded that similar complexes are formed for tantalum and niobium, independent of the cation. Each metal has three catH$_2$ ligands binding in a chelating manner, but based on charge balance one of the cat ligands must possess a hydroxy group. This H atom was not located in the final structure and must be disordered over several sites.
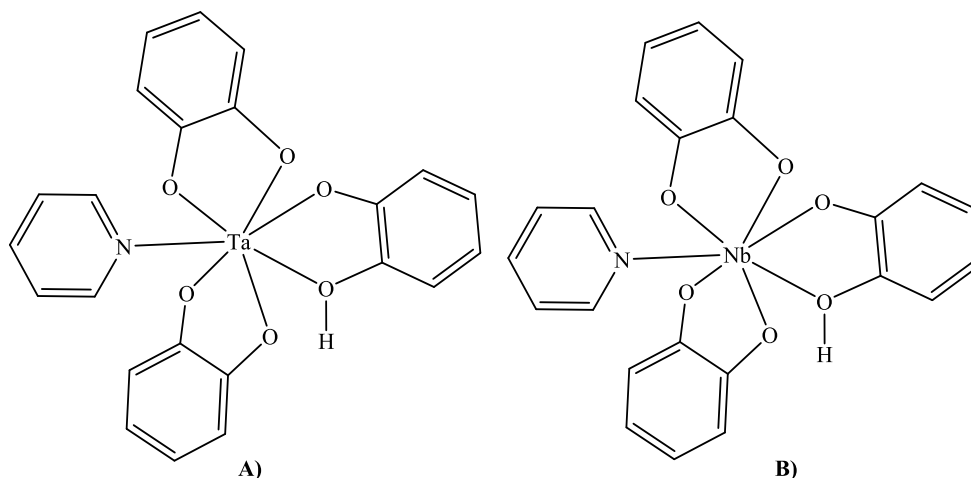
Figure 2.9 Proposed structure of **(A)** [Ta(cat)$_2$(cat-H)py] and **(B)** [Nb(cat)$_2$(cat-H)py].

2.7.4.3 Tris(8-quinolinolato-O,N)oxidoniobium(V) (A) and tris(8-quinolinolato-O,N)oxido tantalum(V) (B), dichloromethane disolvate, [NbO(quin)₃]·2CH₂Cl₂ and [TaO(quin)₃]·2CH₂Cl₂

From 2004 to 2005, Amini *et al.*[123,124] published two crystal structures of tris-niobium(V) and tantalum(V) complexes with 8-hydroxyquinoline (quinH) (Figure 2.10). [NbO(quin)₃]·2CH₂Cl₂ and [TaO(quin)₃]. 2CH₂Cl₂ crystallize in the same orthorhombic space group *Pnma* and the complexes are isostructural. Complexes **A** and **B** do not lose the solvent molecules when exposed to air and exist in a pentagonal bipyramidal geometry.

In complex **A** the Nb-O bond lengths vary from 1.732(3) Å to 2.054(3) Å, with the average Nb-O bond distance as 2.053(6) Å and Nb-N bond distances vary from 2.366(2)Å to 2.386(3)Å, with the average Nb-N bond distance as 2.373(6) Å. The O-Nb-N bite angles vary from 70.80(1)° to 72.50(1)° with the average O-Nb-N bite angle of 71.37(6)°. In complex **B** the Ta-O bond lengths vary from 1.747(3) Å to 2.049(3) Å, with the average Ta-O bond distance being 2.040(3) Å. Ta-N bond distances vary from 2.342(3) Å to 2.356(3) Å, with an average Ta-N bond distance of 2.347(6) Å. The O-Ta-N bite angles vary from 71.2(1)° to 72.7(1)° with the average O-Ta-N bite angle of 71.7(1)°. The bond dimensions of the molecule in the dichloromethane solvate were almost identical to those of the chloroform solvate,[125] but both solvates are unstable with respect to loss of the solvent.

[123] M.M. Amini, T. Tamizkar, M. Mirzaee, S.W. Ng, *Acta Cryst.,* **E60**, m147-m148, 2004.

[124] M.M. Amini, T. Tamizkar, M. Mirzaee, S.W. Ng, *Acta Cryst.,* **E61**, m1053-m1054, 2005.

[125] S. Garcia-Granda, M.R. Doaaz, L. Serra, A. Sanz-Medel, F. Goamez-Beltraan, *Acta Cryst.*, **C46**, 753-755, 1990.
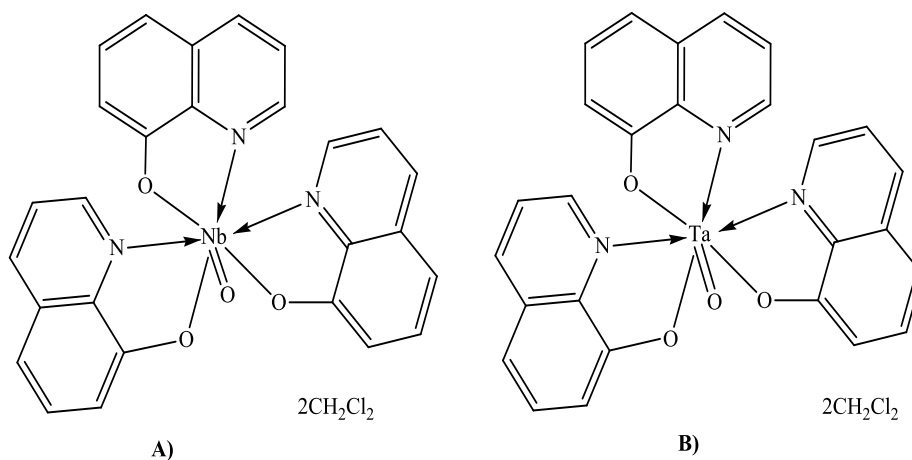
Figure 2.10 Proposed structure of **(A)** [NbO(quin)$_3$]·2CH$_2$Cl$_2$ and **(B)** [TaO(quin)$_3$]·2CH$_2$Cl$_2$.

2.7.5 Cyclo-bridged niobium(V) (*β*-diketonate) and O,O'-and O,N-bidentate complexes

2.7.5.1 Tetrakis(acetylacetonato)octakis(etoxy)tetrakis(*μ²*-oxo)tetraniobium(V), [Nb(acac)(OEt)₂(*μ²*-O)]₄

In 2011, Herbst et *al.*[126] published the crystal structure for the 4-coordinated niobium acetylacetone complex (Figure 2.11). According to a CSD search, it is the only *β*-diketonate crystal structure of this kind published.[102] The complex crystallized in the monoclinic space group $P2_1/c$ with two independent molecules in the unit cell. The Nb-O distances vary between 1.817(2) Å to 2.201(3) Å and the O-Nb-O angles between 78.86(10)° and 102.79(11)°, illustrating the significant distortion from ideal octahedral geometry. The four niobium atoms and the four bridging oxygen atoms form a slightly distorted square with Nb-Nb distances of 3.834(1) Å and 3.823(9) Å respectively and O-Nb-O angles of 93.53(1)° and 97.12(1)°.

---

[126] L. Herbst, H.G. Visser, A. Roodt, T.J. Muller, *Acta Cryst.*, **E67**, m1669-m1670, 2011.
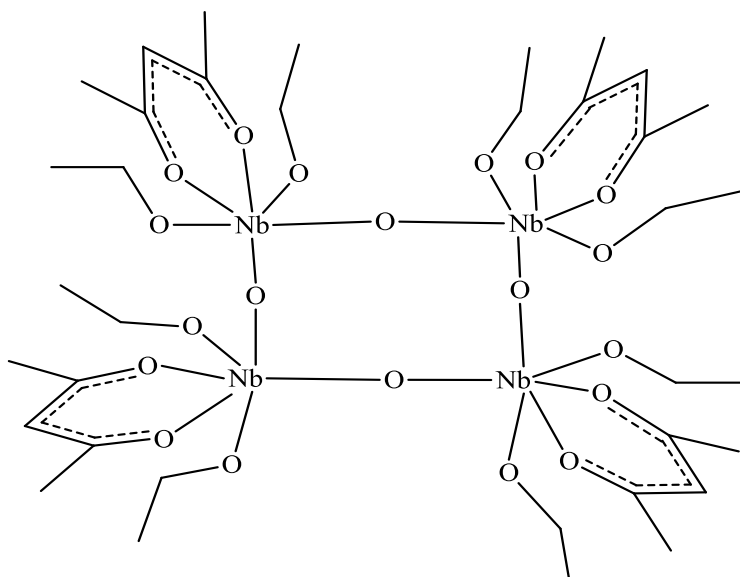
Figure 2.11 Proposed structure of [Nb(acac)(OEt)$_2$(μ^2-O)]$_4$.

2.7.5.2   Bis(8-quinolinolato-O,N)octakis(etoxy)bis(μ-etoxy)tetrakis(μ^2-oxo)tetraniobium(V), [Nb$_4$(μ-O)$_4$(μ-OEt)$_2$(R-quin)$_2$(OEt)$_8$], (where R1= Cl and R2 = Me)

In 2015, Amini *et al.*[127] published the crystal structure of two niobium(V) complexes with bis (5-chloro-8-hydroxyquinolinol and 2-methyl-8-hydroxyquinolinol) ligand (where quinH = 8-hydroxyquinolinol). Tetranuclear heteroleptic niobium complexes, [Nb$_4$(μ-O)$_4$(μ-OEt)$_2$(Cl-quin)$_2$ (OEt)$_8$] **(A)** and [Nb$_4$(μ-O)$_4$(μ-OEt)$_2$(Me-quin)$_2$(OEt)$_8$] **(B)** contain oxo, ethoxo, and quinolinate chelate rings.

The complexes **A** and **B** crystallize in the monoclinic space group *P*2$_1$/*n* and their crystal structures are similar. These crystal structures consist of centrosymmetric tetranuclear molecules and contain a pair of edge-sharing distorted bi-octahedral units that are linked by two oxo ligands (Figure 2.12). The geometry of the Nb atoms in the complex in respect to each other is a parallelogram. Each Nb(V) atom was octahedrally coordinated, and there were two different coordination environments in a bi-octahedral unit. Each metallic centre consists of one bridged ethoxo and two oxo ligands but differs from each other in the other three ligands.

---

[127] M.M. Amini, Y. Fazaeli, G. Mohammadnezhad, H.R. Khavasi, *Spectrochim. Acta Part A*, **144**, 192-199, 2015.

One Nb centre consists of three terminal ethoxides in facial type geometry, and the other one consists of one terminal ethoxo and a bidentate Me-quin or Cl-quin (where quin = 8-hydroxyquinolinol) moiety.

The coordination environment of the chiral niobium centre in both complexes was affected by the Me and Cl substituents of the quinolinate ring. Due to the vicinity of the methyl group to the chelating nitrogen in Me-quin, a steric hindrance is imposed by this group and the bond distance of Nb-N in complex **B** became longer than that of **A** by 0.044 Å, but the presence of electron-withdrawing groups at the para position of phenolic oxygen led to conjugation of the benzene ring with oxygen.[128]

The bond lengths of Nb-O in complex **A** and **B** were nearly similar, and their differences were in the range of 0.008-0.021 Å. The quinolinate bite angles of O-Nb-N for **A** and **B** were 71.71° and 72.18° respectively. The N…O bite distances in these complexes were shorter than uncoordinated ones and are close to the such values found in other metal complexes.[129,130]

The Nb-O-Nb angles in complexes **A** and **B** were 177.4(2)° and 176.58(1)° respectively and Nb-O distances in the Nb-O-Nb moiety were 1.807 and 2.094 Å for **B**, and 1.819 and 2.080 Å for **A** (Figure 2.13). There was a large difference, 0.287 and 0.261 Å, in the bond lengths of Nb-O which leads to asymmetric oxo-bridged complexes. Usually, these type of linearity is known for the alkoxide complexes of pentavalent metals of Nb[131,132,133] and Ta.[134] The Nb…Nb separations were 3.248 and 3.233 Å in compound **B** and **A**, respectively. These values exceed the theoretical value of 2.94 Å calculated from the corresponding metallic radius, but they were shorter than such a distance found in Nb_2Cl_{10} (3.951 Å) for a nonbonding interaction.[48]

[128] G. Mohammadnezhad, M.M. Amini, V. Langer, M. Adineh, *Z. Kristallogr.*, **230**(3), 157-165, 2015.

[129] M.M. Amini, G. Mohammadnezhad, H.R. Khavasi, *J. Coord. Chem.*, **65**(16), 2945-2956, 2012.

[130] E. Sattarzadeh, G. Mohammadnezhad, M.M. Amini, S.W. Ng, *Acta Crystallogr. Sect.*, **E65**, m553, 2009.

[131] V. Lorenz, S. Blaurock, H. Girls, F.T. Edelmann, *Organometallics*, **25**(25), 5922-5926, 2006.

[132] B.L. Ooi, I. Sotofte, *Inorg. Chim. Acta*, **357**, 3780-3784, 2004.

[133] O.A. Nikonova, V.G. Kessler, G.A. Seisenbaeva, *J. Solid State Chem.*, **181**(12), 3294-3302, 2008.

[134] O.A. Nikonova, V.G. Kessler, D.V. Drobot, P.A. Shcheglov, G.A. Seisenbaeva, *Polyhedron*, **26**(4), 862-866, 2007.

The Nb-O distances of these oxo ligands were 1.902 and 1.972 Å for complex **B** and 1.888 and 1.996 Å for **A**. In spite of the smaller difference observed (0.070 and 0.108 Å), these bonds are still considered as asymmetric oxo-bridges. They reported comparisons with other tetranuclear complexes of niobium, such as $[Nb_4(\mu\text{-O})_2(\mu\text{-OEt})_4Cl_4(OEt)_4(EtOH)_4]$[135] and $[Nb_4(\mu\text{-O})_2(\mu\text{-OEt})_2Cl_8(OEt)_2(THF)_4]$,[136] which contain metal-oxygen-metal bonds and also heterobimetallic structures of rhenium, $[Nb_4(\mu\text{-O})_2(\mu\text{-OR})_4(OR)_{10}(ReO_4)_2$ (R = OMe, OEt)]. These complexes have a nearly identical core structure in which Nb-O-Nb angles were approached linearity. In general, Nb-O distances for bridged ethoxo ligands are nearly symmetric with the differences of 0.018 and 0.005 Å for complexes **B** and **A**, respectively.

Almost all Nb-O distances reveal that they are strongly influenced by the *trans* ligands. Obviously, the shortest bonds are directed *trans* to the longest ones. The symmetric nature of the ethoxo-bridged ligand arises from the two similar terminal ethoxo groups in its *trans* position, while other bridges have different ligands in their trans positions. Furthermore, π-donation of ethoxide ligands is responsible for the increase of the bond order in terminal ethoxides and asymmetric bonding of the bridging ligands. The asymmetric unit of these complexes contains two niobium centres and due to the aforementioned discussions, one of these centres was chiral. The centrosymmetric nature of these tetranuclear complexes make them achiral, although two Nb centres with different chirality are present in their structures.

---

[135] R.P. Bontchev, E.L. Venturini, M. Nyman, *Inorg. Chem.*, **46**(11), 4483-4491, 2007.
[136] F.A. Cotton, M.P. Diebold, W.J. Roth, *Inorg. Chem.*, **26**, 3323-3327, 1987.
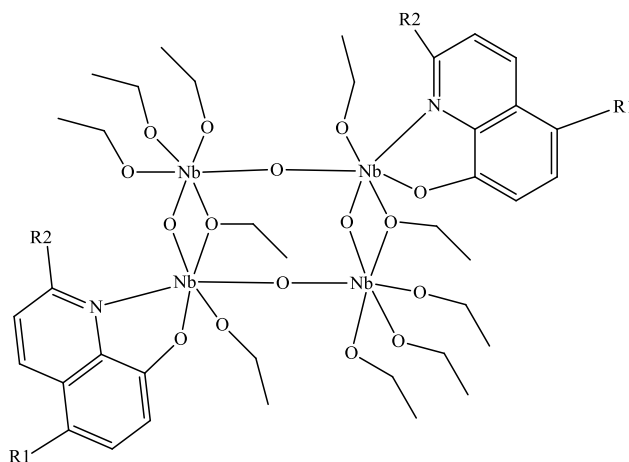
Figure 2.12 Proposed structure of [Nb$_4$(μ-O)$_4$(μ-OEt)$_2$(R-quin)$_2$(OEt)$_8$], (where R1= Cl for **A** and R2 = Me for **B**).

2.7.5.3   2-Hydroxybenzaldehydeoximato- tantalum(V) and tantalum(V) complexes, [Ta$_2$(μ-O)(hbo)$_2$(OEt)$_4$] and [Nb$_2$(μ-O)(hbo)$_2$(OEt)$_4$]

In 2004, Amini *et al*.[137] and 2011, Mirzaee *et al*.[138] published the first molecular structures of μ-oxo-bis-tantalum and niobium(V) complexes with 2-hydroxybenzaldehydeoxime, (hbo) (sometimes called salicylaldoximate) ligand (Figure 2.13). Complexes **A** and **B** were iso-structural and crystallize in the triclinic space group *P*-1 with *Z* = 2 but the unit cell volume of **A** was 1296.8 Å^3, somewhat was smaller than **B**, 1335.6 Å^3. These require longer unit cell dimensions of **B** in comparison with **A**.

The geometry at the niobium and tantalum in these complexes atoms was similar, the metal centre was a distorted octahedral which shared an apex through the bridged oxygen. Each dianionic salicylaldoximate ligand was chelated to the one metal through its phenolic oxygen and oxime nitrogen atoms, and to another metal through its oximate oxygen atom. One ethoxide at each metal centre was *trans* to oximate nitrogen and another one was *trans* to the oximate oxygen (Figure 2.13).

[137] M.M. Amini, M. Mirzaee, S.W. Ng*, Acta Cryst*, **E60**, m53-m55, 2004.
[138] M. Mirzaee, T. Tamizkar, G. Mohammadnezhad, H.R. Khavasi, M.M. Amini, *Comptes Rendus Chimie*, **14**(10), 927-933, 2011.

The shortest bond lengths observed in **A** are Ta-N_{oxim}: 2.296(4) and 2.309(4) Å, which are comparable to Nb-N_{oxim} in **B**, 2.333(2) and 2.337(2) Å and Mo-N_{oxim} in [MoO(O$_2$)$_2$(OC$_6$H$_4$CH = NOH)], 2.374(2) Å.[139] The Ta-O_{oxim} bond lengths in **A** are 2.048(4) and 2.055(4) Å, which are comparable with Nb-O_{oxim} in **B**, 2.061(1) and 2.071(1) Å, and V-O_{oxim} in [(η^5-C$_5$H$_4$CH$_3$)$_2$V(ONC(CN)$_2$)$_2$], 2.0354(9) Å.[140] The Ta-$O_{phenolic}$ bond lengths in **A** were 1.955(4) and 1.958(3) Å and Nb-$O_{phenolic}$ in **B** were 1.969(1) and 1.971(1) Å, which were very close to one other. Furthermore, the Ta-O_{oxo} bond lengths in **A**, 1.920(3) and 1.928(3) Å and Nb-O_{oxo} lengths in **B**, 1.930(1) and1.940 (1) Å were very similar.

In general, the bond lengths of two metal ions in both compound **A** and **B** were similar to some extent. However, the Ta-O_{ethoxy} bond lengths in **A** vary from 1.875(4) Å to 1.896(4) Å and Nb-O_{ethoxy} bond lengths vary from 1.882(2) Å to 1.897(2) Å in **B**, which were comparable to terminal M-O_{alkoxy}, but when compared to Ta-N_{oxim}, Ta-O_{oxim}, Ta-$O_{phenolic}$, Ta-$O_{oxo,}$ and Nb-N_{oxim}, Nb-O_{oxim}, Nb-$O_{phenolic}$, Nb-O_{oxo} have the shortest bond length. The O-Ta-N bite angles in **A** vary from 78.31(14)° to 78.41(14)° with the average O-Ta-N bite angle being 78.36(14)°, whereas the O-Nb-N bite angles in **B** vary from 78.1(1)° to 78.0(1)° with an average O-Ta-N bite angle of 78.05(1)°.
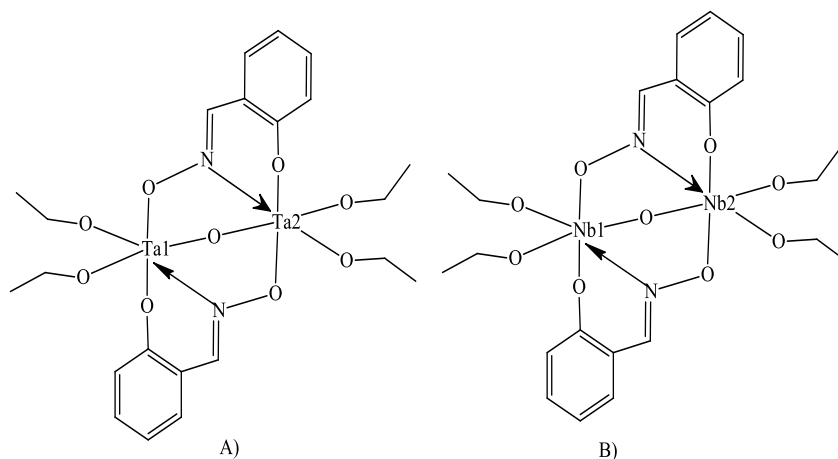
Figure 2.13 Proposed structure of [Ta$_2$(μ-O)(hbo)$_2$(OEt)$_4$] **(A)** and [Nb$_2$(μ-O)(hbo)$_2$(OEt)$_4$] **(B)**.

---

[139] N. Gharah, S. Chakraborty, A.K. Mukherjeeb, R. Bhattacharyya, *Chem. Com.*, **22**, 2630-2632, 2004.

[140] J. Honzcek, J. Vinklarek, I. Csarova, M. Erben, *Inorg. Chim. Acta*, **362**, 83-88, 2009.

2.7.6   Mono (*β*-diketonate) niobium(V) and tantalum(V) complexes

A detailed review of the literature shows that there are more mono-coordinated (*β*-diketonate) niobium(V) and tantalum(V) complexes compared to tris- and tetrakis-(*β*-diketonate) niobium(V) and tantalum(V) complexes.[59,113,122,141,142,143]

2.7.6.1   (Acetylacetonato)chloridotrimethoxidoniobium(V) (A), (Acetylacetonato)di-chloridobis(methoxido)niobium(V) (B), (Benzoylacetonato)dichloridodimethoxido-niobium(V) (C) and (2-(benzoyl)phenolato)-*trans*-dichlorido-*cis*-bis(methoxido)-niobium(V) (D) complexes

From 2010 to 2015 Herbst *et al*.[59,144,145,146,147] published mono-coordinated β-diketonate niobium(V) complexes (Figure 2.14). The aim of these studies was niobium(V) complex formation with various *β*-diketone ligands and to investigate the interaction of transition metals used in the nuclear and separations industries.[148,149] In complexes **A, B, C,** and **D** distorted octahedral coordination geometries were observed around the niobium centre.

Complex **A** crystallizes in the orthorhombic space group *Pbca*. The Nb-O$_{acac}$ bond distances vary between 2.084(2) and 2.108(2) Å, Nb-O$_{methoxy}$ bond distances vary from 1.860(2) to 1.881(2) Å, and the Nb-Cl bond distance was 2.469(9) Å. The O-Nb-O acac bite angle was 80.74(6)°, while the trans Cl-Nb-O angle was 167.60(5)°, which are comparable with *fac*-[Nb(NCS)-(Opr)$_3$(dbm)], where dbm = dibenzoylmethanato, NCS = thiocyanato, and Opr = isopropoxy groups.

[141] R. Koen, *High oxidation state tantalum coordination chemistry, a solution and solid state investigation,* M.Sc. Dissertation, University of the Free State, South Africa, 2012.

[142] P. Wendrup, V.G. Kessler, *J. Chem. Soc, Dalton Trans*, 574-579, 2001.

[143] E.L. Lippert, M.R. Truter, *J. Chem. Soc.A*, **33**, 309-311, 1960.

[144] L. Herbst, R. Koen, A. Roodt, H.G. Visser, *Acta Cryst,* **E66**, m801-m802, 2010.

[145] L. Herbst, H.G. Visser, A. Roodt, C. Pretorius, *Acta Cryst,* E**68**, m1392-m1393, 2012.

[146] L. Herbst, H.G. Visser, A. Roodt, *Z. Kristallogr. NCS*, **228**, 451-452, 2013.

[147] L. Herbst, H.G. Visser, A. Roodt, M. Steyn, N. Loganathan, *Z. Kristallogr. NCS,* **230**(4), 345-347, 2015.

[148] M. Steyn, A. Roodt, G. Steyl, *Acta Cryst.*, **E64**, m827, 2008.

[149] J.A. Viljoen, H.G. Visser, A. Roodt, M. Steyn, *Acta Cryst.*, **E65**, m1514-m1515, 2009a.

The Nb-O$_{dpm}$ bond distances vary from 2.087-2.083 Å and Nb-O$_{Opr}$ bond distances vary between 1.828 and 1.845 Å, with a Nb-N bond distance of 2.176 Å.[150]

Complex **B** crystallizes in the monoclinic space group $P2_1/c$. The Nb-O$_{acac}$ bond distances vary from 2.043(2)-2.089(2) Å and Nb-Cl bond distances vary from 2.399(1)-2.402(12) Å. The O-Nb-O acac bite angle is 81.36(7)°, while the trans Cl-Nb-Cl angle is 167.34(2)°. Complex **C** crystallizes in the triclinic space group P-1 and Nb-O$_{phacac}$ distances vary from 2.047(1) to 2.076(1) Å, while Nb-O$_{methoxy}$ distances vary between 1.836(1) and 1.841(1) Å. The *trans* axial Nb-Cl distances are between 2.407(7) and 2.419(7) Å. The O-Nb-O phacac bite angle is 80.47(5)°, with a *trans* Cl-Nb-Cl angle of 171.83(1)°.

Complex **D** crystallizes in the monoclinic crystal system, space group $P2_1/n$. The Nb-O$_{2-bp}$ bond distances vary from 2.153(2) Å-1.964(2) Å and Nb-O$_{methoxy}$ bond distances vary between 1.828(3) Å and 1.835(2) Å, with the *trans*-axial Nb-Cl distances varying from 2.387(1) Å-2.411(1) Å. The O-Nb-O$_{2-bp}$ bite angle was 79.47(9)°, with a *trans* Cl-Nb-Cl angle of 166.79(4)° (Figure 2.14).

The crystal stabilization was influenced by intermolecular π-π interactions of the phenyl ring on the 2-*bp* ligand and its neighbouring, symmetry generated counterparts were *-x, 1-y, 1-z*. Due to the disorder of the phenyl groups two centroid-centroid distances of 3.54(1) Å and 3.64(2) Å were observed. In conclusion, the *trans* Cl-Nb-Cl angles of complex **C** were relatively larger than complex **B** and **D**, but the rest all the bond distances and angles were nearly similar.

---

[150] F. Dahan, R. Kergoat, M. Senechal-Tocquer, J.E. Guerchais, *J. Chem. Soc*, *Dalton Trans*, 2202-2204, 1976.
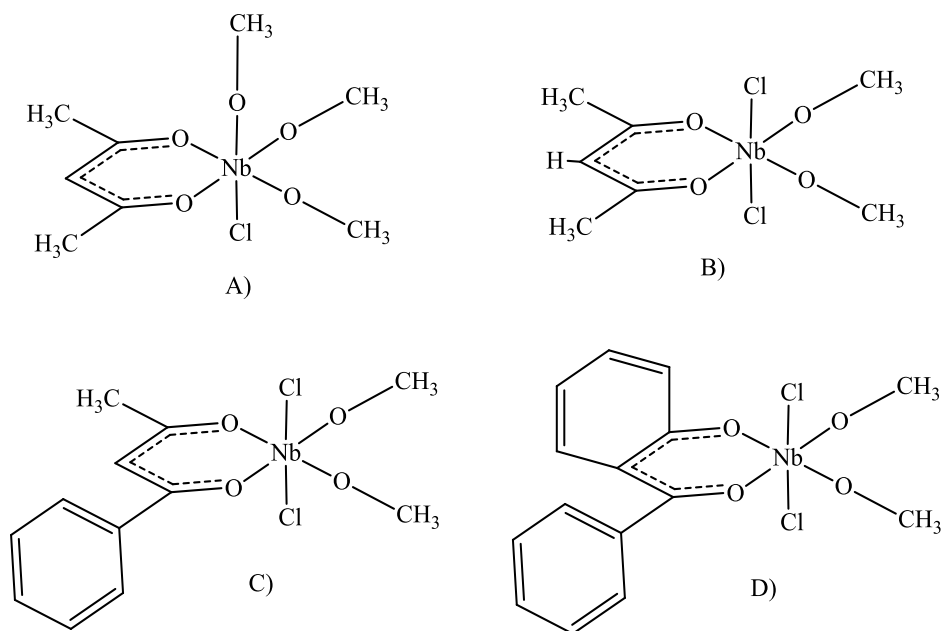
Figure 2.14 Proposed structures of [Nb(acac)(OMe)$_3$Cl]**(A)**, [Nb(acac)(OMe)$_2$Cl$_2$]**(B)**, [Nb(phacac)(OMe)$_2$Cl$_2$]**(C)**, and [Nb(2-bp)(OMe)$_2$Cl$_2$]**(D)**. Where acac = acetylacetonate, phacac = 1-phenyl-1,3-butanedionate and 2-bp = 2-(benzoyl)-phenolato.

2.7.6.2 trans, cis-[TaCl$_2$(OMe)$_2$(tmhd)] and -[TaCl$_2$(OMe)$_2$(acac)], [Ta(OMe)$_4$(tmhd)] and [Ta(OMe)$_4$(acac)]

In 1999, Davies *et al.*[107] published the total four crystal structures of mono coordinated tantalum(V) complexes with 2,2,6,6-tetramethylheptane-3,5-dione (tmhdH) and 2,4-pentanedione or acetylacetone (acacH). The aim of the study was the synthesis and structural characterisation of the coordination complexes for further development of the chemistry of tantalum(V) *β*-diketonates and their application in chemical vapour deposition (CVD) (Figure 2.15).

In complexes **A**, **B**, **C**, and **D** distorted octahedral coordination geometries were observed around the tantalum centre in the solid state, as well as tight chelate ring bite angles. Complex **A** crystallizes in the monoclinic space group *P*2$_1$/*c*. The Ta-O$_{tmhd}$ bond distances vary between 2.051(1) Å and 2.055(9) Å, Ta-O$_{methoxy}$ bond distances from 1.833(1) Å and 1.853(1) Å, and Ta-Cl bond distances between 2.347(5) Å and 2.401(5) Å. The O-Ta-O tmhd bite angle was

79.7(4)°, while the trans Cl-Ta-Cl angle was 169.9(2)° and the *cis* O-Ta-O*methoxy* angle was 100.6(5)°. Complex **B** crystallizes in the orthorhombic space group *Pbca*. The Ta-O*tmhd* bond distances vary from 2.101(6) Å to 2.112(6) Å, and the Ta-O*methoxy* bond distances from 1.861(7) Å to 1.912(7) Å. The O-Ta-O tmhd bite angle was 79.3(2)°. Complex **C** crystallizes in the monoclinic space group *P2₁/n*. The Ta-O*acac* bond distances vary between 2.026(10) Å and 2.083(12)Å, the Ta-O*methoxy* bond distances from 1.810(2) Å to 1.855(1) Å, and the Ta-Cl bond distances between 2.387(9) Å and 2.412(9) Å. The O-Ta-O acac bite angle was 82.2(5)°, while the trans Cl-Ta-Cl angle was 169.0(2)°, and the *cis* O-Ta-O*methoxy* angle was 99.2(7)°. The relatively bite angle of acacH complex **C** was higher when compared to thmdH complex **A**, but the rest of the bond distances and angles were nearly similar. Complex **D** crystallizes in the orthorhombic space group *Pbca*, with the Ta-O*acac* bond distances varying from 2.087(1) Å to 2.095(1) Å, Ta-O*methoxy* bond distances from 1.877(1) Å to 1.915(1) Å. The O-Ta-O*acac* bite angle was 78.9(5)°. In general, all compounds the bond distances and angles were comparable with Herbst *et al.*[59,144,145,146,147]
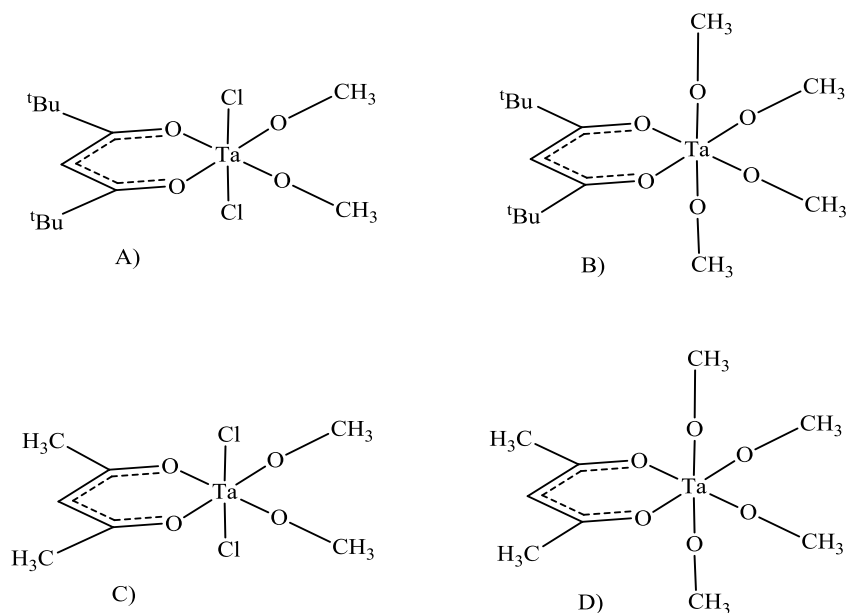
Figure 2.15 Proposed structure of *trans*, *cis*-[TaCl₂(OMe)₂(tmhd)] **(A)**, [Ta(OMe)₄(tmhd)] **(B)**, trans, *cis*-[TaCl₂(OMe)₂(acac)] **(C)**, and [Ta(OMe)₄(acac)] **(D)**, where tmhdH = 2,2,6,6-tetra-methylheptane-3,5-dione, while acacH = acetylacetone.

2.8   Mechanistic studies of niobium(V) and tantalum(V) complexes

Chemical kinetics (reaction kinetics) is the study of rates of chemical processes and includes investigations of how different experimental conditions can influence the speed of a chemical reaction, yield information about the reaction's mechanism and transition states, as well as the construction of mathematical models that can describe the characteristics of a chemical reaction.[151] Separation and purification of niobium from tantalum by means of mechanistic studies of bidentate ligand coordination to niobium(V) and tantalum(V) complexes is important for using in advanced materials for high technology applications. A few literature studies will be discuss here.

2.8.1   Fast and slow reaction between *trans*-[TaCl$_2$(OMe)$_3$(MeOH)] and acacH

In 2014 Koen *et al*.[152] published a paper in which they performed a kinetic study on the coordination of acetylacetone (acacH) to solvated tantalum pentachloride ([TaCl$_5$]$_2$) in methanol at different temperatures. The aim of the study was the coordination of novel, hard ligand systems to tantalum(V) and niobium(V) metal centers, which provided a better understanding in avoiding the use of a dangerous acid, HF and finding other methods to simplify separation (Figure 2.16). They followed the kinetics of the substitution reaction of *trans*-[TaCl$_2$(OMe)$_2$(acac)] of which the crystal structure was obtained by single crystal X-Ray diffraction. The kinetic runs were performed with the ligand concentration in at least ten-fold excess to ensure *pseudo* first-order reaction conditions and the ligand concentrations were varied by one order-of-magnitude.

Similar work to identify the substitution products formed in the solvolysis of [NbCl$_5$]$_2$ and [TaCl$_5$]$_2$ by MeOH was reported by Karaliota *et al*.[153] Figure 2.16 shows the reaction involving a fast initial reaction where acacH substitutes the labile solvated MeOH to form an intermediate mono-coordinated species, which undergoes ring-closure in a second, slower, rate-determining step.

[151] B.E. Norcross, *Advanced organic chemistry: reactions, mechanisms, and structure*, 4th ed., Jerry March, Wiley, New York, NY, *J. Chem. Educ*., **70** (2), 89-174, 1993.
[152] R. Koen, A. Roodt, H.G. Visser, *Adv. Mat.Res.*, **1019**, 426-432, 2014.
[153] A. Karaliota, M. Kamariotaki, D. Hatzipanayioti, *Transition Met. Chem.*, **22**, 411-417, 1997.
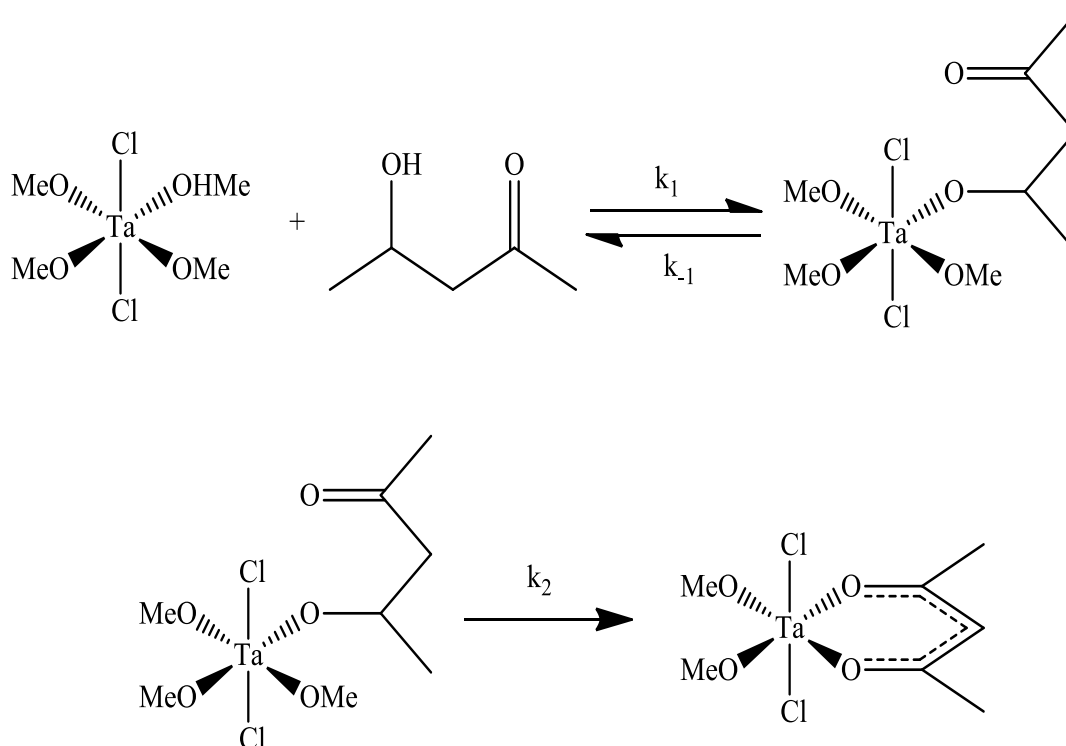
Figure 2.16 Proposed reaction mechanism for the reaction of solvated $[TaCl_5]_2$ and acacH in MeOH.

Tables 2.2 and 2.3 indicate that the stability constant for final product of *trans*-$[TaCl_2(OMe)_3(\eta^1\text{-}acacH)]$ was $K_1 = 2.4 \pm 0.3 \times 10^3$ M^{-1} at 25 °C. The second order rate constant, k_1 is $3.1 \pm 0.1 \times 10^2$ M^{-1}s^{-1} at 25 °C. The slower reaction yielded a K_1 value of $1.7 \pm 0.2 \times 10^3$ M^{-1}s^{-1}. Comparison of k_1 and k_2 indicated that the first reaction was 10^6 times faster than the second, rate determining step.

Table 2.2 Calculated k_1, k_{-1}, K_1, $\Delta S^{\ne}{}_{k1}$ and $\Delta H^{\ne}{}_{k1}$ values for the fast reaction between *trans*-[TaCl$_2$(OMe)$_3$(MeOH)] and acacH in MeOH at different temperatures. Where k_1 = second order forward rate constant, k_{-1} = reverse rate constant, k_2 = rate constant, K_1 = equilibrium constant, $\Delta S^{\ne}{}_{k1}$ = entropy and $\Delta H^{\ne}{}_{k1}$ = enthalpy.

	5.0 °C	15.0 °C	25.0 °C	35.0 °C	$\Delta S^{\ne}{}_{k1}$ (J K^{-1} mol^{-1})	$\Delta H^{\ne}{}_{k1}$ (kJ mol^{-1})
k_1 (M^{-1}s^{-1})	67(2)	151(7)	316(9)	755(13)	-14(10)	54(3)
k_{-1} (s^{-1})	0.03(1)	0.07(4)	0.14(5)	0.32(7)		
K_1 (M^{-1})	2233(745)	2157(573)	2328(358)	2484(219)		

Table 2.3 Calculated k_2, K_1, $\Delta S^{\ne}{}_{k2}$, values for the slow reaction between *trans*-[TaCl$_2$(OMe)$_3$(MeOH)] and acacH in MeOH at different temperatures.

	15.0 °C	25.0 °C	36.0 °C	45.0 °C	$\Delta S^{\ne}{}_{k2}$ (J K^{-1} mol^{-1})	$\Delta H^{\ne}{}_{k2}$ (kJ mol^{-1})
k_2 (x 10^{-5} s^{-1})	2.17(3)	4.43(7)	10.02(5)	18.41(7)	-56(7)	52(2)
K_1 (M^{-1})	1755(185)	1708(208)	2258(452)	2272(111)		

In general, they reported a comparison of the kinetic data at 25 °C with the parallel study on *trans*-[NbCl$_2$(OMe)$_3$(MeOH)] and acacH in MeOH. Different products were formed in spite of the fact that the starting metal complexes are similar. In the case of tantalum(V), both the chlorido ligands remained intact, but this was not the case for the niobium(V) study , where one chlorido ligand was substituted. The rate laws were similar for both studies, except that the k_{-2} step in the tantalum(V) study was negligible. The k_1 values for tantalum(V) was 316(9) M^{-1}s^{-1} while k_1 for niobium(V) was 237(4) M^{-1}s^{-1}, which showed that tantalum was a factor 1.3 faster than niobium. Stability constant values of niobium(V) (1975(201) M^{-1}) is lower than tantalum(V) (2157(573) M^{-1}) (Table 2.2 and 2.3). The k_2 value of the ring closure step for niobium was 3.7(3) x 10^{-5} M^{-1}, similar to the value for Ta(V), 4.43(7) x 10^{-5} M^{-1} (Table 2.2 and 2.3). Therefore these results showed that the niobium(V) reactions to be faster than that for the tantalum(V) because

tantalum(V) is a much stronger Lewis acid than niobium(V). So, these differences in kinetic studies were indicative of a good separation technique for future study.

2.8.2 Displacement reaction of [NbCl₂(OEt)₂(ᵗBuacac)](A) and [NbCl₂(OEt)₂(phacac)](B) with acacH

In 2000, Antinolo *et al.*[154] published a paper on the reactivity of alkoxo-niobium(V) compounds towards *O,O-* or *S,S*-enolate ligands. The aim of the study was to investigate the synthesis, kinetics and structural characterisation of some *β*-diketonate or dialkyl(aryl)dithiocarbamato anions containing alkoxides niobium(V) complexes [NbCl₃(OR)₂]₂ towards some *β*-diketones, namely MeCOCH₂COMe (acacH), ᵗBuCOCH₂COᵗBu (dpmH) **(A)** and PhCOCH₂COPh (dbmH) **(B)** in deuterated chloroform at room temperature (Figure 2.17 and 2.18).

Similar work was reported earlier.[155] The molecular structure of [NbCl₂(OEt)₂(phacac)] **(B)** was revealed by an X-ray diffraction and the kinetic study on these exchange processes was carried out as a function of time and temperature by ^{1}H-NMR spectroscopy. Complex **B** crystallises in the monoclinic space group *P*2₁/*n* and it is described as displaying a *pseudo*-octahedral geometry.

The Nb-O*phacac* bond distances vary between 2.045(4) Å-2.085(4) Å, the Nb-O*ethoxy* bond distances from 1.804(5) Å-1.809(5) Å, and the Nb-Cl bond distances between 2.392(2) Å-2.403(2) Å. The O-Nb-O*phacac* bite angle was 79.72(16)°, while the trans Cl-Nb-Cl angle was 170.23(8)° and the *cis* O-Nb-O*ethoxy* angle was 100.7(2)°. The bond distances and angles are comparable with Herbst *et al.*[59,144,145,146,147] and Davies *et al.*[107]

The calculated values of the *pseudo*-first order rate constants, k_1, at five temperatures, and the rate constant data at 313 K for different molar ratios [acacH]/ [NbCl₂(OEt)₂(ᵗBuacac)] **(A)** are displayed in Table 2.4 and Table 2.5 respectively. Figure 2.17 shows that for molar ratios

[154] A. Antinolo, F. Carrillo-Hermosilla, J. Fernandez-Baeza, S. Garcia-Yuste, A. Otera, E. Palomares, A.M. Rodriguez, L.F. Sanchez-Barba, *J. Organomet. Chem.*, **603**, 194-202, 2000.

[155] G. Wilkinson, R.D. Gillard, J.A. McCleverty (Eds.), *Comprehensive Coordination Chemistry*, 3rd ed., Pergamon, Oxford, 1987.

[acacH]/[complex **A**] higher than 4:1, a negligible dependence on the rate constant can be considered. The k_1 values were fitted to an Arrhenius plot, $k_1 = A_{exp}(-E_a/RT)$, and the E_a values for the two processes were calculated (Table 2.4). The activation parameters, $\Delta H^{\ddagger}$ and $\Delta S^{\ddagger}$, were determined from the Eyring plot. The differences in the activation energy of the two processes were attributed to the more stable bond between the dbmH ligand and the niobium atom for complex **B**, through a delocalized π-system due to the phenyl rings of the ligand, than in compound **A** with the dpmH ligand. In summary, they conclude that equilibrium was reached at more than 24 h between reagents and products. Equilibrium constants near 0.45 at 20 °C were obtained (complex **A**: $K_{eq} = 0.44$; complex **B**: $K_{eq} = 0.46$), which were similar for both niobium complexes, **A** and **B**.
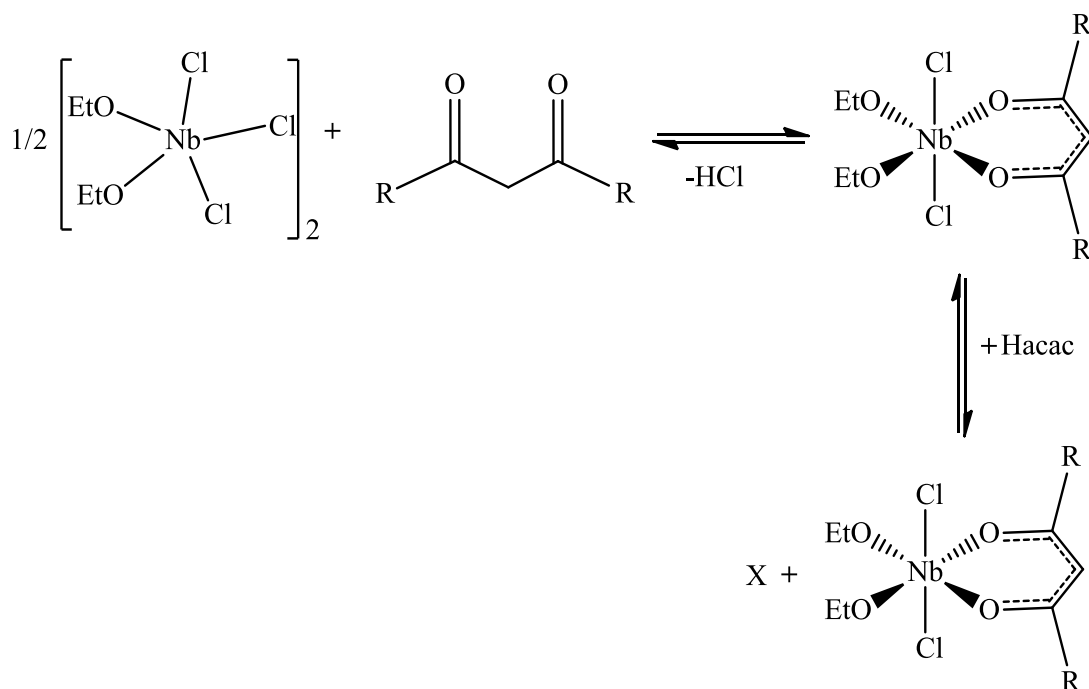
Figure 2.17 Displacement reaction of [NbCl$_2$(OEt)$_2$(^{t}Buacac)] **(A)** and [NbCl$_2$(OEt)$_2$(Phacac)] **(B)** with acacH in CDCl$_3$, where R = ^{t}Bu**(A)** or Ph**(B)** and X = dpmH (3-methyl-2,4-pentanedione).
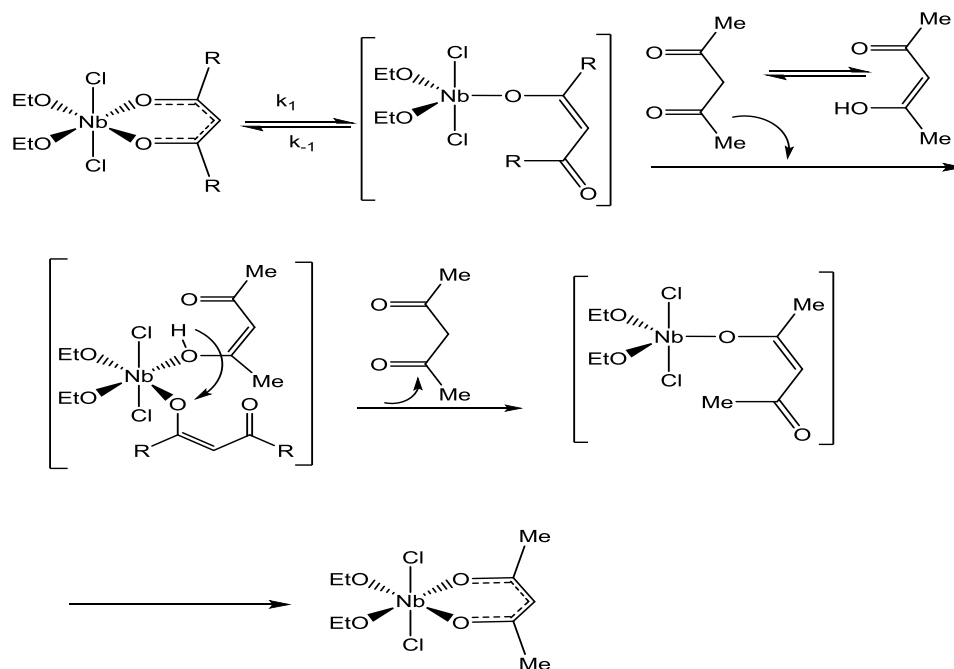
Figure 2.18 A possible mechanism of the displacement reaction of [NbCl$_2$(OEt)$_2$(^{t}Buacac)] **(A)** and [NbCl$_2$(OEt)$_2$(Phacac)] **(B)** with acacH in CDCl$_3$.

Table 2.4 Kinetic and thermodynamic parameters on the displacement reactions of [NbCl$_2$(OEt)$_2$ (^{t}Buacac)] **(A)** and [NbCl$_2$(OEt)$_2$(Phacac)] **(B)** with acacH in CDCl$_3$.

Complex	k_{app} x 10^3 (s^{-1})	T (K)	E_a (kJ mol^{-1})	$\Delta H^{\ddagger}$ (kJ mol^{-1})	$\Delta S^{\ddagger}$ (J mol^{-1} K^{-1})
	0.3 ± 0.2	293			
	0.6 ± 0.2	298			
A	1.2 ± 0.2	303	90.3 ± 0.1	87.8 ± 0.1	-11 ± 4
	2.1 ± 0.2	308			
	3.1 ± 0.2	313			
	0.1 ± 0.2	293			
	0.2 ± 0.2	298			
B	0.5 ± 0.2	303	105.5 ± 0.1	102.9 ± 0.1	31 ± 4
	0.9 ± 0.2	308			
	1.5 ± 0.2	313			

Table 2.5 Values of constant at 313 K for different molar ratios [acacH]/ [NbCl$_2$(OEt)$_2$-('Buacac)] **(A)** in CDCl$_3$.

[Complex A] (M)	[acacH]	[acacH]/Complex A	k_1 x 10^3
0.09	0.09	1:1	0.7(2)
0.09	0.18	2:1	2.0(2)
0.09	0.36	4:1	3.1(2)
0.09	0.45	5:1	3.1(2)
0.09	0.63	7:1	3.1(2)

2.8.3   Conclusion

Both niobium and tantalum metals have recently become vital to industry. The production and use of niobium and tantalum have increased rapidly over the last two decades together with the development of new technologies and materials and the creation of a wide range of products made of these elements. The above described a detailed literature review, showing a considerable shortage of knowledge with relation to the coordination behaviour of tantalum and niobium with different organic bidentate or multidentate ligands. Most of the niobium(V) and tantalum(V) complexes synthesis methods entails dry nitrogen atmosphere, using standard Schlenk techniques and glove boxes. Thus, these techniques show that it is a problem to get stable complexes due to hydrolysis.[156,157,158] A few of the mechanistic studies of solid and solution state behaviour of tantalum and niobium with selected coordination agents showed a clearer image of how improvements on known methods can be achieved.

According to the literature review shown, there is still a shortage of knowledge regarding the twin elements niobium and tantalum, there is still a stability problem and they exhibit nearly identical chemical and physical behaviour. These similarities in chemical and physical properties

[156] P.A. Williams, A.C. Jones, P.J. Wright, M.J. Crosbie, *Chem. Vap. Dep*, **8**, 110-116, 2002.

[157] F. Preuss, G. Lambing, S. Mueller-Becker, *Z. Anorg. Allg. Chem,* **620**, 1812-1821, 1994.

[158] C.K. Gupta, A.K. Suri, *Extractive Metallurgy of Niobium*, CRC Press, Boca Raton, U.S, 1993.

are the reason for the difficult separation of the two elements during the processing of tantalum and niobium containing minerals on industrial level.

One of the aims of this PhD study is investigating whether reactions performed under atmospheric conditions could improve the stability and ease of formation of the corresponding coordination compounds, and if simplified separation of these two elements could possibly be found in the differences in the physico-chemical properties of two similar organic chelated moieties of these metals. This additional information will be helpful in gaining knowledge about physico-chemical behaviour of niobium(V) and tantalum(V) and will be discussed in Chapters 4-8. This further study will provide a novel, safe and more environmentally friendly way to separate the two metals for use in advanced materials for high technology applications.

3 Chemical Synthesis and Characterisation of Niobium(V) and Tantalum(V) Complexes

3.1 Introduction

It is interesting and challenging in science to synthesize new compounds and explore their potential for useful application. Due to increasing interest in niobium and tantalum, stable products of these two metals are required for the development of potentially improved industrial processes for separation of niobium and tantalum from their mineral ores. The synthesis of these new compounds enables us to obtain new physicochemical properties, functionalities and, as a result, create new concepts. The synthesis, as a crucial protocol to form and break various atomic (covalent) bonds, provides new values based on the material resources. In recent years there has been an increasing focus on new materials designed by utilising supramolecular interactions rather than covalent bonds, to prepare functional, crystalline solids. These may include sensing/signalling materials,[1] porous frameworks for molecular sponges,[2] for gas storage or separation,[3] and catalysts.[4] However, the physicochemical properties of such complexes are influenced by the selection of both the metal centre and the organic ligand. Therefore, there is still a gap in the knowledges base of the separation and purification of niobium(V) from tantalum(V) at industrial level by attempting novel, easy, safe, and environmental friendly ways.

[1] J. Scott, K. Tanaka, *Cryst. Grow. Des.*, **5**, 1209-1213, 2005.

[2] C. Aakeroy, A. Beatty, D. Leinen, *Angew. Chem. Int. Edn*., **38**, 1815-1819, 1999.

[3] O. Yaghi, M. O'Keeffe, N. Ockwig, H. Chae, M. Eddaoudi, J. Kim, *Nature*, **423**, 705-714, 2003, b) J. Rowsell, A. Millward, K. Park, O. Yaghi, *J. Am. Chem. Soc.*, **126**, 5666-5667, 2004.

[4] J. Seo, D. Wand, H. Lee, S. Jun, J. Oh, Y. Jeon, K. Kim, *Nature*, **404,** 982-986, 2000, b) M. Fujita, Y.J. Kwon, S. Washizu, K. Ogura, *J. Am. Chem. Soc*., **116**(3), 1151-1152, 1994.

In this chapter all methods applied for both niobium(V) and tantalum(V) complex synthesis are discussed. As mentioned in Chapter 2, most of the previous literature reviews reported synthesis methods involving Schlenk techniques and employing a glove box under dry inert gas. The synthesised product was unstable and easily hydrolysed; production of these complexes is complicated due to the metal's affinity to readily form oxides. In the last few years, Prof. Andreas Roodt's research group has been investigating complexes with different chelating ligands, with and without employing Schlenk techniques. However, these did not yield much information regarding the control of ligand coordination and stability during reactions. This study was aimed at using new synthon techniques and all reactions were carried out in atmospheric conditions by using Et_4NCl as the counter ion. These complexes show enhanced chemical reactivity and were also used as starting material. In an effort to unravel their coordination chemistry, the reaction mechanisms of niobium and tantalum complexes with O,O- and O,N-bidentate ligands were also investigated.

Different types of complexes are produced through selective adjustment of the variables that play a role in the separation of niobium from tantalum. Since no literature method was found that specifically investigates and describes the dependence of niobium complex formation on the specific reaction conditions, a range of methods were attempted and evaluated during this study. Generally, all reactions were carried out in atmospheric conditions, and each method reported and discussed in this chapter is easy, clear and the products formed were relatively more stable than with the previously reported methods. Table 3.1 lists different O,O'-, O,N- and O,S-bidentate ligands, employed in this study.

Table 3.1 O,O'-, O,N-, O,S- and N,N-bidentate ligands, employed in this study.

S/N	L,L'-Bidentate ligands
1	2,5-dichloro-3,6-dihydroxy-2,5-cyclohexadiene-1,4-dione or chloranilic acid (caH_2)
2	2-hydroxypyridine-N-oxide (hopoH)
3	2-mercaptopyridine-N-oxide (mpoH)
4	ammonium salt of N-nitroso-N-phenylhydroxylamine or cupferron (cupfH)
5	ammonium salt of N-hydroxy-N-nitroso-1-naphthylamine, neocupferron (neocupfH)
6	2,5-dihydroxy-1,4-benzoquinone ($dhbqH_2$)
7	8-quinolinol-N-oxide (quinH)
8	picolinic acid N-oxide (picoH)
9	α-pyridoin (pyrH)
10	2,2'-dipyridyl-N-oxide (dipy)
11	2,2':6',2"-terpyridine (terpy)

3.2 Synthesis and spectroscopic characterization

All synthesized complexes of niobium(V) and tantalum(V) were characterised using various techniques such as nuclear magnetic resonance (NMR), ultraviolet-visible (UV-Vis), Fourier transform infrared (FTIR) spectroscopy, as well as single crystal X-ray diffraction (XRD) when suitable crystals were obtained. A detailed discussion of these characterised complexes are presented in Chapters 4-6.

3.2.1 Overview of most used chemicals and instrumentation

All reagents used for the synthesis and characterisation were of analytical grade and were purchased from Sigma-Aldrich, South Africa, unless otherwise stated. Some reagents were used as received without further purification. All organic solvents were purified and dried according to literature.[5] All the infrared spectra of the complexes were recorded on a Bruker Tensor 27 Standard System spectrophotometer utilizing a He-Ne laser at 632.6 nm at a range of

---

[5] D.D. Perrin, W.L.F. Armarego, *Purification of Laboratory Chemicals*, 4th *ed*., Bath Press, Britain, 1-544, 1996.

4000-600 cm^{-1}. All samples were analysed as solid state species via Attenuated Total Reflection (ATR) mode infrared spectrophotometry and all data were recorded at room temperature. No solution or KX (where X = I, Cl, Br) solid salt pellets were utilized since halogen interaction was expected from the solution cell and the KX pellet preparation technique.

^{1}H, ^{31}P and ^{13}C NMR spectra were obtained in deuterated CD$_3$OD, D$_2$O, CD$_3$CN, and (CD$_3$)$_2$SO on a Bruker AVANCE II 600 MHz (^{1}H: 600.28 MHz; ^{31}P: 242.99 MHz; ^{13}C: 150.95 MHz) (probe for ^{1}H and ^{13}C is 5 mm DUAL ^{13}C-^{1}H/D with z-gradients, while for ^{31}P and ^{1}H is 5 mm TBI^{1}H/^{31}P/D-BB with Z-gradients), AVANCE III 400 MHz (^{1}H: 400.13 MHz; ^{13}C: 100.61 MHz; ^{31}P: 161.97 MHz) (for solid state 4 mm VTN multinuclear double resonance magic angle spinning probe and for liquid state 5 mm BBI H-BB-D probe with z-gradients) and FOURIER 300 MHz (^{1}H: 300.18 MHz; ^{13}C: 75.48 MHz) (5 mm ^{13}C/^{1}H high resolution NMR probe equipped with Z-gradient coil) nuclear magnetic resonance spectrometers operating at 25 ^{o}C.

Chemical shifts are reported relative to tetramethylsilane using the CD$_3$CN (^{1}H NMR: 1.94 ppm; ^{13}C NMR: 1.32 and 118.26 ppm), CD$_3$OD (^{1}H NMR: 3.31 ppm; ^{13}C NMR: 49.1 ppm), CD$_3$CN (^{1}H NMR: 1.94 ppm; ^{13}C NMR: 1.32 and 118.26 ppm), (CD$_3$)$_2$SO (^{1}H NMR: 2.50 ppm; ^{13}C NMR: 39.52 ppm) and D$_2$O (^{1}H NMR: 4.79 ppm) peaks. ^{31}P spectra were collected at 360 scans per spectrum, with chemical shifts reported relative to 85% H$_3$PO$_4$ (0 ppm). The applicable resonance frequency was located at 146.93 MHz.

All UV/Vis spectra were recorded using a Varian Cary 50 Conc UV-Visible spectrophotometer equipped with a Julabo F12-mV temperature cell regulator (accurate within 0.1 °C) in a 1.000 ± 0.001 cm quartz cuvette cell. All the synthesised complexes were completely dried *in vacuo* (Buchi Rotavapor R-210 Rotary Evaporator and Heidolph Laborota 4000 Rotary Evaporator).

All concentrations of the solutions and the equivalents added in the reactivity and bonding studies were calculated and are expressed with respect to the quantity of niobium and tantalum ions in solution.

3.2.2 Synthesis of selected niobium(V) and tantalum(V) complexes

3.2.2.1 Synthesis of semi-stable starting materials, $(Et_4N)[NbCl_6]$ and $(Et_4N)[TaCl_6]$

Tetraethylammoniumhexachloridotantalate(V), $(Et_4N)[TaCl_6]$ and tetraethylammoniumhexa-chloridoniobate (V), $(Et_4N)[NbCl_6]$ were prepared by modifying the known procedures.[6,7,8] A solution of $NbCl_5$ (0.2701 g, 1.0 mmol) was carefully (exothermic reaction) dissolved in acetonitrile (10 mL), and then treated with Et_4NCl (0.1657 g, 1.0 mmol). The mixture was refluxed overnight at 90 ^{o}C and the solvent was removed under vacuum, yielding a yellow $(Et_4N)[NbCl_6]$ solid. A solution of $TaCl_5$ (0.3582 g, 1.0 mmol) was carefully (exothermic reaction) dissolved in acetonitrile (10 mL), and then treated with Et_4NCl (0.1657 g, 1.0 mmol). The mixture was refluxed overnight and the solvent was removed under vacuum, yielding a white $(Et_4N)[TaCl_6]$ solid. The reaction can be represented as follows:

$$(Et_4NCl) + [MCl_5] \xrightarrow[\text{90 }^o\text{C / 10-12 hr}]{\text{MeCN}} (Et_4N)[MCl_6], \text{ where M = Nb and Ta}$$
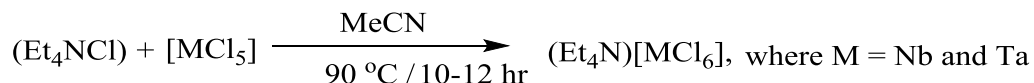
Spectroscopic data for $(Et_4N)[NbCl_6]$

IR (ATR): $\nu_{(N-C)}$ = 1171 cm^{-1}, **UV/Vis**: λ_{max} = 284 nm, ε = 2.663 x 10^3 M^{-1}cm^{-1}. **^{1}H NMR** (300.18 MHz, $(CD_3)_2SO$): δ_{ppm} = 3.18-3.26 (q, 8H), 1.13-1.19 (m, 12H). **^{13}C NMR** (75.48 MHz, $(CD_3)_2SO$): δ_{ppm} = 7.00, 51.29 (Yield: 0.398 g, 94.3%).

Spectroscopic data for $(Et_4N)[TaCl_6]$

IR (ATR): $\nu_{(N-C)}$ = 1174 cm^{-1}, **UV/Vis**: λ_{max} = 274 nm, ε = 1.083 x 10^3 M^{-1}cm^{-1}. **^{1}H NMR** (300.18 MHz, $(CD_3)_2SO$): δ_{ppm} = 3.17-3.25 (q, 8H), 1.12-1.18 (m, 12H). **^{13}C NMR** (75.48 MHz, $(CD_3)_2SO$): δ_{ppm} = 7.02, 51.33 (Yield: 0.478 g, 91.2%).

---

[6] R. Koen, H.G. Visser, A. Roodt. *Z. Kristallogr. NCS.,* **231**(1), 227-229, 2016.

[7] R. Kergoat, J.E. Guerchais, *J. Less Com. Met.*, **39,** 91-98, 1975.

[8] J.C. Daran, Y. Jeanin, R. Kergoat, J.E. Guerchais, *Inorg. Chim. Acta*, **33**, 81-86, 1979.

3.2.2.2 Preparation of tris(N-nitroso-N-phenylhydroxylaminato-k^2O,O')oxidoniobium(V), [NbO(cupf)₃]

(Et₄N)[NbCl₆] (0.1600 g, 0.3791 mmol) was dissolved in methanol (10 mL), and treated with the ammonium salt of N-nitroso-N-phenylhydroxylamine (or cupferron, cupfH) (0.1760 g, 1.1370 mmol) at room temperature. The resulting mixture was stirred for 4 h, and then the volatile material was removed *in vacuo*. The resulting residue was washed with diethyl ether (2x10 mL), giving a grey solid which was dissolved in methanol/acetonitrile and left to stand at 255 K for a few days after which red chunky crystals, suitable for X-ray diffraction, were obtained. An aliquot of this solid was analysed by ^{1}H NMR and ^{13}C NMR (CD₃OD solution), which revealed the presence of a mixture of products. The crystallographic structural characterization of [NbO(cupf)₃] is discussed in Chapter 6 section 6.3. The reaction and proposed product can be represented as in Figure 3.1.
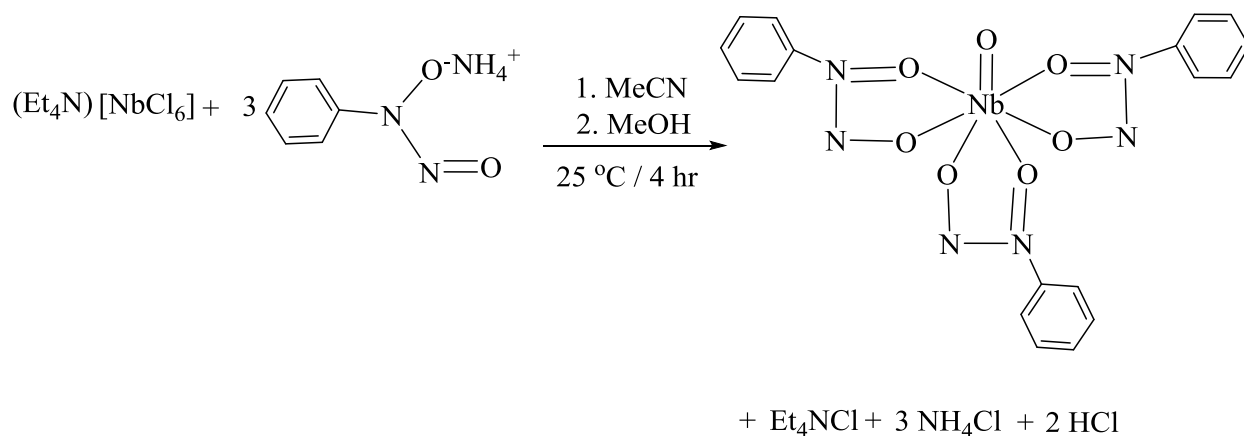
Figure 3.1 Representation of the reaction for the formation of [NbO(cupf)₃].

IR (ATR): $v_{(Nb=O)}$ = 924 cm^{-1}, **UV/Vis:** λmax = 300 nm, ε = 5.729 x 10^3 M^{-1}cm^{-1}, **^{1}H NMR** (300.18 MHz, CD₃OD): δ$_{ppm}$ = 6.54 (d, Ph-2H), 6.08 (m, Ph-13H). **^{13}C NMR** (75.48 MHz, CD₃OD): δ$_{ppm}$ = 128.02, 127.12, 126.95, 118.08, (Yield: 0.165 g, 83.8%).

3.2.2.3   Preparation of tris(N-nitroso-N-phenylhydroxylaminato-k^2O,O')oxidotantalum(V), [TaO(cupf)$_3$]

(Et$_4$N)[TaCl$_6$] (0.1700 g, 0.3244 mmol) was dissolved in acetonitrile (10 mL) and treated with the ammonium salt of N-nitroso-N-phenylhydroxylamine (or cupferron, cupfH) (0.1509 g, 0.9732 mmol) which was dissolved in methanol (10 mL) at room temperature. The resulting mixture was stirred for 8 h, and then the volatile material was removed *in vacuo*. The resulting residue was washed with diethyl ether (2x10 mL), giving a dark yellow powdery solid. An aliquot of this solid was analysed by ^{1}H NMR and ^{13}C NMR (CD$_3$OD solution), which revealed the presence of a mixture of products. This complex was unsuitable for crystallographic structural characterization. The reaction and proposed product can be represented as in Figure 3.2.
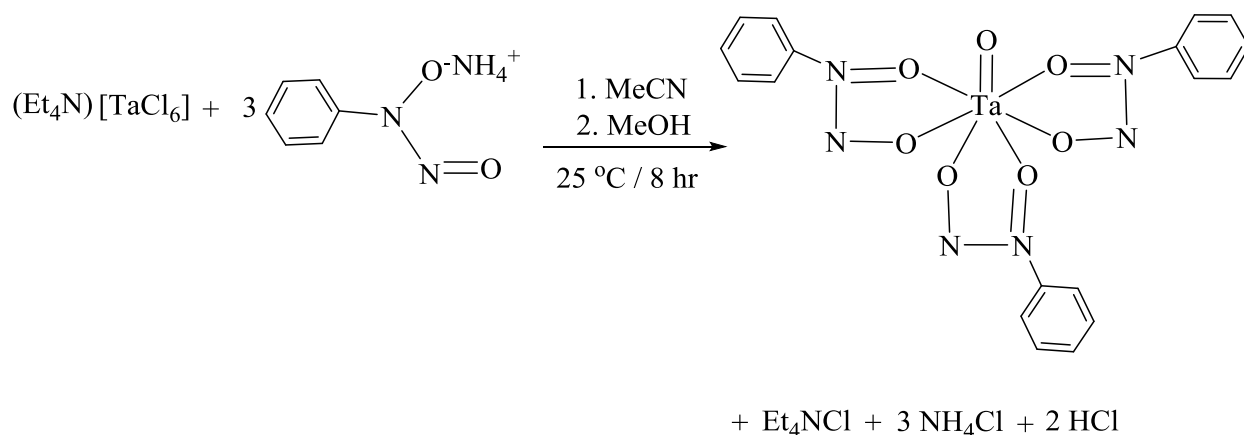
Figure 3.2 Representation of the reaction for the formation of [TaO(cupf)$_3$].

IR (ATR): $v_{(Ta=O)}$ = 941cm^{-1}, **UV/Vis:** λ_{max} = 291 nm, ε = 1.003 x 10^4 M^{-1}cm^{-1}, **^{1}H NMR** (300.18 MHz, CD$_3$OD): δ$_{ppm}$ = 6.98-7.45 (m, Ph-5H). **^{13}C NMR** (75.48 MHz, CD$_3$OD): δ$_{ppm}$ = 128.39, 123.81, 119.85, (Yield: 0.143 g, 72.6%).

3.2.2.4 Preparation of tetrakis(2-hydroxypyridinato-N-oxide-κ^2O,O')tantalum(V) chloride, [Ta(hopo)$_4$]Cl

(Et$_4$N)[TaCl$_6$] (0.1700 g, 0.3244 mmol) was dissolved in acetonitrile (10 mL), and treated with 2-hydroxypyridine N-oxide (hopoH) (0.1441 g, 1.2976 mmol) at room temperature. The resulting mixture was stirred for 6 h, after which the volatile material was removed *in vacuo*. The resulting residue was washed with diethyl ether (2x10 mL), giving a brown solid which was dissolved in a MeOH/MeCN mixture and left to stand at 255 K for five days after which yellow block crystals, suitable for X-ray diffraction were obtained. An aliquot of this solid was analysed by ^{1}H NMR and ^{13}C NMR (DMSO solution), which revealed the presence of a mixture of products. The crystallographic structural characterization of [Ta(hopo)$_4$]Cl is discussed in Chapter 6 section 6.4. The reaction and proposed product can be represented as in Figure 3.3.
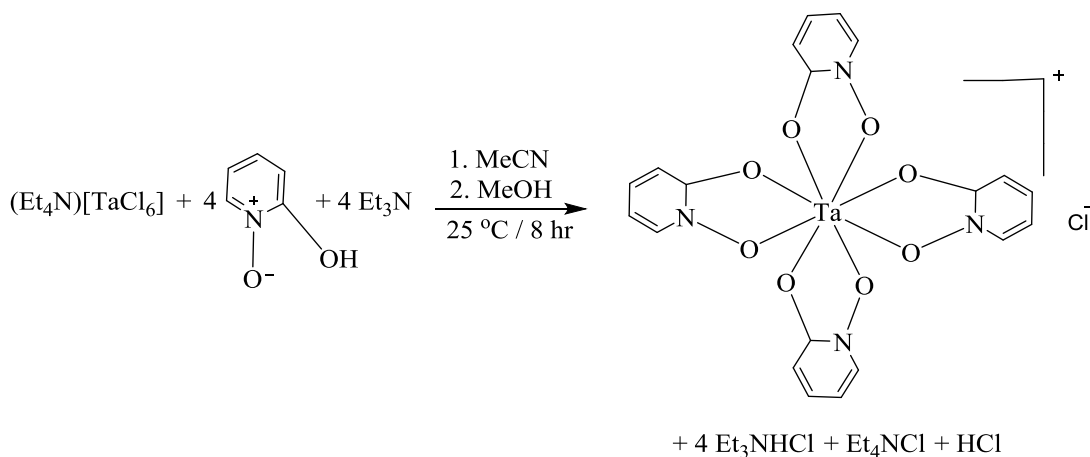
Figure 3.3 Representation of the reaction for the formation of [Ta(hopo)$_4$]Cl.

UV/Vis: λ_{max} = 303 nm, ε = 1.217 x 10^4 M^{-1}cm^{-1}, **^{1}H NMR** (600.28 MHz, (CD$_3$)$_2$SO): δ$_{ppm}$ = 8.49 (d, Ph-1H), 7.86 (t, Ph-1H), 7.19 (t, Ph-1H), 7.08 (d, Ph-1H). **^{13}C NMR** (150.95 MHz, (CD$_3$)$_2$SO): δ$_{ppm}$ = 158.30, 139.48, 134.67, 115.54, 113.90, (Yield: 0.172 g, 85.4%).

3.2.2.5 **Preparation of tris(2-hydroxypyridinato-N-oxide-κ^2O,O')oxidotantalum(V), [TaO(hopo)$_3$]**

2-Hydroxypyridine N-oxide (hopoH) (0.1081 g, 0.9732 mmol) was dissolved in methanol (10 mL) at room temperature and Et$_3$N (0.0985 g, 0.9732 mmol) was added drop-wise. The white-yellow colour of the hopoH solution changed to white-grey as a precipitate formed. This was followed by the addition of (Et$_4$N)[TaCl$_6$] (0.1700 g, 0.3244 mmol) in acetonitrile (10 mL). After *ca*.10 minute of stirring the temperature was increased to 40 ^{o}C and the resulting mixture was stirred overnight. The volatile material was removed *in vacuo*. The resulting white-grey residue was washed with diethyl ether (2x10 mL) and the Et$_3$NHCl salt was removed from the resulting product by washing with cold chloroform (2 x 10 mL) and drying *in vacuo*. The product was dissolved in MeOH/THF (2:3), the extracts filtered through Celite and the solution was left to stand at room temperature for a few days after which colorless needle crystals, suitable for X-ray diffraction, were obtained. The crystallographic structural characterization of [TaO(hopo)$_3$] is discussed in Chapter 6 section 6.5. The reaction and proposed product can be represented as in Figure 3.4.
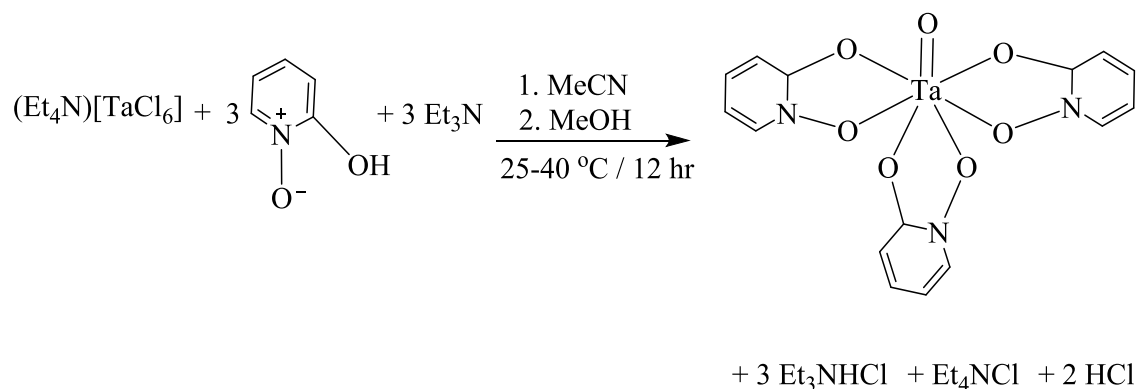
Figure 3.4 Representation of the reaction for the formation of [TaO(hopo)$_3$].

IR (ATR): $\nu_{(Ta=O)}$ = 891, 773 cm^{-1}, **UV/Vis:** λ_{max} = 305 nm, ε = 1.107 x 10^4 M^{-1}cm^{-1}, **^{1}H NMR** (300.18 MHz, (CD$_3$)$_2$SO): δ_{ppm} = 8.39 (d, Ph-1H), 7.70(t, Ph-1H), 6.99 (t, Ph-1H), 6.89 (d, Ph-

1H). ^{13}**C NMR** (75.48 MHz, (CD$_3$)$_2$SO): δ_{ppm} = 159.57, 137.65, 135.69, 114.69, 113.39 (Yield: 0.123 g, 71.9%).

3.2.2.6 Preparation of tris(2-hydroxypyridinato-N-oxide-κ^2O,O')oxidoniobium(V), [NbO(hopo)$_3$]

A methanol solution of 2-hydroxypyridine N-oxide (hopoH) (0.1339 g, 1.2060 mmol in 10 mL MeOH) was added drop-wise to a solution of (Et$_4$N)[NbCl$_6$] (0.1700g, 0.4020 mmol in 10 mL MeCN) at room temperature. The resulting mixture was stirred for 9 hr after which the volatile material was removed *in vacuo*. The resulting yellow oily residue was washed with diethyl ether (10 mL) and cyclohexane (10 mL) and dried *in vacuo*. The product was dissolved in MeCN/MeOH (3:3), the extracts were filtered through Celite and the solution was left to stand at room temperature for one week after which colorless needle crystals, suitable for X-ray diffraction, were obtained. The crystallographic structural characterization of [NbO(hopo)$_3$] is discussed in Chapter 6.4. The reaction and proposed product can be represented as in Figure 3.5.
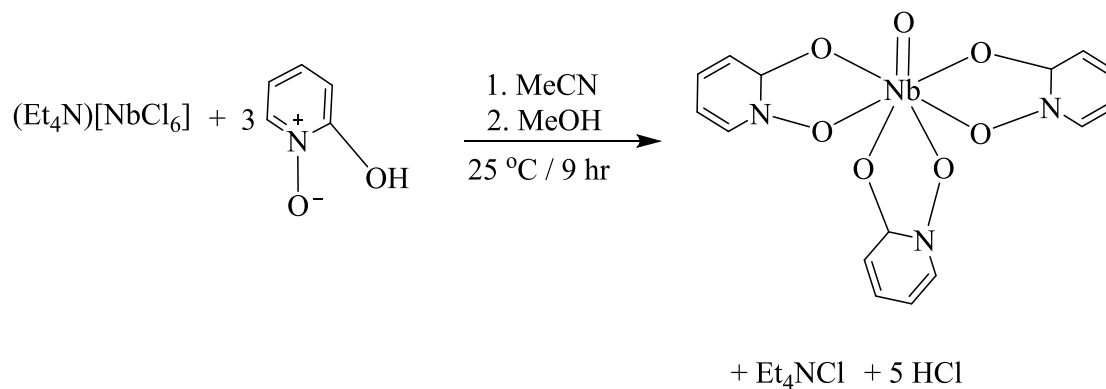
Figure 3.5 Representation of the reaction for the formation of [NbO(hopo)$_3$].

IR (ATR): $\nu_{(Nb=O)}$ = 805, 754 cm^{-1}, **UV/Vis:** λ_{max} = 302 nm, ε = 5.036 x 10^3 M^{-1}cm^{-1}, ^{1}**H NMR** (300.18 MHz, (CD$_3$OD): δ_{ppm} = 8.34 (d, 3H), 7.94 (t, 3H), 7.16 (t, 6H). ^{13}**C NMR** (75.48 MHz, CD$_3$OD): δ_{ppm} = 159.19, 139.45, 133.84, 115.14, 113.64 (Yield: 0.171 g, 96.1%).

3.2.2.7 Preparation of tris(N-hydroxy-N-nitroso-1-naphthylaminato-k^2O,O')oxido-tantalum(V), [TaO(neocupf)₃]

(Et₄N)[TaCl₆] (0.1700 g, 0.3244 mmol) was dissolved in acetonitrile (10 mL) and treated with the ammonium salt of N-hydroxy-N-nitroso-1-naphthylamine, (neocupferron, neocupfH) (0.1997 g, 0.9732 mmol) which was dissolved in acetone (10 mL) at room temperature. The resulting mixture was stirred for 7 h, after which the volatile material was removed *in vacuo*. The resulting residue was washed with hexane fraction (2x10 mL). An aliquot of this solid was analysed by ^{1}H NMR and ^{13}C NMR (DMSO solution), which revealed the presence of a mixture of products. This complex was unsuitable for crystallographic structural characterization. The reaction and proposed product can be represented as in Figure 3.6.
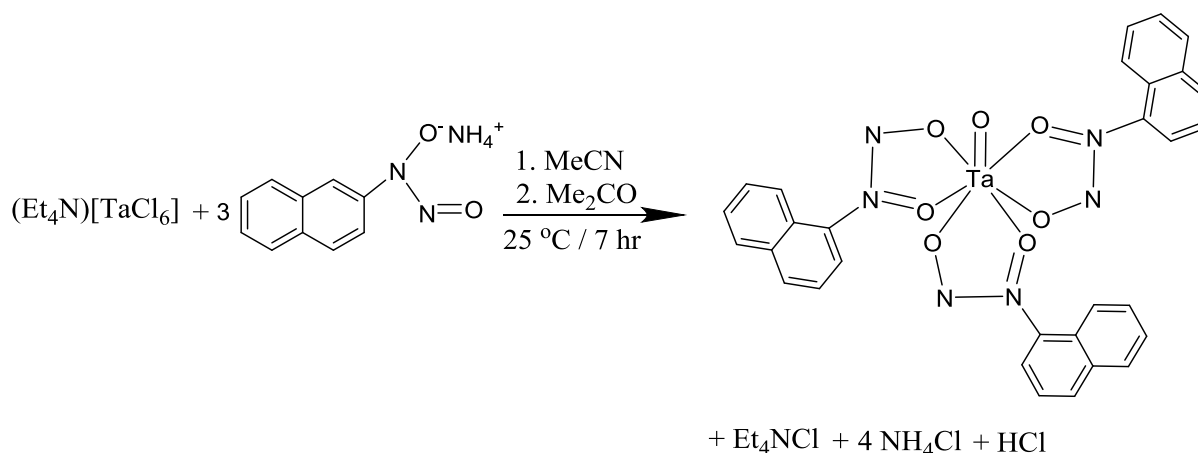
Figure 3.6 Representation of the reaction for the formation of [TaO(neocupf)₃].

IR (ATR): $v_{(Ta=O)}$ = 849 cm^{-1}, **UV/Vis:** λ_{max} = 294 nm, ε = 1.123 x 10^4 M^{-1}cm^{-1}, **^{1}H NMR** (300.18 MHz, (CD₃)₂SO): δ_{ppm} = 7.37 (d, naphthyl-12H), 7.03-7.20 (m, naphthyl-9H). **^{13}C NMR** (75.48 MHz, (CD₃)₂SO): δ_{ppm} = 154.50, 133.75, 132.00, 131.53, 127.33, 125.27, 121.42, 106.00, 99.84 (Yield: 0.172 g, 87.3%).

3.2.2.8 Preparation of tris(N-hydroxy-N-nitroso-1-naphthylaminato-k^2O,O')oxido-niobium(V), [NbO(neocupf)$_3$]

A solution of (Et$_4$N)[NbCl$_6$] (0.1700 g, 0.4020 mmol) was dissolved in acetonitrile (10 mL) and treated with the ammonium salt of N-hydroxy-N-nitroso-1-naphthylamine, (neocupferron, neocupfH) (0.2475 g, 1.2060 mmol) was which dissolved in acetone (10 mL) at room temperature. The resulting mixture was stirred for 13 h, after which the volatile material was removed *in vacuo*. The resulting residue was washed with diethyl ether (2x10 mL), giving a dark brown powder. The resulting product was analysed by ^{1}H NMR and ^{13}C NMR (DMSO solution), which revealed the presence of a mixture of products. This complex was unsuitable for crystallographic structural characterization. The reaction and proposed product can be represented as in Figure 3.7.
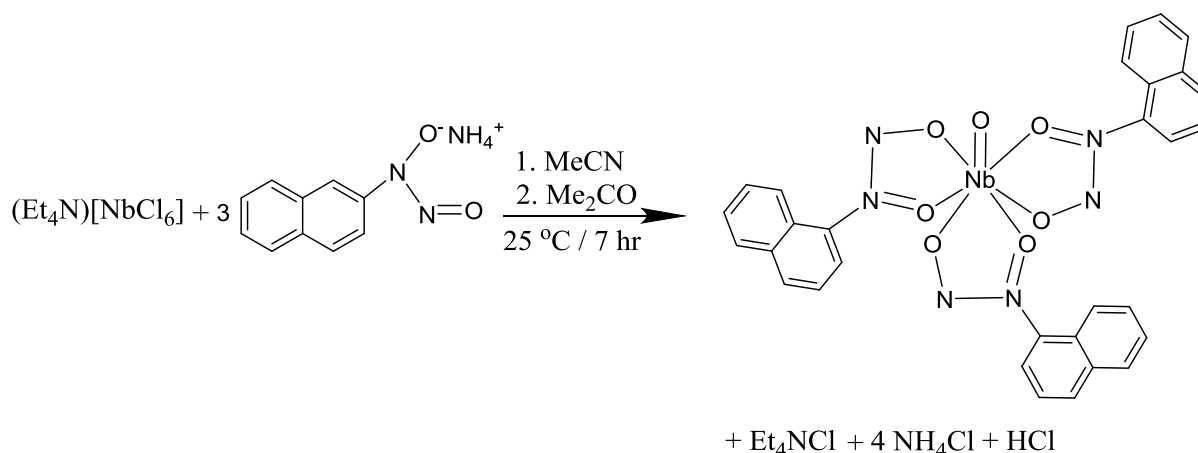
Figure 3.7 Representation of the reaction for the formation of [NbO(neocupf)$_3$].

IR (ATR): $v_{(Nb=O)}$ = 924 cm^{-1}, **UV/Vis**: λ_{max} = 286 nm, ε = 1.867 x 10^4 M^{-1}cm^{-1}, **^{1}H NMR** (300.18 MHz, (CD$_3$)$_2$SO): δ_{ppm} = 7.39 (d, naphthyl-12H), 7.05-7.22 (m, naphthyl-9H). **^{13}C NMR** (75.48 MHz, (CD$_3$)$_2$SO): δ_{ppm} = 140.34, 133.61, 131.02, 130.09, 128.91, 126.07, 120.86, 114.89, 106.21, 93.58 (Yield: 0.243 g, 90.3%).

3.2.2.9 Preparation of bis(2-mercaptopyridinato-N-oxide-κ^2O,O')oxidothiol triphenylphosphineoxideniobium(V), [NbOS(mpo)$_2$OPPh$_3$]

(Et$_4$N)[NbCl$_6$] (0.1700 g, 0.4020 mmol) was dissolved in acetonitrile (10 mL), and 2-mercaptopyridine-N-oxide (mpoH) (0.1533 g, 1.2060 mmol) was dissolved in methanol (10 mL) at room temperature. After *ca*. 40 minutes OPPh$_3$ (0.1119 g, 0.4020 mmol) was added to the solution. The resulting mixture was stirred for 15 h, after which the volatile material was removed *in vacuo*. The resulting residue was washed with diethyl ether (2x10 mL), giving a orange solid which was dissolved in a MeOH/MeCN mixture and left to stand at 255 K for a few days after which yellow block crystals, suitable for X-ray diffraction, were obtained. An aliquot of this solid was analysed by ^{1}H NMR and ^{13}C NMR (DMSO solution), which revealed the presence of a mixture of products. Crystals suitable for X-ray diffraction determination was found and the structure of [NbOS(mpo)$_2$OPPh$_3$] solved. Figure 3.8 gives a representation of the reaction followed, as well as the molecular structure of the product.

$(Et_4N)[NbCl_6] + 3$ [pyridine-N-oxide-2-thiol structure] $+ OPPh_3$ → [product structure]

1. MeCN
2. MeOH
25 °C / 15 hr

$+ Et_4NCl + 5 HCl$
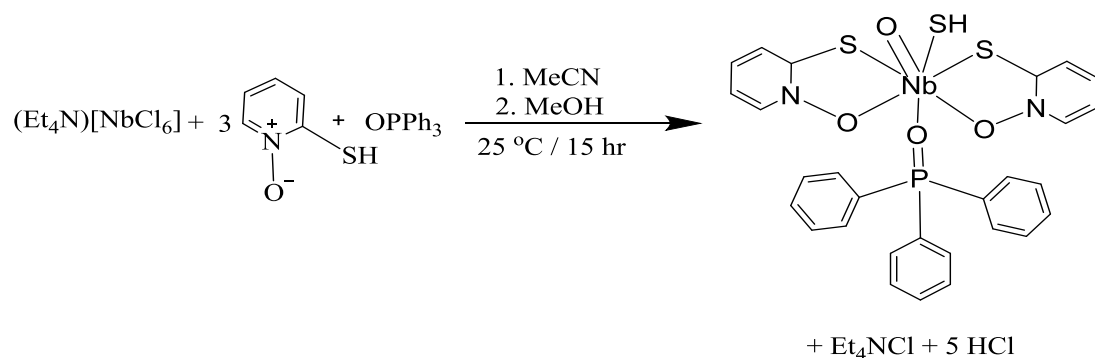
Crystal system, space group: Monclinic, $P2_1$

Rint: 0.0855

R1: 0.0870

wR^2 : 0.2168

Z: 2

Goodness-of-fit on F^2: 1.092

$\Delta\rho_{max}$ and $\Delta\rho_{min}$ (e.Å^{-3}): 1.571 and -4.458

Completeness (%): 99.9
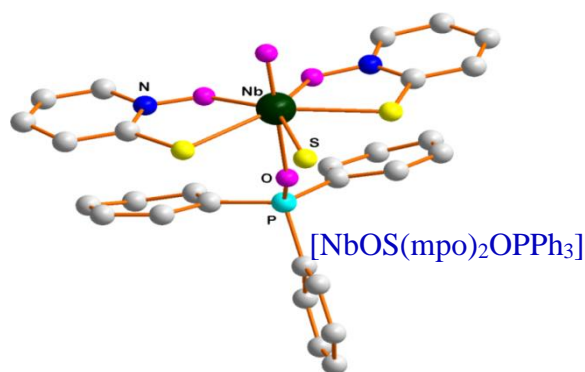
[NbOS(mpo)$_2$OPPh$_3$]

Figure 3.8 Representation of the reaction for the formation of [NbOS(mpo)$_2$OPPh$_3$],with the molecular structure of the product.

IR (ATR): $\nu_{(Nb=O)}$ = 891 cm^{-1}, **UV/Vis:** λ_{max} = 339 nm, ε = 5.44 x 10^3 M^{-1}cm^{-1}, **^{1}H NMR** (600.28 MHz, DMSO): δ_{ppm} = 8.74 (d, 2H, Py), 7.82 (d, 2H, Py), 7.79 (t, 2H, Py), 7.44 (t, 2H, Py), 7.76-7.57 (m, 15H, Ph). **^{31}P** (242.99 MHz, CD$_3$CN: δ_{ppm} = 29.84. **^{13}C NMR** (150.95 MHz, (CD$_3$)$_2$SO): δ_{ppm} = 156.76, 138.05, 135.10, 133.44, 132.76, 131.98, 129.28, 127.13, 120.18, (Yield: 0.198 g, 84.9%).

3.2.2.10 Preparation of 2,5-dichloro-3,6-dihydroxycyclohexa-2,5-diene-1,4-dione triphenylphosphineoxide, [OPPh$_3$(caH$_2$)]

Triphenylphosphine oxide, OPPh$_3$ (0.0999 g, 0.3591 mmol) was dissolved in acetonitrile (5 mL), and treated with 2,5-dichloro-3,6-dihydroxy-2,5-cyclohexadiene-1,4-dione (caH$_2$) (0.0750 g, 0.3591 mmol) in methanol (5 mL) at room temperature. The resulting mixture was stirred for 6 h,

and the volatile material was removed *in vacuo*. The resulting red residue was washed with diethyl ether (2x10 mL), and dried *in vacuo*. The product was dissolved in acetonitrile/methanol (4:1); the solution was left to stand at 255 K for a few days after which orange plate crystals, suitable for X-ray diffraction, were obtained. The crystallographic structural characterization of [OPPh₃(caH₂)] is discussed in Chapter 4 section 4.4. The reaction and proposed product can be represented as in Figure 3.9.
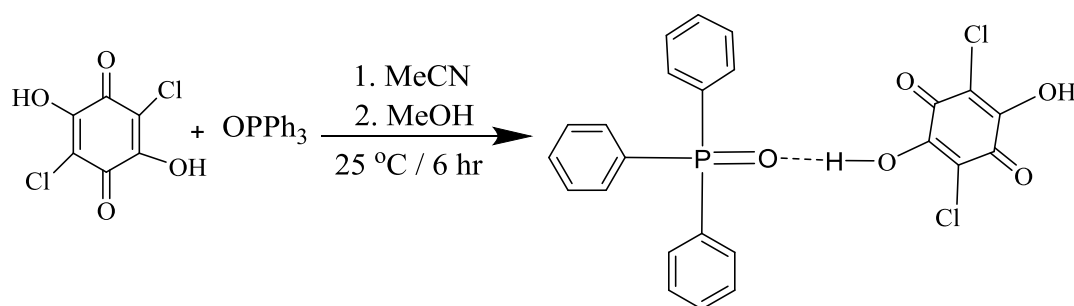
Figure 3.9 Representation of the reaction for the formation of [OPPh₃(caH₂)].

IR (ATR): $v_{(P=O)}$ = 979 (vs), 1118.32 (m) cm^{-1}, **UV/Vis:** λ_{max} = 306, ε = 1.08 x 10^4 M^{-1}cm^{-1}, **^{1}H NMR** (300.18 MHz, (CD₃)₂SO): δ_{ppm} = 8.45 (s, 2 O-H, H₂CA), 7.52-7.66 (m, 15 H, Ph). **^{31}P NMR** (161.97 MHz, (CD₃)₂SO): δ_{ppm} = 25.71 (s, 1 P). **^{13}C NMR** (75.48 MHz, (CD₃)₂SO): δ_{ppm} = 166.16 (C=O; C-OH, H₂CA), 133.85, 132.50, 132.00, 131.87, 129.29, 129.13(Ph) 109.49(C-Cl, H₂CA) (Yield: 0.131 g, 74.3%).

3.2.2.11 Preparation of 2,5-dichloro-3,6-dihydroxycyclohexa-2,5-diene-1,4-dione-4-N,N-dimethylaminopyridinium, [caH₂(DMAP)₂]

This compound was synthesized according to the same procedure as described in 3.2.2.10, from one to two molar amount of chloranilic acid (caH₂) (0.0750 g, 0.3591 mmol) and 4-(dimethylamino)pyridine (DMAP) (0.0876 g, 0.7172 mmol) dissolved in mixtures of acetonitrile and tetrahydrofuran. Purple, cuboid crystals were obtained from a solution of the product in a mixture of acetonitrile and methanol (3:2) using a slow evaporation technique.

The crystallographic structural characterization of [caH$_2$(DMAP)$_2$] is discussed in Chapter 4 section 4.6. The reaction and proposed product can be represented as in Figure 3.10.
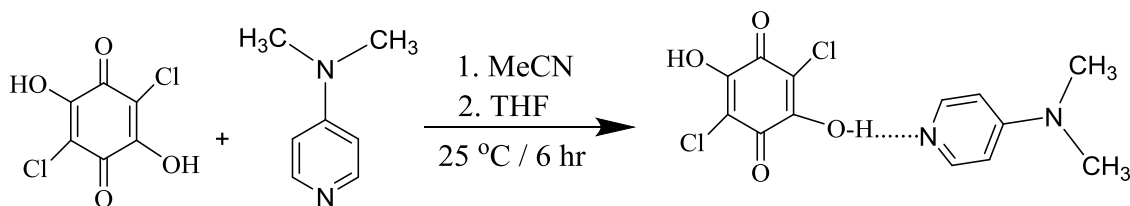
Figure 3.10 Representation of the reaction for the formation of [caH$_2$(DMAP)$_2$].

IR(ATR): $\nu_{(N-H\cdots O)}$ = 1750-3089 cm^{-1}, **UV/Vis:** λ_{max} = 524 nm, ε = 1.755 x 10^3 M^{-1}cm^{-1}, **^{1}H NMR** (300.18 MHz, CD$_3$OD): δ_{ppm} = 8.11 (d, 4H, py), 6.98 (d, 4H, py), 3.26 (s, 12H, CH$_3$). **^{13}C NMR** (75.48 MHz, CD$_3$OD): δ_{ppm} = 166.47 (C=O; C-OH, caH$_2$), 158.35, 138.58, 107.57 (py) 106.79(C-Cl, caH$_2$) (Yield: 0.128 g, 78.5%).

3.2.2.12 Preparation of tetraethylammoniumaquabis(2,5-dichloro-3,6-dihydroxy-1,4-benzoquinonato-κ^2O,O')oxidotriphenylphosphineoxideniobate(V), (Et$_4$N)cis-[NbO(ca)$_2$(H$_2$O)OPPh$_3$] (5)

2,5-dichloro-3,6-dihydroxy-2,5-cyclohexadiene-1,4-dione (caH$_2$) (0.1680 g, 0.8039 mmol) was dissolved in chloroform (10 mL) and Et$_3$N (0.1627 g, 1.6078 mmol) was added drop-wise to the clear solution of caH$_2$ upon which the violet colour changed to dark brown as a precipitate formed. This was followed by the addition of (Et$_4$N)[NbCl$_6$] (0.1700 g, 0.4020 mmol) dissolved in acetonitrile (10 mL). After 30 minutes, OPPh$_3$ (0.112 g, 0.402 mmol) was added to the solution at room temperature. The resulting mixture was stirred overnight, after which the volatile material was removed *in vacuo*. The purple-violet residue was washed with hexane (2x10 mL) and dried *in vacuo*. The product was dissolved in THF/methanol (1:1) and the solution was left to stand at 25 °C for a few days after which red cuboid crystals, suitable for X-ray diffraction, were obtained. The crystallographic structural characterization of *cis*-(Et$_4$N)[NbO(ca)$_2$(H$_2$O)OPPh$_3$] is discussed in Chapter 5 section 5.3. The two step reaction and proposed product can be represented as in Figure 3.11.
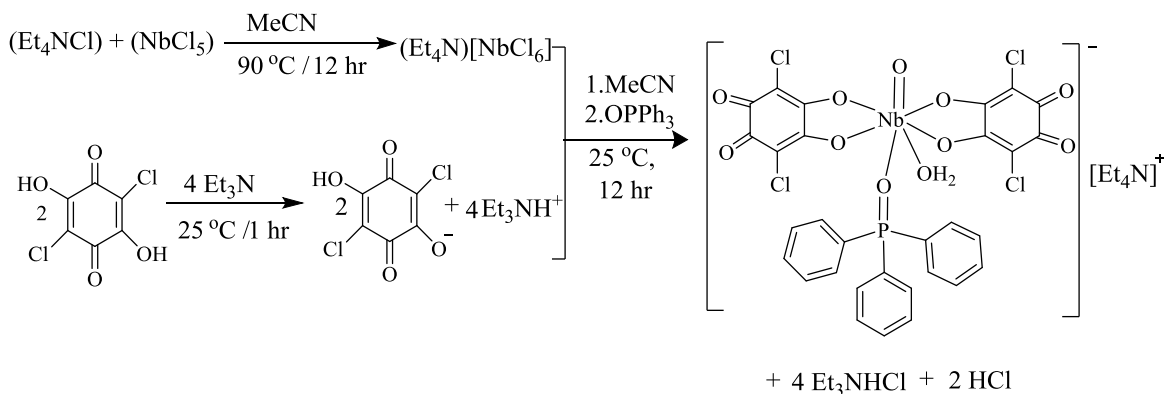
Figure 3.11 Representation of the reaction for the formation of *cis*-(Et$_4$N)[NbO(ca)$_2$OPPh$_3$].

IR(ATR): $\nu_{(Nb=O)}$ = 923 cm^{-1}, ν_{co} = 1537.32 (s) cm^{-1}, **UV/Vis:** λmax = 530 nm, ε = 2.008 x 10^3 M^{-1}cm^{-1}, **^{1}H NMR** (600.28 MHz, CD$_3$CN): δ_{ppm} = 7.57-7.74(m, 15H, Ph), 3.20-3.36 (m, 8H, Et$_4$N, CH$_2$), 1.29-1.32 (m, 12H, Et$_4$N, CH$_3$). **^{31}P** (243 MHz, CD$_3$CN): δ_{ppm} = 45.81, 38.99.
^{13}C NMR (150.95 MHz, CD$_3$CN): δ_{ppm} = 173.56 (C=O; C-O, ca), 132.40 (*ipso*-Ph), 131.71, 131.65, 129.24, 128.65, 128.55, 110.90 (C-Cl, ca), 51.81(CH$_2$, Et$_4$N), 6.15 (CH$_3$, Et$_4$N), (Yield: 0.312 g, 81.7%).

3.2.2.13 Preparation of tetratetraethylammoniumoctachloridocyclo-di-*μ*-oxido-di-*μ*-(2,5-dichloro-3,6-dihydroxy-1,4-benzoquinonato-*κ²O,O'*)tetraoxidoniobate(V), (Et$_4$N)$_4$[Nb$_4$O$_4$(ca)$_2$(*μ²*-O)$_2$Cl$_8$]

Et$_3$N (0.0967 g, 0.9564 mmol) was added drop-wise to a dichloromethane solution of 2,5-dichloro-3,6-dihydroxy-2,5-cyclohexadiene-1,4-dione (caH$_2$) (0.0999 g, 0.4782 mmol in 10 mL CH$_2$Cl$_2$) at 10 °C. After *ca*. 0.5 hr a solution of (Et$_4$N)[NbCl$_6$] (0.4036 g, 0.9564 mmol in 10 mL CH$_3$CN) was added drop-wise to a black-violet clear solution (careful: exothermic reaction); the colour changed to chocolate brown as a precipitate formed. The resulting mixture was stirred overnight, and the temperature was slowly increased to 40 °C. The volatile material was removed *in vacuo*. The resulting dark brown residue was washed with diethyl ether (2x10 mL) and the Et$_3$NHCl salt was removed from the resulting product by washing with cold chloroform (2x10 mL) and dried *in vacuo*. The product was dissolved in MeOH/THF (2:3), the extracts were

filtered through Celite, and the solution was left to stand at room temperature for a few weeks after which brown rhomboid crystals, suitable for X-ray diffraction, were obtained. The crystallographic structural characterization of $(Et_4N)_4[Nb_4O_4(ca)_2(\mu^2\text{-}O)_2Cl_8]$ is discussed in Chapter 5 section 5.4. The reaction and proposed product can be represented as in Figure 3.12.
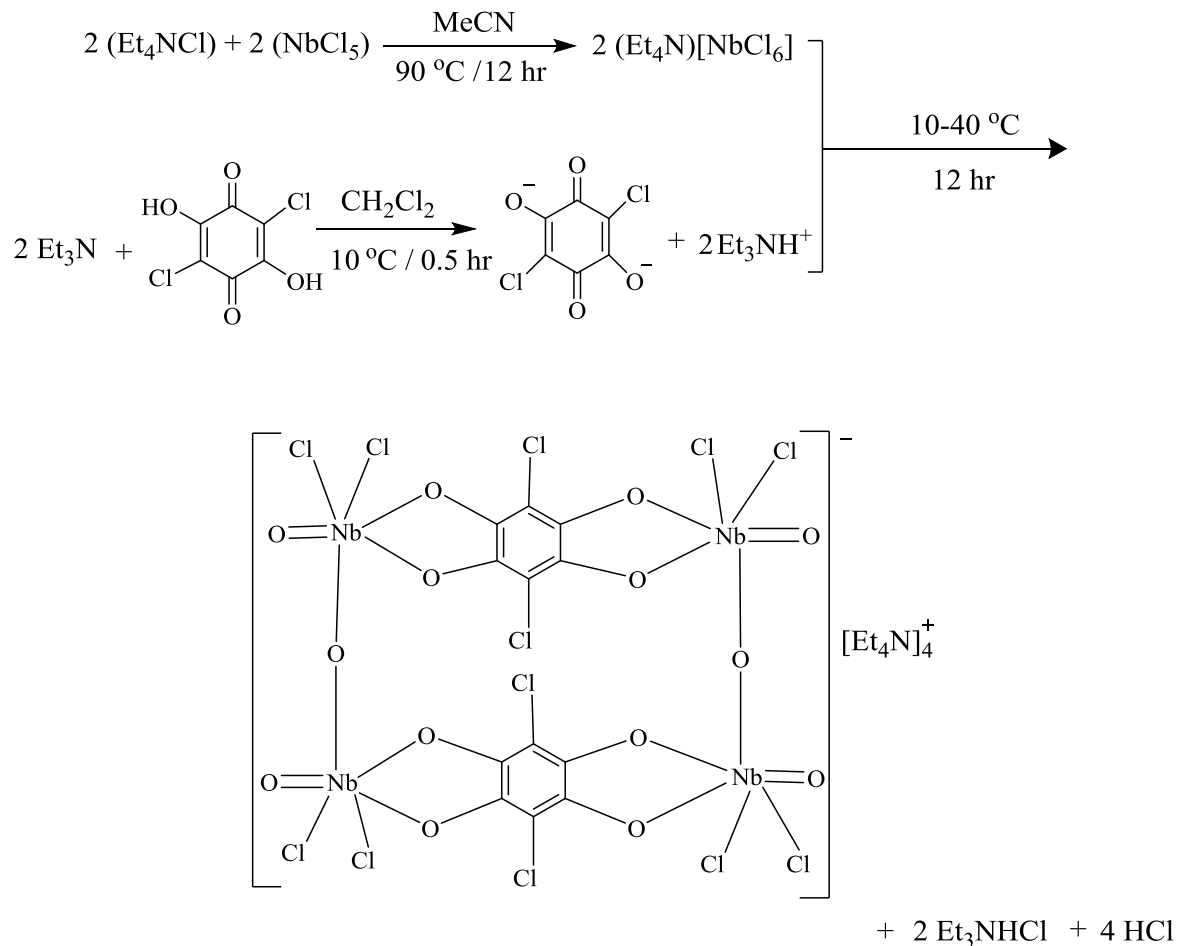
Figure 3.12 Representation of the reaction for the formation of $(Et_4N)_4[Nb_4O_4(ca)_2(\mu^2\text{-}O)_2Cl_8]$.

IR (ATR): $\nu_{(Nb=O)}$ = 949 cm^{-1}, ν_{CO} = 1548(s) cm^{-1}, **UV/Vis**: λ_{max} = 329 nm, ε = 1.464 x 10^4 M^{-1}cm^{-1}, **^{1}H NMR** (300.18 MHz, (CD$_3$)$_2$SO): δ_{ppm} = 3.02-3.21 (m, 32H, Et$_4$N, CH$_2$), 1.15-1.21 (m, 48H, Et$_4$N, CH$_3$). **^{13}C NMR** (75.48 MHz, (CD$_3$)$_2$SO): δ_{ppm} = 172.21 (C-O, ca), 103.33 (C-Cl, ca), 51.87, 45.71(CH$_2$, Et$_4$N), 8.87, 7.64 (CH$_3$, Et$_4$N), (Yield: 0.201 g, 85.6%).

3.2.2.14 Preparation of tris(2,5-dichloro-3,6-dihydroxy-1,4-benzoquinonato-κ^2O,O')

oxidotantalum(V), [TaO(caH)$_3$]

A solution of 2,5-dichloro-3,6-dihydroxy-2,5-cyclohexadiene-1,4-dione (caH$_2$) (0.2034 g, 0.9732 mmol) was dissolved in dichloromethane (10 mL) at 10 °C and Et$_3$N (0.0985 g, 0.9732 mmol) was added drop-wise to a suspended solution of caH$_2$ and stirred for 20 minutes. The red colour changed to purple-red. Addition of (Et$_4$N)[TaCl$_6$] (0.1700 g, 0.3244 mmol) in acetonitrile (10 mL) followed, after which the colour changed to purple violet. After stirring for *ca.* 30 minute the temperature was increased to 40 °C and the resulting mixture was stirred overnight. The volatile material was then removed *in vacuo*. The resulting purple-violet residue was washed with cold diethyl ether (10 mL) and THF (10 mL). Et$_3$NHCl salt was removed from the product by washing with cold chloroform (2x10 mL) and dried *in vacuo*. This complex was unsuitable for crystallographic structural characterization. The reaction and proposed product can be represented as in Figure 3.13.
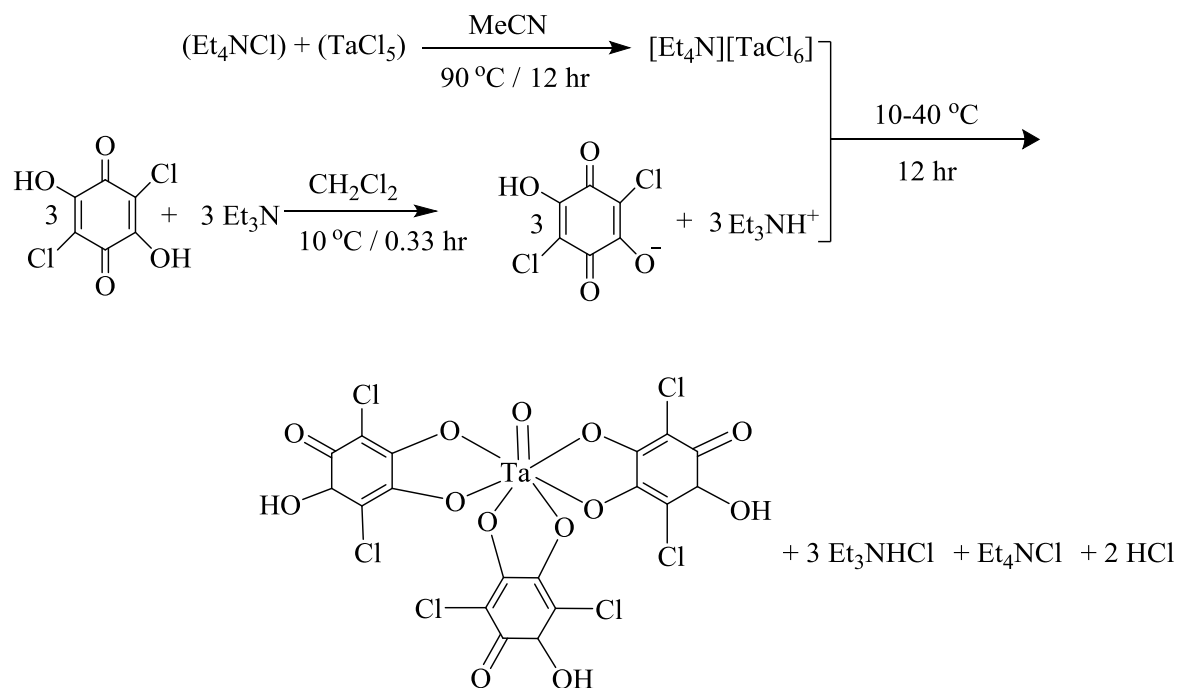
Figure 3.13 Representation of the reaction for the formation of [TaO(caH)$_3$].

IR (ATR): $v_{(Ta=O)}$ = 848 cm^{-1}, v_{co} = 1507(s) cm^{-1}, **UV/Vis:** λ_{max} = 331 nm, ε = 1.631 x 10^4 M^{-1}cm^{-1}, **^{13}C NMR** (75.48 MHz, (CD$_3$)$_2$SO): δ_{ppm} = 171.68 (C=O, C-O, ca), 104.80 (C-Cl, ca), (Yield: 0.189 g, 92.2%).

3.2.2.15 Preparation of tris(2,5-dichloro-3,6-dihydroxy-1,4-benzoquinonato-$\kappa^2 O,O'$)oxido niobium(V), [NbO(caH)$_3$]

This compound was synthesized following the same procedure as described in 3.2.2.14. This complex was unsuitable for crystallographic structural characterization. The reaction and proposed product can be represented in Figure 3.14.
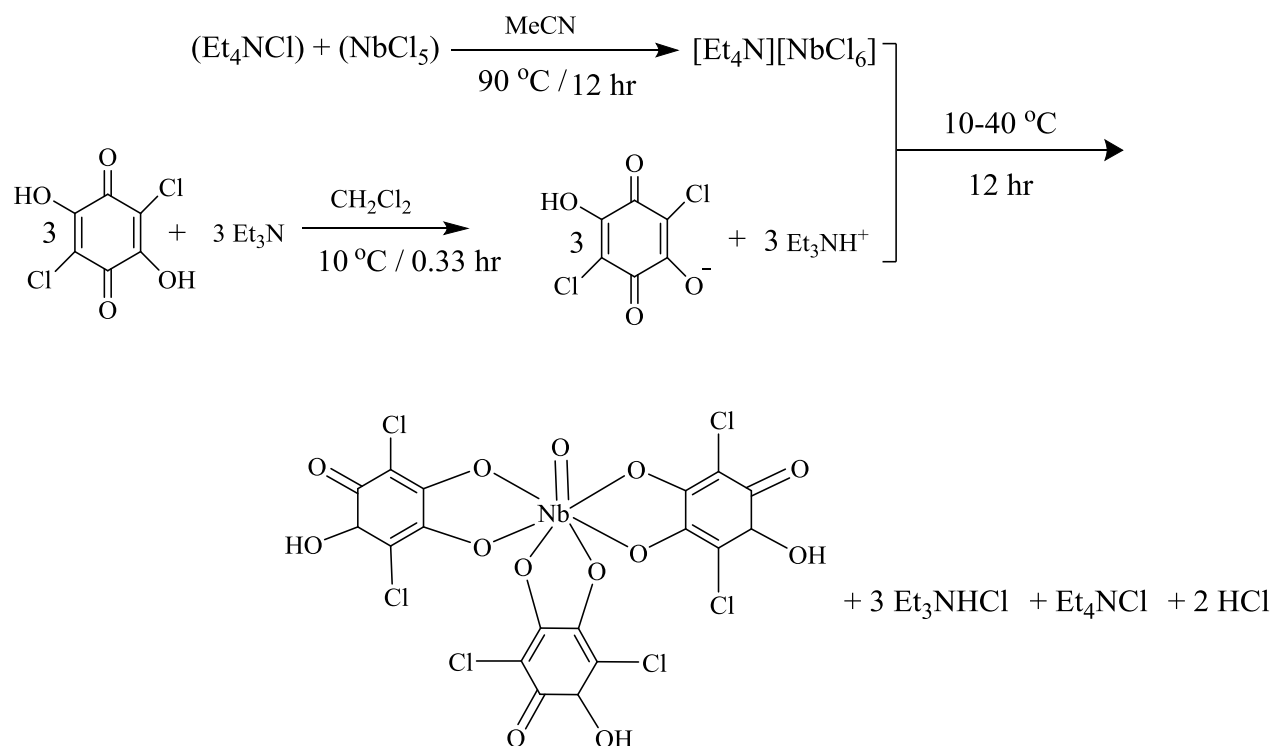
Figure 3.14 Representation of the reaction for the formation of [NbO(caH)$_3$].

IR (ATR): $v_{(Nb=O)}$ = 934 cm^{-1}, v_{co} = 1538(s) cm^{-1}, **UV/Vis:** λmax = 333 nm, ε = 1.915 x 10^4 M^{-1}cm^{-1}, **^{13}C NMR** (75.48 MHz, (CD$_3$)$_2$SO): δ_{ppm} = 173.69 (C=O, C-O, ca), 106.22 (C-Cl, ca), (Yield: 0.281 g, 94.9%).

3.2.2.16 Preparation of tris(2,5-dihydroxy-1,4-benzoquinonato-$\kappa^2 O,O'$)oxidoniobium(V), [NbO(dhbqH)₃]

2,5-dihydroxy-1,4-benzoquinone (dhbqH$_2$) (0.1689 g, 1.2060 mmol) was dissolved in DMF (10 mL) at room temperature and KOH (0.0677 g, 1.2060 mmol) dissolved in ethanol (5 mL) was added drop-wise to a solution of dhbqH$_2$, the brown colour changed to chocolate brown. After stirring for *ca.* 30 minute, (Et$_4$N)[NbCl$_6$] (0.1700 g, 0.4020 mmol) in acetonitrile (10 mL) was added to the reaction mixture (careful: exothermic reaction); the colour changed to black-brown and the resulting mixture was stirred overnight. The volatile material was then removed *in vacuo*. The resulting dark violet residue was washed with diethyl ether (2x10 mL) and the KCl and Et$_4$NCl salts were removed from the product by washing with cold water (10 mL) and drying *in vacuo*. This complex was unsuitable for crystallographic structural characterization. The reaction and proposed product can be represented in Figure 3.15.
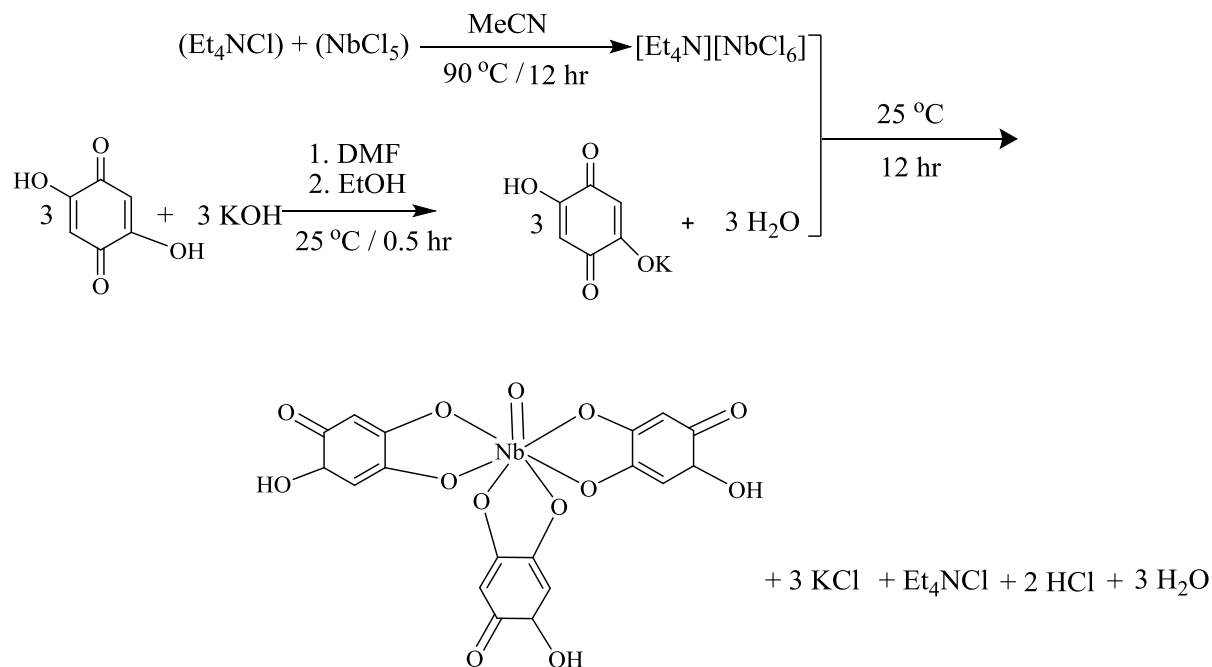
Figure 3.15 Representation of the reaction for the formation of [NbO(dhbqH)₃].

IR (ATR): $v_{(Nb=O)} = 818$ cm^{-1}, $v_{co} = 1558$ cm^{-1}, **UV/Vis:** $\lambda_{max} = 485$ nm, $\varepsilon = 1.641$ x 10^3 M^{-1}cm^{-1}, **¹H NMR** (300.18 MHz, (CD₃)₂SO): $\delta_{ppm} = 5.04$ (s, 3H, dhbq-OH). **¹³C NMR** (75.48 MHz, (CD₃)₂SO): $\delta_{ppm} = 181.38, 178.82, 100.00$ (Yield: 0.197 g, 92.5%).

3.2.2.17 Preparation of tris(2,5-dihydroxy-1,4-benzoquinonato-κ^2O,O')oxidotantalum(V), [TaO(dhbqH)₃]

This compound was synthesized according to the same procedure as described in 3.2.2.16. This complex was unsuitable for crystallographic structural characterization. The reaction and proposed product can be represented as in Figure 3.16.
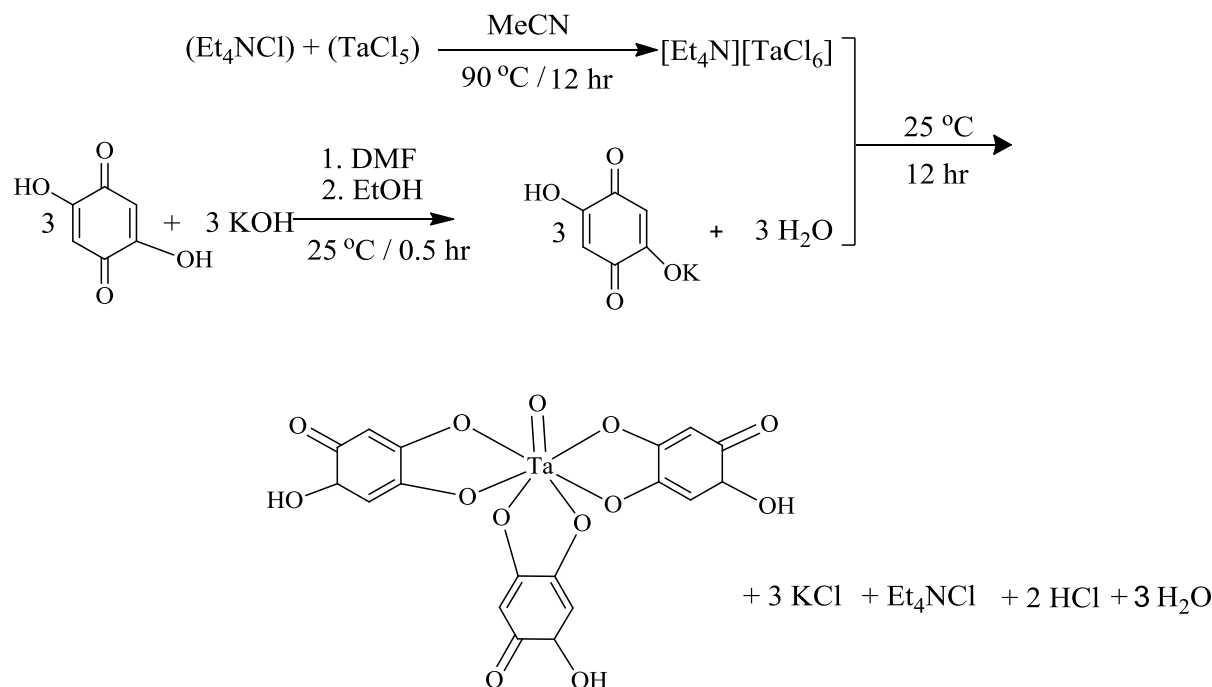
Figure 3.16 Representation of the reaction for the formation of [TaO(dhbqH)₃].

IR (ATR): $v_{(Ta=O)} = 810$ cm^{-1}, $v_{co} = 1548$ cm^{-1}, **UV/Vis:** $\lambda_{max} = 490$ nm, $\varepsilon = 2.346$ x 10^3 M^{-1}cm^{-1}, **¹H NMR** (300.18 MHz, (CD₃)₂SO): $\delta_{ppm} = 5.11$ (s, 3H, dhbq-OH). **¹³C NMR** (75.48 MHz, (CD₃)₂SO): $\delta_{ppm} = 181.11, 108.86, 176.40, 101.01, 79.72$ (Yield: 0.179 g, 89.5%).

3.2.2.18 Preparation of oxidotris(8-quinolinolato-κ^2O,O')niobium(V), [NbO(quin)₃]

A solution of 8-quinolinol-N-oxide (quinH) (0.1944 g, 1.2060 mmol) in acetonitrile (10 mL) was added dropwise to a 10 mL acetonitrile solution of (Et₄N)[NbCl₆] (0.1700 g, 0.4020 mmol), causing the colour to change to yellowish. The mixture was further stirred overnight at room temperature to ensure a complete reaction after which the volatile material was removed *in vacuo*. The resulting yellowish residue was washed with diethyl ether (2x10 mL) and dried *in vacuo*. This complex was unsuitable for crystallographic structural characterization. The reaction and proposed product can be represented as in Figure 3.17.
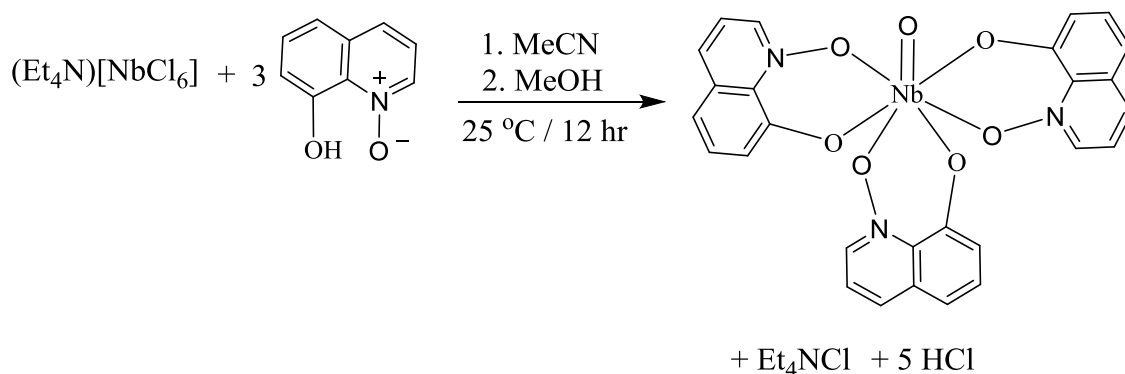
Figure 3.17 Representation of the reaction for the formation of [NbO(quin)₃].

IR (ATR): $\nu_{(Nb=O)}$ = 816 cm⁻¹, **UV/Vis:** λ_{max} = 348 nm, ε = 3.785 x 10³ M⁻¹cm⁻¹, **¹H NMR** (300.18 MHz, CD₃OD): δ_{ppm} = 8.58 (d, 3H, qun), 8.42 (d, 3H, Qu), 8.09 (d, 3H, qun), 7.75 (s, 2H, qun), 7.38-7.54 (m, 4H, Qu), 7.02 (d, 3H, qun) . **¹³C NMR** (75.48 MHz, CD₃OD): δ_{ppm} = 152.80, 149.75, 138.81, 137.86, 135.74, 132.27, 131.39, 130.77, 130.31, 129.36, 129.03, 120.61, 119.74, 117.40, 114.66 (Yield: 0.196 g, 83.1%).

3.2.2.19 Preparation of oxidotris(8-quinolinolato-κ^2O,O')tantalum(V), [TaO(quin)₃]

This complex was synthesized according to the same procedure as described in 3.2.2.18. This complex was unsuitable for crystallographic structural characterization. The reaction and proposed product can be represented in Figure 3.18.
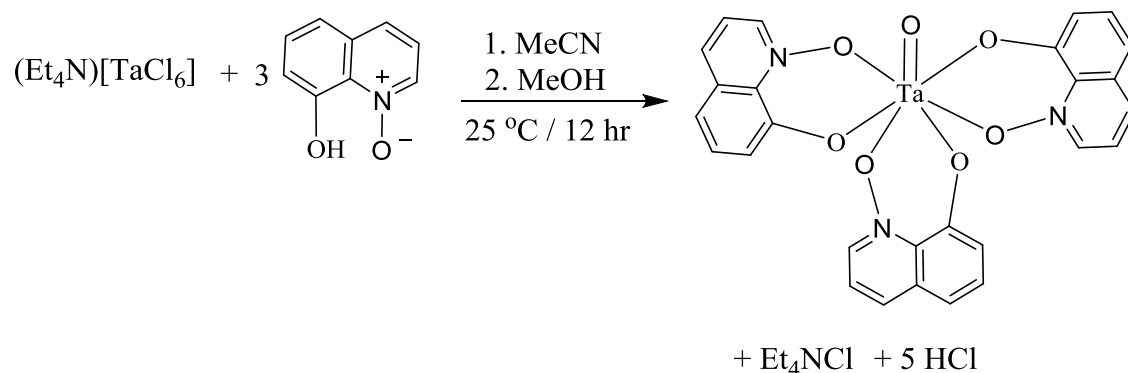
Figure 3.18 Representation of the reaction for the formation of [TaO(quin)$_3$].

IR (ATR): $v_{(Ta=O)}$ = 857 cm^{-1}, **UV/Vis:** λ_{max} = 361 nm, ε = 5.756 x 10^3 M^{-1}cm^{-1}, **^{1}H NMR** (300.18 MHz, (CD$_3$)$_2$SO): δ_{ppm} = 8.48 (d, 3H, qun), 8.08 (d, 3H, qun), 7.38-7.55 (m, 9H, qun), 6.98 (d, 3H, qun). **^{13}C NMR** (75.48 MHz, (CD$_3$)$_2$SO): δ_{ppm} = 153.48, 135.90, 132.43, 130.92, 129.01, 122.18, 117.65, 114.56 (Yield: 0.174 g, 79.5%).

3.2.2.20 Preparation of oxidotris(picolinato-κ^2O,O')niobium(V), [NbO(pico)$_3$]

A solution of picolinic acid-N-oxide (picoH) (0.1678 g, 1.2060 mmol) in acetonitrile/methanol (10 mL) was added dropwise to a 10 mL acetonitrile solution of (Et$_4$N)[NbCl$_6$] (0.1700g, 0.4020 mmol), causing the colorless solution to change to white-yellowish. The mixture was stirred for 9 hr at room temperature to ensure a complete reaction and the volatile material was subsequently removed *in vacuo*. The resulting white-yellowish residue was washed with diethyl ether (2x10 mL) and dried *in vacuo*. This complex was unsuitable for crystallographic structural characterization. The reaction and proposed product can be represented as in Figure 3.19.
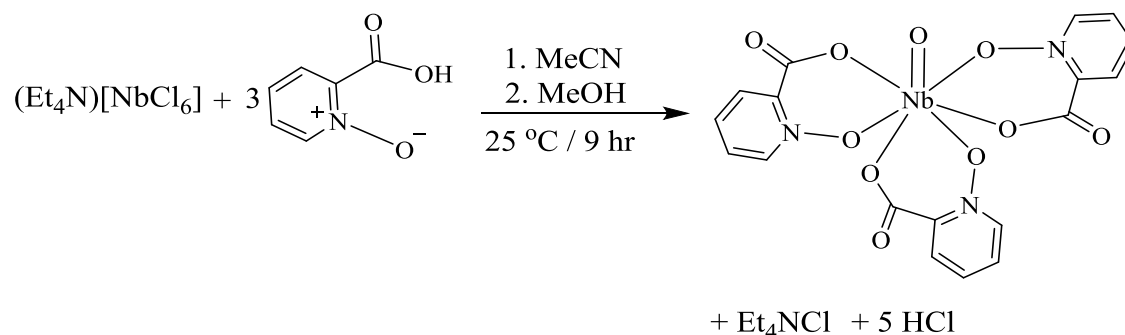
Figure 3.19 Representation of the reaction for the formation of [NbO(pico)$_3$].

IR (ATR): $v_{(Nb=O)}$ = 926 cm^{-1}, **UV/Vis:** λ_{max} = 313 nm, ε = 2.395 x 10^3 M^{-1}cm^{-1}, **^{1}H NMR** (300.18 MHz, (CD$_3$)$_2$SO): δ_{ppm} = 8.78 (d, 3H, py), 8.34 (d, 3H, py), 7.89-7.98 (m, 6H, py). **^{13}C NMR** (75.48 MHz, (CD$_3$)$_2$SO): δ_{ppm} = 161.45, 139.55, 136.42, 133.39, 130.67, 129.16 (Yield: 0.175 g, 82.9%).

3.2.2.21 Preparation of oxidotris(picolinato-$\kappa^2 O,O'$) tantalum(V), [TaO(pico)$_3$]

This compound was synthesized according to the same procedure as described in 3.2.2.20. This complex was unsuitable for crystallographic structural characterization. The reaction and proposed product can be represented as in Figure 3.20.
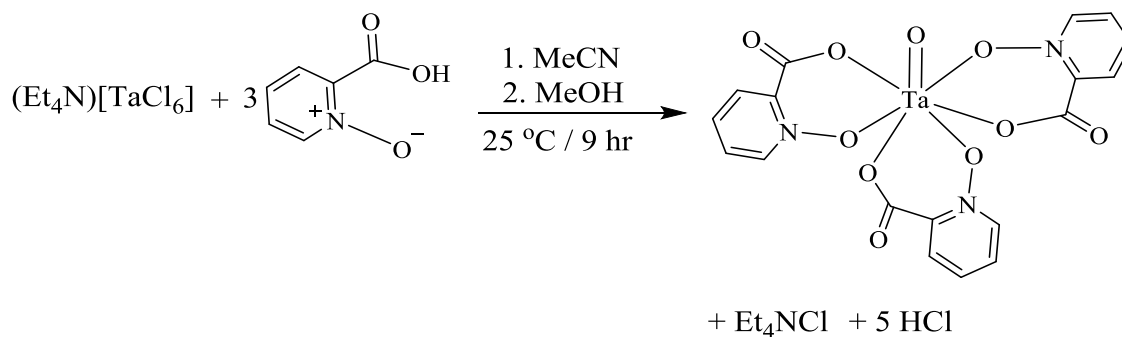
Figure 3.20 Representation of the reaction for the formation of [TaO(pico)$_3$].

IR (ATR): $\nu_{(Ta=O)}$ = 874 cm^{-1}, **UV/Vis:** λ_{max} = 318 nm, ε = 2.132 x 10^3 M^{-1}cm^{-1}, **^{1}H NMR** (300.18 MHz, (CD$_3$)$_2$SO): δ_{ppm} = 8.75 (d, 2H, py), 8.31 (d, 3H, py), 7.89-7.97 (m, 4H, py), 7.38-7.73 (m, 3H, py). **^{13}C NMR** (75.48 MHz, (CD$_3$)$_2$SO): δ_{ppm} = 160.41, 159.30, 139.63, 138.22, 137.39, 134.24, 131.29, 128.54, 126.99, 126.46, 124.05, 116.40 (Yield: 0.132 g, 66.7%).

3.2.3 General procedure for synthesis of substituted L-L' bidentate ligands (cupferron derivatives)

Substituted cupferrate ligands like 2-methylcupferrate, 4-methylcupferrate, 3,5-dichlorocupferrate and 3-acetylcupferrate were prepared by slightly modified published procedures.[9,10] Para, meta or orto-nitrotoluene or nitrobenzene (0.0142 g, 0.1151 mmol) was added with ammonium chloride (11.0 g, 0.2056 mol) to 400 ml of water (or 30% of ethanol aqueous solution). The mixture was subsequently refluxed for 2-5 hr. During the reaction progress zinc dust (13.10 g) was added slowly over a period of 20 minutes with vigorous stirring, which helps to maintain the temperature around 60 °C due to the exothermic nature of the reaction. The progress of the reaction was monitored by TLC for maximum conversion of the starting compound. After completion of the reaction, the solution was cooled to below 35 °C and filtered with suction. It was then extracted by using a separation funnel and about 50 ml of cold water which was added to di-ethereal solution. The solid was filtered and washed with 3x60 ml of solvent ether. The filtrate was extracted with 100 ml portions of ether, repeated three times. All the ether extracts were collected and dried over anhydrous sodium sulphate. The ether solution was transferred to a one liter three-necked round-bottomed flask fitted with a thermometer, a separatory funnel and a gas inlet. The flask was cooled in an ice-salt bath at 0 °C. When the temperature had fallen to 0 ºC, anhydrous ammonia from a compressed gas cylinder was bubbled through the solution for 10 minutes. The addition of ammonia was continued and butyl nitrite (10 ml) was added slowly for about 5 minutes. The solution was stirred for another 50 minutes for completion of the nitrosation reaction. The residue solid (*p*-, *m*-, or *o*-cupferron derivatives) were filtered, washed with cool diethyl ether, and weighed. The yield varied between 20 and 80%.

[9] J.A. Hrabie, L. K. Keefer., *Chem. Rev.,* **102***,* 1135-1154, 2002.

[10] A.D. McGill, W. Zhang, J. Wittbrodt, J. Wang, H.B. Schlegel, P.G. Wang. *Bioorg. Med. Chem.,* **8**, 405-412, 2000.

The *p*-, *m*-, or *o*-cupferron derivatives were recrystallized from methanol. The reaction and proposed product can be represented as in Figure 3.21.
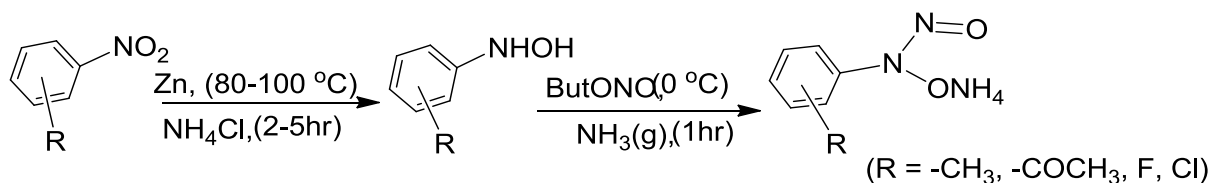
Figure 3.21 Proposed mechanism of general substituted cupferron ligand reactions.

3.2.3.1 3-Acetylcupferron

3-Acetylcupferron was synthesized according to the same procedure as described in Figure 3.21.

IR (ATR): $\nu_{(O-N-N=O)}$ = 960(s), 787(m) cm^{-1}, **UV/Vis:** λ_{max} = 338 nm, 8.476 x 10^3 M^{-1}cm^{-1}, **^{1}H NMR** (300.18 MHz, (CD$_3$)$_2$SO): δ_{ppm} = 8.41 (s, 1H, ph), 8.13 (d, 1H, ph), 7.86 (d, 1H, ph), 7.53 (t, 1H, ph), 2.61 (s, 3H, CH$_3$).. **^{13}C NMR** (75.48 MHz, (CD$_3$)$_2$SO): δ_{ppm} = 197.98, 145.01, 137.64, 129.42, 126.61, 122.50, 117.52, 27.31 (Yield: 7.13 g, 72.3%).

Due to solubility problems, the synthesized substituted cupferrons could not be utilized as ligands for the niobium and tantalum complexes.

3.3 Conclusion

By using various systematic synthon methods a range of novel different niobium(V) and tantalum(V) complexes with O,O'-, O,N- and O,S-bidentate ligands were successfully synthesized and characterized by IR, NMR and UV-vis spectroscopy in atmospheric conditions. This chapter focuses on the establishment of a new methodology to synthesise various new niobium(V) and tantalum(V) complexes and satisfactory results were obtained.

Due to unstable (e.g unreactive and hydrolysis) nature of the starting materials niobium pentachloride, NbCl$_5$, and tantalum pentachloride, TaCl$_5$, tetraethylammoniumchloride was used as a counter ion for the novel synthons tetraethylammoniumhexachloridoniobate, (Et$_4$N)[NbCl$_6$]

and tetraethylammoniumhexachloridotantalite, $(Et_4N)[TaCl_6]$. Compared to $NbCl_5$ and $TaCl_5$ without counter-ions, these synthons are more stable and useful in understanding the physicochemical characteristics of bidentate ligands coordinated to the niobium and tantalum metal centres. However, some of the synthesised niobium and tantalum complexes were not suitable for crystallographic structural characterization in atmospheric conditions, hampering efforts in the further development of these two metals. The realities of these results were shown as the reason for the difficult separation of the two elements during the processing of tantalum and niobium containing minerals.

The special interest ligand of this study was 2,5-dichloro-3,6-dihydroxy-p-benzoquinone, caH_2, which has different coordination chemistry modes. Its suitability as ligand was investigated by forming coordination complexes with niobium(V) and tantalum(V) metal centres. This ligand, together with the rest of the different ligands listed yielded different types of new niobium and tantalum complexes by selective adjustment of the variables that may play a role in separation of niobium from tantalum. No literature method was found that specifically investigated and described the dependence of niobium complex formation on the specific reaction conditions. Therefore, all methods applied for both niobium(V) and tantalum(V) complex synthesis have been reported in this chapter to provide a novel, safe and more environmentally friendly way to separate the two metals.

In the next chapters, the crystallographic structures of selected free ligands and their inter- and/or intra- molecular interaction, bond angles, and bond lengths will be discussed in detail. Table 3.2 summarises the spectroscopic data of the synthesised oxo-niobium(V) and -tantalum(V) complexes. Preliminary results from Nb(V) and Ta(V) complexes not mentioned in the synthon section above, are also included.

Table 3.2 Summary of spectroscopic data for oxo-niobium(V) and-tantalum(V) complexes.

Compounds	$\nu_{(M=O)}$ cm^{-1}	λ_{max}(nm)	ε (M^{-1}cm^{-1})
[NbO(cupf)$_3$]	924	300	5.729 x 10^3
[TaO(cupf)$_3$]	941	291	1.003 x 10^4
[TaO(hopo)$_3$]	891 and 773	305	1.107 x 10^4
[NbO(hopo)$_3$]	805 and 754	302	5.036 x 10^3
[TaO(neocupf)$_3$]	849	294	1.123 x 10^4
[NbO(neocupf)$_3$]	924	286	1.867 x 10^4
[NbOSH(mpo)$_2$OPPh$_3$]	891	339	5.440 x 10^3
[TaO(mpo)$_3$]	835	345	6.272 x 10^3
Cis-(Et$_4$N)[NbO(ca)$_2$(H$_2$O)OPPh$_3$]	923	530	2.008 x 10^3
(Et$_4$N)$_4$[Nb$_4$O$_4$(ca)$_2$(μ^2-O)$_2$Cl$_8$]	949	329	1.464 x 10^4
[TaO(caH)$_3$]	848	331	1.631 x 10^4
[NbO(caH)$_3$]	934	333	1.915 x 10^4
[NbO(dhbqH)$_3$]	818	485	1.641 x 10^3
[TaO(dhbqH)$_3$]	810	490	2.346 x 10^3
[NbO(terpy)$_3$]	784	322	2.208 x 10^4
[TaO(terpy)$_3$]	769	324	1.771 x 10^4
[NbO(pyr)$_3$]	776	457	2.473 x 10^4
[TaO(pyr)$_3$]	948	463	8.690 x 10^3
[NbO(qno)$_3$]	816	348	3.785 x 10^3
[TaO(qno)$_3$]	857	361	5.756 x 10^3
[NbO(pico)$_3$]	926	313	2.395 x 10^3
[TaO(pico)$_3$]	874	318	2.132 x 10^3
[NbO(dipy)$_3$]	826	349	2.265 x 10^3
[TaO(dipy)$_3$]	886	353	3.045 x 10^3

4 X-Ray Crystallographic Studies of Different O,O'-Bidentate Ligands

4.1 Introduction

As was reported in Chapters 1 and 2, the versatility of various O,O'-bidentate ligands can be explored fully in coordination chemistry. Special attention was paid to choose powerful chelating ligands which are essential for the determination of the nature and stability of transition metal complexes, especially for hard metals i.e. Nb(V) and Ta(V). Crystal engineers place emphasis on the design and synthesis of pre-organized ligands, which can control the structure and hence the properties of these complexes.[1]

In this chapter, structures of two selected O,O-bidentate ligands, 2,5-dichloro-3,6-dihydroxy-2,5-cyclohexadiene-1,4-dione (chloranilic acid, caH_2) and 2-hydroxypyridine-N-oxide (hopoH), as well as that of two co-crystals will be discussed in detail. These crystal structures are an important example of prominent representatives and it gives more information on niobium(V) and tantalum(V) complex formation, and are also used for the separation of niobium from tantalum. Surprisingly, caH_2 (Chapter 1, Figure 1.1-1.3) was a unique multifunctional ligand system when compared to the rest of the ligands mentioned above, because it possesses hydrogen bonding and ionic interaction sites as well as π-π inter- and/or intramolecular interactions, affording rich coordination chemistry. It also acts as a strong proton donor and acceptor.[2] Taking into account the significance of the above two ligands when implemented in coordination chemistry and in separation applications, crystal structures of these two ligands were

---

[1] M. Elhabiri, J. Haracek, J. Bünzli and A. Gary, Eur. *Inorg. Chem.*, 51-62, 2004, b) J. Kim, M. Hong, J. Ahn and M. Lee, *Angew. Chem., Int. Edn.*, **44**, 328-332, 2005.

[2] K. Molcanov, B. Kojic-Prodicand, A. Meden, *Croat. Chem. Acta*, **82**(2), 387-396, 2009.

redetermined at the lower temperature of 100(2) K since it was previously determined at room temperature, 298.15(2) K.[3]

The structures of two novel co-crystals from 2,5-dichloro-3,6-dihydroxy-2,5-cyclohexadiene-1,4-dione (caH_2) with triphenylphosphineoxide ($OPPh_3$) and 4-N,N-dimethylaminopyridine (DMAP) were investigated by single crystal X-ray diffraction methods at 100(2) K (Table 4.1) for coordination in new Nb(V) and Ta(V) complexes. The compounds discussed above ensure a better understanding of the coordination behaviour and physico-chemical characteristics of new synthesised niobium(V) and tantalum(V) complexes at corresponding environmental conditions. These chemical characteristics and crystal structures of synthesised Nb(V) and Ta(V) complexes will be discussed in Chapters 5 and 6 in detail.

In general, the solid state structures of 2,5-dichloro-3,6-dihydroxycyclohexa-2,5-diene-1,4-dione (½(caH_2)·H_2O)(**1**), triphenylphosphineoxide-2,5-dichloro-3,6-dihydroxycyclohexa-2,5-diene-1,4-dione ($OPPh_3(caH_2)$) (**2**), 2-hydroxypyridine N-oxide (hopoH) (**3**), and 2,5-dichloro-3,6-dihydroxycyclohexa-2,5-diene-1,4-dione-4-N,N-dimethylaminopyridinium (2½(caH_2)(DMAP)$_6$· 11H_2O) (**4**) have been determined by single crystal X-ray crystallographic studies. The crystal structures with focus on the intra- and/or inter molecular interactions, bond distances and angles, as well as packing of the crystals, are presented.

4.2 Experimental

The X-ray intensity data was collected on a Bruker X8 Apex II 4K Kappa CCD area detector diffractometer, equipped with a graphite monochromator and MoKα finefocus sealed tube (λ = 0.71073 Å, T = 100(2) K operated at 2.0 kW (50 kV, 40 mA). The initial unit cell determinations and data collections were done by the APEX2[4] software package. The collected frames were integrated using a narrow-frame integration algorithm and reduced with the Bruker SAINT-Plus and XPREP software packages[5] respectively.

[3] C.R. Groom, I.J. Bruno, M.P. Lightfoot, S.C. Ward, *Acta. Cryst.*, **B72**, 171-179, 2016.

[4] Bruker Apex2 (Version 2011.4-1). Bruker AXS Inc., Madison, Wisconsin, USA, 2011.

[5] Bruker SAINT-Plus Version 6.02 (including XPREP), *Bruker AXS Inc. Area-Detector Integration Software*,

Analysis of the data showed no significant decay during the data collection. Data was corrected for absorption effects using the multi-scan technique SADABS,[6] and the structure was solved by the direct methods package SIR 97[7] and refined using the WinGX[8] software incorporating SHELXL.[9]

The final anisotropic full-matrix least-squares refinement was done on F^2. All H-atoms were positioned geometrically idealized positions and refined using the riding model with fixed C-H distances for aromatic C-H of 0.93 Å (C-H) [U_{iso} (H) = 1.2 U_{eq}]. Non-hydrogen atoms were refined with anisotropic displacement parameters. The graphics were done using the DIAMOND[10] program with 50% probability ellipsoids for all non-hydrogen atoms.

A summary of crystal data and refinement parameters are presented in Table 4.1. A complete list of atomic coordinates, equivalent isotropic parameters, bond distances and anisotropic displacement parameters and hydrogen coordinates for each individual dataset is given in Appendix A. All CIF files were checked for errors using the free on-line Checkcif service provided by the International Union of Crystallography.[11]

Madison, Wisconsin, USA, 2012.

[6] Bruker SADABS Version 2004/1. *Bruker AXS Inc. Area Detector Absorption Correction Software,* Madison, Wisconsin, USA, 1998.

[7] A. Altomare, M.C. Burla, M. Camalli, G.L. Cascarano, C. Giacovazzo, A. Guagliardi, A.G.G. Moliterni, G. Polidori, R. Spagna, *J. Appl. Cryst.*, **32,** 115-119, 1999.

[8] L.J. Farrugia, *J. Appl. Cryst.*, **45**, 849-854, 2012.

[9] G.M. Sheldrick, SHELXL, *Acta Crystall.,* **C71**, 3-8, 2015.

[10] K. Brandenburg, H. Putz, *DIAMOND*, Release 3.0e, Crystal Impact GbR, Bonn, Germany, 2006.

[11] Available on the web at http://www.iucr.org/acs/checkcif.html. Accessed in 2016, 2017.

Table 4.1 Overall crystal data and refinement parameters of ½(caH$_2$)·H$_2$O (**1**), ½(caH$_2$)OPPh$_3$ (**2**), hopoH (**3**), and 2½(caH$_2$)(DMAP)$_6$·11H$_2$O (**4**).

Identification code	(1)	(2)	(3)	(4)
Empirical formula	C$_3$H$_3$ClO$_3$	C$_{24}$H$_{17}$Cl$_2$O$_5$P	C$_5$H$_5$NO$_2$	C$_{57}$H$_{87}$Cl$_5$N$_{12}$O$_{21}$
Formula weight	122.50	382.76	111.10	1453.63
Temperature (K)	100(2)	100(2)	100(2)	100(2)
Wavelength (Å)	0.71073	0.71073	0.71073	0.71073
Crystal system, space group	Monoclinic, $P2_1/c$	Triclinic, $P\bar{1}$	Monoclinic, $C2/c$	Triclinic, $P\bar{1}$
Unit cell dimensions				
a (Å)	8.557(2)	8.467(1)	8.169(3)	13.382(2)
b (Å)	10.315(2)	9.725(1)	10.992(3)	13.452(2)
c (Å)	5.135(9)	12.243(2)	11.171(3)	19.048(2)
α (°)	90.000	69.887(6)	90.00	86.01(4)
β (°)	104.420(6)	77.758(6)	101.67(2)	88.82(4)
γ (°)	90.000	74.915(6)	90.00	86.37(4)
Volume (Å^3)	438.97(1)	905.5(2)	982.3(5)	3413.0(2)
Z	4	2	4	2
Density$_{calc}$ (g.cm^{-3})	1.854	1.404	1.503	1.414
μ (mm^{-1})	0.740	0.317	0.118	0.294
F(000)	248	396	464.0	1532
Crystal size (mm)	0.119 x 0.329 x 0.448	0.251 x 0.316 x 0.537	0.386 × 0.222 × 0.118	0.252 x 0.173 x 0.130
Theta range (°)	2.46 to 28.40	1.79 to 28.00	3.39 to 28.00	1.52 to 28.00
Index ranges	-11 ≤ h ≤ 11	-11 ≤ h ≤ 11	-10 ≤ h ≤ 10	-12 ≤ h ≤ 17
	-8 ≤ k ≤ 13	-12 ≤ k ≤ 12	-14 ≤ k ≤ 14	-17 ≤ k ≤ 17
	-6 ≤ l ≤ 6	-16 ≤ l ≤ 16	-14 ≤ l ≤ 14	-24 ≤ l ≤ 25
Reflections collected/unique	10003/1097	33617/4369	15280/1180	59603/16428
R$_{int}$	0.0375	0.0420	0.0577	0.0518
Completeness (%)	99.7	100.0	99.5	99.7
Max. and min. transmission	0.746, 0.684	0.746, 0.708	0.746, 0.651	0.746/0.705
Refinement method	Full-matrix least-squares on F^2	Full-matrix least-squares on F^2	Full-matrix least-squares on F^2	Full-matrix least-squares on F2
Data / restraints / parameters	1097 / 0 / 72	4369 / 1 / 239	1180 / 0 / 74	16428/35/948
Goodness-of-fit on F^2	1.3540	1.235	1.128	1.036
Final R indices [$I > 2\sigma(I)$]	$R1 = 0.0253$	$R1 = 0.0347$	$R1 = 0.0363$	$R1 = 0.0508$
	$wR2 = 0.0869$	$wR2 = 0.1157$	$wR2 = 0.1013$	$wR2 = 0.1285$
R indices (all data)	$R1 = 0.0312$	$R1 = 0.0444$	$R1 = 0.0467$	$R1 = 0.0905$
	$wR2 = 0.1297$	$wR2 = 0.1553$	$wR2 = 0.1096$	$wR2 = 0.1641$
$\Delta\rho_{max}$ and $\Delta\rho_{min}$ (e.Å^{-3})	0.390, -0.527	0.505, -0.946	0.21, -0.26	0.738, -0.724

4.3   Crystal structure of 2,5-dichloro-3,6-dihydroxy-2,5-cyclohexadiene-1,4-dione, ½(caH₂).H₂O (1)

The crystal structure of 2,5-dichloro-3,6-dihydroxy-2,5-cyclohexadiene-1,4-dione, caH_2, was first described by Andersen in 1967[12,13] and was collected at room temperature using visually estimated intensities. This structure was redetermined at 100(2) K. ½(caH_2)·H_2O (1) crystallises in the monoclinic space group $P2_1/c$ with Z = 4. The compound (1) lies on an inversion centre; the numbering system is shown in Figure 4.1. Prominent bond distances and angles are reported in Table 4.2 with hydrogen interactions reported in Table 4.3.
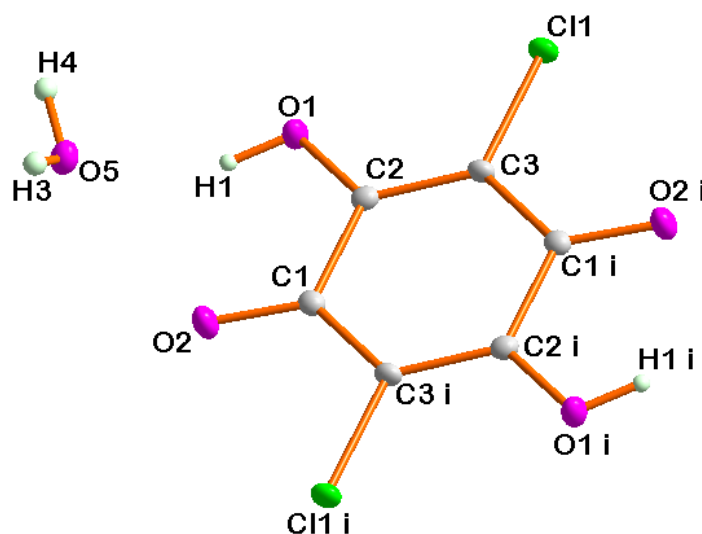
Figure 4.1 DIAMOND[10] view of ½(caH_2)·H_2O (1) with atom numbering system shown and thermal ellipsoids drawn at a 50% probability displacement. Atoms generated by symmetry are indicated by lower case roman numerals corresponding to the symmetry operator (i) 1-x, -y, -z.

[12] E.K Andersen, *Acta Cryst.*, **22**, 188-191, 1967a.
[13] E.K Andersen, *Acta Cryst.*, **22**, 191-196, 1967b.

Table 4.2 Selected bond lengths and angles of ½(caH$_2$)·H$_2$O (**1**).

Bond lengths (Å)			
C1-O2	1.228(7)		
C2-O1	1.317(6)		
C3-Cl1	1.717(1)		
Bond angles (°)			
O1-C2-C3	122.03(2)	O2-C1-C2	118.04(2)
O1-C2-C1	117.89(1)	CL1-C3-C2	121.07(2)
O2-C1-C3i	123.67(2)	CL1i-C3i-C1	117.30(1)

Table 4.2 shows that the C1-O2 and C2-O1 bond lengths are 1.228(7) Å and 1.317(6) Å, which corresponds to C=O and C-OH respectively, while the C3-Cl1 bond length is 1.717(1) Å. Figure 4.2 illustrates two planes, one comprising the four atoms O1, C2, C1 and O2 (green) and the other passing through the six atoms of the chloranilic acid ring C1, C2, C3, C1i, C2i, and C3i (pink), intersecting at O1. The dihedral angle between the two planes is 1.128(8)°, indicating a slight tilt of O1 and O2 from the acid ring along C1 - C2.
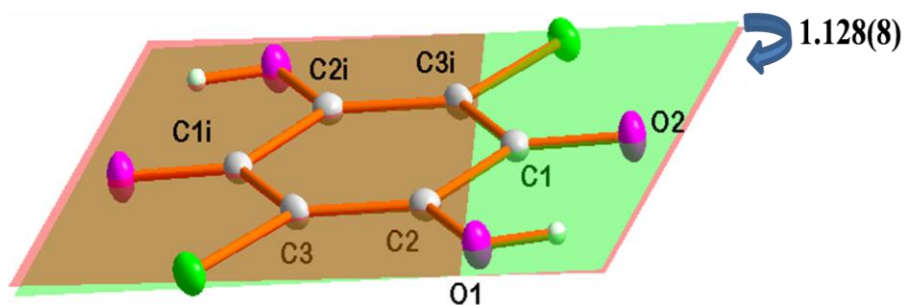
Figure 4.2 Representation of the plane passing through the four atoms O1, C2, C1 and O2 (plane 1, green) and the plane passing through the six atoms of chloranilic acid ring C1, C2, C3, C1i, C2i, and C3i (plane 2, pink). The solvated water molecule is omitted for clarity.

Hydrogen bonding and π-π stacking interactions play an important role in crystal packing, molecular recognition, and the stability of suprastructures, although they are weaker than the

covalent force.[14,15] In the case of hydrogen-bond supported supramolecular compounds, the flexibility in proton donation and/or acceptance of the donor and acceptor allows the formation of new compounds with well-designed geometries.[16]

The asymmetric unit of ½(caH$_2$)·H$_2$O (**1**) contains half of a molecule of 2,5-dichloro-3,6-dihydroxy-2,5-cyclohexadiene-1,4-dione that is located on an inversion centre and its symmetry-generated counterparts are linked by hydrogen-bonds to solvated water molecule (Figure 4.3 and Table 4.3). This generates an infinite network of hydrogen bonds which can be characterised as strong O-H···O hydrogen bonds, forming a zigzag chain. Inter- and intramolecular hydrogen bonds are observed between O1-H···O5 (1.870 Å) and O5-H3...O2ii (2.33(4) Å) as reported in Table 4.3. Sandwich-like π-π stacking is observed between adjacent molecules as illustrated in Figure 4.4, with a distance of 5.1352(2) Å (1-x, -y, 1-z) between parallel chloranilic acid ring planes.

Table 4.3 General hydrogen-bond distances (Å) and angles (°) of ½(caH$_2$)·H$_2$O (**1**).

D-H···A	d(D-H) (Å)	D(H···A) (Å)	d(D···A) (Å)	D-H···A (°)
O1-H1···O5	0.82	1.87	2.632(2)	154
O1-H1···O2	0.82	2.25	2.703(2)	115
O5-H4···O5i	0.91(4)	1.99(4)	2.898(2)	178(3)
O5-H3···O2ii	0.62(4)	2.33(4)	2.938(2)	167(5)

Symmetry code: (i) x, ½ - y, z + ½ (ii) -x, -y, -z,

[14] C.B. Aakeroy, A.M. Beatty, B.A. Helfrich, *J. Am. Chem. Soc.,* **124,** 14425-14432, 2002.

[15] G.S. Papaefstathiou, A. Tsohos, C.P. Raptopoulou, A. Terzis, V. Psycharis, D. Gatteschi, S.P Perlepes, *Cryst. Growth Design*, **1**, 191-194, 2001.

[16] M. Nieuwenhuyzen, T.E. Keyes, J.F. Gallagher, J.G. Vos, *Acta Cryst.*, **C53**, 1873-1875, 1997.
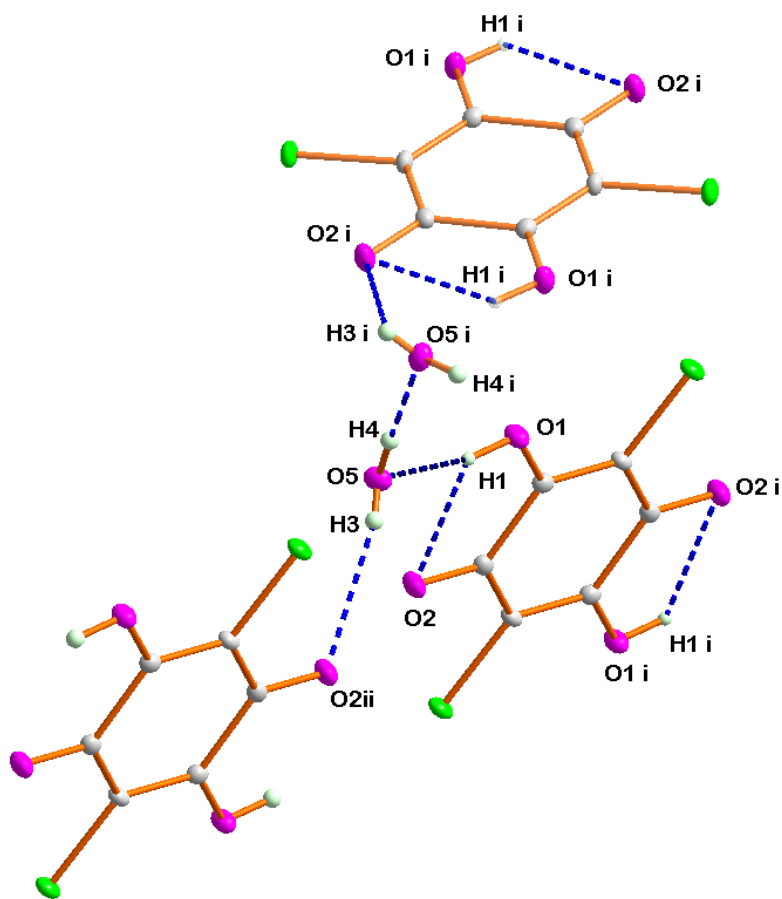
Figure 4.3 Inter-and intramolecular interactions of ½(caH$_2$)·H$_2$O (**1**). The blue dashed lines indicate O-H···O hydrogen bonds. [Symmetry codes: -x, -y, -z, x, ½ - y, z + ½].
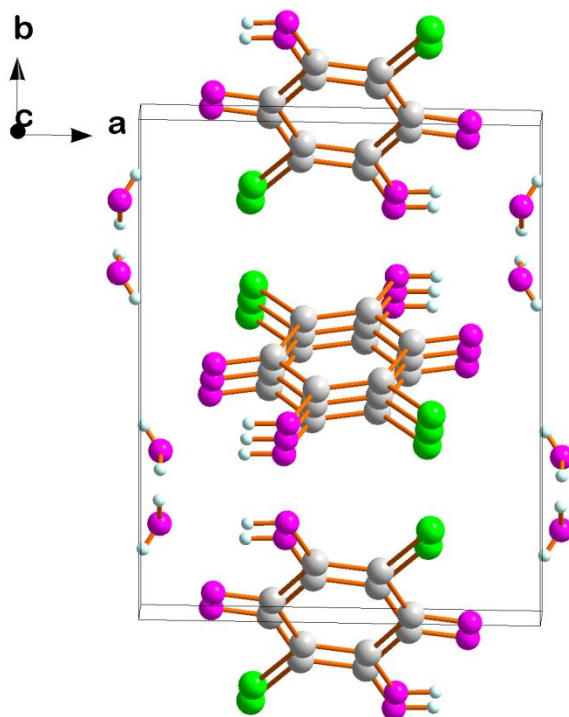
Figure 4.4 Unit cell for ½(caH₂)·H₂O (**1**) showing π-π stacking interactions along the c-axis.

4.4   Crystal structure of 2,5-dichloro-3,6-dihydroxycyclohexa-2,5-diene-1,4-dione triphenylphosphineoxide, OPPh₃½(caH₂) (2)

Triphenylphosphineoxide, $OPPh_3$ is a good proton acceptor that is known to form complexes in solution with a wide variety of organic molecules.[17,18,19] $OPPh_3$½(caH_2) (**2**) crystallises in the triclinic space group, $P\bar{1}$, with $Z = 2$. Figure 4.5 illustrates the numbering system of compound (**2**), with the caH_2 molecule on an inversion center. Selected bond distances and angles are reported in Table 4.4.

[17] E.M. Arnett, E.J. Mitchell, T.S.S.R. Murty, *J. Am. Chem. Soc.*, **96**, 3875-3891, 1974.

[18] D. Hadzi, R. Smerkolj, *J. Am. Chem. Soc.*, *Faraday Trans*, **1** 1188-1191, 1976.

[19] E.M. Arnett, L. Joris, E.J, Mitchell, T.S.S.R. Murty, T.M. Gorrie, P.V.R. Schleyer, *J. Am. Chem. Soc.*, **92**, 2365-2377, 1970.
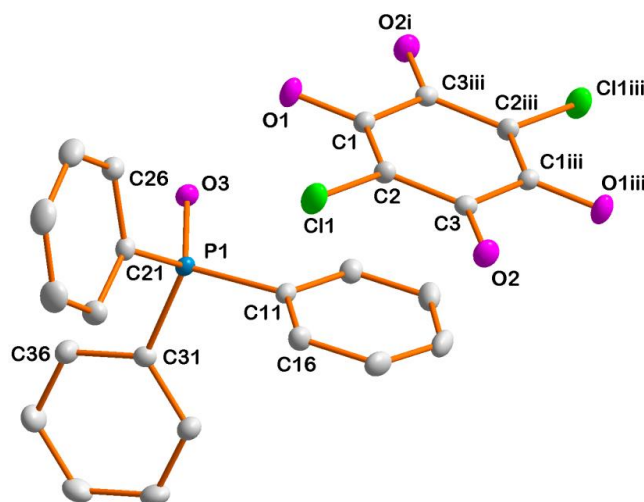
Figure 4.5 DIAMOND[10] view of OPPh$_3$½(caH$_2$) (**2**) with atom numbering system shown and thermal ellipsoids drawn at the 50% probability level. For the phenyl rings, the first digit refers to the ring number, while the second digit refers to the C-atom in the ring. H-atoms are omitted for clarity. Atoms generated by symmetry are indicated by lower case Roman numerals corresponding to the symmetry operator (iii) 1-x, -y, 2-z.

Table 4.4 Selected bond lengths and angles of OPPh$_3$½(caH$_2$) (**2**).

Bond lengths (Å)			
C1-O1	1.316(2)	P1-C11	1.800(3)
C3-O2	1.221(1)	P1-C21	1.79(3)
C2-Cl1	1.719(2)	P1-C31	1.81(2)
P1-O3	1.493(2)		
Bond angles (°)			
O1-C1-C3i	117.99(1)	Cl1-C2-C1	120.18(8)
O1-C1-C2	121.43(1)	O3-P1-C11	110.89(8)
O2-C3-C1i	118.48(9)	O3-P1-C21	113.34(8)
O2-C3-C2	124.16(1)	O3-P1-C31	112.46(6)
Cl1-C2-C3	117.75(1)		

From Table 4.4 it is observed that the C3-O2 and C1-O1 bond lengths are 1.221(1) Å and 1.316(2) Å, corresponding to C=O and C-OH, while the C2-Cl1 and P1-O3 bond lengths are 1.719(2) Å and 1.493(2) Å. These C=O and C-OH bond lengths closely resembles those of compound (**1**) which are 1.228(7) Å and 1.317(6) Å. The asymmetric unit of **2** contains one half of 2,5-dichloro-3,6-dihydroxy-2,5-cyclohexadiene-1,4-dione or chloranilic acid (caH$_2$), sitting on an inversion centre and its symmetry generated counterparts are linked by hydrogen bonds to the O=P of triphenylphosphineoxide molecules (Figure 4.6).

The guest acceptor, OPPh$_3$, co-crystallises with chloranilic acid (caH$_2$) through hydrogen-bonding between the O-H neutral chloranilic acid protons acting as a donor to the acceptor group of the P=O triphenylphosphineoxide. This generates an infinite hydrogen-bonding network which can be characterized as weak hydrogen bonds. The π-π stacking interaction (centroid-centroid) distance between caH$_2$ and phenyl rings is 3.465(9) Å and the inter- and intramolecular hydrogen bonds were observed between O1-H1···O2 (2.7102(14) Å; (iv) 1-x, - y, 2-z and O1-H1···O3 (2.530(13) Å; (v) 1-x, 1- y, 2-z (Table 4.5 and Figure 4.6).[20] A head to tail packing style can be observed.

Table 4.5 General hydrogen-bond distances (Å) and angles (°) of OPPh$_3$½(caH$_2$) (**2**).

D-H···A	d(D-H) (Å)	D(H···A) (Å)	d(D···A) (Å)	D-H···A (°)
O1-H1···O2[iv]	0.82	2.27	2.710(1)	114
O1-H1···O3[v]	0.82	1.83	2.530(1)	143

Symmetry code: (iv) 1-x, - y, 2-z, (v) 1-x, 1- y, 2-z

[20] A.N. Belay, J.A. Venter, A. Roodt, *Z. Kristallogr. NCS*., **232**(2), 163-164, 2017.
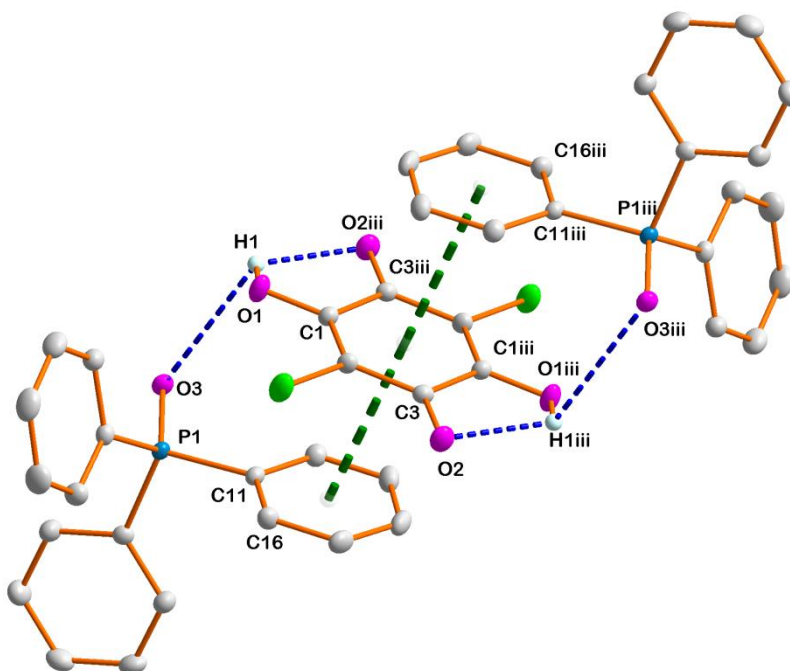
Figure 4.6 Inter-and intramolecular interaction of OPPh$_3$½(caH$_2$) (**2**). The blue dashed lines indicate O-H$_{...}$O hydrogen bonds and the green dashed lines indicate π-π stacking interactions, found between OPPh$_3$ and caH$_2$ obtained by symmetry-generated procedure [Symmetry codes: 1-x, -y, 2-z].

Figure 4.7 illustrates two planes, one through the six carbon atoms of one of the phenyl rings on P, C11 to C16 (blue) another one through the six atoms of the chloranilic acid ring, C1, C2, C3, C1iii, C2iii, and C3iii (green). The dihedral angle between the two planes is 7.994(1)°.
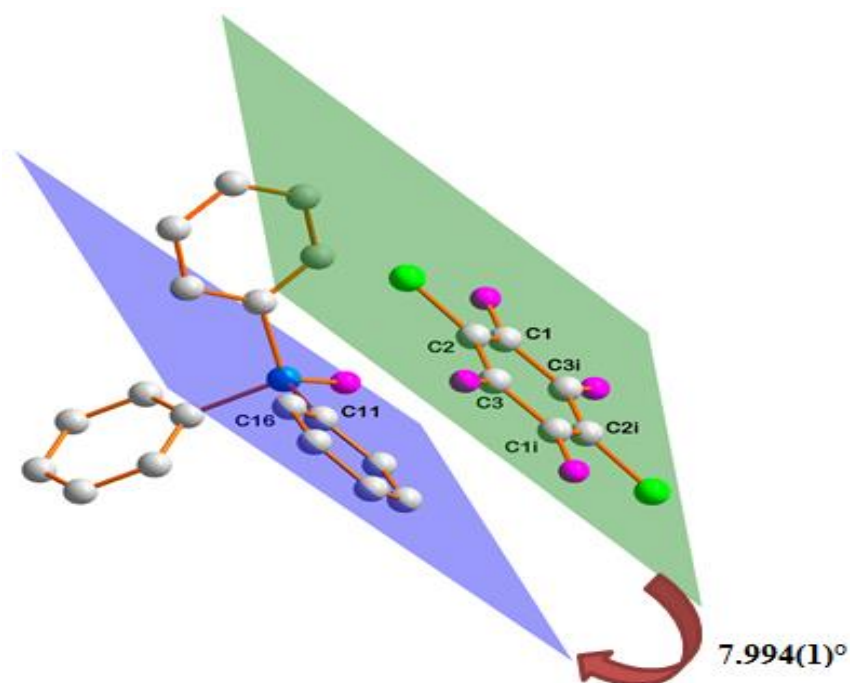
Figure 4.7 Representation of the plane (plane 1, green) passing through the chloranilic acid ring's C1, C2, C3 C1iii, C2iii, and C3iii and the plane passing through the six carbon atoms of the phenyl ring, C11-C16 (plane 2, blue). H-atoms are omitted for clarity.

4.5 Crystal structure of 2-hydroxypyridine-N-oxide (hopoH), $C_5H_5NO_2$ (3)

Previous studies reported that 2-hydroxypyridine-N-oxide (hopoH) has the potential to assist in the formation of amide bonds of active pharmaceutical ingredients (APIs) which are considered non-mutagenic reagents. It is widely employed in several industrial fields, mostly to prevent microbial degradation and deterioration of manufacturing materials (e.g., plastics, polymers, and latexes).[21,22] Moreover, hopoH also acts as a strong bidentate chelating agent in coordination chemistry.[23,24]

[21] D.E. Audette, R.J. Fenn, J.C. Ritter, G. Polson, P.A. Turley, *The Euro-Mediterranean Centre on Insular Coastal Dynamics, Costs and Benefits, Foundation for International Studies*, Malta 4-6 December, 1995.

[22] N.L. Reeder, J. Kaplan, J. Xu, R.S. Youngquist, J. Wallace, P. Hu, K.D. Juhlin, J.R. Schwartz, R.A. Grant, A. Fieno, S. Nemeth, T. Reichling, J.P. Tiesman, T. Mills, M. Steinke, S.L Wang, C.W. Saunders, *Antimicrob. Agents Chemother*., **55**, 5753-5760, 2011.

[23] D. Hubbard, G.R. Eaton, S.S. Eaton, *Inorg. Nucl. Chem. Lett.,* **15**, 255-258, 1979.

The crystal structure of hopoH, $C_5H_5NO_2$, at room temperature was first described by Ballesteros *et al*., in 1990 using visually estimated intensities.[25] Gardner and Katritzky also reported on 2-hydroxypyridine *N*-oxide using UV and IR spectroscopy and showed it exists in solution mainly as the 1-hydroxypyridin-2-one tautomer with a pK_a value of -0.8.[26] A search in Cambridge Structural Database (CSD) yielded no results for the free ligand at lower temperatures.[3] The structure of this compound was redetermined by single crystal X-ray diffraction methods at 100(2) K.

HopoH (**3**) crystallises in the monoclinic space group, *C*2/*c*, with Z = 4. Figure 4.8 illustrates the numbering system of compound (**3**). Selected bond distances and angles are reported in Table 4.6 with hydrogen interactions reported in Table 4.7.
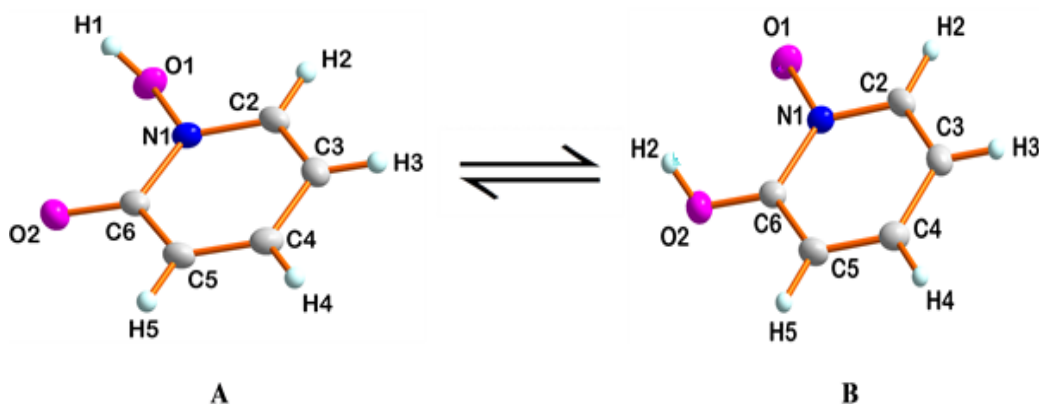
Figure 4.8 DIAMOND[10] view of hopoH (**3**), illustrating the two tautomeric forms of 1-hydroxypyridin-2-one (**A**) and 2-hydroxypyridine-N-oxide (**B**), showing the atom numbering system with the thermal ellipsoids drawn at a 50% probability level.

[24] X. Li, L. Yi-Zhi, L. San-Hui, C. Xue-Tai, Z. Jain-Hao, *Acta Cryst*., **E61**, m364-m366, 2005.

[25] P. Ballesteros, R.M. Claramount, T. Canada, *J. Chem. Soc. Perkin Trans*, **2**, 1215-1219, 1990.

[26] J.N. Gardner, A.R. Katritzky, *J. Chem. Soc.,* 4375-4385, 1957.

Table 4.6 Selected bond lengths and angles of hopoH (**3**).

Bond lengths (Å)			
N1-O1	1.384(3)	C4-C5	1.365(4)
N1-C2	1.359(4)	C5-C6	1.422(3)
C2-C3	1.359(3)	C6-N1	1.382(4)
C3-C4	1.409(3)	C6-O2	1.262(3)
Bond angles (°)			
C6-N1-O1	117.99(1)	O2-C6-C5	125.08(1)
O2-C6-N1	120.72(1)	N1-C6-C5	114.20(1)
N1-C2-C3	119.73(1)	C2-N1-O1	116.82(1)
C2-C3-C4	118.78(1)	C2-N1-C6	125.02(1)
C4-C5-C6	121.88(1)	C5-C4-C3	120.32(1)

The N1-O1, N1-C2, C3-C4 and C5-C6 bond distances of 1.384(3) Å, 1.359(4) Å, 1.409(3) Å and 1.422(3) Å are indicative of single bonds, whereas C2-C3, C4-C5 and C6-O2 distances of 1.359(3) Å, 1.365(4) Å and 1.262(3) Å indicate double bonds. HopoH (**3**) crystallises as 1-hydroxypyridin-2-one (tautomer **A**) with an intermolecular hydrogen-bond between the hydroxyl and pyridin-2-one groups. The N-O, O-H, and C-O bond distances in (**A**) compare well with distances at higher temperature (Ballesteros *et al*., in 1990)[25] for N-O and O-H single and C=O double bonds [N1-O1 = 1.384(3) Å compare (cf.) N-O = 1.384(2) Å; O1-H1 = 0.840(2) Å cf. O-H = 1.000(4) Å; C6-O2 = 1.262(3) Å cf. C=O = 1.252(2) Å]. In both cases the N-O bond lengths are the same, but the O-H single and C=O double bond lengths are respectively 0.16 Å shorter and 0.01 Å longer than the previously reported structure. The unit-cell dimensions in (**A**) are comparable to those of the previously determined compound [a = 8.169(3) Å, b = 10.992(3) Å, c = 11.171(3) Å, β = 101.67(2)°, and V = 982.3(5)Å^3, Z = 4 cf. a = 8.321(3) Å, b = 11.041(4) Å, c = 11.313(4) Å, β = 103.31(3)°, and V = 1011.3(1)Å^3, Z = 8].

Table 4.7 General hydrogen-bond distances (Å) and angles (°) of hopoH (**3**).

D-H···A	d(D-H) (Å)	D(H···A) (Å)	d(D···A) (Å)	D-H···A (°)
O1-H1···O1vi	0.84	2.55	3.0004(2)	114
O1-H1···O2vi	0.84	1.73	2.5563(2)	167
C2-H2···O2vii	0.95	2.50	3.4480(2)	172

Symmetry code: (vi) -x + 1, y, -z + ½, (vii) x + ½, -y + ½, z + ½

H1 is involved in strong intermolecular hydrogen-bonds to the pyridin-2-one group through O1-H1···O2^{vi} (1.73 Å and O1-H1···O2^{vi} (78.84(1)° as well as O1-H1···O1^{vi} (2.55 Å and O1-H1$_{...}$O2^{vi} (114.39(1)°. A third inter molecular hydrogen-bond is observed with another hopoH molecule through C2-H2···O2^{vii} (2.50 Å) and C2-H2···O2^{vi} (172.28(1)°). These are illustrated in Figure 4.9.

Small significant changes in the bond lengths of atoms affected by hydrogen bonding are very important in inferring the position of the hydrogen (OH). The evidence for strong intermolecular hydrogen-bonding in Figure 4.9 is an indication that structure **A** represents the most important tautomeric form.

Head to tail π-π stacking is observed between adjacent molecules as illustrated in Figure 4.10, with a distance of 3.671(2) Å (1/2-x, 1/2-y, 1-z) between parallel hopoH ring planes.
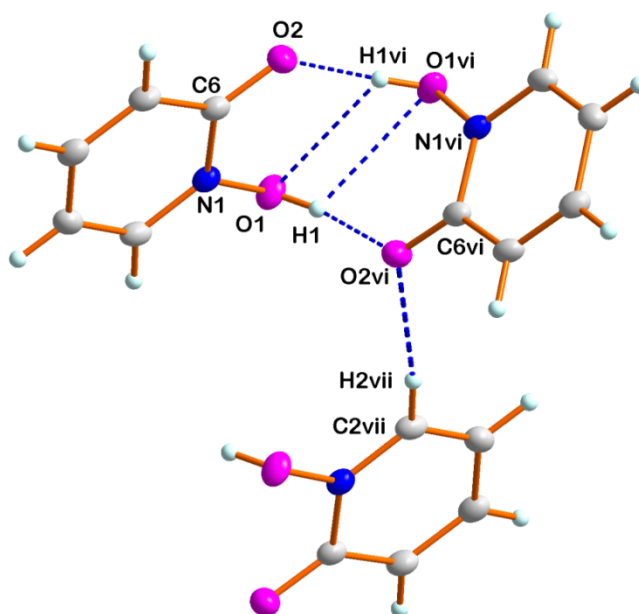
Figure 4.9 Inter- and intramolecular interactions of hopoH (**3**). The blue dashed lines indicate zigzag or v-shaped bifurcated hydrogen-bonds to atoms obtained by symmetry generation [Symmetry codes: (vi) 1-x, y, 1-z (vii) 3/2-x, ½-y, 1-z].
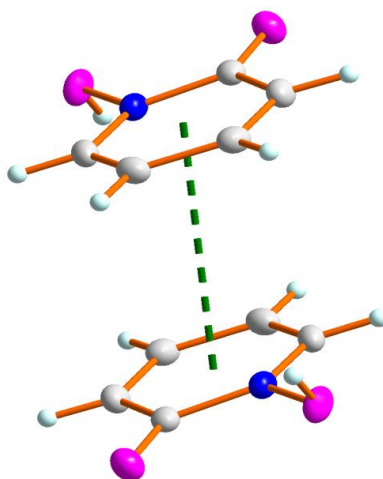
Figure 4.10 π-π interaction between adjacent molecules of hopoH (**3**), indicated by a dashed line [centroid-centroid distance = 3.671(2) Å; ½ - x, ½ - y, 1-z].

Figure 4.11 illustrates two planes, one through the six atoms of the hopoH ring, N1-C6 (pink) and the other passing through the four atoms O1, N1, C6 and O2 (blue) intersecting through N1 and C6. The dihedral angle between two planes is 2.580(1)°, indicating a slight tilt of O1 and O2 away from the hopoH ring.
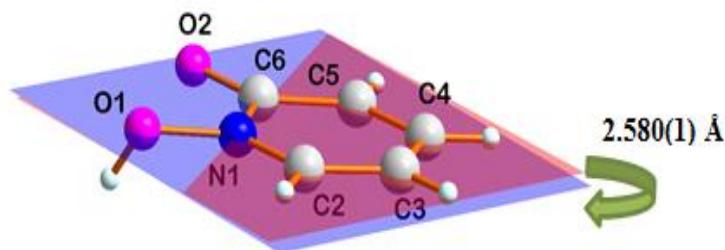
Figure 4.11 Representation of the plane passing through the six atoms of the hopoH ring, N1-C6 (plane 1, pink) and the plane passing through the four atoms O1, N1,C6 and O2 (plane 2, blue).

4.6   Crystal structure of 2,5-dichloro-3,6-dihydroxycyclohexa-2,5-diene-1,4-dione-4-N,N-dimethylaminopyridinium, $2½(caH_2)(DMAP)_6 \cdot 11H_2O$ (4)

2,5-Dichloro-3,6-dihydroxy-2,5-cyclohexadiene-1,4-dione, or chloranilic acid (caH_2), is a good proton donor as well as acceptor that is known to form complexes and co-crystals (Chapter 1, Chapter 4 sections 4.3 and 4.4). $2½(caH_2)(DMAP)_6 \cdot 11H_2O$ (4) crystallises in the triclinic space group, $P\bar{1}$, with $Z = 2$. The asymmetric unit of compound (4) contains six 4-N,N-dimethylaminopyridinium and three chloranilic acid (caH_2) molecules; both are neutral (Figure 4.12). The determination of the structure of compound (4) forms part of our systematic investigation concerning a π-π stacking interactions and an infinite extended network of hydrogen-bonds; this information provides insight into the behaviour of a stable niobium(V) and tantalum(V) complex crystal lattice (Chapters 5 and 6).

Figure 4.12 illustrates the numbering system of compound (4), with the caH_2 molecules that lie on an inversion center. Selected bond distances and angles are reported in Table 4.8 with hydrogen interactions reported in Table 4.9.

The hydrogen atoms of 11 solvated water molecules found in compound (**4**) were constrained at a distance of 0.85 Å from their parent O atoms to best fit the electron density from the Fourier map
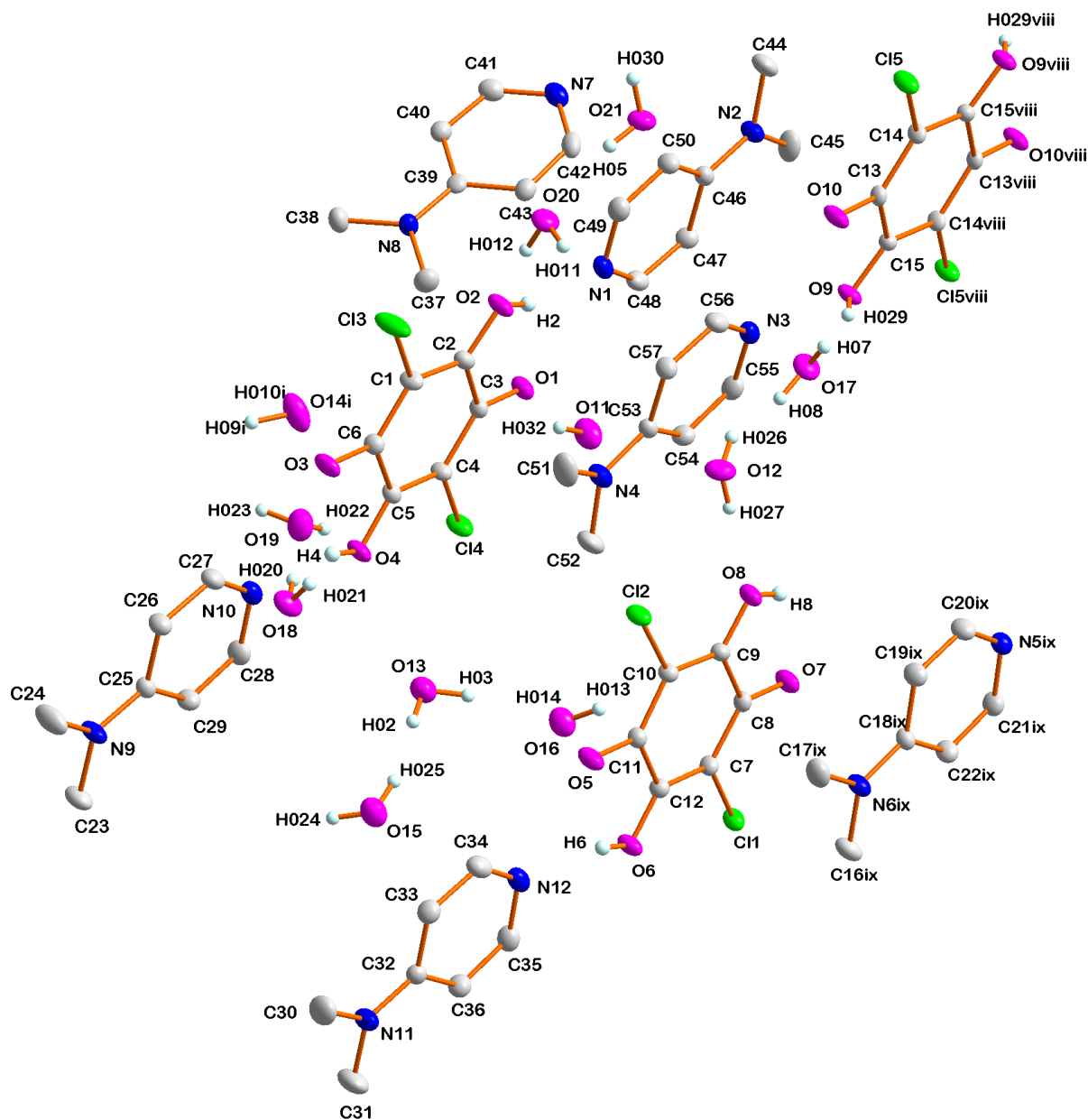
Figure 4.12 DIAMOND[10] view of 2½(caH$_2$)(DMAP)$_6$·11H$_2$O (**4**) with atom numbering system shown and thermal ellipsoids drawn at a 50% probability displacement. Atoms generated by symmetry are indicated by lower case roman numerals corresponding to the symmetry operator (viii) 2-x, 1-y, 1-z (ix) 1-x, 2-y, 1-z. H-atoms are omitted for clarity.

Table 4.8 Selected bond lengths and angles of $2\frac{1}{2}(caH_2)(DMAP)_6 \cdot 11H_2O$ (**4**).

Bond lengths (Å)			
C2-O2	1.251(3)	C10-Cl2	1.736(4)
C3-O1	1.239(3)	C1-Cl3	1.731(4)
C5-O4	1.261(3)	C4-Cl4	1.735(4)
C6-O3	1.243(3)	C14-Cl5	1.738(4)
C8-O7	1.238(3)	C46-N2	1.345(3)
C9-O8	1.253(3)	C53-N4	1.342(3)
C11-O5	1.253(3)	C18ix-N6ix	1.341(3)
C12-O6	1.248(3)	C39-N8	1.364(3)
C13viii-O10viii	1.248(3)	C25-N9	1.339(3)
C15viii-O9viii	1.250(3)	C32-N11	1.338(3)
C7-Cl1	1.742(4)		
Bond angles (°)			
C44-N2-C45	118.54(3)	C37-N8-C38	117.44(3)
C51-N4-C52	116.89(3)	C24-N9-C23	116.35(3)
C16ix-N6ix-C17ix	118.64(3)	C30-N11-C31	116.63(3)

From Table 4.8 it is known that the C8-O7, C3-O1, C6-O3, and C12-O6 bond lengths are 1.238(3) Å, 1.239(3) Å, 1.243(3) Å, and 1.248(2) Å with an average of 1.242(3) Å, corresponding to C=O. The C2-O2, C5-O4, C9-O8, and C15viii-O9viii bond lengths are 1.251(3) Å, 1.261(3) Å, 1.253(3) Å, and 1.250(2) Å with an average of 1.255(3) Å, corresponding to C-OH. The average C-OH bond length for $2\frac{1}{2}(caH_2)(DMAP)_6 \cdot 11H_2O$ (**4**) is shorter than those of $\frac{1}{2}(caH_2) \cdot H_2O$ (**1**) (1.317(6) Å) and $\frac{1}{2}(caH2)OPPh_3$ (**2**) (1.316(2) Å), but the average C=O bond length is longer than for compounds (**1**) (1.228(7) Å) and (2) (1.221(1) Å). The average C-Cl bond length of compound (**4**) is 1.736(4) Å, slightly longer than for compounds (**1**) (1.717(1) Å) and (**2**) (1.719(2) Å).

The asymmetric unit of (**2**) contains one half of 2,5-dichloro-3,6-dihydroxy-2,5-cyclohexadiene-1,4-dione, or chloranilic acid (caH$_2$), sitting on an inversion centre and its symmetry generated counterparts are linked by the network of extended infinite hydrogen-bonds to the 4-N,N-dimethylaminopyridine (DMAP) and solvated aqua cluster molecules (Figure 4.13).

Similar to compound (**2**), the guest acceptor 4-N,N-dimethylaminopyridine (DMAP) cocrystallises with chloranilic acid, caH$_2$, through hydrogen-bonding between the O-H neutral chloranilic acid protons acting as a donor to the nitrogen acceptor group of the DMAP. In addition, compound (**4**) is stabilised by an eleven aqua cluster. This generates an infinite network of hydrogen-bonds which can be characterized as strong and weak hydrogen bonds.

The 2½(caH$_2$)(DMAP)$_6$·11H$_2$O (**4**) crystal is characterised by 36 inter- and intramolecular O-H···O, O-H···Cl, C-H···Cl, O-H···N and C-H···N hydrogen interactions, as illustrated in Figure 4.13 and Table 4.9. The crystal packing is reinforced by the formation of an extended network of hydrogen bonds; similar observations are reported in section 4.2. Different v-shaped bifurcated strong hydrogen-bonds are present, which show H014 bonded to Cl2 and O5, and H029 bonded to N3 and O10 between solvated aqua molecules and chloranilic acid (caH$_2$) as well as DMAP molecules (Figure 4.13).

Table 4.9 General hydrogen-bond distances and angles of 2½(caH$_2$)(DMAP)$_6$·11H$_2$O (**4**).

D-H···A	d(D-H) (Å)	D(H···A) (Å)	d(D···A) (Å)	D-H···A (°)
O2-H2···O1	0.82	2.19	2.668(3)	118
O21-H05···O20	0.83(3)	1.94(3)	2.755(3)	170(4)
O14-H010···O3[viii]	0.91(3)	2.21(3)	3.039(3)	152(3)
O4-H4···O3	0.82	2.18	2.662(3)	118
O16-H013···O14	0.83(3)	2.05(3)	2.879(3)	170(4)
O16-H014···O5	0.84(4)	2.04(4)	2.839(3)	158(4)
O6-H6···O5	0.82	2.16	2.650(3)	118
O20-H012···O2	0.84(2)	2.04(2)	2.855(3)	163(3)

O18-H020···O19	0.84(2)	1.87(2)	2.706(3)	178(5)
O8-H8···O7	0.82	2.18	2.664(3)	118
O18-H021···O4	0.82(2)	2.04(2)	2.840(3)	169(3)
O13-H03···O16	0.86(3)	1.88(3)	2.732(3)	170(3)
O13-H02···O15	0.90(3)	1.95(4)	2.762(3)	150(5)
O17-H08···O12	0.85(4)	1.87(4)	2.713(3)	174(8)
O17-H07···O09	0.84(2)	1.98(3)	2.814(3)	172(3)
O19-H022···O10^{ix}	0.82(3)	2.12(3)	2.908(3)	159(4)
O19-H023···O21^{ix}	0.84(3)	1.89(3)	2.729(3)	175(4)
O20-H011···O15^{viii}	0.89(3)	1.90(3)	2.768(3)	166(3)
O15-H024···O18^{x}	0.81(3)	2.01(3)	2.788(3)	161(3)
O15-H025···O13	0.84(3)	1.95(3)	2.762(3)	163(4)
O12-H027···O8	0.87(3)	1.96(3)	2.821(3)	177(4)
O12-H026···O17	0.87(3)	2.01(4)	2.713(3)	137(4)
O9-H029···O10	1.16(8)	2.05(8)	2.650(3)	108(5)
O21-H030···O6^{xi}	0.87(3)	1.89(3)	2.761(3)	176(3)
O11-H032···O1	0.82(3)	2.11(3)	2.883(3)	157(4)
O11-H042···O17^{xii}	0.84(4)	1.89(5)	2.703(3)	166(2)
O14-H09···N7^{xii}	0.88(3)	2.05(3)	2.897(3)	160(3)
O2-H2···N1	0.82	2.12	2.905(3)	161
O4-H4···N10	0.82	2.02	2.793(3)	157
O6-H6···N12	0.82	2.17	2.966(3)	163
O8-H8···N5	0.82	2.04	2.816(3)	159
O9-H029···N3	1.16(8)	2.06(8)	2.906(3)	127(6)
C20-H20···N8^{xiii}	0.93	2.58	3.480(4)	162
C16-H16B···Cl1^{xiv}	0.96	2.75	3.620(3)	151
O14-H010···Cl3^{viii}	0.91(3)	2.74(3)	3.263(3)	118(2)
O16-H014···Cl2	0.84(4)	2.78(4)	3.344(3)	126 (3)

Symmetry code: (viii) -x +1, -y +1, -z, (ix) x-1, y, z, (x) -x, -y +1, -z, (xi) x +1, y -1, z, (xii) -x +1, -y +1, -z +1, (xiii) x, y +1, z, (xiv) -x +1, -y +2, -z +1(As with previous compounds)

The π-π stacking interaction (centroid-centroid) distances between respective sets of DMAP rings are 3.626(2) Å, 3.641(2) Å and 3.739(2) Å.

Inter- and intramolecular hydrogen-bonds were observed in the range of (i) O-H···O (1.87(2) Å-1.87(2) Å, (ii) O-H···N (2.02 Å - 2.17 Å, and (iii) O-H···Cl (2.74(3) Å - 2.78(4) Å, as well as (iv) C-H···Cl (2.75 Å) and (v) C-H···N (2.58 Å), respectively (Figure 4.13 and Table 4.9).
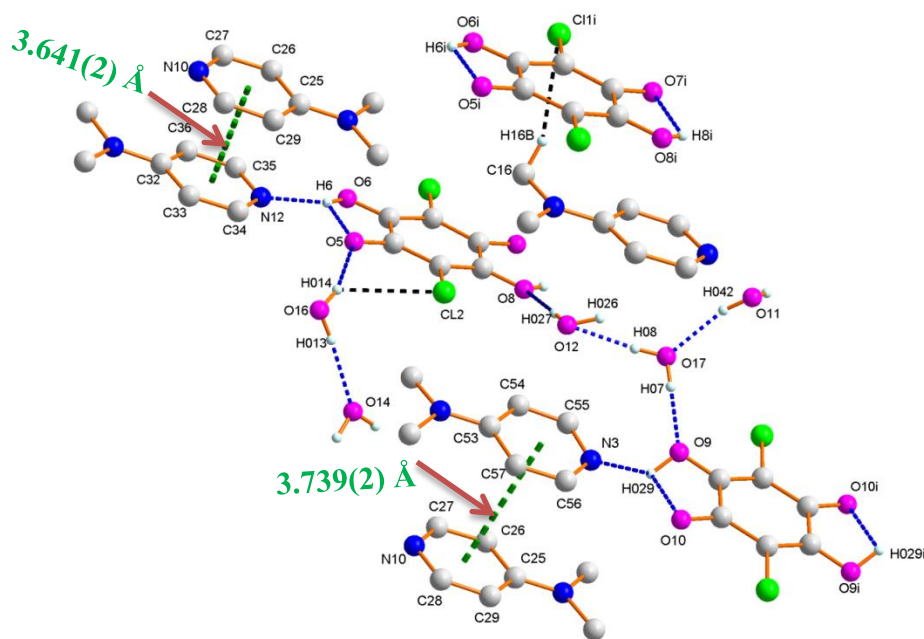
Figure 4.13 Selected molecular structure of 2½(caH₂)(DMAP)₆·11H₂O (**4**) showing the head to tail network of infinite intermolecular interactions. The blue dashed lines indicate O-H···O, O-H···N, and C-H···N hydrogen-bonds, the black dashed lines indicate O-H···Cl and C-H···Cl halogen bonds, while the green dashed lines indicate the π-π stacking interaction [centroid-centroid = 3.641(2) Å and 3.739(2) Å] distance between two DMAP rings on N3-C56 and N10-C28 as well as N10-C28 and N12-C35 [Symmetry codes: (viii) 2-x, 1-y, 1-z (ix) 1-x, 2-y, 1-z]. Uninvolved H-atoms are omitted for clarity.

4.7 Conclusion

In this chapter four crystal structures, those of two different free O,O'-bidentate compounds ½(caH$_2$)·H$_2$O (**1**) and hopoH (**3**) as well as two novel co-crystal structures, OPPh$_3$½(caH$_2$) (**2**), and 2½(caH$_2$)(DMAP)$_6$·11H$_2$O (**4**), were successfully characterized by single crystal X-ray diffraction at 100(2) K. These determinations of the structures of compounds (**2**) and (**4**) form part of our systematic investigation concerning π-π stacking interactions and an infinite extended network of hydrogen-bonds; this information provides insight into the behaviour of a stable niobium(V) and tantalum(V) complex crystal lattice (Chapters 5 and 6). Additionally, comparisons were drawn with similar structures from literature and the significant chemical difference as was observed with [hopoH] (**3**) crystal structure as compared to the literature equivalent at higher temperature (283-303 K).

Comparison of bond distances and angles to those of published works revealed a good correlation. These results are imperative for the identification and evaluation of new synthesised niobium(V) and tantalum(V) complexes in the corresponding environment, since the comparison of the most important bond lengths and angles, space group, hydrogen-bonding, and π-π stacking as obtained from these ligands, ½(caH$_2$)·H$_2$O (**1**) and hopoH (**3**) could assist interpretation of complexes formed by these and related ligands coordinated to the Nb(V) and Ta(V) centers.

In general, from these four crystal structures, different examples of intra- and intermolecular hydrogen bonding as well as π-π stacking interactions which contribute to the stabilization and rigidity of crystal lattice were observed. Coordination of these ligands to hard niobium(V) and tantalum(V) metal centres, with an accompanying understanding of their exact physical and chemical behaviour, will increase the potential of finding safe and environmentally friendly separation techniques.

In Chapter 5 two novel coordination modes of Nb(V) with 2,5-dichloro-3,6-dihydroxy-2,5-cyclohexadiene-1,4-dione, or chloranilic acid (caH$_2$) (**1**) crystal structures will be discussed.

5 X-Ray Crystallographic Studies of Niobium(V) Chloranilato Complexes

5.1 Introduction

As mentioned in Chapter two, literature reveals that only a small number of O- and N- donor ligands have been successfully coordinated to niobium(V) and tantalum(V) centers and their structures characterized by X-Ray crystallography. These reactions were performed under purified argon using standard Schlenk techniques and glove boxes, but it did not yield stable complexes when coordinated to bidentate ligands in atmospheric conditions. This instability in atmospheric conditions has been attributed to the hydrolysis of the various metal chloride precursor starting materials.

In this study it was hypothesized that by using harder ligand systems one might be more successful. Thus some of the synthesised complexes of niobium(V) and tantalum(V) with caH$_2$, hopoH, cupfH, and mpoH have been successfully coordinated in high percent yields and could be unequivocally characterized by X-Ray crystallography. A small number of the newly synthesised Nb(V) and Ta(V) crystals are unstable and not suitable for crystallographic structural characterization following loss of solvents. This instability is part of the reason why a study of the separation of these two metals is complicated and remains a challenge, compared to group (IV) and some other transition metals. Nevertheless, the new Nb(V) and Ta(V) complexes have been successfully characterised by spectroscopic techniques and these result shows different chemical characteristics (Chapter 3). These new Nb(V) and Ta(V) complexes which could not be characterized crystallographically will be discussed in Chapter 9 for potential future studies. Overall, the results obtained indicate that there is a good chance of purification and separation of niobium from tantalum which should be pursued in further studies and could open new routes

with industrial application. In this chapter the focus is on Nb(V) complexes with caH_2 (2,5-dichloro-3,6-dihydroxy-2,5-cyclohexadiene-1,4-dione) ligands in different coordination modes, and the rest of the Nb(V) and Ta(V) complexes with the two other chelating ligands, hopoH and cupfH will be discussed in Chapter 6 in detail.

As discussed in Chapter 1, caH_2, also known as chloranilic acid, is a unique multifunctional ligand system.[1] Four oxygen donors along with orbitals of delocalized electrons of tetraoxolene enable the ligand to bind to metal centres in different coordination modes. Furthermore, the organic molecule does not only coordinate to metal centres via oxygen donors, but also interact through carbanions and π-bonding in order to bind metal centres to its carbon skeleton. In fact, there are five possible coordination modes for caH_2 and its analogues which are shown in Chapter 1 (Figure 1.1-1.3). With the help of hydrogen bonding exerted by the ligand itself and some guest molecules, for instance water, coordination polymers with 1D, 2D, and 3D structures composed of mono or dinuclear complex units are accessible.[2,3]

In this study different coordination behaviour and chemical characteristics of two newly synthesised Nb(V) complexes are presented. The solid state structures of $(Et_4N)cis$-[NbO(ca)$_2$-(H$_2$O)OPPh$_3$]·3H$_2$O.THF (**5**) and $(Et_4N)_4[Nb_4O_4(ca)_2(\mu^2$-O)$_2Cl_8$]·2CH$_3$CN (**6**) have been determined by single crystal X-ray crystallographic studies. Intra- and/or inter molecular interactions, bond distances/angles and packing of the crystals are presented.

5.2 Experimental

The X-ray intensity data was collected on a Bruker X8 Apex II 4K Kappa CCD area detector diffractometer, equipped with a graphite monochromator and MoKα fine focus sealed tube (λ = 0.71073 Å, T = 100(2) K and 298(2) K) operated at 2.0 kW (50 kV, 40 mA). The initial unit cell

[1] K. Molcanov, B. Kojic-Prodic, A. Meden, *Croat. Chem. Acta*, **82**(2), 387-396, 2009.

[2] P.C.A. Bruijnincx, M. Viciano-Chumillas, M. Lutz, A.L. Spek, J. Reedijk, G. Van Koten, R.J.M.K. Gebbink, *Chem. Eur. J.*, **14**(18), 5567-5576, 2008.

[3] S. Kitagawa, S. Kawata, *Coord. Chem. Rev*., **224**, 11-34, 2002.

determinations and data collections were done using the APEX2[4] software package. The collected frames were integrated using a narrow-frame integration algorithm and reduced with the Bruker SAINT-Plus and XPREP software packages,[5] respectively. Analysis of the data showed no significant decay during the data collection. The data was corrected for absorption effects using the multi-scan technique SADABS,[6] and the structure was solved by the direct methods package SIR 97[7] and refined using the WinGX[8] software incorporating SHELXL.[9] The final anisotropic full-matrix least-squares refinement was done on F^2.

All H-atoms were positioned on geometrically idealized positions and refined using the riding model with fixed C-H distances for aromatic C-H of 0.93 Å (C-H) [$U_{iso}(H) = 1.2 U_{eq}$], for methyl C-H of 0.96 Å (C-H) [$U_{iso}(H) = 1.5 U_{eq}$], for methylene C-H of 0.97 Å (C-H) [$U_{iso}(H) = 1.5 U_{eq}$], for methine C-H of 0.98 Å (C-H) [$U_{iso}(H) = 1.5 U_{eq}$]. Non-hydrogen atoms were refined with anisotropic displacement parameters. The graphics were done using the DIAMOND[10] program with 50% probability ellipsoids for all non-hydrogen atoms.

A summary of the crystal data and refinement parameters are presented in Table 5.1, while complete list of atomic coordinates, equivalent isotropic parameters, bond distances and anisotropic displacement parameters and hydrogen coordinates for each individual dataset is given in Appendix **B**. All CIF files were checked for errors using the free on-line Checkcif service provided by the International Union of Crystallography.[11]

---

[4] Bruker Apex2 (Version 2011.4-1), Bruker AXS Inc., Madison, Wisconsin, USA. 2011.

[5] Bruker SAINT-Plus Version 6.02 (including XPREP), *Bruker AXS Inc. Area-Detector Integration Software*, Madison, Wisconsin, USA, 2012.

[6] Bruker SADABS Version 2004/1. *Bruker AXS Inc. Area Detector Absorption Correction Software,* Madison, Wisconsin, USA, 1998.

[7] A. Altomare, M.C. Burla, M. Camalli, G.L. Cascarano, C. Giacovazzo, A. Guagliardi, A.G.G. Moliterni, G. Polidori, R. Spagna, *J. Appl. Cryst*., **32,** 115-119, 1999.

[8] L.J. Farrugia, *J. Appl. Cryst*., **45**, 849-854, 2012.

[9] G.M. Sheldrick, SHELXL, *Acta Crystall.,* **C71**, 3-8, 2015.

[10] K. Brandenburg, H. Putz, *DIAMOND*, Release 3.0e, Crystal Impact GbR, Bonn, Germany, 2006.

[11] Available on the web at http://www.iucr.org/acs/ checkcif.html. Accessed in 2016.

Table 5.1 Summary of crystal data and refinement parameters of (Et$_4$N)*cis*-[NbO(ca)$_2$-(H$_2$O)OPPh$_3$]·3H$_2$O.THF (**5**) and (Et$_4$N)$_4$[Nb$_4$O$_4$(ca)$_2$(μ^2-O)$_2$Cl$_8$]·2CH$_3$CN (**6**).

Identification code	(5)	(6)
Empirical formula	C$_{42}$H$_{51}$Cl$_4$NNbO$_{15}$P	C$_{48}$O$_{14}$Cl$_{12}$Nb$_4$N$_6$H$_{86}$
Formula weight	1075.52	1765.85
Temperature (K)	100(2)	100(2)
Wavelength (Å)	0.71073	0.71073
Crystal system, space group	Monoclinic, *P*2$_1$	Monoclinic, *P*2$_1$/*c*
Unit cell dimensions		
a (Å)	10.468(7)	21.601(4)
b (Å)	18.005(1)	10.665(2)
c (Å)	12.584(9)	31.208(6)
α (°)	90.00	90.00
β (°)	92.66(3)	92.24(1)
γ (°)	90.00	90.00
Volume (Å^3)	2369.2(3)	7184(2)
Z	2	4
Density$_{calc}$ (g.cm^{-3})	1.508	1.6326
μ (mm^{-1})	0.580	1.127
F(000)	1108	3582
Crystal size (mm)	0.143 x 0.320 x 0.788	0.6 $\times$ 0.46 $\times$ 0.17
Theta range (°)	3.35 to 28.29	3.40 to 28.08
Index ranges	-10 $\leq$ h $\leq$ 13	-28 $\leq$ h $\leq$ 28
	-23 $\leq$ k $\leq$ 23	-14 $\leq$ k $\leq$ 13
	-16 $\leq$ *l* $\leq$ 16	-41 $\leq$ *l* $\leq$ 41
Reflections collected/unique	52823/11418	210991/17286
R$_{int}$	0.0458	0.0710
Completeness (%)	99.6	99.8
Max. and min. transmission	0.746, 0.695	0.746, 0.641
Refinement method	Full-matrix least-squares on F^2	Full-matrix least-squares on F^2
Data / restraints / parameters	11418/11/601	17286/0/760
Goodness-of-fit on F^2	1.118	1.214
Final *R* indices [*I*>2σ(*I*)]	*R*1 = 0.0230	*R*1 = 0.1129
	*wR*2 = 0.0613	*wR*2 = 0.2506
R indices (all data)	*R*1 = 0.0242	*R*1 = 0.1219
	*wR*2 = 0.0618	*wR*2 = 0.2585
$\Delta\rho_{max}$ and $\Delta\rho_{min}$ (e.Å^{-3})	0.38, -0.49	1.85, -3.33

5.3 Crystal structure of tetraethylammonium aquabis(2,5-dichloro-3,6-dihydroxy-1,4-benzoquinonato-κ^2O,O')oxidotriphenylphosphineoxideniobate(V), trihydrate tetrahydrofuran solvate, (Et$_4$N)cis-[NbO(ca)$_2$(H$_2$O)OPPh$_3$]·3H$_2$O·THF (5)

(Et$_4$N)cis-[NbO(ca)$_2$(H$_2$O)OPPh$_3$]·3H$_2$O·THF (5) crystallises in the monoclinic space group, $P2_1$, with two formula units in the unit cell. In Figure 5.1, the DIAMOND representation of complex (5) is given with 50% ellipsoid probability and the atom numbering shown. All solvents (H$_2$O) had to be DFIX restrained to a target value, the distance between H and O fixed at 0.85 Å and the distance between H and H fixed at 1.35 Å to best fit the experimental electron density in Shelx-97. This crystal structure will be compared to the other crystal structures reported in Chapter 4 sections 4.3 and 4.4.
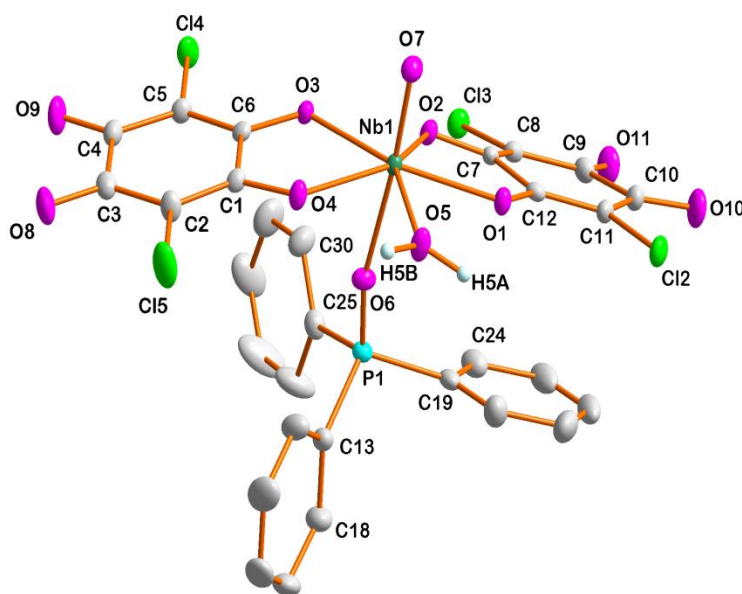
Figure 5.1 Molecular structure of cis-[NbO(ca)$_2$(H$_2$O)OPPh$_3$]$^-$ (5) with atom numbering system shown and the thermal ellipsoids drawn at a 50% probability level. Cation, hydrogen atoms and solvated molecules are omitted for clarity.

Table 5.2 Selected bond lengths and angles of (Et$_4$N)c*is*-[NbO(ca)$_2$(H$_2$O)OPPh$_3$]·3H$_2$O·THF (**5**).

Bond lengths (Å)			
Nb1-O1	2.115(1)	C8-Cl3	1.728(1)
Nb1-O2	2.102(1)	C5-Cl4	1.726(1)
Nb1-O3	2.147(1)	C11-Cl2	1.729(1)
Nb1-O4	2.146(1)	C1-O4	1.286(1)
Nb1-O5	2.109(1)	C3-O8	1.224(1)
Nb1-O6	2.197(1)	C4-O9	1.229(1)
Nb1-O7	1.721(1)	C6-O3	1.283(1)
P1-O6	1.501(1)	C7-O2	1.298(1)
P1-C19	1.796(1)	C9-O11	1.225(1)
P1-C13	1.793(1)	C10-O10	1.223(1)
P1-C25	1.796(1)	C12-O1	1.293(1)
C2-Cl5	1.729(1)		
Bond angles (°)			
O1-Nb1-O2	72.99(4)	O3-Nb1-O7	92.26(4)
O3-Nb1-O4	71.88(4)	O2-Nb1-O7	98.44(4)
O5-Nb1-O7	97.03(5)	O6-P1-C13	108.02(4)
O5-Nb1-O6	86.92(4)	O6-P1-C19	110.55(4)
O4-Nb1-O6	81.18(3)	O6-P1-C25	110.32(4)
O7-Nb1-O6	174.94(4)		

The niobium(V) metal center is coordinated by seven oxygen atoms of two chloranilate dianions (ca^{-2}) bidentate ligands, one triphenylphosphineoxide monodentate ligand, one aqua ligand and one oxido group. The ca^{-2} ligands in (Et$_4$N)c*is*-[NbO(ca)$_2$(H$_2$O)OPPh$_3$]·3H$_2$O·THF (**5**) each form a five-membered coordination ring with a small bite angle. The O-Nb-O bite angles of the ca^{-2} ligands are 71.98(4)° and 73.13(4)°, respectively (Table 5.2 and Figure 5.1). The average bond lengths of C3-O8, C9-O11, C4-O9, and C10-O10 are 1.225(1) Å which correspond to C=O of the uncoordinated site of the ca^{-2} ligand, while the average bond lengths of C6-O3, C12-O1, C1-O4

and C7-O2 are 1.290(1) Å, which corresponds to C-O-Nb. However, as reported in Chapter 4 sections 4.3-4.4 the average C-O bond lengths of the free ligand are 1.228(7) Å and 1.317(6) Å, which correspond to C=O and C-OH respectively. When the average C=O bond lengths of the free ligand are compared to the average bond lengths of C=O and C-O-Nb in the complex (**5**), the C=O average bond length of 1.225(1) Å is nearly same as in the free ligand, while C-O-Nb average bond lengths is slightly shorter than in the free ligand.

The Nb-O ca^{-2} ligand bond lengths Nb-O1, Nb-O2, Nb-O3, and Nb-O4 vary from 2.102(1) Å to 2.147(1) Å, are 2.115(1), 2.102(1), 2.147(1) Å and 2.146(1) Å, respectively compared to Nb-O5 and Nb-O6 with 2.109(1) and 1.197(1) Å, respectively and Nb=O with 1.721(1) Å. The Nb-O(P)$_{trans}$ distance of 2.197(1) Å show the strong *trans* influence of the *trans* oxido ligand and parallel the spectroscopic evidence. Figure 5.1 illustrates the Nb-O distance of the one chloranilato ligand (Nb-O1 and Nb-O2) with average of 2.109(1) Å is significantly shorter than the Nb-O distances of the other chloranilato ligand (Nb-O3 and Nb-O4) with an average of 2.147(1) Å. The C-Cl bond lengths of the chloranilate dianionic (ca^{-2}) bidentate ligands in the complex (**5**) vary from 1.726(1) Å to 1.729(3) Å, whereas the average C-Cl bond length of the free caH$_2$ ligand is 1.717(1) Å, which indicates that the average C-Cl bond lengths of the free caH$_2$ ligand is shorter than those in the complex (**5**).

In 2016 Koen *et al*,[12] reported the Nb-O and Ta-O average bond lengths of [Nb(trop)$_4$Cl] (2.083(1) Å) and [Ta(trop)$_4$Cl] (2.092(1) Å) respectively, whereas the Nb-O average bond lengths of (Et$_4$N)*cis*-[NbO(ca)$_2$(H$_2$O)OPPh$_3$]·3H$_2$O·THF (**5**) was 2.128(1) Å, which showed the average Nb-O bond lengths are slightly longer than in [Nb(trop)$_4$Cl]. In other studies a salt containing an [NbOCl$_4$(OH$_2$)]$^-$ group is reported by Klingelhoefer & Mueller[13] and Schafer *et al*,[14] with a rather long Nb-OH$_2$ distances of 2.49(1) Å, and 2.37(1) Å respectively. We found much shorter Nb-OH$_2$ distances of 2.109(1) Å. In all these structures distances and angles reported are in good correlation with our results.

[12] R. Koen, A. Roodt, H.G. Visser, *J. South .Afr. Inst.Min. Metall.*, **116**, 865-899, 2016.

[13] P. Klingelhoever, U. Mueller, *Z. Anorg. Allg. Chem.*, **516**, 85-87, 1984.

[14] H.N. Schafer, H. Burzlaff, A.M.H. Grimmeiss, R. Weiss, *Acta. Cryst.*, **C**(47), 1808-1811, 1991.

Figure 5.2 illustrates a wing-like limb bending as found far the two ca^{-2} ligands in (Et$_4$N)*cis*-[NbO(ca)$_2$(H$_2$O)OPPh$_3$]·3H$_2$O·THF (**5**). The two planes formed by the five-membered rings of chloranilate (ca^{-2}) ligands, O1-C12-C7-O2 and O3-C6-C1-O4 intersect at the niobium(V) centre. The dihedral angle between two planes is 27.6(6)°.
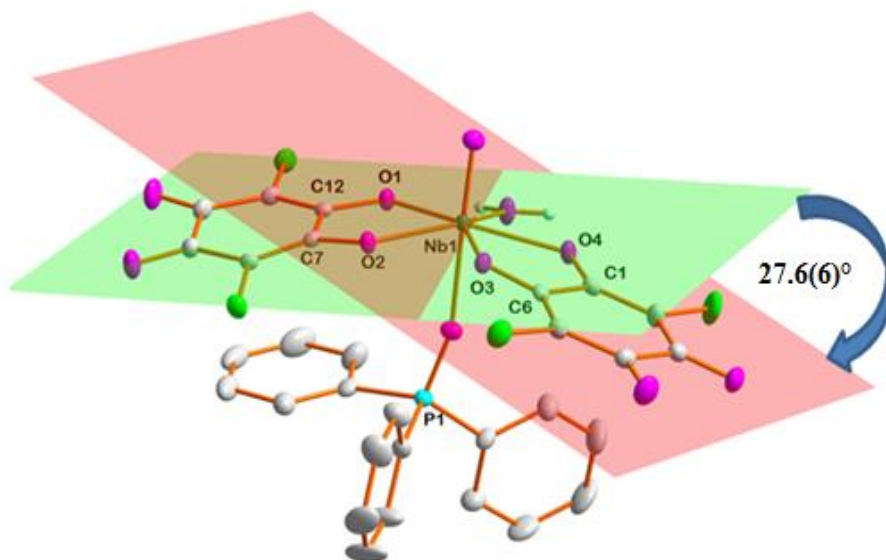
Figure 5.2 Representation of planes through *cis*-[NbO(ca)$_2$(H$_2$O)OPPh$_3$]$^-$. (**5**). Plane 1 (green) passing through the five membered ring of chloranilate ligand in O1, C12, C7 and O2 and plane 2 (pink) passing through the five membered ring of chloranilate ligand (ca) in O3, C6, C1 and O4. H-atoms, counter ions and solvated molecules are omitted for clarity.
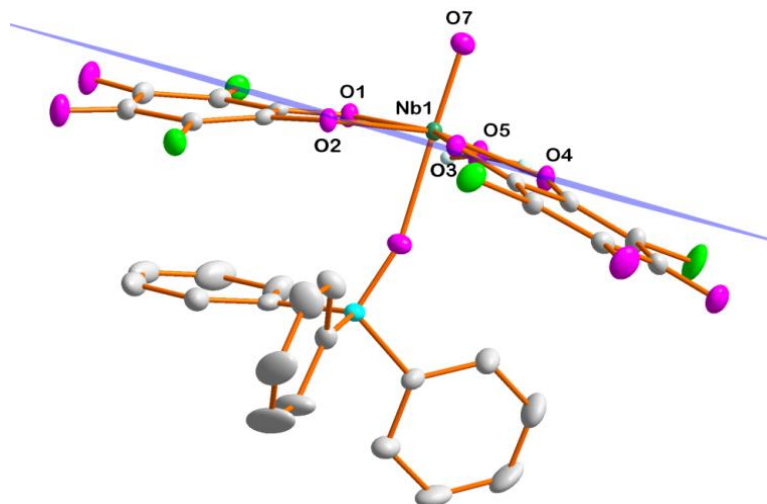
Figure 5.3 Representation of *cis*-[NbO(ca)$_2$(H$_2$O)OPPh$_3$]$^-$ (**5**). The blue plane constructed through the five oxygen atoms O1, O2, O3, O4 and O5 illustrates the distance between the plane and O7. H-atoms, counter ions and solvated molecules are omitted for clarity.

Shown in Figure 5.3 is a plane (blue) that was constructed through the five oxygen atoms O1, O2, O3, O4 and O5 forming a distorted pentagonal planar axis. The distance between the blue plane and O7 is 1.940(2) Å, while the niobium metal centre is slightly elevated above this plane by 0.219(3) Å. This illustrates the distorted D_{5h} pentagonal bipyramidal geometry of the molecule, due to a short oxido ligand distance of 1.721(1) Å, compared to the Nb-O6 distance of 2.197(1) Å (Table 5.2), as well as the large *trans* influence of oxido ligand.

Figure 5.4 illustrates the distorted D_{5h} pentagonal bipyramidal coordination mode of (Et$_4$N)*cis*-[NbO(ca)$_2$(H$_2$O)OPPh$_3$]·3H$_2$O·THF (**5**), which is unusual for both niobium(V) complex structures, as well as for tantalum(V) complexes. The crystal structure of (**5**) is characterised and stabilized by 19 inter- and intramolecular O-H···Cl, O-H···O, C-H···O and C-H···Cl hydrogen interactions, as illustrated in Figure 5.7 and 5.8, and listed in Table 5.3.
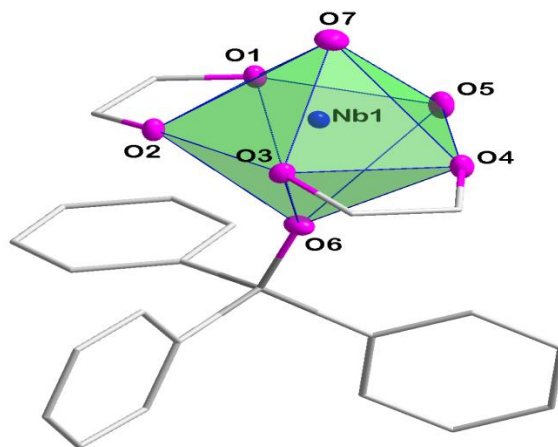
Figure 5.4 Representation of the distorted D_{5h} pentagonal bipyramidal coordination polyhedron formed by oxygen donor atoms surrounding the Nb(V) atoms of *cis*-[NbO(ca)$_2$(H$_2$O)OPPh$_3$]$^-$. H-atoms, counter ions and solvated molecules are omitted for clarity.
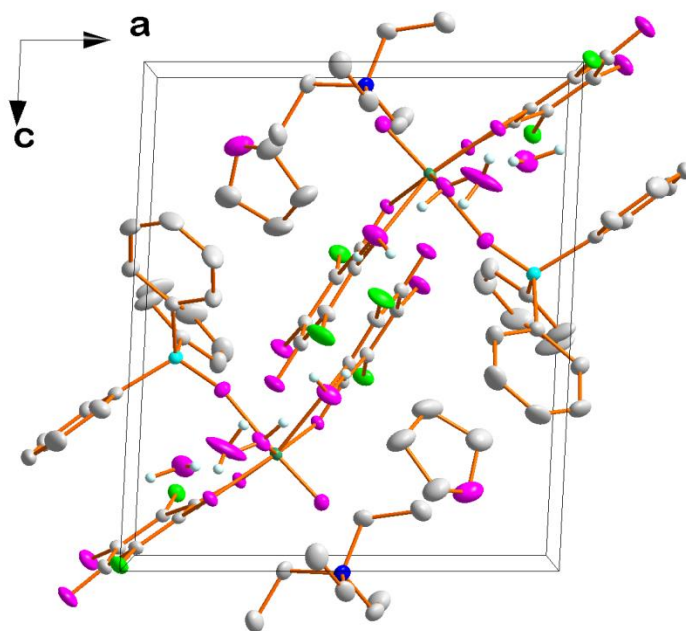
Figure 5.5 Packing diagram of (Et$_4$N)*cis*-[NbO(ca)$_2$(H$_2$O)OPPh$_3$]·3H$_2$O·THF (**5**) showing two molecular formula per unit cell along b-axis. H-atoms are omitted for clarity.

Table 5.3 General hydrogen-bond distances and angles of (Et$_4$N)*cis*-[NbO(ca)$_2$(H$_2$O)OPPh$_3$] ·3H$_2$O·THF (**5**).

Interactions	D-H···A	D-H(Å)	H···A (Å)	D···A (Å)	D-H···A (°)
I	O13-H1···Cl5	0.87(4)	2.52(4)	3.370(2)	166(3)
II	O13-H1···O4	0.87(4)	2.47(4)	2.921(3)	113(3)
III	O13-H2···O9[a]	0.86(4)	1.89(4)	2.739(3)	171(3)
IV	O14-H4···O15[a]	0.85(3)	1.85(3)	2.673(4)	165(5)
V	O15-H5···O8	0.81(3)	2.35(3)	3.062(3)	147(3)
VI	O15-H5···O9	0.81(3)	2.24(3)	2.922(3)	142(3)
VII	O5-H5A···O14	0.92(3)	1.69(3)	2.577(3)	163(3)
VIII	O5-H5B···O13	0.84(4)	2.79(4)	2.608(3)	165(4)
IX	O15-H6···O10[b]	0.85(4)	2.05(4)	2.890(3)	175(5)
X	C14-H14···O6	0.93	2.49	2.918(3)	108
XI	C18-H18···O8[c]	0.93	2.40	3.212(4)	145
XII	C22-H22···O7[c]	0.93	2.44	3.314(4)	157
XIII	C30-H30···O3	0.93	2.52	3.394(3)	156
XIV	C30-H30···O6	0.93	2.57	2.985(3)	108
XV	C31-H31B···O2[d]	0.97	2.57	3.374(4)	140
XVI	C33-H32A···O7[d]	0.96	2.57	3.500(4)	163
XVII	C32-H32B···O11[e]	0.96	2.56	3.522(4)	175
XVIII	C34-H34C···O12[f]	0.96	2.57	3.403(4)	146
XIX	C37-H37A···Cl3[d]	0.97	2.78	3.740(3)	172

Symmetry code: (a) -x+1, y+½, -z+1 (b), x+1, y, z - 1 (c), x-1, y, z (d), x, y+1, (e), x+1, y+1, z (f), -x+1, y+½, -z+2

Figure 5.6 Expanded packing diagram of *cis*-[NbO(ca)$_2$(H$_2$O)OPPh$_3$]$^-$ (**5**) showing extended wing-like orientation chain head to tail π- π stacking interactions along the b-axis. H-atoms, counter ions and solvated molecules are omitted for clarity.

The solid state structure of (**5**) exhibts π-π intramolecular interactions [centroid-centroid distance = 3.552(1) and 3.788(2) Å, -1+x, y, z] between the phenyl ring on the OPPh$_3$ and chloranilate (ca) ligands (Figure 5.9) and different hydrogen bonds were observed; O-H···O, C-H···O, O-H···Cl, and C-H···Cl distances in the range of 1.69(3)-2.47(4) Å, 2.40-2.57 Å , 2.52(4) Å and 2.78 Å respectively are reported in Table 5.3.
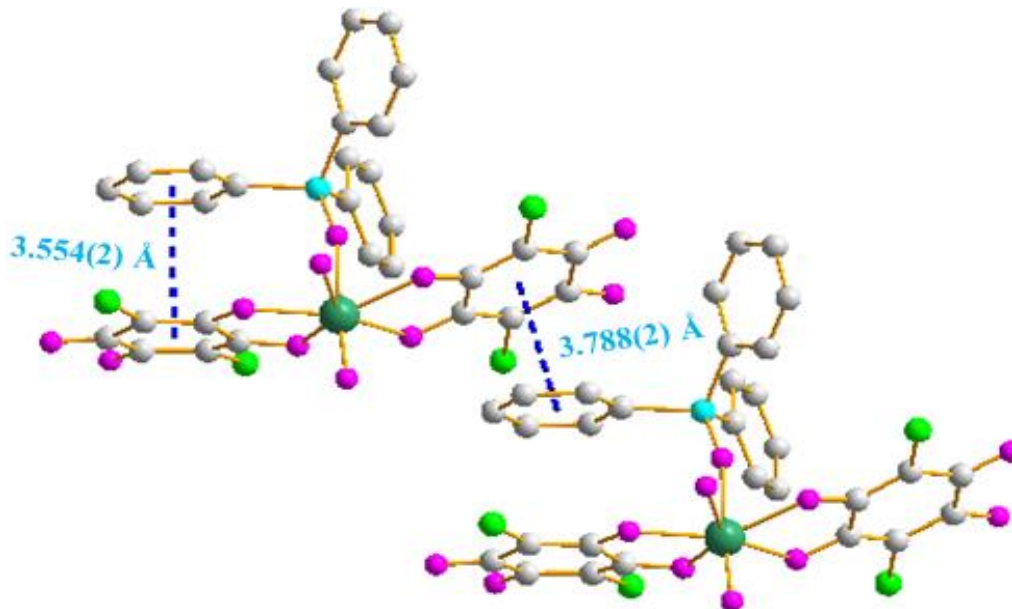
Figure 5.7 Extended structure of *cis*-[NbO(ca)$_2$(H$_2$O)OPPh$_3$]$^-$ (**5**) showing head to tail packing interaction along the b-axis. The thick blue dashed lines indicate π-π stacking interactions [centroid-centroid distance = 3.554(2) and 3.788(2) Å, -1+x, y, z] between a phenyl ring on the OPPh$_3$ and coordinated chloranilate (ca) ligands. H-atoms, counter ions and solvated molecules are omitted for clarity.

The crystal packing is reinforced by the formation of an extended network of hydrogen bonds and similar intractions are reported in Chapter 4.[15] Herein, we present an investigation of different triangle and v-shaped bifurcated strong hydrogen-bonds, which show H1, bonded to Cl5 and O4; H5 bonded to O8 and O9; and H30 bonded to O3 and O6 between solvated water molecules and the generated (Et$_4$N)*cis*-[NbO(ca)$_2$(H$_2$O)OPPh$_3$]·3H$_2$O·THF (**5**) (Figure 5.8 and 5.9).

---

[15] A.N. Belay, J.A. Venter, A. Roodt, *Z. kristallogr. NCS*, **232**(2), 163-164, 2017.
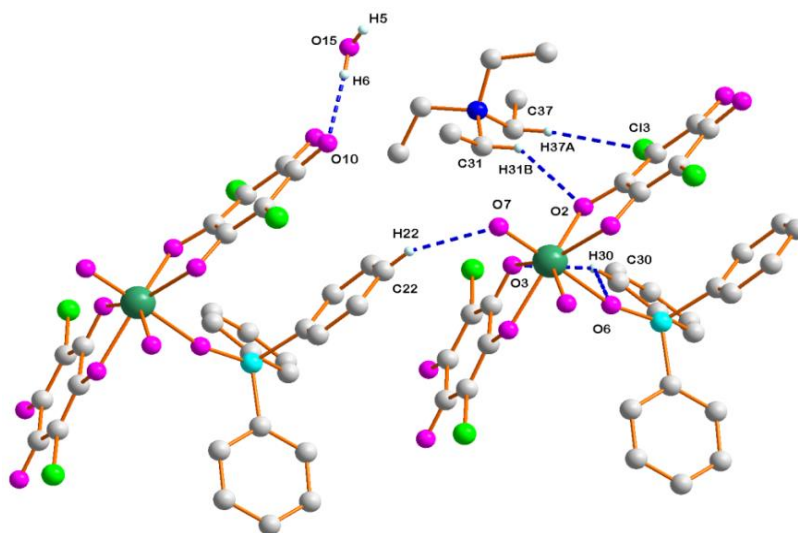
Figure 5.8 Extended structure of $(Et_4N)cis$-$[NbO(ca)_2(H_2O)OPPh_3]\cdot 3H_2O\cdot THF$ (**5**) showing the intra- and intermolecular interactions. The blue dashed lines indicate O-H···O, C-H···O and C-H···Cl hydrogen-bonds [Symmetry codes: Table 5.3].
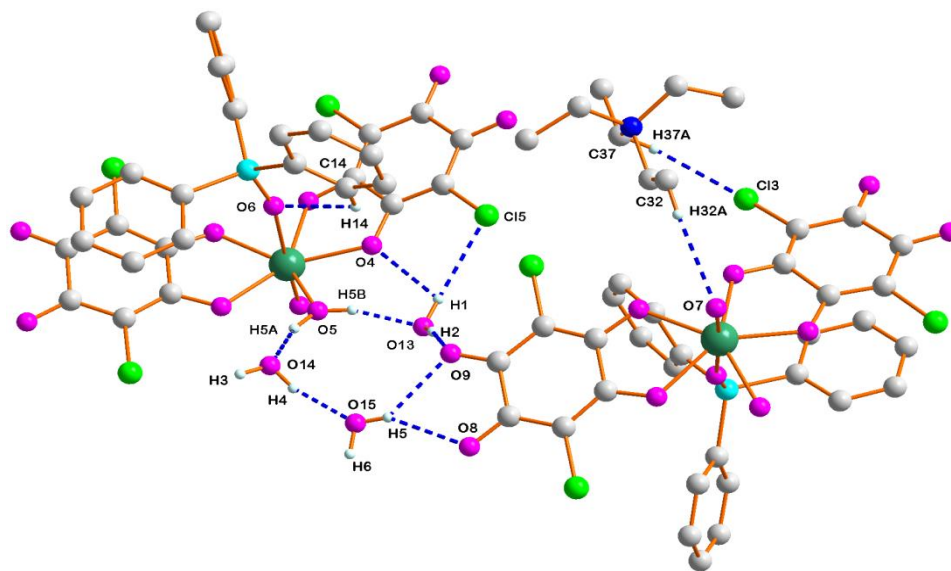
Figure 5.9 Extended structure of $(Et_4N)cis$-$[NbO(ca)_2(H_2O)OPPh_3]\cdot 3H_2O\cdot THF$ (**5**) showing blue dashed lines, indicating different triangle and v-shaped bifurcated hydrogen-bonds found between its symmetry-generated molecules. The rest of the hydrogen atoms are omitted for clarity [Symmetry codes: Table 5.3].

Moreover, infrared spectra of (Et$_4$N)*cis*-[NbO(ca)$_2$(H$_2$O)OPPh$_3$]·3H$_2$O·THF (**5**) recorded in the solid state show a strong band accounting for the P-O stretching, at 979 cm^{-1}. This value appear at lower frequencies with regards to these observed for the free OPPh$_3$ ligand, v(P=O) = 1182 cm^{-1}. The ^{31}P NMR spectrum of this complex shows the signal expected for the unique phosphane present at δ = 45.81 and 38.99 ppm both in solid and solution state, while 26.06 ppm is observed for the free OPPh$_3$ ligand. These chemical shift, δ = 19.75 and 12.39 ppm shows coordination of monodentate OPPh$_3$ ligand to the niobium metal centre. The *trans*-influences of Nb=O groups in this complexes are also shown by the difference in ^{31}P chemical shifts for the *trans* disposed OPPh$_3$ ligands, and similar differences are seen in the v(PO) frequencies in the IR spectra which differ by 203 cm^{-1}. A strong band at 922.60 cm^{-1} is assignable to the terminal Nb=O vibrations. The X-ray crystal structure determination of complex (**5**) (Figure 5.1) confirmed the observed spectroscopic results.

5.4 Crystal structure of tetratetraethylammonium octachloridocyclo-di-*µ*-oxido-di-*µ*-(2,5-dichloro-3,6-dihydroxy-1,4-benzoquinonato-*κ²O,O'*)tetraoxidoniobate(V), diacetonitrile solvate, (Et$_4$N)$_4$[Nb$_4$O$_4$(ca)$_2$(*µ²*-O)$_2$Cl$_8$]·2CH$_3$CN (6)

Chloranilate dianions (abbreviated ca^{-2}), due to their peculiar structure and having different coordination modes are good candidates in coordination chemistry and supramolecular chemistry[16] and potential applications using it for separation of niobium from tantalum. The effective bridging function of µ-chloranilate and the long-distance antiferromagnetic exchange interactions of binuclear copper(II) complexes containing the µ-chloranilate ligand have been illustrated by single-crystal X-ray and magnetic analyses.[17,18,19] However, to our knowledge no binuclear Nb(V) complex bridged by a chloranilate group of this kind has been reported yet. This study reveals a novel Nb(V) tetranuclear complex using the dianion of chloranilate (ca^{-2}) as bridging ligand.

[16] K. Molcanov, B. Kojic-Prodicand, A. Meden, *Croat. Chem. Acta*, **82**(2), 387-396, 2009.

[17] F. Tinti, M. Verdaguer, O. Kahn, J.M. Savariault, *Inorg. Chem.,* **26**, 2380-2384, 1987.

[18] C.L. Deng, Z.H. Jiang, D.Z. Liao, S.P. Yan, G.L. Wang, *Synth. React. Inorg. Met.Org. Chem*., **23**, 247-256, 1993.

[19] S. Kawata, S. Kitagawa, H. Kumagai, C. Kudo, H. Kamesaki, T. Ishiyama, R. Suzuki, M. Konodo, M. Katado, *Inorg. Chem*., **35**(15), 4449-4461, 1996.

$(Et_4N)_4[Nb_4O_4(ca)_2(\mu^2\text{-}O)_2Cl_8]\cdot 2CH_3CN$ (**6**) crystallises in the monoclinic space group, $P2_1/c$, with four molecular complexes in the unit cell. In Figure 5.10, a representation of complex (**6**) is given with ellipsoid probability at 50% and the atom numbering system shown. Selected interatomic bond lengths and angles are presented in Table 5.4.

The high R1 (11%) and wR2 (25%) indicates that the crystals damaged very fast as soon as they were taken out of their mother liquor, even when preventing contact with the atmosphere (or air) using the oil-drop method. Because one of the counter ion of tetraethylammonium(C36) and solvated acetonitrile (N5) indicated a slight disorder. Overall, the poor quality of the structural model is solely related to the degradation of the crystals and disordered solvent area, and that with the crystals at hand this is the best model accessible.

A summary of the general crystallographic data of complex (**5**) and complex (**6**) are presented in Table 5.1. Atomic coordinates, anisotropic displacement parameters, bond distances and angles and hydrogen coordinates, are given in the supplementary data (Appendix **B**).
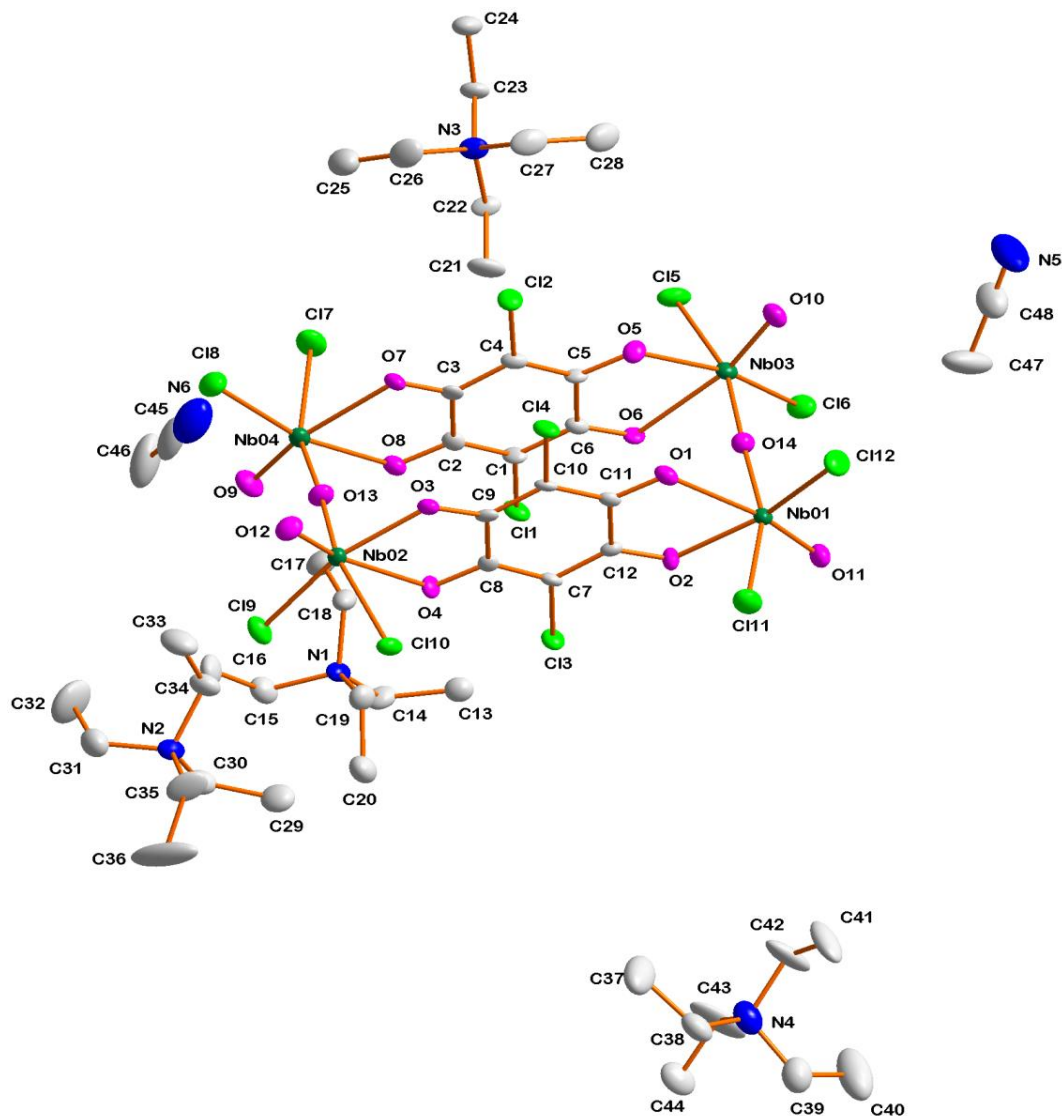
Figure 5.10 Tetranuclear structure of $(Et_4N)_4[Nb_4O_4(ca)_2(\mu^2\text{-}O)_2Cl_8]\cdot 2CH_3CN$ (**6**) showing the atom numbering. Thermal ellipsoids are drawn at the 50% probability level and only hydrogen atoms are omitted for clarity.
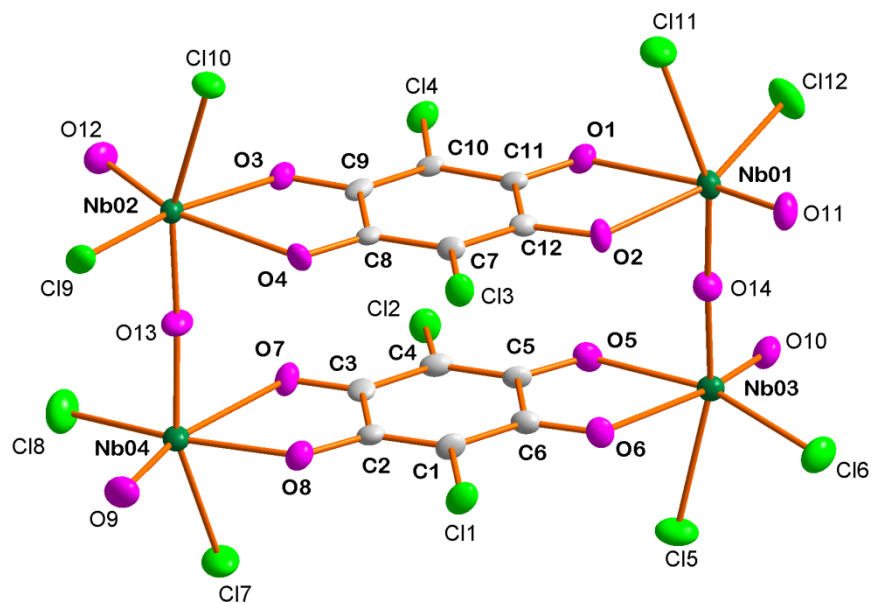
Figure 5.11 Tetranuclear structure of the $[Nb_4O_4(ca)_2(\mu^2\text{-}O)_2Cl_8]^{4-}$ anion of (**6**) with hydrogen atoms, counter ions, and solvated molecules omitted for clarity.

Table 5. 4 Selected bond lengths and angles of $(Et_4N)_4[Nb_4O_4(ca)_2(\mu^2\text{-}O)_2Cl_8]\cdot2CH_3CN$ (**6**).

Bond lengths (Å)			
Nb01-O1	2.381(4)	Nb01-Cl12	2.376(3)
Nb01-O2	2.139(3)	Nb02-Cl9	2.390(3)
Nb01-O11	1.706(2)	Nb02-Cl10	2.461(4)
Nb01-O14	1.920(3)	Nb03-Cl5	2.468(3)
Nb02-O3	2.133(3)	Nb03-Cl6	2.383(3)
Nb02-O4	2.396(4)	Nb04-Cl7	2.449(4)
Nb02-O12	1.728(2)	Nb04-Cl8	2.376(4)
Nb02-O13	1.898(3)	Nb01-Nb02	8.375(2)
Nb03-O5	2.132(3)	Nb01-Nb03	3.820(6)
Nb03-O6	2.391(3)	Nb01-Nb04	9.267(2)
Nb03-O10	1.704(2)	Nb02-Nb04	3.808(2)
Nb03-O14	1.900(3)	Nb02-Nb03	9.130(2)
Nb04-O7	2.402(3)	Nb03-Nb04	8.406(6)
Nb04-O8	2.145(4)	C1-Cl1	1.748(3)
Nb04-O9	1.716(2)	C4-Cl2	1.723(3)
Nb04-O13	1.912(3)	C7-Cl3	1.715(3)
Nb01-Cl11	2.465(4)	C10-Cl4	1.729(3)
Bond angles (°)			
O1-Nb01-O2	70.93(1)	O11-Nb01-Cl12	102.59(2)
O3-Nb02-O4	70.13(1)	O12-Nb02-Cl9	102.42(2)
O5-Nb03-O6	69.93(1)	O10-Nb03-Cl6	103.12(2)
O7-Nb04-O8	69.74(1)	O9-Nb04-Cl8	100.52(2)
O1-Nb01-O14	80.10(1)	Cl12-Nb01-Cl11	88.90(1)
O3-Nb02-O13	89.28(2)	Cl9-Nb02-Cl10	88.50(1)
O6-Nb03-O14	82.73(1)	Cl5-Nb03-Cl6	88.21(1)
O8-Nb04-O13	87.76(2)	Cl7-Nb04-Cl8	89.37(1)

The title tetranuclear niobium(V) complex, $(Et_4N)_4[Nb_4O_4(ca)_2(\mu^2\text{-}O)_2Cl_8]\cdot 2CH_3CN$ (**6**), contains four niobium(V) atoms, separated by two bridging oxido ligands, two bridging chloranilate bidentate ligands, eight terminal chlorido ligands and four terminal oxido ligands (Figure 5.10 and 5.11). Each niobium atom is six coordinated to one bridging oxido, two chlorido ligands and one μ^2-chloranilato ligand, whereas in complex (**5**) the niobium atom is seven coordinated.

The μ-chloranilate ligand forms a five-membered ring with a small bite angle when coordinated to the Nb(V) center in complex (**6**). The O-Nb$_{(n)}$-O bite angles(where n = 1, 2, 3 and 4) of complex (**6**) are 70.93(1)°, 70.13(1)°, 69.93(1)° and 69.74(1)°, respectively with the average O-Nb$_{(n)}$-O bite angle being 70.18(1)° (Table 5.4 and Figure 5.9 and 5.10). In complex (**5**) it was observed the average O-Nb-O bite angle as 72.44(4)°. According to these results, the average O-Nb-O bite angle in complex (**5**) is by account two degree larger than in complex (**6**), assumed to be due to the different coordination modes of the chloranilate dianions ligands (Table 5.2, Figure 5.2, Table 5.4 and Figure 5.10 and 5.11).

The Nb$_{(n)}$-O bond lengths of the μ-chloranilato bidentate ligands in complex (**6**) vary from 2.132(3) Å to 2.402(3) Å with an average of 2.265(3) Å, whereas the average Nb-O bond length of the chloranilato bidentate ligands in complex (**5**) is 2.129(1) Å, which indicate that those in complex (**5**) is significantly shorter than in complex (**6**) (Table 5.2, Figure 5.2, Table 5.4 and Figure 5.10 and 5.11). The average Nb=O bond length in complex (**6**) is 1.714(1) Å, while in complex (**5**) the Nb=O bond length is 1.721(2) Å, which shows it is slightly longer in complex (**5**) than complex (**6**).

The Nb-Nb bond contacts of complex (**6**) vary from 3.808(6) Å to 9.267(2) Å. The C-Cl bond lengths of the μ-chloranilato bidentate ligands in complex (**6**) vary from 1.715(3) Å to 1.748(3) Å with an average of 1.729(3) Å, whereas the average C-Cl bond length of the free caH$_2$ ligand is 1.717(1) Å (Chapter 4 section 4.3), which shows the caH$_2$ free ligand slightly shorter than complex (**6**). Thus, the average C-Cl bond length of complex (5) and complex (6) is the same. As reported in Chapter 4 (sections 4.3-4.4), the C-O bond lengths of free ligand are 1.228(7) Å and 1.317(6) Å, which corresponds to C=O and C-OH respectively.

Comparing the free ligand with the coordinated ligand shows that the average C-O-Nb bond length of the chloranilato bidentate ligands in complex (**5**) is slightly longer than the free ligand, but in complex (**6**) the average C-O-$Nb_{(n)}$ bond length of μ-chloranilato bidentate ligands is 1.260 Å which is slightly shorter than the free caH_2 ligand (Table 4.2, Table 4.4, Table 5.2, Figure 4.2, Figure 4.6, Figure 5.1 and Appendix **B**). Therefore, the effect of the bridging function of the μ^2-chloranilato bidentate ligand causes smaller bite angles as well as an elongation and shortening of bond lengths. All other bond distances and angles are similar to complex (**5**) and other niobium(V) complex structures.

Figure 5.12 illustrates three different type of planes identified in $(Et_4N)_4[Nb_4O_4(ca)_2(\mu^2\text{-}O)_2Cl_8]\cdot2CH_3CN$ (**6**). Plane 1 (**A**) passes through the top of the μ-chloranilate ring, plane 2 (**B**) passes through the bottom of the μ-chloranilate ring and plane 3 (**C**) passes through both the top and bottom of the μ-chloranilate ring. The dihedral angles between the two planes in each representation are 3.6(2)° (**A**), 2.9(5)° (**B**), and 0.8(1)° (**C**), respectively (Figure 5.12).
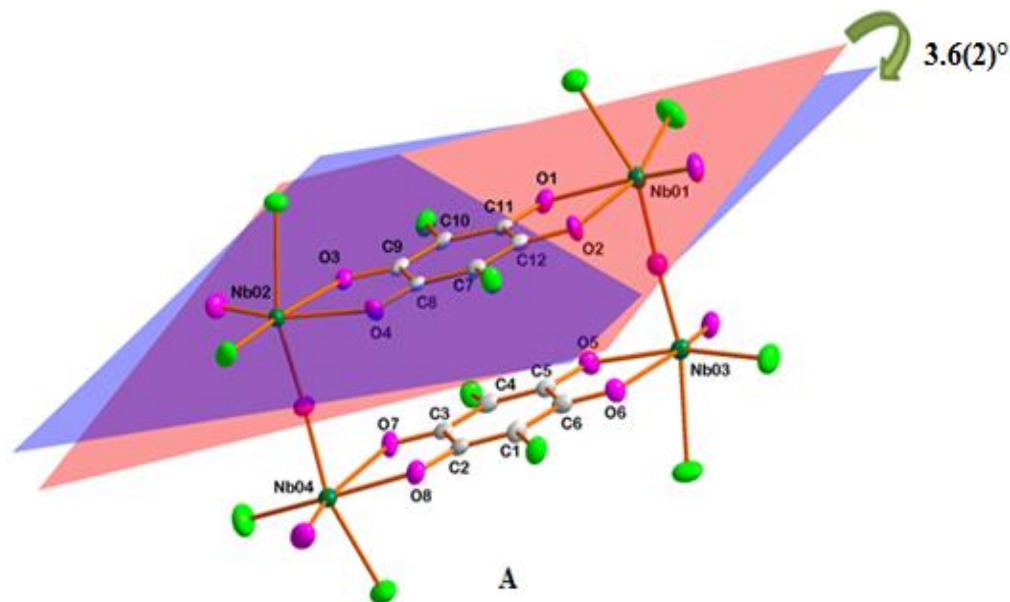
Figure 5.12 (a) Representation of the planes through $[Nb_4O_4(ca)_2(\mu^2\text{-}O)_2Cl_8]^{4-}$ (6), (A) plane 1 (red) passing through the five-membered ring of μ-chloranilate in O1, C11, C12, O2 and Nb01 and plane 2 (blue) passing through the μ-chloranilate ring of C7-C12.
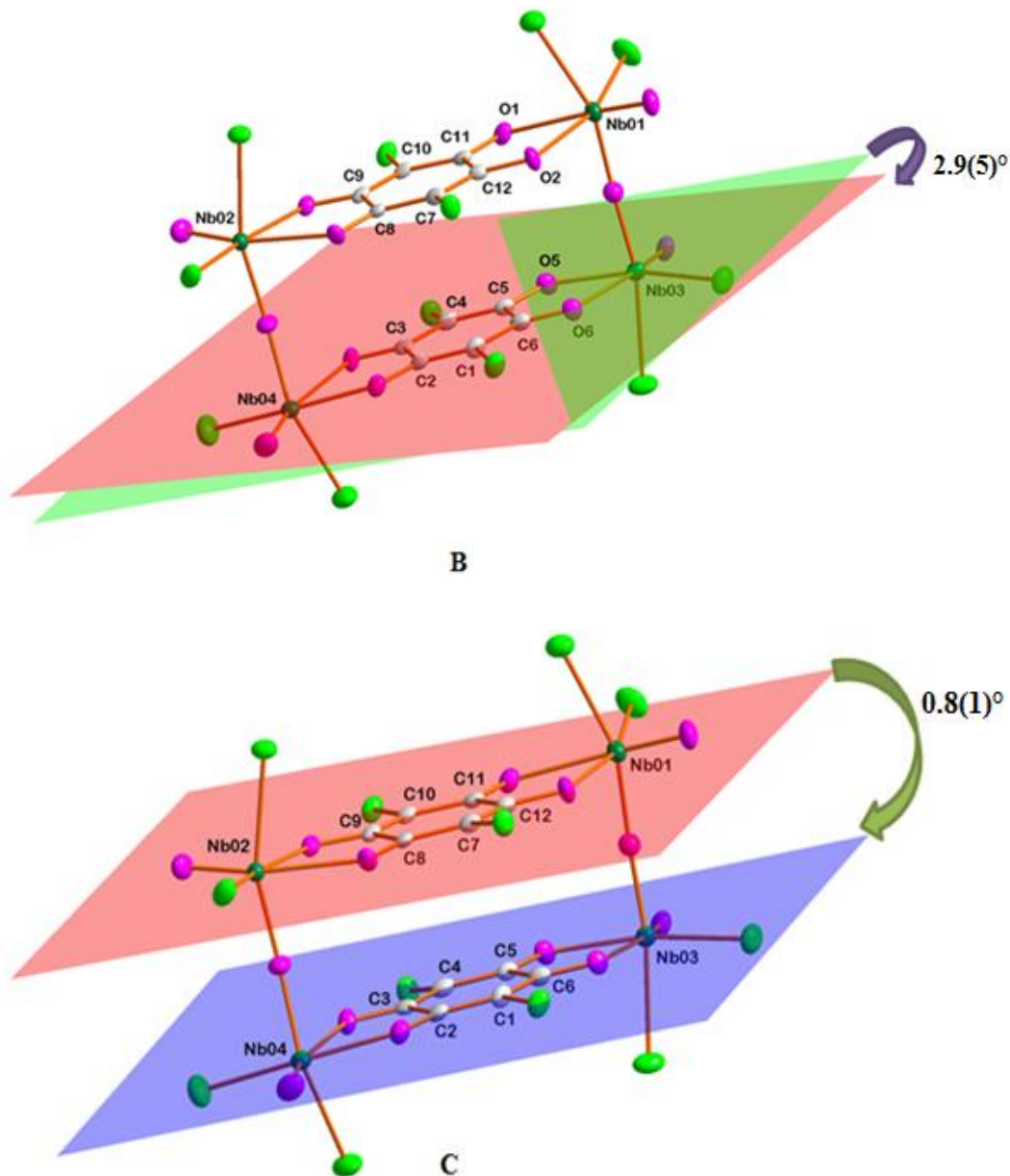
Figure 5.12 (b) Representation of the planes through [Nb$_4$O$_4$(ca)$_2$(μ^2-O)$_2$Cl$_8$]$^{4-}$ (**6**), (**B**) plane 1 (red) passing through the five membered ring of μ-chloranilate in O5, C5, C6, O6 and Nb03 and plane 2 (green) passing through the μ-chloranilate ring of C1-C6; (**C**) plane 1 (red) passing through the top of the μ-chloranilate ring of C7-C12 and plane 2 (blue) passing through the bottom of μ-chloranilate ring of C1-C6. The counter ion, solvated diacetonitrile molecules and H-atoms are omitted for clarity.

A regular octahedral coordination mode of $(Et_4N)_4[Nb_4O_4(ca)_2(\mu^2\text{-}O)_2Cl_8]\cdot 2CH_3CN$ (**6**) (Figure 5.13) is like the coordination modes found in the complex (**5**) unusual[20] for niobium(V) complex structures, as well as for tantalum(V). The crystal system of complex (**6**) is characterised by 13 inter- and intramolecular C-H···Cl and C-H···O hydrogen interactions, as illustrated in Figure 5.16 and listed in Table 5.5.
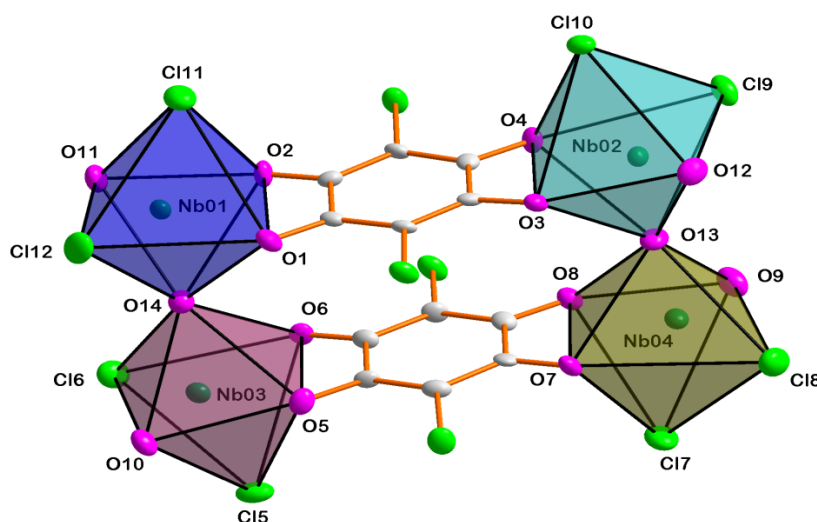
Figure 5.13 Representation of a regular octahedral coordination polyhedron surrounding the Nb(V) atoms of $[Nb_4O_4(ca)_2(\mu^2\text{-}O)_2Cl_8]^{4-}$ (**6**). The counter ion, solvated diacetonitrile molecules and H-atoms are omitted for clarity.

The $(Et_4N)_4[Nb_4O_4(ca)_2(\mu^2\text{-}O)_2Cl_8]\cdot 2CH_3CN$ (**6**) is stabilized by a tetraethylammonium counter-ion, solvated diacetonitrile and there are numerous intra- and intermolecular halogen and hydrogen bonding stabilisation interactions within this molecule. The intermolecular hydrogen bonds also contribute to the stabilization of the crystal lattice. Various different strong halogen (Cl) and hydrogen bonds are observed, with C-H···O and C-H···Cl distances in the range of 2.42 Å to 2.60 Å and 2.35 Å to 2.81 Å respectively (Table 5.5 and Figure 5.16). The crystal packing is reinforced by the formation of an extended network of halogen and hydrogen-bonds as with similar work reported in Chapter 4.

---

[20] T.J. Pannavaia, B.L. Barnett, G. Podolsky, *J. Am. Chem. Soc.*, **97**, 2712-2730, 1975.

Hydrogen and halogen bonds are used as "supramolecular glue" in the construction of these molecular architectures and utilize counter ions and acetonitrile solvent molecules as connectors and/or stabilizers, where efficient hydrogen bonding sites are unavailable between the anion complexes. However, other intermolecular contacts such as π-π interactions (centroid-centroid distance = 3.556(5), 3.506(5), and 3.576(5) Å) (Figure 5.14 and 5.15) also played important roles in controlling the molecular assembly. The tight packing is observed where intermolecular contacts occurred.

Table 5.5 General halogen and hydrogen-bond distances and angles of $(Et_4N)_4[Nb_4O_4(ca)_2(\mu^2-O)_2Cl_8]\cdot2CH_3CN$ (**6**).

Interactions	D-H···A	D-H (Å)	H···A (Å)	D···A (Å)	D-H···A (°)
I	C13-H13B···Cl10[a]	0.98	2.81	3.721(12)	156
II	C14-H14B···O3[b]	0.99	2.60	3.535(14)	158
III	C18-H8A···O9	0.99	2.54	3.288(16)	132
IV	C19-H19B···Cl9	0.99	2.67	3.655(13)	173
V	C22-H22A···O10[c]	0.99	2.42	3.388(14)	167
VI	C34-H34A···Cl9	0.99	2.72	3.568(13)	144
VII	C35-H35B···O11[c]	0.99	2.35	3.060(16)	128
VIII	C41-H41C···Cl7[d]	0.98	2.75	3.715(19)	169
IX	C43-H43A···Cl8[c]	0.99	2.81	3.605(17)	137
X	C46-H46B···Cl8	0.98	2.71	3.650 (2)	161
XI	C46-H46C···Cl11[e]	0.98	2.60	3.574(16)	176
XII	C47-H47B···Cl7[f]	0.98	2.76	3.640(2)	150
XIII	C47-H47B···Cl8[f]	0.98	2.79	3.540(2)	134

Symmetry code: (a) -x + 1, y - ½, - z + ½   (b) x, y -1, z (c), 1- x, y + ½, ½ - z

(d), 1 - x, y + ½ + 1, ½- z (e), x, -y + ½, z - ½ (f), x, -y + ½, z + ½

Figure 5.14 Tetranuclear structure of $[Nb_4O_4(ca)_2(\mu^2\text{-}O)_2Cl_8]^{4-}$ (**6**) anion of with the blue dashed lines indicating π-π stacking interactions between the μ-chloranilate rings (C7-C12 and C1-C6) and five membered rings of μ-chloranilate ligands (Nb02, O3, C9, C8, and O4, and Nb04, O7, C3, C2, and O8, as well as Nb01, O2, C12, C11, and O1, and Nb03, O6, C6, C5, and O5). Hydrogen atoms, counter ions and solvated molecules are omitted for clarity.

Figure 5.14 and 5.15 shows that three different π-π intramolecular interactions or centroid-centroid distances (3.556(5) Å, 3.506(5) Å and 3.576(5) Å) were observed between Nb02, O3, C9, C8, O4 and Nb04, O7, C3, C2, O8 of the five membered rings of μ-chloranilate ligand; the quinone rings of C7-C12 and C1-C6; and Nb01, O2, C12, C11, O1 and Nb03, O6, C6, C5, O5 of the five membered rings of μ-chloranilate ligand respectively. The van der Waal distance of Figure 5.15 is 1.25 Å. The Nb-Nb bond contacts listed in Table 5.4 shows that the average Nb-O-Nb bond distance of 3.814 (2) Å is shorter than the average Nb-ca^{-2}-Nb bond distance of 8.390(2) Å.
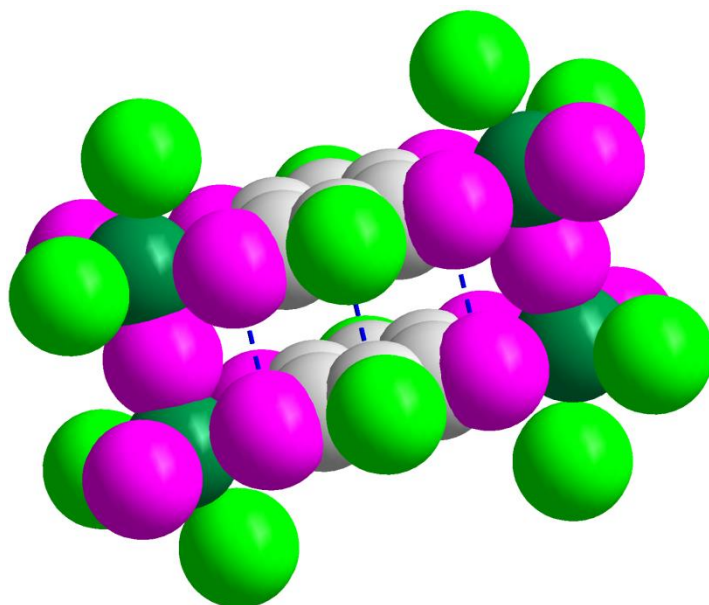
Figure 5.15 Tetranuclear structure of $[Nb_4O_4(ca)_2(\mu_2\text{-}O)_2Cl_8]^{4-}$ (6) presented as space filling model. The blue dashed lines indicating π-π stacking interactions between the μ-chloranilate rings (C7-C12 and C1-C6) and five membered rings of μ-chloranilate ligands (Nb02, O3, C9, C8, and O4 and Nb04, O7, C3, C2, and O8, as well as Nb01, O2, C12, C11, and O1 and Nb03, O6, C6, C5, and O5) (Figure 5.14). Hydrogen atoms, counter ions and solvated molecules are omitted for clarity.
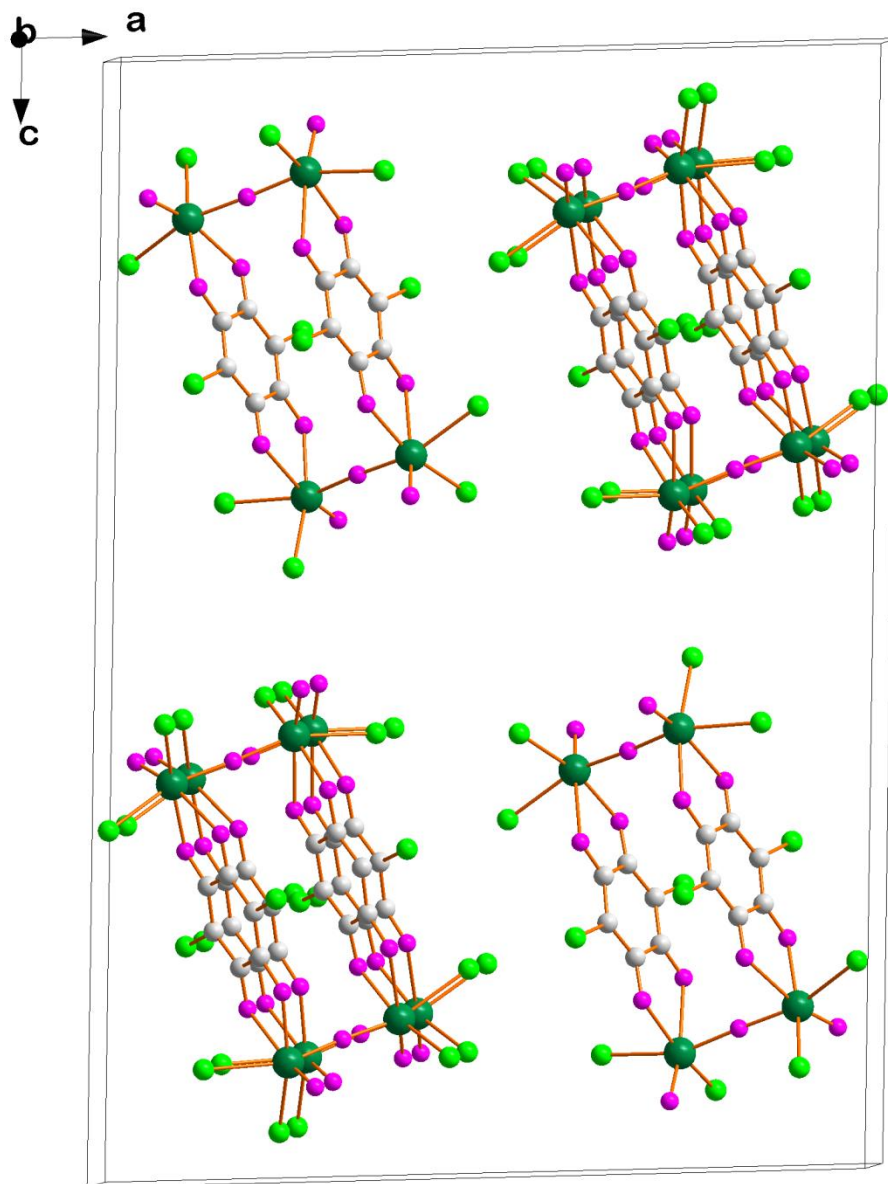
Figure 5.16 Tetranuclear structure of $[Nb_4O_4(ca)_2(\mu^2\text{-}O)_2Cl_8]^{4-}$ anion of (**6**) showing 'sheet-like' crystal packing along the b-axis. H-atoms, counter ions and solvated molecules are omitted for clarity.
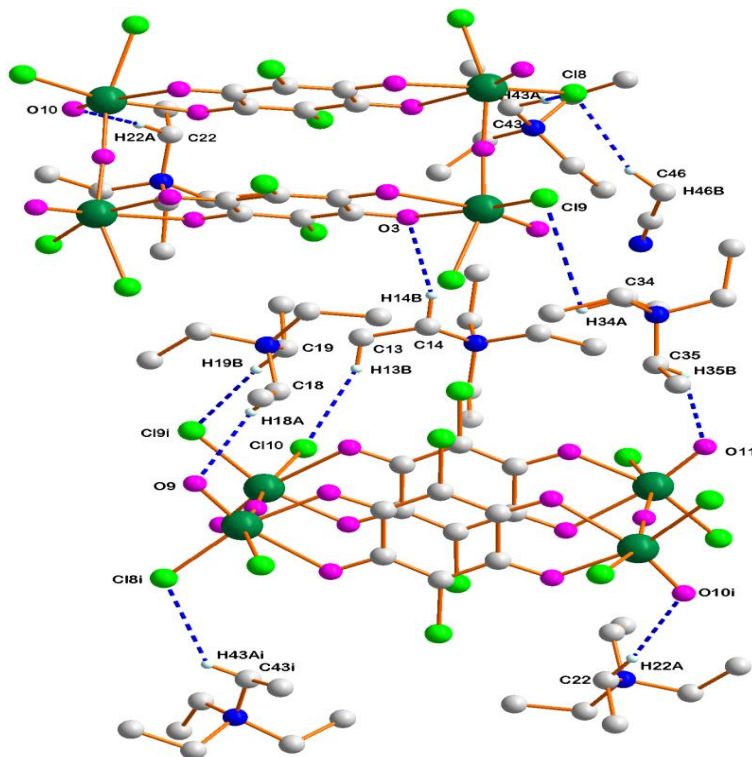
Figure 5.17 Tetranuclear structure of $(Et_4N)_4[Nb_4O_4(ca)_2(\mu^2\text{-}O)_2Cl_8]\cdot 2CH_3CN$ (**6**) showing the intra- and intermolecular interactions. The blue dashed lines indicate C-H···O and C-H···Cl extended halogen and hydrogen-bonds found between its symmetry-generated molecules. The rest of the hydrogen atoms, counter ions and solvated molecules are omitted for clarity [Symmetry codes: Table 5.5].

5.5 Conclusion

In this chapter cis-$(Et_4N)[NbO(ca)_2(H_2O)OPPh_3]\cdot 3H_2O\cdot THF$ (**5**) and $(Et_4N)_4[Nb_4O_4(ca)_2(\mu^2\text{-}O)_2Cl_8]\cdot 2CH_3CN$ (**6**) complexes were successfully characterized by single crystal X-ray diffraction analysis, synthesised complex (**5**) and (**6**) characterization of ^{1}H NMR, ^{13}C NMR and ^{31}P NMR were reported in Chapter 3. These products are fairly air stable in the solid and solution state so as to allow physical measurements and different coordination sites as well as halogen and hydrogen-bonds under environmental conditions were observed. This could be useful in improving the stability of the various niobium(V) complexes, which would allow to further investigation important for the separation of the two metals, Nb(V) and Ta(V).

The small bite angles, the elongation and shorting of bond lengths of complex (**6)** are assumed to be due to the effect of the bridging function of the μ-chloranilate ligand. However, all the bond distances and angles are similar to complex (**5)** and other niobium(V) complex structures.[21] These Nb(V) complexes appear to favour a monoclinic solid state crystal packing system (section 5.3 and 5.4). The steric and electronic properties of the ligands (OPPh$_3$ and caH$_2$) were investigated to evaluate their effect on complex (**5)** and complex (**6)**. However, in spite many efforts, single crystals suitable for X-ray crystallography have not yet been obtained for tantalum(V) complexes, due to the fact that Ta(V) complexes are much less stable than the Nb(V) complexes, which is assumed to be linked to the large tendency of Ta(V) for hydrolysis.

Finally, it is noted that in the last two decades only a small number of O,O'- and N,O-bidentate ligands have successfully been coordinated to Ta(V)- and Nb(V) metal centres and characterized by X-Ray crystallography (as reported in Chapter 2 and 3).[22] These results did not contribute to the knowledge for the separation of niobium from tantalum, because of a different aim of previous studies where metal coordination was more important and ligand effects and stability of products were not considered enough. Due to the hydrolysis of the starting material, novel synthons and stable products are required for the development of potentially improved industrial processes for the separation of Nb(V) and Ta(V) from their mineral ores.

Therefore, as indicated above one of the aims of this project is to investigate the effects of different ligand properties and their coordination on the solution- and solid-state behaviour of tantalum(V) and niobium(V) complexes in an attempt to establish improved methods for the separation of niobium from tantalum at industrial level.

In the next chapter the characterization of the four crystal structures of two Ta(V) complexes and two Nb(V) complexes with different type of ligands hopoH and cupfH will be discussed. A comprehensive evaluation of all the Nb(V) and Ta(V) complexes which form part of this crystallographic study will be presented in later chapters.

---

[21] R. Koen, A. Roodt, H.G. Visser, *Adv. Mat.Res.*, **1019**, 426-432, 2014.

[22] The Cambridge Structural Database, C.R. Groom, I.J. Bruno, M.P. Lightfoot, S.C. Ward, *Acta. Cryst.*, **B72**, 171-179, 2016.

6 X-Ray Crystallographic Studies of Niobium(V) and Tantalum(V) Complexes with O,O'-Bid Ligands

6.1 Introduction

Coordination compounds in which metal centres are bonded to various functional organic ligands (such as O,O'- bidentate ligands), have been attracting different research interests over the past few decades, along with increasing demands for new materials for industrial applications as well as for biological studies. It plays important roles in the purification and identification of metals because most of the metals are not found in the pure state in nature. As was discussed in Chapter 1 bidentate and polydentate ligands that present two or multiple donor atoms for metal bonding provide greater complex stability compared to monodentate analogues due to the chelate effect. This effect can be maximized if the number and size of the chelate rings are optimized for the size of the cation in a way that minimizes steric strain upon metal bonding.[1] The chelate rings form when two donor groups from the same ligand bind to a metal centre and are most favourable for five- and six membered rings. Bidentate and polydentate ligands, however, can induce variable steric strain when ligands contain adjacent five- and six-membered rings.[2] In general, ligands that minimize steric strain in the complex on coordination of the ligand to the metal centre or that reorganise their donor atoms spatially as required for complexation, or both, are preferred for high affinity bonding.[3]

---

[1] A.E. Martell, R.D. Hancock, R.J. Motekaitis, *Coord. Chem. Rev.*, **133**, 39-65, 1994.

[2] A.E. Martell, R.D. Hancock, *Metal Complexes in Aqueous Solution*; Plenum Press: New York, 149-197, 1996.

[3] R.D. Hancock, D.L. Melton, J.M. Harrington, F.C. McDonald, R.T. Gephart, L.L. Boone, S.B. Jones, N.E. Dean, J.R. Whitehead, G.M. Cockrell, *Coord. Chem. Rev.*, **251**(13), 1678-1689, 2007.

Furthermore, the bond lengths, bond angles, intermolecular hydrogen-bonds and number of coordination sites are varied depending on the central metal atom and its oxidation states. However, selecting a good chelating ligand is challenging and an important strategy for this study. Therefore, these physicochemical properties are of utmost importance to establish a more thorough understanding of niobium and tantalum in the most effective, novel and environmental friendly way.

As was mentioned in Chapter 1 and 2, a literature review revealed that only a small number of O,O'- and O,N- donor ligands have been successfully coordinated to niobium(V) and tantalum(V) centers and a few structures were characterized by using single crystal X-Ray diffraction and these how that there is still limited research performed on these two metals.

In this Chapter, for addtional clarification and exploring the physical and chemical difference of four newly synthesised niobium(V) and tantalum(V) complexes with two different O,O'-bidentate ligands, 2-hydroxypyridine N-oxide (hopoH) and cupferron (cupfH), are presented. These Nb(V) and Ta(V) complexes span a range of coordination geometries and are compared with complexes (**5**) and (**6**) from Chapter 5.

The crystal structures of [NbO(cupf)$_3$] (**7**), [NbO(hopo)$_3$]·MeOH (**8**), [TaO(hopo)$_3$]·MeOH (**9**), and [Ta(hopo)$_4$Cl]·2MeCN·2H$_2$O (**10**) were successfully determined using single crystal X-ray diffraction studies and are presented in detail.

6.2 Experimental

The X-ray intensity data was collected on a Bruker X8 Apex II 4K Kappa CCD area detector diffractometer, equipped with a graphite monochromator and MoKα finefocus sealed tube (λ = 0.71073 Å, T = 100(2) K and 298(2) K) operated at 2.0 kW (50 kV, 40 mA). The initial unit cell determinations and data collections were done by the APEX2[4] software package.

---

[4] Bruker Apex2 (Version 2011.4-1). Bruker AXS Inc., Madison, Wisconsin, USA, 2011.

The collected frames were integrated using a narrow-frame integration algorithm and reduced with the Bruker SAINT-Plus and XPREP software packages[5] respectively. Analysis of the data showed no significant decay during the data collection. The data was corrected for absorption effects using the multi-scan technique SADABS,[6] and the structure was solved by the direct method package SIR 97[7] and refined using the WinGX[8] software incorporating SHELXL.[9] The final anisotropic full-matrix least-squares refinement was done on F^2.

All H-atoms were positioned in geometrically idealized positions and refined using the riding model with fixed C-H distances for aromatic C-H of 0.93 Å (C-H) [U_{iso} (H) = 1.2 U_{eq}], for methyl C-H of 0.96 Å (C-H) [U_{iso}(H) = 1.5 U_{eq}], for methylene C-H of 0.97 Å (C-H) [U_{iso} (H) = 1.5 U_{eq}], for methine C-H of 0.98 Å (C-H) [U_{iso} (H) = 1.5 U_{eq}]. Non-hydrogen atoms were refined with anisotropic displacement parameters. The graphics were done using the DIAMOND[10] program with 50% probability ellipsoids for all non-hydrogen atoms. A summary of crystal data and refinement parameters for all four complexes are presented in Table 6.1, while a complete list of atomic coordinates, equivalent isotropic parameters, bond distances and anisotropic displacement parameters and hydrogen coordinates for each individual dataset is given in Appendix **C**. All CIF files were checked for errors using the free on-line Checkcif service provided by the International Union of Crystallography.[11]

---

[5] Bruker SAINT-Plus Version 6.02 (including XPREP), *Bruker AXS Inc. Area-Detector Integration Software*, Madison, Wisconsin, USA, 2012.

[6] Bruker SADABS Version 2004/1. *Bruker AXS Inc. Area Detector Absorption Correction Software,* Madison, Wisconsin, USA, 1998.

[7] A. Altomare, M.C. Burla, M. Camalli, G.L. Cascarano, C. Giacovazzo, A. Guagliardi, A.G.G. Moliterni, G. Polidori, R. Spagna, *J. Appl. Cryst.*, **32,** 115-119, 1999.

[8] L.J. Farrugia, *J. Appl. Cryst.*, **45**, 849-854, 2012.

[9] G.M. Sheldrick, SHELXL, *Acta Crystall., **C71**, 3-8, 2015.

[10] K. Brandenburg, H. Putz, *DIAMOND*, Release 3.0e, Crystal Impact GbR, Bonn, Germany, 2006.

[11] Available on the web at http://www.iucr.org/acs/ checkcif.html. Accessed in 2015, 2016.

Table 6.1 Summary of crystal data and refinement parameters of [NbO(cupf)$_3$] (**7**), [NbO(hopo)$_3$]·MeOH (**8**), [TaO(hopo)$_3$]·MeOH (**9**), and [TaO(hopo)$_4$Cl]·2MeCN·2H$_2$O (**10**).

Identification code	(7)	(8)	(9)	(10)
Empirical formula	C$_{18}$H$_{15}$N$_6$O$_7$ Nb	C$_{16}$H$_{16}$N$_3$O$_8$ Nb	C$_{16}$H$_{16}$N$_3$O$_8$Ta	C$_{24}$H$_{26}$ClN$_6$O$_{10}$Ta
Formula weight	520.27	471.23	559.27	774.91
Temperature (K)	100(2)	100(2)	100(2)	100(2)
Wavelength (Å)	0.71073	0.71073	0.71073	0.71073
Crystal system, space group	Monoclinic, $P2_1/c$	Monoclinic, $P2_1/c$	Monoclinic, $P2_1$	Triclinic, $P\bar{1}$
Unit cell dimensions				
a (Å)	13.070(4)	8.2630(8)	8.294(4)	9.682(2)
b (Å)	10.165(3)	11.043(1)	11.097(6)	12.324(3)
c (Å)	15.109(4)	19.080(2)	9.532(5)	13.339(3)
α (°)	90.00	90.00	90.00	81.063(6)
β (°)	92.20(1)	98.373(4)	97.86(3)	72.902(6)
γ (°)	90.00	90.00	90.00	82.729(7)
Volume (Å^3)	2005.9(9)	1722.5(3)	869.04(8)	1497.2(6)
Z	4	4	2	2
Density$_{calc}$ (g.cm^{-3})	1.723	1.817	2.137	1.719
μ (mm^{-1})	0.656	0.753	6.378	3.822
F(000)	1048	952	540	764
Crystal size (mm)	0.327 x 0.362 x 0.769	0.048 x 0.169 x 0.382	0.585 × 0.101 × 0.091	0.230 x 0.259 x 0.497
Theta range (°)	2.85 to 28.00	3.98 to 27.99	3.06 to 27.99	2.64 to 28.00
Index ranges	-17≤ h ≤ 17	-10 ≤ h ≤ 10	-10 ≤ h ≤ 9	-12 ≤ h ≤ 12
	-13 ≤ k ≤ 11	-11 ≤ k ≤ 14	-14 ≤ k ≤ 14	-16 ≤ k ≤ 16
	-19 ≤ l ≤ 16	-25≤ l ≤ 25	-12 ≤ l ≤ 12	-14 ≤ l ≤ 17
Reflections collected/unique	35221/4825	37897/4129	12913/4082	26764/7199
R$_{int}$	0.0506	0.0347	0.0290	0.0401
Completeness (%)	99.7	99.4	99.0	99.5
Max. and min. transmission	0.746, 0.695	0.746, 0.706	0.746, 0.599	0.746, 0.485
Refinement method	Full-matrix least-squares on F^2	Full-matrix least-squares on F^2	Full-matrix least-squares on F^2	Full-matrix least-squares on F^2
Data / restraints / parameters	4825 / 0 / 289	4129 / 2 / 252	4082 / 6 / 166	7199 / 14 / 386
Goodness-of-fit on F^2	1.042	1.037	1.135	1.065
Final R indices [$I>2\sigma(I)$]	$R1 = 0.0318$	$R1 = 0.0522$	$R1 = 0.0394$	$R1 = 0.0484$
	$wR2 = 0.0824$	$wR2 = 0.1239$	$wR2 = 0.0924$	$wR2 = 0.1359$
R indices (all data)	$R1 = 0.0388$	$R1 = 0.0605$	$R1 = 0.0462$	$R1 = 0.0510$
	$wR2 = 0.0876$	$wR2 = 0.1304$	$wR2 = 0.1014$	$wR2 = 0.1398$
$\Delta\rho_{max}$ and $\Delta\rho_{min}$ (e. Å^{-3})	2.371, -0.646	2.186, -3.468	1.988, -1.675	4.337, -5.559

6.3   Crystal structure of tris(N-nitroso-N-phenylhydroxylaminato-k^2O,O')oxido niobium(V), [NbO(cupf)₃] (7)

The ammonium salt of N-nitroso-N-phenylhydroxylamine is used to synthesise different metal complexes, and the ligand (cupfH) forms stable complexes with various metallic ions.[12] [NbO(cupf)₃] (**7**) crystallises in the monoclinic space group, $P2_1/c$, with four molecules in the unit cell. In Figure 6.1, the DIAMOND representation of the cupferrate complex (**7**) is shown with 50% ellipsoid probability and the atom numbering system shown. This crystal structure will be compared to other crystal structures later presented in this chapter. Important bond distances and angles as well as hydrogen bonds for the cupferrate complex (**7**) are listed in Table 6.2 and 6.3.
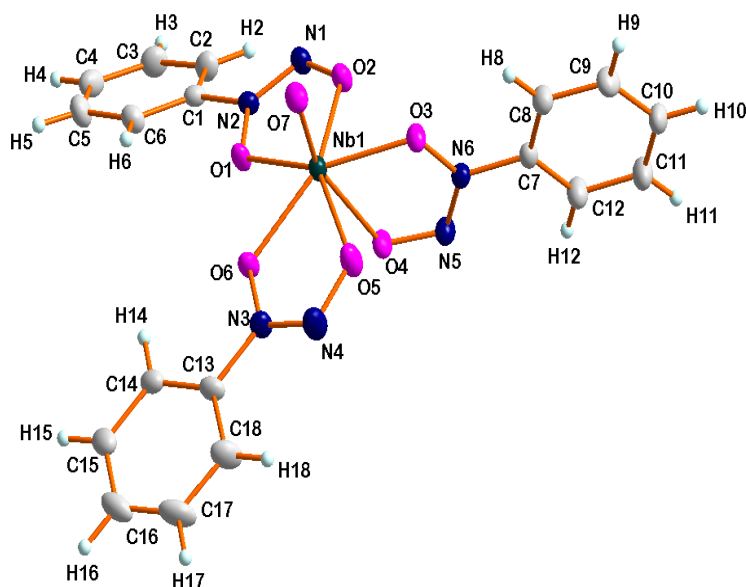
Figure 6.1 Molecular structure of [NbO(cupf)₃] (**7**) showing the atom numbering system with the thermal ellipsoids drawn at the 50% probability level.

Table 6.2 Selected bond lengths and angles of cupferrate [NbO(cupf)$_3$] (**7**).

Bond lengths (Å)			
Nb1-O1	2.081(6)	N1-O2	1.294(3)
Nb1-O2	2.159(7)	N2-O1	1.334(4)
Nb1-O3	2.085(7)	N3-O6	1.325(4)
Nb1-O4	2.227(7)	N4-O5	1.296(3)
Nb1-O5	2.162(6)	N5-O4	1.295(4)
Nb1-O6	2.097(5)	N6-O3	1.328(4)
Nb1-O7	1.711(5)	C1-N2	1.433(4)
N1-N2	1.270(3)	C13-N3	1.442(3)
N3-N4	1.269(4)	C7-N6	1.436(5)
N5-N6	1.284(3)		
Bond angles (°)			
O1-Nb1-O2	69.41(2)	O7-Nb1-O3	88.49(2)
O3-Nb1-O4	70.04(2)	O7-Nb1-O6	103.85(2)
O5-Nb1-O6	69.02(1)	O7-Nb1-O2	96.89(2)
O1-Nb1-O6	68.36(2)	O6-N3-N4	119.92(3)
O2-Nb1-O3	75.07(2)	O1-N2-N1	120.18(3)
O4-Nb1-O5	80.91(2)	O3-N6-N5	121.95(4)
O6-Nb1-O2	135.99(1)	O4-Nb1-O7	158.52(2)
O1-Nb1-O3	143.67(2)	O5-Nb1-O2	148.34(2)

Red block crystals of [NbO(cupf)$_3$] (**7**) crystallise after a few days from a methanol/

tetrahydrofuran (4:3) reaction solution at 255 K containing the synthon of (Et$_4$N)[NbCl$_6$] and

(cupfH).[13] The niobium atom is heptacoordinated by six oxygen atoms of three bidentate

cupferrate ligands and an oxido ligand. The oxido ligand occupies the axial position. Two

chelating cupferrate ligands lies fully in the equatorial plane, with the third cupferrate ligand

---

[13] A.N. Belay, R. Koen, J.A. Venter, R.M. Drost, *Z.kristallogr. NCS*, **231**(2), 513-515, 2016.

coordinated with one oxygen in equatorial plane and the other oxygen in the axial position, trans to the oxido ligand (Figure 6.1).

The cupferrate ligands in [NbO(cupf)$_3$] (**7**) form five-membered rings with small bite angles. The O-Nb-O bite angles of the three cupferrate ligands in complex (**7**) are 69.41(2)°, 70.04(2)° and 69.02(2)° with the average O-Nb-O bite angle being 69.49(4)° (Figure 6.1 and Table 6.2). Complexes (**5**) and (**6**) were reported in Chapter 5 subsection 5.3 and 5.4 with average O-Nb-O bite angles of 72.44(4)° and 70.18(1)° (Table 5.2, Figure 5.1 Table 5.4, and Figure 5.10) respectively. The average O-Nb-O bite angle of the cupferrate ligands in complex (**7**) is 2.95° and 0.69° smaller than that of complex (**5**) and complex (**6**) respectively, with five-membered rings formed by the bidentate ligands in all cases.

The Nb-O bond lengths vary from 2.081(6) Å to 2.227(7) Å with the average Nb-O bond lengths being 2.135(6) Å. The Nb-O bond lengths of the nitroso aminato part of the (Nb1-O1, Nb1-O3 and Nb1-O6) with average of 2.088(6) Å is significantly shorter than the Nb-O distances of the nitroso aminato part of the (Nb1-O2, Nb1-O4 and Nb1-O5) with average of 2.183(6) Å. The N-O bond lengths vary from 1.294(3) Å to 1.334(4) Å with the average N-O bond lengths being 1.312(4) Å. The N-O bond lengths of nitroso aminato part of the (N1-O2, N4-O5 and N5-O4) with average of 1.295(3) Å is significantly shorter than the N-O distances of the other nitroso aminato part of the (N2-O1, N3-O6 and N6-O3) with average of 1.329(4) Å, due to influence of strong oxido ligand (Figure 6.1 and Table 6.2). The Nb1-O7 bond distance is the shortest of all Nb-O bonds at 1.711(5) Å. The trans bond angles of O6-Nb1-O2, O1-Nb1-O3, O4-Nb1-O7 and O5-Nb1-O2 are 135.99(1)°, 143.67(2)°, 158.52(2)°, and 148.34(1)° respectively (Table 6.2 and Figure 6.1).

The average Nb-O bond lengths of 2.135(6) Å in the complex (**7**) is slightly longer than the Nb-O distances of complex (**5**) with average of 2.128(1) Å and shorter than the Nb-O distances of complex (**6**) with average of 2.265(2) Å (Chapter 5, Table 5.2 and 5.4).
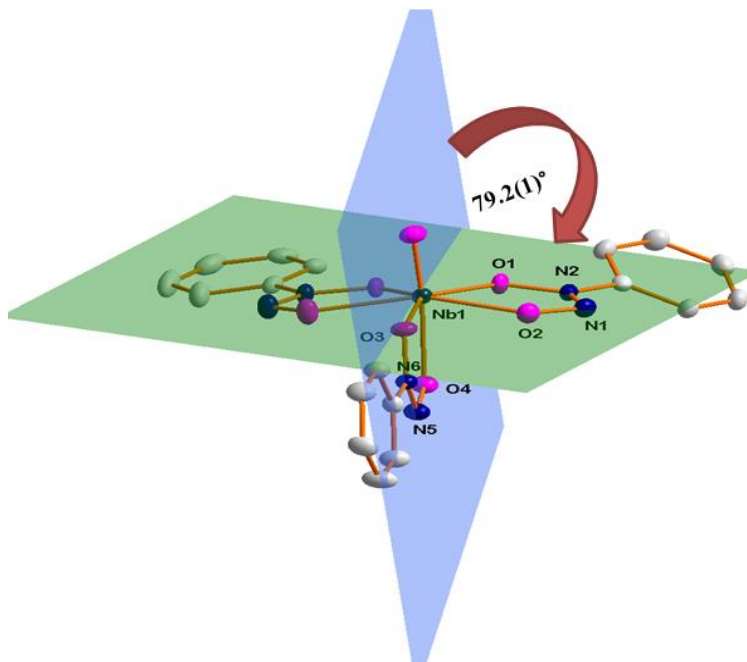
Figure 6.2 Representation of planes through [NbO(cupf)$_3$] (**7**), plane 1 (green) passing through the five membered ring of cupferrate in O1, N2, N1 and O2 and plane 2 (blue) passing through the five membered ring of cupferrate in O4, N5, N6 and O3. H-atoms are omitted for clarity.

Figure 6.2 illustrates the cupferrate complex (**7**) with three coordinated cupferrate ligands, two in the equatorial plane (green) and one in the axial position, as well as the oxido ligand which is also found in axial position. The intersection of the two planes formed by the five membered ligand rings, plane 1 (green) passing through O1, N2, N1 and O2 and plane 2 (blue) passing through O4, N5, N6 and O3 run through the Nb(V) centre. The dihedral angle between the two planes is 79.2(1)°.

Shown in Figure 6.3, a plane (blue) was constructed through the five atoms O1, O2, O3, O5 and O6. The distance between the blue plane and the oxido ligand O7 is 1.946(6) Å. The niobium metal centre is slightly elevated above this plane by 0.235(6) Å. This illustrates the distorted D_{5h} pentagonal bipyramidal geometry of the molecule, indicated by strong oxido ligand (Nb1-O7 distance of 1.711(5) Å), compared to the significantly elongated Nb-O4 distance of 2.227(7) Å (Table 6.2).

It was reported in Chapter 5 that the niobium metal centre in complex (**5**) is slightly elevated above the plane by 0.219(3) Å (Figure 5.3), significantly less than the 0.235(6) Å (Figure 6.3) that was observed in complex (**7**). Both cases illustrate that slightly distorted D_{5h} pentagonal bipyramidal geometry of the molecules, mainly because of the strong oxido bond.
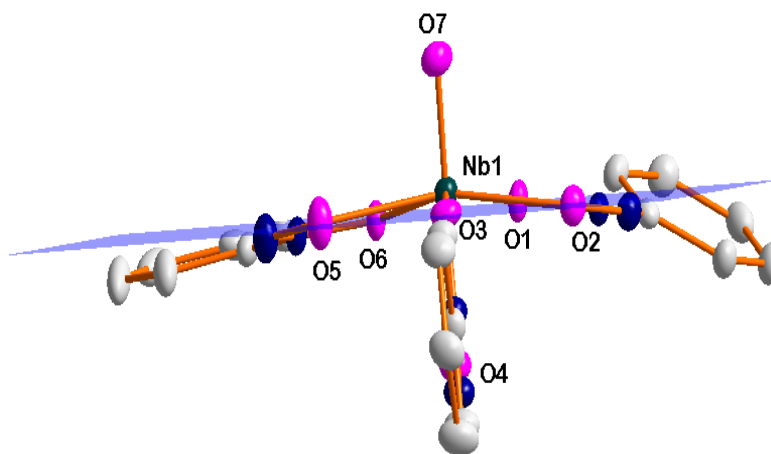
Figure 6.3 Representation of [NbO(cupf)$_3$] (**7**). The blue plane constructed through the five oxygen atoms O1, O2, O3, O5 and O6 illustrates the distance between the plane and O7.

Figure 6.4 illustrates the D_{5h} pentagonal bipyramidal coordination mode of [NbO(cupf)$_3$] (**7**) with the same geometry as complex (**5**) (Chapter 5 Figure 5.4). A regular octahedral geometry is observed with complex (**6**) (Chapter 5 Figure 5.13). This difference may have the potential to lead to a separation of niobium from tantalum. Figure 6.5 shows the packing of [NbO(cupf)$_3$] (**7**) in a unit cell.
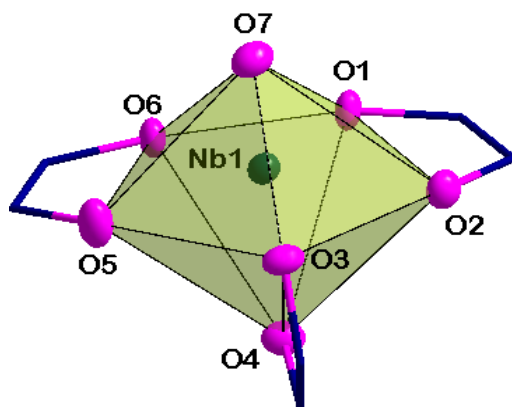
Figure 6.4 Representation of the D_{5h} pentagonal bipyramidal coordination polyhedron surrounding the Nb(V) atom of [Nb(cupf)₃] (**7**).
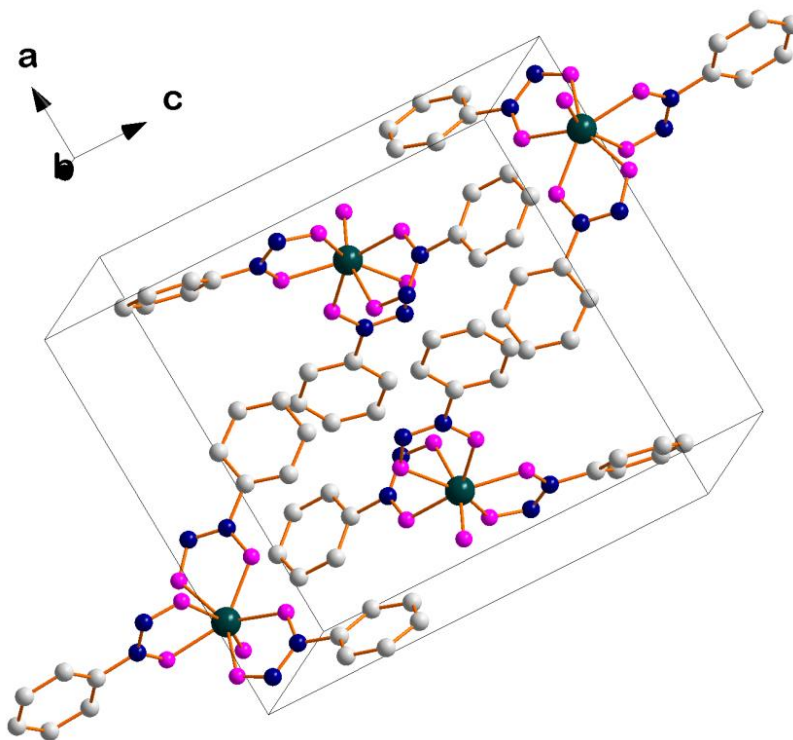
Figure 6.5 Packing structure of [NbO(cupf)₃] (**7**) showing four molecules per unit cell. H-atoms are omitted for clarity.

Figure 6.6 and 6.7 illustrates the molecular structure of [NbO(cupf)$_3$] (**7**), showing head to tail π-π stacking interactions [centroid-centroid distance = 3.926(2) Å] between two phenyl rings on C13-C18 and C7i-C12i obtained by symmetry generated procedures.

The [NbO(cupf)$_3$] (**7**) crystal system is characterised by 4 inter- and intramolecular C-H$_{...}$O hydrogen interactions, as illustrated in Figure 6.8 and Table 6.3.

Table 6.3 General hydrogen-bond distances and angles of [NbO(cupf)$_3$] (**7**).

Interactions	D-H···A	D-H (Å)	H···A (Å)	D···A (Å)	D-H···A(°)
I	C5-H5···O7ii[a]	0.93	2.51	3.357(4)	151
II	C8-H8···O3	0.93	2.37	2.695(3)	100
III	C14-H14···O6	0.93	2.42	2.738(3)	100
IV	C16-H16···O6i[b]	0.93	2.53	3.413(4)	159

Symmetry code: (a) x, -y + ½, z -½ (b) -x + 1, y + ½, -z +3/2

Figure 6.6 Molecular structure of [NbO(cupf)$_3$] (**7**) showing head to tail packing along b-axis. H-atoms are omitted for clarity.
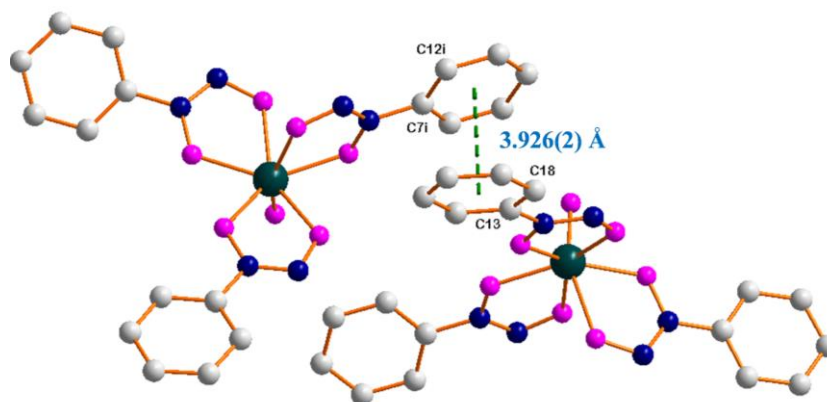
Figure 6.7 Molecular structure of [NbO(cupf)$_3$] (**7**) with the green dashed lines indicating head to tail π-π stacking interactions between two phenyl rings on C13-C18 and C7i-C12i. Hydrogen atoms are omitted for clarity.

Figure 6.8 show the weak inter- and intramolecular hydrogen-bond interactions of [NbO(cupf)₃] (**7**), with C-H⋯O distances in the range of 2.366 Å to 2.531 Å (Table 6.3).
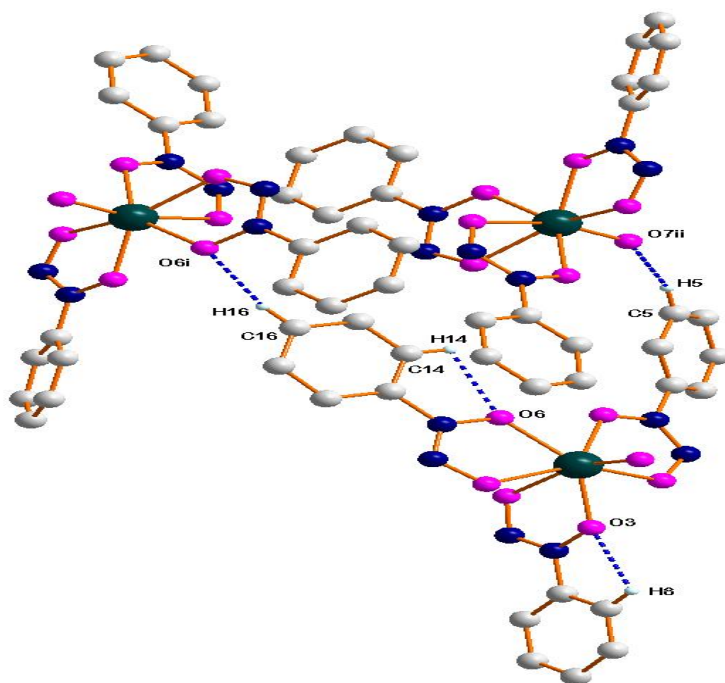
Figure 6.8 Intra- and intermolecular interactions of [NbO(cupf)₃] (**7**). The blue dashed lines indicate important C-H⋯O hydrogen-bonds found between symmetry generated molecules [Symmetry codes: Table 6.3].

6.4 Crystal structure of tris(2-hydroxypyridinato-N-oxide-κ^2O,O')oxidoniobium(V), methanol solvate, [NbO(hopo)₃]·MeOH (8)

[NbO(hopo)₃]·MeOH (**8**) crystallises in the monoclinic space group, $P2_1/c$, with four Nb molecular compounds and MeOH solvate molecules in the unit cell. Figure 6.9 shows the DIAMOND representation of complex (**8**) with ellipsoid probability at 50% and the atom numbering system shown. The solvated methanol molecule found in complex (**8**) displays a 65:35 positional disorder at C02B, and C02A, as well as at O8B and O8A. Moreover, this was found to be DFIX restrained to a target value, the distance between C02A and O8A is fixed at

1.60 Å and the distance between C02B and O8B is fixed at 1.20 Å to best fit the experimental electron density in Shelx-97.

2-Hydroxypyridine-N-oxide (hopoH) (Scheme **A**) ligands represent an interesting class of pyridine derivatives. The chelating properties of hopoH exhibits a hydroxamate function where the nitrogen atom is integrated in the heterocycle and have been previously reported to be an efficient chelator of different metal ions.[14,15,16] Furthermore, 1-hydroxy-6-N-octylcarboxamido-2(1H)-pyridinone (octyl-hopoH) (Figure 6.9 (**B**)) has been demonstrated as an effective ligand and extractant for the selective complexation of lanthanides in traditional solvent extraction processes.[17,18,19]

(A)   (B)
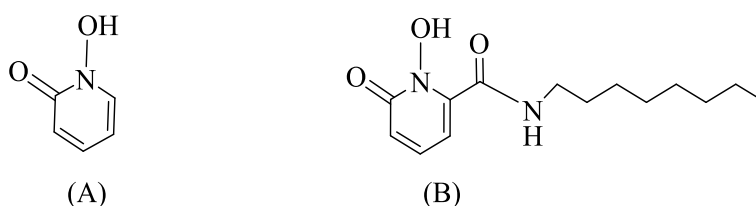
Figure 6.9 Molecular structure of hopoH (**A**) and octyl-hopoH (**B**).

In this section the investigation of various crystal structures of new Nb(V) and Ta(V) complexes with the 2-hydroxypyridine-N-oxide (hopoH) ligand, such as [NbO(hopo)$_3$]·MeOH (**8**), [TaO(hopo)$_3$]·MeOH (**9**), and [Ta(hopo)$_4$Cl]·2MeCN·2H$_2$O (**10**) are presented. This ligand coordinates to Nb(V) and Ta(V) metal centres with different ligand: metal stoichiometry ratios. Crystallographic analyses shown the formation of two types of coordination modes (Figure 6.10, 6.19 and 6.27). Important bond distances and angles as well as hydrogen-bonds for complex (**8**) are listed in Table 6.4 and 6.5.

[14] E. Farkas, E. Enyedi, H. Csoka, *J. Inorg. Biochem.*, **79**, 205-211, 2000.

[15] P.J. Sun, Q. Fernando, H. Freiser, *Anal. Chem.,* **36**, 2485-2486, 1964.

[16] J.L. Yue, A.E. Martell, *Inorg. Chim. Acta,* **214**, 103-111, 1993.

[17] E.G. Moore, J. Xu, C.J. Jocher, I. Castro-Rodriguez, K.N. Raymond, *Inorg. Chem*., **47**, 3105-3118, 2008.

[18] K.N. Raymond, J. Xu, E.G. Moore, E.J. Werner, *Luminescent 1-hydroxy-2-pyridinone chelates of lanthanides*, US Patent, US8557601(**B2**), 2013.

[19] V.V. Romanovski, D.J. White, J. Xu, D.C. Hoffman, K..N. Raymond, *Solvent Extr. Ion. Exch.,* **17**, 55-71, 1999.

(**A**)

(**B**)
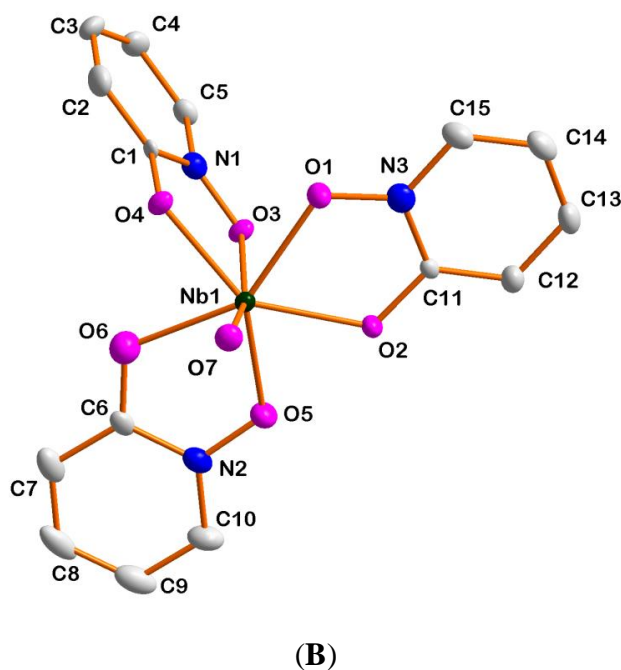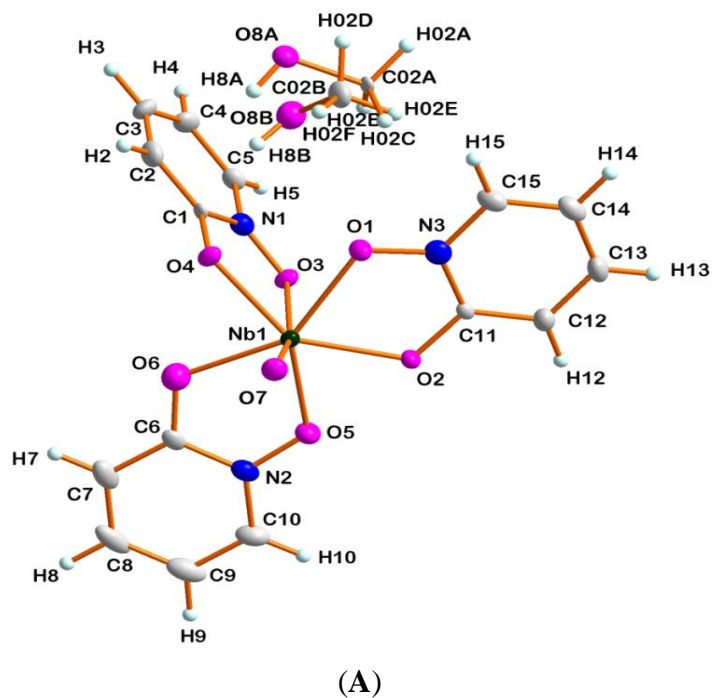
Figure 6.10 Molecular structure of [NbO(hopo)$_3$]·MeOH (**8**) (**A**) showing the atom numbering system with the thermal ellipsoids drawn at a 50% probability level. In (**B**) the atom numbering system is shown with the solvated molecule and hydrogen atoms omitted for clarity.

Table 6. 4 Selected bond lengths and angles of [NbO(hopo)$_3$]·MeOH (**8**).

Bond lengths (Å)			
Nb1-O1	2.169(2)	N2-O5	1.332(1)
Nb1-O2	2.103(1)	N3-O1	1.311(1)
Nb1-O3	2.200(2)	C1-O4	1.339(1)
Nb1-O4	2.089(2)	C6-O6	1.308(1)
Nb1-O5	2.102(1)	C11-O2	1.334(1)
Nb1-O6	2.161(2)	C1-N1	1.367(1)
Nb1-O7	1.722(1)	C6-N2	1.358(1)
N1-O3	1.295(1)	C11-N3	1.354(1)
Bond angles (°)			
O1-Nb1-O2	71.60(3)	O4-Nb1-O6	74.26(3)
O3-Nb1-O4	73.19(3)	O7-Nb1-O1	92.04(4)
O5-Nb1-O6	71.54(3)	O7-Nb1-O3	164.23(4)
O1-Nb1-O3	83.24(4)	O7-Nb1-O5	100.79(3)
O2-Nb1-O5	67.05(3)	O6-Nb1-O2	137.19(4)
O5-Nb1-O1	138.57(5)	O2-Nb1-O4	141.92(3)

The niobium atom in [NbO(hopo)$_3$]·MeOH (**8**) is heptacoordinated by six oxygen atoms of three bidentate 2-hydroxypyridinate-N-oxide ligands and an oxido ligand. Two chelating 2-hydroxypyridinate-N-oxide ligands are positioned in the equatorial plane, while the third ligand occupies the remaining axial position. The oxido ligand occupies an axial position, which is similar to complex (**7**) (Figure 6.2 and 6.11), but the Nb=O bond distance of complex (**8**) (1.722(1) Å) is slightly longer than that of complex (**7**) (1.711(5) Å).

The bidentate hopoH ligand in [NbO(hopo)$_3$]·MeOH (**8**) forms a five-membered ring with a small bite angle and the O-Nb-O bite angles of complex (**8**) are 71.60(3)°, 73.19(3)° and 71.54(3)° with the average O-Nb-O bite angle being 72.11(3)° (Figure 6.10 and Table 6.4). This value is larger than that observed in the cupferrate complex (**7**) with the average O-Nb-O bite

angle of 69.49(4)°. Complex (**6**) was reported in Chapter 5 (section 5.4 and 5.3) with an average O-Nb-O bite angle of 70.18(1)° (Table 5.4 and Figure 5.10), slightly smaller than that of complex (**5**) with an average O-Nb-O bite angle of 72.44(4)° (Table 5.2 and Figure 5.1). A Five-membered rings was formed by the bidentate ligands in all cases. The trans bond angles of O6-Nb1-O2, O5-Nb1-O1 and O2-Nb1-O4 are 137.19(4)°, 143.67(2)°, 138.57(5)°, and 141.92(3)° respectively (Table 6.4 and Figure 6.9).

The Nb-O bond lengths in complex (**8**) vary from 2.089(2) Å to 2.200(2) Å with an average Nb-O bond length of 2.137(2) Å (Figure 6.10 and Table 6.4). This is nearly the same as the average Nb-O bond lengths of complex (**7**) with an average of 2.135(6) Å, slightly longer than the Nb-O distances of complex (**5**) with average of 2.128(1) Å and significantly shorter than the Nb-O distances of complex (**6**) with an average of 2.265(2) Å. The N-O bond lengths in complex (**8**) range from 1.295(1) Å to 1.332(1) Å with the average N-O bond lengths of 1.313(1) Å, significantly shorter than the N-O bond lengths of the free ligand (1.384(3) Å) (Chapter 4 Figure 4.11 and table 4.6). The C-O bond length range from 1.308(1) Å to 1.339(1) Å with an average C-O bond length of 1.327(1) Å (Figure 6.8 and Table 6.5), significantly longer than the C-O bond length of the free ligand (1.262(3) Å). In [NbO(hopo)$_3$]·MeOH (**8**), the average N-O bond length of 1.313(1) Å is slightly shorter than the average C-O bond length of 1.327(1) Å.
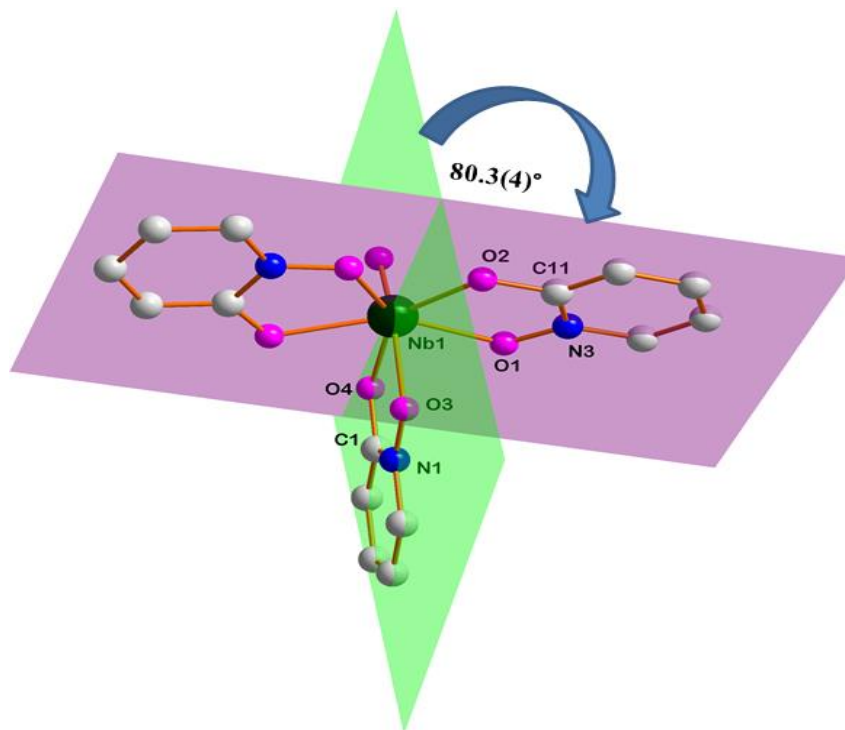
Figure 6.11 Representation of planes through [NbO(hopo)₃] (**8**): plane 1 (violet) passing through the four atoms O2, C11, N3 and O1 and plane 2 (green) passing through the four atoms O3, N1, C1 and O4. Hydrogen atoms and solvated methanol molecule are omitted for clarity.

Figure 6.10 illustrates that [NbO(hopo)₃]·MeOH (**8**), like the cupferrate complex (**7**), has the same coordination mode, three bidentate 2-hydroxypyridinate-n-oxide ligands (hopoH), two in the equatorial plane (violet) and one in the axial position (green), as well as the oxido ligand that occupies the axial position. The two planes such as plane 1 (violet) and plane 2 (green) intersect at the Nb(V) centre. The intersection of the two planes formed by the four atoms of the five-membered ring of hopoH ligands, plane 1(violet) passing through O2, C11, N3 and O1 and plane 2 (green) passing through O3, N1, C1 and O4 runs through the Nb(V) center. The dihedral angle between two planes are 80.3(4)°, which is close to the 79.2(1)° for complex (**7**).

Shown in Figure 6.12 is a plane (blue) that was constructed through the five atoms O5, O6, O4, O1 and O2. The distance between the blue plane and O7 is 1.935(3) Å. The niobium metal centre

is slightly elevated above this plane by 0.213(2) Å. This illustrates the distorted C_3v-capped octahedral (CO) geometry of the molecule, due to a short oxido ligand distance of 1.722(1) Å.

The elevation of the niobium metal centre above the plane by 0.219(3) Å (Chapter 5 Figure 5.3) in complex (**5**) is slightly shorter than the same elevation of 0.235(6) Å (Figure 6.3) in complex (**7**). However, in complex (**8**) the niobium metal centre was slightly elevated above the plane by 0.213(3) Å, nearly the same as in complex (**5**), but significantly shorter than in complex (**7**). Complexes (**5**) and (**7**) are examples of a distorted D_{5h} pentagonal bipyramidal geometry of the molecules, while complex (**8**) illustrates a distorted C_3v-capped octahedral (CO) geometry of the molecule. In all cases the distortion of geometry could be attributed mainly to a short oxido ligand distance.
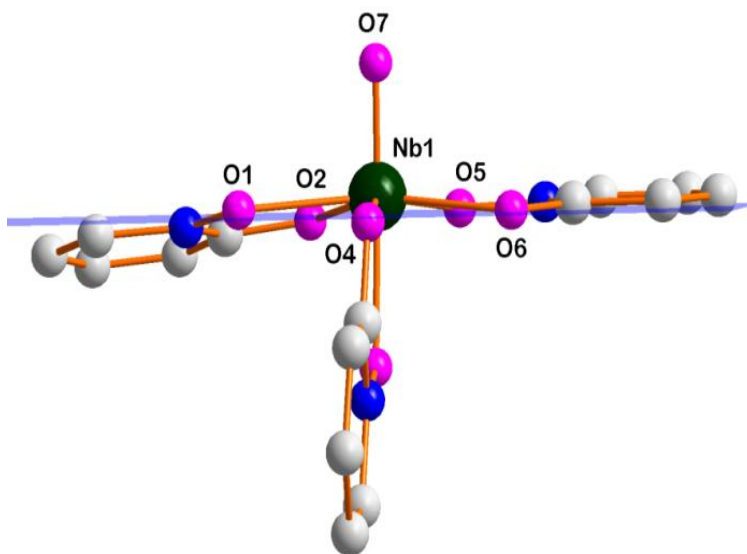
Figure 6.12 Representation of [NbO(hopo)$_3$] (**8**) with a plane (blue) constructed through the five atoms O5, O6, O4, O1 and O2, illustrating the distance between the blue plane and O7. Hydrogen atoms and solvated methanol molecule are omitted for clarity.
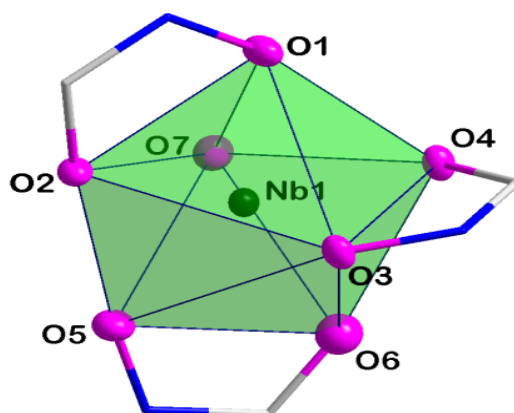
Figure 6.13 Representation of the C_{3v}-capped octahedral coordination polyhedron surrounding the Nb(V) atom of [NbO(hopo)₃] (**8**). Hydrogen atoms and solvated methanol molecule are omitted for clarity.

The C_{3v}-capped octahedral (CO) geometry is next to the D_{5h} pentagonal bipyramidal coordination mode, the second most common representation of the seven-coordinate geometries encountered for larger metal centres (e.g. lanthanides and actinides).[20,21] However, this type of geometry has not been encountered for any tantalum or niobium metal centres before.[20]

With [NbO(hopo)₃]·MeOH (**8**), a C_{3v}-capped octahedral geometry coordination mode has observed (Figure 6.13) and this geometry is different from those observed in complexes (**7**) and (**5**) (D_{5h} pentagonal bipyramidal) (Figure 6.4 and 5.4) as well as in complex (**6**) (a regular octahedral coordination mode) (Figure 5.13). These different geometries observed in complexes (**5**), (**6**), (**7**), and (**8**), may have the potential to be used in future to separate niobium from tantalum.

---

[20] C.S. Erasmus, J.C.A. Boeyens, *J. Cryst. Mol. Struct.*, **1**, 83-87, 1971.

[21] A. Zalkin, D.H. Templeton, D.G. Karraker, *Inorg. Chem.*, **8**, 2680-2689, 1969.
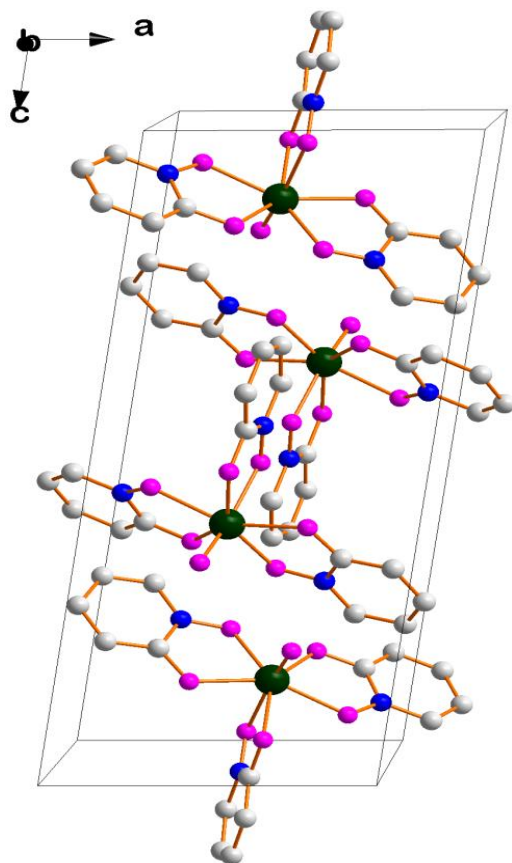
Figure 6.14 Molecular packing of [NbO(hopo)$_3$] (**8**) showing four molecular formula in the unit cell. H-atoms and solvated methanol molecules are omitted for clarity.

The [NbO(hopo)$_3$]·MeOH (**8**) crystal structure is characterised by 7 intermolecular C-H···O hydrogen interactions, as illustrated in Figure 6.15 and 6.16 and presented in Table 6.5.

Table 6.5 General hydrogen-bond distances and angles of [NbO(hopo)₃]·MeOH (**8**).

Interactions	D-H···A	D-H(Å)	H···A(Å)	D···A(Å)	D-H···A(°)
I	C2v-H2v···O6iv[a]	0.95	2.32	3.252(6)	166
II	C5-H5···O2ii[b]	0.95	2.53	3.374(5)	148
III	C02B-H02F···O8B[c]	0.98	2.14	3.013(9)	148
IV	C8-H8···O7i[d]	0.95	2.55	3.287(5)	135
V	C9-H9···O8B[e]	0.95	2.53	3.229(8)	130
VI	C14-H14···O3iii[f]	0.95	2.53	3.247(5)	132
VII	C14-H14···O3iii[g]	0.95	2.54	3.365(5)	146

Symmetry code: (a) -x + 1, -y, -z + 1, (b) -x + 1, -y + 1, -z + 1, (c) -x + 2, -y, -z + 1, (d) x -1, y, z, (e) x-1, -y + ½, -z + ½, (f) x + 1, y, z,(g) -x + 2, -y + 1, -z + 1.

Figure 6.15 Molecular structure of [NbO(hopo)₃] (**8**) showing head to tail intermolecular interactions. The blue dashed lines indicate C-H···O hydrogen-bonds [Symmetry codes: Table 6.5]. H-atoms and solvated methanol molecules are omitted for clarity.
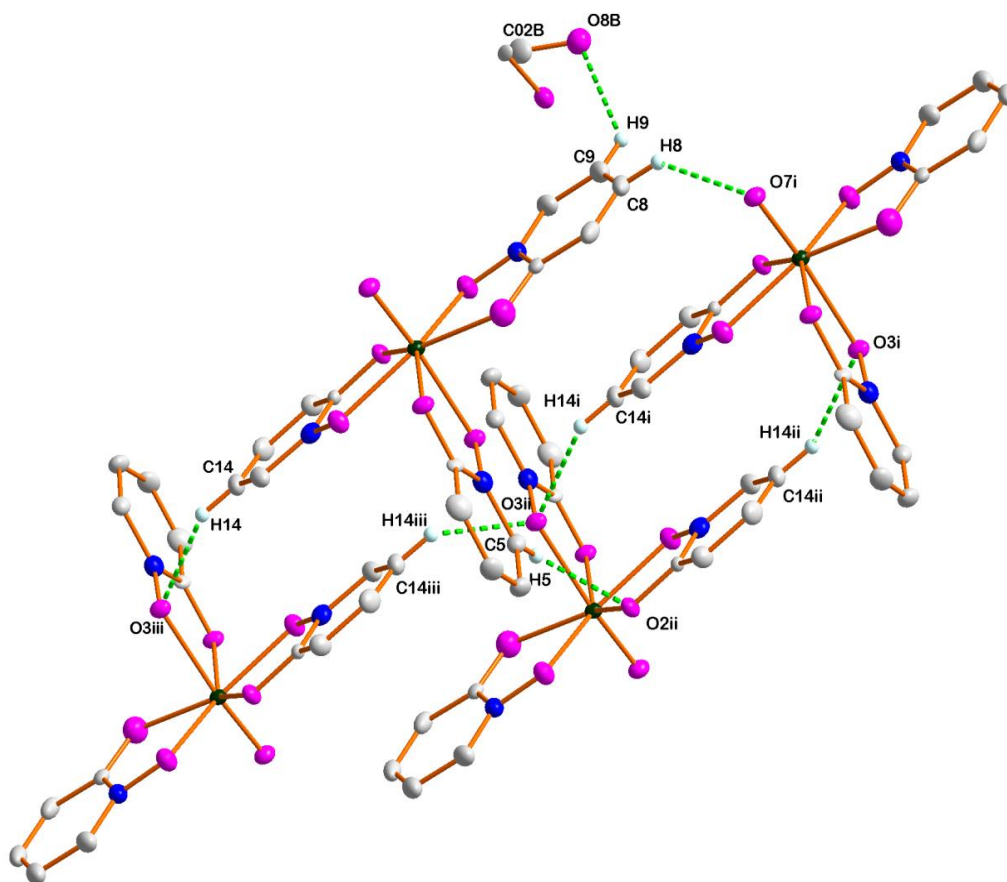
Figure 6.16 Molecular structure of [NbO(hopo)$_3$]·MeOH (**8**) showing the network of infinite intermolecular H-interactions. The green dashed lines indicate C-H···O hydrogen-bonds [Symmetry codes: Table 6.5]. H-atoms and solvated methanol molecule are omitted for clarity.

In [NbO(hopo)$_3$]·MeOH (**8**) (Figure 6.17 and 6.18), both head to head [centroid-centroid distance = 3.450(2) Å] π-π stacking interactions were observed between two 2-hydroxypyridinate-N-oxide rings on N2-C10 and N3i-C15i as well as head to tail [centroid-centroid distance = 3.538(2) Å] π-π stacking interactions between two 2-hydroxypyridinate-N-oxide rings on N3i-C15i and N3ii-C15ii respectively obtained by symmetry generated procedures and the network of infinite intermolecular hydrogen-bonds, which are C-H···O distances in the range of 2.140-2.540 Å as reported in Table 6.5 (Figure 6.15 and 6.16).
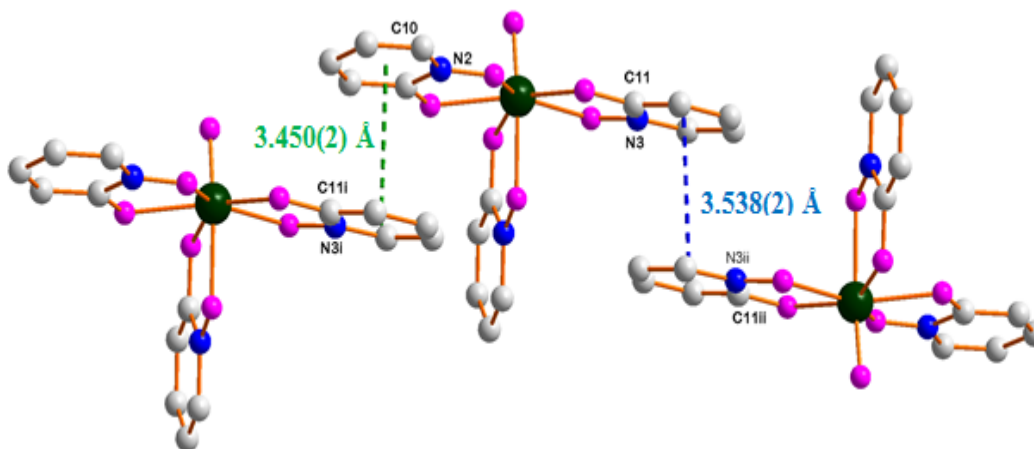
Figure 6.17 Molecular structure of [NbO(hopo)₃] (**8**) showing the green dashed lines which indicate head to head and the blue dashed lines indicating head to tail π-π stacking interactions between two 2-hydroxypyridinate-N-oxide rings on N2-C10 and N3i-C15i; N3i-C15i and N3ii-C15ii respectively. Hydrogen atoms and solvated methanol molecules are omitted for clarity.
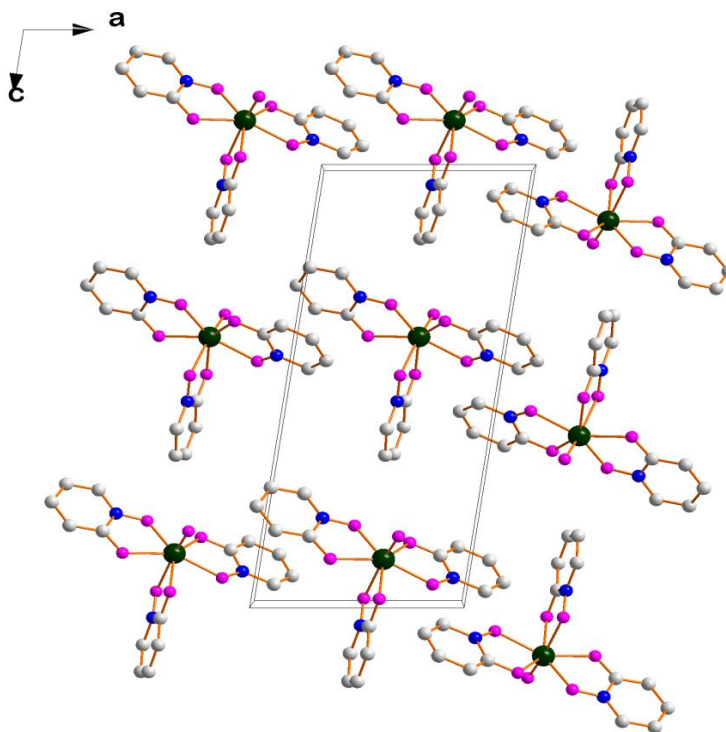
Figure 6.18 Molecular structure of [NbO(hopo)$_3$]·MeOH (**8**) showing head to head and head to tail packing along b-axis. H-atoms and solvated methanol molecules are omitted for clarity.

6.5 Crystal structure of tris(2-hydroxypyridinato-N-oxide-κ^2O,O')oxidotantalum(V), methanol solvate, [TaO(hopo)$_3$]·MeOH (9)

[TaO(hopo)$_3$]·MeOH (**9**) crystallises in the monoclinic space group, $P2_1$, with two molecular formula in the unit cell. In Figure 6.19, a representation of complex (**9**) is given with ellipsoid probability at 50% and atom numbering system shown. The solvated methanol molecule found in the structure of complex (**9**) displays a 60:40 positional disorder at O01A, and O01B. When DFIX restrained to a target value, the distance between C9 and O01A is fixed at 2.10 Å, the distance between C01 and O01A fixed at 1.50 Å, the distance between C01 and O01B fixed at 1.35 Å, the distance between O01A and O01B fixed at 1.10 Å as well as the distance between O01A and C9 fixed at free to best fit the experimental electron density in Shelx-97. Important bond distances and angles as well as hydrogen-bonds for the complex (**9**) are listed in Table 6.6 and 6.7.
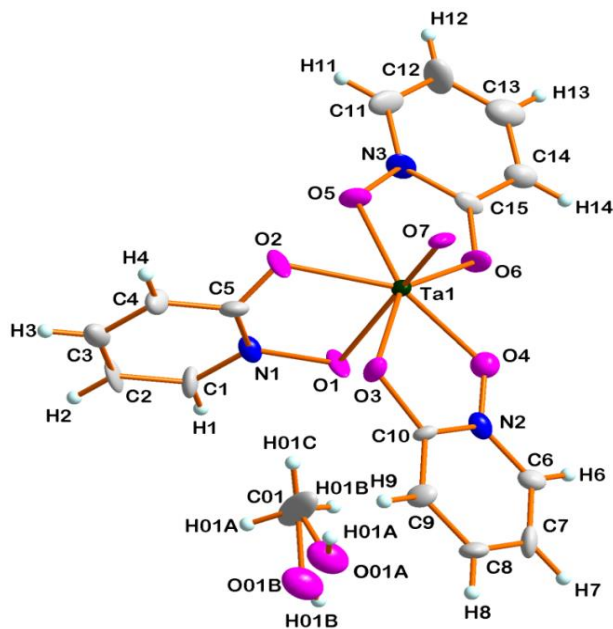
(**A**)
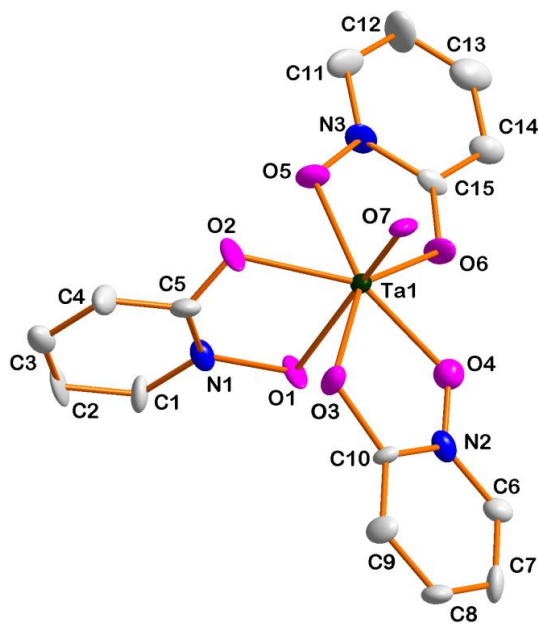
(**B**)

Figure 6.19 Molecular structure of [TaO(hopo)$_3$]·MeOH (**9**) (**A**) showing the atom numbering system. The thermal ellipsoids are drawn at a 50% probability level. In (**B**) the atom numbering system is shown with the solvated molecule and hydrogen atoms omitted for clarity.

Table 6.6 Selected bond lengths and angles of [TaO(hopo)$_3$]·MeOH (**9**).

Bond lengths (Å)			
Ta1-O1	2.092(1)	N2-O4	1.324(1)
Ta1-O2	2.155(1)	N3-O5	1.342(1)
Ta1-O3	2.153(1)	C5-O2	1.173(1)
Ta1-O4	2.107(1)	C10-O3	1.496(1)
Ta1-O5	2.146(1)	C15-O6	1.296(1)
Ta1-O6	2.105(1)	C5-N1	1.390(1)
Ta1-O7	1.725(1)	C10-N2	1.390(1)
N1-O1	1.539(1)	C15-N3	1.413(1)
Bond angles (°)			
O1-Ta1-O2	73.43(1)	O4-Ta1-O6	66.24(1)
O3-Ta1-O4	77.08(2)	O7-Ta1-O1	160.90(2)
O5-Ta1-O6	71.76(2)	O7-Ta1-O3	87.58(2)
O1-Ta1-O3	73.95(2)	O7-Ta1-O5	93.50(2)
O2-Ta1-O5	61.75(2)	O6-Ta1-O2	129.74(2)
O5-Ta1-O4	136.47(2)	O2-Ta1-O4	146.88(2)

The tantalum atom in [TaO(hopo)$_3$]·MeOH (**9**) is heptacoordinated by six oxygen atoms of three bidentate 2-hydroxypyridinate-N-oxide ligands (hopoH) and an oxido ligand. The oxido ligand occupies an axial position. Two chelating 2-hydroxypyridinate-N-oxide ligands are positioned in the equatorial plane, while the third ligand occupies the remaining axial position. This third ligand is one of slightly disordered over the two oxygen atoms (O1 and O2). The oxido ligand in the axial position, is similar to complex (**7**) (Figure 6.2) and complex (**8**) (Figure 6.11), but the Ta=O bond distance of complex (**9**) (1.725(1) Å) is slightly longer than that of complex (**7**) (1.711(5) Å) and complex (**8**) (1.722(5) Å). However, we found complexes (**8**) and (**9**) to be isomorphs (Figure 6.11 and 6.20).

The bidentate ligand in [TaO(hopo)$_3$]·MeOH (**9**) forms a five-membered ring with a small bite angle. The O-Ta-O bite angles of complex (**9**) are 73.43(1)°, 77.08(2)° and 71.76(2)° with an average O-Ta-O bite angle of 74.09(2)° (Figure 6.18 and Table 6.6). This value is significantly larger than those observed in complex (**7**) with the average O-Nb-O bite angle of 69.49(4)°, and in complex (**8**) with the average O-Nb-O bite angle of 72.11(3)°. In Chapter 5, section 5.4 and 5.3, complex (**6**) with the average O-Nb-O bite angle of 70.18(1)° (Table 5.4 and Figure 5.10) as well as complex (**5**) with the average O-Nb-O bite angle of 72.44(4)°) (Table 5.2 and Figure 5.1) were discussed, with five-membered rings formed by the bidentate ligands in all cases. The trans bond angles of O6-Ta1-O2, O5-Ta1-O4, and O2-Ta1-O4 are 129.74(2)°, 136.47(2)° and 146.88(2)° respectively (Table 6.6 and Figure 6.18).

The Ta-O bond lengths vary from 2.092(1) Å to 2.155(1) Å with an average Ta-O bond length of 2.126(1) Å (Figure 6.19 and Table 6.6). This Ta-O bond length of complex (**9**) is nearly the same as the average Nb-O bond length of complex (**5**) with an average of 2.128(1) Å, but shorter than the Nb-O distances of complex (**6**) with an average of 2.265(2) Å, complex (**7**) with an average of 2.135(6) Å as well as complex (**8**) with an average of 2.137(2) Å.

The N-O bond lengths in complex (**9**) range from 1.324(1) Å to 1.539(1) Å with an average of 1.402(1) Å, significantly longer than the N-O bond lengths of the free ligand (1.384(3) Å) (Chapter 4 Figure 4.11 and table 4.6) and the N-O bond length of complex (**8**) with an average of 1.313(1) Å. The C-O bond lengths in complex (**9**) range from 1.173(1) Å to 1.496(1) Å with the an average of 1.322(1) Å (Figure 6.19 and Table 6.6), significantly longer than the C-O bond length of the free ligand (1.262(3) Å), but slightly shorter than that of complex (**8**) with an average of 1.327(1) Å (Figure 6.10 and Table 6.4).

In [TaO(hopo)$_3$]·MeOH (**9**), the average N-O bond lengths of 1.402(1) Å is longer than the average C-O bond lengths of 1.322(1) Å, whereas in complex (**8**), it is the other way round. In general, the average O-M-O bite angle and M-O bond length (where M = Ta or Nb) of all complexes discussed differed from each other and this illustrates the effects of different O,O'-

bidentate chelating ligands. These different chemical properties could lead to the separation of niobium from tantalum.

Figure 6.20 illustrates that [TaO(hopo)$_3$]·MeOH (**9**), like complex (**7**) and (**8**) has the coordination mode of three coordinated 2-hydroxypyridinate-N-oxide ligands, with two in the equatorial plane (green) and one in the axial position (pink), as well as the oxido ligand occupying the axial position.

The intersection of two planes, plane 1 (green) and plane 2 (pink) runs through the Ta(V) centre. The two planes are formed by four atoms of the five-membered ring of 2-hydroxypyridinate-N-oxide ligands, with plane 1(green) passing through O4, N2, C10 and O3 and plane 2 (pink) passing through O1, N1, C5 and O2.

The dihedral angle between the two planes in complex (**9**) (68.5(1)°) (Figure 6.20) is different from the dihedral angle between the same two planes in complex (**7**) (79.9(2)°) (Figure 6.2) and complex (**8**) (80.3(4)°) (Figure 6.11).
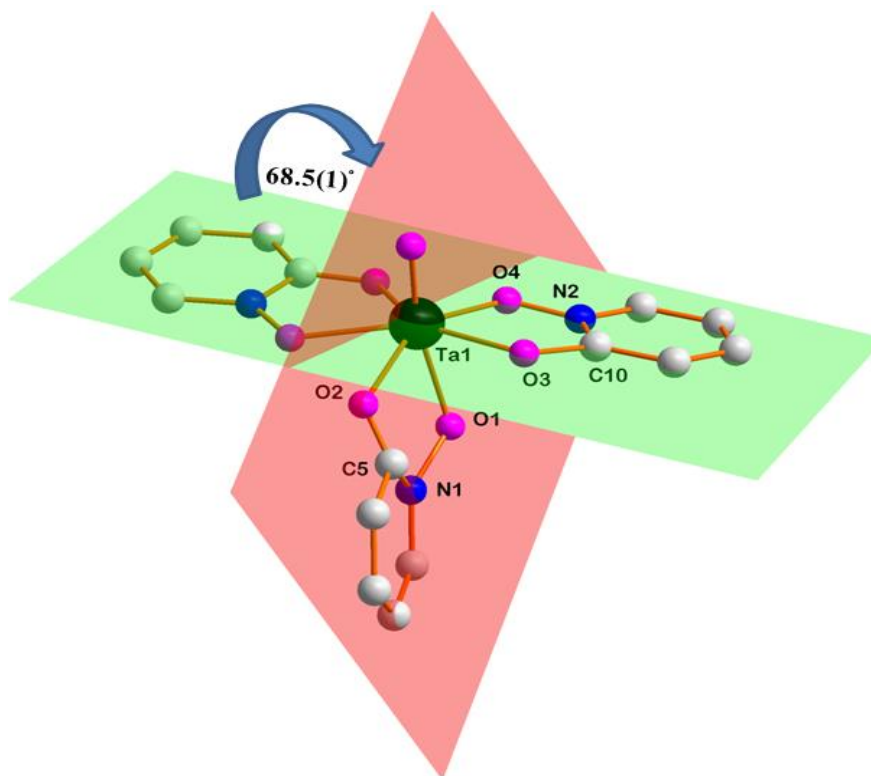
Figure 6.20 Representation of the planes through [TaO(hopo)₃] (**9**). Plane 1(green) passes through the four atoms O4, N2, C10 and O3 and plane 2 (red) passes through the four atoms O1, N1, C5 and O2. H-atoms and solvated methanol molecules are omitted for clarity.

In Figure 6.21 a plane (green) was constructed through the five atoms O3, O4, O2, O5 and O6. The distance between the plane and O7 is 1.986(6) Å. The niobium metal centre is slightly elevated above this plane by 0.261(4) Å. This illustrates the distorted C_2-capped trigonal prismatic geometry of the molecules, due to short oxido ligand bond distance of 1.725(1) Å. The elevation of the niobium metal centre by 0.261(4) Å (Figure 6.21) is slightly more than those observed in complex (**5**) (by 0.219(3) Å, Chapter 5 Figure 5.3) in complex (**7**), (by 0.235(6) Å, Figure 6.3) and in the complex (**8**) (by 0.213(3) Å, Figure 6.12) respectively.
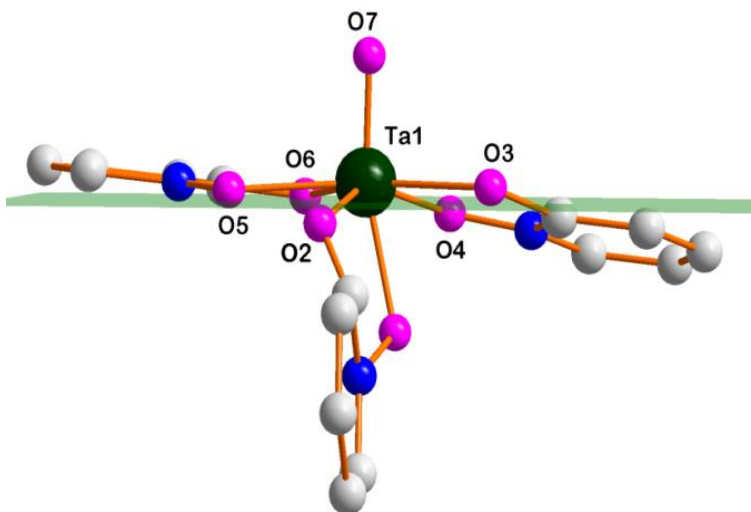
Figure 6.21 Representation of [TaO(hopo)$_3$] (**9**) with the green plane constructed through the five atoms, O3, O4, O2, O5 and O6, illustrating the distance between the plane and O7. H-atoms and solvated methanol molecules are omitted for clarity.
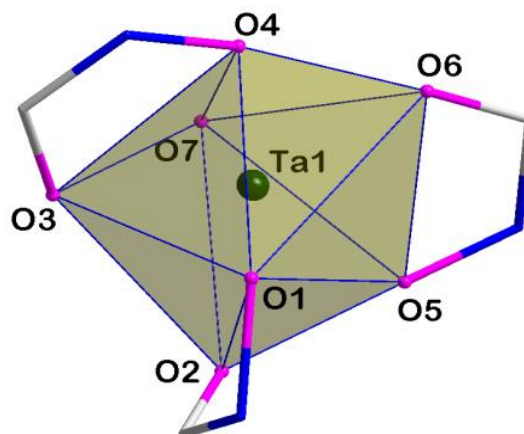
Figure 6.22 Representation of the C_2-capped trigonal prismatic coordination polyhedron surrounding Ta(V) atoms in [TaO(hopo)$_3$] (**9**). H-atoms and solvated methanol molecules are omitted for clarity.

As was discussed in section 6.4, the seven-coordinate [TaO(hopo)$_3$]·MeOH (**9**) has a C_2-capped trigonal prismatic geometry (Figure 6.22), which is a different coordination mode compared to those observed in complexes (**7**) and (**5**) (D_{5h} pentagonal bipyramidal geometry) (Figure 6.4 and

Figure 5.4), complex (**8**) (*C₃v*-capped octahedral geometry) (Figure 6.13) as well as in complex (**6**) (a regular octahedral coordination mode) (Figure 5.13). Therefore, these different geometries found in complex (**5**), (**6**), (**7**), (**8**) and (**9**) describe the shape of complexes with seven oxygen atoms bound to the niobium(V) and tantalum(V) metal centre, and increasing the possibility of a separation of niobium from tantalum and achieving one of the goals of this PhD study.
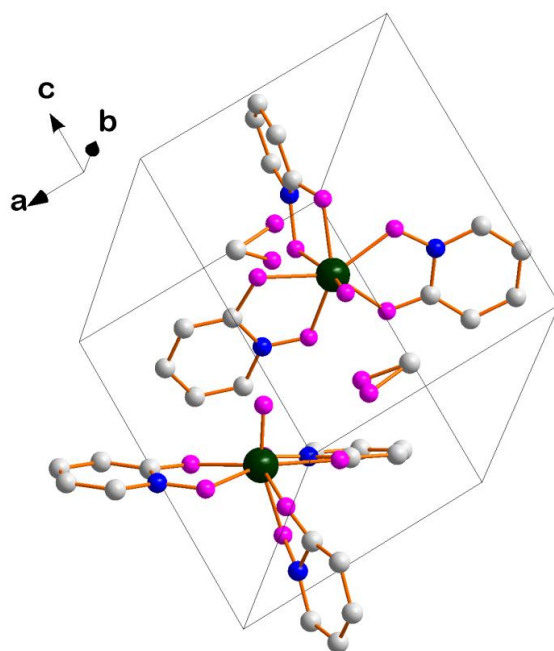
Figure 6.23 Molecular structure of [TaO(hopo)₃]·MeOH (**9**) showing two molecular formula in the unit cell. H-atoms are omitted for clarity.

The [TaO(hopo)₃]·MeOH (**9**) crystal structure is characterised by 4 intermolecular C-H···O hydrogen interactions, as illustrated in Figure 6.24 and listed in Table 6.7.

Table 6.7 General hydrogen-bond distances and angles of [TaO(hopo)₃]·MeOH (**9**).

Interactions	D-H···A	D-H (Å)	H···A (Å)	D···A (Å)	D-H···A (°)
I	C2iii-H2iii···O6ii[a]	0.93	2.30	3.209(5)	166
II	C01ii-H01ii···O3iii[b]	0.96	2.27	3.020(3)	135
III	C8ii-H8ii···O2i[c]	0.93	2.49	3.297(1)	145
IV	C12iv-H12iv···O7iii[d]	0.93	2.55	3.251(6)	133

Symmetry code: (a) x, y, z + 1, (b) x, y, 1 + z, (c) -x + 1, y - ½, -z + 2, (d) x - 1, y, z

Figure 6.24 Molecular structure of [TaO(hopo)₃]·MeOH (**9**) showing the network of intermolecular interactions. The dashed lines indicate C-H···O hydrogen-bonds. H-atoms are omitted for clarity [Symmetry codes: Table 6.7].

As discussed earlier in section 6.4, [NbO(hopo)₃]·MeOH (**8**) have both head to head and head to tail π-π stacking interactions with a centroid-centroid distance of 3.450(2) and 3.538(2) Å

respectively, but [TaO(hopo)$_3$]·MeOH (**9**) has only head to head π-π stacking interactions with a centroid-centroid distance of 3.468(5) Å between the two 2-hydroxypyridinate-N-oxide rings on N2-C10 and N3i-C15i. This indicates a significant difference in the π-π stacking interactions between complex (**9**) (Figure 6.25) and complex (**8**) (Figure 6.17). The implication of this is that the glide plane along c in complex (**8**) is destroyed, leaving only the 2-fold axis. In effect, the unit cell is thereby halved, as manifested in the cell parameters (Table 6.1), *P*2$_1$/c, 4-molecules per unit cell *versus P*2$_1$, 2- molecules per unit cell.

An infinite network of intermolecular hydrogen-bonds was observed, with C-H⋯O distances in the range of 2.300-2.550 Å, as reported in Table 6.7.
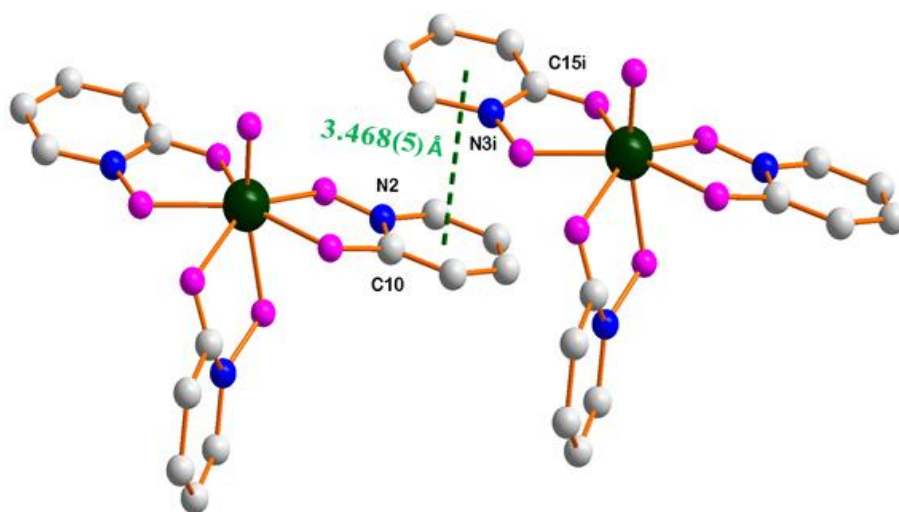
Figure 6.25 Molecular structure of [TaO(hopo)$_3$]·MeOH (**9**) with the dashed lines indicating head to head π-π stacking interactions between two pyridine ring on N2-C10 and N3i-C15i. Hydrogen atoms and solvated methanol molecules are omitted for clarity.
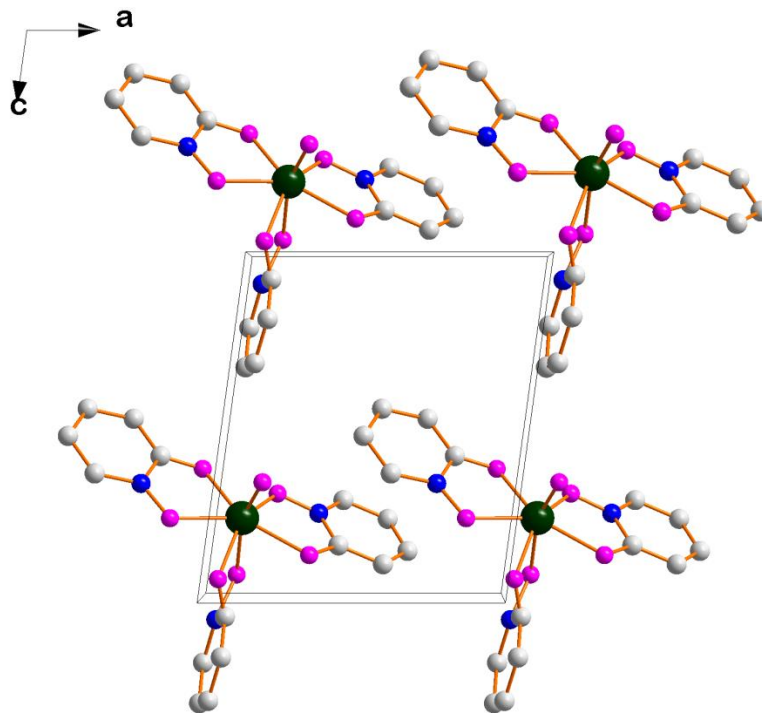
Figure 6.26 Molecular structure of [TaO(hopo)₃]·MeOH (**9**) showing head to head packing along the b-axis. H-atoms and solvated methanol molecules are omitted for clarity.

6.6 Crystal structure of tetrakis(2-hydroxypyridinato-N-oxide-κ^2O,O')tantalum(V) chloride, diacetonitrile and diaqua solvate, [Ta(hopo)₄]Cl·2MeCN·2H₂O (10)

[Ta(hopo)₄]Cl·2MeCN·2H₂O (**10**) crystallises in the triclinic space group, $P\bar{1}$, with two molecular formula units in the unit cell. Figure 6.27 (**B**), shows a representation of complex (**10**) with ellipsoids at the 50% probability level and the atom numbering system. Complex (**10**) is less stable compared to the other complexes and all solvents were found to be disordered. Acetonitrile molecules found to have a static positional disorder at C21B and C21A and C23B and C23A with 82:18 and 89:11 ratios respectively.

These solvated molecules were DFIX restrained to a target value with the distance between (C22 and C21A), (C22 and C21B), (C24 and C23A), and (C24 and C23B) fixed at 1.35 Å, the distance between (O9 and H9A), (O9 and H9B), (O10 and H10A), and (O10 and H10B) fixed at 0.85 Å, the distance between (H9A and H9B) and (H10A and H10B) fixed at 1.40 Å as well as the

177

distance between C24 and N6 is fixed at 0.90 Å to best fit the experimental electron density in Shelx-97. It appeared that the residual electron density is smeared and difficult to refine further, with a fair amount of residual density still observed within the solvent area.

However, the solvated molecules did not significantly affect the bond lengths and bond angles of the crystal structure of complex (**10**). Important bond distances and angles as well as hydrogen-bonds for complex (**10**) are reported in Table 6.8 and 6.9.
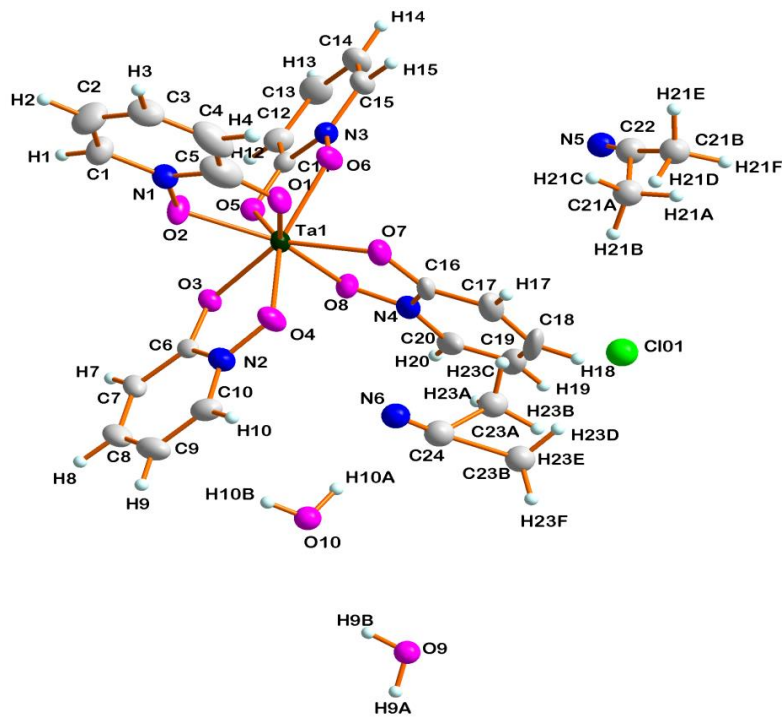
(A)
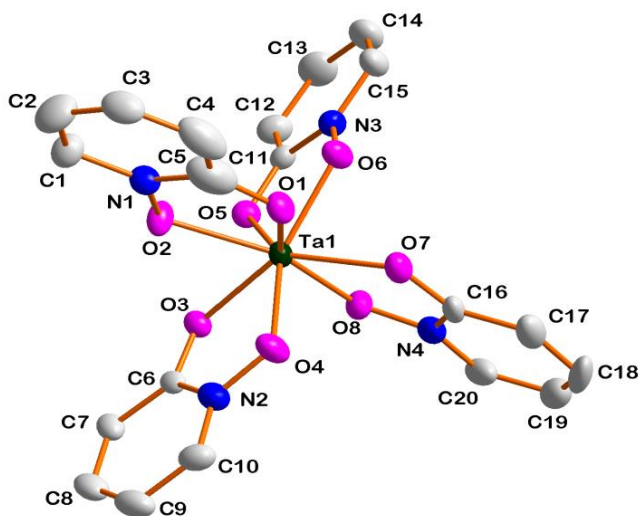
(B)

Figure 6.27 Molecular structure of [Ta(hopo)$_4$]Cl·2MeCN·2H$_2$O (**10**) (**A**) showing the atom numbering system and the thermal ellipsoids drawn at the 50% probability level. In (**B**) the atom numbering system is shown with the chloride counter ion, solvated molecules and hydrogen atoms omitted for clarity.

Table 6.8 Selected bond lengths and angles of $[Ta(hopo)_4]Cl \cdot 2MeCN \cdot 2H_2O$ (**10**).

Bond lengths (Å)			
Ta1-O1	2.099(4)	N3-O6	1.348(3)
Ta1-O2	2.069(3)	N4-O8	1.329(2)
Ta1-O3	2.104(4)	C5-O1	1.303(2)
Ta1-O4	2.076(4)	C6-O3	1.321(2)
Ta1-O5	2.093(4)	C11-O5	1.307(2)
Ta1-O6	2.074(3)	C16-O7	1.322(3)
Ta1-O7	2.103(3)	C5-N1	1.344(2)
Ta1-O8	2.087(4)	C6-N2	1.347(2)
N1-O2	1.345(3)	C11-N3	1.342(2)
N2-O4	1.327(3)	C16-N4	1.345(2)
Bond angles (°)			
O1-Ta1-O2	71.97(9)	O1-Ta1-O5	132.20(1)
O3-Ta1-O4	72.67(9)	O2-Ta1-O3	72.61(1)
O5-Ta1-O6	72.25(9)	O4-Ta1-O8	91.08(9)
O7-Ta1-O8	72.28(9)	O6-Ta1-O7	76.43(9)
O7-Ta1-O5	132.38(1)	O1-Ta1-O3	132.44(1)
O2-Ta1-O8	146.64(1)	O2-Ta1-O4	95.73(1)

The tantalum atom in $[Ta(hopo)_4]Cl \cdot 2MeCN \cdot 2H_2O$ (**10**) is octacoordinated by eight oxygen atoms of four bidentate 2-hydroxypyridinate-N-oxide ligands. Two chelating 2-hydroxypyridinate-N-oxide ligands are positioned in the equatorial plane, while the other two ligands occupies the remaining axial positions (Figure 6.28).

The bidentate ligand in $[Ta(hopo)_4]Cl \cdot 2MeCN \cdot 2H_2O$ (**10**) forms a five-membered ring with a small bite angle and the O-Ta-O bite angles of the complex (**10**) are 71.97(9)°, 72.67(9)°, 72.25(9)° and 72.28(9)° with the average O-Ta-O bite angle of 72.29(9)° (Figure 6.27 and Table 6.8). This value is significantly larger than those observed in complex (**7**) with an average

O-Nb-O bite angle of 69.49(4)°, complex (**8**) an average O-Nb-O bite angle of 72.11(3)° and complex (**6**) with an average O-Nb-O bite angle of 70.18(1)° (Table 5.4 and Figure 5.10). The value of complex (**10**) is, however, smaller than those observed in complex (**5**) with an average O-Nb-O bite angle of 72.44(4)° (Chapter 5 section 5.3, Table 5.2 and Figure 5.1) and complex (**9**) with an average O-Ta-O bite angle of 74.09(2)° (Table 6.6 and Figure 6.19). Five-membered rings are formed by the bidentate ligands in all cases. The trans bond angles of O7-Ta1-O5, O1-Ta1-O3, O2-Ta1-O4 and O2-Ta1-O8 are 132.38(1)°, 132.44(1)°, 95.73(1)° and 146.64(1)° respectively (Table 6.8 and Figure 6.27).

The Ta-O bond lengths vary from 2.074(3) Å to 2.104(4) Å with an average Ta-O bond length of 2.088(4) Å (Figure 6.27 and Table 6.8). This average Ta-O bond length of complex (**10**) is significantly shorter than the Nb-O distances observed in complex (**5**) with an average Nb-O bond lengths of 2.128(1) Å, in complex (**6**) with an average of 2.265(2) Å, in complex (**7**) with an average of 2.135(6) Å, in complex (**8**) with an average of 2.137(2) Å, as well as the average Ta-O distance of 2.126(1) Å in complex (**9**).

The N-O bond lengths in complex (**10**) vary from 1.327(3) Å to 1.348(3) Å with an average of 1.337(3) Å, significantly shorter than the N-O bond lengths of the free ligand (1.384(3) Å) (Chapter 4 Figure 4.11 and table 4.6) and complex (**9**) with the average N-O distances of 1.402(1) Å, but longer than in complex (**8**) with an average of 1.313(1) Å. The C-O bond lengths in complex (**10**) vary from 1.303(2) Å to 1.322(3) Å with an average of 1.313(1) Å (Figure 6.27 and Table 6.8), significantly longer than the C-O bond lengths of the free ligand (1.262(3) Å), but slightly shorter than in complex (**8**) with an average C-O bond length of 1.327(1) Å (Figure 6.10 and Table 6.4). In $[Ta(hopo)_4]Cl \cdot 2MeCN \cdot 2H_2O$ (**10**) and $[TaO(hopo)_3] \cdot MeOH$ (**9**) the average N-O bond lengths of 1.337(3) Å and 1.402(1) Å are longer than the average C-O bond lengths of 1.313(1) Å and 1.322(1) Å respectively, but in complex (**8**) the average C-O bond length of 1.327(1) Å is longer than the average N-O bond length of 1.313(1) Å, This difference might be due to metal effects.

Figure 6.28 (**A**) illustrates the two planes that can be constructed through the two bidentate ligands in the equatorial plane, with plane 1 (blue) passing through O1, C5, N1 and O2 and plane 2 (orange) passing through O7, C16, N4 and O8. The dihedral angle between the two planes is 11.6(6)°. Figure 6.28 (**B**), illustrates the [Ta(hopo)$_4$]Cl·2MeCN·2H$_2$O (**10**) with four 2-hydroxypyridinate N-oxide ligands, of which two occupy the equatorial positions (plane 1 in green passing through O1, C5, N1 and O2) and the other two occupy the axial positions (plane 2 in blue passing through O3, C6, N2 and O4). The dihedral angle between the two planes is 87.5(3)°. The dihedral angle between the ligands in the equatorial plane and the ligands forming part of the axial positions in complex (**10**) (87.5(3)° Figure 6.28 (**B**)) is larger than those observed in complex (**9**) (68.5(1)° Figure 6.20), in complex (**8**) (80.3(4)° Figure 6.11) and in complex (**7**) (79.9(2)° Figure 6.2).

As was discussed in sections 6.3 to 6.5, various coordination modes (geometries) of the seven-coordinate Nb(V) and Ta(V) complexes were characterized and in section 6.6 the eight-coordinate Ta(V) complex (**10**) (Figure 6.29) with D_2 square antiprismatic coordination mode is reported, which significantly differs from the other complexes, (**5**), (**6**), (**7**), (**8**), and (**9**).
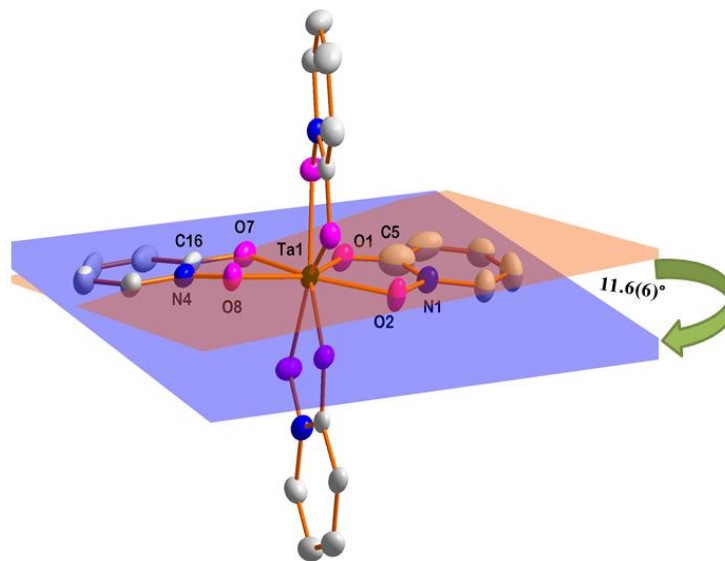
(A)
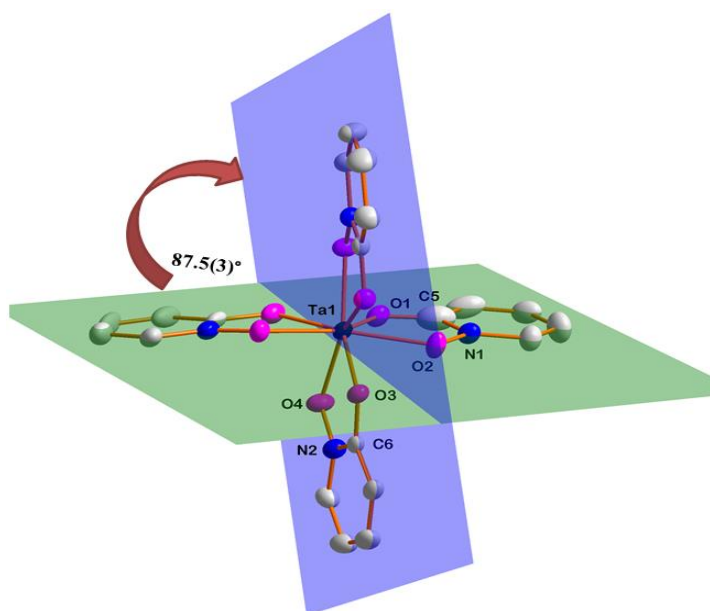
(**B**)

Figure 6.28 Representation of the planes through the [Ta(hopo)₄]Cl (**10**); (**A**) illustrates plane 1(blue) passing through O1, C5, N1 and O2 and plane 2 (orange) passing through O8, N4, C16 and O7. (**B**) illustrates plane 1 (green) passing through O1, C5, N1 and O2 and plane 2 (blue) passing through O3, C6, N2 and O4. Counter ions, H-atoms and solvated acetonitrile molecules are omitted for clarity.
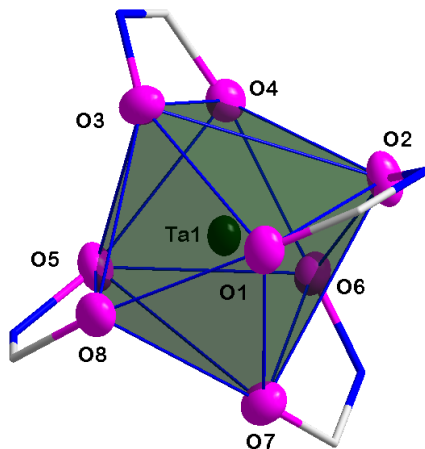
Figure 6.29 Representation of the D_2 square antiprismatic coordination polyhedron surrounding Ta(V) atoms in [Ta(hopo)$_4$] (**10**). Counter ions, H-atoms and solvated acetonitrile molecules are omitted for clarity.
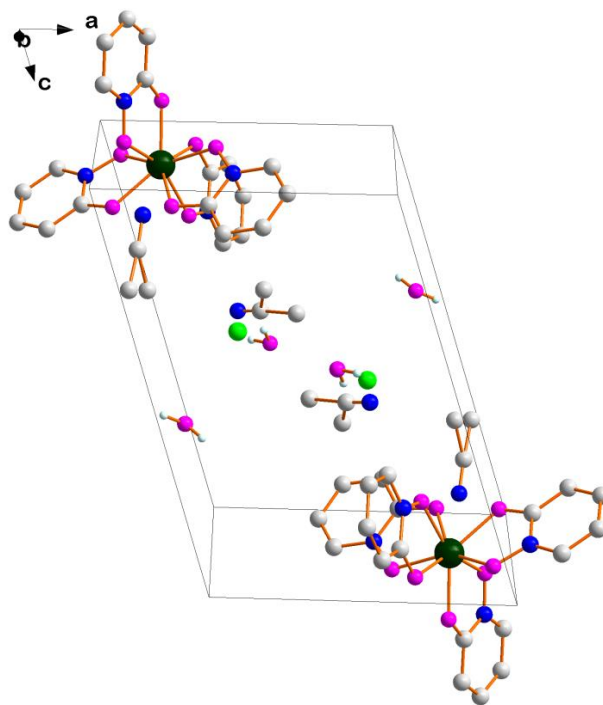
Figure 6.30 Molecular structure of [Ta(hopo)$_4$]Cl·2MeCN·2H$_2$O (**10**) showing two molecular formula in unit cell along the b-axis. H-atoms are omitted for clarity.

The [Ta(hopo)$_4$]Cl·2MeCN·2H$_2$O (**10**) crystal structure is characterised by 9 intra- and intermolecular O-H···O, O-H···N, C-H···O and C-H···N hydrogen interactions, as illustrated in Figure 6.31 (**A**) and (**B**) and listed in Table 6.19.

Table 6.9 General hydrogen-bond distances and angles of [Ta(hopo)$_4$]Cl·2MeCN·2H$_2$O (**10**).

Interactions	D-H···A	D-H (Å)	H···A (Å)	D···A (Å)	D-H···A (°)
I	O9-H9A···O9i[a]	0.89(1)	2.44(1)	3.265(1)	156(7)
II	O9-H9B···O10[b]	0.85(1)	2.46(2)	3.142(1)	137(1)
III	O10-H10A···N6	0.90(9)	1.95(9)	2.832(1)	168(1)
IV	O10-H10B···O9[b]	0.84(9)	2.31(9)	3.142(1)	174(1)
V	C1ii-H1ii···O2i[c]	0.95	2.45	3.373(9)	164
VI	C7-H7···O8ii[d]	0.95	2.48	3.246(8)	137
VII	C15iii-H15iii···O6ii[e]	0.95	2.46	3.373(8)	160
VIII	C15iii-H15iii···O7ii[e]	0.95	2.54	3.300(9)	137
IX	C20ii-H20ii···N5[f]	0.95	2.44	3.364(1)	165

Symmetry code: (a) -x + 2, -y, -z + 1, (b) -x + 1, -y, -z + 1, (c) -x, -y, -z, (d) -x + 1, -y, -z, (e) -x, -y + 1, -z, (f) -x + 1, -y + 1, -z.

As was discussed, in complex (**8**) (Figure 6.17) both head to head and head to tail π-π stacking interactions exist, while in complex (**9**) only head to head π-π stacking interactions is found. In complex (**10**) there are head to tail π-π stacking interactions between two 2-hydroxypyridinate-N-oxide rings on N4-C20 and N4i-C20i with a centroid-centroid distance of 3.541(5) Å [1-x, 1-y,-z] (Figure 6.32). Thus, opposite π-π stacking interactions are observed in complex (**9**) (head to head) and complex (**10**) (head to tail) with the same Ta(V) metal center and ligands. This difference might be due to effects of stoichiometric metal to ligands ratios (1:4).

Bifurcated hydrogen-bonds exist in [Ta(hopo)$_4$]Cl·2MeCN·2H$_2$O (**10**), which shows H15iii bonded to O6ii and O7ii, strong and weak s-shaped intermolecular hydrogen-bond networks between solvated water molecules and acetonitrile molecules with O-H···N and O-H···O distances in the range of 1.950 Å to 2.460 Å, as well as various intermolecular hydrogen-bond

networks, with C-H···O and O-H···N distances in the range of 2.440 Å to 2.480 Å as reported in Table 6.9 (Figure 6.31 (**A)** and 6.31 (**B)**).
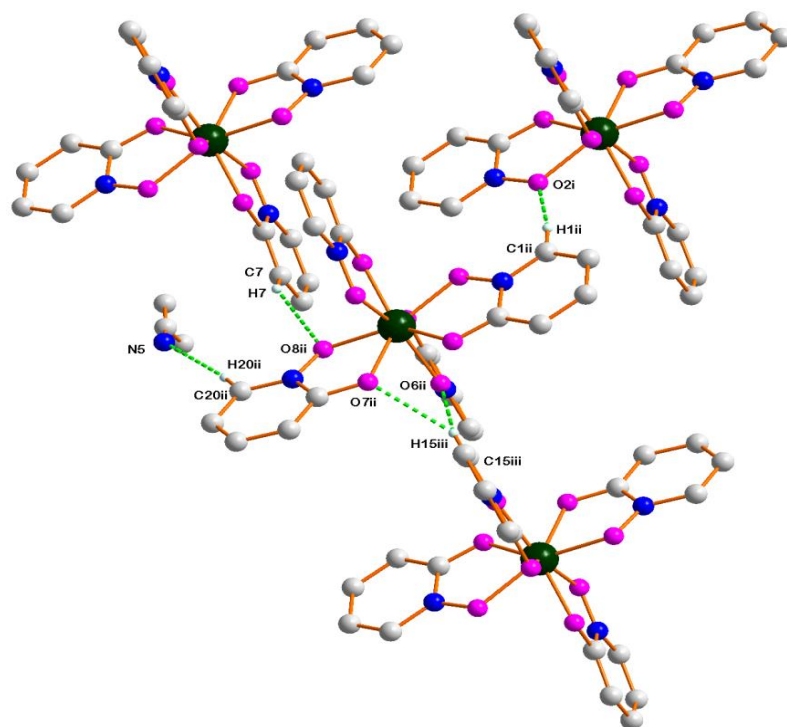
(**A**)
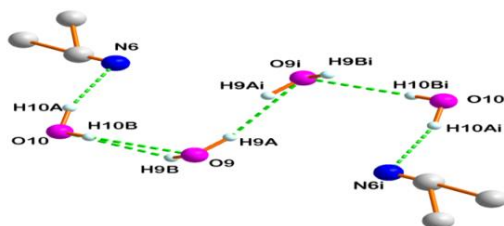
(**B**)

Figure 6.31 Molecular structure of [Ta(hopo)$_4$]Cl·2MeCN·2H$_2$O (**10**) (**A**) showing the network of intermolecular interactions. The dashed lines indicate C-H···N and C-H···O hydrogen-bonds, while (**B**) illustrates partial solvated molecules of O-H···O and O-H···N hydrogen-bond networks. H-atoms are omitted for clarity [Symmetry codes: Table 6.9].
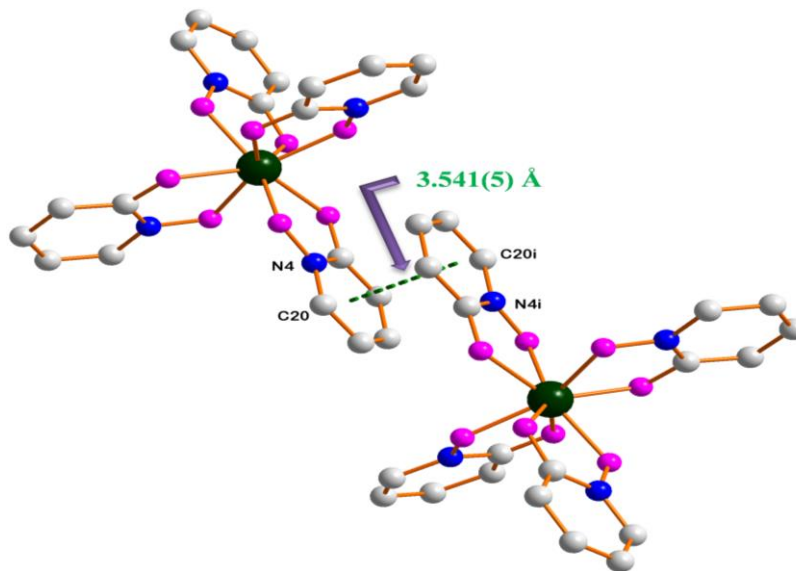
Figure 6.32 Molecular structure of [Ta(hopo)₄]⁺ (**10**) with the green dashed lines indicating side by side π-π stacking interactions between the two 2-hydroxypyridinate rings on N4-C20 and N4i-C20i. Counter ions, hydrogen atoms and solvated acetonitrile molecules are omitted for clarity.
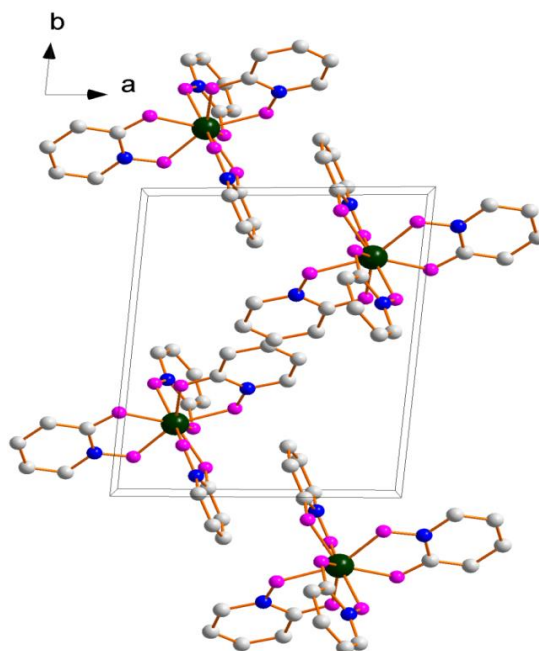
Figure 6.33 Molecular structure of [Ta(hopo)₄]⁺ (**10**) showing side by side packing along the c-axis. Counter ions, H-atoms and solvated acetonitrile molecules are omitted for clarity.

6.7 Correlation of four different complexes in (7), (8), (9) and (10)

Table 6.10 Correlation and summary of selected average (av.) bond lengths and bite angles of Nb(V) and Ta(V) complexes, from this study.

S/N	Compound	Av. Nb-O bond length ($\mathring{A}$)	Av. O-Nb-O bite angle (°)	Nb=O Bond length ($\mathring{A}$)	Type of membered ring ligands
1	[NbO(cupf)$_3$] (**7**)	2.075(4)	69.49(4)	1.711(5)	5
2	[NbO(hopo)$_3$].MeOH (**8**)	2.138(2)	72.11(3)	1.722(1)	5
3	[TaO(hopo)$_3$].MeOH (**9**)	2.126(2)	74.09(2)	1.725(1)	5
4	[Ta(hopo)$_4$]Cl.2MeCN. 2H$_2$O (**10**)	2.088(4)	72.29(9)	---	5

Table 6.10 shows correlation and summary of selected average bond lengths ($\mathring{A}$) and bite angles (°) of four different Nb(V) and Ta(V) complexes. The increasing order of average Nb-O and Ta-O bond lengths of these complexes are (**7**) < (**10**) < (**9**) < (**8**) and increasing order of Nb=O and Ta=O bond lengths are (**7**) < (**8**) < (**9**), while the increasing order of average O-Nb-O and O-Ta-O bite angles are (**7**) < (**8**) < (**10**) < (**9**) respectively, with five membered rings formed by the bidentate ligands in all cases.

In 1986 Basson *et al*,[22,23] have been reported the cupferrate complex of [Rh(cupf)(CO)(PPh$_3$)], which was the average Rh-O bond lengths of 2.044(6) $\mathring{A}$ is significantly shorter than the Nb-O distances of complex (**7**) with average of 2.135(6) $\mathring{A}$. The O-Rh-O bite angles of the cupferrate ligands in [Rh(cupf)(CO)(PPh$_3$)] was 76.6(3)°, which is significantly larger than the O-Nb-O bite angles of complex (**7**) with average of 69.49(4)°. The average N-O bond lengths of the cupferrate ligands in [Rh(cupf)(CO)(PPh$_3$)] was 1.315(8) $\mathring{A}$, which is nearly the same as the N-O distances of complex (**7**) with average of 1.312(4) $\mathring{A}$, with in the experimental error.

---

[22]S.S. Basson, J.G. Leippoldt, A. Roodt, J.A. Venter, *Inorg. Chim. Acta*, **118**, L45-L47, 1986.

[23] J.A. Venter, *Structural and kinetic study of rhodium complexes of N-aryl-N-nitrosohydroxylamines and related complexes*, PhD. Dissertation, University of the Free State, South Africa, 2006.

In overall, the N-N bond distances of cupferrate complex (**7**), being roughly equalized within experimental error, show that delocalization of π-electrons took place.

Figure 6.34 illustrates the general trend for D_{5h}-pentagonal bipyramidal coordination modes of Nb(V) and Ta(V) complexes (**7**, **8** and **9**) with the exception of complex (**10**) that does not fit the relationship. This is clear that complexes (**7**, **8** and **9**) have the seven-coordinate, these complexes geometry was significantly influenced by strong oxido ligand (as was discussed in section 6.3 to 6.7), while complex (**10**) is eight-coordinate. Because of strong oxido ligand complex (**8**) was slightly distorted, but complex (**9**) was highly distorted as compared to complex (**7**). And also different metal to ligand ratio (1:4) of complex (**10**), due to this reason as was reported different coordination modes i.e., the seven-coordinate [TaO(hopo)$_3$]·MeOH (**9**) has a C_2-capped trigonal prismatic geometry (Figure 6.22), which is a different coordination mode compared to those observed in complexes (**7**) and (**5**) (D_{5h} pentagonal bipyramidal geometry) (Figure 6.4 and Figure 5.4), complex (**8**) (C_3v-capped octahedral geometry) (Figure 6.13), in complex (**6**) (a regular octahedral coordination mode) (Figure 5.13) as well as in complex (**10**) (a D_2-square antiprisimatic coordination polyhedron) (Figure 6.29). Therefore, these different geometries found in complex (**5**), (**6**), (**7**), (**8**), (**9**) and (**10**) describe the shape of complexes with seven and eight oxygen atoms bound to the niobium(V) and tantalum(V) metal centre, and this leads potential of a separation of niobium from tantalum.
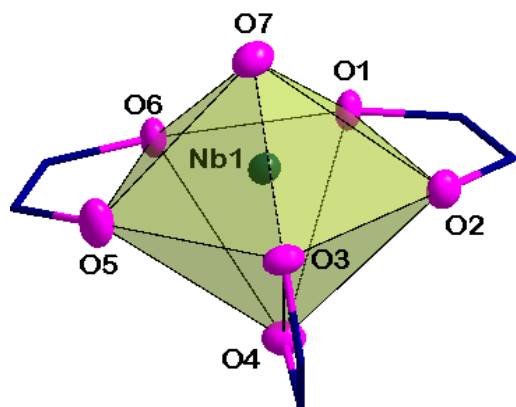
[NbO(cuf)₃] (**7**)
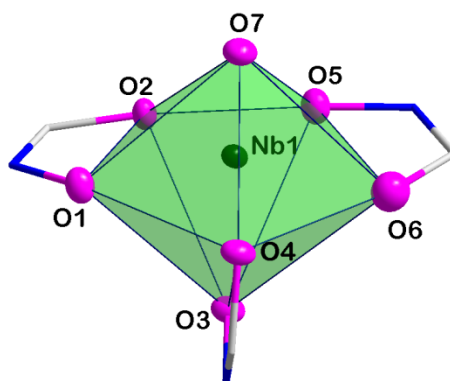
[NbO(hopo)₃]·MeOH (**8**)
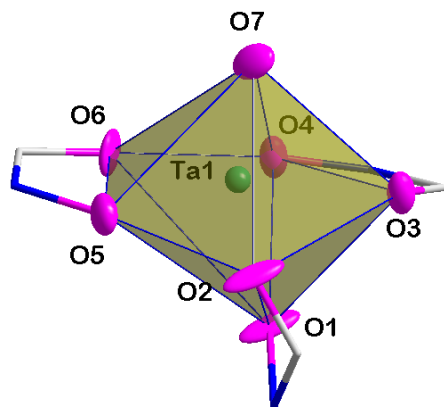
[TaO(hopo)₃]·MeOH (**9**)
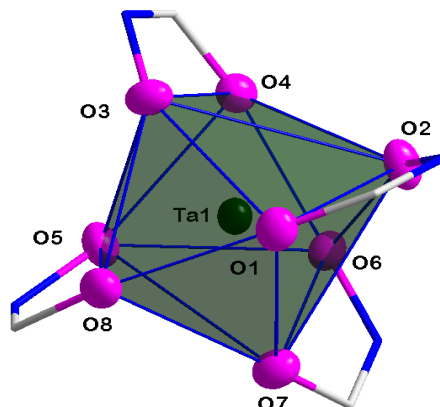
[Ta(hopo)₄]Cl·2MeCN·2H₂O (**10**)

Figure 6.34 Illustration of the general trends for D_{5h}-pentagonal bipyramidal coordination modes of Nb(V) and Ta(V) complexes (**7**, **8** and **9**), with the exception of complex (**10**) that does not fit the relationship (Figure 6.4, 6.13, 6.22 and 6.29).

It makes sense to compare the crystal structure of [NbO(cupf)3] (**7**), [NbO(hopo)₃]·MeOH (**8**) [TaO(hopo)₄]·MeOH (**9**), and [Ta(hopo)₄]Cl·2MeCN·2H₂O (**10**) to that of (Et₄N)*cis*-[NbO(ca)₂(H₂O)OPPh₃]·3H₂O·THF (**5**) and (Et₄N)₄[Nb₄O₄(ca)₂(μ^2-O)₂Cl₈]·2CH₃CN (**6**) as well as the other crystal structures reported from literature. This will be discussed in Chapter 7 with comparing from this study and as found in literature.

6.8 Conclusion

Four new niobium(V) and tantalum(V) complexes were successfully characterized by single crystal X-ray diffraction and their structures reported in this Chapter. One of these has already been published[12], while manuscripts of the remaining crystal structures were already prepared and ready for submission at international journals for publication. Comparisons of all complexes in this study were discussed and it became evident that the crystal stabilization was influenced by intermolecular π-π interactions and inter-and intramolecular hydrogen and/halogen bond networks.

The key to effective separation of Nb(V) and Ta(V) metals could probably be found in the differences in the chemical properties of the two different organic chelated moieties, 2-hydroxypyridinate-N-oxide (hopoH) and cupferrate (cupfH) ligands. In attempt to define a unique chemical state, differences in bond lengths and angles, packing modes, coordination geometries, and intermolecular interactions were presented in detail. These could be crucial to investigate Nb(V) and Ta(V) complexes with hopoH and cupfH ligands for the effective separation of these two identical twin metals.

As was reported in Chapter 5, two Nb(V) complexes (complex (**5**) and (**6**)) with different coordination modes of chloranilate (ca) ligands have successfully been characterized by single crystal X-ray diffraction, but unfortunately due to poor stability of the Ta(V) complexes with chloranilate (ca) ligands, it was not suitable for single crystal X-ray diffraction. However, the two Nb(V) and two Ta(V) complexes with two different coordinated hopoH and cupfH ligands reported here, have been successfully characterized by single crystal X-ray diffraction. Both hopoH and cupfH ligands formed five membered ring chelates.

The synthesis and crystal structures of novel Nb(V) and Ta(V) complexes derived from the hopoH and cupfH ligands demonstrate that (**a**) the hopoH ligand could chelate both Nb(V) and Ta(V) metal centres in bidentate coordination through the oxygen atoms and shown a rich variety of coordination modes. These complexes are air/moisture stable (complexes (**8**), (**9**) and (**10**)). Of these complexes, (**8**) and (**9**) have the same coordination number, but complex (**10**) is different,

because of their ligand: metal stoichiometry which are not equivalent. Complex (**10**) is less stable than complexes (**8**) and (**9**). (**b**) The bidentate cupferrate ligand coordinates through its oxygen atoms and only the Nb(V) complex thereof could be characterised crystallographically. This complex is air/moisture stable. The cupferrate complex of Ta(V) did not form crystals suitable for crystallography. The relative order of stability of these complexes are, complex (**7**) > (**8**) > (**9**) ≥ (**10**). This would be useful to improving the stability of the various Nb(V) and Ta(V) complexes, which would allow to furthering the separation of these two metals.

Seven-coordinate geometries were found in [TaO(hopo)$_3$]·MeOH (**9**) with a C_2-capped trigonal prismatic coordination mode (Figure 6.21), D_{5h} pentagonal bipyramidal geometry were found in [Nb(cupf)$_3$] (**7**) and (Et$_4$N)*cis*-[NbO(ca)$_2$(H$_2$O)OPPh$_3$]·3H$_2$O·THF (**5**) (Figure 6.4 and Figure 5.4), C_{3v}-capped octahedral geometry were found with [NbO(hopo)$_3$]·MeOH (**8**) (Figure 6.12) and D_2 square antiprismatic coordination were found with [Ta(hopo)$_4$]Cl·2MeCN·2H$_2$O (**10**) (Figure 6.28). Six-coordinate geometry was found in (Et$_4$N)$_4$[Nb$_4$O$_4$(ca)$_2$(μ^2-O)$_2$Cl$_8$]·2CH$_3$CN (**6**) with a regular octahedral coordination mode (Figure 5.13). These different geometries found in complexes (**5**), (**6**), (**7**), (**8**), (**9**) and (**10**) describe the shape of these complexes with oxygen atoms bound to the niobium(V) and tantalum(V) metal centre. Making use of differences between the complexes, this may also contribute to attempts to separate niobium from tantalum, and in achieving one of the goals of this study.

In all complexes, the bond distances and angles are similar to each other's as well as to other structures of Nb(V) and Ta(V) complexes. A summary of the general crystallographic data of complexes **7-10** are presented in Table 6.1. Atomic coordinates, anisotropic displacement parameters, bond distances and angles and hydrogen coordinates, are given in the supplementary data section (Appendix **C**). Detailed information of the novel synthetic procedures that yielded these crystals are reported in Chapter 3 section 3.2.2.2, 3.2.2.6, 3.2.2.5, and 3.2.2.4 for complex (**7**), (**8**), (**9**), and (**10**) respectively. In the next Chapter, selected specific data of niobium(V) and tantalum(V) complexes are further combined, compared and correlated with the different chemical properties of each structure, with similar structures of Nb(V) and Ta(V) from literature.

7 Correlation of Crystallographic and Spectroscopic Data of Nb(V) and Ta(V) Complexes

7.1 Introduction

As was discussed and reported in the previous chapters, the chemical similarities between niobium and tantalum complicates the separation and purification of these two metals. In Chapters 4, 5 and 6, the crystallographic investigation of two ligands, two co-crystals and six novel Nb(V) and Ta(V) complexes, ten crystal structures in total, respectively were reported. Various solid state properties such as bond lengths and angles, inter- and intramolecular interactions, crystal packing and coordination modes were discussed in detail. This study also gives more information with regard to coordination preferences, stability of the complexes and the effects of ligand substituents on the crystal systems.

In this chapter, the focus is on integration of selected data to further combine and compare the niobium(V) and tantalum(V) structures from this study as individual entities with those found in literature. Attempts will be made to correlate the different properties within the complexes, such as bond lengths and angles as well as coordination modes. The inter- and intramolecular interactions and crystal packing were dealt with already in previous chapters. As was reported in Chapter 5, the crystallographic investigation of tetraethylammonium aquabis(2,5-dichloro-3,6-dihydroxy-1,4-benzoquinonato-κ^2O,O')oxidotriphenylphosphineoxideniobate(V), trihydrate-tetrahydrofuran solvate, (Et$_4$N)cis-[NbO(ca)$_2$(H$_2$O)OPPh$_3$]·3H$_2$O·THF (**5**) and tetratetraethyl-ammoniumoctachloridocyclo-di-μ-oxido-di-μ-(2,5-dichloro-3,6-dihydroxy-1,4-benzoquinonato-κ^2O,O')tetraoxidoniobate(V), diacetonitrile solvate, (Et$_4$N)$_4$[Nb$_4$O$_4$(ca)$_2$(μ^2-O)$_2$Cl$_8$]·2CH$_3$CN (**6**),

and in Chapter 6, tris(N-nitroso-N-phenylhydroxylaminato-k^2O,O')oxidoniobium(V), [NbO(cupf)₃] (**7**), tris(2-hydroxypyridinato-N-oxide-κ^2O,O')oxidoniobium(V), methanol solvate, [NbO(hopo)₃]·MeOH (**8**), tris(2-hydroxypyridinato-N-oxide-κ^2O,O')oxidotantalum(V), methanol solvate, [TaO(hopo)₃]·MeOH (**9**), as well as tetrakis(2-hydroxypyridinato-N-oxide-κ^2O,O')-tantalum(V)chloride, diacetonitrile and diaqua solvate, [Ta(hopo)₄]Cl.2MeCN.2H₂O (**10**) are briefly summarized and correlated in Figure 7.1, 7.2, 7.3 and 7.4, as well as listed in Table 7.1, 7.2, 7.3, 7.4, 7.5, 7.6 and 7.7.

Table 7.1 Summary of selected spectroscopic data for oxo-niobium(V) and -tantalum(V) complexes (Chapter 3), in this study.

Selected Complexes	v(M=O) cm^{-1}	λ_{max}(nm)	ε (M^{-1}cm^{-1})
[TaO(hopo)₃·MeOH] **(A)**	805	302	5.036 x 10^3
[NbO(hopo)₃·MeOH] **(B)**	891	305	1.107 x 10^4
Cis-(Et₄N)[NbO(ca)₂(H₂O)OPPh₃]·3H₂O·THF **(C)**	923	530	2.008 x 10^3
[NbO(Cupf)₃] **(D)**	924	300	5.729 x 10^3
(Et₄N)₄[Nb₄O₄(ca)₂(µ^2-O)₂Cl₈]·2CH₃CN **(E)**	949	329	1.464 x 10^4

Table 7.2 Correlation of selected average bond lengths and bite angles of Nb(V) complexes, from this study and as found in literature.

S/N	Compound	Av. Nb-O bond length (Å)	Av. O-Nb-O bite angle (°)	Nb=O Bond length (Å)	Type of membered ring ligands	Ref.
1	Cis-(Et$_4$N)[NbO(ca)$_2$(H$_2$O)-OPPh$_3$]·3H$_2$O·THF	2.129(1)	72.55(4)	1.721(1)	5	*
2	(Et$_4$N)$_4$[Nb$_4$O$_4$(ca)$_2$(μ^2-O)$_2$-Cl$_8$]·2CH$_3$CN	2.265(3)	70.18(1)	1.714(2)	5	*
3	[NbO(cupf)$_3$]	2.075(4)	69.49(4)	1.711(5)	5	*
4	[NbO(hopo)$_3$]·MeOH	2.138(2)	72.11(3)	1.722(1)	5	*
5	[Nb(trop)$_4$]Cl	2.083(1)	71.40(2)	---	5	[1,2]
6	[NbO(trop)$_3$]	2.153(2)	71.22(2)	1.754(3)	5	[3]
7	[Nb(trop)$_4$]$_2$[H$_3$OC1$_3$]	2.075(7)	71.20(1)	---	5	[4]
8	[Nb(cat)$_2$(cat-H)py]	2.034(3)	75.44(3)	---	5	[5]
9	[Nb(acac)(OEt)$_2$(μ^2-O)]$_4$	2.143(2)	79.53(1)	---	6	[6]
10	[Nb(acac)(OMe)$_3$Cl]	2.096(2)	80.74(6)	---	6	[7]
11	[Nb(acac)(OMe)$_2$Cl$_2$]	2.066(2)	81.36(7)	---	6	[8]
12	[Nb(phacac)(OMe)$_2$Cl$_2$]	2.062(2)	80.47(5)	---	6	[9]
13	[Nb(2-bp)(OMe)$_2$Cl$_2$]	2.059(2)	79.47(9)	---	6	[10]

The ligands referred to are 2,5-dichloro-3,6-dihydroxy-2,5-cyclohexadiene-1,4-dione (caH$_2$), ammonium salt of N-nitroso-N-phenylhydroxylamine (cupfH), 2-hydroxypyridine-N-oxide (hopoH), tropolone (tropH), catechol (catH$_2$), pyridine (py), oxalate (C$_2$O$_4$), and [β-diketonates = acetylacetonate (acacH),

[1] R. Koen, A. Roodt, H.G. Visser, *J. South. Afr. Inst. Min. Metall.*, **116**, 895-899, 2016.

[2] E.L. Muetterties, C.M. Wright, *J. Am. Chem. Soc.*, **87**(21), 4706-4717, 1965

[3] R. Koen, *High oxidation state niobium and tantalum coordination chemistry: a solution and solid state investigation*, PhD. Dissertation, University of the Free State, South Africa, 2016

[4] A.R. Davis, F.W.B. Einstein. *Inorg. Chem*., **14**(12), 3030-3035, 1975.

[5] T.J. Boyle, L.J. Tribby, T.M. Alam, S.D. Bunge, *Polyhedron*, **24**, 1143-1152, 2005.

[6] L. Herbst, H.G. Visser, A. Roodt, T.J. Muller, *Acta Cryst.*, **E67**, m1669-m1670, 2011.

[7] L. Herbst, R. Koen, A. Roodt, H.G. Visser, *Acta Cryst.,* **E66**, m801-m802, 2010.

[8] L. Herbst, H.G. Visser, A. Roodt, C. Pretorius, *Acta Cryst.,* E**68**, m1392-m1393, 2012.

[9] L. Herbst, H.G. Visser, A. Roodt, *Z. Kristallogr. NCS.*, **228**, 451-452, 2013.

[10] L. Herbst, H.G. Visser, A. Roodt, M. Steyn, N. Loganathan, *Z. Kristallogr. NCS.,* **230**(4), 345-347, 2015.

1-phenyl-1,3-butanedionate (phacacH), 2-hydroxybenzophenone (2-bpH)], and tetraethylammonium (Et$_4$N) as well as * indicate this study.

Table 7.3 Correlation of selected bond lengths and bite angles of Ta(V) complexes, from this study and as found in literature.

S/N	Compound	Av. Ta-O Bond length (Å)	Av. O-Ta-O bite angle (°)	Ta=O Bond length (Å)	Type of membered ring ligands	Ref.
I	[TaO(hopo)$_3$·MeOH]	2.126(2)	74.09(2)	1.725(1)	5	*
II	[Ta(hopo)$_4$Cl]·2MeCN·2H$_2$O	2.088(4)	72.29(9)	---	5	*
III	[Ta (trop)$_4$]Cl	2.092(1)	72.04(2)	---	5	1'2
VI	[Ta(cat)$_2$(cat-H)py]	2.025(5)	75.88(2)	---	5	5
V	[Ta(C$_2$O$_4$)$_4$] [phenH] [Ni(phen)$_3$]·6.5H$_2$O	2.091(4)	73.98(2)	---	5	11
VI	[Ta(tmhd)$_4$][TaCl$_6$]	2.075(9)	77.50(4)	---	6	12
VII	[TaF(tmhd)$_3$][TaF$_6$]	2.030(4)	77.53(1)	---	6	13
VIII	Cis-[TaCl$_2$(OMe)$_2$(tmhd)]	2.053(9)	79.7(4)	---	6	14
IX	[Ta(OMe)$_4$(tmhd)]	2.107(6)	79.3(2)	---	6	14
X	trans, cis- [TaCl$_2$(OMe)$_2$(acac)]	2.055(1)	82.2(5)	---	6	14
XI	[Ta(OMe)$_4$(acac)]	2.091(1)	78.9(5)	---	6	14

The ligands referred to are 2-hydroxypyridine-N-oxide (hopoH), tropolone (tropH), catechol (catH$_2$), pyridine (py), oxalate (C$_2$O$_4$), and [β-diketonates = acetylacetonate (acacH), 2,2,6,6-tetramethylheptane-3,5-dionate (tmhdH), 1-phenyl-1,3-butanedionate (phacacH), 2-hydroxybenzophenone (2-bpH)], 1,10-phenanthroline (phen) and tetraethylammonium (Et$_4$N) as well as * indicate this study.

[11] L. Andros, D. Matkovic-Calogovic, P. Planinic, *Cryst. Eng. Comm.,* **15**, 533-543, 2013.

[12] H.O. Davies, A.C. Jones, M.A. Motevalli, E.A. McKinnell, P.O. Brien, *Inorg. Chem. Com.*, **8**, 585-287, 2005.

[13] F. Marchetti, G. Pampaloni, S. Zacchinib, *Dalton Trans.,* 4343-4351, 2007.

[14] H.O. Davies, A.C. Jones, P.O. Brien, T.J. Leedham, A.J.P. White, D.J. Williams, *Polyhedron*, **18**, 3165, 1999.

Table 7.4 Correlation of selected Nb(V) and Ta(V) complexes of various coordination geometries, from this study and as found in literature.

Complexes	Geometry	Coord. No	Ref.
Cis-(Et$_4$N)[NbO(ca)$_2$(H$_2$O)OPPh$_3$]·3H$_2$O·THF	D_{5h} pentagonal bipyramidal	7	*
(Et$_4$N)$_4$[Nb$_4$O$_4$(ca)$_2$(μ^2-O)$_2$Cl$_8$]·2CH$_3$CN	Regular octahedral	6	*
[NbO(cupf)$_3$]	D_{5h} pentagonal bipyramidal	7	*
[NbO(hopo)$_3$]·MeOH	C_{3v}-capped octahedral	7	*
[TaO(hopo)$_3$]·MeOH	C_2-capped trigonal prismatic	7	*
[Ta(hopo)$_4$Cl]·2MeCN·2H$_2$O	D_2-square antiprismatic	8	*
[Nb(trop)$_4$]Cl	D_2-corner-clipped-square anti-prismatic	8	[1,3]
[Ta(trop)$_4$]Cl	D_2-corner-clipped-square anti-prismatic	8	[1,3]
[NbO(C$_2$O$_4$)$_3$]	D_{5h} pentagonal bipyramidal	7	[15]
[Nb(hfacac)$_4$][TaF$_6$]	D_4-square antiprismatic	8	[16]
[Ta(tmhd)$_4$][TaCl$_6$]	D_4-square antiprismatic	8	[16]
[NbO(trop)$_3$]	D_{5h} pentagonal bipyramidal	7	[3]
[Nb(trop)$_4$]$_2$[H$_3$OCl$_3$]	Irregular bicapped-trigonal prismatic	8	[17]
[Ta(tmhd)$_4$][TaCl$_6$]	Dodecahedral	8	[13]
[Ta(cat)$_2$(catH)py]	C_2-capped trigonal prismatic	7	[5]
[Nb(cat)$_2$(catH)py]	C_2-capped trigonal prismatic	7	[5]

[15] G. Mathern, R. Weiss, *Acta Cryst.*, **B27**, 1610-1618, 1971.

[16] T.J. Pannavaia, B.L. Barnett, G. Podolsky, *J. Am. Chem. Soc.*, **97**, 2712-2730, 1975.

[17] A.R. Davis, F.W.B. Einstein. *Inorg. Chem.*, **14**(12), 3030-3035, 1975.

Table 7.5 Summary of the number of different types of O,O'-bidentate ligands observed from the Nb(V) and Ta(V) complexes listed in Table 7.2 and 7.3.

S/N	Types of Bid ligands	Number of complexes	Percentage (100%)
1	caH_2	2	8
2	hopoH	3	13
3	cupfH	1	4
4	β-diketonates	11	46
5	tropH	4	17
6	$catH_2$	2	8
7	C_2O_4	1	4

The listed number from 1-3 and 4-7 indicate O,O'-bidentate ligands from this study and the as found in literature respectively.

Table 7.6 Summary of inter-and intramolecular hydrogen bonding interactions from the single crystal X-ray diffraction studies in Chapter 5 (Table 5.3 and 5.5) and 6 (Table 6.3, 6.5, 6.7 and 6.9) with different oxygen, chlorine as well as nitrogen donor/accepting atoms.

Selected complexes	Inter-and intramolecular interactions	O	Cl	N	Range of Distances (Å)	Total No of interactions
Cis-(Et$_4$N)[NbO(ca)$_2$(H$_2$O)	O-H···O	x			1.69(3)-2.47(4)	8
OPPh$_3$]·3H$_2$O·THF (**5**)	C-H···O	x			2.40-2.57	9
	O-H···Cl		x		2.52(4)	1
	C-H···Cl		x		2.78	1
(Et$_4$N)$_4$[Nb$_4$O$_4$(ca)$_2$(μ^2-O)$_2$Cl$_8$]·	C-H···O	x			2.42-2.60	4
2CH$_3$CN (**6**)	C-H···Cl		x		2.35-2.81	9
[NbO(cupf)$_3$] (7)	C-H···O	x			2.37-2.53	4
[NbO(hopo)$_3$]·MeOH (**8**)	C-H···O	x			2.14-2.55	7
[TaO(hopo)$_3$]·MeOH (**9**)	C-H···O	x			2.27-2.55	4
[Ta(hopo)$_4$Cl]·2MeCN·2H$_2$O (**10**)	O-H···O	x			2.31(9)-2.46(2)	3
	C-H···O	x			2.45-2.54	4
	O-H···N			x	1.95(9)	1
	C-H···N			x	2.44	1

The purple, green and yellow color indicate inter-and intramolecular hydrogen-bond interactions with oxygen, chlorine and nitrogen donor/accepting atoms respectively, as found in this study.

7.2 Discussion

As mentioned in Table 7.1, 7.2, 7.3, 7.4, 7.5 and 7.6, the data illustrates that the niobium(V) and tantalum(V) complexes of various spectroscopic (Chapter 3) as well as crystallographic studies (Chapter 5-6), compared well with related Nb(V) and Ta(V) complexes found in literature (Chapter 2).
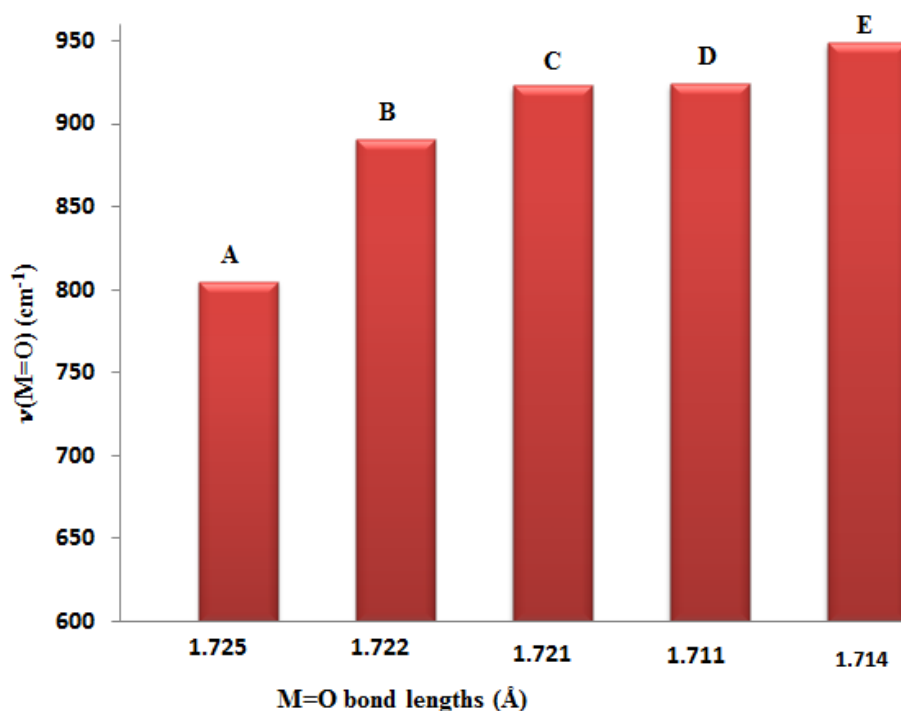
Figure 7.1 Correlation between **M=O bond lengths (Å)** (Table 7.2 and 7.3) and $v_{(M=O)}$ stretching frequencies (Table 7.1) of selected Nb(V) and Ta(V) complexes in this study. B, C, D and E indicate Nb(V) complexes, while A is a Ta(V) complex, as listed in Table 7.1.

Figure 7.1 illustrates the correlation between Nb=O and Ta=O bond length (Å) and $v_{(Nb=O)}$ and $v_{(Ta=O)}$ stretching frequencies (cm^{-1}) of various Nb(V) and Ta(V) complexes (**B, C, D, E** and **A**) (Table 7.1, 7.2 and 7.3). With exception of (**C**) that does not fit the relationship, the graph shows that the $v_{(Nb=O)}$ stretching frequency increases as the Nb=O bond length decrease. A slightly longer Ta=O bond length of complex (**A**) is observed, with the lowest $v_{(Ta=O)}$ stretching frequency when compared to niobium(V) complexes, (**B, C, D** and **E**), indicating a significant structural difference between the niobium and tantalum metals.
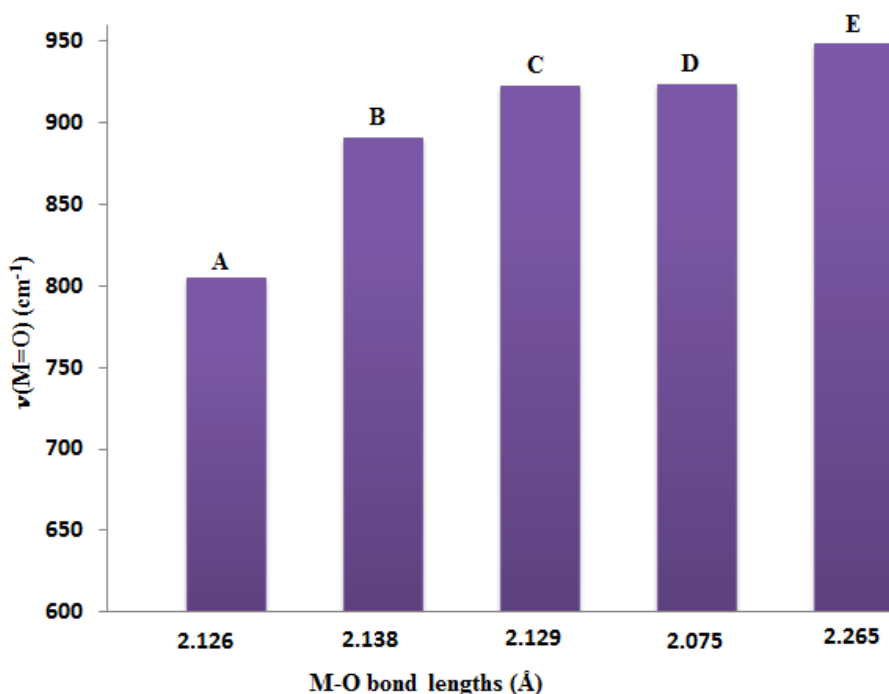
Figure 7.2 Correlation between average **M-O bond lengths (Å)** (Table 7.2 and 7.3) and $v_{(M=O)}$ stretching frequencies (Table 7.1) of selected Nb(V) and Ta(V) complexes in this study. B, C, D and E indicate Nb(V) complexes, while A is a Ta(V) complex, as listed in Table 7.1.

Figure 7.2 illustrates the correlation between average Nb-O and Ta-O bond length (Å) and $v_{(Nb=O)}$ and $v_{(Ta=O)}$ stretching frequencies of various Nb(V) and Ta(V) complexes (**B**, **C**, **D**, **E** and **A**) (Table 7.1, 7.2 and 7.3). There is a general trend for $v_{(Nb=O)}$ stretching frequencies to increase with decreasing Nb-O bond length with the exception of (**E**) that does not fit the relationship. The tantalum complex (**A**) shows the lowest $v_{(M=O)}$ stretching frequency with the shortest M-O bond length when compared to the Nb-O bond lengths of complexes, **B**, **C**, **D** and **E**.
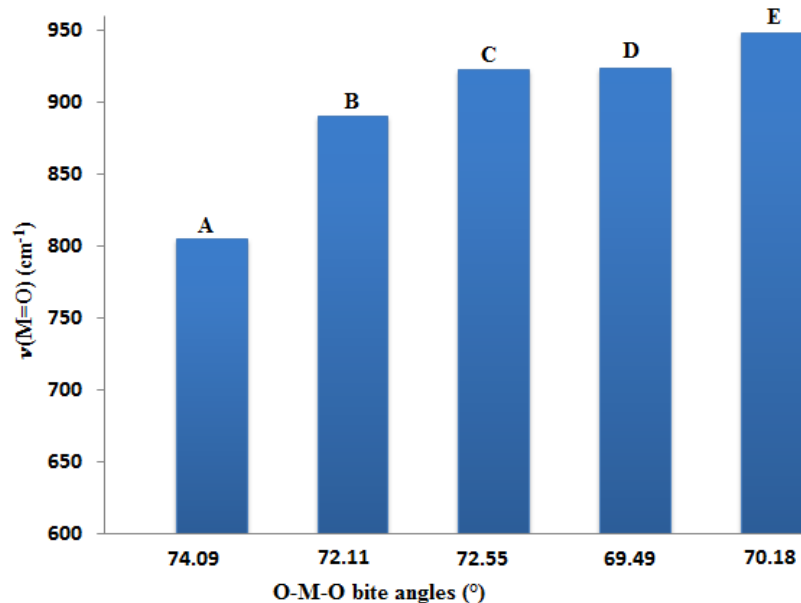
Figure 7.3 Correlation between **O-M-O bite angles** (°) (Table 7.2 and 7.3) and $\nu_{(M=O)}$ stretching frequencies (Table 7.1) of selected Nb(V) and Ta(V) complexes in this study. B, C, D and E indicate Nb(V) complexes, while A is a Ta(V) complex, as listed in Table 7.1.

Figure 7.3 illustrates the correlation between O-Nb-O and O-Ta-O bite angles (°) and $\nu_{(Nb=O)}$ and $\nu_{(Ta=O)}$ stretching frequencies of various Nb(V) and Ta(V) complexes (**B, C, D, E** and **A**) (Table 7.1, 7.2 and 7.3). Comparing the Nb(V) values, it does not seem to fit a relationship, with values scattered, but a clear difference is observed between the Nb(V) and Ta(V) values. The Ta(V) complex (**A**) shows the lowest $\nu_{(M=O)}$ stretching frequency with the largest O-M-O bite angle when compared to the other complexes, **B, C, D** and **E**).

Table 7.4 illustrates the different coordination geometries of novel Nb(V) and Ta(V) complexes with various O,O'-bidentate ligands used in this study, as well as similar geometries from literature. These six-, seven- and eight coordinate geometries were well correlated with each other. Of the different geometries found in this study, as well as those from literature, most have similar coordination numbers, but differ in terms of coordination mode (Table 7.4). The six-coordinate geometry of $(Et_4N)_4[Nb_4O_4(ca)_2(\mu^2\text{-}O)_2Cl_8]\cdot 2CH_3CN$ with a regular octahedral coordination mode is extremely unusual, when compared to other complexes listed in Table 7.4.
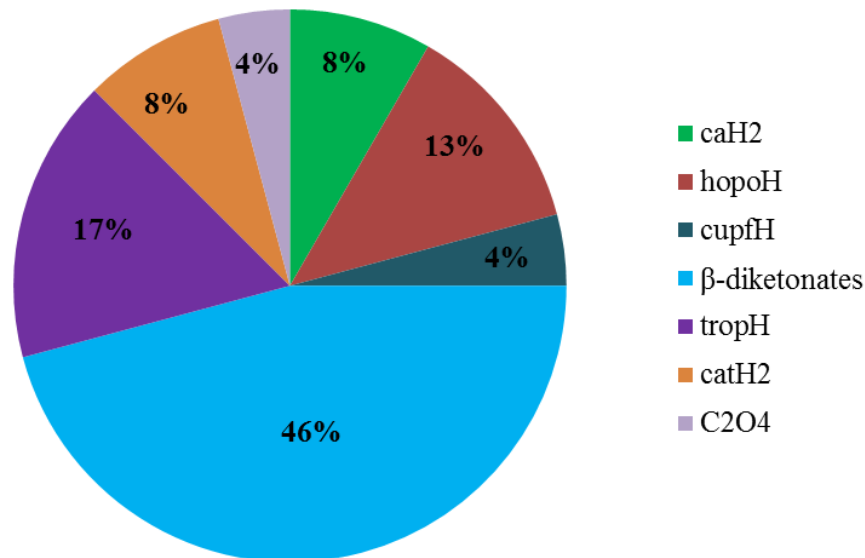
Figure 7.4 Pie chart showing percentages of different ligands used for Nb(V) and Ta(V) complexes in this study and from literature.

Figure 7.4 illustrates the overall percentages of various types of O,O'- bidentate ligands used for di (bis)-, tri (tris)- and tetrakis- Nb(V) and Ta(V) complexes in this study and from literature. This shows that the *β*-diketonate ligands was the most used ligand type, while cupferrate and oxalate ligands were the least used ligands, with chloranilate and catecholate ligands used the second least. The total number crystal structures of Nb(V) and Ta(V) complexes found from those ligands are listed in Table 7.5.

In Table 7.6, various inter- and intramolecular hydrogen interactions with oxygen, chlorine and nitrogen donor/accepting atoms are compared and correlated. This shows 19 non-classical hydrogen interactions noted in complex (**5**), compared to the other complexes (**6**, **7**, **8**, **9** and **10**) listed in Table 7.6. Only 4 non-classical hydrogen interactions are observed in complexes (**7**) and (**9**).

These examples of crystal stabilization was influenced by intermolecular π-π interactions and the networks of inter- and intramolecular hydrogen bonds, interactions with the potential to stabilized the crystal lattice.

7.3 Correlation of selected geometric data in Nb(V) and Ta(V) complexes containing five and six membered metallocycles

As noted in Table 7.2, the average Nb-O bond length in five membered ring ligands of Nb(V) complexes, listed from **1** to **8** in purple, vary from 2.075(4) to 2.265(3) Å. Those of six membered ring ligands, listed from **9** to **13** in green, vary from 2.059(2) to 2.143(2) Å. This shows that the Nb-O average bond lengths of five membered ring ligands have a tendency of being longer than those of six membered ring ligands. This has the consequence, taking ring strain in to account, that the average O-Nb-O bite angle of five membered rings is smaller and vary from 69.49(4) to 75.44(3)° while those of six membered rings is longer and vary from79.49(9) to 81.36(7)°

Shown in Table 7.3, the average Ta-O bond length in five membered ring ligands of Ta(V) complexes listed from **I** to **V** in purple, vary from 2.025(5) to 2.126(2) Å. Those of six membered ring ligands listed from **VI** to **XI** in green, vary from 2.030(4) to 2.107(2) Å. This shows that the average Ta-O bond lengths of five membered ring ligands and six membered ring ligands are nearly the same. However, the average O-Ta-O bite angle of five membered ring ligands is similar to the trend observed with Nb, being smaller and vary from 72.04(9) to 75.88(2)°, while those of six membered ring ligands is larger and vary from 77.50(4) to 82.20(5)°.

It was noted that an increase in inter- and intramolecular hydrogen bonding interactions as listed in Table 7.6 improve the stability of new synthesised niobium(V) and tantalum(V) complexes.

7.4 Conclusion

An overview of the correlation of crystallographic and spectroscopic data of various niobium(V) and tantalum(V) complexes was done and compared with relevant structures from literature. These structures confirmed known theories of niobium and tantalum and coordination with various O,O'-bidentate ligands were successfully obtained and presented.

The correlation between $\nu_{(Nb=O)}$ and $\nu_{(Ta=O)}$ stretching frequencies and Nb=O and Ta=O bond lengths (Å), Nb-O and Ta-O bond lengths (Å) as well as O-Nb-O and O-Ta-O bite angles (°) of various Nb(V) and Ta(V) complexes (Table 7.1, 7.2 and 7.3) were discussed. Physical properties of *cis*-(Et$_4$N)[NbO(ca)$_2$(H$_2$O)OPPh$_3$]·3H$_2$O·THF (**C**), (Et$_4$N)$_4$[Nb$_4$O$_4$(ca)$_2$(μ^2-O)$_2$Cl$_8$]·2CH$_3$CN (**E**), [NbO(cupf)$_3$] (**D**) and [NbO(hopo)$_3$]·MeOH (**B**) show significant differences when compared to [TaO(hopo)$_3$]·MeOH (**A**). The different coordination geometries of novel Nb(V) and Ta(V) complexes from this study and as found in literature were quite well correlated.

Five membered ring ligands of both Nb(V) and Ta(V) complexes have longer bond lengths and smaller bite angles than that of six membered ring ligands. This trend is the same for Nb(V) and Ta(V) and as such cannot be used to distinguish between the two metals.

A synergy was found between the solid state and solution state of these two identical twin metals. Postulation of a reaction mechanism will also assist in the clarification of the chemical behaviour that the metal reveals during substitution with organic ligands in the solution state. One of the aims of this project is to investigate the effects of ligand coordination on the solution state behaviour of tantalum(V) and niobium(V) complexes in an effect to further knowledge for further and open new possibilities of separation of niobium from tantalum. If successful, this could be applied in industry.

The mechanistic study of the substitution reaction of triphenylphosphineoxide in *cis*-[NbO(ca)$_2$(H$_2$O)OPPh$_3$]⁻ (**5**) by five pyridine type ligands are discussed in Chapter 8.

8 Kinetic Investigation of the OPPh₃ substitution in *cis*-[NbO(ca)₂(H₂O)OPPh₃]⁻ by Pyridine type Nucleophiles

8.1 Introduction

As mentioned in Chapter 3, different complexes were synthesised wherein O,O'-bidentate ligands have been successfully coordinated to niobium(V) and tantalum(V) centers and their IR (ATR) and NMR (^{1}H, ^{13}C and ^{31}P) spectroscopy data were reported. In Chapter 4-6 some solid state crystal structures of some of these niobium(V) and tantalum(V) complexes were reported, including the free ligands, which were characterized by detailed single crystal X-ray diffraction studies.

In previous studies the UFS Inorganic research group (see for example Herbst[1] and Koen[2,3]) reported on the mechanism of the formation kinetics of coordination compounds of niobium(V) and tantalum(V) with the acetylacetone (acacH) as entering ligand. The available literature revealed[4] that kinetic investigations of niobium(V) and tantalum(V) complexes were quite challenging and still incomplete, because of the tendency and ease of hydrolysis of ligands from

[1] L. Herbst, *A solution and solid state study of niobium complexes*, *M.Sc. Dissertation*, University of the Free State, South Africa, 2012.

[2] R. Koen, A. Roodt, H.G. Visser, *Advanced Materials Research,* **1019**, 426-432, 2014.

[3] R. Koen, *High oxidation state niobium and tantalum coordination chemistry, PhD. Dissertation*, University of the Free State, South Africa, 2016.

[4] A. Antinolo, F. Carrillo-Hermosilla, J. Fernandez-Baeza, S. Garcia-Yuste, A. Otera, E. Palomares, A. M. Rodriguez, L. F. Sanchez-Barba, *J. Organomet. Chem*, **603**, 194-202, 2000.

these two hard metals. This necessitated a broader kinetic investigation for identifying potential differences in Nb(V) and Ta(V) coordination behaviour which might then potentially be exploited to develop a possible separation method for these metals in an industrial process which may be more environmentally friendly. Thus, in this chapter one of the main objectives of this study is focused on, i.e., (i) the kinetic investigation of the substitution reaction between example complexes synthesised herein, i.e., *cis*-[NbO(ca)$_2$(H$_2$O)OPPh$_3$]$^-$ and pyridine derivatives as entering nucleophiles as well as (ii) a preliminary kinetic study of the reaction of [NbCl$_6$]$^-$ with chloranilic acid (caH$_2$), giving *cis*-[NbO(ca)$_2$(H$_2$O)]$^-$ before triphenylphosphineoxide is added to yield the final product of *cis*-[NbO(ca)$_2$(H$_2$O)OPPh$_3$]$^-$.

Knowledge obtained from this study should increase the understanding of the chemical and physical properties of the various Nb(V) and Ta(V) complexes in the solution state and identify possible differences to apply in future for developing potential separation methods for niobium from tantalum.

8.2 Experimental

8.2.1   General considerations

The preparation and spectroscopic characterization of *cis*-[NbO(ca)$_2$(H$_2$O)OPPh$_3$]$^-$, which is used for the kinetic study reported here were described in Chapter 3 while the crystallographic characterization is reported in Chapter 5. All reagents and chemicals including the various pyridine derivatives as entering ligands were of analytical grade and were purchased from Sigma-Aldrich, South Africa and used as received, without further purification. The acetonitrile was dried and distilled prior to use for the kinetic study.

8.2.2   Kinetic measurements

UV-Vis investigations were performed on a Varian Cary 50 Conc spectrophotometer in a 1.000 ± 0.001 cm quartz tandem cuvette, equipped with a Julabo F12-mV temperature cell regulator (accurate within 0.1 °C). A Stopped-flow kinetic study was attempted on a Hi-Tech SF-61DX2

Stopped-flow instrument equipped with a Julabo F12-mV temperature regulator (accurate within 0.1 °C). The Hi-Tech Stopped-flow instrument is Microsoft Windows operated with Kinet Asyst Stopped-Flow Kinetic Studio software for the acquisition and analysis of kinetic data.[5] Kinetic runs were monitored under *pseudo* first-order conditions and the *pseudo* first-order rate constants (k_{obs}) were determined from least-squares fits of the absorbance versus time data.[6] All the kinetic runs were studied with the ligand concentration in at least ten-fold excess, to ensure *pseudo* first-order reaction conditions. Data analysis was conducted by using the Scientist Micromath program, version 2.01 for all of the data to selected functions.[6]

The kinetic experiments were performed using freshly prepared niobium(V) complexes (*cis*-[NbO(ca)$_2$(H$_2$O)OPPh$_3$]$^-$ and [NbCl$_6$]$^-$), pyridine type ligands ([DMAP], [py], [4-Mepy], [3-Clpy] and [3-Brpy]) as well as chloranilic acid (caH$_2$) solutions.

Two sets of experiments were done:

(i) The substitution of triphenylphosphineoxide by pyridine derivatives was studied in acetonitrile by observing the absorbance change at a suitable fixed wavelength of 430 nm for the complex, *cis*-[NbO(ca)$_2$(H$_2$O)OPPh$_3$]$^-$, as selected from pre-recorded absorbance *versus* wavelength time resolved spectra (Figure 8.1). All the pyridine ligand concentrations were varied between 0.1 and 1.0 M, whereas the *cis*-[NbO(ca)$_2$(H$_2$O)OPPh$_3$]$^-$ concentration of 0.001 M was used. A stock solution of 1.0 M pyridine was prepared and diluted to obtain the appropriate concentrations for the kinetic runs in acetonitrile. The metal complex and ligand stability of solutions in the reaction solvent, acetonitrile (MeCN), was confirmed over a *ca.* 24 hour period, for each of the five pyridine derivative ligands studied.

---

[5] TgK Scientific Kinetic Studio, Version 1.0.8.32278, Copyright © TgK Scientific, 2008.

[6] Micromath Scientist for Windows, Version 2.01, MicroMath, Inc, Copyright© 1986-1995.
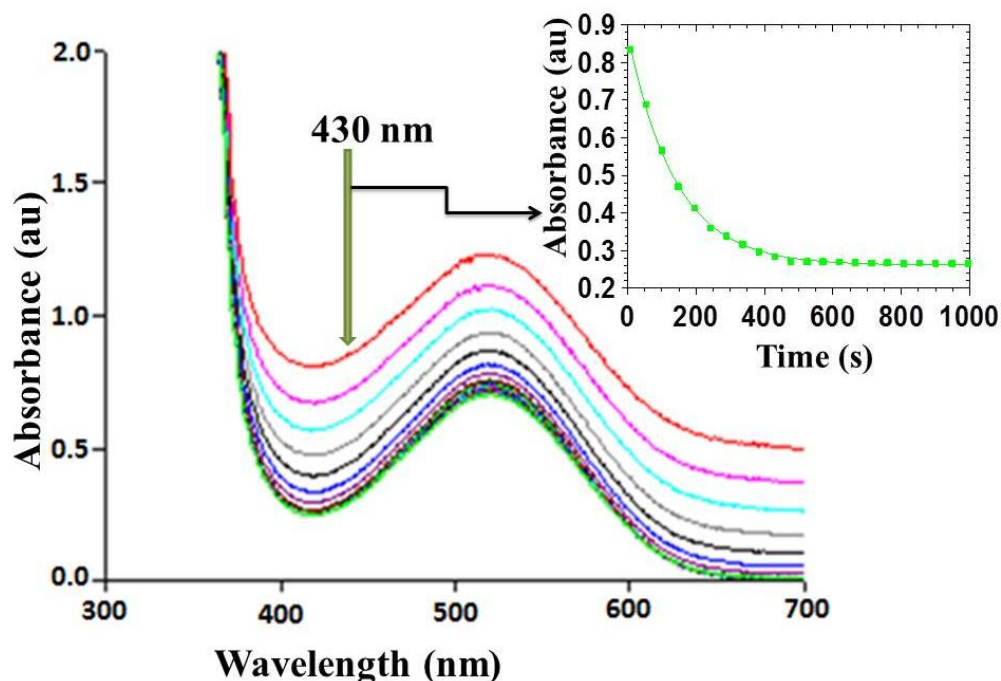
Figure 8.1 UV-Vis spectral change for the substitution reaction between *cis*-[NbO(ca)$_2$-(H$_2$O)OPPh$_3$]$^-$, [0.001 M] and DMAP, [0.70 M] at 31.2 ^{o}C, 430 nm, Δt = 50 s, total time of 1000 s, acetonitrile. The insert indicates the absorbance change *versus* time at 430 nm and the solid line shows the least-squares fit for a first-order reaction (k_{obs} = 0.0076(2) s^{-1}).

(ii) In the second set of experiments, stopped-flow experiments for the preliminary kinetic study of the formation of *cis*-[NbO(ca)$_2$(H$_2$O)]$^-$ from [NbCl$_6$]$^-$, the metal stock solution of 0.0002 M ([NbCl$_6$]$^-$), and chloranilic acid (caH$_2$) ligand solutions were prepared using a stock solution of 0.014 M. Dilution was achieved across a series of 6 solutions (0.0024 to 0.014 M) in methanol (MeOH). The process was monitored by the absorbance change at a suitable fixed wavelength of 530 nm for the formation of the proposed complex, *cis*-[NbO(ca)$_2$(H$_2$O)]$^-$.

8.2.3   NMR experiments

All ^{1}H, ^{31}P and ^{13}C NMR spectra were obtained in deuterated CD$_3$CN on the following nuclear magnetic resonance spectrometers operating at *ca*. 25 ^{o}C, (**i**) a Bruker AVANCE II 600 MHz (^{1}H: 600.28 MHz; ^{31}P: 242.99 MHz; ^{13}C: 150.95 MHz) (probe for ^{1}H and ^{13}C is 5 mm DUAL ^{13}C-

[1]H/D with z-gradients, while for ^{31}P and ^{1}H is 5 mm TBI[1]H/^{31}P/D-BB with Z-gradients) or, (**ii**) Bruker AVANCE III 400 MHz ([1]H: 400.13 MHz; [13]C: 100.61 MHz; [31]P: 161.97 MHz) (for liquid state 5 mm BBI H-BB-D probe with z-gradients) or, (**iii**) Bruker FOURIER 300 MHz ([1]H: 300.18 MHz; [13]C: 75.48 MHz) (5 mm ^{13}C/^{1}H high resolution NMR probe equipped with z-gradient coil). All spectra were obtained by collecting 360 scans per spectrum. [31]P chemical shifts are reported relative to 85% H_3PO_4 (0 ppm); positive shifts are downfield; ^{1}H and ^{13}C chemical shifts are reported relative to tetramethylsilane using the CD_3CN (^{1}H NMR: 1.94 ppm; ^{13}C NMR: 1.32 and 118.26 ppm) peak. The applicable resonance frequency was located at 146.93 MHz. Concentrations of different species used are reported in the captions of the appropriate Figures and Tables below or in the supplementary material.

8.3   Results and discussion

8.3.1   Introduction

Ligand substitution reactions on seven-coordinate metal complexes of the niobium(V) metal centre have been successfully studied using a pre-selected range of pyridine type derivatives as monodentate entering nucleophiles/ligands (see below). The results of these studies almost universally suggested an associative mechanism. The pyridine derivatives which were selected for the substitution kinetic studies span a significant range of electron-donating abilities (as indicted by the almost 7 orders-of-magnitude; see pK_a values) yet keeping the sterics constant. These are pyridine (py), 4-(dimethylamino)pyridine (DMAP), 4-methylpyridine (4-Mepy), 3-chloropyridine(3-Clpy) and 3-bromopyridine(3-Brpy) (Table 8.1).

Table 8.1 The pK_a values of the different pyridine derivatives at 25 $^\circ$C.[7]

S/N	Pyridine derivatives	pK_a	ΔpK_a as compared to pyridine
1	4-(dimethylamino)pyridine (DMAP)	9.60	4.35
2	4-methylpyridine (4-Mepy)	6.02	0.77
3	Pyridine (py)	5.25	-
4	3-chloropyridine(3-Clpy)	2.84	-2.41
5	3-bromopyridine(3-Brpy)	2.84	-2.41

Table 8.1 illustrates the different pK_a values of pyridine ligands, which indicates the highest pK_a value of 4-(dimethylamino)pyridine (DMAP) (the most electron donating), while the lowest pK_a value of 3-chloropyridine (3-Clpy) and 3-bromopyridine (3-Clpy) are the most electron withdrawing (electronic effects) compared to unsubstituted pyridine.

To illustrate thus further, the ΔpK_a values of representative substituted pyridines as compared with pyridine itself are shown in Table 8.1 relative to pyridine. The methyl groups in DMAP are electron donating and due to hyperconjugative and inductive effects and contribution from the amino groups are strong mesomeric electron donors; hence DMAP is a strong base. On the other hand, halogen atoms (Cl and Br) are strong inductive acceptors and weak mesomeric donors and they cause a marked decrease in basicity.[8]

The results of the kinetic studies are presented in this section complete with discussions and interpretations. The effect of concentration on the triphenylphosphineoxide, OPPh$_3$ substitution on *cis*-[NbO(ca)$_2$(H$_2$O)OPPh$_3$]$^-$ at 31.2 $^\circ$C was investigated for five different pyridine ligands and also used in four different temperature studies to determine the activation parameters which govern these reactions.

---

[7] H.C. Brown, D.H. McDaniell and O. Hafliger, Determination of Organic Structures by Physical Methods, ed., E.A. Braude and F.C. Nachod Academic Press Inc., New York, N.Y., 597-662, 1955.

[8] A.R. Katritzky, Handbook of heterocyclic chemistry, University of Florida, first ed., 1985.

8.3.2 Preliminary experiments and arguments from literature to elucidate the stoichiometric reaction process

For this kinetic study the starting material, *cis*-[NbO(ca)$_2$(H$_2$O)OPPh$_3$]$^-$, has been successfully characterized by IR (ATR), ^{1}H NMR, ^{13}C NMR and ^{31}P NMR, as well as by single crystal X-ray diffraction (Chapters 3 and 5).

The kinetic and equilibrium solution of the *cis*-[NbO(ca)$_2$(H$_2$O)OPPh$_3$]$^-$ complex was thus monitored and evaluated by using different experiments as described below.

8.3.2.1 UV-Vis Measurements

As discussed above the starting complex, *cis*-[NbO(ca)$_2$(H$_2$O)OPPh$_3$]$^-$ was fully characterized by IR (ATR), ^{1}H NMR (Chapter 3) and X-ray crystallography (Chapter 5).

(i) Figure 8.1 shown above illustrates the plot of absorbance *versus* wavelength over time for the reaction between *cis*-[NbO(ca)$_2$(H$_2$O)OPPh$_3$]$^-$ and 4-(dimethylamino)pyridine (DMAP) in acetonitrile at 31.2 ^{o}C. The rate constants for the substitution of triphenylphosphineoxide by the DMAP ligand were obtained by monitoring the absorbance changes at 430 nm under *pseudo*-first-order conditions, which indicated that there is only one reaction taking place, with no evidence of either a fast reaction or a second slower reaction step present (Figure 8.1). Acetonitrile was the only solvent in which the starting complex is quite stable and it gave good kinetic results. However, during the NMR (^{1}H and ^{31}P) experiment the starting complex, *cis*-[NbO(ca)$_2$(H$_2$O)OPPh$_3$]$^-$ solubility was not complete in acetonitrile due to the high concentrations required for acceptable peak interpretation, but for the DMAP ligand the solubility is very good.

In another preliminary experiment, triphenylphosphineoxide was added to see if an excess in solution would have an influence on the reaction, but no significant change was observed in the rate of reaction. It is thus clear that consistent and clean kinetics were observed for the substitution reaction (see below).

(ii) Unfortunately, the final substitution reaction product, *cis*-[NbO(ca)$_2$(H$_2$O)(DMAP)]$^-$ could not be crystallysed for analysis by single crystal X-ray diffraction and an expanded attempt using spectroscopy was therefore necessitated and attempted. Before this however, exhaustive attempts to try to crystallise all five pyridine derivatives which were used for the kinetic study by using the same procedure from which the starting complex crystallize structure. This effort, as well as using different crystallization techniques did unfortunately not yield any crystalline substitution products which could be analysed further. However, the reaction is clearly observed by UV/vis, as shown in Figure 8.2, exhibiting a prominent colour change of the substitution reaction between *cis*-[NbO(ca)$_2$(H$_2$O)OPPh$_3$]$^-$ and DMAP (also illustrated in Fig. 8.1).
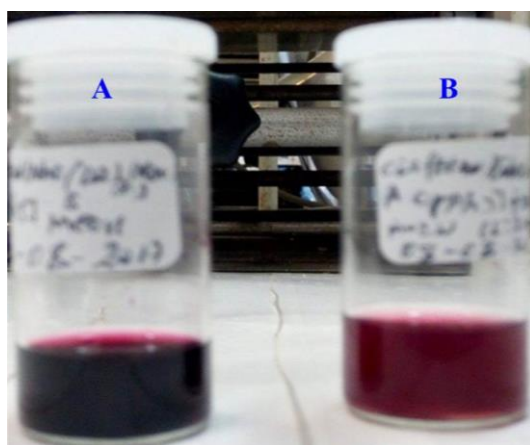
Figure 8.2 The color change observed showing the substitution reaction between *cis*-[NbO(ca)$_2$(H$_2$O)OPPh$_3$]$^-$ and DMAP, where **A** = *cis*-[NbO(ca)$_2$(H$_2$O)OPPh$_3$]$^-$ and **B** = *cis*-[NbO(ca)$_2$(H$_2$O)(DMAP)]$^-$.

8.3.2.2 ^{31}P NMR Studies

As discussed above the starting complex, *cis*-[NbO(ca)$_2$(H$_2$O)OPPh$_3$]$^-$ was fully characterized by IR (ATR), ^{1}H NMR (Chapter 3) and X-ray crystallography (Chapter 5).

(i) A preliminary ^{31}P NMR experiment shown in Figure 8.2 further illustrates complicating factors in the substitution process. Therein, free triphenylphosphineoxide (OPPh$_3$) with

excess water (0.017 M) yields a signal with chemical shift at 32.6 ppm. Moreover, after addition of a 1.0 : 2.2 M ratio of starting complex (**A**) to DMAP, the liberated free triphenylphosphineoxide (OPPh$_3$) signal appears at a chemical shift of 27.8 ppm which means the *cis* aqua ligand in the reactant *cis*-[NbO(ca)$_2$(H$_2$O)OPPh$_3$]$^-$ species is not substituted by DMAP, only the OPPh$_3$. Thus, from this it is concluded that the final product is *cis*-[NbO(ca)$_2$(H$_2$O)(DMAP)]$^-$.
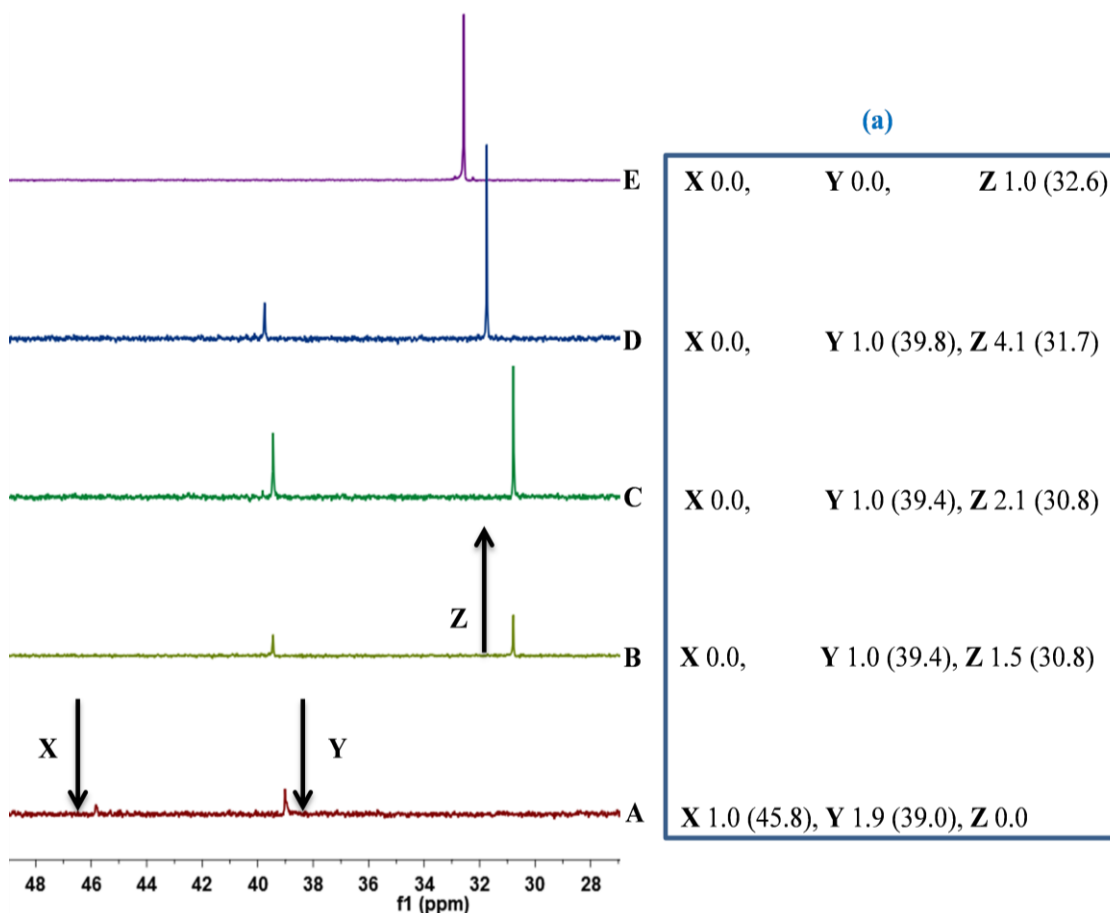
Figure 8.3 Stacked plot of ^{31}P NMR spectral change which is influenced by the addition of water (**B-E**,0.002, 0.004, 0.010 and 0.017 M), respectively to the starting complex (**A**), *cis*-[NbO(ca)$_2$(H$_2$O)OPPh$_3$]$^-$ (0.013 M) in acetonitrile (CD$_3$CN) at 25 $^{\circ}$C. Insert **(a)** illustrates the relative integrals of the signals at **X**, **Y** and **Z** and the chemical shifts of the different signals. **X** = decreasing *cis*-[NbO(ca)$_2$(MeCN)OPPh$_3$]$^-$, **Y** = decreasing *cis*-[NbO(ca)$_2$(H$_2$O)OPPh$_3$]$^-$ and **Z** = increasing liberated free triphenylphosphineoxide (OPPh$_3$) (signal at 32.6 ppm).

In Figure 8.3, the signals at 45.8 and 39.0 ppm represent the coordinated triphenylphosphine-oxide (OPPh$_3$) in *cis*-[NbO(ca)$_2$(MeCN)OPPh$_3$]$^-$ (33%) and *cis*-[NbO(ca)$_2$(H$_2$O)OPPh$_3$]$^-$ (67%) in the starting complex (**A**) respectively. **E** represents the free triphenylphosphineoxide (OPPh$_3$) (signal at 32.6 ppm) upon addition of excess water (0.017 M). **B**, **C**, and **D** shows the *cis*-[NbO(ca)$_2$(MeCN)OPPh$_3$]$^-$ (**Y**) species disappeared and the average signal at 39.6 ppm represent the coordinated triphenylphosphineoxide (OPPh$_3$) in the *cis*-[NbO(ca)$_2$(H$_2$O)OPPh$_3$]$^-$ (**Z**), as well as the average signal at 31.0 ppm, a new species which represents free triphenylphosphineoxide (OPPh$_3$), after addition of excess water (0.002 , 0.004 , and 0.011 M) to the starting complex (**A**) respectively. The additional conclusion from this experiment is that a large amount of water can liberate the OPPh$_3$ from the starting complex (**A**).

(ii) In another preliminary evaluation to confirm that triphenylphosphineoxide, OPPh$_3$ is (or not) substituted by DMAP, a second ^{31}P NMR study was undertaken. The experiment was performed by dissolving the starting complex, *cis*-(Et$_4$N)[NbO(ca)$_2$(H$_2$O)OPPh$_3$], 0.013 M (7.5 mg in 600 µL deuterated acetonitrile), followed by the successive addition of a range of concentrations of DMAP (between 0.013 M and 0.030 M) as illustrated below in Figure 8.4.
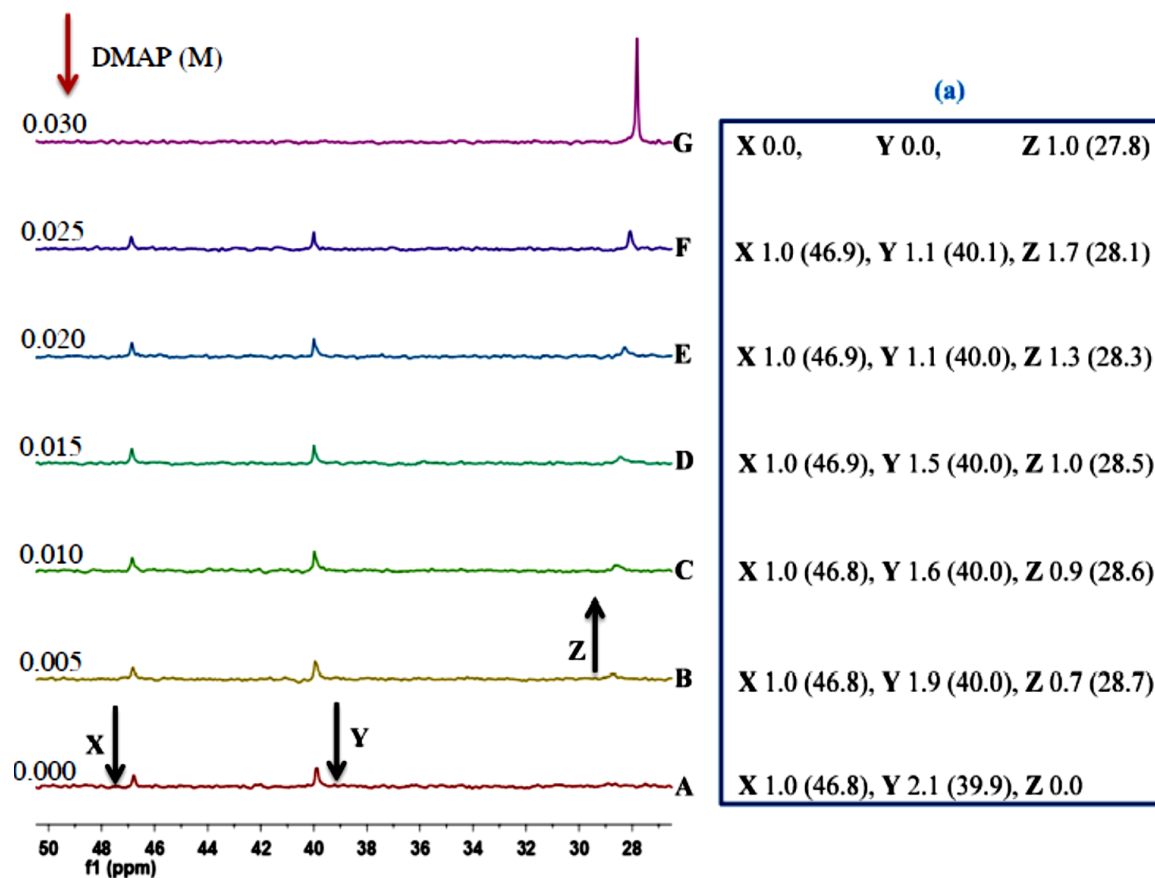
Figure 8.4 Illustration of ^{31}P NMR spectral change for the substitution reaction between *cis*-[NbO(ca)$_2$(H$_2$O)OPPh$_3$]$^-$, (0.013 M) (**A**) and DMAP, (0.005-0.03 M) (**B-G**). Insert (a) illustrates the relative integrals and the chemical shifts of the different signals. **X** = decreasing *cis*-[NbO(ca)$_2$(MeCN)OPPh$_3$]$^-$, **Y** = decreasing *cis*-[NbO(ca)$_2$(H$_2$O)OPPh$_3$]$^-$ and **Z** = increasing liberated free triphenylphosphineoxide (OPPh$_3$) product the signal at 27.8 ppm.

In Figure 8.4, the signals at 46.8 and 39.9 ppm represent coordinated triphenylphosphineoxide 33% of *cis*-[NbO(ca)$_2$(MeCN)OPPh$_3$] and 67% of *cis*-[NbO(ca)$_2$(H$_2$O)OPPh$_3$]$^-$ in the starting complex (**A**) respectively. Here it is concluded that there is an equilibrium between the (MeCN) and (H$_2$O) species. Spectra **B**, **C**, **D**, **E** and **F**, on the other hand, represent the step-wise substitution of triphenylphosphineoxide by DMAP following (0.005, 0.010, 0.015, 0.020, and 0.025 M of added DMAP) respectively.

G represents the complete substitution reaction between *cis*-[NbO(ca)$_2$(H$_2$O)OPPh$_3$]$^-$ and DMAP and gives a new product, *cis*-[NbO(ca)$_2$(H$_2$O)(DMAP)]$^-$ as well as liberated free triphenylphosphineoxide (OPPh$_3$) in acetonitrile (CD$_3$CN) at 25 $^\circ$C. The conclusion from this experiment is that the OPPh$_3$ is being substituted in an equilibrium reaction to finally form the *cis*-[NbO(ca)$_2$(H$_2$O)(DMAP)]$^-$ complex.

8.3.2.3 ^{1}H NMR studies

As discussed in the ^{31}P NMR experiments in Par 8.3.2.2 above, Figure 8.4 illustrated and confirmed the substitution reaction between *cis*-[NbO(ca)$_2$(H$_2$O)OPPh$_3$]$^-$ and DMAP, where in **A** = starting complex, **B** = first intermediate, **G** = new product forming *cis*-[NbO(ca)$_2$(H$_2$O)(DMAP)]$^-$ and liberated free OPPh$_3$.

On the other hand, the ^{1}H NMR experiment which is described below, was designed to attempt to elucidate (i) concentrations and (ii) temperature effects in the reaction.

(i) Concentration effect of DMAP: Figure 8.5 illustrates the ^{1}H NMR spectra showing the concentration dependence of DMAP as entering ligand on the reaction and the changes that are observed in the substitution reaction between *cis*-[NbO(ca)$_2$(H$_2$O)OPPh$_3$]$^-$ (**A**) (0.013 M) and DMAP (0.013-0.068 M) (**B-G**) at 25 $^\circ$C in acetonitrile (CD$_3$CN). This shows that triphenylphosphineoxide (OPPh$_3$) is completely substituted by DMAP at concentrations of 0.026 M (**C**), after addition of an excess of DMAP in the range between 0.03-0.068 M, and there is not a new change observed. However, the spectral results also show some fast exchange and the dynamic nature of the process.
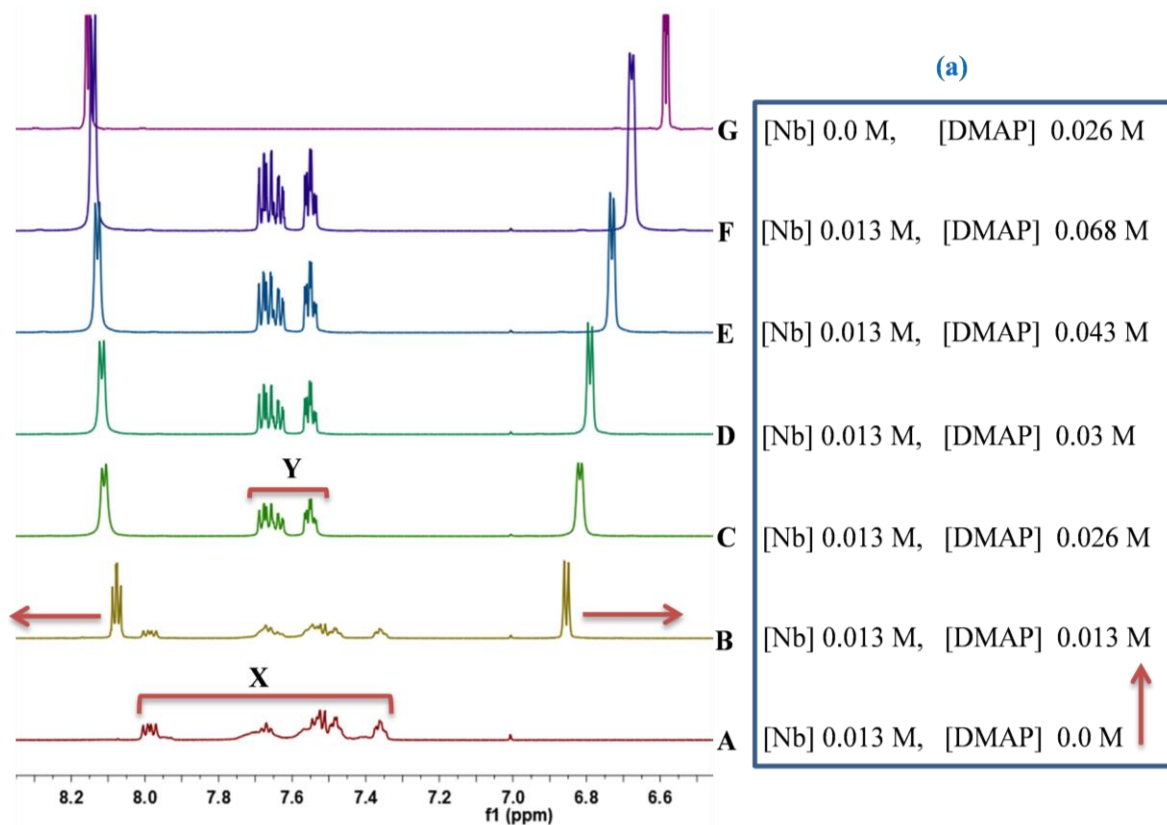
Figure 8.5 ^{1}H NMR spectra showing the changes observed in the substitution reaction between *cis*-[NbO(ca)$_2$(H$_2$O)OPPh$_3$]$^-$ (**A**) (0.013 M) and DMAP (0.013-0.068 M) (**B-G**) at 25 $^{\circ}$C in acetonitrile (CD$_3$CN). Insert **(a)** illustrates the relative concentrations of the starting complex, *cis*-[NbO(ca)$_2$(H$_2$O)OPPh$_3$]$^-$ ([Nb]) and DMAP. X represents coordinated triphenylphosphineoxide in the starting complex (**A**) (0.013 M), while **Y** the step-wise liberated triphenylphosphineoxide upon addition of DMAP (0.03 M) respectively.

(ii) Temperature effect: Figure 8.6 illustrate the temperature dependence of the ^{1}H NMR spectra of pyridine type ligands as entering ligands, the changes that observed the substitution reaction between *cis*-[NbO(ca)$_2$(H$_2$O)OPPh$_3$]$^-$ (**A**) (0.013 M) and DMAP (0.03 M) (**D**, **I-III**) at four different temperatures (25, 10, -10, and -25 $^{\circ}$C) in acetonitrile (CD$_3$CN). This illustrates that the spectra show the same trend from **D**, **I-III**, which means that there is no significant influence of temperature, or the shape of the signals and indicates either (i) a very

218

fast exchange or (ii) no exchange at all, and that the line broadening observed might be due to proton exchange and not substitution processes.
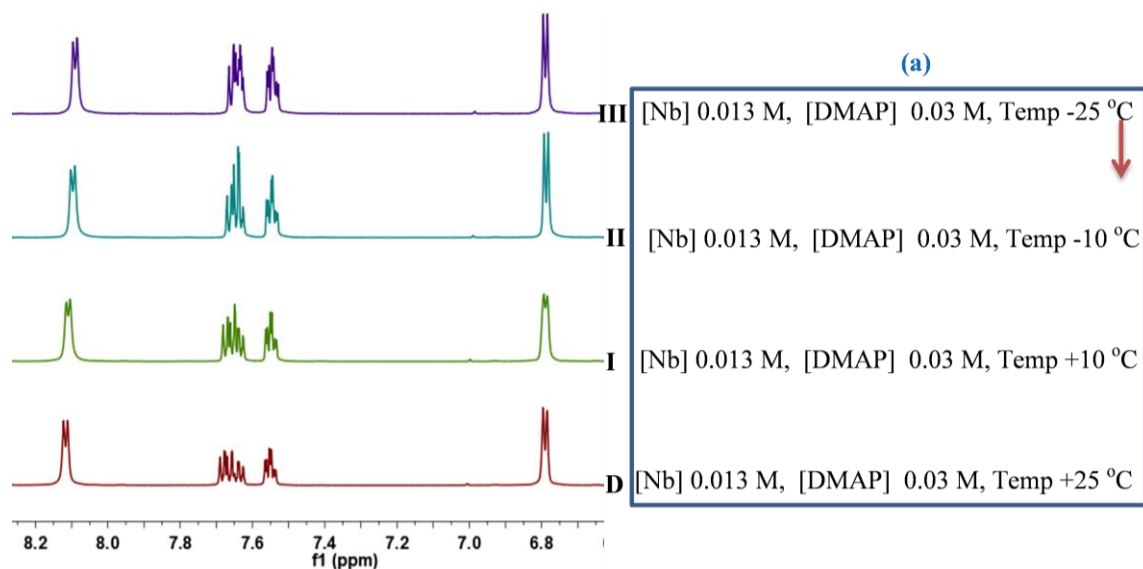
Figure 8.6 ^{1}H NMR spectra showing the changes observed the substitution reaction between *cis*-[NbO(ca)$_2$(H$_2$O)OPPh$_3$]$^-$ (**A**) (0.013 M) and DMAP (0.03 M) (**D, I-III**) at four different temperatures (25, 10, -10, and -25 °C) in acetonitrile (CD$_3$CN). Insert **(a)** illustrates the relative constant concentrations of starting complex, *cis*-[NbO(ca)$_2$(H$_2$O)OPPh$_3$]$^-$ ([Nb]) and DMAP at four different temperatures.

8.3.2.4 Conclusions from UV-Vis and NMR spectral studies

The conclusions from Par 8.3.2.1 (UV-Vis) 8.3.2.2 (^{31}P NMR) and 8.3.2.3 (^{1}H NMR) studies above are as follows:

The UV-Vis observations (Figure 8.1 and 8.2) together with the ^{31}P NMR (Figure 8.3 and 8.4) described above suggest that the new species that forms must be a complex where the triphenylphosphineoxide (OPPh$_3$) is substituted by pyridine type ligands. The final product, *cis*-[NbO(ca)$_2$(H$_2$O)(DMAP)]$^-$ is concluded from the signal peak which appears at 27.8 ppm which indicate that both the liberated triphenylphosphineoxide (OPPh$_3$) and the free triphenylphosphineoxide (OPPh$_3$) have the same chemical shift values.

The overall results from Figure 8.4 (^{31}P NMR) is that triphenylphosphineoxide is substituted from the starting complex by DMAP, while the results shown in Figure 8.5 and 8.6 (^{1}H NMR) agree with this.

It is thus concluded from the UV-Vis, ^{1}H and ^{31}P NMR experiments, as well as preliminary stopped-flow experiments as confirmed by the crystal structure of the starting complex (Chapter 5), that the substitution process with DMAP as entering nucleophile proceeds via a clean, one-step reaction with final Nb-product assumed to be *cis*-[NbO(ca)$_2$(H$_2$O)(DMAP)]$^-$ (and liberated free OPPh$_3$.

The detailed kinetics as describe below, thus assumes this and all interpretations are based on that.

8.4 Mechanism of the substitution of triphenylphosphineoxide (OPPh₃) from *cis*-[NbO(ca)₂(H₂O)OPPh₃]⁻ by pyridine type ligands

8.4.1 Introduction

The above experimental results (Par 8.2-8.3) allowed the proposed simple reaction for the triphenylphosphineoxide (OPPh$_3$) substitution of from *cis*-[NbO(ca)$_2$(H$_2$O)OPPh$_3$]$^-$ by different pyridine type ligands in acetonitrile. It is thus concluded that upon addition of pyridine type ligands to *cis*-[NbO(ca)$_2$(H$_2$O)OPPh$_3$]$^-$, the triphenylphosphineoxide (OPPh$_3$) is substituted according to the reaction in Eq. 8.1, where k_f and k_r represent the forward and reverse rate constants for the simple ligation process, respectively.

$$\text{cis-[NbO(ca)}_2\text{(H}_2\text{O)OPPh}_3]^- + \text{py} \underset{k_r}{\overset{k_f,\, K_1}{\rightleftharpoons}} \text{cis-[NbO(ca)}_2\text{(H}_2\text{O)(py)]}^- + \text{OPPh}_3 \qquad (8.1)$$
$$\textbf{(a)} \qquad\qquad\qquad\qquad\qquad\qquad\qquad \textbf{(b)}$$
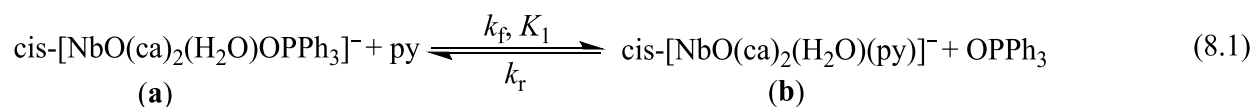
From Eq. 8.1, the rate law to the process can be written as in Eq. 8.2.

$$\text{Rate} = -d[\text{NbP}]/dt = k_f[\text{NbP}][\text{py}] - k_r[\text{Nbpy}][\text{P}] \qquad (8.2)$$

The NbP and Nbpy represent the reactant and product species in Eq. 8.1 (i.e, (**a**) and (**b**)) respectively. By using conditions where [py] >> [Nb] and following integration, the *pseudo* first-order rate constant in Eq. 8.1 is given by Eq. 8.3 below.

$$k_{\mathrm{obs}} = k_{\mathrm{f}}[\mathrm{py}] + k_{\mathrm{r}} \tag{8.3}$$

From general mass balances and Le Chatlier's principle, it follows that

$$K_{\mathrm{eq}} = \frac{k_{\mathrm{f}}}{k_{\mathrm{r}}} \tag{8.4}$$

A systematic study was therefore conducted wherein different pyridine type ligands were utilized and a progressive increase in [py] was studied. The results are presented below in Par 8.4.2.

8.4.2 The effect of pyridine concentration on OPPh₃ substitution from *cis-*[NbO(ca)₂(H₂O)OPPh₃]⁻

In Eq. 8.1 a general simple scheme is represented for the stoichiometric substitution of OPPh₃ from *cis*-[NbO(ca)₂(H₂O)OPPh₃]⁻ and pyridine type ligands such as pyridine (py), 4-methylpyridine (4-Mepy), 4-(dimethylamino)pyridine (DMAP), 3-chloropyridine (3-Clpy) and 3-bromopyridine (3-Brpy). These were investigated in acetonitrile using UV-Vis spectrophotometry.

As mentioned par 8.1, one of the main objectives of this solution mechanistic study was to determine the effect of the different the electron withdrawing and -donating capabilities of entering ligand systems on Nb(V) metal centre (Table 8.1). The following Figure 8.7 shows plot of k_{obs} *versus* concentration for the different pyridine type ligands, based on Eq. 8.3.
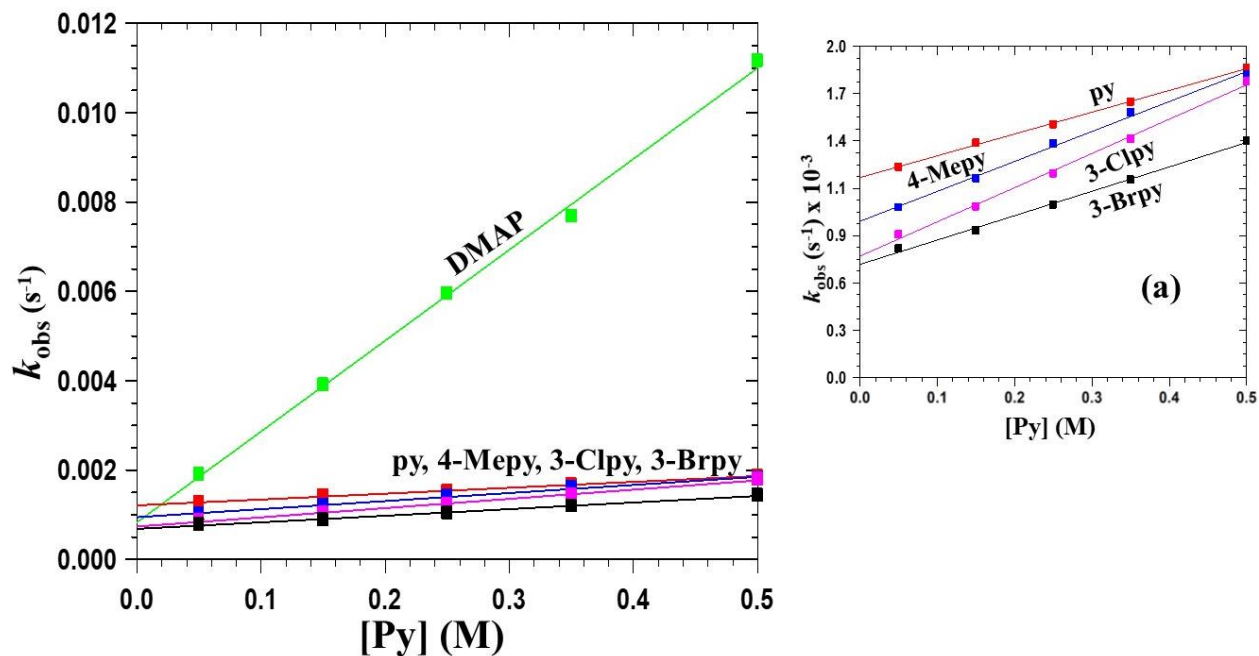
Figure 8.7 Systematic variation of the pyridine type ligand concentration for the reaction *cis*-[NbO(ca)$_2$(H$_2$O)OPPh$_3$]$^-$ in acetonitrile at 31.2 ^{o}C. Insert (a) enlarged perspective of bottom four ligands. Ligand: green DMAP (4-(dimethylamino) pyridine, red py (pyridine), blue 4-Mepy (4-methylpyridine), purple 3-Clpy (3-chloropyridine), and black 3-Brpy (3-bromopyridine). **Py** = pyridine type ligands.

Figure 8.7 above illustrates a plot of the observed *pseudo* first-order rate constant, k_{obs} *versus* Py-concentration. The substitution kinetics yielded straight lines with positive intercepts for all five Py type ligands according to Eq. 8.3.

The highest k_{obs} values are observed for DMAP, while the lowest k_{obs} values are observed for 3-bromopyridine, in agreement with the Bronstead basiscity and the electron donating ability of the ligands. It is interesting to note that a slightly higher k_{obs} value is observed for 3-chloropyridine compared to 3-bromopyridine, even when they have the same pK_a values (Figure 8.7 and Table 8.1). Nevertheless, the general trend is clear.

222

Table 8.2 Equilibrium, pK_a, and second-order rate constants (Eq. 8.3 and 8.4) for *cis*-[NbO(ca)$_2$(H$_2$O)OPPh$_3$]$^-$ and different entering Py-type ligands in acetonitrile at 31.2 ^{o}C

S/N	Entering ligands	pK_a[a]	K_{eq}[b]	k_f (M^{-1}s^{-1}) x 10^{-3} [c]	k_r (s^{-1}) x 10^{-3} [c]
1	4-(dimethylamino)pyridine	9.60	24.42 ± 4.71	20.33 ± 0.526	0.832 ± 0.159
2	4-methylpyridine	6.02	1.92 ± 0.082	1.81 ± 0.062	0.94 ± 0.019
3	Pyridine	5.25	1.09 ± 0.088	1.31 ± 0.0026	1.21 ± 0.008
4	3-chloropyridine	2.84	2.82 ± 0.130	2.07 ± 0.073	0.73 ± 0.022
5	3-bromopyridine	2.84	2.15 ± 0.088	1.47 ± 0.049	0.68 ± 0.015

a) Table 8.1, b) Eq. 8.4, c) Eq. 8.3

Table 8.2 illustrates the comparison of the equilibrium constants K_{eq}, pK_a, and the rate constant values of the substitution of triphenylphosphineoxide (OPPh$_3$) by five different entering ligands from the starting complex, *cis*-[NbO(ca)$_2$(H$_2$O)OPPh$_3$]$^-$. As expected for an Assotiative procces in hard metal centres, DMAP and 3-Brpy are the highest and lowest value observed compared to all five pyridine type ligands, since DMAP and 3-Brpy are more electron donating and withdrawing than the other listed ligands. These entering monodentate ligands were arranged in terms of increasing reactivity values showed as follows: 3-Brpy < 3-Clpy < 4-Mepy < py < DMAP as defined by k_f = 0.147(4) x 10^{-2}, 0.206(7) x 10^{-2}, 0.181(6) x 10^{-2} , 0.131(2) x 10^{-2} and 2.032(2) x 10^{-2} M^{-1}s^{-1} respectively (Figure 8.7).

8.4.3 The effect of temperature on the substitution reaction between *cis*-[NbO(ca)$_2$-(H$_2$O)OPPh$_3$]$^-$ and DMAP

The standard enthalpy change of activation ($\Delta H^{\neq}_{(kf)}$) and the standard entropy change of activation ($\Delta S^{\neq}_{(kf)}$) were determined from the temperature dependence (see Figure 8.8) of the reaction with DMAP, and were then obtained from an Eyring plot (Figure 8.9). Individual second-order rate constants are listed in Table 8.3.
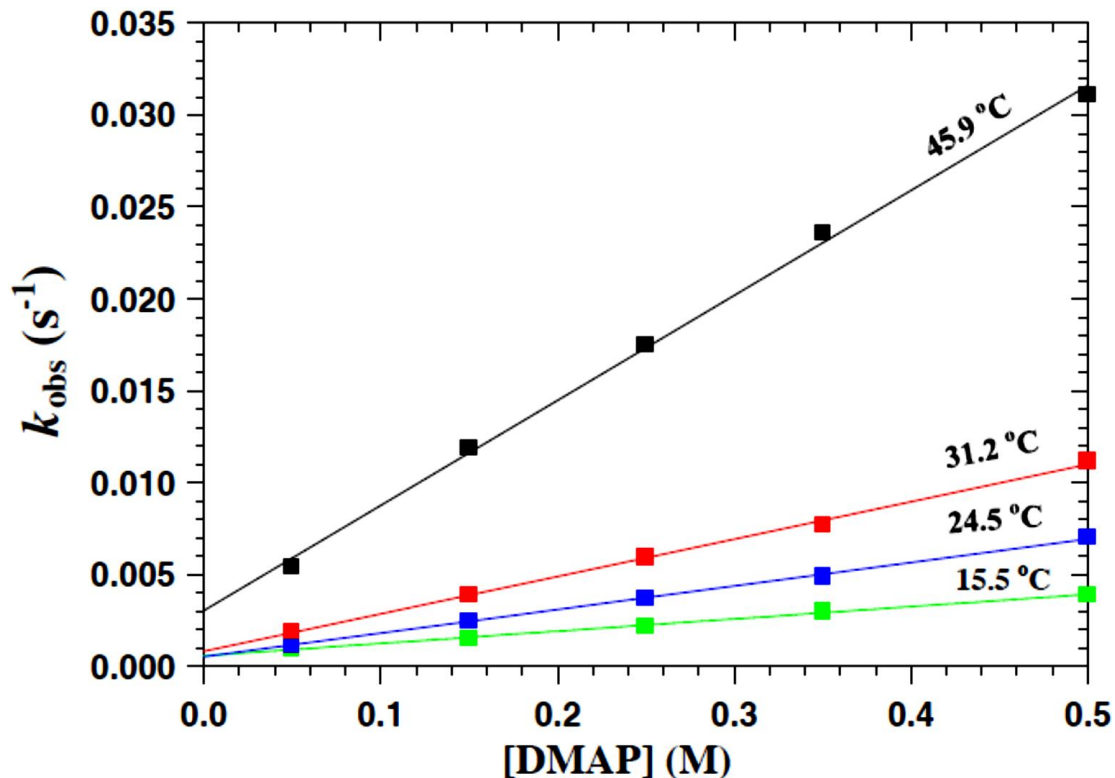
Figure 8.8 Plot of k_{obs} *versus* [DMAP] for the reaction between *cis*-[NbO(ca)$_2$(H$_2$O)OPPh$_3$]$^-$ and DMAP in acetonitrile at four different temperatures, [Nb] = 0.001 M, λ_{max} = 430 nm.

The activation parameters are required to provide an indication of the type of substitution mechanism for this reaction. Values for the standard activation enthalpy change ($\Delta H^{\neq}_{(kf)}$) and the standard activation entropy change ($\Delta S^{\neq}_{(kf)}$) were determined by using the logarithmic form of the Eyring Eq. in Eq. 8.5 below.

$$\ln \frac{k_f}{T} = \frac{-\Delta H^{\neq}}{RT} + \ln \frac{k_B}{h} + \frac{\Delta S^{\neq}}{R} \tag{8.5}$$

Here k_f = experimentally determined second-order rate constant, T = absolute temperature (K), $\Delta H^{\neq}$ = enthalpy change of activation (kJ mol^{-1}), $\Delta S^{\neq}$ = entropy change of activation (J K^{-1} mol^{-1}), R = universal gas constant (8.314 J K^{-1} mol^{-1}), k_B = Boltzmann constant (1.381 × 10^{-23} m^2 kg s^{-2} K^{-1}), h = Planck constant (6.626 × 10^{-34} m^2 kg s^{-1}).

Therefore, the enthalpy change of activation ($\Delta H^{\neq}$) and the entropy change of activation ($\Delta S^{\neq}$), were calculated from the experimental data (Figure 8.8; Table 8.3) by plotting $\left(\ln\frac{k}{T}\right)$ *versus* $\left(\frac{1}{T}\right)$ which gave a linear relationship with a slope of $\left(\frac{-\Delta H^{\neq}}{R}\right)$ and intercept of $\left(\ln\frac{k_B}{h} + \frac{\Delta S^{\neq}}{R}\right)$.

As indicated, the activation parameters were determined primarily to obtain evidence concerning whether or not an associative mechanism of activation was active for the reactions investigated. All the observed rate constants that were calculated for the chemical reactions are reported in the supplementary material (Appendix D), if not documented in the text.

The activation parameters of this reaction were thus determined by fitting the data to Eq. 8.5. It is represented in Figure 8.9 and reported in Table 8.3.

Table 8.3 Summary of the kinetic data for the triphenylphosphineoxide (OPPh$_3$) substitution reaction from *cis*-[NbO(ca)$_2$(H$_2$O)OPPh$_3$]$^-$ by DMAP in acetonitrile at four different temperatures, λ_{max} = 430 nm.

	15.5 ºC	24.5 ºC	31.2 ºC	45.9 ºC
k_f (M^{-1}s^{-1}) x 10^{-3}	6.68 ± 0.202	12.82 ± 0.251	20.33 ± 0.526	57.13 ± 1.526
k_{-r} (s^{-1}) x 10^{-3}	0.59 ± 0.061	0.54 ± 0.076	0.83 ± 0.159	3.06 ± 0.463
K_{eq} (M^{-1})^a	11.28 ± 1.210	23.82 ± 3.390	24.42 ± 4.710	18.70 ± 2.880
$\Delta H^{\neq}_{(kf)}$ (kJ mol^{-1})^b			51.50 ± 0.990	
$\Delta S^{\neq}_{(kf)}$ (J K^{-1} mol^{-1})^b			-107.95 ± 3.290	

a) Eq. 8.4, b) Eq. 8.5
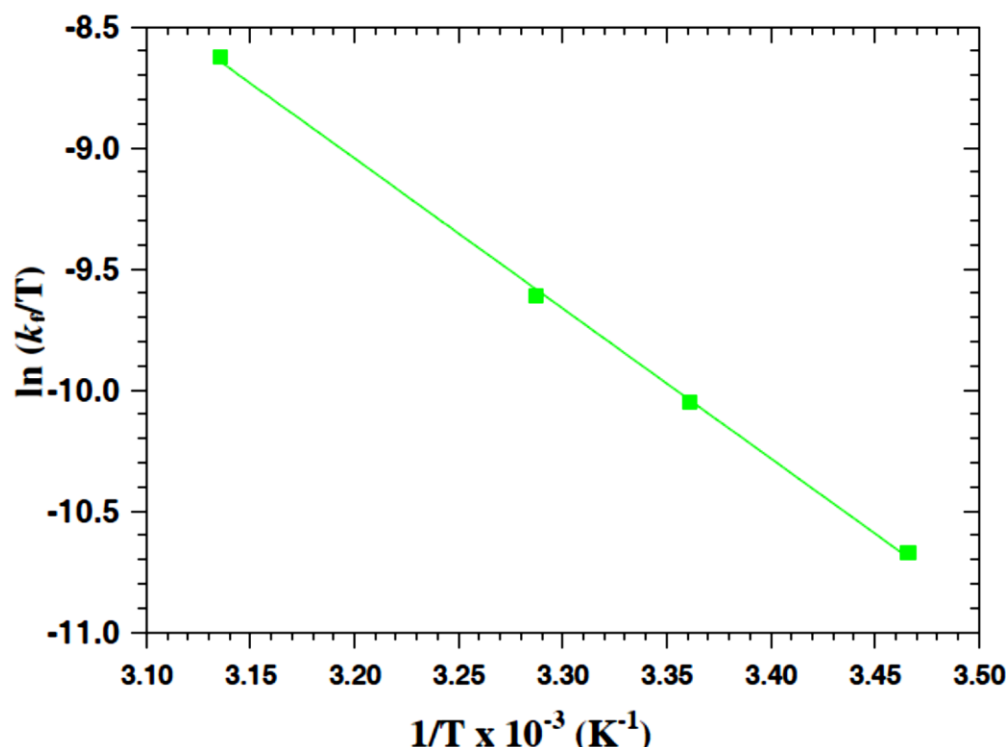
Figure 8.9 Eyring plot for the k_f rate constant of the reaction between *cis*-[NbO(ca)$_2$(H$_2$O)OPPh$_3$]$^-$ with DMAP in acetonitrile.

The activation parameters for the triphenylphosphineoxide substitution reaction from *cis*-[NbO(ca)$_2$(H$_2$O)OPPh$_3$]$^-$ by DMAP were calculated as 51(1) k J mol^{-1} and -108(3) J K^{-1} mol^{-1} for the standard change of enthalpy ($\Delta H^{\neq}_{(kf)}$) and the standard change of entropy ($\Delta S^{\neq}_{(kf)}$) respectively (Figure 8.9 and Table 8.3). The negative entropy of activation implies a more ordered transition state and presumably this substitution reaction involves an associative (A) ligand substitution mechanism. As indicated earlier, this is typical for hard metal such as Nb(V) centres as in this study.

8.5 Preliminary kinetic investigation the formation of *cis*-[NbO(ca)$_2$(H$_2$O)]$^-$ from [NbCl$_6$]$^-$

In this section, preliminary kinetic exeriments of the reaction between [NbCl$_6$]$^-$ and chloranilic acid (caH$_2$) in solution is described, presumably forming *cis*-[NbO(ca)$_2$(H$_2$O)]$^-$ before triphenylphosphineoxide (OPPh$_3$) is added to the final product of *cis*-[NbO(ca)$_2$(H$_2$O)OPPh$_3$]$^-$.

As reported in Chapter 3, the synthesised final product containing the OPPh$_3$ ligand was successfully characterised by IR (ATR), ^{1}H NMR, ^{13}C NMR, and ^{31}P NMR as well as by single crystal X-ray diffraction as reported in Chapter 5. Concrete evidence from these spectroscopic studies and in particular the X-ray diffraction confirms that two chloranilic acid ligands (caH$_2$) coordinated to the niobium(V) centre. The general proposed simple reaction is as follows:

$$[Nb(Cl)_6]^- + 2caH_2 + H_2O \rightleftharpoons cis\text{-}[NbO(ca)_2(H_2O)]^- + 6HCl \qquad (8.6)$$

In this set of experiments, the reaction between [NbCl$_6$]$^-$ and caH$_2$ was monitored at the best selected wavelength (530 nm) for product formation in MeOH at 25 ^{o}C, and is illustrated in Figure 8.10.

Figure 8.10 shows a plot of absorbance *versus* wavelength over time for the reaction between [NbCl$_6$]$^-$ and chloranilic acid (caH$_2$) in methanol (MeOH) at 25 ^{o}C. The rate constants for the formation reaction of *cis*-[NbO(ca)$_2$(H$_2$O)]$^-$ were obtained by measuring the absorbance changes at 530 nm under *pseudo*-first-order conditions and fitting it to the normal first-order exponential. It illustrates that there is only one reaction taking place with no evidence for second slower reaction step preceding the spectrum illustrated in Figure 8.10. It is clear that as in the reaction with pyridine ligands described earlier in the chapter, that it is also a simple reaction, exhibiting clear kinetics observed.

This is obviously an over-simplification of the overall process since the final product contains two chloranilic acid ligands. Nevertheless, the reaction was not analysed in more detail for the purpose of this PhD study, since only preliminarily kinetic were required to be obtained. In spite of this, the clear second-order dependence on the entering chloroanalinic acid is indeed obtained, as described further below.
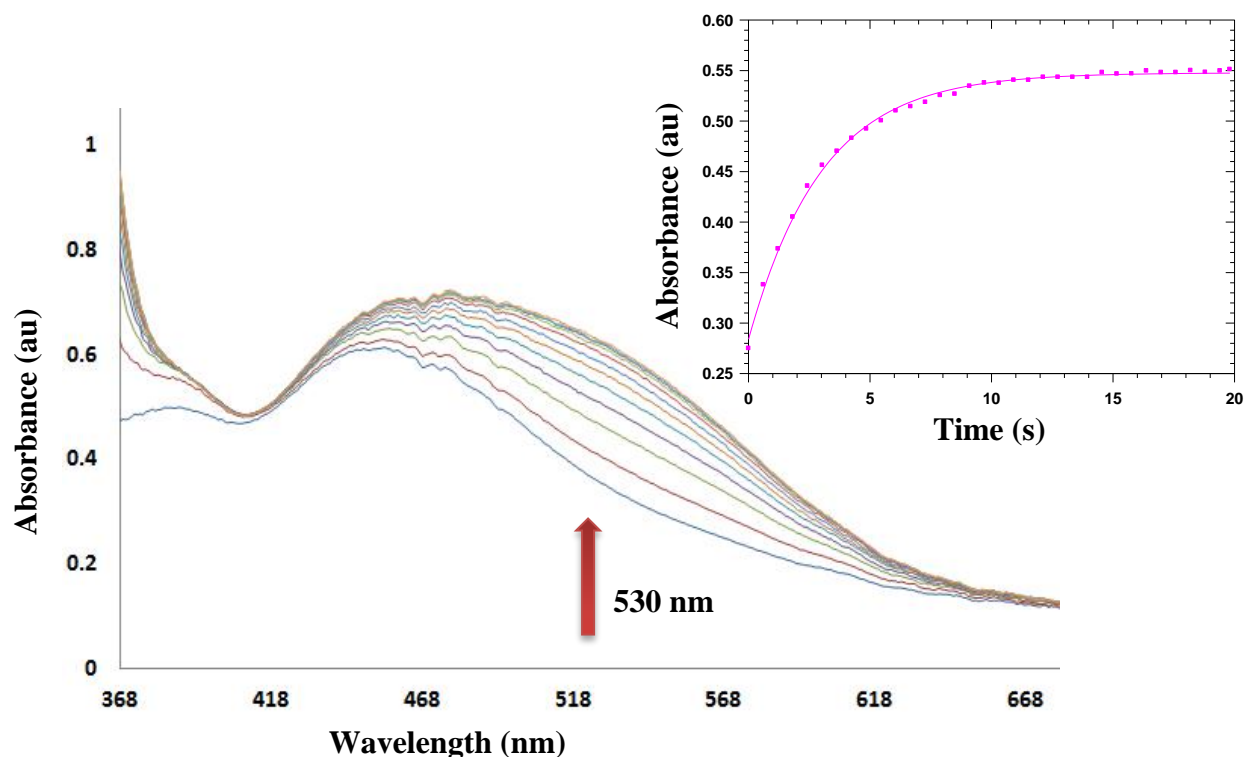
Figure 8.10 Stopped-flow spectra (20 second intervals) for the reaction between $[NbCl_6]^-$ (2×10^{-4} M) and $[caH_2]$ (6×10^{-3} M) for the formation of *cis*-$[NbO(ca)_2(H_2O)]^-$ in MeOH at 25.0 °C, λ_{max} = 530 nm, Δt = 1 s. Insert illustrates the absorbance change *versus* time at 530 nm and the line shows the least-squares fit to a first-order exponential (k_{obs} = 0.3173(6) s^{-1}).

8.5.1 Reaction order for the formation of *cis*-[NbO(ca)₂(H₂O)]⁻ in methanol, MeOH

In this preliminary study, the reaction between $[NbCl_6]^-$ and chloranilic acid (caH_2) in methanol (MeOH) was investigated at four different temperatures between 15 and 45 °C) using Stopped-flow techniques, by monitoring the product formation of *cis*-$[NbO(ca)_2(H_2O)]^-$ at 530 nm.

It is clear that when plotting k_{obs} *versus* $[caH_2]$, an *exponential*, <u>non-linear</u> relationship with respect to $[caH_2]$ is obtained (not shown). However, when plotting k_{obs} *versus* the square of the chloroanilinic acid concentration, $[caH_2]^2$, for these reactions, excellent straight lines as presented in Figure 8.11 below are obtained, clearly confirming a *second-order* dependence on $[caH_2]$.

The data from Figure 8.11 below yielded third-order rate constants which are reported in Table 8.4 below.
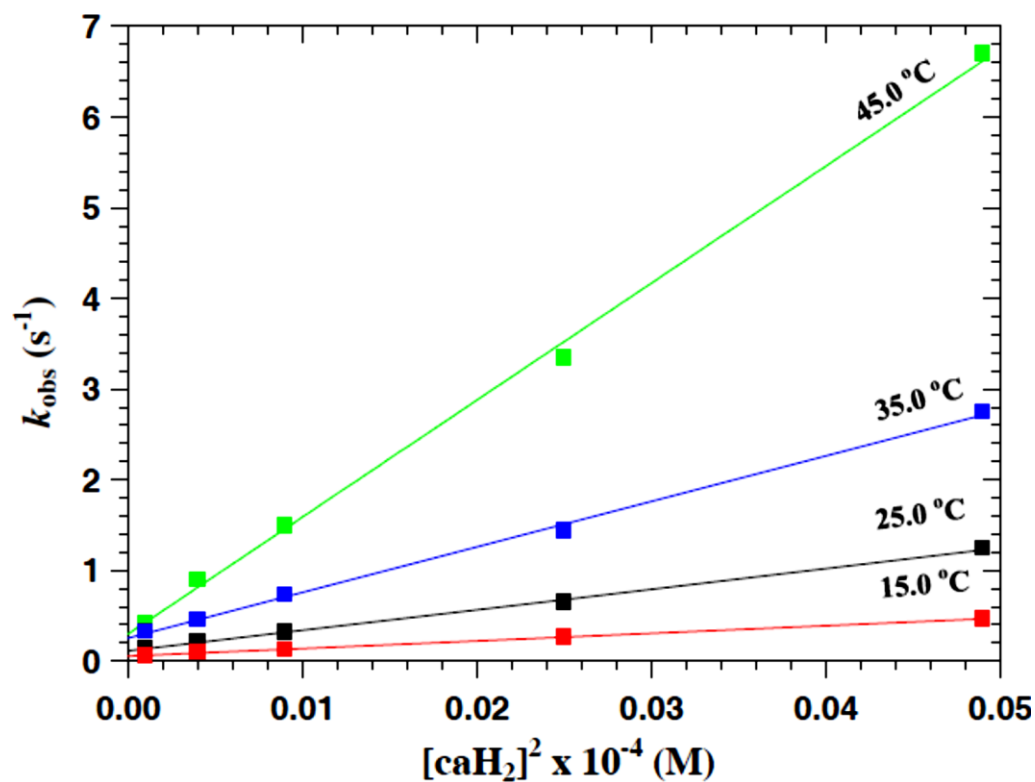
Figure 8.11 Plot of k_{obs} *versus* $[caH_2]^2$ for the formation of *cis*-$[NbO(ca)_2(H_2O)]^-$ in MeOH at four different temperatures (15-45 ºC), $\lambda_{max} = 530$ nm.

Table 8.4 Summary of the kinetic data for the reaction between $[NbCl_6]^-$ and $[caH_2]$ for the formation of *cis*-$[NbO(ca)_2(H_2O)]^-$ in MeOH at four different temperatures.

	15 ºC	25 ºC	35 ºC	45 ºC
k_f (M^{-2}s^{-1})	8361(198)	22691(574)	50208(1218)	129003(3131)
k_{-f} (s^{-1})	0.0533(9)	0.1106(4)	0.2529(4)	0.2980(3)
K_{eq} (M^{-2})	large	large	large	large
$\Delta H^{\neq}_{(kf)}$ (k J mol^{-1})		66(2)		
$\Delta S^{\neq}_{(kf)}$ (J K^{-1} mol^{-1})		60(7)		

The activation parameters governing the k_f step were determined by fitting the k_f *versus* temperature data to the Eyring Eq. 8.5. This is represented in Figure 8.12 and the data is reported in Table 8.4.
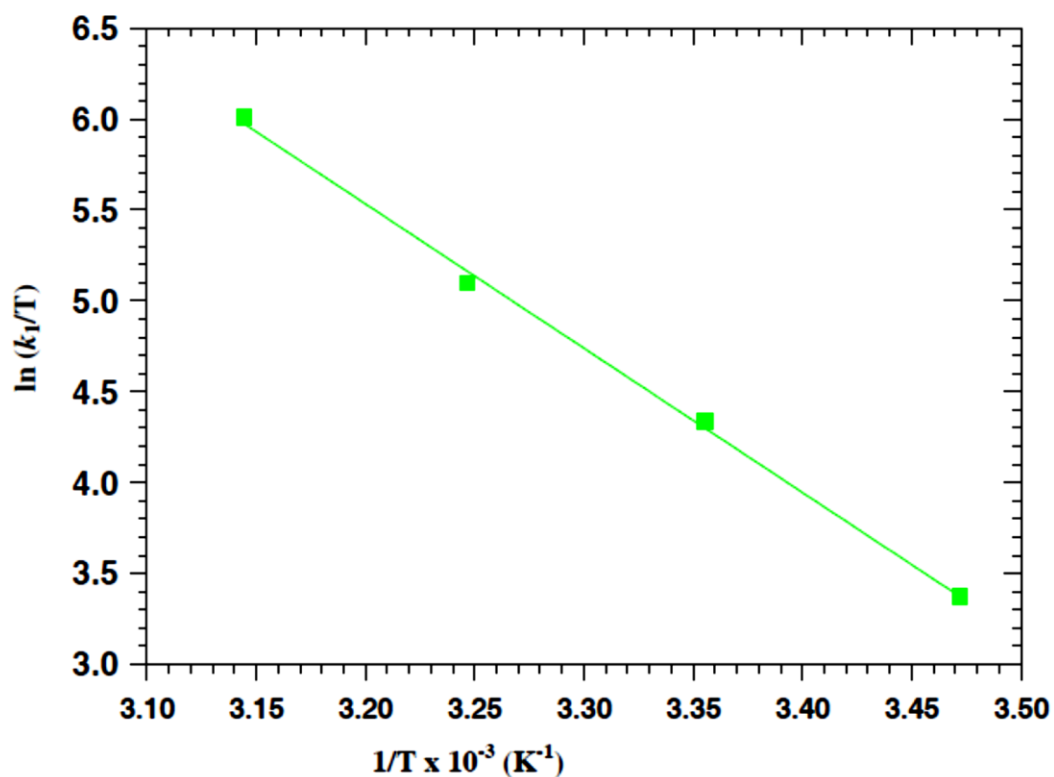
Figure 8.12 Eyring plot for the forward reaction between $[NbCl_6]^-$ and caH_2 in methanol at 15, 25, 35, and 45 °C.

As indicated above, in Figure 8.11, the effect of temperature on the reaction rate as studied by performing the kinetic runs at four different temperatures between 15 and 45 °C is illustrated. The results indicate that the observed third-order rate constant increased significantly with increased temperature (Table 8.4).

The activation parameters for the formation of *cis*-$[NbO(ca)_2(H_2O)]^-$, were calculated as 66(2) kJ mol^{-1} and 60(7) J K^{-1} mol^{-1} for the standard change of enthalpy ($\Delta H^{\neq}_{(kf)}$) and the standard change of entropy ($\Delta S^{\neq}_{(kf)}$) respectively (Figure 8.12 and Table 8.4). The positive entropy of activation

implies a presumably less ordered transition state and this formation kinetic process could involve a dissociative activation.

The fact that it obeys third-order kinetics however complicates the assignment thereof.

According to Scheme 8.6 below the reaction might involve a fast, initial reaction where caH_2 substitutes one leaving Cl^- ligand in an unfavourable equilibrium (small equilibrium constant), followed by rapid ring closing coordination by the caH_2 ligand through a potential dissociative process, thus forcing another Cl^- ligand out of the coordination sphere (8.6a). This process is then succeeded by a second caH_2 substituting yet another 1-2 Cl^- ligands via a very large equilibrium process (thermodynamically favoured) to yield the final cis-$[NbO(ca)_2(H_2O)]^-$ (8.6b).

The preliminary experiments indicate that the two consecutive steps in the *pseudo* first-order process may be written in Eq. s 8.6a and 8.6b below.

$$[NbCl_6]^- + caH_2 \underset{k_{-1}}{\overset{k_1,\,K_1}{\rightleftharpoons}} [Nb(ca)Cl_4]^- + 2HCl \tag{8.6a}$$

$$\text{A} \qquad\qquad\qquad\qquad\qquad\qquad \text{B}$$

$$[Nb(ca)Cl_4]^- + caH_2 \xrightarrow{\;k_2\;} [Nb(ca)_2Cl_2]^- + 2HCl \tag{8.6b}$$

$$\text{B} \qquad\qquad\qquad\qquad\qquad \text{C}$$
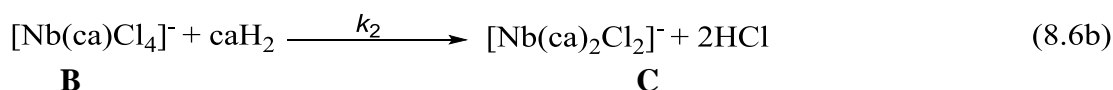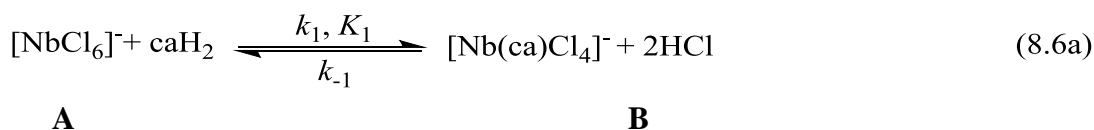
However, to complicate matters, due to the known rapid hydrolysis of Nb(V) species in general, Eq. 8.6c might also be operative in the broader reaction scheme in different parts of the overall reaction sequence.

$$[Nb(ca)_2Cl_2]^- + 2H_2O \xrightarrow{\;k_3\;} cis\text{-}[NbO(ca)_2(H_2O)]^- + 2HCl \tag{8.6c}$$
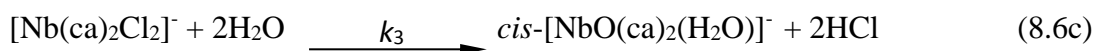
The presence of oxygen (H_2O) in the system and the fact that the final product contains the oxido ligand may clearly be obtained from a version of Eq. 8.6c, followed by deprotonation. In our research group related work reported with β-diketonate ligands utilized with niobium(V) and tantalum(V) centre, and indeed, similar complicated processes could be identified.[3]

To increase the complexity in this case even more, the deprotonation of the chloroanilinic acid is also expected to add yet another uncertainty parameter to be considered when doing a complete analysis of the process.

Nevertheless, by considering the overall formation of the cis-$[NbO(ca)_2(H_2O)]^-$ as indicated in Eq. 8.6b, the rate is given by:

$$d[C]/dt = k_2[B][CaH_2] \tag{8.6ai}$$

In Eq. 8.6.a, by (i) using the equilibrium for the first step $\{K_1 = ([B][HCl]^2)/([A][caH_2])\}$, and (ii) the total $[Nb]_{tot}$ just before the second reaction starts given by: $[Nb]_{tot} = [A] + [B]$, yields upon rearranging and substitution into each other:

$$[B] = ([Nb]_{tot}\, K_1[caH_2])/([HCl]^2 + K_1[caH_2]) \tag{8.6ii}$$

In addition, assuming (iii) that K_1 is small $\{K_1[caH_2]<<[HCl]^2\}$, then, upon substituting Eq. (86.ii) into Eq. (8.6i) and integration under pseudo first-order conditions $\{[caH_2]>>[Nb]\}$, Eq. (8.6iii) is obtained, with accounts for the second-order dependence in $[caH_2]$ as observed in this investigation:

$$k_{obs} = k_2K_1[caH_2]^2/([HCl]^2) \tag{8.6iii}$$

or, $$k_{obs} = k_f[caH_2]^2 + k_{-r} \tag{8.6iv}$$

For this study, $k_f = k_2K_1$, which is not further interpreted due to the complexity thereof. Moreover, note that a reverse reaction was added for completeness, which is by itself equally complicated considering the overall process.

It is clear that very interesting kinetics is prevalent in this process, however, it requires a much more in-depth investigation than that which was possible during this PhD study. This has to be considered when attempting this further in future.

8.6 Conclusion

The broad aims of this chapter included an overview of the reactivity of these complexes and an attempt at a mechanistic investigation of the reactivity of the fascinating complex *cis*-[NbO(ca)$_2$(H$_2$O)OPPh$_3$]$^-$ towards pyridine entering ligands, thus enabling a better understanding of physical and chemical behaviour of niobium and tantalum metals their structure/ reactivity relationships. The triphenylphosphineoxide (OPPh$_3$) substitution reaction from *cis*-[NbO(ca)$_2$(H$_2$O)OPPh$_3$]$^-$ by the pyridine type ligands was investigated and successfully evaluated. An interesting observation was made by comparing the NMR (^{1}H and ^{31}P) data and the kinetic data of the complex. In this study pyridine type ligands were chosen as the entering ligand, since (i) this kind of substitution reaction with Nb(V) and Ta(V) centres is novel and, (ii) the bond between Nb(V) metal centre and triphenylphosphineoxide ligand is long and weak (Chapter 5 Table 5.2). Literature has shown that pyridine type ligand can easily substitute if the bond is weaker.[9]

The rate and equilibrium constants for the substitution of triphenylphosphineoxide (OPPh$_3$) by different pyridine type ligands were determined in acetonitrile solutions at four different temperatures by UV-visible spectroscopy. The *pseudo* first-order rate constants were dependent on concentration and temperature. From the observed kinetic results a suitable mechanism could been proposed. All indications are that the substitution of the OPPh$_3$ by DMAP as studied here proceeds via an associative mechanism, confirmed by the activation parameters.

The preliminary fast (stopped-flow) study of the formation of *cis*-[NbO(ca)$_2$(H$_2$O)]$^-$ from [NbCl$_5$]$^-$ by reacting with chloroanilinic acid, revealed an interesting second-order dependence on [caH$_2$], and thus an overall third-order process. Again, from the observed kinetic results an acceptable mechanism could been proposed. The activation parameters suggested a dissociative intimate process for the substitution of chloride ligand by chloranilic acid (caH$_2$).

---

[9] S. Otto, *PhD. Thesis*. Structural and reactivity relationships in platinum(II) and rhodium(I) complexes, University of the Free State, 1999.

Overall it can be stated that the complex kinetics and equilibria investigated in this PhD project could be quite well studied under the circumstances, and indeed makes a positive contribution towards the structure/ reactivity relationships in these early transition metals, and particular to that of niobium.

9 Evaluation of the Study

9.1 Introduction

The aim of this study was to synthesise, characterise and further investigate novel niobium(V) and tantalum(V) complexes with various O,O'-bidentate ligands. In this study crystallographically (solid state) comparison was focused on selected best candidate ligands, chloranilate dianion (ca), 2-hydroxypyridinate-N-oxide (hopo) and cupferrate (cupf). From these ligands, chloranilate was chosen, coordinated to Nb(V) center and used for the solution state, substitution kinetics study. Substitution reaction kinetics between triphenylphosphineoxide (OPPh$_3$) and pyridine derivatives as entering ligand in a niobium(V) complex, in this case *cis*-[NbO(ca)$_2$(H$_2$O)OPPh$_3$]$^-$ has not been attempted before. The chemical relevance and results of this study are briefly discussed in Chapters 3-8 according to the pre-set aims which were established in Chapter 1.

The range of different coordination modes and geometries, including bond length and angles, π-π stacking as well as inter-and intramolecular interactions were discussed in Chapters 4-6. All complexes which were investigated by solid- and solution state as well as the newly synthesised Nb(V) and Ta(V) complexes that formed part of the preliminary study were successfully characterized by spectroscopic techniques (Chapter 3). Comparisons were drawn with similar niobium(V) and tantalum(V) structures from literature and the structures from this study were found to correlate quite well (Chapter 7). Those differences between the Nb(V) and Ta(V) complexes are quite significant and could translate to an ideal starting point for improved separation of niobium from tantalum. Some of the newly synthesised Nb(V) and Ta(V) complexes that formed part of the preliminary study were not characterized fully crystallographically and kinetically and will be discussed in this chapter as potential starting points for further studies.

9.2 Solid- and solution state investigation of various new niobium(V) and tantalum(V) complexes

9.2.1 Single crystal X-ray diffraction studies

In this study ten crystal structures, consisting of two free ligands, 2,5-dichloro-3,6-dihydroxy-2,5-cyclohexadiene-1,4-dione, or chloranilic acid (caH$_2$), and 2-hydroxypyridine-N-oxide (hopoH), two co-crystals obtained from 2,5-dichloro-3,6-dihydroxy-2,5-cyclohexadiene-1,4-dione (caH$_2$) with triphenylphosphineoxide (OPPh$_3$) and 4-(dimethylamino)pyridine (DMAP) respectively, one Nb(V)-cupferrate complex; three M(V)-2-hydroxypyridinate-N-oxide complexes (where M = Ta and Nb) as well as two Nb(V)-chloranilate complexes were successfully obtained and characterized by single crystal X-ray diffraction at low temperature, 100 K (Chapters 4, 5 and 6).

Due to a lack of stability and poor crystal quality, the crystal structures of tetrakis(2-hydroxypyridinato-N-oxide-κ^2O,O')tantalate(V) chloride, diacetonitrile and diaqua solvate, [Ta(hopo)$_4$]Cl·2MeCN·2H$_2$O (**10**) were not of the same standard when compared to other complexes reported in Chapter 5 and 6. Characterization by single crystal X-ray diffraction of [NbOS(mpo)$_2$OPPh$_3$] for example, was not reported in the crystallographic Chapter due to unfortunately poor crystal quality and a highly disordered (Chapter 3) structure. Various attempts to correct this was not successful.

The six-, seven- and eight coordinate geometries showed different coordination modes, as observed in [TaO(hopo)$_3$]·MeOH (**9**) (*C$_2$*-capped trigonal prismatic geometry), [NbO(hopo)$_3$]·MeOH (**8**) (*C$_{3v}$*-capped octahedral geometry), [Ta(hopo)$_4$]Cl·2MeCN·2H$_2$O (**10**) (*D$_2$*-square antiprismatic geometry), [NbO(cupf)$_3$] (**7**) and (Et$_4$N)*cis*-[NbO(ca)$_2$(H$_2$O)OPPh$_3$] (**5**) (*D$_{5h}$* pentagonal bipyramidal geometry) and (Et$_4$N)$_4$[Nb$_4$O$_4$(ca)$_2$(μ^2-O)$_2$Cl$_8$]·2CH$_3$CN (**6**) (a regular octahedral coordination mode). These coordination geometries were unusual for niobium(V) and tantalum(V) complexes when compared to other complexes from literature (Chapters 2 and 7).

During this study, different networks of infinite hydrogen-bonds, which lead to stabilised crystal lattices and increased stability of Nb(V) and Ta(V) complexes, were observed and discussed in Chapters 4, 5 and 6. The bond lengths and angles of niobium(V) and tantalum(V) complexes as well as that of the free ligands were well correlated.

Overall, these different geometries mentioned, describe the shape of complexes with six-, seven- and eight oxygen atoms bound to the niobium(V) and tantalum(V) centres and increase the possibility of separation of niobium from tantalum because of the differences. Exploiting phenomena like these was one of the goals of this study. In general, tantalum(V) complexes were less stable than niobium(V) complexes under atmospheric conditions.

9.2.2   Mechanistic Study

The substitution reaction between cis-[NbO(ca)$_2$(H$_2$O)OPPh$_3$]$^-$ and pyridine type ligands was successfully evaluated and discussed in Chapter 8. The rate of the reaction was slow, but in the case of the preliminary study, the kinetic substitution study in the formation of cis-[NbO(ca)$_2$(H$_2$O)]$^-$ was fast. ^{31}P NMR kinetics result shows that triphenylphosphineoxide was successfully replaced by DMAP in the starting complex, cis-[NbO(ca)$_2$(H$_2$O)OPPh$_3$]$^-$. However, ^{1}H NMR kinetic results were quite challenging and did not proceed as anticipated because of fast exchange between triphenylphosphineoxide with aqua and DMAP molecules. The concentration and temperature showed quite a significant influence on the rate of the reaction. Moreover, the final substitution reaction product, cis-[NbO(ca)$_2$(DMAP)(H$_2$O)]$^-$ was unfortunately not suitable for single crystal X-ray diffraction. With regard to the pK_a, values of five different pyridine derivatives used as entering ligands in the substitution kinetics, showed that DMAP was the most electron donating, while 3-Clpy and 3-Brpy were the most electron withdrawing of all five pyridine derivatives (Chapter 8 Table 8.2).

The mechanistic information gathered from this basic kinetic study, the investigation of the substitution reaction kinetics of triphenylphosphineoxide (OPPh$_3$) by pyridine type ligands in cis-[NbO(ca)$_2$(H$_2$O)OPPh$_3$]$^-$, could prove the potentially distinct physical and chemical behaviour of this Nb(V) complex, which helps for better understanding and to separate niobium from tantalum

in further studies. As was discussed in Chapter 2, no examples of this type of studies are currently available from literature. A simplified mechanistic study for the entire process of the two chloranilic acid (caH$_2$) ligand coordination to a niobium metal centre was reported in preliminary work (Chapter 8). From this preliminary work, evidence from spectroscopic data (Chapters 3 and 5) and crystallographic data (Chapter 5) show the presence of two chloranilic acid (caH$_2$) ligand in the complex. Overall, the mechanistic information obtained this far proves to be a very important stepping stone for understanding exactly how niobium(V) coordination reactions proceed and by clearly identifying reaction species, a more exact mechanistic theory can be identified and further utilized for separation processes.

9.3 Novel synthon of different new niobium (V)- and tantalum(V) complexes

The Nb(V) and Ta(V) complexes, *cis*-(Et$_4$N)[NbO(ca)$_2$(H$_2$O)OPPh$_3$] (**5**), (Et$_4$N)$_4$[Nb$_4$O$_4$(ca)$_2$(μ^2-O)$_2$Cl$_8$]·2CH$_3$CN (**6**), [NbO(cupf)$_3$] (**7**), [NbO(hopo)$_3$]·MeOH (**8**), [TaO(hopo)$_3$]·MeOH (**9**), and [Ta(hopo)$_4$]Cl·2MeCN·2H$_2$O (**10**) were successfully prepared from caH$_2$, cupfH, and hopoH ligands, using tetraethylammoniumchloride as counter-ion that has led to more stable starting materials, (Et$_4$N)[NbCl$_6$] and (Et$_4$N)[TaCl$_6$] and high percentage yields in atmospheric conditions. These complexes were successfully characterized by ATR-FTIR, UV-Vis, NMR (^{1}H, ^{13}C and ^{31}P) spectroscopy as well as single crystal X-ray diffraction (Chapter 3).

The complex [NbOS(mpo)$_2$OPPh$_3$] was prepared from 2-mercaptopyridine N-oxide (mpoH) as ligand and successfully characterised by ATR-FTIR, UV-Vis, and NMR (^{1}H, ^{13}C and ^{31}P) spectroscopy (Chapter 3). Unfortunately due to poor quality crystals and highly disordered structural data the crystal structure was not included in crystallographic Chapters 4, 5 and 6.

In preliminary synthesis, a range of quite a number of Nb(V) and Ta(V) complexes, [TaO(cupf)$_3$], [TaO(neocupf)$_3$], [NbO(neocupf)$_3$], [TaO(mpo)$_3$], [TaO(caH)$_3$], [NbO(dhbqH)$_3$], [TaO(dhbqH)$_3$], [NbO(qno)$_3$], [TaO(qno)$_3$], [NbO(pico)$_3$] and [TaO(pico)$_3$] were prepared from O,O'-, O,N-, O,S-and N,N'-bidentate ligands, using tetraethylammoniumchloride as counter-ion. These complexes were characterised by NMR (^{1}H, and ^{13}C), UV-Vis and FT-IR (ATR) spectroscopy, but crystals were not suitable for single crystal X-ray diffraction.

However, this preliminary spectroscopic results shown different physical and chemical behaviour of Nb(V) and Ta(V) complexes, which is promising in terms of its potential in the separation of these two metals (Chapter 3, Table 3.1 and 3.2). This has to be explored in further studies.

Overall, as was discussed in Chapter 3, substituted cupferrate ligands like 2-methylcupferrate, 4-methylcupferrate, 3,5-dichlorocupferrate and 3-acetylcupferrate were prepared by slightly modifying published procedures. Unfortunately, the synthesized substituted cupferron ligands were not suitable with niobium and tantalum complexes, because of solubility problems.

9.4 Future Work

A range of investigations undertaken as part of this study, and other evidence from literature, gave results that correlated quite well and begs for further investigation. Suggestion for future studies can be expressed as:

➢ As mentioned earlier in section 9.3, preliminarily synthesised complexes should be further characterised by solution sate (mechanistic) studies. This is of real importance in the furthering of separation studies, because studies using the new synthons have not been explored.

➢ As was mentioned in section 9.2, selection of the best candidates of the O,O'-bidentate ligands, chloranilic acid (caH$_2$), 2-hydroxypyridine N-oxide (hopoH), as well cupferron (cupf) ligands once again should be considered for further studies, to evaluate the influence of different substituents on the O,O'-bidentate ligands coordinating to Nb(V) and Ta(V) centres, as well as to compare electronic and steric effects of substitution reaction kinetics. Hopefully this will give insight into the coordination of different ligands and a better understanding and ease of differentiating of these two metals.

➢ Attempts to extend the range of different Nb(V) and Ta(V) complexes with O,O'-, O,N-, and N,N'-bidentate ligands system should be pursued by computational chemistry. A kinetic study is widely used to characterise the factors that control the reactivity and the mechanisms

of chemical changes that occur. This will provide a useful conceptual framework and expressions for calculation and possibly yield a theoretical construct through direct connection of measurables or easily computed properties of these two identical twin metals. Overall, these concepts of solid state reaction will be useful and effective to solve problems encountered with the poor solubility of Nb(V) and Ta(V) complexes.

10 Supplementary Data

10.1 Supplementary crystallographic data

Supplementary data for the structures discussed in Chapters 4, 5 and 6 are given in this chapter. For each of the structures data which are containing tables with atomic coordinates and equivalent isotropic displacement parameters, all bond distances and angles, anisotropic thermal parameters and hydrogen coordinates.

A.1 Crystal data of 2,5-dichloro-3,6-dihydroxy-2,5-cyclohexadiene-1,4-dione, ½(caH₂)·H₂O (1)

Table A.1 Atomic coordinates (x 10^4) and equivalent isotropic displacement parameters (Å^2x 10^3) for ½(caH₂)·H₂O (1). U(eq) is defined as one third of the trace of the orthogonalized U^{ij} tensor.

	x	y	z	U(eq)
Cl(1)	7186(1)	1425(1)	5045(1)	12(1)
O(1)	3629(2)	1586(1)	3145(3)	13(1)
O(2)	1810(2)	291(1)	-1120(3)	14(1)
C(1)	3276(2)	144(2)	-682(4)	10(1)
C(2)	4335(2)	843(2)	1691(3)	10(1)
C(3)	5956(2)	676(2)	2302(3)	10(1)
O(5)	507(2)	1848(2)	2614(3)	14(1)

Table A.2 Bond lengths (Å) and angles (°) for ½(caH₂)·H₂O (1).

Atoms	Distance (Å)	Atoms	Angle (°)
Cl(1)-C(3)	1.7175(2)	C(2)-O(1)-H(1)	109.5
O(1)-C(2)	1.317(2)	O(2)-C(1)-C(3)#1	123.67(2)
O(1)-H(1)	0.82	O(2)-C(1)-C(2)	118.04(2)
O(2)-C(1)	1.228(2)	C(3)#1-C(1)-C(2)	118.29(2)
C(1)-C(3)#1	1.453(2)	O(1)-C(2)-C(3)	122.02(2)
C(1)-C(2)	1.509(2)	O(1)-C(2)-C(1)	117.89(2)
C(2)-C(3)	1.354(2)	C(3)-C(2)-C(1)	120.07(2)
C(3)-C(1)#1	1.453(2)	C(2)-C(3)-C(1)#1	121.62(2)
O(5)-H(5B)	0.91(4)	C(2)-C(3)-Cl(1)	121.07(1)
O(5)-H(5A)	0.62(4)	C(1)#1-C(3)-Cl(1)	117.30(1)
		H(5B)-O(5)-H(5A)	112(4)

Table A.3 Anisotropic displacement parameters (Å^2 x 10^3) for ½(caH₂)·H₂O (1). The anisotropic displacement factor exponent takes the form: $-2\pi^2[$ $h^2a*^2U^{11}$ + … + 2 h k a* b* $U^{12}]$.

	U^{11}	U^{22}	U^{33}	U^{23}	U^{13}	U^{12}
Cl(1)	12(1)	15(1)	9(1)	-3(1)	1(1)	-4(1)
O(1)	10(1)	16(1)	13(1)	-5(1)	3(1)	0(1)
O(2)	9(1)	18(1)	15(1)	-3(1)	1(1)	0(1)
C(1)	10(1)	10(1)	9(1)	1(1)	2(1)	-1(1)
C(2)	12(1)	9(1)	8(1)	0(1)	3(1)	-1(1)
C(3)	10(1)	10(1)	7(1)	-1(1)	1(1)	-2(1)
O(5)	12(1)	16(1)	16(1)	-3(1)	6(1)	-2(1)

Table A.4 Hydrogen coordinates (x 10^4) and isotropic displacement parameters (Å^2x 10^3) for ½(caH₂)·H₂O (1).

	x	y	z	U(eq)
H(1)	2651	1580	2502	19
H(5B)	490(4)	2270(4)	4160(7)	42(1)
H(5A)	100(5)	1340(4)	2470(8)	34(1)

Table A.5 General hydrogen-bond distances (Å) and angles (°) of ½(caH₂)·H₂O (1).

D-H···A	d(D-H) (Å)	D(H···A) (Å)	d(D···A) (Å)	D-H···A (°)
O1-H1···O5	0.82	1.87	2.632(2)	154
O1-H1···O2	0.82	2.25	2.703(2)	115
O5-H4···O5i	0.91(4)	1.99(4)	2.898(2)	178(3)
O5-H3···O2ii	0.62(4)	2.33(4)	2.938(2)	167(5)

Symmetry code: (i) x, ½ - y, z + ½ (ii) -x, -y, -z,

A.2 Crystal data of triphenylphosphineoxide-2,5-dichloro-3,6-dihydroxy-cyclohexa-2,5-diene-1,4-dione, ½(caH₂)OPPh₃ (2)

Table A.6 Atomic coordinates (x 10^4) and equivalent isotropic displacement parameters (Å^{2}x 10^3) for (caH₂)OPPh₃½ (2). U(eq) is defined as one third of the trace of the orthogonalized U^{ij} tensor.

	x	y	z	U(eq)
Cl(1)	1807(1)	1766(1)	8806(1)	24(1)
C(26)	2474(2)	6104(1)	8624(1)	17(1)
C(23)	1061(2)	6890(2)	6574(1)	25(1)
C(21)	3479(1)	6145(1)	7554(1)	14(1)
C(22)	2769(2)	6560(1)	6524(1)	19(1)
O(3)	6226(1)	5697(1)	8594(1)	16(1)
O(1)	3323(1)	2706(1)	10293(1)	20(1)
O(2)	3987(1)	-1125(1)	8631(1)	21(1)
C(36)	6380(2)	8203(1)	5996(1)	19(1)
C(11)	6262(1)	3667(1)	7513(1)	13(1)
C(3)	4402(1)	-584(1)	9263(1)	14(1)
C(24)	68(2)	6819(2)	7645(1)	25(1)
C(31)	6610(1)	6669(1)	6179(1)	14(1)
C(16)	5477(2)	3146(1)	6884(1)	17(1)
C(32)	7595(2)	6050(1)	5325(1)	18(1)
C(1)	4102(1)	1421(1)	10125(1)	14(1)
C(12)	7601(1)	2727(1)	8072(1)	16(1)
C(2)	3557(1)	836(1)	9455(1)	14(1)
C(25)	765(2)	6448(2)	8665(1)	23(1)
C(15)	6061(2)	1711(1)	6787(1)	20(1)
C(13)	8175(2)	1289(1)	7974(1)	20(1)
C(33)	8313(2)	6962(2)	4292(1)	22(1)
C(35)	7116(2)	9105(1)	4966(1)	22(1)
C(34)	8070(2)	8485(2)	4111(1)	23(1)
C(14)	7416(2)	796(1)	7320(1)	21(1)
P(1)	5669(1)	5566(1)	7562(1)	11(1)

Table A.7 Bond lengths (Å) and angles (°) for ½(caH₂)OPPh₃ (2).

Atoms	Distance (Å)	Atoms	Angle (°)
Cl(1)-C(2)	1.7192(1)	C(25)-C(26)-C(21)	119.73(1)
C(26)-C(25)	1.3915(2)	C(25)-C(26)-H(26)	120.1
C(26)-C(21)	1.3964(2)	C(21)-C(26)-H(26)	120.1
C(26)-H(26)	0.93	C(24)-C(23)-C(22)	119.78(1)
C(23)-C(24)	1.389(2)	C(24)-C(23)-H(23)	120.1
C(23)-C(22)	1.3903(2)	C(22)-C(23)-H(23)	120.1
C(23)-H(23)	0.93	C(26)-C(21)-C(22)	120.05(1)
C(21)-C(22)	1.4001(2)	C(26)-C(21)-P(1)	118.08(9)
C(21)-P(1)	1.7930(1)	C(22)-C(21)-P(1)	121.79(9)
C(22)-H(22)	0.93	C(23)-C(22)-C(21)	119.84(1)
O(3)-P(1)	1.4929(8)	C(23)-C(22)-H(22)	120.1
O(1)-C(1)	1.3157(1)	C(21)-C(22)-H(22)	120.1
O(1)-H(1)	0.82	C(1)-O(1)-H(1)	109.5
O(2)-C(3)	1.2213(1)	C(35)-C(36)-C(31)	120.14(1)
C(36)-C(35)	1.3920(2)	C(35)-C(36)-H(36)	119.9
C(36)-C(31)	1.3962(2)	C(31)-C(36)-H(36)	119.9
C(36)-H(36)	0.93	C(12)-C(11)-C(16)	119.70(1)
C(11)-C(12)	1.3959(2)	C(12)-C(11)-P(1)	118.39(9)
C(11)-C(16)	1.3970(2)	C(16)-C(11)-P(1)	121.82(9)
C(11)-P(1)	1.8019(1)	O(2)-C(3)-C(2)	124.16(1)
C(3)-C(2)	1.4526(2)	O(2)-C(3)-C(1)#1	118.48(1)
C(3)-C(1)#1	1.5089(2)	C(2)-C(3)-C(1)#1	117.35(9)
C(24)-C(25)	1.389(2)	C(25)-C(24)-C(23)	120.64(1)
C(24)-H(24)	0.93	C(25)-C(24)-H(24)	119.7
C(31)-C(32)	1.3980(2)	C(23)-C(24)-H(24)	119.7
C(31)-P(1)	1.8093(1)	C(36)-C(31)-C(32)	119.39(1)
C(16)-C(15)	1.3913(2)	C(36)-C(31)-P(1)	117.35(9)
C(16)-H(16)	0.93	C(32)-C(31)-P(1)	123.20(9)
C(32)-C(33)	1.3929(2)	C(15)-C(16)-C(11)	120.05(1)
C(32)-H(32)	0.93	C(15)-C(16)-H(16)	120
C(1)-C(2)	1.3506(2)	C(11)-C(16)-H(16)	120
C(1)-C(3)#1	1.5088(2)	C(33)-C(32)-C(31)	120.13(1)
C(12)-C(13)	1.3935(2)	C(33)-C(32)-H(32)	119.9
C(12)-H(12)	0.93	C(31)-C(32)-H(32)	119.9
C(25)-H(25)	0.93	O(1)-C(1)-C(2)	121.43(1)
C(15)-C(14)	1.3856(2)	O(1)-C(1)-C(3)#1	117.99(1)

C(15)-H(15)	0.93	C(2)-C(1)-C(3)#1	120.55(1)
C(13)-C(14)	1.3882(2)	C(13)-C(12)-C(11)	119.90(1)
C(13)-H(13)	0.93	C(13)-C(12)-H(12)	120
C(33)-C(34)	1.3854(2)	C(11)-C(12)-H(12)	120
C(33)-H(33)	0.93	C(1)-C(2)-C(3)	122.07(1)
C(35)-C(34)	1.3911(2)	C(1)-C(2)-Cl(1)	120.18(9)
C(35)-H(35)	0.93	C(3)-C(2)-Cl(1)	117.74(8)
C(34)-H(34)	0.93	C(24)-C(25)-C(26)	119.93(1)
C(14)-H(14)	0.93	C(24)-C(25)-H(25)	120
		C(26)-C(25)-H(25)	120
		C(14)-C(15)-C(16)	119.94(1)
		C(14)-C(15)-H(15)	120
		C(16)-C(15)-H(15)	120
		C(14)-C(13)-C(12)	119.95(1)
		C(14)-C(13)-H(13)	120
		C(12)-C(13)-H(13)	120
		C(34)-C(33)-C(32)	120.19(1)
		C(34)-C(33)-H(33)	119.9
		C(32)-C(33)-H(33)	119.9
		C(34)-C(35)-C(36)	120.14(1)
		C(34)-C(35)-H(35)	119.9
		C(36)-C(35)-H(35)	119.9
		C(33)-C(34)-C(35)	119.99(1)
		C(33)-C(34)-H(34)	120
		C(35)-C(34)-H(34)	120
		C(15)-C(14)-C(13)	120.41(1)
		C(15)-C(14)-H(14)	119.8
		C(13)-C(14)-H(14)	119.8
		O(3)-P(1)-C(21)	113.34(5)
		O(3)-P(1)-C(11)	110.90(5)
		C(21)-P(1)-C(11)	107.83(5)
		O(3)-P(1)-C(31)	112.46(5)
		C(21)-P(1)-C(31)	106.57(5)
		C(11)-P(1)-C(31)	105.29(5)

Table A.8 Anisotropic displacement parameters ($Å^2$ x 10^3) for ½(caH$_2$)OPPh$_3$ (2). The anisotropic displacement factor exponent takes the form: $-2\pi^2[\ h^2a^{*2}U^{11} + \ldots + 2\ h\ k\ a^*\ b^*\ U^{12}]$.

	U^{11}	U^{22}	U^{33}	U^{23}	U^{13}	U^{12}
Cl(1)	21(1)	27(1)	30(1)	-16(1)	-15(1)	6(1)
C(26)	18(1)	16(1)	17(1)	-5(1)	-2(1)	-2(1)
C(23)	20(1)	27(1)	30(1)	-9(1)	-12(1)	0(1)
C(21)	13(1)	12(1)	17(1)	-5(1)	-3(1)	-2(1)
C(22)	18(1)	21(1)	18(1)	-7(1)	-5(1)	-1(1)
O(3)	18(1)	17(1)	15(1)	-8(1)	-6(1)	-2(1)
O(1)	21(1)	18(1)	27(1)	-14(1)	-11(1)	3(1)
O(2)	24(1)	21(1)	23(1)	-12(1)	-10(1)	-3(1)
C(36)	21(1)	17(1)	18(1)	-8(1)	0(1)	-4(1)
C(11)	14(1)	13(1)	13(1)	-5(1)	0(1)	-3(1)
C(3)	15(1)	15(1)	12(1)	-5(1)	-2(1)	-5(1)
C(24)	13(1)	24(1)	39(1)	-11(1)	-6(1)	-1(1)
C(31)	13(1)	16(1)	13(1)	-5(1)	-2(1)	-4(1)
C(16)	20(1)	15(1)	17(1)	-6(1)	-5(1)	-4(1)
C(32)	19(1)	18(1)	18(1)	-8(1)	-1(1)	-2(1)
C(1)	14(1)	14(1)	14(1)	-6(1)	-2(1)	-2(1)
C(12)	14(1)	17(1)	19(1)	-6(1)	-2(1)	-4(1)
C(2)	13(1)	16(1)	14(1)	-6(1)	-5(1)	-1(1)
C(25)	17(1)	22(1)	26(1)	-8(1)	4(1)	-3(1)
C(15)	27(1)	18(1)	20(1)	-10(1)	-1(1)	-8(1)
C(13)	16(1)	16(1)	25(1)	-5(1)	-1(1)	-1(1)
C(33)	21(1)	28(1)	17(1)	-10(1)	2(1)	-4(1)
C(35)	27(1)	16(1)	22(1)	-4(1)	-2(1)	-8(1)
C(34)	22(1)	27(1)	17(1)	-2(1)	0(1)	-9(1)
C(14)	24(1)	14(1)	25(1)	-9(1)	4(1)	-4(1)
P(1)	11(1)	12(1)	12(1)	-6(1)	-2(1)	-2(1)

Table A.9 Hydrogen coordinates (x 10^4) and isotropic displacement parameters (Å^{2}x 10^3) for ½(caH$_2$)OPPh$_3$ (2).

	x	y	z	U(eq)
H(26)	2945	5849	9306	21
H(23)	584	7157	5893	30
H(22)	3438	6614	5808	23
H(1)	3846	2937	10672	31
H(36)	5734	8622	6563	22
H(24)	-1074	7022	7679	30
H(16)	4564	3758	6531	20
H(32)	7771	5026	5447	22
H(12)	8110	3059	8508	20
H(25)	91	6429	9374	27
H(15)	5541	1366	6365	24
H(13)	9065	660	8347	24
H(33)	8957	6548	3721	27
H(35)	6969	10124	4850	27
H(34)	8546	9092	3418	27
H(14)	7820	-154	7238	25

Table A.10 General hydrogen-bond distances (Å) and angles (°) for ½(caH$_2$)OPPh$_3$ (2).

D-H···A	d(D-H) (Å)	D(H···A) (Å)	d(D···A) (Å)	D-H···A (°)
O1-H1···O2^{iv}	0.82	2.27	2.7102(14)	114
O1-H1···O3^{v}	0.82	1.83	2.5301(13)	143

Symmetry code: (iv) 1-x, - y, 2-z, (v) 1-x, 1- y, 2-z

A.3 Crystal data of 2-hydroxypyridine-N-oxide (hopoH), C₅H₅NO₂ (3)

Table A.11 Atomic coordinates (x 10^4) and equivalent isotropic displacement parameters (Å^2x 10^3) for [hopoH] (3). U(eq) is defined as one third of the trace of the orthogonalized U^{ij} tensor.

	x	y	z	U(eq)
O(2)	2843(1)	3242(1)	2237(1)	24(1)
C(3)	3602(2)	4131(1)	5860(1)	21(1)
C(2)	4537(2)	3268(1)	5439(1)	20(1)
O(1)	5186(1)	2081(1)	3864(1)	23(1)
C(5)	2118(2)	4483(1)	3800(1)	21(1)
C(6)	3049(2)	3562(1)	3343(1)	18(1)
N(1)	4259(1)	3017(1)	4224(1)	18(1)
C(4)	2373(2)	4754(1)	5016(1)	21(1)

Table A.12 Bond lengths (Å) and angles (°) for hopoH (3).

Atoms	Distance (Å)	Atoms	Angle (°)
O(2)-C(6)	1.2619(2)	C(2)-C(3)-C(4)	118.78(1)
C(3)-C(2)	1.359(2)	C(2)-C(3)-H(3)	120.6
C(3)-C(4)	1.4085(2)	C(4)-C(3)-H(3)	120.6
C(3)-H(3)	0.95	N(1)-C(2)-C(3)	119.73(1)
C(2)-N(1)	1.3590(2)	N(1)-C(2)-H(2)	120.1
C(2)-H(2)	0.95	C(3)-C(2)-H(2)	120.1
O(1)-N(1)	1.3836(1)	N(1)-O(1)-H(1)	109.5
O(1)-H(1)	0.84	C(4)-C(5)-C(6)	121.88(1)
C(5)-C(4)	1.365(2)	C(4)-C(5)-H(5)	119.1
C(5)-C(6)	1.4222(2)	C(6)-C(5)-H(5)	119.1
C(5)-H(5)	0.95	O(2)-C(6)-N(1)	120.72(1)
C(6)-N(1)	1.3824(2)	O(2)-C(6)-C(5)	125.08(1)
C(4)-H(4)	0.95	N(1)-C(6)-C(5)	114.20(1)
		C(2)-N(1)-C(6)	125.02(1)
		C(2)-N(1)-O(1)	116.82(1)
		C(6)-N(1)-O(1)	117.99(1)
		C(5)-C(4)-C(3)	120.32(1)
		C(5)-C(4)-H(4)	119.8
		C(3)-C(4)-H(4)	119.8

Table A.13 Anisotropic displacement parameters ($\mathring{A}^2$ x 10^3) for hopoH (3). The anisotropic displacement factor exponent takes the form: $-2\pi^2[\,h^2a^{*2}U^{11} + \ldots + 2\,h\,k\,a^*\,b^*\,U^{12}]$.

	U^{11}	U^{22}	U^{33}	U^{23}	U^{13}	U^{12}
O(2)	21(1)	28(1)	20(1)	0(1)	2(1)	2(1)
C(3)	20(1)	23(1)	20(1)	-1(1)	2(1)	-4(1)
C(2)	16(1)	20(1)	22(1)	6(1)	0(1)	-1(1)
O(1)	23(1)	19(1)	30(1)	5(1)	10(1)	8(1)
C(5)	16(1)	20(1)	25(1)	2(1)	1(1)	2(1)
C(6)	15(1)	17(1)	21(1)	3(1)	2(1)	-2(1)
N(1)	15(1)	15(1)	22(1)	2(1)	4(1)	2(1)
C(4)	17(1)	19(1)	28(1)	-1(1)	4(1)	-1(1)

Table A.14 Hydrogen coordinates (x 10^4) and isotropic displacement parameters (Å^{2}x 10^3) for hopoH (3).

	x	y	z	U(eq)
H(3)	3774	4309	6709	26
H(2)	5381	2844	5992	24
H(1)	5832	2365	3436	35
H(5)	1296	4923	3244	25
H(4)	1718	5366	5294	25

Table A.15 Torsion angles (°) for hopoH (3).

Torsion angles	Angle (°)
C(4)-C(3)-C(2)-N(1)	-0.72(2)
C(4)-C(5)-C(6)-O(2)	177.78(1)
C(4)-C(5)-C(6)-N(1)	-2.61(2)
C(3)-C(2)-N(1)-C(6)	-1.17(2)
C(3)-C(2)-N(1)-O(1)	-176.35(1)
O(2)-C(6)-N(1)-C(2)	-177.62(1)
C(5)-C(6)-N(1)-C(2)	2.75(2)
O(2)-C(6)-N(1)-O(1)	-2.49(2)
C(5)-C(6)-N(1)-O(1)	177.89(1)
C(6)-C(5)-C(4)-C(3)	1.0(2)
C(2)-C(3)-C(4)-C(5)	0.77(2)

Table A.16 General hydrogen-bond distances (Å) and angles (°) for hopoH (3).

D-H…A	d(D-H) (Å)	D(H…A) (Å)	d(D…A) (Å)	D-H…A (°)
O1-H1…O1vi	0.84	2.55	3.0004(2)	114
O1-H1…O2vi	0.84	1.73	2.5563(2)	167
C2ii-H2ii…O2vii	0.95	2.50	3.4480(2)	172

Symmetry code: (vi) -x + 1, y, -z + ½, (vii) x + ½, -y + ½, z + ½

A.4 Crystal structure of 2,5-dichloro-3,6-dihydroxycyclohexa-2,5-diene-1,4-dione-4-N,N-dimethylaminopyridinium, 2½(caH₂)(DMAP)₆·11H₂O (4)

Table A.17 Atomic coordinates (x 10^4) and equivalent isotropic displacement parameters (Å^2x 10^3) for 2½(caH₂)(DMAP)₆·11H₂O (4). U(eq) is defined as one third of the trace of the orthogonalized U^{ij} tensor.

	x	y	z	U(eq)
Cl(2)	3444(1)	7283(1)	2649(1)	22(1)
Cl(4)	2813(1)	4608(1)	2164(1)	24(1)
O(10)	9598(1)	4507(1)	3694(1)	22(1)
C(52)	4998(2)	5823(2)	1325(2)	34(1)
N(3)	7845(2)	4998(2)	2987(1)	21(1)
C(14)	10703(2)	4362(2)	4641(1)	15(1)
O(6)	574(1)	9927(1)	2590(1)	23(1)
C(57)	7476(2)	4543(2)	1845(1)	18(1)
C(56)	8101(2)	4526(2)	2404(1)	21(1)
C(53)	6528(2)	5079(2)	1871(1)	16(1)
C(54)	6282(2)	5548(2)	2501(1)	19(1)
C(13)	9818(2)	4703(2)	4302(1)	14(1)
N(4)	5898(2)	5143(2)	1328(1)	23(1)
O(2)	6043(1)	2428(1)	2059(1)	22(1)
C(51)	6167(2)	4689(2)	675(1)	31(1)
C(55)	6948(2)	5494(2)	3035(1)	21(1)
C(10)	2765(2)	8273(2)	3008(1)	16(1)
N(12)	105(2)	9136(2)	1227(1)	24(1)
N(11)	-1836(2)	9199(2)	-431(1)	27(1)
C(29)	620(2)	3861(2)	-1123(1)	19(1)
C(4)	3635(2)	3778(2)	1750(1)	16(1)
C(22)	5831(2)	8177(2)	5858(1)	20(1)
N(5)	4378(2)	8898(2)	5285(1)	20(1)
N(6)	6273(2)	8740(2)	6978(1)	21(1)
C(32)	-1199(2)	9184(2)	103(1)	18(1)
C(21)	5185(2)	8247(2)	5310(1)	21(1)
O(4)	2659(1)	3858(1)	733(1)	21(1)
C(34)	316(2)	8555(2)	691(2)	25(1)
C(33)	-300(2)	8558(2)	132(1)	22(1)
C(25)	847(2)	3286(2)	-1709(1)	16(1)

N(1)	6443(2)	3036(2)	3454(1)	22(1)
C(30)	-1639(3)	8613(3)	-1034(2)	36(1)
C(45)	8075(2)	3522(2)	5751(1)	29(1)
N(9)	235(2)	3286(2)	-2256(1)	22(1)
C(18)	5659(2)	8793(2)	6428(1)	17(1)
C(47)	6786(2)	3556(2)	4580(1)	19(1)
C(20)	4193(2)	9498(2)	5814(1)	22(1)
C(6)	4138(2)	2767(2)	716(1)	16(1)
O(5)	1690(1)	8465(2)	2044(1)	24(1)
O(3)	3898(1)	2538(2)	124(1)	24(1)
C(48)	6184(2)	3553(2)	4018(2)	22(1)
C(38)	1315(2)	378(2)	6112(2)	25(1)
O(1)	4719(1)	3636(1)	2705(1)	20(1)
C(27)	2377(2)	2703(2)	-1122(1)	22(1)
C(17)	6066(2)	9352(2)	7569(2)	27(1)
C(42)	3980(2)	1724(2)	7377(2)	24(1)
C(23)	-719(2)	3894(2)	-2292(2)	27(1)
C(16)	7170(2)	8066(2)	6992(2)	27(1)
C(37)	2165(2)	1840(2)	5574(1)	25(1)
C(28)	1267(2)	3824(2)	-584(1)	22(1)
C(12)	1295(2)	9562(2)	2948(1)	16(1)
C(31)	-2782(2)	9817(3)	-428(2)	44(1)
C(40)	2589(2)	369(2)	7306(1)	19(1)
C(35)	-736(2)	9747(2)	1215(1)	23(1)
C(11)	1947(2)	8714(2)	2634(1)	16(1)
C(50)	7981(2)	2473(2)	3982(1)	20(1)
C(36)	-1385(2)	9795(2)	673(1)	21(1)
C(24)	492(2)	2708(3)	-2856(2)	35(1)
N(2)	8336(2)	2965(2)	5139(1)	21(1)
C(2)	5256(2)	2702(2)	1738(1)	16(1)
C(3)	4507(2)	3416(2)	2108(1)	15(1)
C(5)	3415(2)	3520(2)	1078(1)	16(1)
C(1)	5004(2)	2406(2)	1079(1)	18(1)
C(46)	7724(2)	2991(2)	4585(1)	17(1)
C(44)	9253(2)	2311(2)	5154(2)	28(1)
C(49)	7333(2)	2508(2)	3439(1)	22(1)
C(7)	1555(2)	9839(2)	3611(1)	16(1)
N(10)	2133(2)	3252(2)	-575(1)	22(1)

C(19)	4800(2)	9471(2)	6383(1)	21(1)
C(26)	1770(2)	2698(2)	-1692(1)	20(1)
N(7)	3917(2)	1047(2)	7923(1)	25(1)
N(8)	2099(2)	1075(2)	6145(1)	19(1)
C(43)	3397(2)	1780(2)	6786(1)	20(1)
C(39)	2671(2)	1081(2)	6729(1)	16(1)
C(41)	3219(2)	389(2)	7866(1)	23(1)
C(15)	9049(2)	5368(2)	4692(1)	14(1)
O(9)	8246(1)	5608(1)	4382(1)	20(1)
Cl(5)	11564(1)	3628(1)	4177(1)	22(1)
Cl(1)	823(1)	10777(1)	3997(1)	21(1)
O(8)	3792(1)	8226(1)	3997(1)	23(1)
O(7)	2662(1)	9674(2)	4564(1)	24(1)
C(8)	2402(2)	9427(2)	3983(1)	16(1)
C(9)	3051(2)	8585(2)	3652(1)	16(1)
Cl(3)	5827(1)	1578(1)	667(1)	35(1)
O(20)	8008(2)	1808(2)	1585(1)	27(1)
O(21)	9316(2)	1620(2)	2691(1)	26(1)
O(12)	5035(2)	6468(2)	3889(1)	28(1)
O(16)	2848(2)	7607(2)	949(1)	28(1)
O(17)	6354(2)	6158(2)	4957(1)	30(1)
O(19)	420(2)	3263(2)	2607(1)	32(1)
O(18)	646(2)	3906(2)	1238(1)	29(1)
O(13)	1955(2)	5981(2)	530(1)	33(1)
O(14)	4777(2)	8434(2)	983(1)	37(1)
O(15)	1081(2)	6789(2)	-699(1)	31(1)
O(11)	3947(2)	4871(2)	3795(1)	34(1)

Table A. 18 Bond lengths (Å) and angles (°) for 2½(caH₂)(DMAP)₆·11H₂O (4).

Atoms	Distance (Å)	Atoms	Angle (°)
Cl(2)-C(10)	1.736(3)	N(4)-C(52)-H(52A)	109.5
Cl(4)-C(4)	1.735(3)	N(4)-C(52)-H(52B)	109.5
O(10)-C(13)	1.250(3)	H(52A)-C(52)-H(52B)	109.5
C(52)-N(4)	1.466(4)	N(4)-C(52)-H(52C)	109.5
C(52)-H(52A)	0.96	H(52A)-C(52)-H(52C)	109.5
C(52)-H(52B)	0.96	H(52B)-C(52)-H(52C)	109.5
C(52)-H(52C)	0.96	C(55)-N(3)-C(56)	120.1(2)
N(3)-C(55)	1.340(3)	C(13)-C(14)-C(15)#1	123.5(2)
N(3)-C(56)	1.344(4)	C(13)-C(14)-Cl(5)	117.36(2)
C(14)-C(13)	1.397(3)	C(15)#1-C(14)-Cl(5)	119.04(2)
C(14)-C(15)#1	1.398(3)	C(12)-O(6)-H(6)	109.5
C(14)-Cl(5)	1.738(2)	C(56)-C(57)-C(53)	119.7(2)
O(6)-C(12)	1.249(3)	C(56)-C(57)-H(57)	120.1
O(6)-H(6)	0.82	C(53)-C(57)-H(57)	120.1
C(57)-C(56)	1.366(4)	N(3)-C(56)-C(57)	121.9(2)
C(57)-C(53)	1.421(3)	N(3)-C(56)-H(56)	119.1
C(57)-H(57)	0.93	C(57)-C(56)-H(56)	119.1
C(56)-H(56)	0.93	N(4)-C(53)-C(54)	121.6(2)
C(53)-N(4)	1.342(3)	N(4)-C(53)-C(57)	122.0(2)
C(53)-C(54)	1.418(4)	C(54)-C(53)-C(57)	116.3(2)
C(54)-C(55)	1.362(4)	C(55)-C(54)-C(53)	120.3(2)
C(54)-H(54)	0.93	C(55)-C(54)-H(54)	119.9
C(13)-C(15)	1.535(3)	C(53)-C(54)-H(54)	119.9
N(4)-C(51)	1.452(4)	O(10)-C(13)-C(14)	124.7(2)
O(2)-C(2)	1.251(3)	O(10)-C(13)-C(15)	116.6(2)
O(2)-H(2)	0.82	C(14)-C(13)-C(15)	118.7(2)
C(51)-H(51A)	0.96	C(53)-N(4)-C(51)	121.4(2)
C(51)-H(51B)	0.96	C(53)-N(4)-C(52)	120.7(2)
C(51)-H(51C)	0.96	C(51)-N(4)-C(52)	117.0(2)
C(55)-H(55)	0.93	C(2)-O(2)-H(2)	109.5
C(10)-C(9)	1.393(3)	N(4)-C(51)-H(51A)	109.5
C(10)-C(11)	1.397(3)	N(4)-C(51)-H(51B)	109.5
N(12)-C(34)	1.344(4)	H(51A)-C(51)-H(51B)	109.5
N(12)-C(35)	1.350(4)	N(4)-C(51)-H(51C)	109.5
N(11)-C(32)	1.339(3)	H(51A)-C(51)-H(51C)	109.5
N(11)-C(30)	1.448(4)	H(51B)-C(51)-H(51C)	109.5

N(11)-C(31)	1.470(4)	N(3)-C(55)-C(54)	121.6(2)
C(29)-C(28)	1.352(4)	N(3)-C(55)-H(55)	119.2
C(29)-C(25)	1.419(4)	C(54)-C(55)-H(55)	119.2
C(29)-H(29)	0.93	C(9)-C(10)-C(11)	123.1(2)
C(4)-C(5)	1.391(3)	C(9)-C(10)-Cl(2)	119.11(2)
C(4)-C(3)	1.407(3)	C(11)-C(10)-Cl(2)	117.77(2)
C(22)-C(21)	1.363(4)	C(34)-N(12)-C(35)	119.7(2)
C(22)-C(18)	1.417(4)	C(32)-N(11)-C(30)	122.4(2)
C(22)-H(22)	0.93	C(32)-N(11)-C(31)	120.9(2)
N(5)-C(20)	1.344(3)	C(30)-N(11)-C(31)	116.7(2)
N(5)-C(21)	1.345(3)	C(28)-C(29)-C(25)	119.7(2)
N(6)-C(18)	1.340(3)	C(28)-C(29)-H(29)	120.2
N(6)-C(17)	1.452(3)	C(25)-C(29)-H(29)	120.2
N(6)-C(16)	1.457(3)	C(5)-C(4)-C(3)	123.2(2)
C(32)-C(36)	1.415(4)	C(5)-C(4)-Cl(4)	118.84(2)
C(32)-C(33)	1.425(4)	C(3)-C(4)-Cl(4)	117.94(2)
C(21)-H(21)	0.93	C(21)-C(22)-C(18)	120.1(2)
O(4)-C(5)	1.261(3)	C(21)-C(22)-H(22)	119.9
O(4)-H(4)	0.82	C(18)-C(22)-H(22)	119.9
C(34)-C(33)	1.358(4)	C(20)-N(5)-C(21)	119.6(2)
C(34)-H(34)	0.93	C(18)-N(6)-C(17)	121.1(2)
C(33)-H(33)	0.93	C(18)-N(6)-C(16)	120.3(2)
C(25)-N(9)	1.339(3)	C(17)-N(6)-C(16)	118.6(2)
C(25)-C(26)	1.423(3)	N(11)-C(32)-C(36)	121.5(2)
N(1)-C(49)	1.348(3)	N(11)-C(32)-C(33)	122.3(2)
N(1)-C(48)	1.348(4)	C(36)-C(32)-C(33)	116.2(2)
C(30)-H(30A)	0.96	N(5)-C(21)-C(22)	122.0(2)
C(30)-H(30B)	0.96	N(5)-C(21)-H(21)	119
C(30)-H(30C)	0.96	C(22)-C(21)-H(21)	119
C(45)-N(2)	1.454(3)	C(5)-O(4)-H(4)	109.5
C(45)-H(45A)	0.96	N(12)-C(34)-C(33)	121.8(3)
C(45)-H(45B)	0.96	N(12)-C(34)-H(34)	119.1
C(45)-H(45C)	0.96	C(33)-C(34)-H(34)	119.1
N(9)-C(24)	1.449(3)	C(34)-C(33)-C(32)	120.3(3)
N(9)-C(23)	1.472(3)	C(34)-C(33)-H(33)	119.9
C(18)-C(19)	1.421(4)	C(32)-C(33)-H(33)	119.9
C(47)-C(48)	1.352(4)	N(9)-C(25)-C(29)	122.5(2)
C(47)-C(46)	1.425(3)	N(9)-C(25)-C(26)	120.7(2)

C(47)-H(47)	0.93	C(29)-C(25)-C(26)	116.7(2)
C(20)-C(19)	1.365(4)	C(49)-N(1)-C(48)	119.6(2)
C(20)-H(20)	0.93	N(11)-C(30)-H(30A)	109.5
C(6)-O(3)	1.244(3)	N(11)-C(30)-H(30B)	109.5
C(6)-C(1)	1.404(3)	H(30A)-C(30)-H(30B)	109.5
C(6)-C(5)	1.544(3)	N(11)-C(30)-H(30C)	109.5
O(5)-C(11)	1.254(3)	H(30A)-C(30)-H(30C)	109.5
C(48)-H(48)	0.93	H(30B)-C(30)-H(30C)	109.5
C(38)-N(8)	1.455(3)	N(2)-C(45)-H(45A)	109.5
C(38)-H(38A)	0.96	N(2)-C(45)-H(45B)	109.5
C(38)-H(38B)	0.96	H(45A)-C(45)-H(45B)	109.5
C(38)-H(38C)	0.96	N(2)-C(45)-H(45C)	109.5
O(1)-C(3)	1.238(3)	H(45A)-C(45)-H(45C)	109.5
C(27)-N(10)	1.342(4)	H(45B)-C(45)-H(45C)	109.5
C(27)-C(26)	1.369(4)	C(25)-N(9)-C(24)	121.6(2)
C(27)-H(27)	0.93	C(25)-N(9)-C(23)	122.0(2)
C(17)-H(17A)	0.96	C(24)-N(9)-C(23)	116.3(2)
C(17)-H(17B)	0.96	N(6)-C(18)-C(22)	121.8(2)
C(17)-H(17C)	0.96	N(6)-C(18)-C(19)	121.9(2)
C(42)-N(7)	1.340(4)	C(22)-C(18)-C(19)	116.3(2)
C(42)-C(43)	1.378(4)	C(48)-C(47)-C(46)	119.6(2)
C(42)-H(42)	0.93	C(48)-C(47)-H(47)	120.2
C(23)-H(23A)	0.96	C(46)-C(47)-H(47)	120.2
C(23)-H(23B)	0.96	N(5)-C(20)-C(19)	122.1(2)
C(23)-H(23C)	0.96	N(5)-C(20)-H(20)	119
C(16)-H(16A)	0.96	C(19)-C(20)-H(20)	119
C(16)-H(16B)	0.96	O(3)-C(6)-C(1)	125.9(2)
C(16)-H(16C)	0.96	O(3)-C(6)-C(5)	116.5(2)
C(37)-N(8)	1.450(3)	C(1)-C(6)-C(5)	117.6(2)
C(37)-H(37A)	0.96	N(1)-C(48)-C(47)	122.1(2)
C(37)-H(37B)	0.96	N(1)-C(48)-H(48)	118.9
C(37)-H(37C)	0.96	C(47)-C(48)-H(48)	118.9
C(28)-N(10)	1.349(3)	N(8)-C(38)-H(38A)	109.5
C(28)-H(28)	0.93	N(8)-C(38)-H(38B)	109.5
C(12)-C(7)	1.398(3)	H(38A)-C(38)-H(38B)	109.5
C(12)-C(11)	1.540(3)	N(8)-C(38)-H(38C)	109.5
C(31)-H(31A)	0.96	H(38A)-C(38)-H(38C)	109.5
C(31)-H(31B)	0.96	H(38B)-C(38)-H(38C)	109.5

C(31)-H(31C)	0.96	N(10)-C(27)-C(26)	122.0(2)
C(40)-C(41)	1.376(4)	N(10)-C(27)-H(27)	119
C(40)-C(39)	1.413(4)	C(26)-C(27)-H(27)	119
C(40)-H(40)	0.93	N(6)-C(17)-H(17A)	109.5
C(35)-C(36)	1.359(4)	N(6)-C(17)-H(17B)	109.5
C(35)-H(35)	0.93	H(17A)-C(17)-H(17B)	109.5
C(50)-C(49)	1.359(4)	N(6)-C(17)-H(17C)	109.5
C(50)-C(46)	1.411(4)	H(17A)-C(17)-H(17C)	109.5
C(50)-H(50)	0.93	H(17B)-C(17)-H(17C)	109.5
C(36)-H(36)	0.93	N(7)-C(42)-C(43)	125.4(3)
C(24)-H(24A)	0.96	N(7)-C(42)-H(42)	117.3
C(24)-H(24B)	0.96	C(43)-C(42)-H(42)	117.3
C(24)-H(24C)	0.96	N(9)-C(23)-H(23A)	109.5
N(2)-C(46)	1.346(3)	N(9)-C(23)-H(23B)	109.5
N(2)-C(44)	1.464(3)	H(23A)-C(23)-H(23B)	109.5
C(2)-C(1)	1.397(3)	N(9)-C(23)-H(23C)	109.5
C(2)-C(3)	1.539(3)	H(23A)-C(23)-H(23C)	109.5
C(1)-Cl(3)	1.731(3)	H(23B)-C(23)-H(23C)	109.5
C(44)-H(44A)	0.96	N(6)-C(16)-H(16A)	109.5
C(44)-H(44B)	0.96	N(6)-C(16)-H(16B)	109.5
C(44)-H(44C)	0.96	H(16A)-C(16)-H(16B)	109.5
C(49)-H(49)	0.93	N(6)-C(16)-H(16C)	109.5
C(7)-C(8)	1.412(3)	H(16A)-C(16)-H(16C)	109.5
C(7)-Cl(1)	1.742(3)	H(16B)-C(16)-H(16C)	109.5
C(19)-H(19)	0.93	N(8)-C(37)-H(37A)	109.5
C(26)-H(26)	0.93	N(8)-C(37)-H(37B)	109.5
N(7)-C(41)	1.337(4)	H(37A)-C(37)-H(37B)	109.5
N(8)-C(39)	1.364(3)	N(8)-C(37)-H(37C)	109.5
C(43)-C(39)	1.406(4)	H(37A)-C(37)-H(37C)	109.5
C(43)-H(43)	0.93	H(37B)-C(37)-H(37C)	109.5
C(41)-H(41)	0.93	N(10)-C(28)-C(29)	122.7(2)
C(15)-O(9)	1.251(3)	N(10)-C(28)-H(28)	118.7
C(15)-C(14)#1	1.398(3)	C(29)-C(28)-H(28)	118.7
O(9)-H(029)	1.15(8)	O(6)-C(12)-C(7)	126.3(2)
O(8)-C(9)	1.253(3)	O(6)-C(12)-C(11)	116.6(2)
O(8)-H(8)	0.82	C(7)-C(12)-C(11)	117.1(2)
O(7)-C(8)	1.239(3)	N(11)-C(31)-H(31A)	109.5
C(8)-C(9)	1.545(3)	N(11)-C(31)-H(31B)	109.5

O(20)-H(012)	0.840(2)	H(31A)-C(31)-H(31B)	109.5
O(20)-H(011)	0.885(2)	N(11)-C(31)-H(31C)	109.5
O(21)-H(05)	0.827(2)	H(31A)-C(31)-H(31C)	109.5
O(21)-H(030)	0.867(2)	H(31B)-C(31)-H(31C)	109.5
O(12)-H(027)	0.860(2)	C(41)-C(40)-C(39)	119.3(2)
O(12)-H(026)	0.867(2)	C(41)-C(40)-H(40)	120.4
O(16)-H(013)	0.835(2)	C(39)-C(40)-H(40)	120.4
O(16)-H(014)	0.85(4)	N(12)-C(35)-C(36)	121.9(3)
O(17)-H(08)	0.846(2)	N(12)-C(35)-H(35)	119
O(17)-H(07)	0.843(2)	C(36)-C(35)-H(35)	119
O(19)-H(022)	0.825(2)	O(5)-C(11)-C(10)	124.4(2)
O(19)-H(023)	0.841(2)	O(5)-C(11)-C(12)	116.1(2)
O(18)-H(020)	0.837(2)	C(10)-C(11)-C(12)	119.5(2)
O(18)-H(021)	0.816(2)	C(49)-C(50)-C(46)	119.9(2)
O(13)-H(03)	0.856(2)	C(49)-C(50)-H(50)	120
O(13)-H(02)	0.89(2)	C(46)-C(50)-H(50)	120
O(14)-H(09)	0.882(2)	C(35)-C(36)-C(32)	120.2(3)
O(14)-H(010)	0.907(2)	C(35)-C(36)-H(36)	119.9
O(15)-H(024)	0.806(2)	C(32)-C(36)-H(36)	119.9
O(15)-H(025)	0.835(2)	N(9)-C(24)-H(24A)	109.5
O(11)-H(032)	0.819(2)	N(9)-C(24)-H(24B)	109.5
O(11)-H(042)	0.833(2)	H(24A)-C(24)-H(24B)	109.5
		N(9)-C(24)-H(24C)	109.5
		H(24A)-C(24)-H(24C)	109.5
		H(24B)-C(24)-H(24C)	109.5
		C(46)-N(2)-C(45)	121.5(2)
		C(46)-N(2)-C(44)	119.8(2)
		C(45)-N(2)-C(44)	118.5(2)
		O(2)-C(2)-C(1)	125.3(2)
		O(2)-C(2)-C(3)	116.7(2)
		C(1)-C(2)-C(3)	118.0(2)
		O(1)-C(3)-C(4)	124.4(2)
		O(1)-C(3)-C(2)	117.2(2)
		C(4)-C(3)-C(2)	118.4(2)
		O(4)-C(5)-C(4)	124.7(2)
		O(4)-C(5)-C(6)	116.5(2)
		C(4)-C(5)-C(6)	118.8(2)
		C(2)-C(1)-C(6)	123.9(2)

C(2)-C(1)-Cl(3)	118.35(2)
C(6)-C(1)-Cl(3)	117.68(2)
N(2)-C(46)-C(50)	121.9(2)
N(2)-C(46)-C(47)	121.2(2)
C(50)-C(46)-C(47)	116.8(2)
N(2)-C(44)-H(44A)	109.5
N(2)-C(44)-H(44B)	109.5
H(44A)-C(44)-H(44B)	109.5
N(2)-C(44)-H(44C)	109.5
H(44A)-C(44)-H(44C)	109.5
H(44B)-C(44)-H(44C)	109.5
N(1)-C(49)-C(50)	121.8(3)
N(1)-C(49)-H(49)	119.1
C(50)-C(49)-H(49)	119.1
C(12)-C(7)-C(8)	124.0(2)
C(12)-C(7)-Cl(1)	118.74(2)
C(8)-C(7)-Cl(1)	117.28(2)
C(27)-N(10)-C(28)	119.4(2)
C(20)-C(19)-C(18)	119.9(2)
C(20)-C(19)-H(19)	120
C(18)-C(19)-H(19)	120
C(27)-C(26)-C(25)	119.6(2)
C(27)-C(26)-H(26)	120.2
C(25)-C(26)-H(26)	120.2
C(41)-N(7)-C(42)	114.8(2)
C(39)-N(8)-C(37)	121.1(2)
C(39)-N(8)-C(38)	121.1(2)
C(37)-N(8)-C(38)	117.4(2)
C(42)-C(43)-C(39)	119.3(3)
C(42)-C(43)-H(43)	120.4
C(39)-C(43)-H(43)	120.4
N(8)-C(39)-C(43)	121.9(2)
N(8)-C(39)-C(40)	122.2(2)
C(43)-C(39)-C(40)	115.9(2)
N(7)-C(41)-C(40)	125.4(3)
N(7)-C(41)-H(41)	117.3
C(40)-C(41)-H(41)	117.3
O(9)-C(15)-C(14)#1	126.0(2)

O(9)-C(15)-C(13)	116.3(2)
C(14)#1-C(15)-C(13)	117.7(2)
C(15)-O(9)-H(029)	101(4)
C(9)-O(8)-H(8)	109.5
O(7)-C(8)-C(7)	125.3(2)
O(7)-C(8)-C(9)	116.9(2)
C(7)-C(8)-C(9)	117.8(2)
O(8)-C(9)-C(10)	125.2(2)
O(8)-C(9)-C(8)	116.5(2)
C(10)-C(9)-C(8)	118.3(2)
H(012)-O(20)-H(011)	104(2)
H(05)-O(21)-H(030)	104(3)
H(027)-O(12)-H(026)	107(3)
H(013)-O(16)-H(014)	106(4)
H(08)-O(17)-H(07)	108(3)
H(022)-O(19)-H(023)	105(2)
H(020)-O(18)-H(021)	107(3)
H(03)-O(13)-H(02)	98(3)
H(09)-O(14)-H(010)	106(2)
H(024)-O(15)-H(025)	114(3)
H(032)-O(11)-H(042)	108(3)

Symmetry transformations used to generate equivalent atoms: -x +2,-y+1,-z+1

Table A. 19 Anisotropic displacement parameters (Å^2 x 10^3) for 2½(caH$_2$)(DMAP)$_6$·11H$_2$O (4). The anisotropic displacement factor exponent takes the form: -2π^2[h^{2}a*^{2}U^{11} + … + 2 h k a* b* U^{12}].

	U^{11}	U^{22}	U^{33}	U^{23}	U^{13}	U^{12}
Cl(2)	20(1)	26(1)	21(1)	-9(1)	-4(1)	9(1)
Cl(4)	19(1)	32(1)	22(1)	-11(1)	-3(1)	10(1)
O(10)	19(1)	31(1)	15(1)	-10(1)	-5(1)	5(1)
C(52)	24(1)	35(2)	42(2)	0(2)	-15(1)	3(1)
N(3)	21(1)	21(1)	21(1)	0(1)	-5(1)	-4(1)
C(14)	14(1)	16(1)	16(1)	-8(1)	0(1)	1(1)
O(6)	22(1)	28(1)	18(1)	-9(1)	-8(1)	8(1)
C(57)	17(1)	20(1)	18(1)	-6(1)	1(1)	1(1)
C(56)	15(1)	23(1)	26(2)	1(1)	-2(1)	2(1)
C(53)	16(1)	16(1)	16(1)	0(1)	-2(1)	-2(1)
C(54)	18(1)	19(1)	19(1)	-3(1)	1(1)	3(1)
C(13)	14(1)	14(1)	14(1)	-5(1)	0(1)	-2(1)
N(4)	20(1)	30(1)	18(1)	-3(1)	-5(1)	1(1)
O(2)	17(1)	32(1)	16(1)	-9(1)	-6(1)	7(1)
C(51)	38(2)	43(2)	15(1)	-5(1)	-3(1)	-13(1)
C(55)	27(1)	20(1)	16(1)	-6(1)	1(1)	-2(1)
C(10)	14(1)	17(1)	17(1)	-3(1)	-1(1)	2(1)
N(12)	23(1)	29(1)	22(1)	1(1)	-6(1)	-5(1)
N(11)	31(1)	25(1)	26(1)	-7(1)	-13(1)	4(1)
C(29)	18(1)	20(1)	20(1)	-5(1)	-1(1)	4(1)
C(4)	14(1)	18(1)	16(1)	-4(1)	-1(1)	4(1)
C(22)	18(1)	22(1)	22(1)	-7(1)	1(1)	2(1)
N(5)	18(1)	23(1)	21(1)	-3(1)	-2(1)	-1(1)
N(6)	17(1)	28(1)	19(1)	-6(1)	-5(1)	3(1)
C(32)	19(1)	17(1)	18(1)	0(1)	-1(1)	-2(1)
C(21)	22(1)	22(1)	19(1)	-8(1)	1(1)	-1(1)
O(4)	18(1)	30(1)	15(1)	-7(1)	-7(1)	5(1)
C(34)	18(1)	28(2)	28(2)	2(1)	-2(1)	1(1)
C(33)	23(1)	21(1)	22(1)	-5(1)	2(1)	0(1)
C(25)	15(1)	19(1)	15(1)	-1(1)	-1(1)	-2(1)
N(1)	20(1)	24(1)	24(1)	0(1)	-7(1)	-5(1)
C(30)	49(2)	36(2)	26(2)	-9(1)	-13(1)	-1(2)
C(45)	38(2)	33(2)	18(1)	-9(1)	-1(1)	-11(1)
N(9)	19(1)	30(1)	18(1)	-9(1)	-6(1)	8(1)

C(18)	14(1)	20(1)	18(1)	-3(1)	-1(1)	-2(1)
C(47)	18(1)	21(1)	19(1)	-3(1)	1(1)	2(1)
C(20)	19(1)	24(2)	23(1)	-6(1)	-1(1)	5(1)
C(6)	16(1)	18(1)	15(1)	-4(1)	0(1)	0(1)
O(5)	21(1)	32(1)	19(1)	-10(1)	-6(1)	9(1)
O(3)	22(1)	32(1)	16(1)	-10(1)	-9(1)	7(1)
C(48)	15(1)	21(1)	30(2)	1(1)	-3(1)	1(1)
C(38)	22(1)	27(2)	26(2)	-4(1)	-4(1)	-5(1)
O(1)	18(1)	28(1)	16(1)	-9(1)	-4(1)	3(1)
C(27)	16(1)	24(2)	25(2)	-1(1)	-5(1)	2(1)
C(17)	30(2)	35(2)	18(1)	-6(1)	-3(1)	-6(1)
C(42)	19(1)	24(2)	33(2)	-13(1)	0(1)	-2(1)
C(23)	19(1)	34(2)	27(2)	-9(1)	-7(1)	9(1)
C(16)	18(1)	36(2)	26(2)	0(1)	-6(1)	3(1)
C(37)	30(2)	24(2)	20(1)	0(1)	0(1)	-2(1)
C(28)	25(1)	25(2)	16(1)	-6(1)	-2(1)	-1(1)
C(12)	16(1)	16(1)	16(1)	-2(1)	-1(1)	0(1)
C(31)	37(2)	42(2)	53(2)	-9(2)	-25(2)	12(2)
C(40)	17(1)	19(1)	21(1)	-3(1)	2(1)	-1(1)
C(35)	26(1)	26(2)	17(1)	-5(1)	1(1)	-4(1)
C(11)	16(1)	18(1)	14(1)	-4(1)	0(1)	-1(1)
C(50)	19(1)	19(1)	21(1)	-5(1)	-1(1)	3(1)
C(36)	20(1)	21(1)	23(1)	-4(1)	1(1)	0(1)
C(24)	30(2)	51(2)	23(2)	-18(1)	-9(1)	13(1)
N(2)	20(1)	26(1)	18(1)	-5(1)	-6(1)	3(1)
C(2)	14(1)	19(1)	16(1)	0(1)	-2(1)	0(1)
C(3)	15(1)	16(1)	14(1)	-3(1)	-1(1)	-1(1)
C(5)	13(1)	19(1)	16(1)	-2(1)	-1(1)	-1(1)
C(1)	16(1)	20(1)	17(1)	-5(1)	0(1)	6(1)
C(46)	16(1)	17(1)	17(1)	-1(1)	-2(1)	-1(1)
C(44)	20(1)	33(2)	29(2)	-1(1)	-10(1)	3(1)
C(49)	24(1)	22(2)	19(1)	-4(1)	-1(1)	-3(1)
C(7)	15(1)	16(1)	18(1)	-5(1)	0(1)	1(1)
N(10)	21(1)	24(1)	19(1)	-1(1)	-4(1)	-3(1)
C(19)	21(1)	24(2)	19(1)	-8(1)	0(1)	3(1)
C(26)	17(1)	23(1)	21(1)	-5(1)	-2(1)	3(1)
N(7)	21(1)	32(1)	23(1)	-11(1)	-3(1)	4(1)
N(8)	20(1)	21(1)	17(1)	-1(1)	-2(1)	-4(1)

C(43)	19(1)	19(1)	23(1)	-4(1)	3(1)	-1(1)
C(39)	15(1)	15(1)	19(1)	-6(1)	3(1)	3(1)
C(41)	22(1)	28(2)	20(1)	-2(1)	2(1)	4(1)
C(15)	13(1)	14(1)	16(1)	-2(1)	-2(1)	0(1)
O(9)	15(1)	27(1)	18(1)	-6(1)	-6(1)	6(1)
Cl(5)	17(1)	30(1)	20(1)	-12(1)	-3(1)	8(1)
Cl(1)	18(1)	23(1)	22(1)	-10(1)	-2(1)	4(1)
O(8)	21(1)	26(1)	22(1)	-11(1)	-9(1)	6(1)
O(7)	23(1)	30(1)	20(1)	-11(1)	-8(1)	6(1)
C(8)	16(1)	16(1)	16(1)	-4(1)	-1(1)	-2(1)
C(9)	15(1)	16(1)	18(1)	-1(1)	-2(1)	1(1)
Cl(3)	31(1)	49(1)	22(1)	-18(1)	-10(1)	25(1)
O(20)	18(1)	29(1)	33(1)	-5(1)	-2(1)	7(1)
O(21)	24(1)	25(1)	29(1)	-3(1)	-5(1)	8(1)
O(12)	25(1)	30(1)	29(1)	-1(1)	0(1)	11(1)
O(16)	27(1)	36(1)	21(1)	-10(1)	1(1)	-1(1)
O(17)	18(1)	35(1)	36(1)	-10(1)	-1(1)	5(1)
O(19)	38(1)	37(1)	22(1)	-11(1)	2(1)	-6(1)
O(18)	18(1)	40(1)	29(1)	0(1)	-1(1)	1(1)
O(13)	33(1)	31(1)	34(1)	-3(1)	-12(1)	-1(1)
O(14)	28(1)	62(2)	23(1)	-14(1)	-1(1)	-11(1)
O(15)	31(1)	38(1)	25(1)	-4(1)	-3(1)	-5(1)
O(11)	32(1)	41(1)	30(1)	-18(1)	-2(1)	4(1)

Symmetry transformations used to generate equivalent atoms: -x +2,-y+1,-z+1

Table A.20 Hydrogen coordinates (x 10⁴) and isotropic displacement parameters (Å²x 10³) for 2½(caH₂)(DMAP)₆·11H₂O (4).

	x	y	z	U(eq)
H(52A)	4637	5772	900	50
H(52B)	5187	6496	1349	50
H(52C)	4579	5647	1723	50
H(6)	566	9651	2219	34
H(57)	7670	4206	1450	22
H(56)	8723	4177	2381	26
H(54)	5663	5893	2550	23
H(2)	6041	2688	2435	33
H(51A)	5627	4812	350	47
H(51B)	6295	3982	768	47
H(51C)	6758	4972	475	47
H(55)	6777	5809	3444	25
H(29)	28	4262	-1109	23
H(22)	6384	7722	5859	24
H(21)	5306	7833	4943	25
H(4)	2668	3613	351	31
H(34)	899	8140	702	30
H(33)	-133	8149	-232	26
H(30A)	-2183	8730	-1356	55
H(30B)	-1575	7917	-881	55
H(30C)	-1029	8804	-1265	55
H(45A)	8601	3412	6089	43
H(45B)	7462	3299	5959	43
H(45C)	7991	4221	5610	43
H(47)	6589	3924	4960	23
H(20)	3634	9946	5792	26
H(48)	5572	3921	4021	27
H(38A)	996	480	5663	37
H(38B)	829	489	6480	37
H(38C)	1604	-294	6169	37
H(27)	2977	2314	-1115	26
H(17A)	6582	9215	7911	41
H(17B)	5431	9202	7779	41
H(17C)	6048	10045	7406	41

H(42)	4455	2196	7399	29
H(23A)	-1047	3792	-2722	40
H(23B)	-591	4586	-2278	40
H(23C)	-1140	3698	-1899	40
H(16A)	7521	8120	7420	40
H(16B)	7596	8240	6597	40
H(16C)	6983	7392	6967	40
H(37A)	1714	1715	5209	37
H(37B)	2838	1829	5387	37
H(37C)	1988	2483	5747	37
H(28)	1109	4208	-205	26
H(31A)	-3141	9737	-850	66
H(31B)	-2642	10506	-407	66
H(31C)	-3182	9613	-26	66
H(40)	2115	-107	7307	23
H(35)	-875	10147	1588	27
H(50)	8592	2107	3956	23
H(36)	-1954	10230	676	25
H(24A)	-35	2805	-3192	52
H(24B)	576	2014	-2702	52
H(24C)	1104	2924	-3069	52
H(44A)	9604	2381	5581	41
H(44B)	9673	2492	4757	41
H(44C)	9084	1630	5135	41
H(49)	7510	2159	3046	26
H(19)	4652	9896	6741	25
H(26)	1959	2312	-2065	24
H(43)	3483	2276	6428	24
H(41)	3155	-94	8234	28
H(8)	3826	8517	4359	34
H(09)	5150(2)	8740(3)	1265(2)	57(1)
H(05)	8940(2)	1600(3)	2352(1)	46(1)
H(010)	5150(2)	8360(3)	586(1)	65(1)
H(013)	3438(2)	7770(3)	960(2)	65(1)
H(014)	2580(3)	7730(3)	1341(2)	43(1)
H(012)	7397(1)	1980(3)	1633(2)	50(1)
H(020)	580(3)	3720(3)	1664(1)	61(1)
H(021)	1244(2)	3860(3)	1147(2)	53(1)

H(03)	2300(2)	6440(2)	660(2)	51(1)
H(02)	1900(4)	6200(4)	77(1)	360(7)
H(08)	5960(3)	6220(6)	4610(2)	200(4)
H(07)	6939(2)	6050(3)	4796(2)	44(1)
H(022)	320(3)	3560(2)	2968(1)	44(1)
H(023)	80(3)	2760(2)	2660(2)	69(2)
H(011)	8220(2)	2240(2)	1251(2)	63(1)
H(024)	585(2)	6500(2)	-772(2)	40(1)
H(025)	1310(3)	6670(3)	-295(1)	66(1)
H(027)	4650(3)	7000(2)	3940(2)	63(1)
H(026)	5180(3)	6210(4)	4307(2)	340(6)
H(029)	8510(6)	5630(6)	3800(4)	230(4)
H(030)	9700(2)	1075(2)	2680(2)	52(1)
H(032)	3990(3)	4510(2)	3464(1)	41(1)
H(042)	3950(1)	4500(4)	4165(2)	370(7)

Table A.21 Torsion angles (°) for 2½(caH₂)(DMAP)₆·11H₂O (4).

Torsion angles	Angle (°)	Torsion angles	Angle (°)
C(55)-N(3)-C(56)-C(57)	0.9(4)	C(3)-C(4)-C(5)-C(6)	2.5(4)
C(53)-C(57)-C(56)-N(3)	0.4(4)	Cl(4)-C(4)-C(5)-C(6)	-178.88(2)
C(56)-C(57)-C(53)-N(4)	178.0(3)	O(3)-C(6)-C(5)-O(4)	-1.8(3)
C(56)-C(57)-C(53)-C(54)	-1.6(4)	C(1)-C(6)-C(5)-O(4)	177.8(2)
N(4)-C(53)-C(54)-C(55)	-178.1(3)	O(3)-C(6)-C(5)-C(4)	178.2(2)
C(57)-C(53)-C(54)-C(55)	1.6(4)	C(1)-C(6)-C(5)-C(4)	-2.2(4)
C(15)#1-C(14)-C(13)-O(10)	176.9(2)	O(2)-C(2)-C(1)-C(6)	-176.6(3)
Cl(5)-C(14)-C(13)-O(10)	1.0(4)	C(3)-C(2)-C(1)-C(6)	4.0(4)
C(15)#1-C(14)-C(13)-C(15)	-3.1(4)	O(2)-C(2)-C(1)-Cl(3)	1.1(4)
Cl(5)-C(14)-C(13)-C(15)	-178.94(2)	C(3)-C(2)-C(1)-Cl(3)	-178.39(2)
C(54)-C(53)-N(4)-C(51)	178.0(3)	O(3)-C(6)-C(1)-C(2)	178.4(3)
C(57)-C(53)-N(4)-C(51)	-1.7(4)	C(5)-C(6)-C(1)-C(2)	-1.2(4)
C(54)-C(53)-N(4)-C(52)	9.2(4)	O(3)-C(6)-C(1)-Cl(3)	0.7(4)
C(57)-C(53)-N(4)-C(52)	-170.5(3)	C(5)-C(6)-C(1)-Cl(3)	-178.87(2)
C(56)-N(3)-C(55)-C(54)	-0.9(4)	C(45)-N(2)-C(46)-C(50)	178.5(3)
C(53)-C(54)-C(55)-N(3)	-0.4(4)	C(44)-N(2)-C(46)-C(50)	-5.9(4)
C(30)-N(11)-C(32)-C(36)	177.2(3)	C(45)-N(2)-C(46)-C(47)	-0.8(4)
C(31)-N(11)-C(32)-C(36)	-3.1(4)	C(44)-N(2)-C(46)-C(47)	174.7(2)
C(30)-N(11)-C(32)-C(33)	-2.7(4)	C(49)-C(50)-C(46)-N(2)	179.1(3)
C(31)-N(11)-C(32)-C(33)	176.9(3)	C(49)-C(50)-C(46)-C(47)	-1.5(4)
C(20)-N(5)-C(21)-C(22)	-0.2(4)	C(48)-C(47)-C(46)-N(2)	-179.1(3)
C(18)-C(22)-C(21)-N(5)	0.5(4)	C(48)-C(47)-C(46)-C(50)	1.5(4)
C(35)-N(12)-C(34)-C(33)	-0.4(4)	C(48)-N(1)-C(49)-C(50)	0.7(4)
N(12)-C(34)-C(33)-C(32)	-0.2(4)	C(46)-C(50)-C(49)-N(1)	0.5(4)
N(11)-C(32)-C(33)-C(34)	-178.9(3)	O(6)-C(12)-C(7)-C(8)	-177.5(3)
C(36)-C(32)-C(33)-C(34)	1.2(4)	C(11)-C(12)-C(7)-C(8)	3.6(4)
C(28)-C(29)-C(25)-N(9)	179.6(3)	O(6)-C(12)-C(7)-Cl(1)	0.3(4)
C(28)-C(29)-C(25)-C(26)	-0.4(4)	C(11)-C(12)-C(7)-Cl(1)	-178.60(2)
C(29)-C(25)-N(9)-C(24)	178.7(3)	C(26)-C(27)-N(10)-C(28)	-0.5(4)
C(26)-C(25)-N(9)-C(24)	-1.3(4)	C(29)-C(28)-N(10)-C(27)	0.8(4)
C(29)-C(25)-N(9)-C(23)	0.6(4)	N(5)-C(20)-C(19)-C(18)	0.1(4)
C(26)-C(25)-N(9)-C(23)	-179.4(3)	N(6)-C(18)-C(19)-C(20)	-179.7(3)
C(17)-N(6)-C(18)-C(22)	-177.7(3)	C(22)-C(18)-C(19)-C(20)	0.2(4)
C(16)-N(6)-C(18)-C(22)	2.6(4)	N(10)-C(27)-C(26)-C(25)	-0.3(4)
C(17)-N(6)-C(18)-C(19)	2.2(4)	N(9)-C(25)-C(26)-C(27)	-179.3(3)
C(16)-N(6)-C(18)-C(19)	-177.4(3)	C(29)-C(25)-C(26)-C(27)	0.7(4)

C(21)-C(22)-C(18)-N(6)	179.5(3)	C(43)-C(42)-N(7)-C(41)	-0.2(4)
C(21)-C(22)-C(18)-C(19)	-0.4(4)	N(7)-C(42)-C(43)-C(39)	-0.2(4)
C(21)-N(5)-C(20)-C(19)	0.0(4)	C(37)-N(8)-C(39)-C(43)	-4.5(4)
C(49)-N(1)-C(48)-C(47)	-0.7(4)	C(38)-N(8)-C(39)-C(43)	-176.7(2)
C(46)-C(47)-C(48)-N(1)	-0.4(4)	C(37)-N(8)-C(39)-C(40)	177.2(2)
C(25)-C(29)-C(28)-N(10)	-0.3(4)	C(38)-N(8)-C(39)-C(40)	5.0(4)
C(34)-N(12)-C(35)-C(36)	0.1(4)	C(42)-C(43)-C(39)-N(8)	-177.4(2)
C(9)-C(10)-C(11)-O(5)	178.0(3)	C(42)-C(43)-C(39)-C(40)	0.9(4)
Cl(2)-C(10)-C(11)-O(5)	-2.5(4)	C(41)-C(40)-C(39)-N(8)	177.1(2)
C(9)-C(10)-C(11)-C(12)	-2.3(4)	C(41)-C(40)-C(39)-C(43)	-1.2(4)
Cl(2)-C(10)-C(11)-C(12)	177.25(2)	C(42)-N(7)-C(41)-C(40)	-0.1(4)
O(6)-C(12)-C(11)-O(5)	-0.2(3)	C(39)-C(40)-C(41)-N(7)	0.9(4)
C(7)-C(12)-C(11)-O(5)	178.8(2)	O(10)-C(13)-C(15)-O(9)	3.9(3)
O(6)-C(12)-C(11)-C(10)	-180.0(2)	C(14)-C(13)-C(15)-O(9)	-176.1(2)
C(7)-C(12)-C(11)-C(10)	-1.0(4)	O(10)-C(13)-C(15)-C(14)#1	-177.1(2)
N(12)-C(35)-C(36)-C(32)	0.9(4)	C(14)-C(13)-C(15)-C(14)#1	2.9(4)
N(11)-C(32)-C(36)-C(35)	178.6(3)	C(12)-C(7)-C(8)-O(7)	178.3(3)
C(33)-C(32)-C(36)-C(35)	-1.5(4)	Cl(1)-C(7)-C(8)-O(7)	0.5(4)
C(5)-C(4)-C(3)-O(1)	179.8(3)	C(12)-C(7)-C(8)-C(9)	-3.0(4)
Cl(4)-C(4)-C(3)-O(1)	1.2(4)	Cl(1)-C(7)-C(8)-C(9)	179.21(2)
C(5)-C(4)-C(3)-C(2)	0.3(4)	C(11)-C(10)-C(9)-O(8)	-178.3(3)
Cl(4)-C(4)-C(3)-C(2)	-178.35(2)	Cl(2)-C(10)-C(9)-O(8)	2.2(4)
O(2)-C(2)-C(3)-O(1)	-2.6(4)	C(11)-C(10)-C(9)-C(8)	2.9(4)
C(1)-C(2)-C(3)-O(1)	176.9(2)	Cl(2)-C(10)-C(9)-C(8)	-176.58(2)
O(2)-C(2)-C(3)-C(4)	177.0(2)	O(7)-C(8)-C(9)-O(8)	-0.5(4)
C(1)-C(2)-C(3)-C(4)	-3.5(4)	C(7)-C(8)-C(9)-O(8)	-179.3(2)
C(3)-C(4)-C(5)-O(4)	-177.4(2)	O(7)-C(8)-C(9)-C(10)	178.4(2)
Cl(4)-C(4)-C(5)-O(4)	1.2(4)	C(7)-C(8)-C(9)-C(10)	-0.4(4)

Symmetry transformations used to generate equivalent atoms: -x +2,-y+1,-z+1

Table A.22 Hydrogen bonds for 2½(caH₂)(DMAP)₆·11H₂O (4).

D-H···A	d(D-H) (Å)	D(H···A) (Å)	d(D···A) (Å)	D-H···A (°)
O2-H2···O1	0.82	2.19	2.668(3)	118
O21-H05···O20	0.83(3)	1.94(3)	2.755(3)	170(4)
O14-H010···O3ᵃ	0.91(3)	2.21(3)	3.039(3)	152(3)
O4-H4···O3	0.82	2.18	2.662(3)	118
O16-H013···O14	0.83(3)	2.05(3)	2.879(3)	170(4)
O16-H014···O5	0.84(4)	2.04(4)	2.839(3)	158(4)
O6-H6···O5	0.82	2.16	2.650(3)	118
O20-H012···O2	0.84(2)	2.04(2)	2.855(3)	163(3)
O18-H020···O19	0.84(2)	1.87(2)	2.706(3)	178(5)
O8-H8···O7	0.82	2.18	2.664(3)	118
O18-H021···O4	0.82(2)	2.04(2)	2.840(3)	169(3)
O13-H03···O16	0.86(3)	1.88(3)	2.732(3)	170(3)
O13-H02···O15	0.90(3)	1.95(4)	2.762(3)	150(5)
O17-H08···O12	0.85(4)	1.87(4)	2.713(3)	174(8)
O17-H07···O09	0.84(2)	1.98(3)	2.814(3)	172(3)
O19-H022···O10ᵇ	0.82(3)	2.12(3)	2.908(3)	159(4)
O19-H023···O21ᵇ	0.84(3)	1.89(3)	2.729(3)	175(4)
O20-H011···O15ᵃ	0.89(3)	1.90(3)	2.768(3)	166(3)
O15-H024···O18ᶜ	0.81(3)	2.01(3)	2.788(3)	161(3)
O15-H025···O13	0.84(3)	1.95(3)	2.762(3)	163(4)
O12-H027···O8	0.87(3)	1.96(3)	2.821(3)	177(4)
O12-H026···O17	0.87(3)	2.01(4)	2.713(3)	137(4)
O9-H029···O10	1.16(8)	2.05(8)	2.650(3)	108(5)
O21-H030···O6ᵈ	0.87(3)	1.89(3)	2.761(3)	176(3)
O11-H032···O1	0.82(3)	2.11(3)	2.883(3)	157(4)
O11-H042···O17ᵉ	0.84(4)	1.89(5)	2.703(3)	166(2)
O14-H09···N7ᵉ	0.88(3)	2.05(3)	2.897(3)	160(3)
O2-H2···N1	0.82	2.12	2.905(3)	161
O4-H4···N10	0.82	2.02	2.793(3)	157
O6-H6···N12	0.82	2.17	2.966(3)	163
O8-H8···N5	0.82	2.04	2.816(3)	159
O9-H029···N3	1.16(8)	2.06(8)	2.906(3)	127(6)
C20-H20···N8ᶠ	0.93	2.58	3.480(4)	162
C16-H16B···Cl1ᵍ	0.96	2.75	3.620(3)	151
O14-H010···Cl3ᵃ	0.91(3)	2.74(3)	3.263(3)	118(2)
O16-H014···Cl2	0.84(4)	2.78(4)	3.344(3)	126 (3)

Symmetry code: (a) -x +1, -y +1, -z, (b) x-1, y, z, (c) -x, -y +1, -z, (d) x +1, y -1, z, (e) -x +1, -y +1, -z +1, (f) x, y +1, z, (g) -x +1, -y +2, -z +1

B.1 Crystal structure of tetraethylammoniumaquabis(2,5-dichloro-3,6-dihydroxy-1,4-benzoquinonato-$\kappa^2 O,O$')oxidotriphenylphosphineoxide niobate(V), trihydrate tetrahydrofuran solvate, (Et$_4$N)*cis*-[NbO(ca)$_2$(H$_2$O)OPPh$_3$]·3H$_2$O·THF (5)

Table B.1 Atomic coordinates (x 10^4) and equivalent isotropic displacement parameters (Å^{2}x 10^3) for (Et$_4$N) *cis*-[NbO(ca)$_2$(H$_2$O)OPPh$_3$]·3H$_2$O·THF (5). U(eq) is defined as one third of the trace of the orthogonalized U^{ij} tensor.

	x	y	z	U(eq)
Nb(1)	3334(1)	1030(1)	7859(1)	11(1)
Cl(5)	5690(1)	2002(1)	4623(1)	33(1)
Cl(2)	-291(1)	1956(1)	10138(1)	21(1)
P(1)	789(1)	599(1)	5857(1)	15(1)
O(3)	4295(2)	86(1)	7223(1)	14(1)
O(7)	4489(2)	1140(1)	8864(1)	19(1)
O(2)	2461(2)	66(1)	8428(1)	15(1)
O(6)	1960(2)	808(1)	6524(1)	18(1)
O(4)	4457(2)	1407(1)	6581(1)	17(1)
O(9)	6610(2)	-761(1)	4343(2)	28(1)
N(1)	4936(2)	8146(1)	9730(2)	21(1)
O(10)	-1544(2)	548(1)	10849(2)	29(1)
O(11)	-1135(2)	-843(1)	10124(2)	28(1)
O(12)	7940(3)	5041(1)	8565(2)	44(1)
C(11)	60(2)	1048(2)	9812(2)	15(1)
C(2)	5592(2)	1095(2)	5061(2)	19(1)
O(5)	2975(2)	2168(1)	7584(2)	20(1)
O(1)	1805(2)	1380(1)	8780(1)	15(1)
O(8)	6730(2)	631(1)	3638(2)	27(1)
C(9)	-424(2)	-347(2)	9841(2)	18(1)
C(13)	667(2)	1217(1)	4741(2)	19(1)
C(8)	638(2)	-459(1)	9179(2)	14(1)
C(3)	6170(2)	529(2)	4458(2)	18(1)
C(25)	882(3)	-354(2)	5444(2)	20(1)
C(20)	-955(3)	1408(2)	6922(2)	31(1)
C(22)	-2632(3)	890(2)	7934(2)	38(1)

C(24)	-1296(3)	83(2)	6956(2)	27(1)
C(5)	5416(2)	-424(1)	5803(2)	16(1)
C(35)	6313(3)	7873(2)	9777(2)	24(1)
C(34)	3129(3)	8285(2)	11021(3)	33(1)
C(17)	-410(3)	1698(2)	3149(2)	35(1)
C(32)	5552(3)	9500(2)	10109(3)	38(1)
C(10)	-692(2)	462(2)	10228(2)	18(1)
C(7)	1407(2)	115(1)	8929(2)	13(1)
C(12)	1063(2)	895(1)	9191(2)	13(1)
C(31)	4843(3)	8958(2)	9390(2)	28(1)
C(14)	1656(3)	1723(2)	4616(2)	27(1)
C(4)	6086(2)	-287(2)	4872(2)	18(1)
C(39)	8141(4)	4858(2)	7506(3)	48(1)
C(30)	1792(3)	-803(2)	5972(2)	26(1)
C(1)	4988(2)	934(1)	5976(2)	14(1)
C(15)	1601(3)	2209(2)	3768(3)	38(1)
C(42)	7174(4)	5698(2)	8498(3)	42(1)
C(29)	1869(3)	-1546(2)	5715(3)	36(1)
C(36)	6969(3)	7882(2)	8734(3)	35(1)
C(37)	4111(3)	7716(2)	8919(2)	28(1)
C(19)	-620(2)	698(2)	6606(2)	21(1)
C(18)	-382(3)	1212(2)	4004(2)	27(1)
C(6)	4887(2)	151(1)	6358(2)	13(1)
C(16)	570(3)	2193(2)	3038(3)	40(1)
C(41)	6296(4)	5630(3)	7503(3)	52(1)
C(23)	-2304(3)	189(2)	7629(3)	36(1)
C(21)	-1973(3)	1499(2)	7584(3)	42(1)
C(27)	150(5)	-1412(2)	4427(3)	56(1)
C(38)	4025(3)	6886(2)	9092(3)	38(1)
C(40)	6888(4)	4985(3)	6884(3)	58(1)
C(26)	46(4)	-659(2)	4673(2)	39(1)
C(28)	1059(4)	-1848(2)	4944(3)	43(1)
Cl(4)	5352(1)	-1322(1)	6277(1)	24(1)
Cl(3)	921(1)	-1347(1)	8725(1)	20(1)
C(33)	4485(3)	8039(2)	10850(2)	25(1)
O(13)	4546(2)	3029(1)	6606(2)	31(1)
O(14)	1159(2)	3051(1)	8077(2)	34(1)
O(15)	7814(4)	-622(2)	2303(2)	63(1)

Table B. 2 Bond lengths (Å) and angles (°) for (Et₄N)*cis*-[NbO(ca)₂(H₂O)OPPh₃]·3H₂O·THF (5).

Atoms	Distance (Å)	Atoms	Angle (°)
Nb(1)-O(7)	1.7205(2)	O(7)-Nb(1)-O(2)	98.44(8)
Nb(1)-O(2)	2.1022(2)	O(7)-Nb(1)-O(5)	97.03(8)
Nb(1)-O(5)	2.1094(2)	O(2)-Nb(1)-O(5)	141.36(7)
Nb(1)-O(1)	2.1147(2)	O(7)-Nb(1)-O(1)	94.98(7)
Nb(1)-O(4)	2.1462(2)	O(2)-Nb(1)-O(1)	73.00(7)
Nb(1)-O(3)	2.1473(2)	O(5)-Nb(1)-O(1)	70.55(7)
Nb(1)-O(6)	2.1969(2)	O(7)-Nb(1)-O(4)	97.10(8)
Cl(5)-C(2)	1.729(3)	O(2)-Nb(1)-O(4)	141.14(6)
Cl(2)-C(11)	1.729(3)	O(5)-Nb(1)-O(4)	70.64(7)
P(1)-O(6)	1.5007(2)	O(1)-Nb(1)-O(4)	140.42(7)
P(1)-C(13)	1.793(3)	O(7)-Nb(1)-O(3)	92.26(8)
P(1)-C(25)	1.796(3)	O(2)-Nb(1)-O(3)	72.11(7)
P(1)-C(19)	1.796(3)	O(5)-Nb(1)-O(3)	142.19(7)
O(3)-C(6)	1.283(3)	O(1)-Nb(1)-O(3)	145.03(7)
O(2)-C(7)	1.298(3)	O(4)-Nb(1)-O(3)	71.88(6)
O(4)-C(1)	1.287(3)	O(7)-Nb(1)-O(6)	174.94(7)
O(9)-C(4)	1.229(3)	O(2)-Nb(1)-O(6)	80.25(7)
N(1)-C(37)	1.519(4)	O(5)-Nb(1)-O(6)	86.91(7)
N(1)-C(33)	1.519(4)	O(1)-Nb(1)-O(6)	89.32(7)
N(1)-C(35)	1.521(3)	O(4)-Nb(1)-O(6)	81.18(7)
N(1)-C(31)	1.526(4)	O(3)-Nb(1)-O(6)	82.68(7)
O(10)-C(10)	1.223(3)	O(6)-P(1)-C(13)	108.02(1)
O(11)-C(9)	1.225(3)	O(6)-P(1)-C(25)	110.32(1)
O(12)-C(39)	1.398(4)	C(13)-P(1)-C(25)	111.69(1)
O(12)-C(42)	1.429(5)	O(6)-P(1)-C(19)	110.55(1)
C(11)-C(12)	1.365(3)	C(13)-P(1)-C(19)	108.60(1)
C(11)-C(10)	1.430(4)	C(25)-P(1)-C(19)	107.66(1)
C(2)-C(1)	1.370(3)	C(6)-O(3)-Nb(1)	119.87(2)
C(2)-C(3)	1.423(4)	C(7)-O(2)-Nb(1)	120.08(2)
O(5)-H(5A)	0.92(4)	P(1)-O(6)-Nb(1)	164.14(2)
O(5)-H(5B)	0.84(4)	C(1)-O(4)-Nb(1)	120.02(2)
O(1)-C(12)	1.293(3)	C(37)-N(1)-C(33)	111.6(2)
O(8)-C(3)	1.224(3)	C(37)-N(1)-C(35)	111.7(2)
C(9)-C(8)	1.433(3)	C(33)-N(1)-C(35)	105.0(2)
C(9)-C(10)	1.566(4)	C(37)-N(1)-C(31)	105.9(2)
C(13)-C(14)	1.393(4)	C(33)-N(1)-C(31)	111.3(2)

C(13)-C(18)	1.404(4)	C(35)-N(1)-C(31)	111.6(2)
C(8)-C(7)	1.356(3)	C(39)-O(12)-C(42)	104.3(3)
C(8)-Cl(3)	1.729(2)	C(12)-C(11)-C(10)	120.8(2)
C(3)-C(4)	1.561(4)	C(12)-C(11)-Cl(2)	120.3(2)
C(25)-C(26)	1.390(4)	C(10)-C(11)-Cl(2)	118.92(2)
C(25)-C(30)	1.394(4)	C(1)-C(2)-C(3)	121.4(3)
C(20)-C(19)	1.390(4)	C(1)-C(2)-Cl(5)	120.3(2)
C(20)-C(21)	1.392(4)	C(3)-C(2)-Cl(5)	118.29(2)
C(20)-H(20)	0.93	Nb(1)-O(5)-H(5A)	122(2)
C(22)-C(23)	1.367(5)	Nb(1)-O(5)-H(5B)	115(3)
C(22)-C(21)	1.380(6)	H(5A)-O(5)-H(5B)	123(4)
C(22)-H(22)	0.93	C(12)-O(1)-Nb(1)	120.14(2)
C(24)-C(19)	1.395(4)	O(11)-C(9)-C(8)	124.4(2)
C(24)-C(23)	1.397(4)	O(11)-C(9)-C(10)	117.8(2)
C(24)-H(24)	0.93	C(8)-C(9)-C(10)	117.8(2)
C(5)-C(6)	1.378(3)	C(14)-C(13)-C(18)	119.5(2)
C(5)-C(4)	1.415(4)	C(14)-C(13)-P(1)	117.9(2)
C(5)-Cl(4)	1.726(3)	C(18)-C(13)-P(1)	122.6(2)
C(35)-C(36)	1.510(4)	C(7)-C(8)-C(9)	120.9(2)
C(35)-H(35A)	0.97	C(7)-C(8)-Cl(3)	120.99(2)
C(35)-H(35B)	0.97	C(9)-C(8)-Cl(3)	118.10(2)
C(34)-C(33)	1.511(4)	O(8)-C(3)-C(2)	125.0(3)
C(34)-H(34A)	0.96	O(8)-C(3)-C(4)	117.4(2)
C(34)-H(34B)	0.96	C(2)-C(3)-C(4)	117.6(2)
C(34)-H(34C)	0.96	C(26)-C(25)-C(30)	119.9(3)
C(17)-C(16)	1.372(5)	C(26)-C(25)-P(1)	122.6(2)
C(17)-C(18)	1.385(4)	C(30)-C(25)-P(1)	117.5(2)
C(17)-H(17)	0.93	C(19)-C(20)-C(21)	119.3(3)
C(32)-C(31)	1.503(5)	C(19)-C(20)-H(20)	120.4
C(32)-H(32A)	0.96	C(21)-C(20)-H(20)	120.4
C(32)-H(32B)	0.96	C(23)-C(22)-C(21)	120.6(3)
C(32)-H(32C)	0.96	C(23)-C(22)-H(22)	119.7
C(7)-C(12)	1.490(3)	C(21)-C(22)-H(22)	119.7
C(31)-H(31A)	0.97	C(19)-C(24)-C(23)	119.4(3)
C(31)-H(31B)	0.97	C(19)-C(24)-H(24)	120.3
C(14)-C(15)	1.380(4)	C(23)-C(24)-H(24)	120.3
C(14)-H(14)	0.93	C(6)-C(5)-C(4)	121.0(2)
C(39)-C(40)	1.514(6)	C(6)-C(5)-Cl(4)	120.36(2)

C(39)-H(39A)	0.97	C(4)-C(5)-Cl(4)	118.55(2)
C(39)-H(39B)	0.97	C(36)-C(35)-N(1)	115.6(2)
C(30)-C(29)	1.379(4)	C(36)-C(35)-H(35A)	108.4
C(30)-H(30)	0.93	N(1)-C(35)-H(35A)	108.4
C(1)-C(6)	1.495(3)	C(36)-C(35)-H(35B)	108.4
C(15)-C(16)	1.384(5)	N(1)-C(35)-H(35B)	108.4
C(15)-H(15)	0.93	H(35A)-C(35)-H(35B)	107.4
C(42)-C(41)	1.523(5)	C(33)-C(34)-H(34A)	109.5
C(42)-H(42A)	0.97	C(33)-C(34)-H(34B)	109.5
C(42)-H(42B)	0.97	H(34A)-C(34)-H(34B)	109.5
C(29)-C(28)	1.371(5)	C(33)-C(34)-H(34C)	109.5
C(29)-H(29)	0.93	H(34A)-C(34)-H(34C)	109.5
C(36)-H(36A)	0.96	H(34B)-C(34)-H(34C)	109.5
C(36)-H(36B)	0.96	C(16)-C(17)-C(18)	120.0(3)
C(36)-H(36C)	0.96	C(16)-C(17)-H(17)	120
C(37)-C(38)	1.513(5)	C(18)-C(17)-H(17)	120
C(37)-H(37A)	0.97	C(31)-C(32)-H(32A)	109.5
C(37)-H(37B)	0.97	C(31)-C(32)-H(32B)	109.5
C(18)-H(18)	0.93	H(32A)-C(32)-H(32B)	109.5
C(16)-H(16)	0.93	C(31)-C(32)-H(32C)	109.5
C(41)-C(40)	1.544(7)	H(32A)-C(32)-H(32C)	109.5
C(41)-H(41A)	0.97	H(32B)-C(32)-H(32C)	109.5
C(41)-H(41B)	0.97	O(10)-C(10)-C(11)	124.8(2)
C(23)-H(23)	0.93	O(10)-C(10)-C(9)	117.6(2)
C(21)-H(21)	0.93	C(11)-C(10)-C(9)	117.6(2)
C(27)-C(28)	1.375(6)	O(2)-C(7)-C(8)	126.0(2)
C(27)-C(26)	1.396(5)	O(2)-C(7)-C(12)	113.1(2)
C(27)-H(27)	0.93	C(8)-C(7)-C(12)	120.9(2)
C(38)-H(38A)	0.96	O(1)-C(12)-C(11)	125.8(2)
C(38)-H(38B)	0.96	O(1)-C(12)-C(7)	113.0(2)
C(38)-H(38C)	0.96	C(11)-C(12)-C(7)	121.2(2)
C(40)-H(40A)	0.97	C(32)-C(31)-N(1)	115.5(2)
C(40)-H(40B)	0.97	C(32)-C(31)-H(31A)	108.4
C(26)-H(26)	0.93	N(1)-C(31)-H(31A)	108.4
C(28)-H(28)	0.93	C(32)-C(31)-H(31B)	108.4
C(33)-H(33A)	0.97	N(1)-C(31)-H(31B)	108.4
C(33)-H(33B)	0.97	H(31A)-C(31)-H(31B)	107.5
O(13)-H(1)	0.870(2)	C(15)-C(14)-C(13)	119.8(3)

O(13)-H(2)	0.86(2)	C(15)-C(14)-H(14)	120.1
O(14)-H(3)	0.87(2)	C(13)-C(14)-H(14)	120.1
O(14)-H(4)	0.85(2)	O(9)-C(4)-C(5)	125.3(3)
O(15)-H(6)	0.84(2)	O(9)-C(4)-C(3)	116.1(2)
O(15)-H(5)	0.81(2)	C(5)-C(4)-C(3)	118.6(2)
		O(12)-C(39)-C(40)	107.0(3)
		O(12)-C(39)-H(39A)	110.3
		C(40)-C(39)-H(39A)	110.3
		O(12)-C(39)-H(39B)	110.3
		C(40)-C(39)-H(39B)	110.3
		H(39A)-C(39)-H(39B)	108.6
		C(29)-C(30)-C(25)	119.8(3)
		C(29)-C(30)-H(30)	120.1
		C(25)-C(30)-H(30)	120.1
		O(4)-C(1)-C(2)	125.9(2)
		O(4)-C(1)-C(6)	113.3(2)
		C(2)-C(1)-C(6)	120.8(2)
		C(14)-C(15)-C(16)	120.2(3)
		C(14)-C(15)-H(15)	119.9
		C(16)-C(15)-H(15)	119.9
		O(12)-C(42)-C(41)	107.3(3)
		O(12)-C(42)-H(42A)	110.3
		C(41)-C(42)-H(42A)	110.3
		O(12)-C(42)-H(42B)	110.3
		C(41)-C(42)-H(42B)	110.3
		H(42A)-C(42)-H(42B)	108.5
		C(28)-C(29)-C(30)	120.7(3)
		C(28)-C(29)-H(29)	119.7
		C(30)-C(29)-H(29)	119.7
		C(35)-C(36)-H(36A)	109.5
		C(35)-C(36)-H(36B)	109.5
		H(36A)-C(36)-H(36B)	109.5
		C(35)-C(36)-H(36C)	109.5
		H(36A)-C(36)-H(36C)	109.5
		H(36B)-C(36)-H(36C)	109.5
		C(38)-C(37)-N(1)	116.2(2)
		C(38)-C(37)-H(37A)	108.2
		N(1)-C(37)-H(37A)	108.2

C(38)-C(37)-H(37B)	108.2
N(1)-C(37)-H(37B)	108.2
H(37A)-C(37)-H(37B)	107.4
C(20)-C(19)-C(24)	120.1(3)
C(20)-C(19)-P(1)	117.7(2)
C(24)-C(19)-P(1)	121.9(2)
C(17)-C(18)-C(13)	119.7(3)
C(17)-C(18)-H(18)	120.1
C(13)-C(18)-H(18)	120.1
O(3)-C(6)-C(5)	125.7(2)
O(3)-C(6)-C(1)	113.7(2)
C(5)-C(6)-C(1)	120.6(2)
C(17)-C(16)-C(15)	120.7(3)
C(17)-C(16)-H(16)	119.7
C(15)-C(16)-H(16)	119.7
C(42)-C(41)-C(40)	103.5(3)
C(42)-C(41)-H(41A)	111.1
C(40)-C(41)-H(41A)	111.1
C(42)-C(41)-H(41B)	111.1
C(40)-C(41)-H(41B)	111.1
H(41A)-C(41)-H(41B)	109
C(22)-C(23)-C(24)	120.2(3)
C(22)-C(23)-H(23)	119.9
C(24)-C(23)-H(23)	119.9
C(22)-C(21)-C(20)	120.4(3)
C(22)-C(21)-H(21)	119.8
C(20)-C(21)-H(21)	119.8
C(28)-C(27)-C(26)	120.6(3)
C(28)-C(27)-H(27)	119.7
C(26)-C(27)-H(27)	119.7
C(37)-C(38)-H(38A)	109.5
C(37)-C(38)-H(38B)	109.5
H(38A)-C(38)-H(38B)	109.5
C(37)-C(38)-H(38C)	109.5
H(38A)-C(38)-H(38C)	109.5
H(38B)-C(38)-H(38C)	109.5
C(39)-C(40)-C(41)	102.2(3)
C(39)-C(40)-H(40A)	111.3

C(41)-C(40)-H(40A)	111.3
C(39)-C(40)-H(40B)	111.3
C(41)-C(40)-H(40B)	111.3
H(40A)-C(40)-H(40B)	109.2
C(25)-C(26)-C(27)	119.0(3)
C(25)-C(26)-H(26)	120.5
C(27)-C(26)-H(26)	120.5
C(29)-C(28)-C(27)	120.0(3)
C(29)-C(28)-H(28)	120
C(27)-C(28)-H(28)	120
C(34)-C(33)-N(1)	115.4(2)
C(34)-C(33)-H(33A)	108.4
N(1)-C(33)-H(33A)	108.4
C(34)-C(33)-H(33B)	108.4
N(1)-C(33)-H(33B)	108.4
H(33A)-C(33)-H(33B)	107.5
H(1)-O(13)-H(2)	111(3)
H(3)-O(14)-H(4)	102(3)
H(6)-O(15)-H(5)	106(3)

Table B.3 Anisotropic displacement parameters (Å^2 x 10^3) for (Et$_4$N)*cis*-[NbO(ca)$_2$(H$_2$O)OPPh$_3$]·3H$_2$O· THF (5). The anisotropic displacement factor exponent takes the form: $-2\pi^2[\ h^2a^{*2}U^{11} + \ldots + 2\ h\ k\ a^*\ b^*\ U^{12}]$.

	U^{11}	U^{22}	U^{33}	U^{23}	U^{13}	U^{12}
Nb(1)	11(1)	10(1)	13(1)	-1(1)	3(1)	0(1)
Cl(5)	52(1)	18(1)	31(1)	4(1)	22(1)	-7(1)
Cl(2)	23(1)	17(1)	23(1)	-4(1)	7(1)	5(1)
P(1)	14(1)	16(1)	14(1)	1(1)	-1(1)	0(1)
O(3)	13(1)	13(1)	16(1)	1(1)	4(1)	2(1)
O(7)	17(1)	21(1)	20(1)	-3(1)	1(1)	1(1)
O(2)	13(1)	12(1)	19(1)	1(1)	6(1)	0(1)
O(6)	19(1)	15(1)	19(1)	1(1)	-3(1)	0(1)
O(4)	18(1)	13(1)	21(1)	-1(1)	9(1)	-1(1)
O(9)	36(1)	24(1)	27(1)	-7(1)	15(1)	4(1)
N(1)	19(1)	24(1)	20(1)	6(1)	-1(1)	5(1)
O(10)	28(1)	29(1)	31(1)	0(1)	19(1)	-1(1)
O(11)	28(1)	25(1)	32(1)	-1(1)	14(1)	-8(1)
O(12)	60(2)	40(1)	32(1)	3(1)	-9(1)	-5(1)
C(11)	16(1)	16(1)	14(1)	-2(1)	2(1)	4(1)
C(2)	23(1)	14(1)	21(1)	-1(1)	7(1)	-4(1)
O(5)	24(1)	11(1)	28(1)	2(1)	12(1)	0(1)
O(1)	16(1)	12(1)	18(1)	-1(1)	7(1)	-1(1)
O(8)	29(1)	32(1)	20(1)	-3(1)	12(1)	-6(1)
C(9)	18(1)	19(1)	16(1)	1(1)	3(1)	-2(1)
C(13)	18(1)	24(2)	16(1)	4(1)	2(1)	4(1)
C(8)	15(1)	13(1)	14(1)	0(1)	0(1)	0(1)
C(3)	15(1)	22(1)	18(1)	-3(1)	2(1)	-5(1)
C(25)	22(1)	19(1)	19(1)	-3(1)	4(1)	-5(1)
C(20)	34(2)	33(2)	27(2)	2(1)	7(1)	8(1)
C(22)	18(1)	75(3)	21(1)	0(2)	2(1)	6(2)
C(24)	22(1)	36(2)	23(1)	4(1)	-1(1)	-5(1)
C(5)	16(1)	13(1)	19(1)	0(1)	2(1)	-1(1)
C(35)	19(1)	29(2)	26(1)	6(1)	-3(1)	9(1)
C(34)	32(2)	33(2)	33(2)	3(1)	9(1)	3(1)
C(17)	33(2)	50(2)	21(1)	6(1)	-6(1)	15(2)
C(32)	37(2)	23(2)	53(2)	7(1)	4(2)	4(1)
C(10)	16(1)	21(1)	17(1)	0(1)	4(1)	2(1)
C(7)	13(1)	15(1)	10(1)	0(1)	0(1)	3(1)

C(12)	14(1)	15(1)	11(1)	1(1)	-2(1)	-1(1)
C(31)	28(2)	25(2)	32(2)	15(1)	4(1)	10(1)
C(14)	21(1)	32(2)	28(2)	12(1)	1(1)	1(1)
C(4)	15(1)	21(1)	18(1)	-4(1)	2(1)	0(1)
C(39)	50(2)	55(2)	38(2)	5(2)	3(2)	-14(2)
C(30)	22(1)	21(1)	34(2)	-5(1)	0(1)	0(1)
C(1)	12(1)	12(1)	18(1)	-2(1)	1(1)	-2(1)
C(15)	34(2)	40(2)	42(2)	22(2)	10(1)	0(1)
C(42)	48(2)	39(2)	38(2)	5(2)	-10(2)	-1(2)
C(29)	36(2)	20(2)	51(2)	-7(1)	5(2)	2(1)
C(36)	24(2)	43(2)	38(2)	7(1)	5(1)	9(1)
C(37)	24(1)	35(2)	24(1)	2(1)	-5(1)	7(1)
C(19)	17(1)	31(1)	13(1)	3(1)	-2(1)	2(1)
C(18)	23(1)	34(2)	23(1)	4(1)	-2(1)	3(1)
C(6)	9(1)	15(1)	15(1)	0(1)	0(1)	-1(1)
C(16)	45(2)	48(2)	27(2)	22(2)	9(1)	16(2)
C(41)	53(2)	65(3)	36(2)	4(2)	-16(2)	-5(2)
C(23)	17(1)	64(2)	25(2)	7(2)	1(1)	-7(2)
C(21)	37(2)	56(2)	33(2)	-6(2)	3(2)	23(2)
C(27)	99(3)	30(2)	36(2)	-4(2)	-27(2)	-26(2)
C(38)	38(2)	37(2)	39(2)	-3(1)	-7(1)	-2(2)
C(40)	65(3)	81(3)	28(2)	-5(2)	-4(2)	-30(2)
C(26)	59(2)	29(2)	29(2)	1(1)	-21(2)	-11(2)
C(28)	76(3)	20(2)	35(2)	-8(1)	2(2)	-9(2)
Cl(4)	33(1)	14(1)	24(1)	0(1)	8(1)	6(1)
Cl(3)	23(1)	12(1)	25(1)	-1(1)	5(1)	-2(1)
C(33)	30(2)	24(1)	21(1)	7(1)	2(1)	2(1)
O(13)	44(1)	17(1)	32(1)	3(1)	15(1)	-2(1)
O(14)	38(1)	29(1)	34(1)	2(1)	7(1)	14(1)
O(15)	114(3)	39(2)	42(2)	8(1)	53(2)	19(2)

Table B.4 Hydrogen coordinates (x 10^4) and isotropic displacement parameters (Å^{2}x 10^3) for (Et$_4$N)*cis*-[NbO(ca)$_2$(H$_2$O)OPPh$_3$]·3H$_2$O·THF (5).

	x	y	z	U(eq)
H(20)	-503	1819	6694	37
H(22)	-3305	956	8382	45
H(24)	-1078	-393	6742	32
H(35A)	6805	8179	10282	29
H(35B)	6329	7369	10049	29
H(34A)	2929	8193	11746	49
H(34B)	2550	8011	10554	49
H(34C)	3048	8806	10872	49
H(17)	-1095	1688	2651	42
H(32A)	5433	9994	9836	57
H(32B)	6447	9380	10141	57
H(32C)	5231	9471	10810	57
H(31A)	5165	9002	8683	34
H(31B)	3947	9099	9344	34
H(14)	2351	1733	5104	33
H(39A)	8401	4343	7451	57
H(39B)	8806	5170	7230	57
H(30)	2346	-602	6495	31
H(15)	2259	2548	3686	46
H(42A)	7714	6134	8451	51
H(42B)	6674	5745	9124	51
H(29)	2477	-1844	6068	43
H(36A)	7828	7701	8843	52
H(36B)	6987	8380	8464	52
H(36C)	6510	7569	8231	52
H(37A)	3252	7919	8910	34
H(37B)	4440	7801	8221	34
H(18)	-1055	883	4088	32
H(16)	542	2521	2467	48
H(41A)	6290	6086	7091	62
H(41B)	5428	5514	7685	62
H(23)	-2754	-218	7870	43
H(21)	-2209	1974	7791	51
H(27)	-402	-1620	3908	67

H(38A)	3479	6669	8542	57
H(38B)	3678	6790	9772	57
H(38C)	4863	6671	9074	57
H(40A)	6350	4546	6887	70
H(40B)	7027	5125	6154	70
H(26)	-575	-366	4326	47
H(28)	1125	-2348	4771	52
H(33A)	4559	7517	11032	30
H(33B)	5055	8311	11339	30
H(3)	400(30)	3120(20)	8310(40)	59(13)
H(4)	1450(40)	3489(17)	8070(40)	62(14)
H(6)	7970(50)	-260(20)	1900(30)	78(16)
H(5)	7430(40)	-450(20)	2790(20)	59(13)
H(1)	4920(40)	2720(20)	6190(30)	65(14)
H(2)	4170(40)	3380(19)	6250(30)	65(15)
H(5A)	2270(30)	2403(19)	7830(30)	29(9)
H(5B)	3490(40)	2380(20)	7190(30)	46(11)

Table B.5 Torsion angles (°) for (Et₄N)*cis*-[NbO(ca)₂(H₂O)OPPh₃]·3H₂O·THF (5).

Torsion angles	Angle (°)	Torsion angles	Angle (°)
C(13)-P(1)-O(6)-Nb(1)	143.5(4)	O(8)-C(3)-C(4)-O(9)	1.0(4)
C(25)-P(1)-O(6)-Nb(1)	-94.1(4)	C(2)-C(3)-C(4)-O(9)	-179.0(2)
C(19)-P(1)-O(6)-Nb(1)	24.8(4)	O(8)-C(3)-C(4)-C(5)	-178.5(2)
O(6)-P(1)-C(13)-C(14)	4.9(2)	C(2)-C(3)-C(4)-C(5)	1.6(3)
C(25)-P(1)-C(13)-C(14)	-116.6(2)	C(42)-O(12)-C(39)-C(40)	-41.2(4)
C(19)-P(1)-C(13)-C(14)	124.8(2)	C(26)-C(25)-C(30)-C(29)	0.9(4)
O(6)-P(1)-C(13)-C(18)	-174.7(2)	P(1)-C(25)-C(30)-C(29)	177.4(2)
C(25)-P(1)-C(13)-C(18)	63.8(3)	Nb(1)-O(4)-C(1)-C(2)	171.49(2)
C(19)-P(1)-C(13)-C(18)	-54.8(3)	Nb(1)-O(4)-C(1)-C(6)	-8.1(3)
O(11)-C(9)-C(8)-C(7)	-177.8(2)	C(3)-C(2)-C(1)-O(4)	178.9(2)
C(10)-C(9)-C(8)-C(7)	2.1(3)	Cl(5)-C(2)-C(1)-O(4)	-0.2(4)
O(11)-C(9)-C(8)-Cl(3)	1.4(4)	C(3)-C(2)-C(1)-C(6)	-1.5(4)
C(10)-C(9)-C(8)-Cl(3)	-178.68(2)	Cl(5)-C(2)-C(1)-C(6)	179.45(2)
C(1)-C(2)-C(3)-O(8)	-179.6(2)	C(13)-C(14)-C(15)-C(16)	-0.3(5)
Cl(5)-C(2)-C(3)-O(8)	-0.6(4)	C(39)-O(12)-C(42)-C(41)	34.4(4)
C(1)-C(2)-C(3)-C(4)	0.3(4)	C(25)-C(30)-C(29)-C(28)	0.1(5)
Cl(5)-C(2)-C(3)-C(4)	179.35(2)	C(33)-N(1)-C(37)-C(38)	-57.8(3)
O(6)-P(1)-C(25)-C(26)	-168.5(2)	C(35)-N(1)-C(37)-C(38)	59.3(3)
C(13)-P(1)-C(25)-C(26)	-48.3(3)	C(31)-N(1)-C(37)-C(38)	-179.0(3)
C(19)-P(1)-C(25)-C(26)	70.8(3)	C(21)-C(20)-C(19)-C(24)	-0.4(4)
O(6)-P(1)-C(25)-C(30)	15.1(2)	C(21)-C(20)-C(19)-P(1)	-174.3(2)
C(13)-P(1)-C(25)-C(30)	135.2(2)	C(23)-C(24)-C(19)-C(20)	-0.4(4)
C(19)-P(1)-C(25)-C(30)	-105.6(2)	C(23)-C(24)-C(19)-P(1)	173.3(2)
C(37)-N(1)-C(35)-C(36)	55.7(3)	O(6)-P(1)-C(19)-C(20)	65.5(2)
C(33)-N(1)-C(35)-C(36)	176.8(3)	C(13)-P(1)-C(19)-C(20)	-52.9(3)
C(31)-N(1)-C(35)-C(36)	-62.6(3)	C(25)-P(1)-C(19)-C(20)	-174.0(2)
C(12)-C(11)-C(10)-O(10)	174.5(2)	O(6)-P(1)-C(19)-C(24)	-108.3(2)
Cl(2)-C(11)-C(10)-O(10)	-3.7(4)	C(13)-P(1)-C(19)-C(24)	133.3(2)
C(12)-C(11)-C(10)-C(9)	-6.8(3)	C(25)-P(1)-C(19)-C(24)	12.2(3)
Cl(2)-C(11)-C(10)-C(9)	174.93(2)	C(16)-C(17)-C(18)-C(13)	-1.4(5)
O(11)-C(9)-C(10)-O(10)	4.7(4)	C(14)-C(13)-C(18)-C(17)	1.3(4)
C(8)-C(9)-C(10)-O(10)	-175.2(2)	P(1)-C(13)-C(18)-C(17)	-179.1(2)
O(11)-C(9)-C(10)-C(11)	-174.0(2)	Nb(1)-O(3)-C(6)-C(5)	-172.28(2)
C(8)-C(9)-C(10)-C(11)	6.1(3)	Nb(1)-O(3)-C(6)-C(1)	8.6(3)
Nb(1)-O(2)-C(7)-C(8)	168.37(2)	C(4)-C(5)-C(6)-O(3)	-177.9(2)
Nb(1)-O(2)-C(7)-C(12)	-9.6(3)	Cl(4)-C(5)-C(6)-O(3)	-1.6(4)

C(9)-C(8)-C(7)-O(2)	172.8(2)	C(4)-C(5)-C(6)-C(1)	1.1(4)
Cl(3)-C(8)-C(7)-O(2)	-6.4(3)	Cl(4)-C(5)-C(6)-C(1)	177.41(2)
C(9)-C(8)-C(7)-C(12)	-9.4(4)	O(4)-C(1)-C(6)-O(3)	-0.3(3)
Cl(3)-C(8)-C(7)-C(12)	171.42(2)	C(2)-C(1)-C(6)-O(3)	-180.0(2)
Nb(1)-O(1)-C(12)-C(11)	178.89(2)	O(4)-C(1)-C(6)-C(5)	-179.5(2)
Nb(1)-O(1)-C(12)-C(7)	-0.7(3)	C(2)-C(1)-C(6)-C(5)	0.9(3)
C(10)-C(11)-C(12)-O(1)	-179.7(2)	C(18)-C(17)-C(16)-C(15)	0.6(5)
Cl(2)-C(11)-C(12)-O(1)	-1.5(3)	C(14)-C(15)-C(16)-C(17)	0.3(5)
C(10)-C(11)-C(12)-C(7)	-0.1(3)	O(12)-C(42)-C(41)-C(40)	-14.3(4)
Cl(2)-C(11)-C(12)-C(7)	178.07(2)	C(21)-C(22)-C(23)-C(24)	-0.1(5)
O(2)-C(7)-C(12)-O(1)	6.5(3)	C(19)-C(24)-C(23)-C(22)	0.6(4)
C(8)-C(7)-C(12)-O(1)	-171.6(2)	C(23)-C(22)-C(21)-C(20)	-0.7(5)
O(2)-C(7)-C(12)-C(11)	-173.1(2)	C(19)-C(20)-C(21)-C(22)	0.9(5)
C(8)-C(7)-C(12)-C(11)	8.8(3)	O(12)-C(39)-C(40)-C(41)	31.0(4)
C(37)-N(1)-C(31)-C(32)	177.8(3)	C(42)-C(41)-C(40)-C(39)	-9.3(4)
C(33)-N(1)-C(31)-C(32)	56.4(3)	C(30)-C(25)-C(26)-C(27)	-1.1(5)
C(35)-N(1)-C(31)-C(32)	-60.5(3)	P(1)-C(25)-C(26)-C(27)	-177.5(3)
C(18)-C(13)-C(14)-C(15)	-0.5(4)	C(28)-C(27)-C(26)-C(25)	0.5(6)
P(1)-C(13)-C(14)-C(15)	180.0(2)	C(30)-C(29)-C(28)-C(27)	-0.7(6)
C(6)-C(5)-C(4)-O(9)	178.3(3)	C(26)-C(27)-C(28)-C(29)	0.5(6)
Cl(4)-C(5)-C(4)-O(9)	2.0(4)	C(37)-N(1)-C(33)-C(34)	-59.9(3)
C(6)-C(5)-C(4)-C(3)	-2.3(4)	C(35)-N(1)-C(33)-C(34)	178.9(3)
Cl(4)-C(5)-C(4)-C(3)	-178.64(2)	C(31)-N(1)-C(33)-C(34)	58.1(3)

Table B.6 General hydrogen-bond distances (Å) and angles (°) of (Et$_4$N)*cis*-[NbO(ca)$_2$(H$_2$O)OPPh$_3$]· 3H$_2$O·THF (5).

Interactions	D-H⋯A	D-H(Å)	H⋯A (Å)	D⋯A (Å)	D-H⋯A (°)
I	O13-H1⋯Cl5	0.87(4)	2.52(4)	3.370(2)	166(3)
II	O13-H1⋯O4	0.87(4)	2.47(4)	2.921(3)	113(3)
III	O13-H2⋯O9[a]	0.86(4)	1.89(4)	2.739(3)	171(3)
IV	O14-H4⋯O15[a]	0.85(3)	1.85(3)	2.673(4)	165(5)
V	O15-H5⋯O8	0.81(3)	2.35(3)	3.062(3)	147(3)
VI	O15-H5⋯O9	0.81(3)	2.24(3)	2.922(3)	142(3)
VII	O5-H5A⋯O14	0.92(3)	1.69(3)	2.577(3)	163(3)
VIII	O5-H5B⋯O13	0.84(4)	2.79(4)	2.608(3)	165(4)
IX	O15-H6⋯O10[b]	0.85(4)	2.05(4)	2.890(3)	175(5)
X	C14-H14⋯O6	0.93	2.49	2.918(3)	108
XI	C18-H18⋯O8[c]	0.93	2.40	3.212(4)	145
XII	C22-H22⋯O7[c]	0.93	2.44	3.314(4)	157
XIII	C30-H30⋯O3	0.93	2.52	3.394(3)	156
XIV	C30-H30⋯O6	0.93	2.57	2.985(3)	108
XV	C31-H31B⋯O2[d]	0.97	2.57	3.374(4)	140
XVI	C33-H32A⋯O7[d]	0.96	2.57	3.500(4)	163
XVII	C32-H32B⋯O11[e]	0.96	2.56	3.522(4)	175
XVIII	C34-H34C⋯O12[f]	0.96	2.57	3.403(4)	146
XIX	C37-H37A⋯Cl3[d]	0.97	2.78	3.740(3)	172

Symmetry code: (a) -x+1, y+½, -z+1 (b), x+1, y, z - 1 (c), x-1, y, z (d), x, y+1, (e), x+1, y+1, z (f), -x+1, y+½, -z+2

B.2 Crystal structure of tetratetraethylammoniumoctachloridocyclo-di-μ-oxido-di-μ-(2,5-dichloro-3,6-dihydroxy-1,4-benzoquinonato-κ^2O,O') tetraoxidoniobate(V), diacetonitrile solvate, (Et$_4$N)$_4$[Nb$_4$O$_4$(ca)$_2$(μ^2-O)$_2$Cl$_8$]· 2CH$_3$CN (6)

Table B.7 Atomic coordinates (x 10^4) and equivalent isotropic displacement parameters (Å^{2}x 10^3) for (Et$_4$N)$_4$[Nb$_4$O$_4$(ca)$_2$(μ^2-O)$_2$Cl$_8$]·2CH$_3$CN (6). U(eq) is defined as one third of the trace of the orthogonalized U^{ij} tensor.

	x	y	z	U(eq)
C(36)	2559(8)	2370(2)	758(9)	93(1)
N(5)	9795(1)	7000(2)	5006(6)	96(9)
Nb(01)	7452(1)	1477(1)	3963(1)	17(1)
Nb(02)	6048(1)	1434(1)	1424(1)	17(1)
Cl(10)	5180(1)	2141(2)	1851(1)	22(1)
Cl(2)	8832(1)	2492(2)	2109(1)	24(1)
Cl(1)	7561(1)	-2711(2)	2534(1)	24(1)
Cl(11)	6424(1)	2480(3)	3965(1)	33(1)
Cl(12)	7880(2)	3286(3)	4306(1)	35(1)
O(2)	6982(3)	372(7)	3480(2)	21(2)
O(3)	6612(3)	2393(7)	1893(2)	18(1)
O(7)	7991(3)	909(7)	1549(2)	20(2)
O(6)	8325(3)	-1030(7)	3116(2)	18(1)
C(1)	7879(5)	-1248(9)	2420(3)	17(2)
C(5)	8520(4)	647(9)	2650(3)	14(2)
C(7)	6528(4)	161(9)	2784(3)	15(2)
C(2)	7802(4)	-777(10)	2017(3)	18(2)
O(5)	8822(4)	1136(7)	2962(2)	22(2)
O(8)	7497(3)	-1268(7)	1701(2)	21(2)
C(6)	8227(4)	-641(10)	2747(3)	18(2)
C(3)	8082(4)	498(10)	1920(3)	17(2)
C(4)	8446(5)	1142(9)	2242(4)	19(2)
O(1)	7462(3)	2566(7)	3298(2)	21(2)
C(9)	6730(4)	1965(9)	2270(3)	15(2)
C(12)	6879(4)	767(9)	3097(3)	15(2)
O(4)	6164(3)	182(7)	2059(2)	19(1)

C(10)	7075(4)	2569(9)	2578(3)	14(2)
C(8)	6460(4)	682(9)	2368(3)	15(2)
Cl(4)	7413(1)	4003(2)	2477(1)	22(1)
C(11)	7170(4)	2043(9)	2995(3)	14(2)
Cl(3)	6149(1)	-1201(2)	2901(1)	22(1)
Cl(9)	5363(1)	-41(3)	1079(1)	27(1)
Nb(03)	8988(1)	243(1)	3567(1)	17(1)
Nb(04)	7426(1)	-478(1)	1069(1)	20(1)
Cl(5)	9768(1)	-924(3)	3170(1)	31(1)
Cl(6)	9057(1)	-1348(3)	4103(1)	30(1)
Cl(7)	8497(1)	-1209(3)	1027(1)	38(1)
Cl(8)	7557(2)	754(3)	445(1)	37(1)
O(9)	7047(4)	-1754(8)	851(3)	31(2)
O(12)	6023(4)	2679(8)	1069(3)	27(2)
O(14)	8222(4)	876(7)	3753(2)	23(2)
O(13)	6755(3)	521(8)	1260(2)	25(2)
O(11)	7353(4)	482(8)	4383(2)	27(2)
O(10)	9481(4)	1369(8)	3764(2)	26(2)
N(1)	5706(4)	-3762(9)	1687(3)	22(2)
N(2)	3679(4)	1904(8)	665(3)	22(2)
N(3)	637(4)	9878(9)	1733(3)	23(2)
C(22)	262(5)	8797(9)	1906(4)	21(2)
C(23)	1290(5)	9363(1)	1669(4)	25(2)
C(14)	5723(6)	-4851(1)	2004(4)	28(2)
C(21)	-396(5)	9130(1)	1985(5)	36(3)
C(19)	5342(6)	-2635(1)	1844(4)	30(3)
C(13)	5932(6)	-4491(1)	2459(4)	28(2)
C(27)	660(6)	10987(1)	2037(4)	35(3)
C(24)	1758(6)	10350(1)	1517(4)	34(3)
C(18)	6356(6)	-3262(1)	1617(4)	31(3)
C(26)	351(6)	10388(1)	1318(4)	37(3)
C(15)	5429(6)	-4279(1)	1267(4)	30(3)
C(16)	5361(7)	-3352(1)	900(4)	37(3)
C(30)	3613(6)	691(1)	911(4)	32(3)
C(33)	4496(7)	3606(2)	536(5)	49(4)
C(31)	3609(6)	1622(1)	195(4)	39(3)
C(34)	4320(6)	2423(1)	773(4)	33(3)
C(17)	6814(7)	-4200(2)	1446(4)	41(3)

C(20)	4682(6)	-2957(2)	1954(4)	42(3)
C(29)	3621(7)	806(1)	1402(5)	40(3)
C(28)	928(7)	10692(1)	2486(5)	41(3)
C(25)	262(7)	9425(2)	969(5)	47(4)
C(35)	3203(6)	2886(1)	792(5)	43(4)
C(32)	4092(1)	740(20)	12(6)	72(6)
N(4)	1253(6)	9476(1)	4398(4)	40(3)
C(38)	908(6)	10325(1)	4085(5)	38(3)
C(45)	6405(9)	4165(2)	203(5)	57(5)
C(39)	813(8)	9421(2)	4777(5)	48(4)
C(44)	794(7)	7453(1)	4093(5)	43(3)
C(46)	6317(1)	2891(2)	98(6)	78(7)
C(41)	1918(1)	11235(2)	4740(6)	72(7)
C(42)	1877(6)	10029(2)	4548(7)	63(6)
C(40)	1082(1)	8610(2)	5145(7)	90(8)
C(43)	1356(7)	8184(2)	4243(8)	76(7)
C(37)	1251(1)	10550(2)	3660(6)	76(7)
C(48)	9383(8)	6358(2)	4973(5)	51(4)
C(47)	8848(8)	5490(2)	4923(7)	79(7)
N(6)	6470(9)	5213(2)	287(5)	70(5)

Table B.8 Bond lengths (Å) and angles (°) for (Et₄N)₄[Nb₄O₄(ca)₂(μ^2-O)₂Cl₈]·2CH₃CN (6).

Atoms	Distance (Å)	Atoms	Angle (°)
C(36)-C(35)	1.50(2)	C(35)-C(36)-H(36A)	109.5
C(36)-H(36A)	0.98	C(35)-C(36)-H(36B)	109.5
C(36)-H(36B)	0.98	H(36A)-C(36)-H(36B)	109.5
C(36)-H(36C)	0.98	C(35)-C(36)-H(36C)	109.5
N(5)-C(48)	1.12(2)	H(36A)-C(36)-H(36C)	109.5
Nb(01)-O(11)	1.706(8)	H(36B)-C(36)-H(36C)	109.5
Nb(01)-O(14)	1.920(8)	O(11)-Nb(01)-O(14)	101.0(4)
Nb(01)-O(2)	2.139(7)	O(11)-Nb(01)-O(2)	97.4(3)
Nb(01)-Cl(12)	2.376(3)	O(14)-Nb(01)-O(2)	88.2(3)
Nb(01)-O(1)	2.380(7)	O(11)-Nb(01)-Cl(12)	102.6(3)
Nb(01)-Cl(11)	2.465(3)	O(14)-Nb(01)-Cl(12)	95.7(3)
Nb(02)-O(12)	1.728(8)	O(2)-Nb(01)-Cl(12)	158.5(2)
Nb(02)-O(13)	1.898(7)	O(11)-Nb(01)-O(1)	168.3(3)
Nb(02)-O(3)	2.130(7)	O(14)-Nb(01)-O(1)	80.1(3)
Nb(02)-Cl(9)	2.386(3)	O(2)-Nb(01)-O(1)	70.9(3)
Nb(02)-O(4)	2.396(7)	Cl(12)-Nb(01)-O(1)	88.9(2)
Nb(02)-Cl(10)	2.461(3)	O(11)-Nb(01)-Cl(11)	97.3(3)
Cl(2)-C(4)	1.723(1)	O(14)-Nb(01)-Cl(11)	159.6(2)
Cl(1)-C(1)	1.747(1)	O(2)-Nb(01)-Cl(11)	80.7(2)
O(2)-C(12)	1.278(1)	Cl(12)-Nb(01)-Cl(11)	88.90(1)
O(3)-C(9)	1.279(1)	O(1)-Nb(01)-Cl(11)	80.1(2)
O(7)-C(3)	1.246(1)	O(12)-Nb(02)-O(13)	103.1(4)
O(7)-Nb(04)	2.402(7)	O(12)-Nb(02)-O(3)	94.2(3)
O(6)-C(6)	1.234(1)	O(13)-Nb(02)-O(3)	89.3(3)
O(6)-Nb(03)	2.390(7)	O(12)-Nb(02)-Cl(9)	102.4(3)
C(1)-C(2)	1.358(1)	O(13)-Nb(02)-Cl(9)	91.8(3)
C(1)-C(6)	1.403(1)	O(3)-Nb(02)-Cl(9)	162.6(2)
C(5)-O(5)	1.266(1)	O(12)-Nb(02)-O(4)	163.3(3)
C(5)-C(4)	1.380(1)	O(13)-Nb(02)-O(4)	83.0(3)
C(5)-C(6)	1.547(1)	O(3)-Nb(02)-O(4)	70.1(3)
C(7)-C(12)	1.374(1)	Cl(9)-Nb(02)-O(4)	92.75(2)
C(7)-C(8)	1.415(1)	O(12)-Nb(02)-Cl(10)	96.1(3)
C(7)-Cl(3)	1.715(1)	O(13)-Nb(02)-Cl(10)	160.3(3)
C(2)-O(8)	1.278(1)	O(3)-Nb(02)-Cl(10)	84.7(2)
C(2)-C(3)	1.524(1)	Cl(9)-Nb(02)-Cl(10)	88.50(1)
O(5)-Nb(03)	2.132(7)	O(4)-Nb(02)-Cl(10)	77.26(2)

O(8)-Nb(04)	2.144(7)	C(12)-O(2)-Nb(01)	122.6(7)
C(3)-C(4)	1.428(1)	C(9)-O(3)-Nb(02)	123.4(6)
O(1)-C(11)	1.247(1)	C(3)-O(7)-Nb(04)	114.8(7)
C(9)-C(10)	1.354(1)	C(6)-O(6)-Nb(03)	115.8(6)
C(9)-C(8)	1.523(1)	C(2)-C(1)-C(6)	123.1(9)
C(12)-C(11)	1.537(1)	C(2)-C(1)-Cl(1)	118.9(8)
O(4)-C(8)	1.255(1)	C(6)-C(1)-Cl(1)	117.9(8)
C(10)-C(11)	1.425(1)	O(5)-C(5)-C(4)	126.2(9)
C(10)-Cl(4)	1.729(9)	O(5)-C(5)-C(6)	114.6(8)
Nb(03)-O(10)	1.704(8)	C(4)-C(5)-C(6)	119.2(9)
Nb(03)-O(14)	1.900(8)	C(12)-C(7)-C(8)	120.1(9)
Nb(03)-Cl(6)	2.383(3)	C(12)-C(7)-Cl(3)	120.1(8)
Nb(03)-Cl(5)	2.468(3)	C(8)-C(7)-Cl(3)	119.7(7)
Nb(04)-O(9)	1.716(8)	O(8)-C(2)-C(1)	127.2(1)
Nb(04)-O(13)	1.912(8)	O(8)-C(2)-C(3)	114.1(9)
Nb(04)-Cl(8)	2.375(3)	C(1)-C(2)-C(3)	118.7(9)
Nb(04)-Cl(7)	2.449(3)	C(5)-O(5)-Nb(03)	124.2(6)
N(1)-C(15)	1.523(1)	C(2)-O(8)-Nb(04)	124.4(7)
N(1)-C(18)	1.524(1)	O(6)-C(6)-C(1)	126.2(9)
N(1)-C(14)	1.525(1)	O(6)-C(6)-C(5)	115.2(9)
N(1)-C(19)	1.529(2)	C(1)-C(6)-C(5)	118.5(9)
N(2)-C(31)	1.499(2)	O(7)-C(3)-C(4)	123.3(1)
N(2)-C(30)	1.515(2)	O(7)-C(3)-C(2)	116.7(9)
N(2)-C(34)	1.518(1)	C(4)-C(3)-C(2)	120.0(9)
N(2)-C(35)	1.531(1)	C(5)-C(4)-C(3)	120.4(9)
N(3)-C(26)	1.513(2)	C(5)-C(4)-Cl(2)	120.2(8)
N(3)-C(27)	1.517(2)	C(3)-C(4)-Cl(2)	119.3(8)
N(3)-C(22)	1.521(1)	C(11)-O(1)-Nb(01)	115.0(6)
N(3)-C(23)	1.532(1)	O(3)-C(9)-C(10)	124.6(9)
C(22)-C(21)	1.494(1)	O(3)-C(9)-C(8)	116.1(9)
C(22)-H(22A)	0.99	C(10)-C(9)-C(8)	119.3(9)
C(22)-H(22B)	0.99	O(2)-C(12)-C(7)	125.5(9)
C(23)-C(24)	1.548(2)	O(2)-C(12)-C(11)	115.3(9)
C(23)-H(23A)	0.99	C(7)-C(12)-C(11)	119.2(9)
C(23)-H(23B)	0.99	C(8)-O(4)-Nb(02)	115.6(6)
C(14)-C(13)	1.523(2)	C(9)-C(10)-C(11)	121.1(9)
C(14)-H(14A)	0.99	C(9)-C(10)-Cl(4)	121.0(8)
C(14)-H(14B)	0.99	C(11)-C(10)-Cl(4)	117.9(7)

C(21)-H(21A)	0.98	O(4)-C(8)-C(7)	124.7(9)
C(21)-H(21B)	0.98	O(4)-C(8)-C(9)	114.6(8)
C(21)-H(21C)	0.98	C(7)-C(8)-C(9)	120.6(9)
C(19)-C(20)	1.517(2)	O(1)-C(11)-C(10)	124.6(9)
C(19)-H(19A)	0.99	O(1)-C(11)-C(12)	115.9(9)
C(19)-H(19B)	0.99	C(10)-C(11)-C(12)	119.4(8)
C(13)-H(13A)	0.98	O(10)-Nb(03)-O(14)	100.3(4)
C(13)-H(13B)	0.98	O(10)-Nb(03)-O(5)	94.9(3)
C(13)-H(13C)	0.98	O(14)-Nb(03)-O(5)	89.7(3)
C(27)-C(28)	1.53(2)	O(10)-Nb(03)-Cl(6)	103.1(3)
C(27)-H(27A)	0.99	O(14)-Nb(03)-Cl(6)	94.0(2)
C(27)-H(27B)	0.99	O(5)-Nb(03)-Cl(6)	160.6(2)
C(24)-H(24A)	0.98	O(10)-Nb(03)-O(6)	164.7(3)
C(24)-H(24B)	0.98	O(14)-Nb(03)-O(6)	82.7(3)
C(24)-H(24C)	0.98	O(5)-Nb(03)-O(6)	69.9(3)
C(18)-C(17)	1.518(2)	Cl(6)-Nb(03)-O(6)	91.61(2)
C(18)-H(18A)	0.99	O(10)-Nb(03)-Cl(5)	96.2(3)
C(18)-H(18B)	0.99	O(14)-Nb(03)-Cl(5)	162.4(2)
C(26)-C(25)	1.50(2)	O(5)-Nb(03)-Cl(5)	82.8(2)
C(26)-H(26A)	0.99	Cl(6)-Nb(03)-Cl(5)	88.21(1)
C(26)-H(26B)	0.99	O(6)-Nb(03)-Cl(5)	79.78(2)
C(15)-C(16)	1.515(2)	O(9)-Nb(04)-O(13)	102.1(4)
C(15)-H(15A)	0.99	O(9)-Nb(04)-O(8)	94.0(4)
C(15)-H(15B)	0.99	O(13)-Nb(04)-O(8)	87.8(3)
C(16)-H(16A)	0.98	O(9)-Nb(04)-Cl(8)	100.5(3)
C(16)-H(16B)	0.98	O(13)-Nb(04)-Cl(8)	93.6(3)
C(16)-H(16C)	0.98	O(8)-Nb(04)-Cl(8)	164.8(2)
C(30)-C(29)	1.534(2)	O(9)-Nb(04)-O(7)	163.5(3)
C(30)-H(30A)	0.99	O(13)-Nb(04)-O(7)	80.6(3)
C(30)-H(30B)	0.99	O(8)-Nb(04)-O(7)	69.7(3)
C(33)-C(34)	1.518(2)	Cl(8)-Nb(04)-O(7)	95.52(2)
C(33)-H(33A)	0.98	O(9)-Nb(04)-Cl(7)	99.4(3)
C(33)-H(33B)	0.98	O(13)-Nb(04)-Cl(7)	157.4(3)
C(33)-H(33C)	0.98	O(8)-Nb(04)-Cl(7)	83.8(2)
C(31)-C(32)	1.53(2)	Cl(8)-Nb(04)-Cl(7)	89.37(1)
C(31)-H(31A)	0.99	O(7)-Nb(04)-Cl(7)	76.8(2)
C(31)-H(31B)	0.99	Nb(03)-O(14)-Nb(01)	177.6(5)
C(34)-H(34A)	0.99	Nb(02)-O(13)-Nb(04)	175.7(5)

C(34)-H(34B)	0.99	C(15)-N(1)-C(18)	109.7(9)
C(17)-H(17A)	0.98	C(15)-N(1)-C(14)	106.4(8)
C(17)-H(17B)	0.98	C(18)-N(1)-C(14)	111.2(9)
C(17)-H(17C)	0.98	C(15)-N(1)-C(19)	111.7(9)
C(20)-H(20A)	0.98	C(18)-N(1)-C(19)	105.0(9)
C(20)-H(20B)	0.98	C(14)-N(1)-C(19)	112.9(9)
C(20)-H(20C)	0.98	C(31)-N(2)-C(30)	108.6(9)
C(29)-H(29A)	0.98	C(31)-N(2)-C(34)	110.4(9)
C(29)-H(29B)	0.98	C(30)-N(2)-C(34)	107.6(9)
C(29)-H(29C)	0.98	C(31)-N(2)-C(35)	110.4(1)
C(28)-H(28A)	0.98	C(30)-N(2)-C(35)	112.0(9)
C(28)-H(28B)	0.98	C(34)-N(2)-C(35)	107.9(1)
C(28)-H(28C)	0.98	C(26)-N(3)-C(27)	104.9(9)
C(25)-H(25A)	0.98	C(26)-N(3)-C(22)	111.8(9)
C(25)-H(25B)	0.98	C(27)-N(3)-C(22)	111.9(9)
C(25)-H(25C)	0.98	C(26)-N(3)-C(23)	111.4(9)
C(35)-H(35A)	0.99	C(27)-N(3)-C(23)	110.7(9)
C(35)-H(35B)	0.99	C(22)-N(3)-C(23)	106.3(8)
C(32)-H(32A)	0.98	C(21)-C(22)-N(3)	113.7(9)
C(32)-H(32B)	0.98	C(21)-C(22)-H(22A)	108.8
C(32)-H(32C)	0.98	N(3)-C(22)-H(22A)	108.8
N(4)-C(43)	1.480(2)	C(21)-C(22)-H(22B)	108.8
N(4)-C(38)	1.509(2)	N(3)-C(22)-H(22B)	108.8
N(4)-C(42)	1.526(2)	H(22A)-C(22)-H(22B)	107.7
N(4)-C(39)	1.55(2)	N(3)-C(23)-C(24)	114.3(1)
C(38)-C(37)	1.56(2)	N(3)-C(23)-H(23A)	108.7
C(38)-H(38A)	0.99	C(24)-C(23)-H(23A)	108.7
C(38)-H(38B)	0.99	N(3)-C(23)-H(23B)	108.7
C(45)-N(6)	1.15(3)	C(24)-C(23)-H(23B)	108.7
C(45)-C(46)	1.41(3)	H(23A)-C(23)-H(23B)	107.6
C(39)-C(40)	1.53(2)	C(13)-C(14)-N(1)	114.4(9)
C(39)-H(39A)	0.99	C(13)-C(14)-H(14A)	108.7
C(39)-H(39B)	0.99	N(1)-C(14)-H(14A)	108.7
C(44)-C(43)	1.502(2)	C(13)-C(14)-H(14B)	108.7
C(44)-H(44A)	0.98	N(1)-C(14)-H(14B)	108.7
C(44)-H(44B)	0.98	H(14A)-C(14)-H(14B)	107.6
C(44)-H(44C)	0.98	C(22)-C(21)-H(21A)	109.5
C(46)-H(46A)	0.98	C(22)-C(21)-H(21B)	109.5

C(46)-H(46B)	0.98	H(21A)-C(21)-H(21B)	109.5
C(46)-H(46C)	0.98	C(22)-C(21)-H(21C)	109.5
C(41)-C(42)	1.42(2)	H(21A)-C(21)-H(21C)	109.5
C(41)-H(41A)	0.98	H(21B)-C(21)-H(21C)	109.5
C(41)-H(41B)	0.98	C(20)-C(19)-N(1)	113.2(1)
C(41)-H(41C)	0.98	C(20)-C(19)-H(19A)	108.9
C(42)-H(42A)	0.99	N(1)-C(19)-H(19A)	108.9
C(42)-H(42B)	0.99	C(20)-C(19)-H(19B)	108.9
C(40)-H(40A)	0.98	N(1)-C(19)-H(19B)	108.9
C(40)-H(40B)	0.98	H(19A)-C(19)-H(19B)	107.7
C(40)-H(40C)	0.98	C(14)-C(13)-H(13A)	109.5
C(43)-H(43A)	0.99	C(14)-C(13)-H(13B)	109.5
C(43)-H(43B)	0.99	H(13A)-C(13)-H(13B)	109.5
C(37)-H(37A)	0.98	C(14)-C(13)-H(13C)	109.5
C(37)-H(37B)	0.98	H(13A)-C(13)-H(13C)	109.5
C(37)-H(37C)	0.98	H(13B)-C(13)-H(13C)	109.5
C(48)-C(47)	1.49(2)	N(3)-C(27)-C(28)	114.5(1)
C(47)-H(47A)	0.98	N(3)-C(27)-H(27A)	108.6
C(47)-H(47B)	0.98	C(28)-C(27)-H(27A)	108.6
C(47)-H(47C)	0.98	N(3)-C(27)-H(27B)	108.6
		C(28)-C(27)-H(27B)	108.6
		H(27A)-C(27)-H(27B)	107.6
		C(23)-C(24)-H(24A)	109.5
		C(23)-C(24)-H(24B)	109.5
		H(24A)-C(24)-H(24B)	109.5
		C(23)-C(24)-H(24C)	109.5
		H(24A)-C(24)-H(24C)	109.5
		H(24B)-C(24)-H(24C)	109.5
		C(17)-C(18)-N(1)	115.8(1)
		C(17)-C(18)-H(18A)	108.3
		N(1)-C(18)-H(18A)	108.3
		C(17)-C(18)-H(18B)	108.3
		N(1)-C(18)-H(18B)	108.3
		H(18A)-C(18)-H(18B)	107.4
		C(25)-C(26)-N(3)	114.2(1)
		C(25)-C(26)-H(26A)	108.7
		N(3)-C(26)-H(26A)	108.7
		C(25)-C(26)-H(26B)	108.7

N(3)-C(26)-H(26B)	108.7
H(26A)-C(26)-H(26B)	107.6
C(16)-C(15)-N(1)	115.9(1)
C(16)-C(15)-H(15A)	108.3
N(1)-C(15)-H(15A)	108.3
C(16)-C(15)-H(15B)	108.3
N(1)-C(15)-H(15B)	108.3
H(15A)-C(15)-H(15B)	107.4
C(15)-C(16)-H(16A)	109.5
C(15)-C(16)-H(16B)	109.5
H(16A)-C(16)-H(16B)	109.5
C(15)-C(16)-H(16C)	109.5
H(16A)-C(16)-H(16C)	109.5
H(16B)-C(16)-H(16C)	109.5
N(2)-C(30)-C(29)	116.2(1)
N(2)-C(30)-H(30A)	108.2
C(29)-C(30)-H(30A)	108.2
N(2)-C(30)-H(30B)	108.2
C(29)-C(30)-H(30B)	108.2
H(30A)-C(30)-H(30B)	107.4
C(34)-C(33)-H(33A)	109.5
C(34)-C(33)-H(33B)	109.5
H(33A)-C(33)-H(33B)	109.5
C(34)-C(33)-H(33C)	109.5
H(33A)-C(33)-H(33C)	109.5
H(33B)-C(33)-H(33C)	109.5
N(2)-C(31)-C(32)	116.3(1)
N(2)-C(31)-H(31A)	108.2
C(32)-C(31)-H(31A)	108.2
N(2)-C(31)-H(31B)	108.2
C(32)-C(31)-H(31B)	108.2
H(31A)-C(31)-H(31B)	107.4
C(33)-C(34)-N(2)	116.0(1)
C(33)-C(34)-H(34A)	108.3
N(2)-C(34)-H(34A)	108.3
C(33)-C(34)-H(34B)	108.3
N(2)-C(34)-H(34B)	108.3
H(34A)-C(34)-H(34B)	107.4

C(18)-C(17)-H(17A)	109.5
C(18)-C(17)-H(17B)	109.5
H(17A)-C(17)-H(17B)	109.5
C(18)-C(17)-H(17C)	109.5
H(17A)-C(17)-H(17C)	109.5
H(17B)-C(17)-H(17C)	109.5
C(19)-C(20)-H(20A)	109.5
C(19)-C(20)-H(20B)	109.5
H(20A)-C(20)-H(20B)	109.5
C(19)-C(20)-H(20C)	109.5
H(20A)-C(20)-H(20C)	109.5
H(20B)-C(20)-H(20C)	109.5
C(30)-C(29)-H(29A)	109.5
C(30)-C(29)-H(29B)	109.5
H(29A)-C(29)-H(29B)	109.5
C(30)-C(29)-H(29C)	109.5
H(29A)-C(29)-H(29C)	109.5
H(29B)-C(29)-H(29C)	109.5
C(27)-C(28)-H(28A)	109.5
C(27)-C(28)-H(28B)	109.5
H(28A)-C(28)-H(28B)	109.5
C(27)-C(28)-H(28C)	109.5
H(28A)-C(28)-H(28C)	109.5
H(28B)-C(28)-H(28C)	109.5
C(26)-C(25)-H(25A)	109.5
C(26)-C(25)-H(25B)	109.5
H(25A)-C(25)-H(25B)	109.5
C(26)-C(25)-H(25C)	109.5
H(25A)-C(25)-H(25C)	109.5
H(25B)-C(25)-H(25C)	109.5
C(36)-C(35)-N(2)	111.3(1)
C(36)-C(35)-H(35A)	109.4
N(2)-C(35)-H(35A)	109.4
C(36)-C(35)-H(35B)	109.4
N(2)-C(35)-H(35B)	109.4
H(35A)-C(35)-H(35B)	108
C(31)-C(32)-H(32A)	109.5
C(31)-C(32)-H(32B)	109.5

H(32A)-C(32)-H(32B)	109.5
C(31)-C(32)-H(32C)	109.5
H(32A)-C(32)-H(32C)	109.5
H(32B)-C(32)-H(32C)	109.5
C(43)-N(4)-C(38)	115.0(1)
C(43)-N(4)-C(42)	108.5(1)
C(38)-N(4)-C(42)	112.0(1)
C(43)-N(4)-C(39)	108.6(1)
C(38)-N(4)-C(39)	102.5(1)
C(42)-N(4)-C(39)	110.1(1)
N(4)-C(38)-C(37)	113.9(1)
N(4)-C(38)-H(38A)	108.8
C(37)-C(38)-H(38A)	108.8
N(4)-C(38)-H(38B)	108.8
C(37)-C(38)-H(38B)	108.8
H(38A)-C(38)-H(38B)	107.7
N(6)-C(45)-C(46)	179(2)
C(40)-C(39)-N(4)	111.6(2)
C(40)-C(39)-H(39A)	109.3
N(4)-C(39)-H(39A)	109.3
C(40)-C(39)-H(39B)	109.3
N(4)-C(39)-H(39B)	109.3
H(39A)-C(39)-H(39B)	108
C(43)-C(44)-H(44A)	109.5
C(43)-C(44)-H(44B)	109.5
H(44A)-C(44)-H(44B)	109.5
C(43)-C(44)-H(44C)	109.5
H(44A)-C(44)-H(44C)	109.5
H(44B)-C(44)-H(44C)	109.5
C(45)-C(46)-H(46A)	109.5
C(45)-C(46)-H(46B)	109.5
H(46A)-C(46)-H(46B)	109.5
C(45)-C(46)-H(46C)	109.5
H(46A)-C(46)-H(46C)	109.5
H(46B)-C(46)-H(46C)	109.5
C(42)-C(41)-H(41A)	109.5
C(42)-C(41)-H(41B)	109.5
H(41A)-C(41)-H(41B)	109.5

C(42)-C(41)-H(41C)	109.5
H(41A)-C(41)-H(41C)	109.5
H(41B)-C(41)-H(41C)	109.5
C(41)-C(42)-N(4)	121.2(1)
C(41)-C(42)-H(42A)	107
N(4)-C(42)-H(42A)	107
C(41)-C(42)-H(42B)	107
N(4)-C(42)-H(42B)	107
H(42A)-C(42)-H(42B)	106.8
C(39)-C(40)-H(40A)	109.5
C(39)-C(40)-H(40B)	109.5
H(40A)-C(40)-H(40B)	109.5
C(39)-C(40)-H(40C)	109.5
H(40A)-C(40)-H(40C)	109.5
H(40B)-C(40)-H(40C)	109.5
N(4)-C(43)-C(44)	117.1(1)
N(4)-C(43)-H(43A)	108
C(44)-C(43)-H(43A)	108
N(4)-C(43)-H(43B)	108
C(44)-C(43)-H(43B)	108
H(43A)-C(43)-H(43B)	107.3
C(38)-C(37)-H(37A)	109.5
C(38)-C(37)-H(37B)	109.5
H(37A)-C(37)-H(37B)	109.5
C(38)-C(37)-H(37C)	109.5
H(37A)-C(37)-H(37C)	109.5
H(37B)-C(37)-H(37C)	109.5
N(5)-C(48)-C(47)	179(3)
C(48)-C(47)-H(47A)	109.5
C(48)-C(47)-H(47B)	109.5
H(47A)-C(47)-H(47B)	109.5
C(48)-C(47)-H(47C)	109.5
H(47A)-C(47)-H(47C)	109.5
H(47B)-C(47)-H(47C)	109.5
C(35)-C(36)-H(36A)	109.5

Table B.9 Anisotropic displacement parameters ($Å^2$ x 10^3) for (Et$_4$N)$_4$[Nb$_4$O$_4$(ca)$_2$(μ^2-O)$_2$Cl$_8$]·2CH$_3$CN (6). The anisotropic displacement factor exponent takes the form: $-2\pi^2[$ $h^2a^{*2}U^{11}$ + … + 2 h k a* b* U^{12}].

	U^{11}	U^{22}	U^{33}	U^{23}	U^{13}	U^{12}
C(36)	28(9)	96(2)	160(2)	88(2)	29(1)	23(1)
N(5)	99(2)	121(2)	65(1)	34(1)	-29(1)	-78(1)
Nb(01)	16(1)	20(1)	16(1)	-1(1)	0(1)	-5(1)
Nb(02)	16(1)	19(1)	15(1)	1(1)	0(1)	2(1)
Cl(10)	16(1)	23(1)	28(1)	-5(1)	5(1)	-1(1)
Cl(2)	29(1)	17(1)	26(1)	4(1)	0(1)	-10(1)
Cl(1)	22(1)	15(1)	33(1)	3(1)	-5(1)	-7(1)
Cl(11)	24(1)	39(2)	37(2)	-7(1)	2(1)	7(1)
Cl(12)	42(2)	33(2)	31(1)	-14(1)	2(1)	-16(1)
O(2)	28(4)	22(4)	13(3)	2(3)	-3(3)	-6(3)
O(3)	12(3)	20(4)	20(3)	4(3)	0(3)	-1(3)
O(7)	15(3)	24(4)	20(3)	5(3)	-4(3)	-5(3)
O(6)	20(3)	15(3)	20(3)	1(3)	2(3)	-9(3)
C(1)	17(4)	10(4)	24(5)	5(4)	2(4)	-4(4)
C(5)	14(4)	8(4)	22(5)	1(3)	4(3)	-3(3)
C(7)	9(4)	14(4)	23(5)	-2(4)	0(3)	-3(3)
C(2)	14(4)	16(5)	23(5)	-2(4)	0(4)	4(4)
O(5)	30(4)	15(4)	21(4)	1(3)	3(3)	-4(3)
O(8)	18(3)	21(4)	24(4)	2(3)	-3(3)	-1(3)
C(6)	14(4)	14(5)	25(5)	-3(4)	2(4)	-2(4)
C(3)	7(4)	23(5)	22(5)	-2(4)	2(3)	3(4)
C(4)	14(4)	14(5)	30(5)	0(4)	4(4)	0(4)
O(1)	17(3)	20(4)	25(4)	2(3)	-5(3)	-1(3)
C(9)	8(4)	16(5)	21(5)	5(4)	4(3)	2(3)
C(12)	13(4)	14(4)	19(5)	1(4)	5(3)	0(3)
O(4)	26(4)	13(3)	16(3)	-4(3)	-2(3)	-4(3)
C(10)	7(4)	11(4)	23(5)	1(4)	2(3)	-1(3)
C(8)	11(4)	15(4)	18(4)	0(4)	2(3)	5(3)
Cl(4)	18(1)	17(1)	30(1)	6(1)	-2(1)	-6(1)
C(11)	9(4)	13(4)	21(5)	-2(4)	1(3)	1(3)
Cl(3)	26(1)	15(1)	24(1)	2(1)	-2(1)	-9(1)
Cl(9)	31(1)	18(1)	31(1)	-6(1)	-11(1)	2(1)
Nb(03)	16(1)	14(1)	21(1)	-1(1)	0(1)	-3(1)
Nb(04)	16(1)	23(1)	20(1)	-2(1)	0(1)	3(1)

Cl(5)	21(1)	26(1)	46(2)	-5(1)	12(1)	0(1)
Cl(6)	30(1)	27(1)	34(1)	12(1)	1(1)	-1(1)
Cl(7)	23(1)	51(2)	41(2)	-9(1)	-1(1)	13(1)
Cl(8)	34(2)	50(2)	28(1)	12(1)	3(1)	-4(1)
O(9)	30(4)	23(4)	38(5)	-9(4)	-7(4)	-1(3)
O(12)	32(4)	23(4)	27(4)	8(3)	5(3)	1(3)
O(14)	22(4)	25(4)	23(4)	0(3)	1(3)	-1(3)
O(13)	20(4)	29(4)	26(4)	1(3)	4(3)	8(3)
O(11)	28(4)	33(5)	19(4)	5(3)	-5(3)	-5(3)
O(10)	23(4)	28(4)	26(4)	1(3)	-8(3)	1(3)
N(1)	22(4)	18(4)	26(5)	-6(4)	3(3)	-6(4)
N(2)	21(4)	14(4)	31(5)	-4(4)	2(4)	0(3)
N(3)	20(4)	16(4)	34(5)	5(4)	2(4)	7(3)
C(22)	23(5)	6(4)	34(6)	1(4)	9(4)	2(4)
C(23)	13(5)	26(6)	35(6)	0(5)	4(4)	0(4)
C(14)	36(6)	14(5)	34(6)	2(4)	10(5)	-5(4)
C(21)	13(5)	32(7)	61(9)	-4(6)	5(5)	3(5)
C(19)	32(6)	29(6)	28(6)	-7(5)	4(5)	1(5)
C(13)	28(6)	22(6)	34(6)	2(5)	2(5)	3(5)
C(27)	40(7)	12(5)	53(8)	-5(5)	15(6)	3(5)
C(24)	24(6)	42(7)	38(7)	-5(6)	8(5)	-10(5)
C(18)	32(6)	38(7)	24(6)	-3(5)	5(5)	-15(5)
C(26)	36(7)	35(7)	42(7)	16(6)	3(6)	15(6)
C(15)	33(6)	22(6)	36(6)	-7(5)	-3(5)	0(5)
C(16)	50(8)	39(8)	22(6)	-12(5)	-4(5)	-8(6)
C(30)	30(6)	22(6)	43(7)	-3(5)	0(5)	-3(5)
C(33)	39(8)	45(9)	61(1)	12(7)	-8(7)	-18(7)
C(31)	39(7)	44(8)	34(7)	6(6)	-7(5)	-5(6)
C(34)	22(6)	36(7)	42(7)	3(6)	-4(5)	-3(5)
C(17)	41(8)	48(9)	34(7)	5(6)	12(6)	-3(6)
C(20)	37(7)	55(9)	35(7)	-9(6)	-3(6)	-10(7)
C(29)	44(8)	31(7)	45(8)	11(6)	4(6)	-6(6)
C(28)	49(8)	30(7)	45(8)	-16(6)	16(6)	-5(6)
C(25)	42(8)	61(1)	39(8)	14(7)	2(6)	-10(7)
C(35)	40(7)	28(7)	61(9)	9(6)	20(7)	25(6)
C(32)	95(2)	70(1)	54(1)	-21(1)	32(1)	17(1)
N(4)	49(7)	28(6)	40(6)	-2(5)	-13(5)	0(5)
C(38)	34(7)	32(7)	46(8)	-4(6)	-13(6)	-4(6)
C(45)	78(1)	69(1)	25(7)	8(7)	6(7)	38(1)

C(39)	64(1)	41(8)	39(8)	-4(6)	-4(7)	-5(7)
C(44)	47(8)	26(7)	56(9)	-15(6)	-9(7)	-1(6)
C(46)	140(2)	66(1)	34(9)	-4(8)	5(10)	31(1)
C(41)	96(1)	61(1)	55(1)	17(9)	-43(1)	-53(1)
C(42)	20(6)	66(1)	101(1)	-43(1)	-19(8)	4(7)
C(40)	140(2)	57(1)	66(1)	17(1)	-42(1)	-44(1)
C(43)	20(7)	52(1)	150(2)	-49(1)	-31(9)	19(7)
C(37)	106(2)	80(1)	43(9)	-15(9)	2(1)	-57(1)
C(48)	69(1)	39(8)	45(8)	13(7)	-12(7)	-15(8)
C(47)	38(9)	92(2)	110(2)	-43(1)	27(1)	-26(1)
N(6)	91(1)	66(1)	54(9)	13(8)	12(8)	32(1)

Table B.10 Hydrogen coordinates (x 10^4) and isotropic displacement parameters (Å^{2}x 10^3) for (Et$_4$N)$_4$[Nb$_4$O$_4$(ca)$_2$(μ^2-O)$_2$Cl$_8$]·2CH$_3$CN (6).

	x	y	z	U(eq)
H(36A)	2452	2172	458	140
H(36B)	2268	3002	861	140
H(36C)	2534	1614	933	140
H(22A)	267	8094	1699	25
H(22B)	463	8503	2178	25
H(23A)	1261	8677	1455	30
H(23B)	1450	9000	1943	30
H(14A)	5303	-5222	2011	33
H(14B)	6005	-5504	1899	33
H(21A)	-610	8395	2096	53
H(21B)	-602	9403	1716	53
H(21C)	-406	9811	2196	53
H(19A)	5560	-2282	2101	35
H(19B)	5331	-1981	1619	35
H(13A)	5933	-5237	2642	42
H(13B)	5648	-3865	2570	42
H(13C)	6352	-4140	2458	42
H(27A)	235	11317	2063	42
H(27B)	912	11658	1911	42
H(24A)	2162	9951	1483	51
H(24B)	1799	11023	1730	51
H(24C)	1610	10701	1241	51
H(18A)	6322	-2549	1414	38
H(18B)	6527	-2931	1893	38
H(26A)	-57	10760	1378	45
H(26B)	618	11068	1214	45
H(15A)	5691	-4983	1175	36
H(15B)	5014	-4625	1322	36
H(16A)	5180	-3776	646	56
H(16B)	5770	-3019	834	56
H(16C)	5091	-2662	982	56
H(30A)	3953	123	834	38
H(30B)	3218	289	815	38
H(33A)	4917	3858	628	73

H(33B)	4205	4279	601	73
H(33C)	4480	3444	227	73
H(31A)	3621	2424	36	47
H(31B)	3194	1251	138	47
H(34A)	4351	2598	1085	40
H(34B)	4629	1766	713	40
H(17A)	7215	-3789	1413	62
H(17B)	6659	-4516	1167	62
H(17C)	6864	-4900	1648	62
H(20A)	4472	-2200	2051	64
H(20B)	4689	-3586	2183	64
H(20C)	4460	-3293	1699	64
H(29A)	3572	-28	1529	60
H(29B)	3280	1348	1485	60
H(29C)	4016	1170	1504	60
H(28A)	928	11453	2662	62
H(28B)	1354	10385	2466	62
H(28C)	675	10046	2618	62
H(25A)	76	9824	712	71
H(25B)	-12	8759	1066	71
H(25C)	665	9066	902	71
H(35A)	3298	3159	1091	51
H(35B)	3234	3628	604	51
H(32A)	4002	616	-296	108
H(32B)	4078	-73	159	108
H(32C)	4506	1105	55	108
H(38A)	840	11144	4224	45
H(38B)	497	9953	4013	45
H(39A)	741	10281	4883	58
H(39B)	409	9070	4676	58
H(44A)	922	6625	3993	65
H(44B)	579	7904	3858	65
H(44C)	516	7352	4331	65
H(46A)	5899	2635	171	117
H(46B)	6622	2382	260	117
H(46C)	6369	2772	-210	117
H(41A)	2352	11431	4813	108
H(41B)	1680	11242	5002	108
H(41C)	1748	11865	4539	108

H(42A)	2070	9428	4754	76
H(42B)	2141	10045	4295	76
H(40A)	793	8604	5379	135
H(40B)	1479	8965	5248	135
H(40C)	1144	7757	5042	135
H(43A)	1570	7706	4477	91
H(43B)	1642	8228	4003	91
H(37A)	1003	11108	3473	115
H(37B)	1310	9746	3515	115
H(37C)	1655	10934	3726	115
H(47A)	8580	5758	4679	119
H(47B)	8612	5496	5185	119
H(47C)	8999	4637	4871	119

Table B.11 Torsion angles (°) for (Et$_4$N)$_4$[Nb$_4$O$_4$(ca)$_2$(μ^2-O)$_2$Cl$_8$]·2CH$_3$CN (6).

Torsion angles	Angle (°)	Torsion angles	Angle (°)
C(6)-C(1)-C(2)-O(8)	179.6(1)	C(9)-C(10)-C(11)-O(1)	-177.2(9)
Cl(1)-C(1)-C(2)-O(8)	2.4(2)	Cl(4)-C(10)-C(11)-O(1)	2.6(1)
C(6)-C(1)-C(2)-C(3)	-2.6(2)	C(9)-C(10)-C(11)-C(12)	0.4(1)
Cl(1)-C(1)-C(2)-C(3)	-179.8(7)	Cl(4)-C(10)-C(11)-C(12)	-179.8(7)
C(4)-C(5)-O(5)-Nb(03)	-174.1(8)	O(2)-C(12)-C(11)-O(1)	-1.6(1)
C(6)-C(5)-O(5)-Nb(03)	4.4(12)	C(7)-C(12)-C(11)-O(1)	177.2(9)
C(1)-C(2)-O(8)-Nb(04)	-177.8(8)	O(2)-C(12)-C(11)-C(10)	-179.4(9)
C(3)-C(2)-O(8)-Nb(04)	4.3(1)	C(7)-C(12)-C(11)-C(10)	-0.6(1)
Nb(03)-O(6)-C(6)-C(1)	176.9(8)	C(26)-N(3)-C(22)-C(21)	-57.8(1)
Nb(03)-O(6)-C(6)-C(5)	-3.4(1)	C(27)-N(3)-C(22)-C(21)	59.5(1)
C(2)-C(1)-C(6)-O(6)	-178.4(1)	C(23)-N(3)-C(22)-C(21)	-179.5(1)
Cl(1)-C(1)-C(6)-O(6)	-1.1(2)	C(26)-N(3)-C(23)-C(24)	61.4(1)
C(2)-C(1)-C(6)-C(5)	1.9(2)	C(27)-N(3)-C(23)-C(24)	-55.0(1)
Cl(1)-C(1)-C(6)-C(5)	179.2(7)	C(22)-N(3)-C(23)-C(24)	-176.7(1)
O(5)-C(5)-C(6)-O(6)	-0.2(13)	C(15)-N(1)-C(14)-C(13)	-174.6(1)
C(4)-C(5)-C(6)-O(6)	178.5(9)	C(18)-N(1)-C(14)-C(13)	66.0(1)
O(5)-C(5)-C(6)-C(1)	179.6(9)	C(19)-N(1)-C(14)-C(13)	-51.7(1)
C(4)-C(5)-C(6)-C(1)	-1.8(1)	C(15)-N(1)-C(19)-C(20)	63.9(1)
Nb(04)-O(7)-C(3)-C(4)	175.4(7)	C(18)-N(1)-C(19)-C(20)	-177.2(1)
Nb(04)-O(7)-C(3)-C(2)	-2.6(1)	C(14)-N(1)-C(19)-C(20)	-55.9(1)
O(8)-C(2)-C(3)-O(7)	-0.6(1)	C(26)-N(3)-C(27)-C(28)	179.2(1)
C(1)-C(2)-C(3)-O(7)	-178.7(9)	C(22)-N(3)-C(27)-C(28)	57.8(1)
O(8)-C(2)-C(3)-C(4)	-178.7(9)	C(23)-N(3)-C(27)-C(28)	-60.5(1)
C(1)-C(2)-C(3)-C(4)	3.2(14)	C(15)-N(1)-C(18)-C(17)	-58.2(1)
O(5)-C(5)-C(4)-C(3)	-179.0(9)	C(14)-N(1)-C(18)-C(17)	59.2(1)
C(6)-C(5)-C(4)-C(3)	2.5(1)	C(19)-N(1)-C(18)-C(17)	-178.4(1)
O(5)-C(5)-C(4)-Cl(2)	5.2(2)	C(27)-N(3)-C(26)-C(25)	-178.1(1)
C(6)-C(5)-C(4)-Cl(2)	-173.3(7)	C(22)-N(3)-C(26)-C(25)	-56.6(1)
O(7)-C(3)-C(4)-C(5)	178.8(9)	C(23)-N(3)-C(26)-C(25)	62.1(1)
C(2)-C(3)-C(4)-C(5)	-3.2(1)	C(18)-N(1)-C(15)-C(16)	-60.1(1)
O(7)-C(3)-C(4)-Cl(2)	-5.4(1)	C(14)-N(1)-C(15)-C(16)	179.6(1)
C(2)-C(3)-C(4)-Cl(2)	172.6(7)	C(19)-N(1)-C(15)-C(16)	56.0(1)
Nb(02)-O(3)-C(9)-C(10)	-178.4(7)	C(31)-N(2)-C(30)-C(29)	-175.4(1)
Nb(02)-O(3)-C(9)-C(8)	1.9(1)	C(34)-N(2)-C(30)-C(29)	65.2(1)
Nb(01)-O(2)-C(12)-C(7)	-173.1(7)	C(35)-N(2)-C(30)-C(29)	-53.2(2)
Nb(01)-O(2)-C(12)-C(11)	5.6(1)	C(30)-N(2)-C(31)-C(32)	-62.1(2)
C(8)-C(7)-C(12)-O(2)	-178.5(9)	C(34)-N(2)-C(31)-C(32)	55.5(2)

Cl(3)-C(7)-C(12)-O(2)	3.8(1)	C(35)-N(2)-C(31)-C(32)	174.8(1)
C(8)-C(7)-C(12)-C(11)	2.9(1)	C(31)-N(2)-C(34)-C(33)	58.2(2)
Cl(3)-C(7)-C(12)-C(11)	-174.9(7)	C(30)-N(2)-C(34)-C(33)	176.4(1)
O(3)-C(9)-C(10)-C(11)	178.0(9)	C(35)-N(2)-C(34)-C(33)	-62.6(2)
C(8)-C(9)-C(10)-C(11)	-2.3(1)	C(31)-N(2)-C(35)-C(36)	67.9(2)
O(3)-C(9)-C(10)-Cl(4)	-1.8(1)	C(30)-N(2)-C(35)-C(36)	-53.2(2)
C(8)-C(9)-C(10)-Cl(4)	177.9(6)	C(34)-N(2)-C(35)-C(36)	-171.4(1)
Nb(02)-O(4)-C(8)-C(7)	173.3(7)	C(43)-N(4)-C(38)-C(37)	-62.1(2)
Nb(02)-O(4)-C(8)-C(9)	-4.0(10)	C(42)-N(4)-C(38)-C(37)	62.3(2)
C(12)-C(7)-C(8)-O(4)	177.9(9)	C(39)-N(4)-C(38)-C(37)	-179.7(1)
Cl(3)-C(7)-C(8)-O(4)	-4.3(1)	C(43)-N(4)-C(39)-C(40)	59.0(2)
C(12)-C(7)-C(8)-C(9)	-4.9(1)	C(38)-N(4)-C(39)-C(40)	-178.9(1)
Cl(3)-C(7)-C(8)-C(9)	172.9(7)	C(42)-N(4)-C(39)-C(40)	-59.6(2)
O(3)-C(9)-C(8)-O(4)	1.8(12)	C(43)-N(4)-C(42)-C(41)	-176(2)
C(10)-C(9)-C(8)-O(4)	-177.9(9)	C(38)-N(4)-C(42)-C(41)	56(2)
O(3)-C(9)-C(8)-C(7)	-175.7(9)	C(39)-N(4)-C(42)-C(41)	-57(2)
C(10)-C(9)-C(8)-C(7)	4.6(1)	C(38)-N(4)-C(43)-C(44)	-56(2)
Nb(01)-O(1)-C(11)-C(10)	175.2(7)	C(42)-N(4)-C(43)-C(44)	178.1(2)
Nb(01)-O(1)-C(11)-C(12)	-2.5(1)	C(39)-N(4)-C(43)-C(44)	59(2)

Table B.12 General hydrogen-bond distances and angles for (Et₄N)₄[Nb₄O₄(ca)₂(μ^2-O)₂Cl₈]·2CH₃CN (6).

Interactions	D-H···A	D-H (Å)	H···A (Å)	D···A (Å)	D-H···A (°)
I	C13-H13B···Cl10[a]	0.98	2.81	3.721(12)	156
II	C14-H14B···O3[b]	0.99	2.60	3.535(14)	158
III	C18-H8A···O9	0.99	2.54	3.288(16)	132
IV	C19-H19B···Cl9	0.99	2.67	3.655(13)	173
V	C22-H22A···O10[c]	0.99	2.42	3.388(14)	167
VI	C34-H34A···Cl9	0.99	2.72	3.568(13)	144
VII	C35-H35B···O11[c]	0.99	2.35	3.060(16)	128
VIII	C41-H41C···Cl7[d]	0.98	2.75	3.715(19)	169
IX	C43-H43A···Cl8[c]	0.99	2.81	3.605(17)	137
X	C46-H46B···Cl8	0.98	2.71	3.650 (2)	161
XI	C46-H46C···Cl11[e]	0.98	2.60	3.574(16)	176
XII	C47-H47B···Cl7[f]	0.98	2.76	3.640(2)	150
XIII	C47-H47B···Cl8[f]	0.98	2.79	3.540(2)	134

Symmetry code: (a) -x + 1, y - ½, - z + ½ (b) x, y -1, z (c), 1- x, y + ½, ½ - z
(d), 1 - x, y + ½ + 1, ½- z (e), x, -y + ½, z - ½ (f), x, -y + ½, z + ½

C.1 Crystal data of tris(N-nitroso-N-phenylhydroxylaminato-k^2O,O')

oxidoniobium(V), [NbO(cupf)₃] (7)

Table C.1 Atomic coordinates (x 10⁴) and equivalent isotropic displacement parameters (Å²x 10³) for [NbO(cupf)₃] (7). U(eq) is defined as one third of the trace of the orthogonalized U^{ij} tensor.

	x	y	z	U(eq)
Nb(1)	7803(1)	1232(1)	9999(1)	16(1)
O(7)	8698(1)	2430(2)	10215(1)	25(1)
O(4)	6733(1)	-415(2)	10261(1)	22(1)
O(6)	6817(1)	2076(2)	9029(1)	19(1)
O(5)	6596(1)	2335(2)	10598(1)	29(1)
O(1)	8147(1)	608(2)	8733(1)	20(1)
O(3)	7909(1)	721(2)	11336(1)	20(1)
O(2)	8842(1)	-419(2)	10066(1)	22(1)
N(5)	6725(2)	-894(2)	11056(1)	22(1)
N(6)	7344(1)	-285(2)	11594(1)	17(1)
N(1)	9161(2)	-965(2)	9354(1)	21(1)
N(2)	8786(1)	-407(2)	8663(1)	17(1)
N(3)	6060(2)	2828(2)	9294(1)	20(1)
C(1)	9024(2)	-818(2)	7787(2)	18(1)
C(7)	7410(2)	-614(2)	12518(1)	19(1)
C(18)	4579(2)	4188(3)	8896(2)	31(1)
C(13)	5415(2)	3468(2)	8629(2)	21(1)
C(9)	8074(2)	-157(3)	13975(2)	26(1)
C(4)	9459(2)	-1577(3)	6095(2)	26(1)
N(4)	5923(2)	2975(2)	10116(1)	28(1)
C(14)	5662(2)	3362(2)	7750(2)	21(1)
C(10)	7509(2)	-1194(3)	14302(2)	27(1)
C(5)	9139(2)	-301(2)	6258(2)	26(1)
C(15)	5060(2)	4023(2)	7117(2)	27(1)
C(8)	8031(2)	134(2)	13076(2)	23(1)
C(11)	6899(2)	-1934(3)	13726(2)	31(1)
C(12)	6838(2)	-1653(3)	12827(2)	26(1)
C(3)	9558(2)	-2461(2)	6787(2)	26(1)
C(16)	4233(2)	4760(2)	7366(2)	32(1)
C(2)	9358(2)	-2093(2)	7645(2)	23(1)
C(17)	3997(2)	4841(3)	8248(2)	36(1)
C(6)	8904(2)	81(2)	7105(2)	22(1)

Table C.2 Bond lengths (Å) and angles (°) for [NbO(cupf)₃] (7).

Atoms	Distance (Å)	Atoms	Angle (°)
Nb(1)-O(7)	1.7107(2)	O(7)-Nb(1)-O(1)	102.81(8)
Nb(1)-O(1)	2.0805(2)	O(7)-Nb(1)-O(3)	88.49(7)
Nb(1)-O(3)	2.0850(2)	O(1)-Nb(1)-O(3)	143.67(6)
Nb(1)-O(6)	2.0974(2)	O(7)-Nb(1)-O(6)	103.85(7)
Nb(1)-O(2)	2.1593(2)	O(1)-Nb(1)-O(6)	68.36(6)
Nb(1)-O(5)	2.1621(2)	O(3)-Nb(1)-O(6)	142.65(6)
Nb(1)-O(4)	2.2266(2)	O(7)-Nb(1)-O(2)	96.89(8)
O(4)-N(5)	1.296(3)	O(1)-Nb(1)-O(2)	69.41(6)
O(6)-N(3)	1.325(2)	O(3)-Nb(1)-O(2)	75.06(6)
O(5)-N(4)	1.296(3)	O(6)-Nb(1)-O(2)	136.00(6)
O(1)-N(2)	1.334(2)	O(7)-Nb(1)-O(5)	93.20(8)
O(3)-N(6)	1.328(2)	O(1)-Nb(1)-O(5)	136.89(6)
O(2)-N(1)	1.294(3)	O(3)-Nb(1)-O(5)	75.29(7)
N(5)-N(6)	1.283(3)	O(6)-Nb(1)-O(5)	69.02(6)
N(6)-C(7)	1.436(3)	O(2)-Nb(1)-O(5)	148.34(6)
N(1)-N(2)	1.270(3)	O(7)-Nb(1)-O(4)	158.52(7)
N(2)-C(1)	1.433(3)	O(1)-Nb(1)-O(4)	95.37(6)
N(3)-N(4)	1.269(3)	O(3)-Nb(1)-O(4)	70.04(6)
N(3)-C(13)	1.442(3)	O(6)-Nb(1)-O(4)	93.37(6)
C(1)-C(6)	1.381(3)	O(2)-Nb(1)-O(4)	78.77(7)
C(1)-C(2)	1.387(3)	O(5)-Nb(1)-O(4)	80.91(7)
C(7)-C(8)	1.376(3)	N(5)-O(4)-Nb(1)	118.36(1)
C(7)-C(12)	1.385(3)	N(3)-O(6)-Nb(1)	118.06(1)
C(18)-C(17)	1.386(4)	N(4)-O(5)-Nb(1)	121.02(1)
C(18)-C(13)	1.388(3)	N(2)-O(1)-Nb(1)	117.86(1)
C(18)-H(18)	0.93	N(6)-O(3)-Nb(1)	117.35(1)
C(13)-C(14)	1.382(3)	N(1)-O(2)-Nb(1)	121.07(1)
C(9)-C(10)	1.389(3)	N(6)-N(5)-O(4)	112.22(2)
C(9)-C(8)	1.389(3)	N(5)-N(6)-O(3)	121.94(2)
C(9)-H(9)	0.93	N(5)-N(6)-C(7)	121.10(2)
C(4)-C(3)	1.381(4)	O(3)-N(6)-C(7)	116.85(2)
C(4)-C(5)	1.388(4)	N(2)-N(1)-O(2)	111.48(2)
C(4)-H(4)	0.93	N(1)-N(2)-O(1)	120.18(2)
C(14)-C(15)	1.388(3)	N(1)-N(2)-C(1)	122.61(2)
C(14)-H(14)	0.93	O(1)-N(2)-C(1)	117.21(2)
C(10)-C(11)	1.381(4)	N(4)-N(3)-O(6)	119.92(2)
C(10)-H(10)	0.93	N(4)-N(3)-C(13)	121.89(2)

C(5)-C(6)	1.383(3)	O(6)-N(3)-C(13)	118.18(2)
C(5)-H(5)	0.93	C(6)-C(1)-C(2)	122.0(2)
C(15)-C(16)	1.378(4)	C(6)-C(1)-N(2)	118.3(2)
C(15)-H(15)	0.93	C(2)-C(1)-N(2)	119.7(2)
C(8)-H(8)	0.93	C(8)-C(7)-C(12)	121.9(2)
C(11)-C(12)	1.387(3)	C(8)-C(7)-N(6)	118.6(2)
C(11)-H(11)	0.93	C(12)-C(7)-N(6)	119.5(2)
C(12)-H(12)	0.93	C(17)-C(18)-C(13)	117.7(3)
C(3)-C(2)	1.383(3)	C(17)-C(18)-H(18)	121.2
C(3)-H(3)	0.93	C(13)-C(18)-H(18)	121.2
C(16)-C(17)	1.381(4)	C(14)-C(13)-C(18)	122.4(2)
C(16)-H(16)	0.93	C(14)-C(13)-N(3)	118.9(2)
C(2)-H(2)	0.93	C(18)-C(13)-N(3)	118.7(2)
C(17)-H(17)	0.93	C(10)-C(9)-C(8)	120.5(2)
C(6)-H(6)	0.93	C(10)-C(9)-H(9)	119.8
		C(8)-C(9)-H(9)	119.8
		C(3)-C(4)-C(5)	119.6(2)
		C(3)-C(4)-H(4)	120.2
		C(5)-C(4)-H(4)	120.2
		N(3)-N(4)-O(5)	111.88(2)
		C(13)-C(14)-C(15)	118.5(2)
		C(13)-C(14)-H(14)	120.8
		C(15)-C(14)-H(14)	120.8
		C(11)-C(10)-C(9)	119.4(2)
		C(11)-C(10)-H(10)	120.3
		C(9)-C(10)-H(10)	120.3
		C(6)-C(5)-C(4)	120.4(2)
		C(6)-C(5)-H(5)	119.8
		C(4)-C(5)-H(5)	119.8
		C(16)-C(15)-C(14)	120.3(3)
		C(16)-C(15)-H(15)	119.8
		C(14)-C(15)-H(15)	119.8
		C(7)-C(8)-C(9)	118.8(2)
		C(7)-C(8)-H(8)	120.6
		C(9)-C(8)-H(8)	120.6
		C(10)-C(11)-C(12)	121.0(2)
		C(10)-C(11)-H(11)	119.5
		C(12)-C(11)-H(11)	119.5

C(7)-C(12)-C(11)	118.4(2)
C(7)-C(12)-H(12)	120.8
C(11)-C(12)-H(12)	120.8
C(4)-C(3)-C(2)	121.2(2)
C(4)-C(3)-H(3)	119.4
C(2)-C(3)-H(3)	119.4
C(15)-C(16)-C(17)	120.2(2)
C(15)-C(16)-H(16)	119.9
C(17)-C(16)-H(16)	119.9
C(3)-C(2)-C(1)	118.1(2)
C(3)-C(2)-H(2)	121
C(1)-C(2)-H(2)	121
C(16)-C(17)-C(18)	121.0(2)
C(16)-C(17)-H(17)	119.5
C(18)-C(17)-H(17)	119.5
C(1)-C(6)-C(5)	118.8(2)
C(1)-C(6)-H(6)	120.6
C(5)-C(6)-H(6)	120.6

Table C.3 Anisotropic displacement parameters (Å^2 x 10^3) for [NbO(cupf)$_3$] (7). The anisotropic displacement factor exponent takes the form: $-2\pi^2[\,h^2a^{*2}U^{11} + \ldots + 2\,h\,k\,a^*\,b^*\,U^{12}]$.

	U^{11}	U^{22}	U^{33}	U^{23}	U^{13}	U^{12}
Nb(1)	19(1)	16(1)	14(1)	0(1)	0(1)	1(1)
O(7)	28(1)	21(1)	25(1)	2(1)	-2(1)	-2(1)
O(4)	24(1)	26(1)	16(1)	0(1)	-2(1)	-4(1)
O(6)	20(1)	20(1)	18(1)	-2(1)	1(1)	9(1)
O(5)	34(1)	34(1)	19(1)	0(1)	3(1)	14(1)
O(1)	23(1)	19(1)	17(1)	1(1)	0(1)	10(1)
O(3)	24(1)	19(1)	18(1)	2(1)	-2(1)	-6(1)
O(2)	25(1)	23(1)	19(1)	2(1)	-1(1)	6(1)
N(5)	23(1)	25(1)	17(1)	-1(1)	0(1)	-5(1)
N(6)	18(1)	16(1)	18(1)	1(1)	1(1)	-1(1)
N(1)	23(1)	20(1)	20(1)	2(1)	-1(1)	4(1)
N(2)	16(1)	16(1)	20(1)	0(1)	0(1)	4(1)
N(3)	21(1)	19(1)	21(1)	-3(1)	2(1)	6(1)
C(1)	14(1)	19(1)	20(1)	-3(1)	-1(1)	0(1)
C(7)	19(1)	21(1)	16(1)	1(1)	2(1)	2(1)
C(18)	26(1)	31(1)	35(1)	-11(1)	-4(1)	11(1)
C(13)	18(1)	16(1)	29(1)	-1(1)	-4(1)	4(1)
C(9)	27(1)	31(1)	21(1)	-2(1)	-4(1)	-5(1)
C(4)	23(1)	33(1)	21(1)	-8(1)	2(1)	2(1)
N(4)	31(1)	31(1)	24(1)	-3(1)	4(1)	12(1)
C(14)	17(1)	19(1)	29(1)	3(1)	-1(1)	-1(1)
C(10)	27(1)	37(1)	16(1)	4(1)	1(1)	-4(1)
C(5)	32(1)	28(1)	18(1)	1(1)	-3(1)	2(1)
C(15)	23(1)	25(1)	32(1)	6(1)	-4(1)	-7(1)
C(8)	25(1)	23(1)	21(1)	2(1)	0(1)	-3(1)
C(11)	32(1)	37(2)	23(1)	9(1)	-1(1)	-10(1)
C(12)	29(1)	28(1)	20(1)	2(1)	-2(1)	-7(1)
C(3)	27(1)	22(1)	30(1)	-6(1)	4(1)	6(1)
C(16)	31(1)	21(1)	43(2)	2(1)	-17(1)	0(1)
C(2)	26(1)	18(1)	26(1)	1(1)	3(1)	5(1)
C(17)	26(1)	30(1)	51(2)	-14(1)	-12(1)	14(1)
C(6)	25(1)	18(1)	22(1)	-1(1)	-3(1)	3(1)

Table C.4 Hydrogen coordinates (x 10^4) and isotropic displacement parameters (Å^2x 10^3) for [NbO(cupf)$_3$] (7).

	x	y	z	U(eq)
H(18)	4415	4230	9488	37
H(9)	8484	346	14361	32
H(4)	9605	-1836	5523	31
H(14)	6218	2859	7587	26
H(10)	7542	-1389	14904	32
H(5)	9083	301	5795	31
H(15)	5214	3969	6523	32
H(8)	8414	822	12855	27
H(11)	6523	-2631	13943	37
H(12)	6423	-2150	12441	31
H(3)	9763	-3319	6675	31
H(16)	3834	5203	6940	39
H(2)	9445	-2682	8112	28
H(17)	3438	5341	8409	44
H(6)	8669	927	7214	26

Table C.5 General hydrogen-bond distances (Å) and angles (°) for [NbO(cupf)$_3$] (7).

Interactions	D-H···A	D-H (Å)	H···A (Å)	D···A (Å)	D-H···A(°)
I	C5-H5···O7ii[a]	0.93	2.51	3.357(4)	151
II	C8-H8···O3	0.93	2.37	2.695(3)	100
III	C14-H14···O6	0.93	2.42	2.738(3)	100
IV	C16-H16···O6i[b]	0.93	2.53	3.413(4)	159

Symmetry code: (a) x, -y + ½, z -½ (b) -x + 1, y + ½, -z +3/2

C.2 Crystal data of tris(2-hydroxypyridinato-N-oxide-κ^2O,O') oxido niobium(V), methanol solvate, [NbO(hopo)₃]·MeOH (8)

Table C.6 Atomic coordinates (x 10^4) and equivalent isotropic displacement parameters (Å^{2}x 10^3) for [NbO(hopo)₃].MeOH (8). U(eq) is defined as one third of the trace of the orthogonalized U^{ij} tensor.

	x	y	z	U(eq)
O(8A)	11079(1)	81(8)	5947(5)	23(1)
C(02A)	11571(1)	1209(1)	5606(6)	11(1)
O(8B)	9689(6)	1000(5)	5623(3)	31(1)
C(02B)	11223(9)	829(7)	5539(4)	26(1)
Nb(1)	5863(1)	2479(1)	3869(1)	13(1)
O(1)	8331(3)	2605(2)	4434(2)	19(1)
N(1)	5318(4)	2993(3)	5359(2)	21(1)
O(3)	5259(3)	3564(2)	4763(1)	16(1)
O(2)	6973(3)	4034(3)	3516(1)	17(1)
O(4)	5972(3)	1311(2)	4736(1)	16(1)
O(5)	4277(4)	3486(3)	3126(2)	23(1)
O(6)	3408(4)	1790(3)	3849(2)	31(1)
O(7)	6397(4)	1321(3)	3343(2)	20(1)
C(1)	5701(4)	1790(3)	5354(2)	11(1)
C(5)	5034(5)	3517(4)	5996(2)	18(1)
C(4)	5172(5)	2827(4)	6602(2)	22(1)
N(2)	2742(4)	3106(3)	2952(2)	21(1)
C(3)	5575(5)	1595(4)	6579(2)	23(1)
C(6)	2280(5)	2181(4)	3348(2)	16(1)
C(7)	676(5)	1763(4)	3214(2)	26(1)
C(2)	5838(5)	1090(4)	5954(2)	26(1)
C(10)	1704(5)	3635(4)	2411(2)	26(1)
C(9)	124(6)	3222(5)	2271(3)	32(1)
N(3)	9227(4)	3532(3)	4298(2)	21(1)
C(12)	9254(5)	5349(4)	3625(2)	21(1)
C(15)	10836(5)	3731(4)	4603(2)	21(1)
C(11)	8490(4)	4320(3)	3808(2)	11(1)
C(13)	10829(5)	5576(4)	3931(2)	24(1)
C(14)	11634(5)	4750(4)	4420(2)	23(1)
C(8)	-382(5)	2284(5)	2678(3)	32(1)

Table C.7 Bond lengths (Å) and angles (°) for [NbO(hopo)₃]·MeOH (8).

Atoms	Distance (Å)	Atoms	Angle (°)
O(8A)-C(02A)	1.488(1)	C(02A)-O(8A)-H(8A)	109.5
O(8A)-H(8A)	0.84	O(8A)-C(02A)-H(02A)	109.5
C(02A)-H(02A)	0.98	O(8A)-C(02A)-H(02B)	109.5
C(02A)-H(02B)	0.98	H(02A)-C(02A)-H(02B)	109.5
C(02A)-H(02C)	0.98	O(8A)-C(02A)-H(02C)	109.5
O(8B)-C(02B)	1.314(8)	H(02A)-C(02A)-H(02C)	109.5
O(8B)-H(8B)	0.84	H(02B)-C(02A)-H(02C)	109.5
C(02B)-H(02D)	0.98	C(02B)-O(8B)-H(8B)	109.5
C(02B)-H(02E)	0.98	O(8B)-C(02B)-H(02D)	109.5
C(02B)-H(02F)	0.98	O(8B)-C(02B)-H(02E)	109.5
Nb(1)-O(7)	1.722(3)	H(02D)-C(02B)-H(02E)	109.5
Nb(1)-O(4)	2.089(3)	O(8B)-C(02B)-H(02F)	109.5
Nb(1)-O(5)	2.103(3)	H(02D)-C(02B)-H(02F)	109.5
Nb(1)-O(2)	2.103(3)	H(02E)-C(02B)-H(02F)	109.5
Nb(1)-O(6)	2.161(3)	O(7)-Nb(1)-O(4)	91.05(1)
Nb(1)-O(1)	2.169(3)	O(7)-Nb(1)-O(5)	100.79(1)
Nb(1)-O(3)	2.200(3)	O(4)-Nb(1)-O(5)	144.19(1)
O(1)-N(3)	1.311(4)	O(7)-Nb(1)-O(2)	104.98(1)
N(1)-O(3)	1.295(4)	O(4)-Nb(1)-O(2)	141.92(1)
N(1)-C(1)	1.367(5)	O(5)-Nb(1)-O(2)	67.05(1)
N(1)-C(5)	1.396(5)	O(7)-Nb(1)-O(6)	92.75(1)
O(2)-C(11)	1.334(4)	O(4)-Nb(1)-O(6)	74.26(1)
O(4)-C(1)	1.339(4)	O(5)-Nb(1)-O(6)	71.54(1)
O(5)-N(2)	1.331(4)	O(2)-Nb(1)-O(6)	137.19(1)
O(6)-C(6)	1.308(5)	O(7)-Nb(1)-O(1)	92.04(1)
C(1)-C(2)	1.373(6)	O(4)-Nb(1)-O(1)	73.56(1)
C(5)-C(4)	1.376(6)	O(5)-Nb(1)-O(1)	138.57(1)
C(5)-H(5)	0.95	O(2)-Nb(1)-O(1)	71.60(1)
C(4)-C(3)	1.403(6)	O(6)-Nb(1)-O(1)	147.53(1)
C(4)-H(4)	0.95	O(7)-Nb(1)-O(3)	164.23(1)
N(2)-C(6)	1.358(5)	O(4)-Nb(1)-O(3)	73.19(1)
N(2)-C(10)	1.372(5)	O(5)-Nb(1)-O(3)	92.58(1)
C(3)-C(2)	1.363(6)	O(2)-Nb(1)-O(3)	87.85(1)
C(3)-H(3)	0.95	O(6)-Nb(1)-O(3)	83.53(1)
C(6)-C(7)	1.392(5)	O(1)-Nb(1)-O(3)	83.24(1)
C(7)-C(8)	1.372(7)	N(3)-O(1)-Nb(1)	118.0(2)

C(7)-H(7)	0.95	O(3)-N(1)-C(1)	116.4(3)
C(2)-H(2)	0.95	O(3)-N(1)-C(5)	125.0(3)
C(10)-C(9)	1.372(6)	C(1)-N(1)-C(5)	118.6(3)
C(10)-H(10)	0.95	N(1)-O(3)-Nb(1)	115.6(2)
C(9)-C(8)	1.394(8)	C(11)-O(2)-Nb(1)	119.1(2)
C(9)-H(9)	0.95	C(1)-O(4)-Nb(1)	117.4(2)
N(3)-C(11)	1.354(5)	N(2)-O(5)-Nb(1)	118.6(2)
N(3)-C(15)	1.389(5)	C(6)-O(6)-Nb(1)	117.6(3)
C(12)-C(11)	1.369(5)	O(4)-C(1)-N(1)	117.3(3)
C(12)-C(13)	1.370(6)	O(4)-C(1)-C(2)	120.5(3)
C(12)-H(12)	0.95	N(1)-C(1)-C(2)	122.1(4)
C(15)-C(14)	1.375(6)	C(4)-C(5)-N(1)	119.9(4)
C(15)-H(15)	0.95	C(4)-C(5)-H(5)	120
C(13)-C(14)	1.401(6)	N(1)-C(5)-H(5)	120
C(13)-H(13)	0.95	C(5)-C(4)-C(3)	120.1(4)
C(14)-H(14)	0.95	C(5)-C(4)-H(4)	119.9
C(8)-H(8)	0.95	C(3)-C(4)-H(4)	119.9
		O(5)-N(2)-C(6)	115.6(3)
		O(5)-N(2)-C(10)	121.5(4)
		C(6)-N(2)-C(10)	122.9(4)
		C(2)-C(3)-C(4)	119.5(4)
		C(2)-C(3)-H(3)	120.2
		C(4)-C(3)-H(3)	120.2
		O(6)-C(6)-N(2)	115.3(3)
		O(6)-C(6)-C(7)	125.7(4)
		N(2)-C(6)-C(7)	119.0(4)
		C(8)-C(7)-C(6)	118.9(4)
		C(8)-C(7)-H(7)	120.5
		C(6)-C(7)-H(7)	120.5
		C(3)-C(2)-C(1)	119.7(4)
		C(3)-C(2)-H(2)	120.1
		C(1)-C(2)-H(2)	120.1
		C(9)-C(10)-N(2)	118.5(5)
		C(9)-C(10)-H(10)	120.7
		N(2)-C(10)-H(10)	120.7
		C(10)-C(9)-C(8)	119.5(4)
		C(10)-C(9)-H(9)	120.2
		C(8)-C(9)-H(9)	120.2

O(1)-N(3)-C(11)	115.4(3)
O(1)-N(3)-C(15)	125.0(4)
C(11)-N(3)-C(15)	119.6(4)
C(11)-C(12)-C(13)	119.2(4)
C(11)-C(12)-H(12)	120.4
C(13)-C(12)-H(12)	120.4
C(14)-C(15)-N(3)	119.2(4)
C(14)-C(15)-H(15)	120.4
N(3)-C(15)-H(15)	120.4
O(2)-C(11)-N(3)	115.9(3)
O(2)-C(11)-C(12)	122.0(3)
N(3)-C(11)-C(12)	122.1(3)
C(12)-C(13)-C(14)	119.6(4)
C(12)-C(13)-H(13)	120.2
C(14)-C(13)-H(13)	120.2
C(15)-C(14)-C(13)	120.2(4)
C(15)-C(14)-H(14)	119.9
C(13)-C(14)-H(14)	119.9
C(7)-C(8)-C(9)	121.1(4)
C(7)-C(8)-H(8)	119.4
C(9)-C(8)-H(8)	119.4

Table C.8 Anisotropic displacement parameters (Å^2 x 10^3) for [NbO(hopo)$_3$]·MeOH (8). The anisotropic displacement factor exponent takes the form: -2π^2[h^{2}a*^{2}U^{11} + … + 2 h k a* b* U^{12}].

	U^{11}	U^{22}	U^{33}	U^{23}	U^{13}	U^{12}
O(8A)	18(1)	26(1)	23(1)	3(1)	0(1)	-2(1)
C(02A)	13(1)	8(1)	10(2)	-2(1)	1(1)	-6(1)
O(8B)	31(1)	33(2)	30(2)	3(1)	5(1)	-3(1)
C(02B)	27(2)	18(2)	32(2)	3(2)	0(2)	-8(1)
Nb(1)	15(1)	12(1)	11(1)	0(1)	2(1)	-2(1)
O(1)	19(1)	14(1)	22(1)	3(1)	-1(1)	-1(1)
N(1)	18(2)	21(2)	22(2)	-1(1)	2(1)	-2(1)
O(3)	23(1)	11(1)	14(1)	2(1)	2(1)	2(1)
O(2)	14(1)	19(1)	17(1)	3(1)	0(1)	-4(1)
O(4)	24(1)	12(1)	13(1)	-1(1)	4(1)	0(1)
O(5)	18(1)	26(1)	23(1)	3(1)	0(1)	-2(1)
O(6)	31(1)	33(2)	30(2)	3(1)	5(1)	-3(1)
O(7)	24(1)	19(1)	17(1)	-4(1)	5(1)	-1(1)
C(1)	13(1)	8(1)	10(2)	-2(1)	1(1)	-6(1)
C(5)	17(2)	18(2)	19(2)	-5(2)	3(1)	-2(1)
C(4)	22(2)	31(2)	14(2)	-2(2)	5(2)	-3(2)
N(2)	17(2)	26(2)	19(2)	-5(1)	1(1)	1(1)
C(3)	24(2)	28(2)	16(2)	8(2)	3(2)	-4(2)
C(6)	14(2)	19(2)	14(2)	-8(1)	4(1)	-2(1)
C(7)	20(2)	34(2)	28(2)	-14(2)	11(2)	-8(2)
C(2)	27(2)	18(2)	32(2)	3(2)	0(2)	-8(1)
C(10)	22(2)	32(2)	21(2)	-4(2)	-2(2)	8(2)
C(9)	20(2)	46(3)	27(2)	-14(2)	-2(2)	9(2)
N(3)	23(2)	20(2)	21(2)	-5(1)	5(1)	0(1)
C(12)	21(2)	22(2)	20(2)	1(2)	3(2)	-6(2)
C(15)	18(2)	20(2)	23(2)	-6(2)	-1(2)	3(2)
C(11)	10(2)	14(2)	11(2)	-2(1)	2(1)	-1(1)
C(13)	21(2)	28(2)	26(2)	-2(2)	7(2)	-9(2)
C(14)	14(2)	29(2)	25(2)	-8(2)	3(2)	-1(2)
C(8)	15(2)	50(3)	31(2)	-23(2)	5(2)	-4(2)

Table C.9 Hydrogen coordinates (x 10^4) and isotropic displacement parameters (Å^{2}x 10^3) for [NbO(hopo)₃]· MeOH (8).

	x	y	z	U(eq)
H(8A)	10351	-276	5669	34
H(02A)	12554	1544	5889	16
H(02B)	10682	1802	5577	16
H(02C)	11802	1022	5129	16
H(8B)	9090	508	5369	47
H(02D)	11895	742	6004	39
H(02E)	11608	1524	5290	39
H(02F)	11309	92	5261	39
H(5)	4747	4348	6011	21
H(4)	4993	3185	7037	27
H(3)	5664	1116	6997	27
H(7)	319	1127	3490	32
H(2)	6115	257	5934	31
H(10)	2072	4273	2140	31
H(9)	-620	3574	1901	38

Table C.10 Torsion angles (°) for [NbO(hopo)₃]·MeOH (8).

Torsion angles	Angle (°)	Torsion angles	Angle (°)
C(1)-N(1)-O(3)-Nb(1)	-1.7(4)	O(4)-C(1)-C(2)-C(3)	179.3(4)
C(5)-N(1)-O(3)-Nb(1)	177.8(3)	N(1)-C(1)-C(2)-C(3)	0.5(6)
Nb(1)-O(4)-C(1)-N(1)	2.3(4)	O(5)-N(2)-C(10)-C(9)	-178.2(4)
Nb(1)-O(4)-C(1)-C(2)	-176.6(3)	C(6)-N(2)-C(10)-C(9)	0.9(6)
O(3)-N(1)-C(1)-O(4)	-0.3(5)	N(2)-C(10)-C(9)-C(8)	0.0(6)
C(5)-N(1)-C(1)-O(4)	-179.8(3)	Nb(1)-O(1)-N(3)-C(11)	-0.1(4)
O(3)-N(1)-C(1)-C(2)	178.5(4)	Nb(1)-O(1)-N(3)-C(15)	-178.6(3)
C(5)-N(1)-C(1)-C(2)	-1.0(5)	O(1)-N(3)-C(15)-C(14)	-179.2(4)
O(3)-N(1)-C(5)-C(4)	-178.3(4)	C(11)-N(3)-C(15)-C(14)	2.3(6)
C(1)-N(1)-C(5)-C(4)	1.1(5)	Nb(1)-O(2)-C(11)-N(3)	2.9(4)
N(1)-C(5)-C(4)-C(3)	-0.8(6)	Nb(1)-O(2)-C(11)-C(12)	-177.0(3)
Nb(1)-O(5)-N(2)-C(6)	8.8(4)	O(1)-N(3)-C(11)-O(2)	-1.8(5)
Nb(1)-O(5)-N(2)-C(10)	-172.1(3)	C(15)-N(3)-C(11)-O(2)	176.8(3)
C(5)-C(4)-C(3)-C(2)	0.4(6)	O(1)-N(3)-C(11)-C(12)	178.2(3)
Nb(1)-O(6)-C(6)-N(2)	-8.5(5)	C(15)-N(3)-C(11)-C(12)	-3.2(6)
Nb(1)-O(6)-C(6)-C(7)	174.0(3)	C(13)-C(12)-C(11)-O(2)	-178.3(4)
O(5)-N(2)-C(6)-O(6)	0.0(5)	C(13)-C(12)-C(11)-N(3)	1.7(6)
C(10)-N(2)-C(6)-O(6)	-179.0(4)	C(11)-C(12)-C(13)-C(14)	0.7(6)
O(5)-N(2)-C(6)-C(7)	177.7(3)	N(3)-C(15)-C(14)-C(13)	-0.1(6)
C(10)-N(2)-C(6)-C(7)	-1.4(6)	C(12)-C(13)-C(14)-C(15)	-1.4(6)
O(6)-C(6)-C(7)-C(8)	178.5(4)	C(6)-C(7)-C(8)-C(9)	-0.4(7)
N(2)-C(6)-C(7)-C(8)	1.1(6)	C(10)-C(9)-C(8)-C(7)	-0.2(7)
C(4)-C(3)-C(2)-C(1)	-0.2(6)		

Table C.11 General hydrogen-bond distances (Å) and angles (°) for [NbO(hopo)₃]·MeOH (8).

Interactions	D-H⋯A	D-H(Å)	H⋯A(Å)	D⋯A(Å)	D-H⋯A(°)
I	C2v-H2v⋯O6iv[a]	0.95	2.32	3.252(6)	166
II	C5-H5⋯O2ii[b]	0.95	2.53	3.374(5)	148
III	C02B-H02F⋯O8B[c]	0.98	2.14	3.013(9)	148
IV	C8-H8⋯O7i[d]	0.95	2.55	3.287(5)	135
V	C9-H9⋯O8B[e]	0.95	2.53	3.229(8)	130
VI	C14-H14⋯O3iii[f]	0.95	2.53	3.247(5)	132
VII	C14-H14⋯O3iii[g]	0.95	2.54	3.365(5)	146

Symmetry code: (a) -x + 1, -y, -z + 1, (b) -x + 1, -y + 1, -z + 1, (c) -x + 2, -y, -z + 1, (d) x -1, y, z, (e) x-1, -y + ½, -z + ½, (f) x + 1, y, z,(g) -x + 2, -y + 1, -z + 1.

C.3 Crystal data of tris(2-hydroxypyridinato-N-oxide-κ^2O,O') oxido tantalum(V), methanol solvate, [TaO(hopo)$_3$]·MeOH (9)

Table C.12 Atomic coordinates (x 10^4) and equivalent isotropic displacement parameters (Å^{2}x 10^3) for [TaO(hopo)$_3$].MeOH (9). U(eq) is defined as one third of the trace of the orthogonalized U^{ij} tensor.

	x	y	z	U(eq)
N(1)	448(3)	-577(1)	10808(1)	19(2)
C(1)	206(5)	-1054(1)	12111(2)	25(2)
C(2)	280(6)	-309(1)	13290(1)	32(6)
C(3)	596(6)	913(1)	13166(2)	29(4)
C(4)	839(5)	1391(1)	11864(2)	29(4)
C(5)	765(3)	646(1)	10684(1)	26(2)
N(2)	3430(3)	-1854(1)	7659(3)	19(2)
C(6)	4206(4)	-2892(1)	7284(4)	21(3)
C(7)	5811(4)	-3116(1)	7855(5)	25(2)
C(8)	6640(3)	-2302(1)	8802(5)	26(2)
C(9)	5864(2)	-1264(1)	9177(4)	22(3)
C(10)	4259(2)	-1040(1)	8605(3)	14(3)
N(3)	-2698(1)	294(1)	6737(3)	24(4)
C(11)	-4294(1)	756(1)	6433(4)	34(4)
C(12)	-5394(2)	251(1)	5327(5)	43(7)
C(13)	-4897(3)	-717(1)	4524(4)	42(5)
C(14)	-3301(3)	-1179(1)	4827(4)	27(3)
C(15)	-2201(2)	-674(1)	5934(3)	18(3)
O(1)	933(2)	-1190(1)	9479(2)	33(3)
O(2)	367(3)	1056(1)	9556(2)	33(3)
O(3)	3320(1)	69(1)	8870(2)	23(2)
O(4)	1939(2)	-1573(1)	7068(2)	23(2)
O(7)	1421(2)	1134(1)	6691(2)	25(3)
O(6)	-713(2)	-1020(1)	6320(2)	23(2)
O(5)	-1546(1)	686(1)	7762(2)	25(2)
Ta(1)	875(1)	0(1)	7771(1)	12(1)
O(01A)	6408(1)	-1587(2)	11223(2)	40(5)
O(01B)	6030(3)	-2280(2)	11890(4)	40(5)
C(01)	4700(2)	-1510(2)	11330(3)	81(1)

Table C.13 Bond lengths (Å) and angles (°) for [TaO(hopo)₃]·MeOH (9).

Atoms	Distance (Å)	Atoms	Angle (°)
N(1)-C(5)	1.39	C(5)-N(1)-C(1)	120
N(1)-C(1)	1.3901	C(5)-N(1)-O(1)	106.8
N(1)-O(1)	1.5385	C(1)-N(1)-O(1)	130.7
C(1)-C(2)	1.3897	C(2)-C(1)-N(1)	120
C(1)-H(1)	0.93	C(2)-C(1)-H(1)	120
C(2)-C(3)	1.39	N(1)-C(1)-H(1)	120
C(2)-H(2)	0.93	C(1)-C(2)-C(3)	120
C(3)-C(4)	1.3895	C(1)-C(2)-H(2)	120
C(3)-H(3)	0.93	C(3)-C(2)-H(2)	120
C(4)-C(5)	1.3901	C(4)-C(3)-C(2)	120
C(4)-H(4)	0.93	C(4)-C(3)-H(3)	120
C(5)-O(2)	1.1727	C(2)-C(3)-H(3)	120
N(2)-O(4)	1.3238	C(3)-C(4)-C(5)	120
N(2)-C(6)	1.39	C(3)-C(4)-H(4)	120
N(2)-C(10)	1.3902	C(5)-C(4)-H(4)	120
C(6)-C(7)	1.3899	O(2)-C(5)-N(1)	115.1
C(6)-H(6)	0.93	O(2)-C(5)-C(4)	119.1
C(7)-C(8)	1.3902	N(1)-C(5)-C(4)	120
C(7)-H(7)	0.93	O(4)-N(2)-C(6)	121.6
C(8)-C(9)	1.3902	O(4)-N(2)-C(10)	118.3
C(8)-H(8)	0.93	C(6)-N(2)-C(10)	120
C(9)-C(10)	1.3899	C(7)-C(6)-N(2)	120
C(9)-H(9)	0.93	C(7)-C(6)-H(6)	120
C(10)-O(3)	1.4962	N(2)-C(6)-H(6)	120
N(3)-O(5)	1.3423	C(6)-C(7)-C(8)	120
N(3)-C(11)	1.4125	C(6)-C(7)-H(7)	120
N(3)-C(15)	1.4126	C(8)-C(7)-H(7)	120
C(11)-C(12)	1.4127	C(7)-C(8)-C(9)	120
C(11)-H(11)	0.93	C(7)-C(8)-H(8)	120
C(12)-C(13)	1.4125	C(9)-C(8)-H(8)	120
C(12)-H(12)	0.93	C(10)-C(9)-C(8)	120
C(13)-C(14)	1.4126	C(10)-C(9)-H(9)	120
C(13)-H(13)	0.93	C(8)-C(9)-H(9)	120
C(14)-C(15)	1.4127	C(9)-C(10)-N(2)	120
C(14)-H(14)	0.93	C(9)-C(10)-O(3)	125
C(15)-O(6)	1.2963	N(2)-C(10)-O(3)	114.9

O(1)-Ta(1)	2.0924	O(5)-N(3)-C(11)	125.8
O(2)-Ta(1)	2.1548	O(5)-N(3)-C(15)	114.2
O(3)-Ta(1)	2.153	C(11)-N(3)-C(15)	120
O(4)-Ta(1)	2.1073	N(3)-C(11)-C(12)	120
O(7)-Ta(1)	1.7248	N(3)-C(11)-H(11)	120
O(6)-Ta(1)	2.1048	C(12)-C(11)-H(11)	120
O(5)-Ta(1)	2.1457	C(13)-C(12)-C(11)	120
O(01A)-C(01)	1.44(2)	C(13)-C(12)-H(12)	120
O(01A)-H(01A)	0.82	C(11)-C(12)-H(12)	120
O(01B)-C(01)	1.44(2)	C(12)-C(13)-C(14)	120
O(01B)-H(01B)	0.82	C(12)-C(13)-H(13)	120
C(01)-H(01A)	0.96	C(14)-C(13)-H(13)	120
C(01)-H(01B)	0.96	C(13)-C(14)-C(15)	120
C(01)-H(01C)	0.96	C(13)-C(14)-H(14)	120
		C(15)-C(14)-H(14)	120
		O(6)-C(15)-N(3)	114.1
		O(6)-C(15)-C(14)	125.9
		N(3)-C(15)-C(14)	120
		N(1)-O(1)-Ta(1)	112.4
		C(5)-O(2)-Ta(1)	116.9
		C(10)-O(3)-Ta(1)	111.5
		N(2)-O(4)-Ta(1)	117.8
		C(15)-O(6)-Ta(1)	120.9
		N(3)-O(5)-Ta(1)	117.4
		O(7)-Ta(1)-O(1)	160.9
		O(7)-Ta(1)-O(6)	101.1
		O(1)-Ta(1)-O(6)	96.8
		O(7)-Ta(1)-O(4)	105
		O(1)-Ta(1)-O(4)	76
		O(6)-Ta(1)-O(4)	66.2
		O(7)-Ta(1)-O(5)	93.5
		O(1)-Ta(1)-O(5)	98.6
		O(6)-Ta(1)-O(5)	71.8
		O(4)-Ta(1)-O(5)	136.5
		O(7)-Ta(1)-O(3)	87.6
		O(1)-Ta(1)-O(3)	74
		O(6)-Ta(1)-O(3)	143.3
		O(4)-Ta(1)-O(3)	77.1

O(5)-Ta(1)-O(3)	143.9
O(7)-Ta(1)-O(2)	99.8
O(1)-Ta(1)-O(2)	73.4
O(6)-Ta(1)-O(2)	129.7
O(4)-Ta(1)-O(2)	146.9
O(5)-Ta(1)-O(2)	61.7
O(3)-Ta(1)-O(2)	82.5
C(01)-O(01A)-H(01A)	109.5
C(01)-O(01B)-H(01B)	109.5
O(01A)-C(01)-H(01A)	109.5
O(01A)-C(01)-H(01B)	109.5
H(01A)-C(01)-H(01B)	109.5
O(01A)-C(01)-H(01C)	109.5
H(01A)-C(01)-H(01C)	109.5
H(01B)-C(01)-H(01C)	109.5

Table C.14 Anisotropic displacement parameters ($Å^2$ x 10^3) for [TaO(hopo)$_3$]·MeOH (9). The anisotropic displacement factor exponent takes the form: $-2\pi^2[h^2a^{*2}U^{11} + \ldots + 2\,h\,k\,a^*\,b^*\,U^{12}]$.

	U^{11}	U^{22}	U^{33}	U^{23}	U^{13}	U^{12}
N(1)	20(5)	23(4)	16(4)	0(3)	3(3)	-10(4)
C(1)	34(7)	27(6)	16(5)	-8(4)	13(5)	-6(5)
C(2)	22(8)	70(2)	8(6)	-2(6)	10(5)	-5(7)
C(3)	21(9)	48(1)	19(8)	4(7)	4(6)	10(8)
C(4)	42(1)	30(9)	19(8)	8(6)	16(7)	11(7)
C(5)	26(6)	24(6)	27(6)	5(5)	0(5)	13(5)
N(2)	20(5)	23(4)	16(4)	0(3)	3(3)	-10(4)
C(6)	21(8)	20(7)	21(7)	7(6)	2(6)	-1(6)
C(7)	34(7)	27(6)	16(5)	-8(4)	13(5)	-6(5)
C(8)	26(6)	24(6)	27(6)	5(5)	0(5)	13(5)
C(9)	21(8)	14(6)	31(8)	-2(6)	1(6)	-2(5)
C(10)	12(7)	11(6)	21(7)	2(5)	3(5)	4(5)
N(3)	3(5)	43(1)	26(6)	5(5)	3(4)	-3(4)
C(11)	25(1)	39(9)	42(1)	17(8)	22(8)	10(7)
C(12)	21(8)	80(2)	28(8)	-13(9)	-5(6)	-1(8)
C(13)	32(1)	51(1)	44(1)	22(9)	10(9)	2(9)
C(14)	19(8)	31(8)	31(9)	10(7)	3(6)	-3(6)
C(15)	10(7)	26(8)	18(7)	11(6)	1(5)	-8(5)
O(1)	81(8)	5(3)	12(3)	3(4)	0(4)	3(4)
O(2)	81(8)	5(3)	12(3)	3(4)	0(4)	3(4)
O(3)	15(3)	29(4)	24(3)	-12(4)	1(3)	3(4)
O(4)	15(3)	29(4)	24(3)	-12(4)	1(3)	3(4)
O(7)	29(7)	23(6)	25(6)	5(4)	5(5)	17(5)
O(6)	17(6)	21(5)	29(6)	-10(4)	-12(4)	-2(4)
O(5)	13(6)	26(6)	33(6)	2(5)	-1(5)	4(4)
Ta(1)	13(1)	10(1)	14(1)	0(1)	1(1)	0(1)
O(01A)	31(1)	47(1)	42(1)	14(8)	3(8)	-11(8)
O(01B)	31(1)	47(1)	42(1)	14(8)	3(8)	-11(8)
C(01)	57(2)	100(2)	71(2)	-62(2)	-36(1)	47(2)

Table C.15 Hydrogen coordinates (x 10^4) and isotropic displacement parameters (Å^{2}x 10^3) for [TaO(hopo)₃]·MeOH (9).

	x	y	z	U(eq)
H(1)	-6	-1872	12194	30
H(2)	117	-629	14161	38
H(3)	646	1412	13955	35
H(4)	1051	2209	11781	35
H(6)	3652	-3436	6651	25
H(7)	6331	-3811	7605	30
H(8)	7714	-2452	9184	31
H(9)	6418	-720	9810	26
H(11)	-4621	1393	6962	41
H(12)	-6445	555	5127	51
H(13)	-5621	-1050	3795	50
H(14)	-2974	-1817	4299	33
H(01A)	6735	-928	10990	60
H(01B)	5749	-2984	11797	60
H(01A)	4534	-1620	12301	122

Table C.16 Torsion angles (°) **for [TaO(hopo)₃]·MeOH (9).**

Torsion angles	Angle (°)	Torsion angles	Angle (°)
O(1)-N(1)-C(1)-C(2)	159.5	C(13)-C(14)-C(15)-O(6)	179.6
C(1)-N(1)-C(5)-O(2)	-152.9	C(5)-N(1)-O(1)-Ta(1)	-24.3
O(1)-N(1)-C(5)-O(2)	43.1	C(1)-N(1)-O(1)-Ta(1)	174.2
O(1)-N(1)-C(5)-C(4)	-163.9	N(1)-C(5)-O(2)-Ta(1)	-42.4
C(3)-C(4)-C(5)-O(2)	151.8	C(4)-C(5)-O(2)-Ta(1)	164.4
O(4)-N(2)-C(6)-C(7)	175.6	C(9)-C(10)-O(3)-Ta(1)	-179.5
C(8)-C(9)-C(10)-O(3)	-176.9	N(2)-C(10)-O(3)-Ta(1)	3.5
O(4)-N(2)-C(10)-C(9)	-175.8	C(6)-N(2)-O(4)-Ta(1)	178.3
O(4)-N(2)-C(10)-O(3)	1.4	C(10)-N(2)-O(4)-Ta(1)	-6.0
C(6)-N(2)-C(10)-O(3)	177.2	N(3)-C(15)-O(6)-Ta(1)	-10.1
O(5)-N(3)-C(11)-C(12)	-179.5	C(14)-C(15)-O(6)-Ta(1)	170.3
O(5)-N(3)-C(15)-O(6)	-0.1	C(11)-N(3)-O(5)-Ta(1)	-170.7
C(11)-N(3)-C(15)-O(6)	-179.7	C(15)-N(3)-O(5)-Ta(1)	9.8
O(5)-N(3)-C(15)-C(14)	179.5		

Table C.17 General hydrogen-bond distances and angles of [TaO(hopo)₃]·MeOH (9).

Interactions	D-H⋯A	D-H (Å)	H⋯A (Å)	D⋯A (Å)	D-H⋯A (°)
I	C2iii-H2iii⋯O6ii[a]	0.93	2.30	3.209(5)	166
II	C01ii-H01ii⋯O3iii[b]	0.96	2.27	3.020(3)	135
III	C8ii-H8ii⋯O2i[c]	0.93	2.49	3.297(1)	145
IV	C12iv-H12iv⋯O7iii[d]	0.93	2.55	3.251(6)	133

Symmetry code: (a) x, y, z + 1, (b) x, y, 1 + z, (c) -x + 1, y - ½, -z + 2, (d) x - 1, y, z

C.4 Crystal data of chloridetetrakis(2-hydroxypyridinato-N-oxide-κ^2O,O') tantalum(V), diacetonitrile and dihydrate solvate, [Ta(hopo)$_4$]Cl· 2MeCN·2H$_2$O (10)

Table C.18 Atomic coordinates (x 10^4) and equivalent isotropic displacement parameters ($\mathring{A}^2$x 10^3) for [Ta(hopo)$_4$]Cl·2MeCN·2H$_2$O (10). U(eq) is defined as one third of the trace of the orthogonalized U^{ij} tensor.

	x	y	z	U(eq)
C(21A)	670(4)	7444(2)	2956(2)	34(1)
C(21B)	159(1)	8411(9)	2775(8)	49(2)
C(23A)	4250(5)	3890(3)	3570(3)	38(1)
C(23B)	5108(1)	3824(7)	4166(7)	52(2)
Ta(1)	1850(1)	2246(1)	734(1)	21(1)
O(8)	3943(5)	2762(4)	173(4)	31(1)
O(1)	-186(5)	2634(3)	1776(3)	27(1)
O(3)	3107(4)	742(3)	459(3)	24(1)
O(5)	2502(4)	2060(3)	-876(3)	25(1)
O(6)	949(5)	3605(3)	-57(3)	29(1)
O(2)	468(4)	1110(4)	699(3)	30(1)
O(7)	1931(5)	3550(3)	1556(3)	31(1)
O(4)	2233(5)	1534(4)	2154(3)	32(1)
N(3)	1375(5)	3737(4)	-1122(4)	25(1)
N(1)	-942(5)	1249(4)	1233(4)	27(1)
N(2)	2823(6)	503(4)	2217(4)	31(1)
N(4)	4321(6)	3449(4)	702(5)	35(1)
C(6)	3284(5)	72(4)	1294(4)	20(1)
C(11)	2233(6)	2887(5)	-1553(4)	22(1)
C(5)	-1274(1)	2085(8)	1824(7)	57(2)
C(7)	3896(6)	-998(5)	1257(5)	27(1)
C(10)	2981(7)	-78(6)	3143(5)	33(1)
C(16)	3218(7)	3882(5)	1448(5)	29(1)
C(15)	933(8)	4658(5)	-1684(5)	34(1)
C(1)	-1919(7)	576(6)	1180(5)	34(1)
C(4)	-2688(1)	2275(7)	2435(6)	52(2)
C(20)	5728(8)	3717(6)	473(7)	44(2)
C(8)	4034(7)	-1599(5)	2183(6)	37(1)
C(2)	-3316(8)	756(8)	1773(7)	49(2)

C(12)	2727(7)	2953(6)	-2649(5)	31(1)
C(9)	3605(7)	-1143(6)	3124(6)	40(2)
C(13)	2307(8)	3901(6)	-3230(5)	41(2)
C(3)	-3708(7)	1599(6)	2407(5)	38(1)
C(14)	1410(9)	4742(6)	-2765(6)	40(2)
C(19)	6025(1)	4455(6)	1012(8)	51(2)
C(17)	3494(1)	4635(6)	2025(6)	47(2)
C(18)	4913(1)	4898(7)	1799(8)	62(3)
Cl(01)	6854(1)	3918(4)	5795(4)	207(4)
C(22)	779(1)	7828(1)	1878(9)	66(3)
N(5)	1252(1)	7476(1)	1078(9)	80(3)
O(9)	9180(7)	626(8)	4134(5)	90(3)
O(10)	3651(1)	530(9)	5593(6)	83(2)
N(6)	3037(1)	2510(8)	4386(8)	76(3)
C(24)	3849(1)	2945(8)	4283(8)	57(2)

Table C.19 Bond lengths (Å) and angles (°) for [Ta(hopo)₄]Cl·2MeCN·2H₂O (10).

Atoms	Distance (Å)	Atoms	Angle (°)
C(21A)-C(22)	1.419(2)	C(22)-C(21A)-H(21A)	109.5
C(21A)-H(21A)	0.98	C(22)-C(21A)-H(21B)	109.5
C(21A)-H(21B)	0.98	H(21A)-C(21A)-H(21B)	109.5
C(21A)-H(21C)	0.98	C(22)-C(21A)-H(21C)	109.5
C(21B)-C(22)	1.430(1)	H(21A)-C(21A)-H(21C)	109.5
C(21B)-H(21D)	0.98	H(21B)-C(21A)-H(21C)	109.5
C(21B)-H(21E)	0.98	C(22)-C(21B)-H(21D)	109.5
C(21B)-H(21F)	0.98	C(22)-C(21B)-H(21E)	109.5
C(23A)-C(24)	1.40(2)	H(21D)-C(21B)-H(21E)	109.5
C(23A)-H(23A)	0.98	C(22)-C(21B)-H(21F)	109.5
C(23A)-H(23B)	0.98	H(21D)-C(21B)-H(21F)	109.5
C(23A)-H(23C)	0.98	H(21E)-C(21B)-H(21F)	109.5
C(23B)-C(24)	1.689(1)	C(24)-C(23A)-H(23A)	109.5
C(23B)-H(23D)	0.98	C(24)-C(23A)-H(23B)	109.5
C(23B)-H(23E)	0.98	H(23A)-C(23A)-H(23B)	109.5
C(23B)-H(23F)	0.98	C(24)-C(23A)-H(23C)	109.5
Ta(1)-O(2)	2.069(4)	H(23A)-C(23A)-H(23C)	109.5
Ta(1)-O(6)	2.074(4)	H(23B)-C(23A)-H(23C)	109.5
Ta(1)-O(4)	2.076(4)	C(24)-C(23B)-H(23D)	109.5
Ta(1)-O(8)	2.087(4)	C(24)-C(23B)-H(23E)	109.5
Ta(1)-O(5)	2.093(4)	H(23D)-C(23B)-H(23E)	109.5
Ta(1)-O(1)	2.099(4)	C(24)-C(23B)-H(23F)	109.5
Ta(1)-O(7)	2.103(4)	H(23D)-C(23B)-H(23F)	109.5
Ta(1)-O(3)	2.104(4)	H(23E)-C(23B)-H(23F)	109.5
O(8)-N(4)	1.329(7)	O(2)-Ta(1)-O(6)	98.21(2)
O(1)-C(5)	1.303(1)	O(2)-Ta(1)-O(4)	95.76(2)
O(3)-C(6)	1.321(6)	O(6)-Ta(1)-O(4)	146.20(2)
O(5)-C(11)	1.307(7)	O(2)-Ta(1)-O(8)	146.67(2)
O(6)-N(3)	1.348(6)	O(6)-Ta(1)-O(8)	93.83(2)
O(2)-N(1)	1.345(6)	O(4)-Ta(1)-O(8)	91.08(2)
O(7)-C(16)	1.322(8)	O(2)-Ta(1)-O(5)	79.27(2)
O(4)-N(2)	1.326(7)	O(6)-Ta(1)-O(5)	72.25(2)
N(3)-C(11)	1.342(7)	O(4)-Ta(1)-O(5)	140.90(2)
N(3)-C(15)	1.355(8)	O(8)-Ta(1)-O(5)	75.03(2)
N(1)-C(5)	1.344(1)	O(2)-Ta(1)-O(1)	71.97(2)
N(1)-C(1)	1.358(8)	O(6)-Ta(1)-O(1)	75.04(2)

N(2)-C(6)	1.347(8)	O(4)-Ta(1)-O(1)	80.36(2)
N(2)-C(10)	1.367(8)	O(8)-Ta(1)-O(1)	141.36(2)
N(4)-C(16)	1.345(9)	O(5)-Ta(1)-O(1)	132.20(2)
N(4)-C(20)	1.377(9)	O(2)-Ta(1)-O(7)	140.83(2)
C(6)-C(7)	1.377(7)	O(6)-Ta(1)-O(7)	76.43(2)
C(11)-C(12)	1.391(8)	O(4)-Ta(1)-O(7)	73.33(2)
C(5)-C(4)	1.384(1)	O(8)-Ta(1)-O(7)	72.28(2)
C(7)-C(8)	1.371(9)	O(5)-Ta(1)-O(7)	132.41(2)
C(7)-H(7)	0.95	O(1)-Ta(1)-O(7)	69.16(2)
C(10)-C(9)	1.374(1)	O(2)-Ta(1)-O(3)	72.61(2)
C(10)-H(10)	0.95	O(6)-Ta(1)-O(3)	141.01(2)
C(16)-C(17)	1.390(8)	O(4)-Ta(1)-O(3)	72.67(2)
C(15)-C(14)	1.370(1)	O(8)-Ta(1)-O(3)	78.48(2)
C(15)-H(15)	0.95	O(5)-Ta(1)-O(3)	68.82(2)
C(1)-C(2)	1.362(1)	O(1)-Ta(1)-O(3)	132.41(2)
C(1)-H(1)	0.95	O(7)-Ta(1)-O(3)	134.10(2)
C(4)-C(3)	1.381(1)	N(4)-O(8)-Ta(1)	118.2(4)
C(4)-H(4)	0.95	C(5)-O(1)-Ta(1)	119.2(5)
C(20)-C(19)	1.349(1)	C(6)-O(3)-Ta(1)	117.2(3)
C(20)-H(20)	0.95	C(11)-O(5)-Ta(1)	118.8(3)
C(8)-C(9)	1.384(1)	N(3)-O(6)-Ta(1)	118.2(3)
C(8)-H(8)	0.95	N(1)-O(2)-Ta(1)	119.0(3)
C(2)-C(3)	1.387(1)	C(16)-O(7)-Ta(1)	117.6(4)
C(2)-H(2)	0.95	N(2)-O(4)-Ta(1)	118.2(4)
C(12)-C(13)	1.383(1)	C(11)-N(3)-O(6)	114.5(5)
C(12)-H(12)	0.95	C(11)-N(3)-C(15)	124.4(5)
C(9)-H(9)	0.95	O(6)-N(3)-C(15)	121.1(5)
C(13)-C(14)	1.367(1)	C(5)-N(1)-O(2)	114.3(6)
C(13)-H(13)	0.95	C(5)-N(1)-C(1)	124.1(6)
C(3)-H(3)	0.95	O(2)-N(1)-C(1)	121.6(5)
C(14)-H(14)	0.95	O(4)-N(2)-C(6)	115.1(5)
C(19)-C(18)	1.388(2)	O(4)-N(2)-C(10)	122.8(6)
C(19)-H(19)	0.95	C(6)-N(2)-C(10)	122.1(5)
C(17)-C(18)	1.386(1)	O(8)-N(4)-C(16)	114.7(5)
C(17)-H(17)	0.95	O(8)-N(4)-C(20)	121.9(7)
C(18)-H(18)	0.95	C(16)-N(4)-C(20)	123.3(6)
C(22)-N(5)	1.159(1)	O(3)-C(6)-N(2)	115.4(5)
O(9)-H(9B)	0.85(2)	O(3)-C(6)-C(7)	123.9(5)

O(9)-H(9A)	0.89(2)	N(2)-C(6)-C(7)	120.7(5)
O(10)-H(10A)	0.89(2)	O(5)-C(11)-N(3)	115.1(5)
O(10)-H(10B)	0.84(2)	O(5)-C(11)-C(12)	126.4(5)
N(6)-C(24)	0.972(1)	N(3)-C(11)-C(12)	118.5(5)
		O(1)-C(5)-N(1)	115.1(7)
		O(1)-C(5)-C(4)	126.0(8)
		N(1)-C(5)-C(4)	118.9(9)
		C(8)-C(7)-C(6)	117.9(6)
		C(8)-C(7)-H(7)	121.1
		C(6)-C(7)-H(7)	121.1
		N(2)-C(10)-C(9)	118.3(6)
		N(2)-C(10)-H(10)	120.9
		C(9)-C(10)-H(10)	120.9
		O(7)-C(16)-N(4)	115.5(5)
		O(7)-C(16)-C(17)	125.3(7)
		N(4)-C(16)-C(17)	119.2(7)
		N(3)-C(15)-C(14)	118.1(6)
		N(3)-C(15)-H(15)	120.9
		C(14)-C(15)-H(15)	120.9
		N(1)-C(1)-C(2)	117.6(6)
		N(1)-C(1)-H(1)	121.2
		C(2)-C(1)-H(1)	121.2
		C(3)-C(4)-C(5)	118.6(8)
		C(3)-C(4)-H(4)	120.7
		C(5)-C(4)-H(4)	120.7
		C(19)-C(20)-N(4)	118.8(9)
		C(19)-C(20)-H(20)	120.6
		N(4)-C(20)-H(20)	120.6
		C(7)-C(8)-C(9)	121.4(6)
		C(7)-C(8)-H(8)	119.3
		C(9)-C(8)-H(8)	119.3
		C(1)-C(2)-C(3)	120.4(7)
		C(1)-C(2)-H(2)	119.8
		C(3)-C(2)-H(2)	119.8
		C(13)-C(12)-C(11)	117.6(6)
		C(13)-C(12)-H(12)	121.2
		C(11)-C(12)-H(12)	121.2
		C(10)-C(9)-C(8)	119.6(6)

C(10)-C(9)-H(9)	120.2
C(8)-C(9)-H(9)	120.2
C(14)-C(13)-C(12)	122.4(6)
C(14)-C(13)-H(13)	118.8
C(12)-C(13)-H(13)	118.8
C(4)-C(3)-C(2)	120.4(6)
C(4)-C(3)-H(3)	119.8
C(2)-C(3)-H(3)	119.8
C(13)-C(14)-C(15)	119.0(6)
C(13)-C(14)-H(14)	120.5
C(15)-C(14)-H(14)	120.5
C(20)-C(19)-C(18)	119.0(8)
C(20)-C(19)-H(19)	120.5
C(18)-C(19)-H(19)	120.5
C(18)-C(17)-C(16)	117.5(8)
C(18)-C(17)-H(17)	121.2
C(16)-C(17)-H(17)	121.2
C(17)-C(18)-C(19)	122.1(7)
C(17)-C(18)-H(18)	119
C(19)-C(18)-H(18)	119
N(5)-C(22)-C(21A)	136.4(2)
N(5)-C(22)-C(21B)	171.6(2)
H(9B)-O(9)-H(9A)	106(3)
H(10A)-O(10)-H(10B)	109(3)
N(6)-C(24)-C(23A)	129.1(2)
N(6)-C(24)-C(23B)	173.0(1)

Table C.20 Anisotropic displacement parameters (Å² x 10³) for [Ta(hopo)₄]Cl·2MeCN·2H₂O (10). The anisotropic displacement factor exponent takes the form: $-2\pi^2[h^2a^{*2}U^{11} + \ldots + 2\,h\,k\,a^*\,b^*\,U^{12}]$.

	U^{11}	U^{22}	U^{33}	U^{23}	U^{13}	U^{12}
C(21A)	28(3)	36(3)	36(3)	-9(3)	-3(2)	-8(2)
C(21B)	30(3)	61(4)	55(3)	-11(3)	-7(2)	-14(3)
C(23A)	26(3)	42(4)	37(3)	0(3)	2(2)	2(3)
C(23B)	66(4)	38(3)	33(3)	-4(2)	5(2)	13(3)
Ta(1)	23(1)	16(1)	23(1)	-5(1)	-5(1)	-2(1)
O(8)	29(2)	25(2)	41(2)	-6(2)	-11(2)	-6(2)
O(1)	30(2)	21(2)	28(2)	-9(2)	-1(2)	-1(2)
O(3)	24(2)	20(2)	26(2)	-2(1)	-4(2)	-2(1)
O(5)	23(2)	24(2)	25(2)	-7(2)	-3(1)	-1(1)
O(6)	39(2)	23(2)	24(2)	-7(2)	-9(2)	3(2)
O(2)	22(2)	28(2)	37(2)	-16(2)	3(2)	-6(2)
O(7)	43(2)	22(2)	29(2)	-6(2)	-12(2)	-4(2)
O(4)	42(2)	23(2)	28(2)	-3(2)	-9(2)	4(2)
N(3)	30(2)	23(2)	24(2)	-5(2)	-9(2)	-2(2)
N(1)	22(2)	25(2)	30(2)	-5(2)	-1(2)	-1(2)
N(2)	28(2)	26(2)	36(3)	0(2)	-8(2)	-2(2)
N(4)	41(3)	23(2)	46(3)	4(2)	-22(2)	-7(2)
C(6)	12(2)	19(2)	27(2)	0(2)	-4(2)	-3(2)
C(11)	21(2)	23(2)	23(2)	-4(2)	-7(2)	-5(2)
C(5)	64(4)	52(4)	46(3)	-6(3)	-9(3)	13(3)
C(7)	17(2)	21(3)	40(3)	-3(2)	-5(2)	-1(2)
C(10)	29(3)	39(3)	31(3)	1(2)	-12(2)	-4(2)
C(16)	45(3)	15(2)	33(3)	0(2)	-21(3)	-7(2)
C(15)	45(4)	22(3)	39(3)	-5(2)	-19(3)	1(2)
C(1)	28(3)	36(3)	36(3)	-9(3)	-3(2)	-8(2)
C(4)	66(4)	38(3)	33(3)	-4(2)	5(2)	13(3)
C(20)	40(4)	27(3)	70(5)	13(3)	-30(4)	-12(3)
C(8)	24(3)	28(3)	56(4)	2(3)	-13(3)	2(2)
C(2)	30(3)	61(4)	55(3)	-11(3)	-7(2)	-14(3)
C(12)	28(3)	39(3)	25(3)	-6(2)	-4(2)	-2(2)
C(9)	31(3)	38(4)	46(4)	11(3)	-13(3)	-3(3)
C(13)	48(4)	47(4)	26(3)	3(3)	-6(3)	-11(3)
C(3)	26(3)	42(4)	37(3)	0(3)	2(2)	2(3)
C(14)	53(4)	30(3)	40(3)	5(3)	-19(3)	-6(3)

C(19)	62(5)	33(4)	72(5)	7(4)	-41(5)	-16(3)
C(17)	82(6)	26(3)	45(4)	-4(3)	-37(4)	-7(3)
C(18)	108(8)	34(4)	71(6)	10(4)	-64(6)	-36(5)
Cl(01)	428(12)	70(2)	74(2)	1(2)	-20(4)	25(4)
C(22)	41(4)	85(7)	78(7)	-9(6)	-19(4)	-30(5)
N(5)	49(5)	106(8)	93(7)	-15(6)	-20(5)	-35(5)
O(9)	44(4)	159(8)	33(3)	30(4)	4(2)	30(4)
O(10)	86(6)	106(7)	49(4)	11(4)	-25(4)	9(5)
N(6)	90(7)	54(5)	68(6)	1(4)	3(5)	-16(5)
C(24)	64(4)	52(4)	46(3)	-6(3)	-9(3)	13(3)

Table C.21 Hydrogen coordinates (x 10^4) and isotropic displacement parameters (Å^{2}x 10^3) for [Ta(hopo)$_4$]Cl· 2MeCN·2H$_2$O (10).

	x	y	z	U(eq)
H(21A)	665	8069	3331	51
H(21B)	1503	6916	3003	51
H(21C)	-229	7083	3277	51
H(21D)	105	7901	3424	73
H(21E)	-819	8731	2769	73
H(21F)	764	9001	2747	73
H(23A)	4798	3673	2874	57
H(23B)	4850	4301	3824	57
H(23C)	3374	4359	3501	57
H(23D)	4663	4583	4128	77
H(23E)	5900	3734	3521	77
H(23F)	5492	3664	4781	77
H(7)	4212	-1309	611	32
H(10)	2668	247	3782	39
H(15)	310	5230	-1338	41
H(1)	-1638	0	744	41
H(4)	-2952	2857	2864	62
H(20)	6477	3386	-56	53
H(8)	4433	-2343	2179	44
H(2)	-4027	301	1753	58
H(12)	3330	2368	-2986	38
H(9)	3740	-1564	3753	48
H(13)	2656	3969	-3979	50
H(3)	-4683	1713	2825	46
H(14)	1122	5375	-3186	49
H(19)	6983	4669	855	61

H(17)	2739	4958	2555	56
H(18)	5131	5397	2196	74
H(9B)	8720(110)	250(60)	3870(90)	68
H(9A)	9750(90)	150(60)	4440(80)	68
H(10A)	3620(110)	1140(50)	5130(70)	68
H(10B)	3020(100)	130(70)	5590(90)	68

Table C.22 Torsion angles (°) for [Ta(hopo)₄]Cl·2MeCN·2H₂O (10).

Torsion angles	Angle (°)	Torsion angles	Angle (°)
Ta(1)-O(6)-N(3)-C(11)	7.1(6)	Ta(1)-O(7)-C(16)-N(4)	9.0(6)
Ta(1)-O(6)-N(3)-C(15)	-173.7(4)	Ta(1)-O(7)-C(16)-C(17)	-171.8(5)
Ta(1)-O(2)-N(1)-C(5)	-5.8(7)	O(8)-N(4)-C(16)-O(7)	1.0(7)
Ta(1)-O(2)-N(1)-C(1)	175.3(5)	C(20)-N(4)-C(16)-O(7)	179.0(5)
Ta(1)-O(4)-N(2)-C(6)	8.2(6)	O(8)-N(4)-C(16)-C(17)	-178.2(5)
Ta(1)-O(4)-N(2)-C(10)	-173.1(4)	C(20)-N(4)-C(16)-C(17)	-0.2(9)
Ta(1)-O(8)-N(4)-C(16)	-10.7(6)	C(11)-N(3)-C(15)-C(14)	-1.2(1)
Ta(1)-O(8)-N(4)-C(20)	171.3(5)	O(6)-N(3)-C(15)-C(14)	179.7(6)
Ta(1)-O(3)-C(6)-N(2)	-9.8(6)	C(5)-N(1)-C(1)-C(2)	-0.8(1)
Ta(1)-O(3)-C(6)-C(7)	170.4(4)	O(2)-N(1)-C(1)-C(2)	178.0(6)
O(4)-N(2)-C(6)-O(3)	1.2(7)	O(1)-C(5)-C(4)-C(3)	-178.8(8)
C(10)-N(2)-C(6)-O(3)	-177.6(5)	N(1)-C(5)-C(4)-C(3)	-0.4(12)
O(4)-N(2)-C(6)-C(7)	-179.0(5)	O(8)-N(4)-C(20)-C(19)	177.3(6)
C(10)-N(2)-C(6)-C(7)	2.2(8)	C(16)-N(4)-C(20)-C(19)	-0.5(1)
Ta(1)-O(5)-C(11)-N(3)	-8.8(6)	C(6)-C(7)-C(8)-C(9)	-1.4(9)
Ta(1)-O(5)-C(11)-C(12)	172.3(5)	N(1)-C(1)-C(2)-C(3)	-0.1(1)
O(6)-N(3)-C(11)-O(5)	1.1(7)	O(5)-C(11)-C(12)-C(13)	179.4(6)
C(15)-N(3)-C(11)-O(5)	-178.1(5)	N(3)-C(11)-C(12)-C(13)	0.5(9)
O(6)-N(3)-C(11)-C(12)	-179.9(5)	N(2)-C(10)-C(9)-C(8)	-0.8(1)
C(15)-N(3)-C(11)-C(12)	1.0(9)	C(7)-C(8)-C(9)-C(10)	2.2(1)
Ta(1)-O(1)-C(5)-N(1)	4.5(9)	C(11)-C(12)-C(13)-C(14)	-1.7(1)
Ta(1)-O(1)-C(5)-C(4)	-177.1(7)	C(5)-C(4)-C(3)-C(2)	-0.4(1)
O(2)-N(1)-C(5)-O(1)	0.8(10)	C(1)-C(2)-C(3)-C(4)	0.7(1)
C(1)-N(1)-C(5)-O(1)	179.6(6)	C(12)-C(13)-C(14)-C(15)	1.5(1)
O(2)-N(1)-C(5)-C(4)	-177.8(7)	N(3)-C(15)-C(14)-C(13)	-0.1(1)
C(1)-N(1)-C(5)-C(4)	1.1(12)	N(4)-C(20)-C(19)-C(18)	1.8(1)
O(3)-C(6)-C(7)-C(8)	179.0(5)	O(7)-C(16)-C(17)-C(18)	-179.4(6)
N(2)-C(6)-C(7)-C(8)	-0.8(8)	N(4)-C(16)-C(17)-C(18)	-0.2(9)
O(4)-N(2)-C(10)-C(9)	179.9(6)	C(16)-C(17)-C(18)-C(19)	1.5(1)
C(6)-N(2)-C(10)-C(9)	-1.4(9)	C(20)-C(19)-C(18)-C(17)	-2.3(1)

Table C.23 General hydrogen-bond distances (Å) and angles (°) for [Ta(hopo)₄]Cl·2MeCN·2H₂O (10).

Interactions	D-H···A	D-H (Å)	H···A (Å)	D···A (Å)	D-H···A (°)
I	O9-H9A···O9i[a]	0.89(1)	2.44(1)	3.265(1)	156(7)
II	O9-H9B···O10[b]	0.85(1)	2.46(2)	3.142(1)	137(1)
III	O10-H10A···N6	0.90(9)	1.95(9)	2.832(1)	168(1)
IV	O10-H10B···O9[b]	0.84(9)	2.31(9)	3.142(1)	174(1)
V	C1ii-H1ii···O2i[c]	0.95	2.45	3.373(9)	164
VI	C7-H7···O8ii[d]	0.95	2.48	3.246(8)	137
VII	C15iii-H15iii···O6ii[e]	0.95	2.46	3.373(8)	160
VIII	C15iii-H15iii···O7ii[e]	0.95	2.54	3.300(9)	137
IX	C20ii-H20ii···N5[f]	0.95	2.44	3.364(1)	165

Symmetry code: (a) -x + 2, -y, -z + 1, (b) -x + 1, -y, -z + 1, (c) -x, -y, -z, (d) -x + 1, -y, -z,

(e) -x, -y + 1, -z, (f) -x + 1, -y + 1, -z.

10.2 Supplementary kinetic data

Supplementary kinetic data for the complex, *cis*-[NbO(ca)$_2$(H$_2$O)OPPh$_3$]$^-$ discussed in Chapter 8 is listed in Table D.1. The triphenylphosphineoxide (OPPh$_3$) substitution reactions between *cis*-[NbO(ca)$_2$(H$_2$O)OPPh$_3$]$^-$ and pyridine derivatives; pyridine (py), 4-(dimetylamino)pyridine (DMAP), 4-methylpyridine (4-Mepy), 3-chloropyridine(3-Clpy) and 3-bromopyridine(3-Brpy) as entering ligands were followed. The reaction was followed at four different temperatures (15.5, 24.5, 31.2 and 45.9 °C) and the niobium concentration was kept constant at 1.0 x 10^{-3} M throughout.

Table D.1 Temperature and [DMAP] dependence of the *pseudo* first-order reaction between *cis*-[NbO(ca)$_2$(H$_2$O)OPPh$_3$]$^-$ and 4-(dimethylamino)pyridine. [Nb] = 1.0 x 10^{-3} M, λ$_{max}$ = 430 nm, MeCN.

	10^{-3} k$_{obs}$(s^{-1})			
[DMAP] M	15.5 ºC	24.5 ºC	31.2 ºC	45.9 ºC
0.05	0.9897(6)	1.2030(8)	1.9043(7)	5.4333(4)
0.15	1.5219(9)	2.4965(7)	3.9020(6)	11.8946(1)
0.25	2.2155(3)	3.7257(5)	5.9448(2)	17.5026(9)
0.35	2.9891(5)	4.9062(1)	7.6794(3)	23.5853(6)
0.50	3.9313(9)	7.0311(8)	11.1549(4)	31.1322(7)

Table D.2 Substituent dependence of the *pseudo* first-order reaction between *cis*-[NbO(ca)$_2$(H$_2$O)OPPh$_3$]$^-$ and pyridine derivative ligands (Py). [Nb] = 1.0 x 10^{-3} M, λ$_{max}$ = 430 nm, 31.2 ºC, MeCN.

	10^{-3} k$_{obs}$(s^{-1})				
[Py] M	py	DMAP	4-Mepy	3-Clpy	3-Brpy
0.05	1.2711(1)	1.9042(7)	1.0268(6)	0.8918(4)	0.7767(8)
0.15	1.4161(4)	3.9020(6)	1.2020(5)	1.0325(2)	0.8871(9)
0.25	1.5678(2)	5.9447(2)	1.4125(6)	1.2321(2)	1.0426(3)
0.35	1.6634(9)	7.6794(3)	1.5989(4)	1.4383(1)	1.1935(8)
0.50	1.8693(3)	11.1549(4)	1.8279(9)	1.7897(4)	1.4306(1)

Table D. 3 Temperature and [caH$_2$] dependence of the *pseudo* first-order reaction between [NbCl$_6$]$^-$ and chloranilic acid. [Nb] = 2.0 x 10^{-4} M, λ_{max} = 530 nm, MeOH.

[caH$_2$] M	$k_{obs}(s^{-1})$			
	15.0 ºC	**25.0 ºC**	**35.0 ºC**	**45.0 ºC**
0.001	0.06603(4)	0.14331(3)	0.32399(1)	0.41648(7)
0.002	0.09256(1)	0.20666(5)	0.45177(3)	0.89292(1)
0.003	0.12124(4)	0.31727(2)	0.72468(5)	1.49113(4)
0.005	0.25477(2)	0.64382(6)	1.43655(6)	3.34264(6)
0.007	0.46758(8)	1.23874(5)	2.74561(9)	6.69908(7)